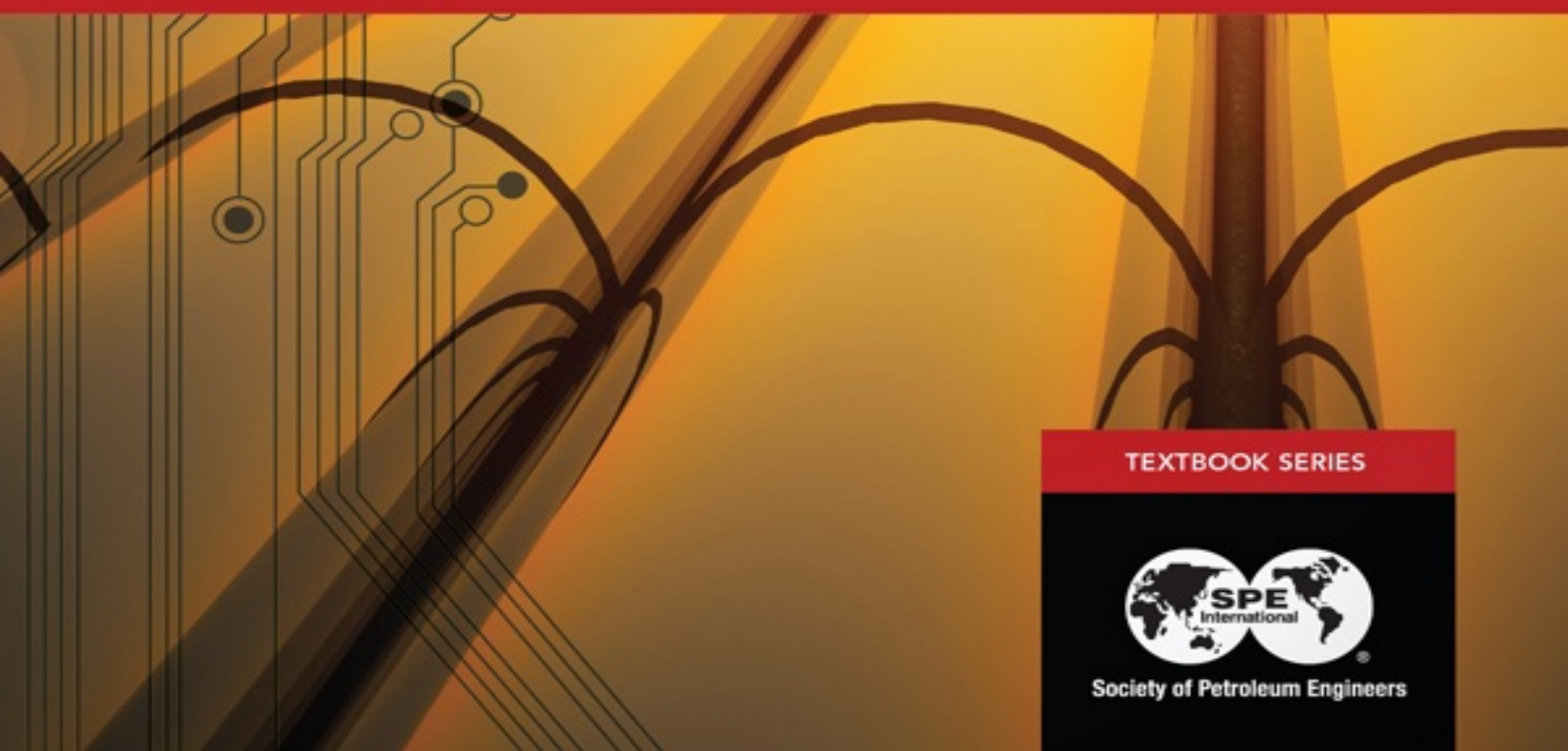


NODAL ANALYSIS

of Oil and Gas Production Systems

Jan-Dirk Jansen



TEXTBOOK SERIES



Society of Petroleum Engineers

Nodal Analysis of Oil and Gas Production Systems

Nodal Analysis of Oil and Gas Production Systems

Jan Dirk Jansen

The MATLAB software accompanying the book can be downloaded from www.tudelft.nl/nodal

Society of Petroleum Engineers

© Copyright 2017 Society of Petroleum Engineers

All rights reserved. No portion of this book may be reproduced in any form or by any means, including electronic storage and retrieval systems, except by explicit, prior written permission of the publisher except for brief passages excerpted for review and critical purposes.

Printed in the United States of America.

Disclaimer

This book was prepared by members of the Society of Petroleum Engineers and their well-qualified colleagues from material published in the recognized technical literature and from their own individual experience and expertise. While the material presented is believed to be based on sound technical knowledge, neither the Society of Petroleum Engineers nor any of the authors or editors herein provide a warranty either expressed or implied in its application. Correspondingly, the discussion of materials, methods, or techniques that may be covered by letters patents implies no freedom to use such materials, methods, or techniques without permission through appropriate licensing. Nothing described within this book should be construed to lessen the need to apply sound engineering judgment nor to carefully apply accepted engineering practices in the design, implementation, or application of the techniques described herein.

ISBN 978-1-61399-564-8

First Printing 2017

Society of Petroleum Engineers
222 Palisades Creek Drive
Richardson, TX 75080-2040 USA

Promizer.ir | salmani.sgh@gmail.com | Sadegh Salmani

<http://www.spe.org/store>

service@spe.org

1.972-952.9393

Preface

This book is based on material used in a three-month course for first-year graduate students in the Petroleum Engineering MSc program at Delft University of Technology (TU Delft). This course aims at providing skills in the development and use of mathematical and computer models for flow through the various parts of an oil and gas production system. The underlying idea is that a basic understanding of the numerical implementation of theoretical concepts should be an important element in the education of all engineering students, even though only a few of them will become tool developers and most of them will just use software tools whose inner workings are hidden behind slick user interfaces.

Although the book is primarily intended for classroom use, it may also be of value for practicing engineers or researchers who want to get acquainted with the essentials of nodal analysis or learn more about the underlying theory.* Prerequisites are a basic understanding of physical transport phenomena; calculus, including first-order differential equations; and preferably an acquaintance with hydrocarbon properties and oil and gas well completions.

Questions and exercises are provided at the end of each chapter. Some of those involve computations that can be performed by hand with a calculator, while others require the use of a computer to run the MATLAB routines that accompany the book. MATLAB questions and assignments form an important ingredient of the course, and a basic level in computer programming will therefore be of help to benefit maximally from the book. Hand calculations are primarily seen as a means to obtain quick order-of-magnitude estimates or to verify the results of computer simulations. However, the theory is presented in the book to be understandable without the reader going through the MATLAB exercises. Worked-out answers to all questions are provided in [Appendix G](#).

An early version of this book was based on material written by prof. Peter K. Currie. Since I took over his course in 2001, the text has gradually been rewritten and expanded. During Spring 2011 I revised major parts while teaching a similar course at Stanford University. Very little of the theory described in the text is new, and I acknowledge the contributions of all those who have pioneered the field of nodal analysis and the underlying models for the various production system elements. I have tried to refer to the original sources as far as I am aware of them. Moreover, I acknowledge the contribution of many students and teaching assistants at TU Delft and Stanford who helped to spot errors, inconsistencies, or material that was unclear, both in the text and in the accompanying MATLAB code. No doubt there is still room for further improvement. If you find errors, note missing references, or have other comments, please let me know at j.d.jansen@tudelft.nl.

* Those readers who are just looking for a quick introduction to nodal analysis should read Sections 1.5.1 and 1.6, perform the assignment in [Section 1.8](#) (no MATLAB required), and then jump to [Chapter 8](#), which gives an overview of the most common nodal analysis applications.

Contents

Preface

1 Introduction

- 1.1 What Is Covered in This Chapter?
- 1.2 About This Book
- 1.3 Production Engineering
- 1.4 Oil and Gas Production Systems
- 1.5 System Models
- 1.6 Nodal Analysis
- 1.7 Questions
- 1.8 MATLAB Assignment: Nodal Analysis of a Simple System

2 Properties of Reservoir Fluids

- 2.1 What Is Covered in This Chapter?
- 2.2 Fluid Properties
- 2.3 Production Variables
- 2.4 Pressure/Temperature Phase Diagram
- 2.5 Equations of State
- 2.6 Oil Models
- 2.7 Fluid Property Calculations
- 2.8 Questions
- 2.9 MATLAB Assignment: Hydrocarbon Properties

3 Single-Phase Flow in Wells and Pipelines

- 3.1 What Is Covered in This Chapter?
- 3.2 Governing Equations
- 3.3 Single-Phase Oil Flow
- 3.4 Single-Phase Gas Flow
- 3.5 Tubing Performance and Intake Curves
- 3.6 Flow in an Annular Geometry
- 3.7 Questions
- 3.8 MATLAB Assignment: Single-Phase Gas Flow

4 Multiphase Flow in Wells and Pipelines

- 4.1 What Is Covered in This Chapter?
- 4.2 Multiphase Flow Concepts

- 4.3 Pressure Drop Analysis
- 4.4 Tubing Intake Curves
- 4.5 Lift Tables
- 4.6 Questions
- 4.7 MATLAB Assignment: Drift Flux

5 Flow Through Restrictions

- 5.1 What Is Covered in This Chapter?
- 5.2 Restrictions
- 5.3 Single-Phase Oil Flow
- 5.4 Single-Phase Gas Flow
- 5.5 Multiphase Flow: Empirical Models
- 5.6 Multiphase Flow: Theoretical Models
- 5.7 Questions
- 5.8 MATLAB Assignment: Choke Flow

6 Inflow Performance: The Basics

- 6.1 What Is Covered in This Chapter?
- 6.2 The Importance of Inflow Performance
- 6.3 Well Operation and Reservoir Flow Stages
- 6.4 Governing Equations
- 6.5 Single-Phase Oil Flow
- 6.6 The Skin Factor
- 6.7 Single-Phase Gas Flow
- 6.8 Multiphase Flow: Empirical Models
- 6.9 Multilayer Inflow Performance
- 6.10 Related Topics Not Considered in This Chapter
- 6.11 Questions
- 6.12 MATLAB Assignment: Commingled Production With a Smart Well

7 Inflow Performance: Further Topics

- 7.1 What Is Covered in This Chapter?
- 7.2 Two-Dimensional Reservoir Flow
- 7.3 Horizontal Wells, Part 1
- 7.4 Horizontal Wells, Part 2
- 7.5 Semi-Analytical Approach
- 7.6 Multiphase Flow: Theoretical Models
- 7.7 Related Topics Not Considered in This Chapter

7.8 Questions

7.9 MATLAB Assignment: Horizontal Well Inflow and Pressure Drop ...

8 Well Performance

8.1 What Is Covered in This Chapter?

8.2 Analyzing Well Performance

8.3 Field Development Planning and Field Management

8.4 Artificial Lift

8.5 Related Topics Not Considered in This Chapter

8.6 Questions

8.7 MATLAB Assignment: Well Performance

Appendix A: SI Units and Field Units

A-1 Conversion Factors

A-2 SI Prefixes

A-3 Standard Conditions

A-4 Pitfalls in Unit Conversion

Appendix B: Fluid Properties and Correlations

B-1 Fluid Properties

B-2 Oil Correlations

B-3 Gas Correlations

B-4 Water Properties

Appendix C: Wellbore Surveying

C-1 Coordinates

C-2 Survey Evaluation

C-3 Numerical Implementation

Appendix D: Numerical Methods

D-1 Root Finding

D-2 Differential Equations

Appendix E: Multiphase Flow Correlations

E-1 Hagedorn and Brown

E-2 Mukherjee and Brill

E-3 Drift Flux Models

Appendix F: Relative Permeabilities

F-1 Physics

F-2 Corey Expressions

Appendix G: Answers to Questions

- G-1 Answers for Chapter 1, Introduction
- G-2 Answers for Chapter 2, Properties of Reservoir Fluids
- G-3 Answers for Chapter 3, Single-Phase Flow in Wells and Pipelines
- G-4 Answers for Chapter 4, Multiphase Flow in Wells and Pipelines
- G-5 Answers for Chapter 5, Flow Through Restrictions
- G-6 Answers for Chapter 6, Inflow Performance: The Basics
- G-7 Answers for Chapter 7, Inflow Performance: Further Topics
- G-8 Answers for Chapter 8, Well Performance

Appendix H: MATLAB Files

- H-1 Guidance for Use
- H-2 Conversion Factors
- H-3 Survey
- H-4 Fluid Properties
- H-5 Pipe Flow
- H-6 Lift Tables
- H-7 Choke Flow
- H-8 Reservoir Flow
- H-9 Systems
- H-10 Questions
- H-11 Graphical User Interface
- H-12 Demo

Nomenclature

Glossary

References

Index

Chapter 1

Introduction

1.1 What Is Covered in This Chapter?

This introductory chapter is meant to clarify the scope and objectives of the book, give a brief overview of the field of production engineering and the relevant hardware, describe the basic concepts used in oil and gas production system modeling, and introduce the method of nodal analysis.

1.2 About This Book

1.2.1 Objectives. Oil and gas wells are essential elements of oil and gas *production systems*. A production system can be roughly defined as the equipment required to produce hydrocarbons from a subsurface reservoir to the point of sale. The activities related to the conceptual design and the operation of a production system are collectively referred to as *production engineering*. An important element of production engineering is the quantification of pressures, temperatures, and flow rates inside the production system for various operating conditions, an activity that usually requires some mathematical model of the system, either in the form of written equations or implemented in a computer program. A particular form of modeling, known as *nodal analysis*, describes the system as a collection of separate elements with distinct flow properties (Brown 1984; Brown and Lea 1985; Beggs 1991) and builds on theory developed in the classic paper of Gilbert (1954). (Note that literature references are listed alphabetically in the References section of this book.) Nodal analysis has proven to be an effective tool for analyzing production system performance, and forms the basis of several commercial and proprietary software packages.

The objectives of this book are:

- To provide an understanding of the concepts used in computer models for the nodal analysis of flow through a production system. This includes understanding the physics, capturing the essential physics in the form of mathematical expressions, and coding these in a computer model.
- To provide basic skills in using a production system computer model to perform production engineering calculations. This concerns, in particular, generating predictions of pressures and flow rates and using them to optimize the design of the production system.

1.2.2 Scope. This book is not explicitly meant to give a complete overview of the field

of production engineering, but, rather, to treat some essential concepts in enough detail to achieve the objectives listed above. In particular, it concentrates on the modeling of the flow in a well system, including the near-well reservoir, but does not treat surface facilities in any detail, nor complex networks of multiple wells. Also, the treatment of the physical principles is aimed at explaining the essential concepts but does not completely cover all aspects involved. For example, the book does treat the equations for pressure drops in various elements of a well system and demonstrates how they can be implemented in a simple computer code. However, it does not cover the temperature drops in those elements, because the equations and the computer implementation are analogous to those for pressure drops, and the details can be found in specialized books. Another example concerns the models for multiphase flow in pipes covered in [Chapter 4](#). There, rather than cover the vast range of available models and correlations, the book describes just a few typical models, not necessarily the most accurate ones, to explain the underlying concepts. Understanding the essential concepts in nodal analysis of a well system should provide the readers with enough knowledge to use commercial nodal analysis software for more complex systems, explore the literature in this field, and expand their knowledge as required. Moreover, the scope of this book does not include a detailed description of hardware components. Several other books are available for this purpose, such as Bellarby (2009); various chapters in the *SPE Petroleum Engineering Handbook* (Lake 2007) also contain good descriptions of hardware components.

1.2.3 Empiricism and First-Principles Modeling. Many textbooks on production engineering present a large number of formulas without their derivation. In the present book, I tried, wherever feasible, to avoid this approach and instead present the derivation of formulas starting from first principles. However, many production engineering calculations are performed with empirical correlations, or at least semiempirical ones with coefficients “tuned” through experiments; in those instances the presentation of equations without derivation is, of course, unavoidable. Moreover, the description of full physical models would sometimes be too involved and outside the scope of this book—e.g., as in the case of fully “mechanistic” multiphase pipe flow models. Therefore, in such cases the book will revert to (semi)empirical approaches.

1.2.4 MATLAB Routines. Many of the equations developed here have been programmed in MATLAB routines that can be downloaded from the website accompanying the book. MATLAB is a programming language for numerical computing with extensive plotting capabilities and a large number of pre-programmed routines for mathematical operations. For an overview and tutorials, see MATLAB (2017). The understanding and use of the routines accompanying the book requires basic programming skills, but no advanced MATLAB knowledge. In particular, the use of compact vector notation as offered by the MATLAB programming language has mostly

been avoided, thus somewhat sacrificing computational and notational efficiency for the benefit of readability and educational value. Questions are provided at the end of the chapters. Some of these can be answered through reasoning, others by performing calculations by hand or with a simple calculator, others require the use of MATLAB routines. In line with modern production engineering practice, hand calculations are seen primarily as a means to obtain quick order-of-magnitude estimates or to verify the results of computer simulations.

1.2.5 Unit Systems and Notation Conventions. Formulas, data, and example calculations will be presented primarily in consistent SI units. Occasionally the corresponding field units are added to allow easy comparison with results from literature or to give the reader a feel for units still used in oil field practice. In the oil industry, the expression “SI units” is often loosely used to indicate both “strict” (consistent) SI units and “allowable” (possibly inconsistent) SI units. The strict units can be subdivided into the seven base SI units (m, kg, s, A, K, mol, and cd) and derived SI units such as N, Pa, °C, or J. Allowable SI units typically include d (day) and a (year), and are defined in the SPE Metric Standard (SPE 1982).

A brief list of conversion factors is given in [Appendix A](#) (for a more extensive list, see SPE 1982). In addition, a number of MATLAB “m-files” for unit conversion can be downloaded from the website accompanying the book (web address listed on title page at time of printing). These have a self-explanatory syntax. Thus, e.g., to convert a value of 1,000 psi into Pa, type:

```
» from_psi_to_Pa(1000)
```

which produces the answer

```
ans = 6894757
```

SI units will be used directly in the text. Non-SI units will be enclosed in round brackets when necessary to avoid confusion. To distinguish between temperatures expressed in °C (or °F) and absolute temperatures expressed in K (or °R), absolute temperatures will be labeled with a subscript: T_{abs} . Following the SPE Style Guide (SPE, 2015), different notations, expressed in either SI or field units, can be used for the same unit. For example, “day” is indicated with “d” in SI units, while it is indicated with “D” in field units. Oil volumes in field units are indicated with “bbl”, but in combined units with “B”, such that oil flow rates in field units are expressed in B/D. Also, products of units in the denominators of fractional expressions are indicated with a “.” in SI units and a “-” in field units. Thus, $\text{kg}/(\text{m}^3 \cdot \text{s})$ should be read as $\text{kg}/(\text{m}^3 \times \text{s})$ and $\text{lbs}/(\text{ft}^3 \cdot \text{s})$ as $\text{lbs}/(\text{ft}^3 \times \text{s})$. Dimensions will be enclosed in square brackets, as, for example, in “ J_s ” is expressed in $\text{m}^2/\text{s} \cdot \text{Pa}$ (B/D-psi-ft) and has dimensions of $[\text{L}^3 \text{ m}^{-1} \text{ t}]$.

Dimensions appear as follows, using the SPE Symbols Standard (Lake 2007, Vol. 7, pp. 103-140):

L	length
---	--------

m	mass
M	money
n	amount of substance
q	electrical charge
t	time
T	temperature

Following the SPE Style Guide (SPE 2015), variables are always written in *italics*, while subscripts are italicized when they represent SPE standard symbols or acronyms; they are written in Roman font when they represent abbreviations. For example, p_{mf} and p_{sep} are used to indicate ‘manifold pressure’ and ‘separator pressure’ respectively.

1.3 Production Engineering

Fig. 1.1 displays a high-level overview of activities during oil and gas *exploration and production*, known as E&P. This process diagram, often referred to as the *petroleum life cycle model*, can of course be refined to display subactivities at deeper levels. The material in this book is of relevance to the production engineering activities during the development and production phases of the petroleum life cycle, in particular to the sub-activities involving field development planning, detailed design of wells and facilities, and operation of wells and facilities.

1.3.1 Development. Unlike what is suggested in **Fig. 1.1**, the petroleum life cycle is not just a sequential process. In particular, during the design phase, a lot of activities are performed in an iterative fashion. **Fig. 1.2**, e.g., displays some of the activities involved in designing a well during a field development project, clearly indicating the iterative nature of the process. At a higher level, several cycles of reappraisal (e.g., based on production performance or new seismic data); redevelopment (e.g., through either the recompletion of existing wells or in-fill drilling of new ones); and production may take place during the life of a field. Each of these activities involves aspects of production engineering.



Fig. 1.1—Petroleum life cycle model.

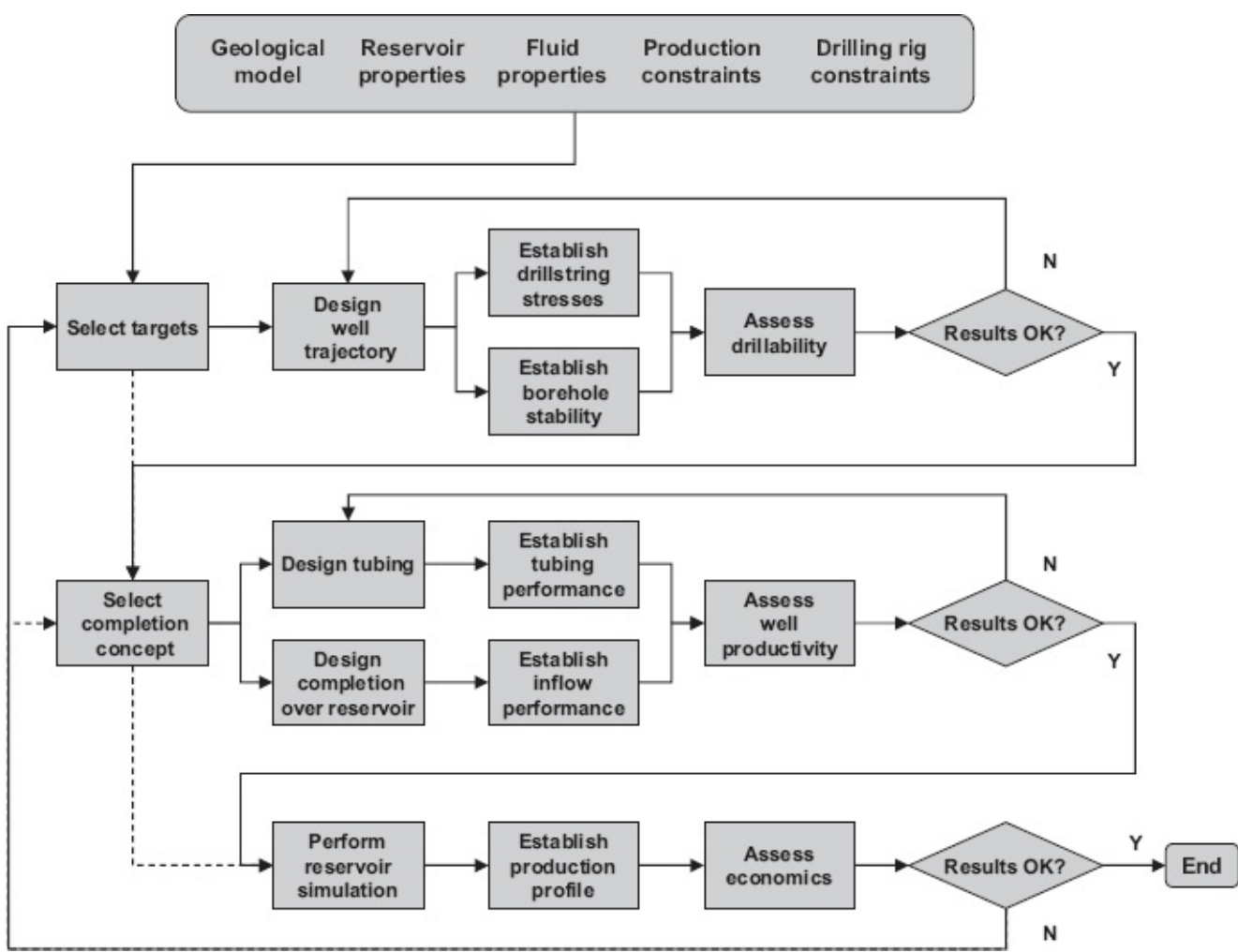


Fig. 1.2—An example of iterative processes during well design in a field development project. Not shown are the links to other iterative activities during the development process such as geological modeling or design of surface facilities.

The key objective during field development is maximizing the economic benefits within the constraints of the project. This optimization process involves comparing multiple development concepts, usually in combination with multiple subsurface models to reflect geological uncertainties. Early cooperation between geophysicists, geologists, reservoir engineers, production engineers, and well engineers, supported by the appropriate organizational structure and systems (software), is essential to achieve the objective.

Traditionally, the concept of production optimization is used in a somewhat narrower context. For example, the textbooks of Brown (1984) and Beggs (1991) focus on optimizing the various components in the flow path from the reservoir to the separator, and elaborate on the detailed analysis of flow in flowlines, chokes, wells, and the near-well section of the reservoir. This book takes a similar approach. All optimization activities require the use of some kind of model of the production system. Traditionally, these models consisted of relatively simple mathematical equations, accessible to hand analysis, sometimes with the aid of charts or tables. Now, the models are usually much more complicated and require the use of a computer.

1.3.2 Production. Apart from its seemingly linear character, Fig. 1.1 has another flaw. It suggests that all phases of the petroleum life cycle are equally important, or that they take similar amounts of time. In reality, the majority of the life of an oil field is spent in the production phase (see Fig. 1.3). Just as during the design phase, various repetitive processes occur during the production phase. This is illustrated in Fig. 1.4, which represents oil and gas production as a feedback control process, involving measurement, modeling, and control. Two major feedback cycles occur, each on its own timescale (see, e.g., Rossi et al. 2000).

- *Daily Production Control.* On a scale of days to weeks, typical input variables are wellhead chokesettings, water-injection pressures, or lift-gas rates. Measured output from the process includes production variables such as tubing-head pressures and oil, gas, and water rates. Control will often be driven by short-term optimization objectives—e.g., production targets or utilization rates of surface facilities. Models of flow through wells and surface facilities can play an important role in the process of optimizing daily production (Bieker et al. 2007). A typical short-term optimization problem is maximizing oil production by distributing a limited amount of lift gas over a number of producing wells.
- *Reservoir Management.* On a time scale of months to years, the production process consists essentially of draining the reservoir. In addition to the variables that control daily production, input includes production engineering activities such as water or gas shutoff, recompletion, stimulation, or even sidetracking or infill drilling.

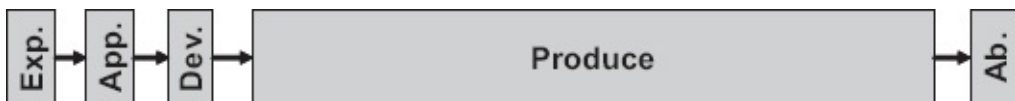
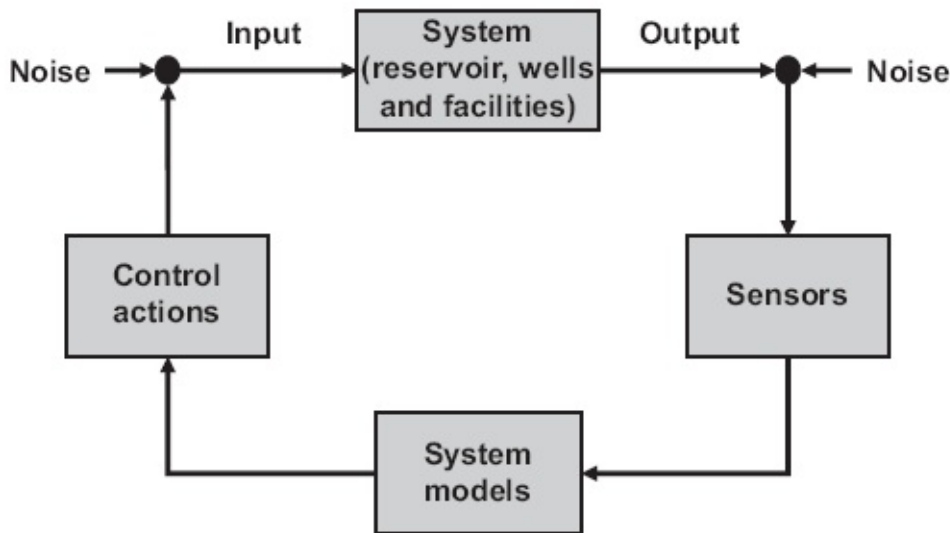


Fig. 1.3—Petroleum life cycle model emphasizing the importance of the production phase.

Control Measure



Model

Fig. 1.4—Oil and gas production represented as a feedback control process, involving measurement, modeling, and control.

Measured output includes *production histories* (i.e., records of wellhead pressures and well flow rates over time), and the results of *well tests* (i.e., measurements of downhole pressure buildup after a well is shut in) and *production logs* (i.e., downhole measurements of pressure, temperature, and flow rates made with a tool run on a wireline), and reservoir images obtained from *time-lapse seismic data* (i.e., the results of seismic measurements repeated over time to monitor the movement of fluid fronts). Control is usually focused on maximizing the asset revenues, by maximizing ultimate recovery and minimizing operating expenditures.

System modeling will often involve extensive reservoir simulation, in addition to wellbore- and surface-flow modeling. In particular, when redevelopment activities are initiated at a later stage in the producing life of a field, the reservoir management process coincides in many aspects with the field development process described above (Jansen et al. 2008). Sometimes short-term production optimization is considered to be an activity for production engineers only, whereas reservoir management would be the domain of the reservoir engineering and production geology disciplines. Such a distinction is somewhat artificial because these activities are linked. An important production engineering activity is *surveillance*, the systematic collection and analysis of well and facilities performance data. Such production data are essential not only for optimizing the production system but also managing the reservoir over the long term. In turn, understanding the long-term objectives of field

development is essential to optimizing the depletion of a reservoir. Because of the need to integrate the short- and long-term optimization activities, many oil companies have reorganized their production organizations around assets, rather than around the traditional disciplines.

1.4 Oil and Gas Production Systems

The main functions of an oil and gas production system are to:

- Provide a conduit for the flow of fluids from the reservoir to the off-take point at the surface, or from the surface back to the subsurface
- Separate the produced reservoir fluids from each other
- Minimize the production of and the negative effects of byproducts
- Store the produced fluids if they cannot be exported immediately
- Measure the amounts of fluids produced and control the production process
- Provide (part of) the energy required to transport fluids through the system

The basic elements of a production system are shown in **Figs. 1.5 through 1.7**:

- *Near-wellbore region* of the reservoir, i.e., a zone of several meters in a radial direction around the wells throughout at the depth of the reservoir
- *Wells*, from the reservoir to the wellheads at the surface
- *Flowlines*, from the wellheads to the surface facilities
- *Surface facilities*, consisting of gas/liquid separators, pumps, compressors, and other equipment for treatment and measurement
- *Storage tanks* (also called *stock tanks*) and *pipelines* (also called *trunk lines*) up to the off-take point (also called the sales point), which can, e.g., be a valve at the entrance of a gas transport pipeline or the off-loading point of an oil terminal that supplies tankers

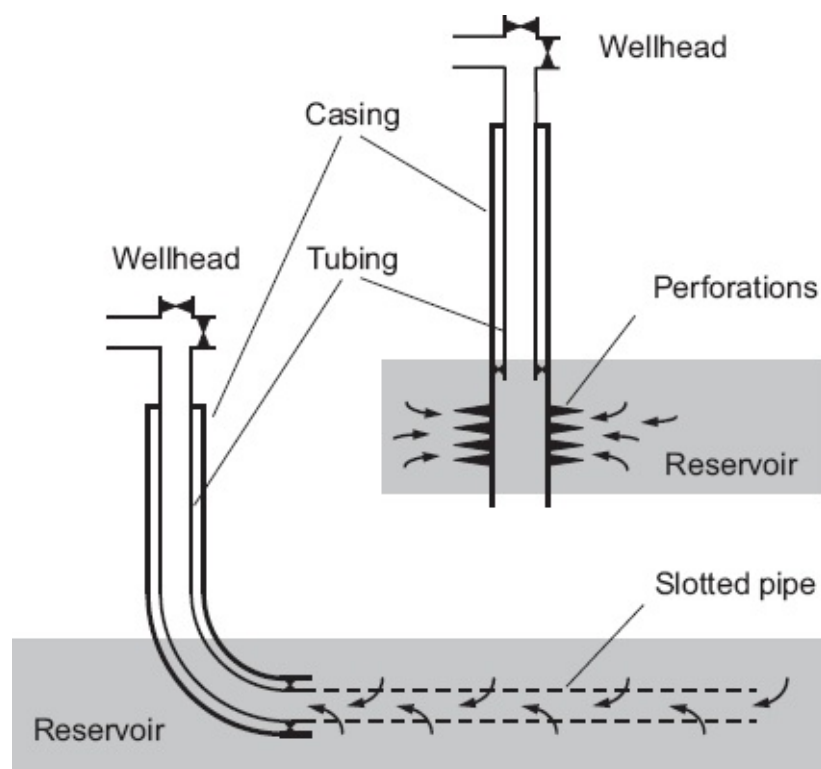


Fig. 1.5—Schematics of a vertical and a horizontal well. The vertical well (top right) is completed with a tubing, a packer, and a perforated casing. The horizontal well (bottom left) is completed with a tubing, a packer, and an uncemented slotted pipe.

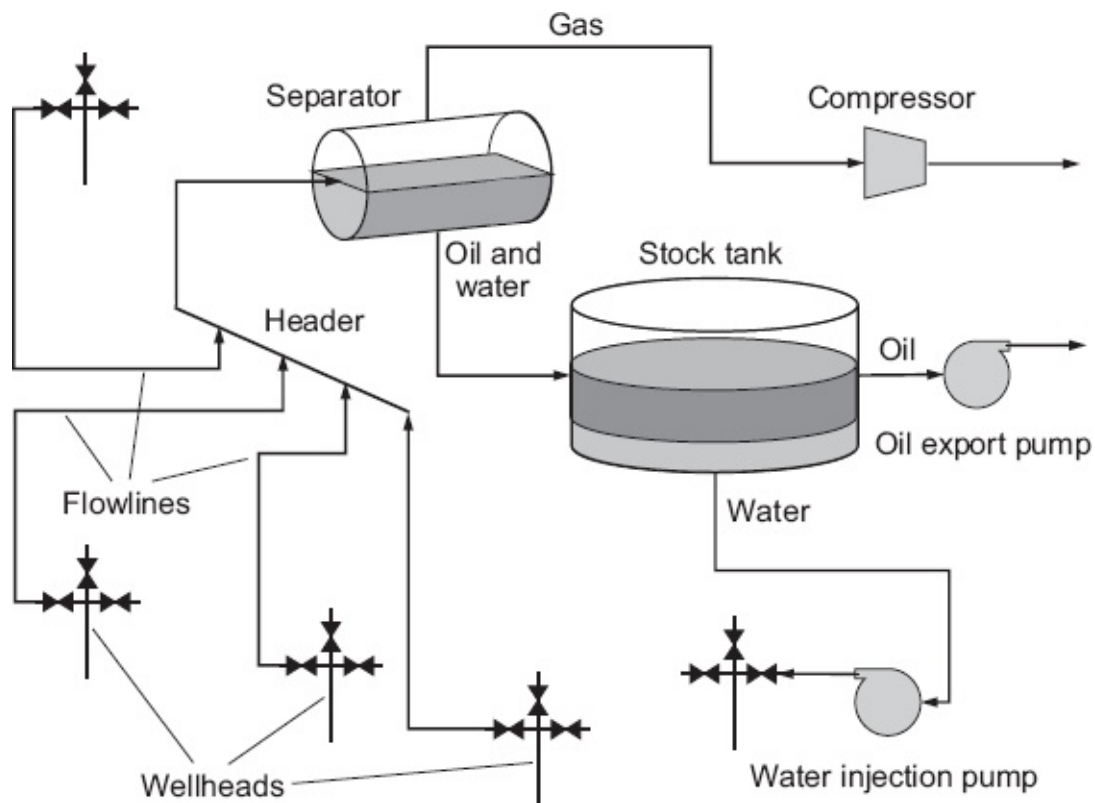


Fig. 1.6—Surface facilities. The five wellheads are connected to four production wells and one water injection well. Oil is exported to a terminal, gas into an export pipeline.

Each element of the system can be subdivided into subelements. In particular, the flow path through the wellbore may consist of:

- *Perforations* (“perfs”) in the formation, in the cement around the casing, and in the casing itself
- *Sand control equipment*, consisting of densely-packed gravel or metal screens at the bottom of the well
- *Tubing*, a pipe running from the bottom of the well to surface
- *Surface-controlled subsurface safety valve (SCSSV)*, to close in the well if surface control is accidentally lost
- *Wellhead* (often called *Christmas tree* or *tree*), consisting of manually or remotely controlled valves to shut in the well and allow access with wireline tools. One of the valves is usually a *choke valve* or *bean*, which is a variable-sized restriction used to control the flow from the well

The downhole equipment in a well is usually referred to as the *completion*. Some wells are not completed with a cemented production casing over their entire depth but instead have an *openhole completion*, which is an open, uncased hole in the producing unit, also called a *barefoot completion*; or they may have a perforated or slotted pipe. There is always a cemented *casing* running from the top of the reservoir (i.e., the *seal* or the *caprock*) to the surface to avoid uncontrolled flow or co-mingling of reservoir fluids. The tubing is usually anchored to the casing just above the reservoir with the aid of an inflatable rubber *packer*. As opposed to the casing, which is cemented in place, the tubing can be replaced if it is worn or corroded, or if the flow rate of the well can be increased by changing the tubing diameter. Some wells have a *dual completion*, which means two tubings are installed, each producing from a different reservoir at a different depth.

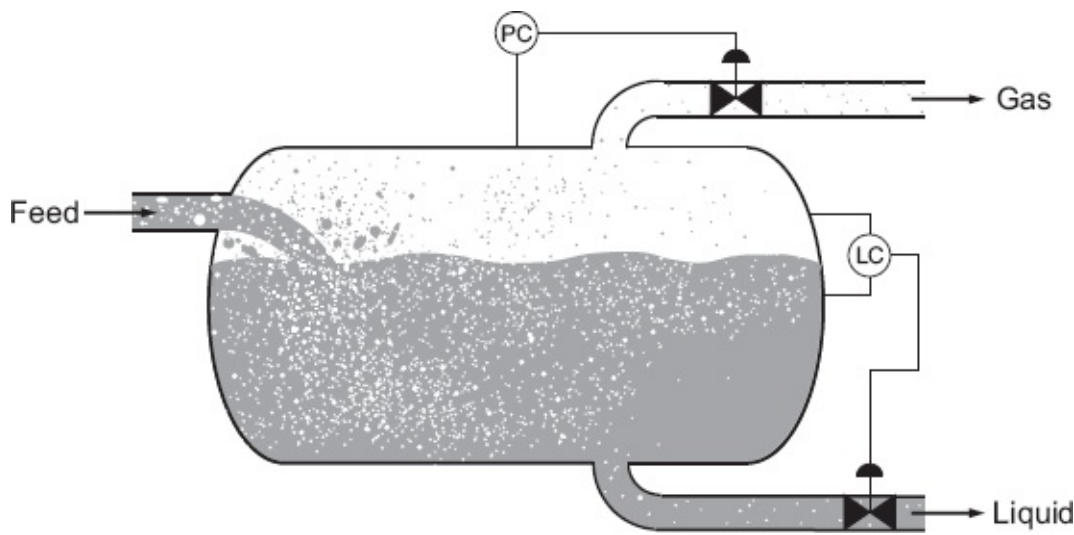


Fig. 1.7—Schematic representation of a gas/liquid separator. The throughput is controlled with the aid of a pressure controller (PC) and a level controller (LC).

The surface facilities are usually more complicated than those depicted in Fig. 1.6. Often, two or more separators are mounted in series to allow a stepwise reduction of the pressure, rather than a single pressure drop. These steps are performed in order to maximize the amount of oil produced. During separation of light and heavy hydrocarbon components, a certain amount of the intermediate components disappears with the lighter ones. The lower the pressure drop, the lower the amounts of intermediate components that disappear. A multiple separator configuration also allows coping with a drop in *tubinghead pressure* (i.e., the pressure in the tubing at the wellhead), an effect that often occurs during the life of a well when water production increases and oil production drops. In that case it is possible to connect the well to the low-pressure separator directly while those wells that still produce at high tubinghead pressures remain connected to the high-pressure separator. The pressure in the stock tank is always atmospheric because *crude oil* (degassed and dewatered oil) is transported under atmospheric conditions.

A special role is played by the *test separator*, which is another, smaller separator equipped to measure oil, gas, and water flow rates. Individual wells can be rerouted to the test separator for these measurements. Such a *production test*, which takes several hours to obtain accurate data, is typically performed once a month for each well. This has traditionally been the only way to assess a well's production. Increasingly, however, more continuous measurements are being taken with the aid of multiphase flowmeters directly connected to the flowlines. Some form of continuous measurement of pressures and temperatures at various parts of the surface production system is quite common. Downhole measurements with the aid of *permanent downhole gauges* (PDGs) are less common, although their application is steadily increasing. Automatic measurements are usually stored in an electronic control system, which can allow full control of the surface facilities from a local or even remote control room. This level of instrumentation and automated process control is quite common in expensive, high-production operations, typically in an offshore environment. However, many production facilities, especially those on land, are relatively simple and are still operated manually.

Gas production often requires specialized treatment facilities to dry the gas and remove corrosive components such as hydrogen sulfide (H_2S) or carbon dioxide (CO_2). Furthermore, various types of pumps and compressors, both centrifugal and reciprocating, are applied to export oil and gas or to reinject produced water or gas into the subsurface. Gas compression is also often used to enable *gas lift*, which is the injection of gas into the wellbore to reduce the hydrostatic head of the liquid and thus increase production. This is an example of *artificial lift*, the process of supplying external energy to force the wellbore liquid from the reservoir to surface. Artificial lift is required when the reservoir pressure is too low to make the well flow naturally, a situation that often occurs at a later stage in the life of the reservoir. The most well-known methods, apart from gas lift, are pumping with *beam pumps* ("nodding donkeys") or *electrical submersible pumps* (ESPs). For further information on surface facilities, see, e.g., Chilingarian et al. (1987) or Arnold and Stewart (1998).

For further information on artificial lift, see, e.g., Bellarby (2009) or Economides et al. (2013).

1.5 System Models

1.5.1 Topology. Flow through a complicated system, such as a production system, must be broken down into its component parts for analysis. In this book we will examine the flow behavior in several of the component parts: inflow into the wells, flow within the wells, and flow through chokes and flowlines. In performing these detailed analyses it is essential to realize that we are looking only at separate components of a larger system. Optimizing the performance of each component will not normally result in an optimized system. For example, if we improve the well inflow so much that the tubing is unable to handle the production, we have wasted money.

We can describe the components of a production system as a network of elements connected at nodes. For example, the flow from the reservoir through the well, the surface facilities, and the pipeline can be represented as a series of elements and nodes as shown in [Fig. 1.8](#). This figure represents the simplest form of a network: a *cascade*, i.e., a chain of elements in which each node is connected to not more than two elements. In reality, a production system is not a cascade, and the associated network has a more complex topology. It may, for example, contain *branches*, i.e., three or more elements connected at a node. A next step in complexity involves *loops*, which are a chain of elements with a beginning and ending connected to the same node. [Fig. 1.9](#) displays a production system with several nested loops formed by multiple wells, one of which is a multilateral well, connecting two reservoirs to a single production facility. If we look in detail at some of the other components of the system, we can further refine the system model. Thus, for example, the manifold may be more complex, the facilities may consist of many components, or the pipeline may have branches with flow coming in from other fields.

1.5.2 Flow and Effort Variables. If we consider the flow of single-phase fluid through a network, the interaction between the various elements can usually be described in terms of two pairs of variables: *pressure* and *flow rate*, and *temperature* and *heat flow*, respectively. These are examples of pairs of *effort and flow variables*, concepts that play a key role in the branch of engineering known as systems dynamics. Other familiar pairs of effort and flow variables are the electric potential and current used in electrical network analysis, force and velocity used in mechanical systems analysis, and torque and angular velocity used also in mechanics. A common feature of most pairs of effort and flow variables is that their product represents *power*, also known as *energy rate* or energy per unit time:

$$P = \frac{dE}{dt} = p \times q = V \times I = F \times v = M \times \omega, \dots \quad (1.1)$$

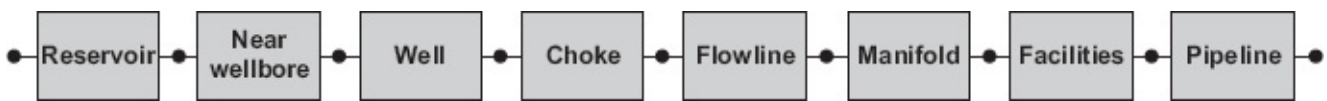


Fig. 1.8—Network representation of a simple production system.

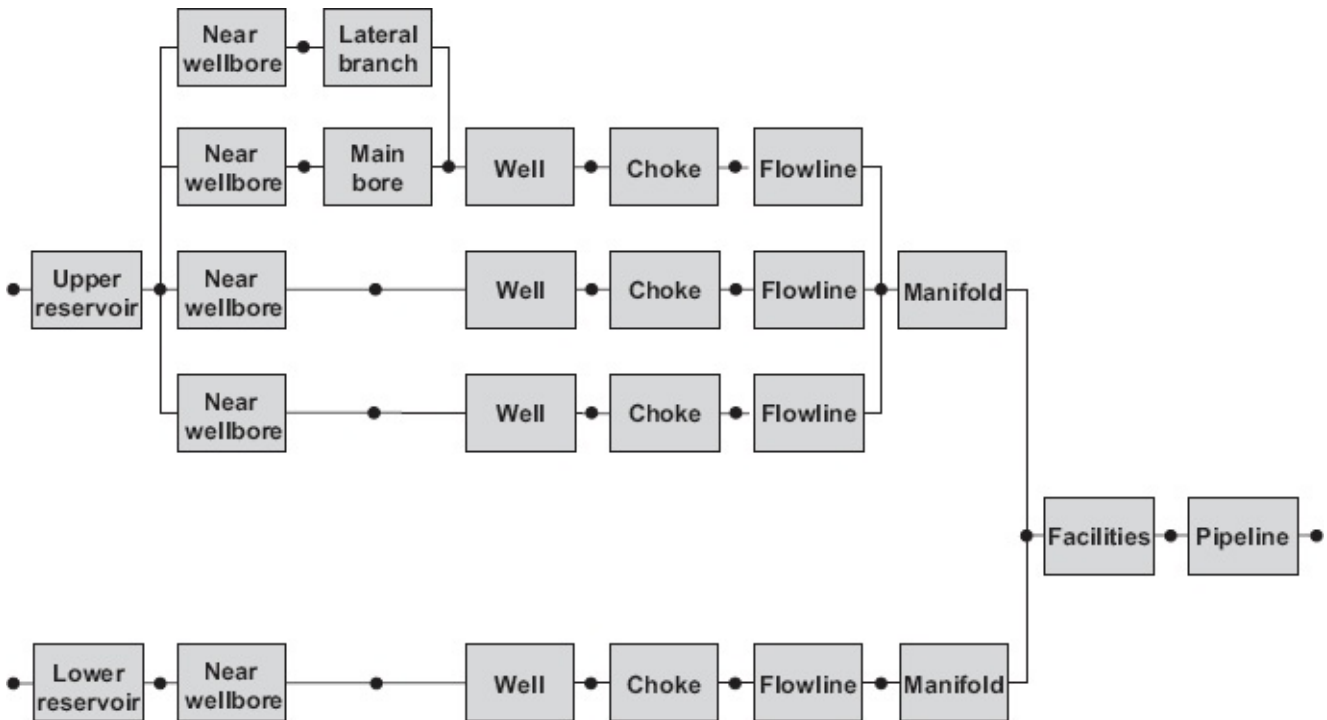


Fig. 1.9—More complex production system forming a network with branches and loops.

where P is power, E is energy, t is time and where the other symbols have been defined in [Table 1.1](#), together with their SI units and physical dimensions. [Eq. 1.1](#) is valid only for consistent sets of units, such as SI units. For use with field units it will be necessary to introduce numerical factors, for example to account for differences between quantities expressed in feet and inches. Furthermore, it should be noted that the product of temperature and heat flow is *not* power. (Note that a more consistent formulation of thermal systems is possible in terms of temperature and *entropy flow*, an effort and flow variable pair whose product does represent power.) For an in-depth treatment of system dynamics, see Karnopp et al. (2000).

1.5.3 Element Equations. In the following, we will consider single-phase flow of a fluid with density and viscosity that are functions of pressure and temperature. For the sake of simplicity, we will neglect the occurrence of heat flow and assume that the temperature distribution within the system is known.

Within an element of a production system, pressure and temperature will generally be functions of time t and spatial coordinates x , y , and z . Most elements, however, can be represented as 1D systems with a single spatial coordinate s . Furthermore, we generally restrict ourselves to the analysis of *steady-state flow*—i.e., flow independent of t . If we consider a wellbore element, for instance, we can then

describe the flow behavior with the following variables:

pressure $p(q, \rho, s, z, \alpha, T)$, flow rate $q(p, \rho, s, z, \alpha, T)$, density $\rho(p, T)$, viscosity $\mu(p, T)$, (1.2)

	Hydraulics	Electricity	Translation	Rotation	Heat Flow
Effort	Pressure	Potential	Force	Torque	Temperature
Symbol	p	V	F	M	T_{abs}
SI units	Pa	V	N	N · m	K
Dimension	[L ⁻¹ m t ⁻²]	[L ² m q ⁻¹ t ⁻²]	[L m t ⁻²]	[L ² m t ⁻²]	[T]
Flow	Flow rate	Current	Velocity	Angular velocity	Heat flow rate
Symbol	q	I	v	ω	Q
SI units	m ³ /s	A	m/s	rad/s	J/s
Dimension	[L ³ t ⁻¹]	[q t ⁻¹]	[L t ⁻¹]	[t ⁻¹]	[L ² m t ⁻³]
Product	$p \times q = dE/dt$	$V \times I = dE/dt$	$F \times v = dE/dt$	$M \times \omega = dE/dt$	$T_{abs} \times Q \neq dE/dt$

Table 1.1—Analogies between system variables in different domains.

where round brackets indicate functional relationships, and where along-hole distance s is the independent variable, while vertical depth from surface $z(s)$, wellbore inclination $\alpha(s)$, and temperature $T(s)$ are given functions of s .

We need four equations to solve for the four unknowns p , q , ρ , and μ . In [Chapter 3](#) we will discuss the nature of these equations in detail. Here we state only that it is generally possible to solve the equations over the length of an element and express the pressure and flow rate at one end of the element in terms of the pressure and flow rate at the other end with *input/output relationships*:

$$\begin{cases} p_{out} = f_1(p_{in}, q_{in}) \\ q_{out} = f_2(p_{in}, q_{in}) \end{cases}, \quad \dots \quad (1.3)$$

where f_1 and f_2 are functions. They are usually strongly nonlinear such that they cannot be obtained in closed form but have to be determined numerically, as will be treated in more detail in [Chapter 3](#). Density and viscosity can be computed anywhere in the element because they are a function of p and T only. We could have expressed [Eq. 1.3](#) in terms of mass flow rates $\dot{m}_{in} = q_{in}\rho_{in}$ and $\dot{m}_{out} = q_{out}\rho_{out}$ instead of volume flow rates q_{in} and q_{out} . In that case we would have found that $\dot{m}_{out} = \dot{m}_{in}$ because we are considering a steady-state situation, where no mass can accumulate in an element. The same result could have been reached by expressing q_{in} and q_{out} in terms of a reference flow rate at a given pressure and temperature. In the oil industry such a reference flow rate is usually defined at *standard conditions*, representing “typical” atmospheric conditions of 15°C and 100 kPa. In that case [Eq. 1.3](#) reduces to

$$p_{out} = f_3(p_{in}, q_{sc}), \quad \dots \quad (1.4)$$

where f_3 is another nonlinear function and where the subscript sc indicates standard

conditions. Eq. 1.4 illustrates that single-phase flow through an element can be completely determined with a single relation between pressure and flow rate. In theory it is also possible to derive the flow rate from the pressure drop with the aid of the inverse relation:

$$q_{sc} = f_3^{-1}(p_{in}, p_{out}) = f_4(p_{in}, p_{out}), \dots \quad (1.5)$$

although in practice this can hardly ever be done directly and requires an iterative procedure. Moreover, for flow in oil and gas production systems, the situation is usually more complex because we encounter *multiphase flow*—i.e., flow involving a gas phase, one or two liquid phases (oil and water), and sometimes even solid phases (e.g., wax, asphaltenes, hydrates, ice). As a result, we cannot use a single rate q to characterize the flow.

Both oil and the gas phases may contain a large number of hydrocarbon components in compositions that vary with pressure and temperature. However, in this book we restrict ourselves by assuming that the oil and gas phases are composed of just two *pseudocomponents* that are present in a variable ratio depending on the local pressure and temperature. Each of the phases will have its own density and viscosity, while in addition the interfacial tension σ comes into play. Often the pseudocomponents chosen are the gas and oil that result from surface separation at standard conditions. We can then express the input/output relationships either in terms of local oil- and gas-phase flow rates q_o and q_g , or in terms of the reference pseudocomponent flow rates $q_{o,sc}$ and $q_{g,sc}$:

$$\begin{cases} p_{out} = f_5(p_{in}, q_{o,in}, q_{g,in}) \\ q_{o,out} = f_6(p_{in}, q_{o,in}, q_{g,in}) \\ q_{g,out} = f_7(p_{in}, q_{o,in}, q_{g,in}) \end{cases}, \dots \quad (1.6)$$

or

$$p_{out} = f_8(p_{in}, q_{o,sc}, q_{g,sc}). \dots \quad (1.7)$$

As was the case in single-phase flow, at steady-state conditions the difference between flow-in and flow-out vanishes in the equations expressed in (pseudocomponent) flow rates at standard conditions, i.e., $q_{o,sc,in} = q_{o,sc,out} = q_{o,sc}$, and $q_{g,sc,in} = q_{g,sc,out} = q_{g,sc}$. Eq. 1.7 shows that, just like for single-phase flow, for two-phase flow the pressure drop over an element can be reduced to a single expression in terms of the flow rates. In this case, however, we cannot reconstruct the flow rates from the pressure drop using the inverse of Eq. 1.7 alone, and we need a second equation that provides information about the ratio of the flow rates $q_{o,sc}$ and $q_{g,sc}$.

1.5.4 System Equations. The input/output representations (Eqs. 1.3, 1.4, 1.6, and

[1.7](#)) are of course perfectly suited for the analysis of cascade systems with the aid of a marching algorithm. We can then start from the known values for pressure and flow rate(s) at one end of the system and work our way through to the other end by using the input/output relations f_i for the elements one after another. A system with branches but without loops can also be analyzed using this approach. For a system with loops, however, the situation is more complicated and requires solving a system of nonlinear equations in an iterative fashion. The same approach can be used for the analysis of fluid-flow networks with multiple components, and obviously the number of equations increases with the number of components taken into account. Furthermore, the analysis could be extended to include the temperature T and heat flow rate Q in the system. Mass flow and heat flow are strongly coupled through convective heat transport and viscous dissipation. Therefore, in the most general situation of thermal compositional network analysis, we end up with a large system of coupled nonlinear equations that may require considerable computing power. Such an analysis is outside the scope of this book.

1.6 Nodal Analysis

1.6.1 Principle. The analysis of cascade systems with the aid of a marching algorithm is known in the oil industry as *nodal analysis*. Written in capitals, NODAL™ analysis has even been registered as a trademark by a major service company. For any given cascade network, we can march between the system boundaries—i.e., between the ends of the cascade, from beginning to end or vice versa. If we know the pressure *and* the flow rate at one of the ends, such a one-pass analysis is sufficient to obtain the pressures and flow rates at all nodes. However, we often only know the value of one variable at each end of the cascade. For example, we may know the reservoir pressure and the separator pressure at the ends of a cascade representing a single well. In that case we need to guess the flow rate at one of the ends and repeat the marching algorithm several times, either upward or downward, to establish the correct flow rate in an iterative fashion. (Note that “correct flow rate” means the flow rate that gives the correct pressure at the other end.) Instead of marching all the way from one end to the other, we could just as well perform two shorter marches, each one starting at an end and finishing in a *joint node*, also referred to as the *analysis node* (see [Fig. 1.10](#)).

Furthermore, instead of performing the iteration automatically, we could plot both pressures (top-down and bottom-up) at that particular node for a large number of flow rates, and determine the correct flow rate graphically. This is indeed the approach followed in traditional nodal analysis of production systems, which was developed in the 1950s and relied on tabulated pressure drop values and graphical analysis rather than computer methods.

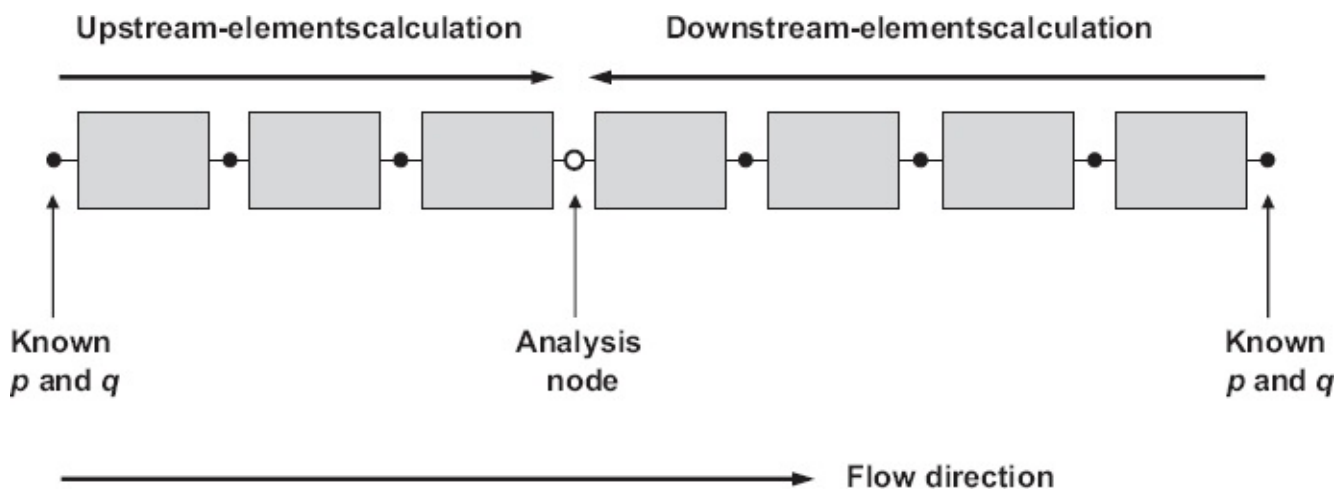


Fig. 1.10—Procedure for nodal analysis.

1.6.2 Classic Procedure. In traditional nodal analysis, popular locations for the analysis node are those corresponding to any of the following types of pressures:

- Flowing bottomhole pressure, p_{wf} , at the bottom of the tubing (see [Fig. 1.11](#))
- Flowing tubinghead pressure, p_{tf} , just upstream of the wellhead choke
- Flowline pressure, p_f , at the entrance of the flowline just downstream of the wellhead choke
- Manifold pressure, p_m , at the end of the flowline

Frequently-used abbreviations for (flowing) tubinghead pressure and (flowing) bottomhole pressure are (F)THP and (F)BHP, in which the adjective “flowing” is used to distinguish the pressures from the *closed-in* values (also referred to as the *static* values) for THP and BHP. These occur when the well is closed in at the surface, and are sometimes abbreviated as CTHP and CBHP.

Suppose we want to determine the production rate $q_{o,sc}$ of the oil well depicted in [Fig. 1.11](#) at given values of the reservoir pressure p_R and separator pressure p_{sep} . We choose the analysis node at the bottom of the hole and take a first guess for $q_{o,sc}$. Starting from p_{sep} , we compute the pressure increase over the manifold, the flowline, the choke, the top part of the tubing, the safety valve, and finally the bottom part of the tubing, resulting in the FBHP p_{wf} —the pressure at the analysis node. Repeating this procedure for different flow rates, we can plot a *performance curve* representing the relationship between $q_{o,sc}$ and p_{wf} ; as determined by the system elements downstream of the analysis node. Similarly, starting from the reservoir, we can perform pressure drop calculations for the near-well reservoir and the perforations, and determine a second performance curve for the upstream part of our system. (Note that upstream and downstream performance curves are sometimes referred to as *inflow* and *outflow curves*, respectively. Moreover, the downstream performance curve, which is the outflow curve, is sometimes referred to as the *intake curve*.) The upstream and downstream performance curves can be plotted on the same p - q

graph. In general, there will be two possibilities:

1. *The two curves do not intersect.* The system cannot be operated under the assumed conditions (i.e., the given reservoir and manifold pressures).
2. *The curves intersect at one or more points.* Usually we simply find a single intersection, which is referred to as the *operating point* or *working point* (see Fig. 1.12). The desired value of the flow rate can be read from the horizontal axis and the corresponding pressure from the vertical axis.

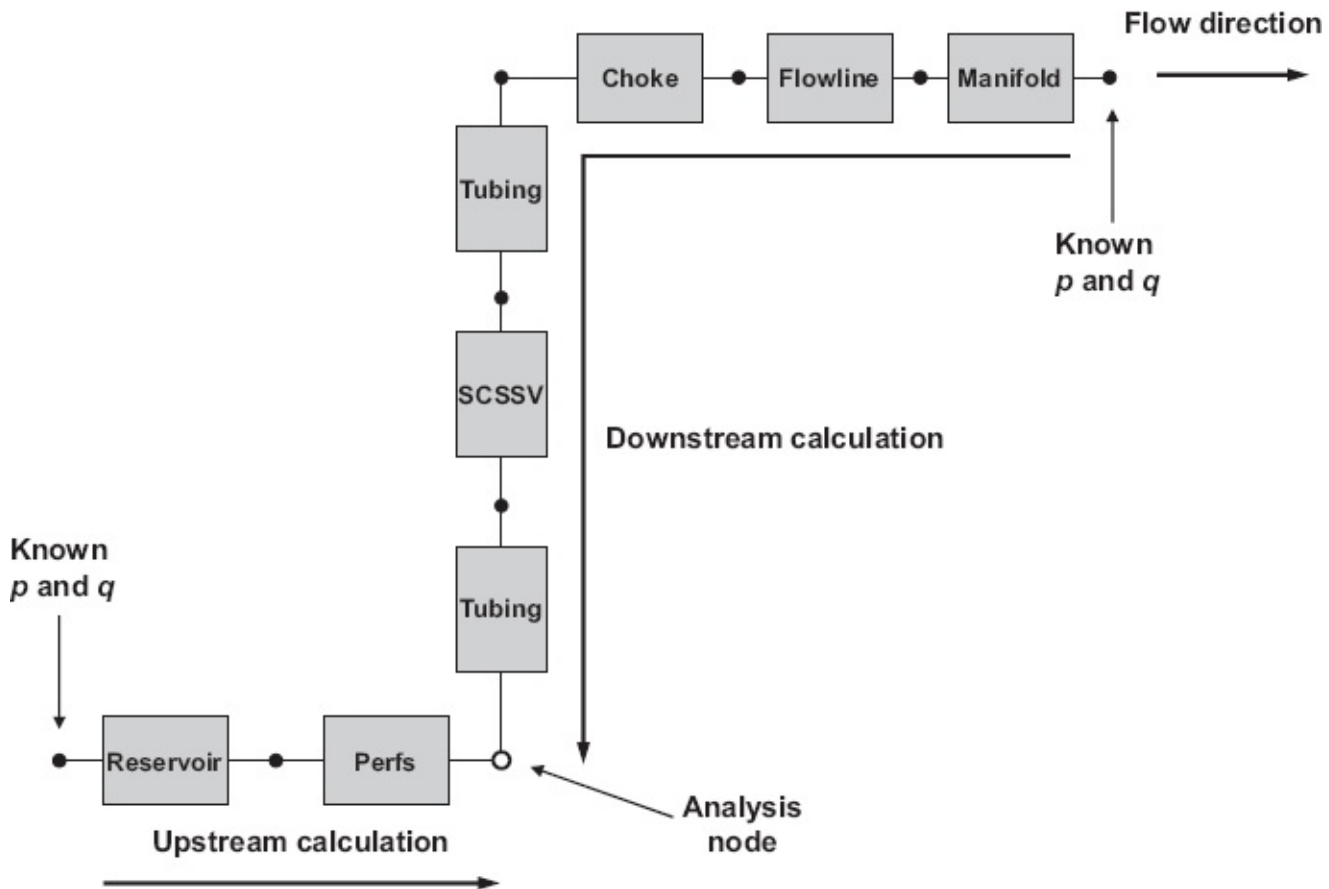


Fig. 1.11—Example of nodal analysis configuration with analysis node at the well bottom.

Note that we could have chosen any other node as the analysis node, but we would have found an identical value for $q_{o,sc}$. However, it is sometimes convenient to choose a specific location for the analysis node to investigate the performance of a specific element or combination of elements. Moreover, as will be discussed in later chapters, the particular flow behavior or modeling assumptions in certain elements may prohibit marching in either an upstream or downstream direction over those elements which restricts the freedom to select the analysis node.

1.6.3 Production Optimization. Nodal analysis can be used during the FDP phase to optimize the design of the production system, and in particular to optimize the configuration and the dimensions of the various system components. Later, during the

production phase, nodal analysis can be used to analyze production measurements and to optimize system performance through the design of modifications to the system components. Nodal analysis is particularly useful for *debottlenecking*, aimed at removing or modifying those elements in the production system that form the largest restrictions to flow. Other forms of production optimization involve more than just nodal analysis and can be framed as formal mathematical optimization problems. These require maximizing or minimizing one or more objectives by systematically changing *control variables* (also known as *manipulated* or *input variables*) under the presence of constraints. A classic example is gas-lift optimization, which involves optimizing the distribution of a limited amount of available lift gas over a set of oil producers. Note, however, that in this book we will not cover production optimization beyond nodal analysis.

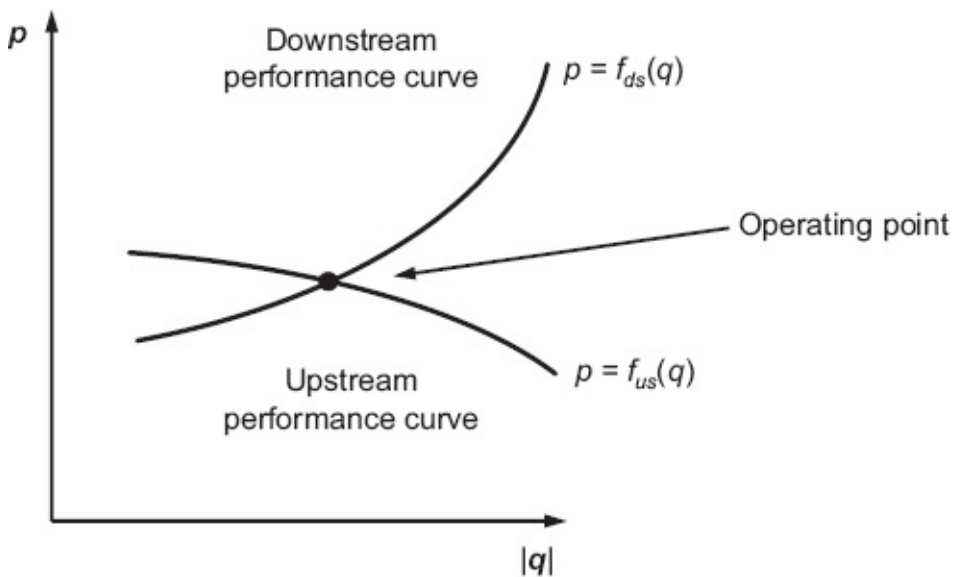


Fig. 1.12—Nodal analysis using performance curves. The intersection between the downstream and upstream performance curves defines the operating point.

1.7 Questions

Note that answers to all questions can be found in [Appendix G](#).

- 1.1 What is displayed on the axes of performance curves used in nodal analysis?
- 1.2 Why can the two performance curves for an analysis node intersect in more than one point?
- 1.3 Under steady-state flow conditions in a well, the mass flow rates of oil and gas (pseudo)components do not change over the depth of the well. However, the volume flow rates of the oil and gas phase rates will change. Why?
- 1.4 For each of the following wells, would it be theoretically possible to determine the gas, oil, and/or water flow rates from two pressure measurements, one at the wellhead and one at the bottom of the well, through iterative use of a wellbore flow simulator? Assume that you have full knowledge of the fluid

properties (e.g., densities, viscosities), the wellbore geometry, and the temperature profile along the wellbore. Briefly explain your answers.

- (a) Water injection well.
 - (b) Single-phase gas production well.
 - (c) “Dead oil” production well (i.e., without gas production) with known water/oil ratio.
 - (d) “Live oil” production well (i.e., with gas production) and with known water/oil ratio but unknown gas/oil ratio.
- 1.5 An electric motor operates with 90% efficiency at 300 V and draws a current of 16 A. The shaft of the motor rotates with 240 revolutions per minute (rpm) and drives an oil pump by means of a reduction gear with an efficiency of 98%. The pump creates a pressure differential of 160 kPa at a flow rate of $22 \times 10^{-3} \text{ m}^3/\text{s}$. What is the torque generated by the motor? What is the efficiency of the pump?

Questions 1.6 through 1.10 involve unit conversions. Consult [Appendix A](#) for conversion factors and further information. In addition, you may want to make use of the MATLAB “m-files” for unit conversion (see [Appendix H](#) for an overview).

- 1.6 A well produces 12,000 STB/D of oil at a gas/oil ratio (GOR) of 15,000 scf/STB. The oil gravity is 38°API and the gas gravity is 0.82. What are the oil and gas production rates and densities in SI units?
- 1.7 A mixture of 1 lbm mol of C_1H_4 and 0.3 lbm mol of CO_2 is kept at a temperature of 83°R and a pressure of 30 psig. What are the mass, the temperature, and the pressure of the gas mixture in SI units?
- 1.8 Calculate the pressure in Pa and in psi in a well open to the atmosphere and filled with salt water (specific gravity 1.03) at a depth of 2000 m.
- 1.9 The pressure drop over a choke for an incompressible liquid is given by

$$\Delta p = \rho v^2 / (288g_c C^2),$$

where Δp is the pressure drop expressed in psi, ρ is the liquid density in lbm/ft³, v is the liquid velocity in ft/s, and C is a dimensionless choke coefficient. The nature of the dimensional constant g_c is discussed in [Appendix A](#). Convert the expression to SI units.

- 1.10 [Fig. 1.13](#) depicts a vertical well penetrating a reservoir containing gas, oil, and water. The acronyms GOC and OWC indicate the gas/oil contact and the oil/water contact respectively. The aquifer is hydrostatic. The atmospheric pressure is 100 kPa. The oil has a 30°API gravity, and the water gradient is 0.45 psi/ft. The top perforations are 50 ft below the GOC. The total perforation height is 100 ft. What is the pressure at the GOC in SI units?

1.8 MATLAB Assignment: Nodal Analysis of a Simple System

1.8.1 Objectives.

- Get a first impression of the use of nodal analysis to determine the pressure drop and flow rate in a simple production system.
- Become aware of some typical, and sometimes surprising, features of nodal analysis.
- Get a first impression of the use of MATLAB to perform nodal analysis.

1.8.2 Assignment. Note that if you do not have access to MATLAB, you can run the executable file `nodal.exe`. This requires first installing the free-of-charge MATLAB runtime compiler by running `MyAppInstaller_web.exe`. Both files are located in directory “Demo.” (Keep in mind that depending on the speed of your computer, the installation of the runtime compiler and the startup of the application may require some patience.)

Task 1.

- Download the MATLAB files listed in [Appendix H](#) and store them in a working directory (possibly with subdirectories). If necessary adjust the path to the directory (and the subdirectories) using the command “Set Path” under the tab “File” in the MATLAB workspace.
- Type the command `nodal` in the MATLAB workspace. This should result in the appearance of the graphical user interface (GUI) shown in [Fig. 1.14](#).

At the left side of [Fig. 1.14](#) a schematic is displayed of a simple production system consisting of a near-well reservoir, a vertical tubing, a wellhead choke (usually represented by two touching triangles in process engineering drawings), and a horizontal flowline. The sliders at the center can be used to set the pressures at the boundaries of the system—i.e., the reservoir pressure, p_R , and the separator pressure, p_{sep} . The analysis node has been chosen at the top of the tubing; the corresponding FTHP, p_{tf} , is one of the two desired outcomes of the nodal analysis, the other one being the oil flow rate at standard conditions, $q_{o,sc}$. These output quantities are displayed on the axes of the graph at the right. Note that in this book we use the convention that the flow in production wells is negative (because we define the flow in injection wells as positive). The graph also depicts two curves, an upstream (dashed) and a downstream (solid) pressure drop curve. As explained in [Section 1.6](#), the intersection between the downstream and upstream curves should define the operating point, but in this case there is clearly no intersection and therefore no flow through the system.

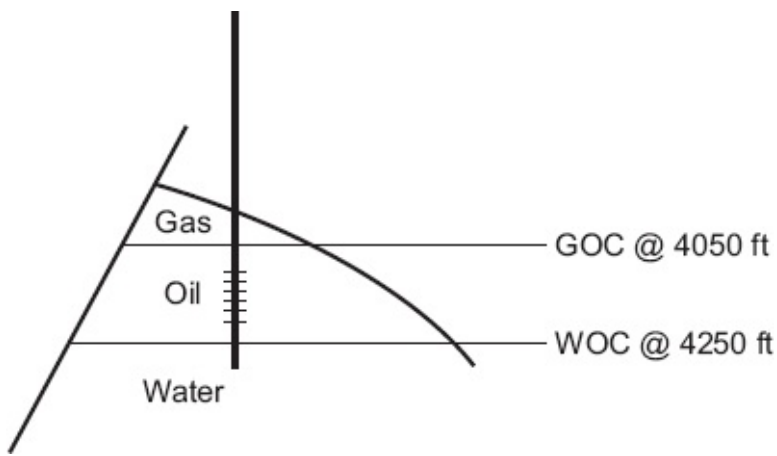


Fig. 1.13—Oil reservoir with gas cap and aquifer.

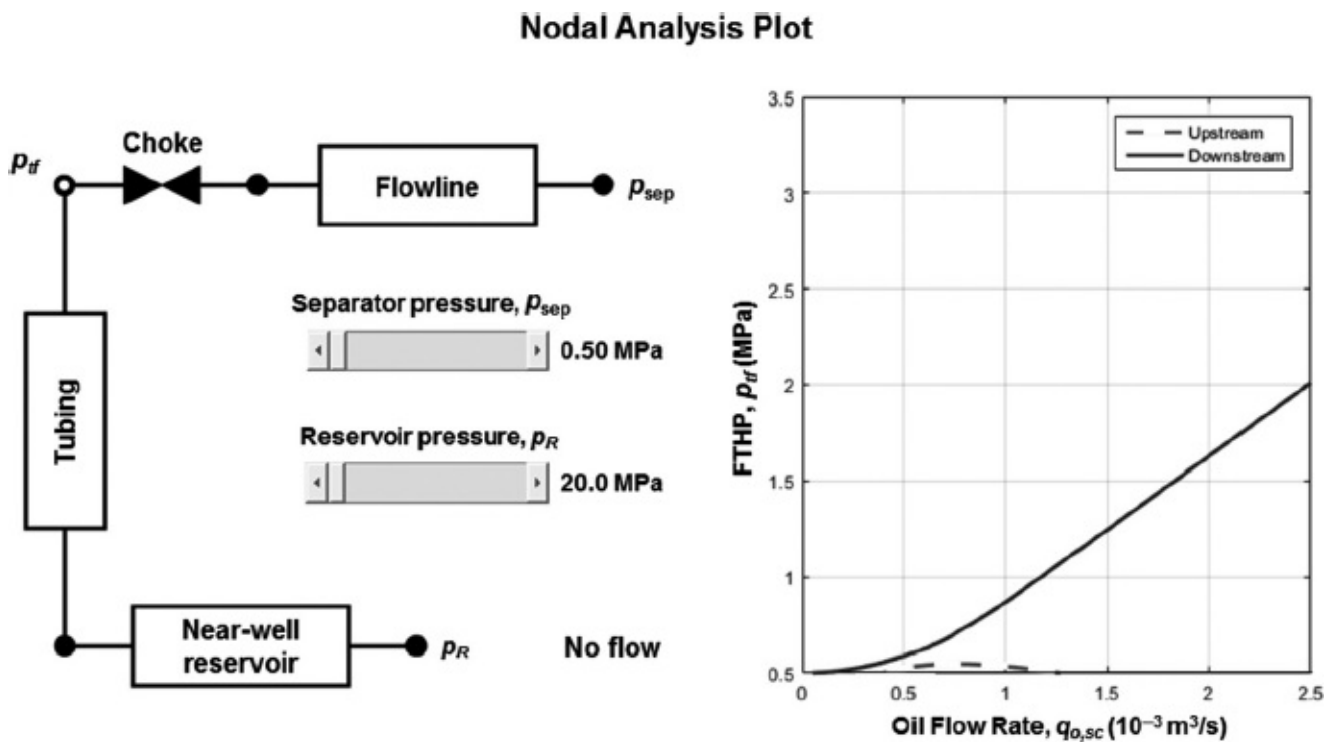


Fig. 1.14—GUI for a simple production system. The upstream (dashed) and downstream (solid) pressure drop curves do not intersect, indicating that for the present system configuration and boundary conditions, flow through the system is not possible.

Question 1. Which system elements contribute to the upstream and downstream pressure drops respectively?

Task 2.

- Move the sliders to see what happens. Note that depending on the speed of your computer, the response to the slider movements may be more or less delayed.
- Set the sliders to (approximately) reproduce the situation shown in Fig. 1.15.

Question 2.

- 2(a) What are new values of the system boundary conditions p_R and p_{sep} ?
- 2(b) What are the values of the corresponding FTHP, p_{tf} , and oil flow rate, $q_{o,sc}$?
- 2(c) Verify, with the aid of the downstream curve, that for a zero flow rate the FTHP, p_{tf} , becomes equal to p_{sep} . Why?

Task 3.

- Determine what will happen if you reduce the reservoir pressure. Is the flow rate going to increase or decrease?
 - Check your reasoning with the aid of the bottom slider. Note that at low reservoir pressures two intersections occur. Only the one corresponding to the highest flow rate is physically relevant. This is not immediately obvious and requires a dynamic analysis—i.e., a more complex analysis than the steady-state pressure drop approach used in our nodal analysis—to prove this.
- Learning point:

Nodal analysis requires understanding of the underlying physical mechanisms and assumptions to correctly interpret its results.

Task 4.

- Restore the situation as in Fig. 1.15.
Determine what will happen if you reduce the separator pressure. Is the flow rate going to increase or decrease?
- Check your reasoning with the aid of the top slider. Surprised? Learning point:

Nodal analysis requires understanding of the behavior of the individual system components to explain the behavior of the total system.

Task 5 (only if you have access to MATLAB)

- Close the GUI.
- Type the command `system_01` in the MATLAB workspace. This invokes the running of MATLAB m-file `system_01.m` (which is located in the subfolder “systems”) and should result in a figure popping up similar to the one in the GUI. In fact, the GUI is based on a slightly modified version of `system_01.m`.

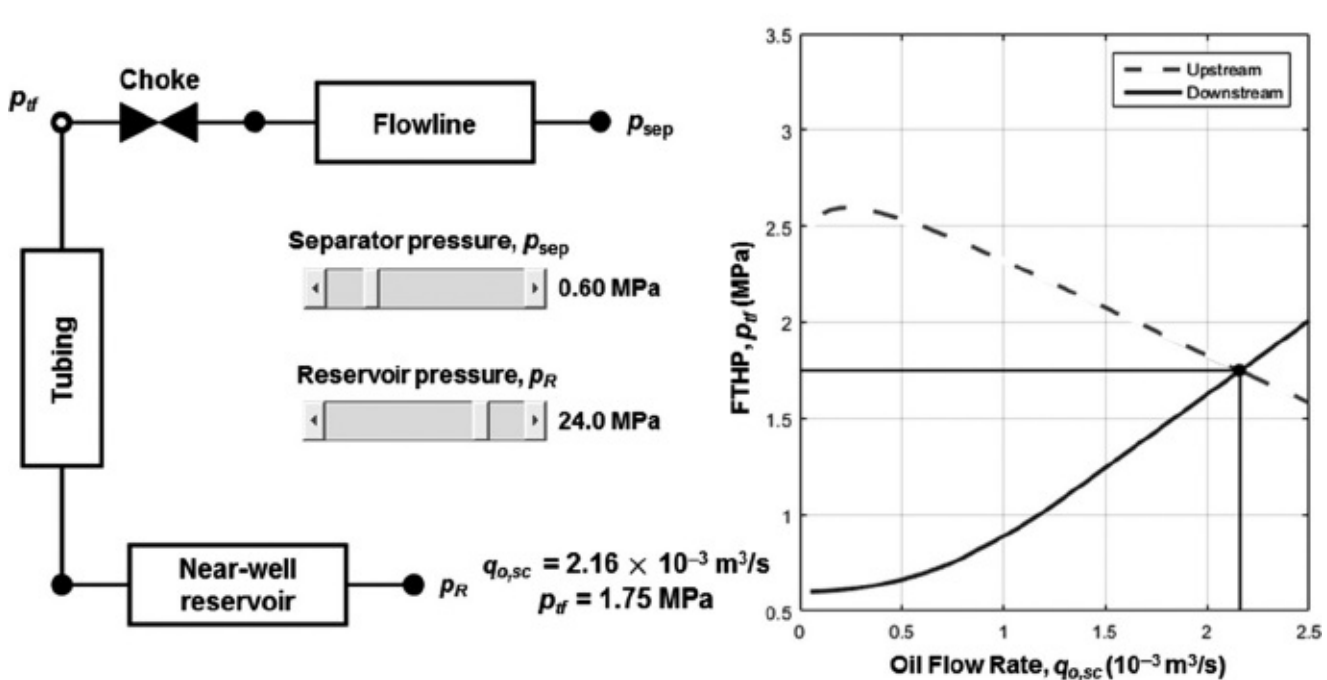
Nodal Analysis Plot

Fig. 1.15—GUI for the same production system as in [Fig. 1.14](#), but with different boundary conditions. Now the upstream and downstream pressure drop curves do intersect, resulting in an operating point indicated with a black dot. The values of the corresponding FTHP, p_{tf} , and oil flow rate, $-q_{o,sc}$, can be read off from the axes and are also displayed at the bottom of the GUI.

- Open the m-file in the MATLAB editor and save it under a different name in the same folder (e.g., `system_01_test.m`). Rather than by using the GUI, you can now change the reservoir and separator pressures by editing them in the (renamed) m-file. Give it a try and rerun the renamed file to inspect the results. Moreover, you now have the freedom to change many more parameters.
- Choose $p_R = 21.5 \text{ MPa}$ and $p_{sep} = 0.7 \text{ MPa}$.
- Read off the corresponding oil flow rate in the graph (it should be approximately $1.2 \times 10^{-3} \text{ m}^3/\text{s}$). Determine what would happen if you increase the tubing size. Do you expect the well to produce more or less oil?
- Verify your reasoning by changing the tubing diameter d_w in the renamed m-file from 0.07600 m to 0.10053 m (which corresponds to replacing a 3½-in.-diameter tubing by a 4½-in.-diameter one.) Surprised? See the learning points stated above.

Chapter 2

Properties of Reservoir Fluids

2.1 What Is Covered in This Chapter?

The two-phase (gas/liquid) behavior of hydrocarbons is a major reason for the nonlinear relationship between flow rate and pressure drop in the various production system elements. Single-phase reservoir oil will start to boil on its journey to the surface and will separate into oil and gas phases as a result of reducing pressure. Consequently, the oil shrinks while the gas massively expands at reducing pressures. Likewise, single-phase reservoir gas may experience condensation when brought to the surface and thus also may separate in two phases.

We will focus on relatively simple models for hydrocarbon phase behavior in which the many components that make up the oil and gas phases are reduced to a mixture of two pseudocomponents. These two are conveniently chosen as stock-tank oil and stock-tank gas, which are the oil and gas phases at ambient pressure and temperature (also known as *standard conditions*). The so-called black oil or volatile oil models that we will consider in detail are capable of describing the local density and flow rate of the gas and oil phases at any combination of pressure and temperature in terms of the two pseudocomponents. That is, they allow us to express all flow equations for oil, gas, and water at downhole conditions in terms of just three (pseudo)components (stock-tank oil, stock-tank gas, and water) with constant properties. This will simplify the flow equations in the subsequent chapters because at steady-state conditions the flow rates of the three (pseudo)components in a well remain constant throughout their journey from reservoir to surface.

Accompanying this chapter is [Appendix B](#), which provides a number of (semi)empirical correlations to compute the relevant hydrocarbon properties required to perform production engineering calculations.

2.2 Fluid Properties

The thermodynamic properties of reservoir fluids, such as pressure, temperature, density, or viscosity, can have a strong influence on the flow in a well and the production rate. For engineering-oriented information see, e.g., Whitson and Brûlé (2000), Danesh (1998), or McCain (1990); for a more theoretical treatment see Firoozabadi (1999). During the exploration and appraisal phase of an oil or gas field, determination of the fluid properties is an important activity. Fluid samples, often called *bottomhole samples*, can be collected from the bottom of the wellbore with the aid of specialized wireline tools. Specialized laboratories perform pressure/volume/temperature (PVT) analyses to determine the *composition*—i.e.,

type and relative quantity of each component in the fluid mixture—and the properties of the fluids at a wide range of pressures and temperatures. The composition is usually specified in terms of fractions of the various components per mol (or lbm/mol) of fluid sample. For a good description of the reporting of other properties, see Whitson and Brûlé (2000). Some important properties of the most frequently encountered reservoir fluid components have been reproduced in [Tables B-1](#) and [B-2](#) in [Appendix B](#).

To analyze multiphase flow of hydrocarbons in production systems, we need to know the state—i.e., thermodynamic condition—of the fluid mixture in each point of the production system. Apart from the thermodynamic properties of the components, this requires knowledge of the *phase behavior* of the mixture. We usually distinguish three distinct phases: gas, oil, and water, where we consider oil and water as different phases because they are immiscible. In this book we will not consider the effect of the presence of a solid phase as may occur when, e.g., asphaltenes or waxes are present. To what extent the various components of a reservoir fluid mixture are in the liquid or the gas phase is fully determined by the composition of the mixture and by a minimal set of fluid properties, called *state variables* (i.e., PVT). The state variables are related to each other through an algebraic relationship known as the *equation of state* (EOS), as will be discussed in [Section 2.5](#). As a result it suffices to know only two of the three variables to completely specify the state of an oil/gas mixture. It is customary to specify fluid properties at a reference state. In the E&P industry this is done through the definition of standard conditions: a pressure $p_{sc} = 100 \text{ kPa}$ (14.7 psi) and a temperature $T_{sc} = 15^\circ\text{C}$ (60°F), which can be considered as typical for atmospheric conditions in temperate climates. Oil at standard conditions is often referred to as *stock-tank oil*, gas at surface conditions sometimes as *stock-tank gas*. The term *separator gas* usually refers to gas at a slightly higher than atmospheric pressure and should not be confused with gas at standard conditions. The fluid properties that are of most interest for production engineering calculations are these:

- *Oil density at standard conditions* $\rho_{o,sc}$. In SI units, this is the density of the oil in kg/m^3 . In field units, oil density is usually specified by the oil specific gravity y_o , which is the density of the oil relative to that of pure water, both measured at standard conditions: $\rho_{w,sc} = 999 \text{ kg/m}^3$ (62.4 lbm/ft^3 or 8.34 lbm/gal). However, it is also common to use the API gravity y_{API} , which is related to the specific gravity as $\rho_o = 141.5 / (131.5 + y_{API})$ and therefore to the density as $\rho_o = 141.5 \times 10^3 / (131.5 + y_{API})$. Closely related to the oil density is the oil *gradient* g_o , defined as the pressure gradient in an oil column: $g_o = \rho_o g \text{ Pa/m}$ (psi/ft), where g is the acceleration of gravity: $g = 9.80665 \text{ m/s}^2$ (32.174 ft/s^2).
- *Gas density at standard conditions* $\rho_{g,sc}$ or *gas specific gravity* y_g . The latter is the density of the gas relative to air, both measured at standard conditions: $\rho_{air,sc} = 1.23 \text{ kg/m}^3$ ($76.3 \times 10^{-3} \text{ lbm/ft}^3$). This is equal to the ratio of the gas

molar mass M (expressed in kg/mol) to the molar mass of air, where $M_{\text{air}} = 28.97 \times 10^{-3}$ kg/mol. Alternatively, it is the ratio of the gas molecular weight M_w (expressed in g/mol or lbm/(lbm mol)) to the molecular weight of air, where $M_{w,\text{air}} = 28.97$ g/mol [lbm/(lbm mol)]. In an analogy to the oil gradient, the gas gradient is $g_g = \rho_g g$ Pa/m (psi/ft).

- *Water density at standard conditions* $\rho_{w,\text{sc}}$ or *water specific gravity* y_w , which is the density of the formation water relative to that of pure water, both measured at standard conditions. The water gradient follows as $g_w = \rho_w g$ Pa/m (psi/ft). Formation water will contain many dissolved salts. An equivalent measurement for density is therefore the NaCl equivalent water salinity.
- *Bubblepoint pressure* p_b . This is the pressure at which first gas is formed when oil is subjected to a decreasing pressure at a given temperature. If the pressure at the top of a reservoir is above the bubblepoint pressure, all gas is dissolved in the oil. However, if the top part of the reservoir is below bubblepoint pressure, a gas cap exists and the oil is gas saturated. The bubblepoint pressure is therefore also known as the *saturation pressure*.
- *Solution gas/oil ratio* R_s . This is the volume of stock-tank gas, which will dissolve in a unit volume of stock-tank oil when both are transferred to the given pressure and temperature conditions. R_s , also referred to as *gas solubility*, is a ratio of volumes and hence is dimensionless, but it is dependent on the choice of units (m^3/m^3 or scf/STB). The abbreviation "scf" indicates standard cubic feet, or " ft^3 at standard conditions"; "STB" indicates stock-tank barrel or standard barrel, or "bbl at standard conditions." We will indicate the solution gas/oil ratio (GOR) at the bubblepoint pressure with the symbol R_{sb} . If the pressure is increased to above the bubblepoint pressure, R_s remains equal to R_{sb} and the oil becomes undersaturated. Oil with a zero GOR—i.e., with a bubblepoint pressure equal to atmospheric pressure p_{sc} —is referred to as *dead oil*. All other oil is known as *live oil*. Both p_b and R_{sb} are strongly dependent on the composition of the oil.
- *Solution oil/gas ratio* r_s . This is the volume of stock-tank oil that will vaporize in a unit volume of stock-tank gas when both are transferred to the given pressure and temperature conditions. The oil/gas ratio (OGR) plays an important role in the production of gas condensates and is therefore also referred to as *condensate/gas ratio* (CGR). Yet another name is *volatilized oil/gas ratio*, which leads to the use of the symbol R_v (instead of r_s) in some publications. Also r_s is a ratio of volumes, and hence dimensionless, but it is dependent on the choice of units (m^3/m^3 or STB/ scf). Gas with a very low CGR is referred to as *dry gas*.
- *Oil formation volume factor* B_o . This is the volume occupied by one stock-tank unit volume of oil, transferred to another condition with a given pressure p and temperature T . The oil volume will change because of compression, thermal

expansion, and, in particular, the uptake of gas. The net effect is an increase of oil volume with increasing depth. In reservoir engineering, B_o is usually specified at reservoir conditions p_R and T_R ; but in production engineering, B_o may also be specified at other conditions that occur between the reservoir and the separator. B_o is a ratio of volumes and hence is dimensionless; unlike the GOR and OGR, it is independent of the choice of units (m^3/m^3 or bbl/STB).

- *Gas formation volume factor B_g .* This is the volume occupied by a unit volume of gas at standard conditions, transferred to another condition with a given pressure p and temperature T . (Note that this definition concerns the dry gas formation volume factor. As discussed later, there is also a wet gas formation volume factor.) The gas volume will change because of compression, thermal expansion, dissolution in the oil phase, or uptake of condensate. The net effect is a decrease of gas volume with increasing depth. B_g is also a dimensionless ratio of volumes, but in field units different definitions can be used, leading to a dependency on the choice of units (m^3/m^3 , ft^3/scf , or bbl/scf).
- *Water formation volume factor B_w .* Not surprisingly, this is the volume occupied by a unit volume of water at standard conditions, transferred to another condition with a given pressure p and temperature T . Also B_w is dimensionless, but like B_o , independent of the choice of units (m^3/m^3 or bbl/STB). B_w usually has a value close to one, because of the low compressibility and low gas solubility capacity of water.
- *Oil, gas, and water viscosities μ_o , μ_g , μ_w :* Usually the dynamic viscosities are used, with SI units ($\text{Pa}\cdot\text{s}$) or field units (cp). The viscosities are strongly varying functions of temperature.
- *Interfacial tensions σ_{og} , σ_{ow} , σ_{gw} .* These quantities play a role in multiphase flow behavior in production systems, but to a much lesser extent than in flow through porous media.
- *Specific heat capacities.* These quantities play a role in the flow of gas through restrictions. A unit increase in temperature of a unit mass of an ideal gas at constant volume (and increasing pressure) results in an increase of energy with $c_v \text{ J}$, where c_v is the specific heat capacity (or specific heat) at constant volume. The specific heat capacity is therefore expressed in $\text{J/kg} \cdot \text{K}$ ($\text{lbf-ft/lbm} \cdot ^\circ\text{R}$). Similarly, an increase in temperature at constant pressure (and increasing volume) results in an increase of energy with $c_p \text{ J/kg} \cdot \text{K}$ ($\text{lbf-ft/lbm} \cdot ^\circ\text{R}$), where c_p is the specific heat at constant pressure.

A simple interpretation of the oil and gas formation volume factors is depicted in **Fig. 2.1**. When an amount of $B_o \text{ m}^3$ of reservoir oil is brought to surface it yields 1 m^3 of stock-tank oil, and $R_s \text{ m}^3$ of stock-tank gas. Or, when 1 m^3 of reservoir oil is brought to surface it yields $1/B_o \text{ m}^3$ of stock-tank oil and $R_s/B_o \text{ m}^3$ of stock-tank gas. (This stock-tank gas originating from reservoir oil is referred to as *solution gas*.) Although the oil itself slightly expands under reducing pressure, the escaping solution

gas makes the oil effectively shrink when it comes to surface. Therefore the ratio $1/B_o$ is known as the *shrinkage factor*, where $1/B_o < 1$.

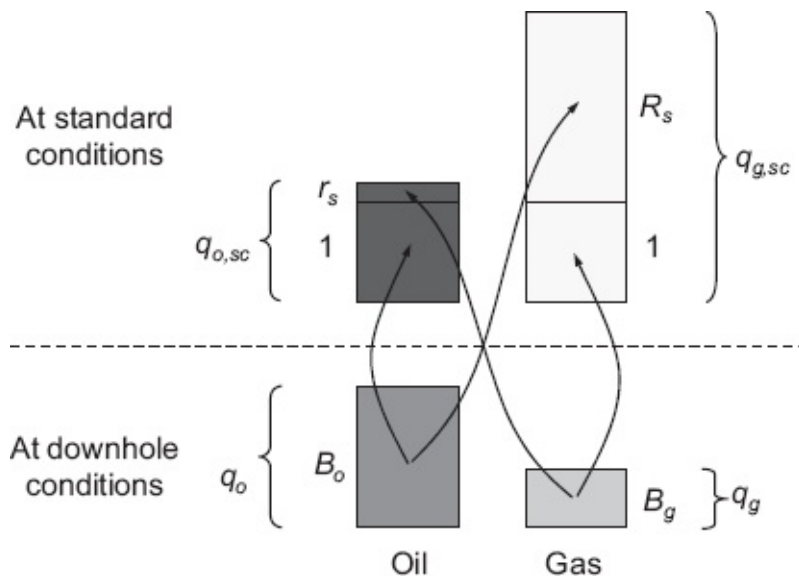


Fig. 2.1—Oil and gas volume flow rates at different two-phase conditions. (Volume flow rates q are used instead of volumes V based on the underlying assumption that the flow rates are steady-state, i.e., time invariant.)

Similarly, when an amount of B_g m³ of reservoir gas is brought to surface, it yields 1 m³ of stock-tank gas and r_s m³ of stock-tank oil. (This stock-tank oil originating from reservoir gas is referred to as *condensate* or *volatilized oil*.) Even at large amounts of condensate dropout, the gas still expands so much under reducing pressure that the ratio $1/B_g$ is always much larger than unity. In gas engineering it is common practice to use the symbol E to indicate this *gas expansion factor*, $E = 1/B_g$. Values for R_s , r_s , B_o , and B_g as a function of p and T can be determined from a laboratory analysis of a bottomhole sample in a so-called *flash test*, in which oil at reservoir pressure and temperature is brought to standard conditions through a stepwise reduction of pressure and temperature. Different types of flash tests are in use, and we refer to the references mentioned at the beginning of this chapter for a detailed treatment.

2.3 Production Variables

Related to the fluid properties R_s and r_s defined above are two frequently used production process variables:

- *Producing gas/oil ratio R_{go}* . This is the instantaneous ratio of the gas and oil flow rates measured at surface during production: $R_{go} = q_{g,sc} / q_{o,sc}$. If water is present in the production stream, we can extend the concept of the producing GOR to a producing gas/liquid ratio (GLR) $R_{gl} = q_{g,sc} / (q_{o,sc} + q_{w,sc})$. These

quantities are also referred to as the *instantaneous* GOR and GLR. The producing GOR should not be confused with the *produced* GOR R_p , as used by reservoir engineers in material-balance calculations, which refers to the cumulative ratio of gas and oil produced from the reservoir since the start of production. Many publications use R , without subscript, to indicate the instantaneous producing GOR; but confusingly, some also use R_p . When producing oil from a reservoir above bubble-point pressure, R_{go} will be identical to R_{sb} —i.e., to R_s at bubblepoint pressure and reservoir temperature. If during production the reservoir pressure drops below bubblepoint pressure, R_{go} could in theory drop below R_{sb} . In practice, however, usually the opposite occurs because the gas viscosity is much lower than the liquid viscosity, which makes the gas flow to the well much more easily than the oil. In addition, *gas coning* may occur, which implies that free gas is pulled in from the gas cap. Together with the associated gas that is released from the oil during its travel up the wellbore, this may result in an R_{go} that is significantly higher than R_{sb} .

- *Producing oil/gas ratio r_{og}* . In analogy to the producing GOR, this is the instantaneous ratio of the oil and gas flow rates measured at surface: $r_{og} = q_{o,sc} / q_{g,sc}$. As mentioned before, the OGR plays an important role in the production of gas condensates and is therefore also referred to as the producing CGR or the *condensate yield*. Note that in reporting field production we could either use R_{go} (the usual choice for black or volatile oil reservoirs) or r_{og} (the usual choice for gas/condensate reservoirs).

A third production variable that is frequently used concerns the combined production of water and oil:

- *Water/oil ratio R_{wo}* . This is the volume of water produced at surface together with a unit volume of oil, both measured at standard conditions, or, in terms of flow rates: $R_{wo} = q_{w,sc} / q_{o,sc}$. An alternative measure is the *water cut*, which is the fraction (or percentage) of water in the total volume of produced liquids (oil and water) measured at standard conditions: $f_{w,sc} = q_{w,sc} / (q_{o,sc} + q_{w,sc})$. Both measures are dimensionless and are independent on the choice of units (m^3/m^3 or STB/STB). Oil with a zero or very low water/oil ratio (WOR) is often referred to as *dry oil*. Sometimes the concept of ‘base sediment and water’ (BSW) is used to indicate the amount of solids and water as a fraction of the total amount of solids and liquids in the wellbore flow. Because the amount of solids is usually very low, the BSW value is in practice almost identical to the water cut.

2.4 Pressure/Temperature Phase Diagram

Fig. 2.2 displays the phase diagram for a hydrocarbon mixture. To the left of the

bubblepoint line, the system acts as a single-phase liquid and all the gas is dissolved. To the right of the *dewpoint line*, the system acts as a gas. If the bubblepoint line is crossed when coming from the liquid phase, gas is liberated to form a two-phase system. Moving farther toward the dewpoint line, an increasing amount of gas comes out of solution. Conversely, if the dewpoint line is crossed when coming from the gas phase, liquid condenses. At the *critical point*, the distinction between liquid and gas cannot be made because at that particular pressure and temperature the liquid and gas phases have identical densities. In general, at pressures above the *cricondenbar* (the maximum pressure at which two phases can coexist) in combination with temperatures above the *cricondentherm* (the maximum temperature at which two phases can coexist), the fluid is in a supercritical state, also known as *dense phase*.

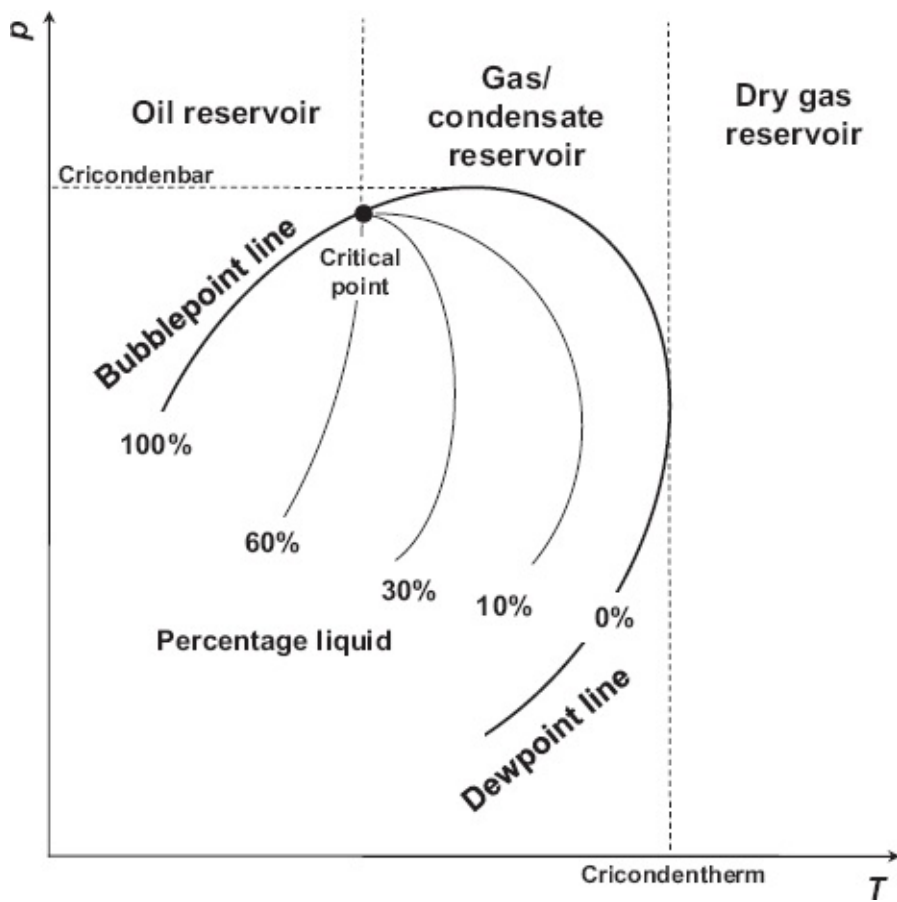


Fig. 2.2—Phase diagram for a hydrocarbon mixture.

Fig. 2.2 also indicates a classification of reservoir types based on the phase diagram:

- *Undersaturated oil reservoirs* have initial pressures above the bubblepoint line and temperatures to the left of the critical point. During production of a reservoir, the reservoir pressure will drop while the reservoir temperature remains unchanged. This can be represented by a vertical line in p - T space. When the line crosses the bubblepoint line, gas is coming out of solution.

- *Saturated oil reservoirs*, also known as *gas cap reservoirs*, have initial pressures already below the bubblepoint line.
- *Gas condensate reservoirs* have initial pressures above the dewpoint line and initial temperatures between the critical temperature and the cricondentherm. During production of a gas/condensate reservoir, condensation occurs when the pressure drops below the dewpoint line. This effect, which is called *retrograde condensation*, may seem somewhat counterintuitive because we usually experience condensation when the pressure of a gas/liquid mixture increases rather than decreases. Although it appears from the phase diagram that at even lower pressures the condensate would return to the gas phase again, this is usually not the case. Because the condensed liquids are much less mobile than the gas, they stay behind in the formation while the gas is produced. As a result, the reservoir fluid composition changes and the entire phase diagram changes its form and moves to the right such that vaporization of the remaining condensate may never occur.
- *Dry gas reservoirs* have temperatures to the right of the cricondentherm and do not experience this problem.

Using a similar terminology but a slightly different classification, we can distinguish four categories of hydrocarbon fluids:

- *Black oil*: oil for which, at reservoir conditions, the solution GOR $R_s < 350 \text{ m}^3/\text{m}^3$ (approximately 2000 scf/STB)
- *Volatile oil*: oil for which $R_s > 350 \text{ m}^3/\text{m}^3$ (approximately 2000 scf/STB)
- *Wet gas (or condensate gas)*: gas for which the condensate/gas ratio $r_s > 30 \text{ m}^3/\text{million m}^3$ (approximately 5 STB/million scf)
- *Dry gas*: gas for which the condensate/gas ratio $r_s < 30 \text{ m}^3/\text{million m}^3$ (approximately 5 STB/million scf)

As shown in [Fig. 2.3](#), when oil flows up the production tubing, it follows a path in p-T space in which gas is liberated and expands as it goes up the tubing. As a result, the amount of liquid decreases, so there is a shrinkage in the volume of oil. Furthermore, unlike the pressure drop in the reservoir, which is isothermal, the pressure drop in the tubing is accompanied by a drop in temperature. When producing from a wet gas reservoir, this may result in condensate dropout and *liquid loading* of the wells.

2.5 Equations of State

2.5.1 Vapor/Liquid Equilibrium. As discussed in [Section 2.2](#), an EOS specifies an algebraic relationship between the state variables pressure, volume, and temperature. With the aid of such an EOS, all properties of hydrocarbon mixtures as used in production engineering can be determined, provided an accurate

compositional description is available from laboratory experiments on fluid samples. In particular, we can use an EOS to determine the so-called equilibrium factors (K values) that are needed to describe the equilibrium between components in the liquid and the vapor phase. The K values allow us to compute the composition of the liquid and the gas phases in a multiphase fluid mixture at any given pressure and temperature. These so-called *flash calculations* or vapor/liquid equilibrium (VLE) calculations, which use an EOS to determine the K values, require a level of numerical computation outside the scope of this book. For more information on the EOS-based approach, see the references mentioned at the beginning of this chapter. Although we do not discuss multiphase EOS definitions, we will use simple expressions for the EOS of single-phase fluids as discussed in the following two sections.

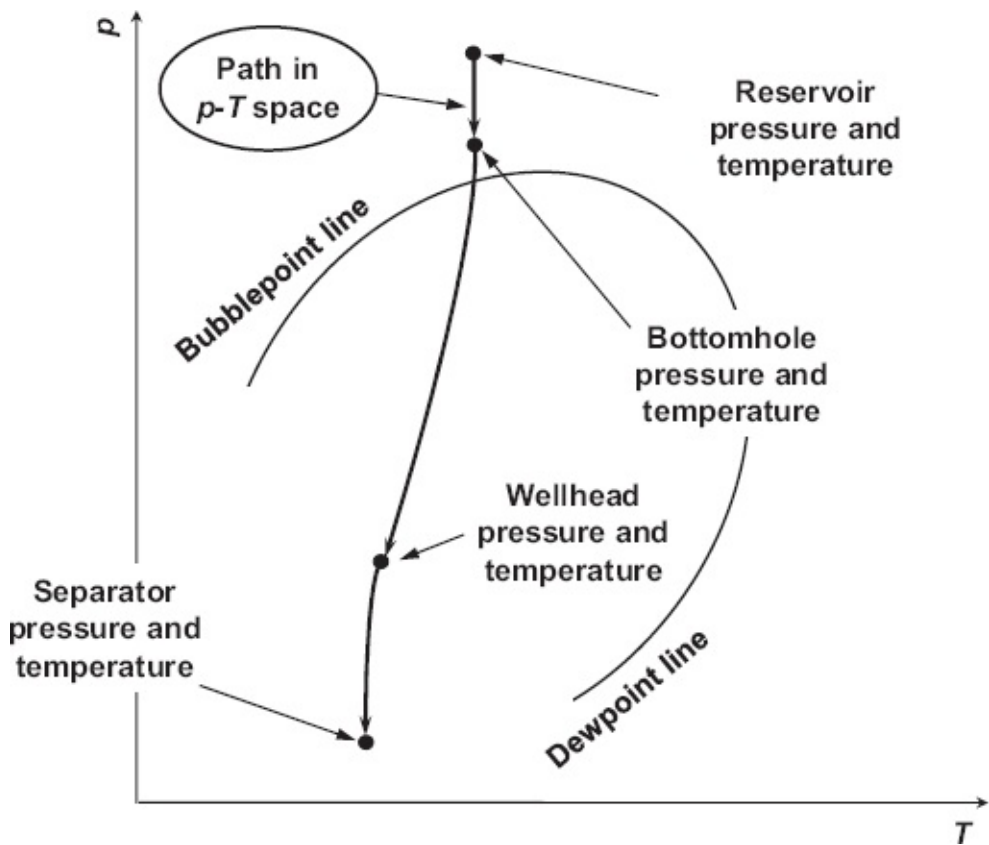


Fig. 2.3—Path in p - T space as the oil/gas mixture flows from the reservoir to the terminal.

2.5.2 Single-Phase Gas. The relationship between pressure, volume, and temperature of an ideal gas is given by an EOS known as the *ideal-gas law*, which can be expressed in different forms in SI units as

$$pV = nRT_{\text{abs}}, \dots \quad (2.1)$$

$$pV = \frac{mRT_{\text{abs}}}{M}, \dots \quad (2.2)$$

$$\frac{p}{\rho_g} = \frac{RT_{\text{abs}}}{M}, \dots \quad (2.3)$$

or in field units as

$$pV = nRT_{\text{abs}}, \dots \quad (2.4)$$

$$pV = \frac{mRT_{\text{abs}}}{M_w} \quad \dots \dots \dots \quad (2.5)$$

$$\frac{p}{\rho_w} = \frac{RT_{abs}}{M_w}, \dots \quad (2.6)$$

where p is pressure, Pa, (psia); V is volume, m³; (ft³), n is amount of gas, mol, (lbm/mol); R is the universal gas constant equal to 8.314 J/K·mol, (10.73 psia-ft³/°R-lbm/mol); T_{abs} is absolute temperature, K, (°R); m is mass, kg, (lbm); ρ_g is gas density, kg/m³, (lbm/ft³); M is molar mass, kg/mol; M_w is molecular weight, (lbm/lbm·mol). See Section A-4.2 of [Appendix A](#) for the numerical relationship between the molar mass M , the molecular weight M_w , the specific gravity y_g , and the density $\rho_{g,sc}$:

The ideal-gas law is valid only at pressures much below those normally encountered in the E&P industry. Approximate relationships, valid at higher pressures, are given in SI units by

$$pV = nZRT_{\text{abs}}, \dots \quad (2.7)$$

$$pV = \frac{mZRT_{\text{abs}}}{M}, \quad \dots \dots \dots \quad (2.8)$$

and in field units by

$$pV = nZRT_{\text{abs}}, \dots \quad (2.10)$$

$$pV = \frac{mZRT_{\text{abs}}}{M_w}, \quad \dots \dots \dots \quad (2.11)$$

$$\frac{p}{\rho_g} = \frac{ZRT_{abs}}{M_w}, \dots \quad (2.12)$$

where Z is the *gas deviation factor*, also known as the *gas compressibility factor* or simply the *Z factor*. Correlations developed by Standing and Katz (1942) are normally used to extend this relationship to hydrocarbon gas mixtures (see [Appendix B](#)).

2.5.3 Single-Phase Oil. The relationship between pressure, volume, and temperature of single-phase oil is given by an EOS in the form of an expression for compressibility. Isothermal oil compressibility is defined as the decrease in volume per unit of pressure, $-dV/dp$, per unit of volume V (or the increase in density per unit volume, $dp/d\rho$, per unit of density ρ) at constant temperature T :

$$c_o = -\frac{1}{V} \frac{dV}{dp} \Big|_T = \frac{1}{\rho} \frac{dp}{d\rho} \Big|_T, \dots \quad (2.13)$$

where c_o is the compressibility coefficient, which typically is itself a function of pressure and temperature. The large heat capacity of an oil reservoir justifies the assumption that oil expansion in the reservoir during production is an isothermal process. When flowing through the wellbore to the surface, the fluid mixture gradually cools down, but it is often still assumed that the expansion occurs pseudothermally with a compressibility coefficient that gradually changes with decreasing pressure and temperature. (An empirical correlation for c_o is given in Section B-2.6 in [Appendix B](#).) [Eq. 2.13](#) can be interpreted as a differential equation in V and p that allows for separation of variables:

$$\frac{dV}{V} = -c_o dp. \dots \quad (2.14)$$

We specify a boundary condition in the form of

$$p = p_{\text{ref}} : V = V_{\text{ref}}, \dots \quad (2.15)$$

and we assume that the dependence of c_o on p is small enough to linearize the right side of [Eq. 2.14](#). The solution can then be written as

$$V = V_{\text{ref}} \exp[-c_o(p - p_{\text{ref}})]. \dots \quad (2.16)$$

Remembering that c_o is a function of p and T , [Eq. 2.16](#) can be interpreted as an EOS that describes the PVT behavior of single-phase oil. Because the density ρ_o is inversely proportional to the volume V , we can also write [Eq. 2.16](#) as

$$\rho_o = \rho_{o,\text{ref}} \exp[c_o(p - p_{\text{ref}})]. \dots \quad (2.17)$$

Single-phase oil is at a pressure above the bubblepoint pressure, and a natural choice for the reference pressure p_{ref} is therefore the bubblepoint pressure at a certain temperature T , leading to

$$\rho_o = \rho_{ob} \exp[c_o(p - p_b)] \text{ for } p > p_b, \dots \quad (2.18)$$

where the values of p_b and ρ_{ob} can be determined from laboratory experiments or from empirical correlations as discussed in [Appendix B](#). A special case is obtained for dead oil, which has a bubblepoint pressure equal to the atmospheric pressure, in which case $p_{\text{ref}} = p_{sc}$.

2.6 Oil Models

2.6.1 Compositional Models. In a compositional model of a multiphase hydrocarbon mixture, the compositions of the liquid and the gas phases are functions of pressure and temperature and need to be determined from experiments, possibly combined with flash calculations using an EOS. Hydrocarbon mixtures may consist of many tens of components, and a full compositional analysis taking into account all components would be very time consuming. Furthermore, it is often quite difficult to accurately establish the amount and the properties of all components, in particular those with a high molar mass, the so-called heavy fractions. Therefore it is customary to lump these into a pseudocomponent. This is typically done for heptane and all heavier fractions, in which case the pseudocomponent is referred to as C_{7+} . In its most simple form, a compositional model consists of only two pseudocomponents, one for the lighter and one for the heavier hydrocarbons, often referred to as *heavies* and *lights*. Such a two-component model, also known as a *binary-mixture model*, is too crude to accurately describe the behavior of gas/condensate systems. However, it is usually sufficient to describe the behavior of black oils or even volatile oils.

2.6.2 Volatile Oil Model. The *volatile oil model* is a two-component model that accounts for compositional variations in both the liquid and the gas phase. Other names are *modified black oil model*, *extended black oil model*, or *volatilized oil model*. The pseudocomponents in the volatile oil model are stock-tank oil and stock-tank gas (“heavies” and “lights”), which can each be characterized with just a single parameter per pseudocomponent: $\rho_{o,sc}$ and $\rho_{g,sc}$ in SI units, or y_o (or y_{API}) and y_g in field units. Note that this is an assumption. In a more accurate model, it should be taken into account that the properties of stock-tank gas originating from reservoir gas are different from those of stock-tank gas originating from reservoir oil (i.e., solution gas). The same holds for the properties of stock-tank oil resulting from reservoir oil or from reservoir gas (i.e., condensate). The difference may be of relevance—e.g., for the accurate design of separation facilities for condensates or volatile oils. However, for most reservoir engineering or production engineering calculations, the assumption is acceptable.

The composition of the oil at or above bubblepoint pressure is fully defined by the bubblepoint GOR R_{sb} . The compositions of the oil and the gas at pressures below bubblepoint are specified by the solution GOR R_s and the solution OGR r_s , which are both functions of pressure and temperature. To describe the change in density (or volume) of the oil and gas phases with changing pressure and temperature, we need two additional variables, the oil and gas formation volume factors B_o and B_g . With the aid of Fig. 2.1 we can derive the mass balance equations for oil and gas that are brought from downhole conditions (also known as *local* or *in-situ conditions*) to standard conditions:

$$B_o \rho_o = \rho_{o,sc} + R_s \rho_{g,sc}, \dots \quad (2.19)$$

$$B_g \rho_g = \rho_{g,sc} + R_s \rho_{o,sc}, \dots \quad (2.20)$$

which give us the required expressions in terms of densities:

$$\rho_o = \frac{\rho_{o,sc} + R_s \rho_{g,sc}}{B_o}, \dots \quad (2.21)$$

$$\rho_g = \frac{r_s \rho_{o,sc} + \rho_{g,sc}}{B_g}, \dots \quad (2.22)$$

Since B_g , B_o , R_s , and r_s are functions of pressure and temperature, Eqs. 2.21 and 2.22 can be interpreted as EOSs. They can be conveniently written in matrix form, and if we also include the mass balance equation for water,

$$\rho_w = \frac{\rho_{w,sc} + R_{sw} \rho_{g,sc}}{B_w} = \rho_{w,sc}, \dots \quad (2.23)$$

this results in

$$\begin{bmatrix} \rho_g \\ \rho_o \\ \rho_w \end{bmatrix} = \begin{bmatrix} \frac{1}{B_g} & \frac{r_s}{B_g} & 0 \\ \frac{R_s}{B_o} & \frac{1}{B_o} & 0 \\ 0 & 0 & 1 \end{bmatrix} \begin{bmatrix} \rho_{g,sc} \\ \rho_{o,sc} \\ \rho_{w,sc} \end{bmatrix}. \dots \quad (2.24)$$

or

$$\begin{bmatrix} \rho_{g,sc} \\ \rho_{o,sc} \\ \rho_{w,sc} \end{bmatrix} = \begin{bmatrix} \frac{B_g}{1 - R_s r_s} & \frac{-B_o r_s}{1 - R_s r_s} & 0 \\ \frac{-B_g R_s}{1 - R_s r_s} & \frac{B_o}{1 - R_s r_s} & 0 \\ 0 & 0 & 1 \end{bmatrix} \begin{bmatrix} \rho_g \\ \rho_o \\ \rho_w \end{bmatrix}, \dots \quad (2.25)$$

where we have assumed that $B_w = 1$ and $R_{sw} = 0$, which implies that gas solubility, compressibility, and thermal expansion for water are so small that they can be neglected. We can use Fig. 2.1 to derive similar matrix expressions for the volume flow rates, resulting in

$$\begin{bmatrix} q_{g,sc} \\ q_{o,sc} \\ q_{w,sc} \end{bmatrix} = \begin{bmatrix} \frac{1}{B_g} & \frac{R_s}{B_g} & 0 \\ \frac{r_s}{B_o} & \frac{1}{B_o} & 0 \\ 0 & 0 & 1 \end{bmatrix} \begin{bmatrix} q_g \\ q_o \\ q_w \end{bmatrix}, \dots \quad (2.26)$$

or

$$\begin{bmatrix} q_g \\ q_o \\ q_w \end{bmatrix} = \begin{bmatrix} \frac{B_g}{1-R_s r_s} & \frac{-B_g R_s}{1-R_s r_s} & 0 \\ \frac{-B_o r_s}{1-R_s r_s} & \frac{B_o}{1-R_s r_s} & 0 \\ 0 & 0 & 1 \end{bmatrix} \begin{bmatrix} q_{g,sc} \\ q_{o,sc} \\ q_{w,sc} \end{bmatrix}, \dots \quad (2.27)$$

Note that we could equally well have used volumes instead of flow rates. For example, the second row in Eq. 2.26 can also be expressed as $V_{o,sc} = r_s/B_g \times V_g + 1/B_o \times V_o$.

Eqs. 2.24 and 2.27 have been programmed in MATLAB function `local_q_and_rho.m`. Determination of the necessary values of B_g , B_o , R_s , and r_s as functions of pressure and temperature is usually made with the aid of PVT tests and compositional analysis. This is outside the scope of our book, and therefore we will mainly use an even further simplified formulation, the so-called *black oil model* as described in the following section. An example of the use of tabulated volatile oil parameters B_g , B_o , R_s , and r_s is discussed in the MATLAB assignment (Hydrocarbon Properties) at the end of this chapter. Several varieties of the volatile oil model have been developed (for an overview, see Whitson and Brûlé 2000). A graphical representation of the volatile oil parameter definitions as used in our text is given in Fig. 2.4.

2.6.3 Black Oil Model. Just like the volatile oil model, the black oil model is a two-component model. However, it assumes a constant composition of the gas phase and accounts only for compositional variations in the liquid phase. The relevant equations of the model follow directly from those of the volatile oil model by substitution of $r_s = 0$. In particular, Eqs. 2.24 to 2.27 become

$$\begin{bmatrix} \rho_g \\ \rho_o \\ \rho_w \end{bmatrix} = \begin{bmatrix} \frac{1}{B_g} & 0 & 0 \\ \frac{R_s}{B_o} & \frac{1}{B_o} & 0 \\ 0 & 0 & 1 \end{bmatrix} \begin{bmatrix} \rho_{g,sc} \\ \rho_{o,sc} \\ \rho_{w,sc} \end{bmatrix}, \quad \dots \dots \dots \quad (2.28)$$

$$\begin{bmatrix} \rho_{g,sc} \\ \rho_{o,sc} \\ \rho_{w,sc} \end{bmatrix} = \begin{bmatrix} B & 0 & 0 \\ -B_g R_s & B_o & 0 \\ 0 & 0 & 1 \end{bmatrix} \begin{bmatrix} \rho_g \\ \rho_o \\ \rho_w \end{bmatrix}, \quad \dots \dots \dots \quad (2.29)$$

$$\begin{bmatrix} q_{g,sc} \\ q_{o,sc} \\ q_{w,sc} \end{bmatrix} = \begin{bmatrix} \frac{1}{B_g} & \frac{R_s}{B_o} & 0 \\ \frac{B_g}{B_o} & \frac{1}{B_o} & 0 \\ 0 & 0 & 1 \end{bmatrix} \begin{bmatrix} q_g \\ q_o \\ q_w \end{bmatrix}, \quad \dots \dots \dots \quad (2.30)$$

$$\begin{bmatrix} q_g \\ q_o \\ q_w \end{bmatrix} = \begin{bmatrix} B_g & -B_g R_s & 0 \\ 0 & B_o & 0 \\ 0 & 0 & 1 \end{bmatrix} \begin{bmatrix} q_{g,sc} \\ q_{o,sc} \\ q_{w,sc} \end{bmatrix}. \quad \dots \dots \dots \quad (2.31)$$

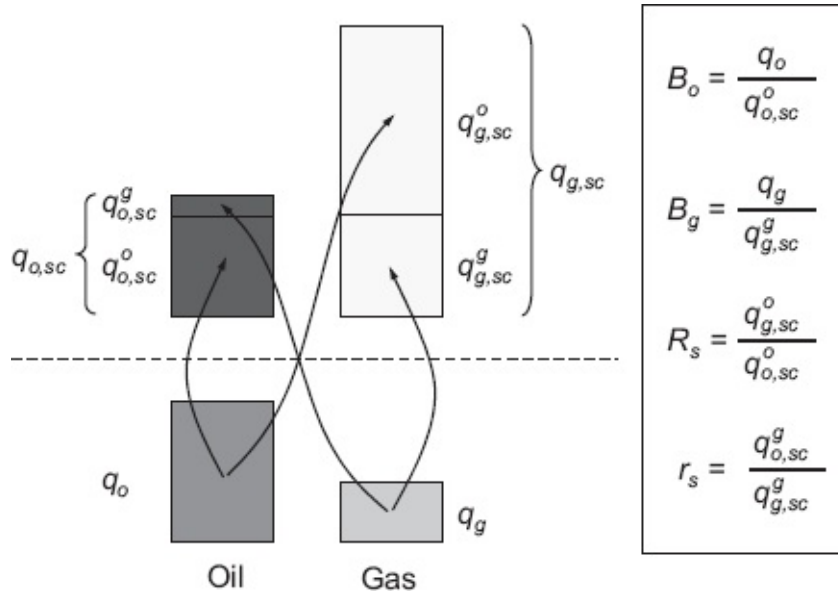


Fig. 2.4—Graphical representation of the volatile oil parameter definitions (after Whitson and Brûlé 2000). Superscripts o and g are used to indicate the origins of contributions to the volume flow rates at standard conditions. For example, $q_{g,sc}^o$ represents the part of the gas phase at standard conditions that originates from the downhole oil phase.

Just as for the volatile oil models, the necessary values of B_g , B_o , and R_s as functions of pressure and temperature may be obtained with the aid of PVT tests and compositional analysis. However, during the early development phase of an oil field no fluid samples may be available. In that case it is necessary to fall back on *correlations*, which are relationships for “typical” oil and gas compositions, based on experimental data. Especially for black oils such correlations can be reasonably accurate. In addition, production engineering calculations based on correlations require much less computational effort than do calculations based on compositional analysis using an EOS. Therefore, black oil correlations are widely used. However, to describe the behavior of volatile oil or gas/condensate systems, correlations are usually of limited value, and thus performing PVT analyses on fluid samples is required to allow proper compositional calculations.

2.7 Fluid Property Calculations

2.7.1 Gas Formation Volume Factor. An expression for the gas formation volume factor follows from Eqs. 2.24 and 2.27 as

$$B_g = \frac{q_g(1 - R_s r_s)}{q_{g,sc} - R_s q_{o,sc}} = \frac{r_s \rho_{o,sc} + \rho_{g,sc}}{\rho_g}. \quad \dots \dots \dots \quad (2.32)$$

For black oil—i.e., for $r_s = 0$ —this reduces to

$$B_g = \frac{q_g}{q_{g,sc} - R_s q_{o,sc}} = \frac{\rho_{g,sc}}{\rho_g}. \quad \dots \dots \dots \quad (2.33)$$

Numerical values for B_g can be computed as follows. With the aid of the gas law for nonideal gases, Eq. 2.7, we obtain

$$B_{gw} = \frac{q_g}{q_{g,sc}} = \frac{V_g}{V_{g,sc}} = \frac{p_{sc} T_{abs} Z}{p T_{sc,abs} Z_{sc}} = \frac{p_{sc} T_{abs} Z}{p T_{sc,abs}}, \quad \dots \dots \dots \quad (2.34)$$

where the last equality results from the fact that, by definition, $Z_{sc} = 1$. Here we added the subscript *w* to indicate that this equation concerns the wet gas formation volume factor, because it is based on the assumption that we consider volumes of identical amounts of substance *n* at downhole and standard conditions. This assumption is fully justified for single-phase gas; but where applying Eq. 2.34 in two-phase computations, take into account that condensate may be present at surface conditions. Usually we are more interested in the dry gas formation volume factor B_g , which is related to its wet gas counterpart according to

$$B_g = B_{gw} (1 + r_s) = \frac{p_{sc} T_{abs} Z}{p T_{sc,abs}} (1 + r_s). \quad \dots \dots \dots \quad (2.35)$$

Note that for black oil and single-phase gas, $r_s = 0$ and therefore $B_g = B_{gw}$.

2.7.2 Oil Formation Volume Factor. An expression for the oil formation volume factor follows from Eqs. 2.24 and 2.27 as

$$B_o = \frac{q_o(1 - R_s r_s)}{q_{o,sc} - r_s q_{g,sc}} = \frac{\rho_{o,sc} + R_s \rho_{g,sc}}{\rho_o}, \quad \dots \dots \dots \quad (2.36)$$

which for black oil, i.e., for $r_s = 0$, reduces to

$$B_o = \frac{q_o}{q_{o,sc}} = \frac{\rho_{o,sc} + R_s \rho_{g,sc}}{\rho_o}. \quad \dots \dots \dots \quad (2.37)$$

The actual computation of B_o is based on either experiments or correlations. For pressures above the bubblepoint pressure the oil formation volume factor is given by

$$\begin{aligned} B_o &= \frac{q_o}{q_{o,sc}} = \frac{\rho_{o,sc} + R_{sb} \rho_{g,sc}}{\rho_o} = \frac{\rho_{o,sc} + R_{sb} \rho_{g,sc}}{\rho_{ob}} \exp[-c_o(p - p_b)] \\ &= B_{ob} \exp[-c_o(p - p_b)] \end{aligned} \quad \dots \dots \dots \quad (2.38)$$

An empirical correlation for c_o is given in [Appendix B](#).

2.7.3 Black Oil Correlations. The standard reference for black oil correlations is Standing (1952), and these “Standing correlations” for p_b , R_s , and B_o have been programmed in the MATLAB function `black_oil_Standings.m`. For details of the correlations see [Appendix B](#), and for an overview of the corresponding MATLAB routines see [Appendix H](#). A flow chart displaying the various computational steps in MATLAB function `black_oil_standing.m` has been displayed in [Fig. 2.5](#). Many other correlations have been developed over the past half-century, and an extensive overview is given in [Appendix B](#) of Brill and Mukherjee (1999); further information can be found in the references mentioned in [Section 2.2](#) above. As an example of an alternative correlation, the “Glasø correlations” (Glasø 1980) have been programmed in MATLAB function `black_oil_Glaso.m`. [Figs. 2.6](#) and [2.7](#) illustrate the typical behavior of B_o and R_s with increasing pressure, reflecting the increasing amount of gas dissolving in the oil. After the bubblepoint pressure has been reached—i.e., after the maximum amount of gas has been dissolved— R_s stays constant (at a value of R_{sb} , by definition). The value of B_o slightly decreases because of compression of the undersaturated oil with increasing pressure.

2.8 Questions

2.1 What is the difference between the solution GOR and the producing GOR in

an oil well?

- 2.2 What is the difference between ordinary and retrograde condensation?
- 2.3 The thermodynamic behavior of a hydrocarbon mixture can be characterized with an EOS if we know its composition (in terms of component fractions) and the thermodynamic properties of the components. A strongly simplified description of hydrocarbon mixtures is the black oil model. How are the EOS, the composition, and the (pseudo)component properties defined in the black oil model?
- 2.4 What is the difference between the oil phase and the oil (pseudo)component in a volatile or black oil model?

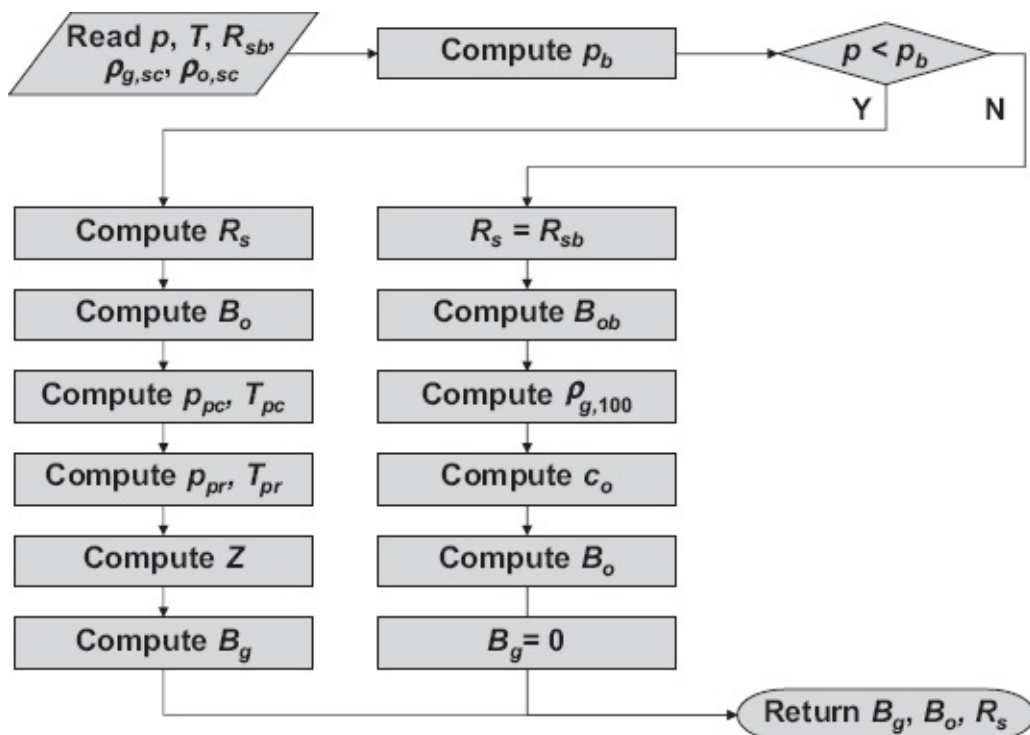


Fig. 2.5—Flow chart displaying the various computational steps in MATLAB function `black_oil_Standing.m`.

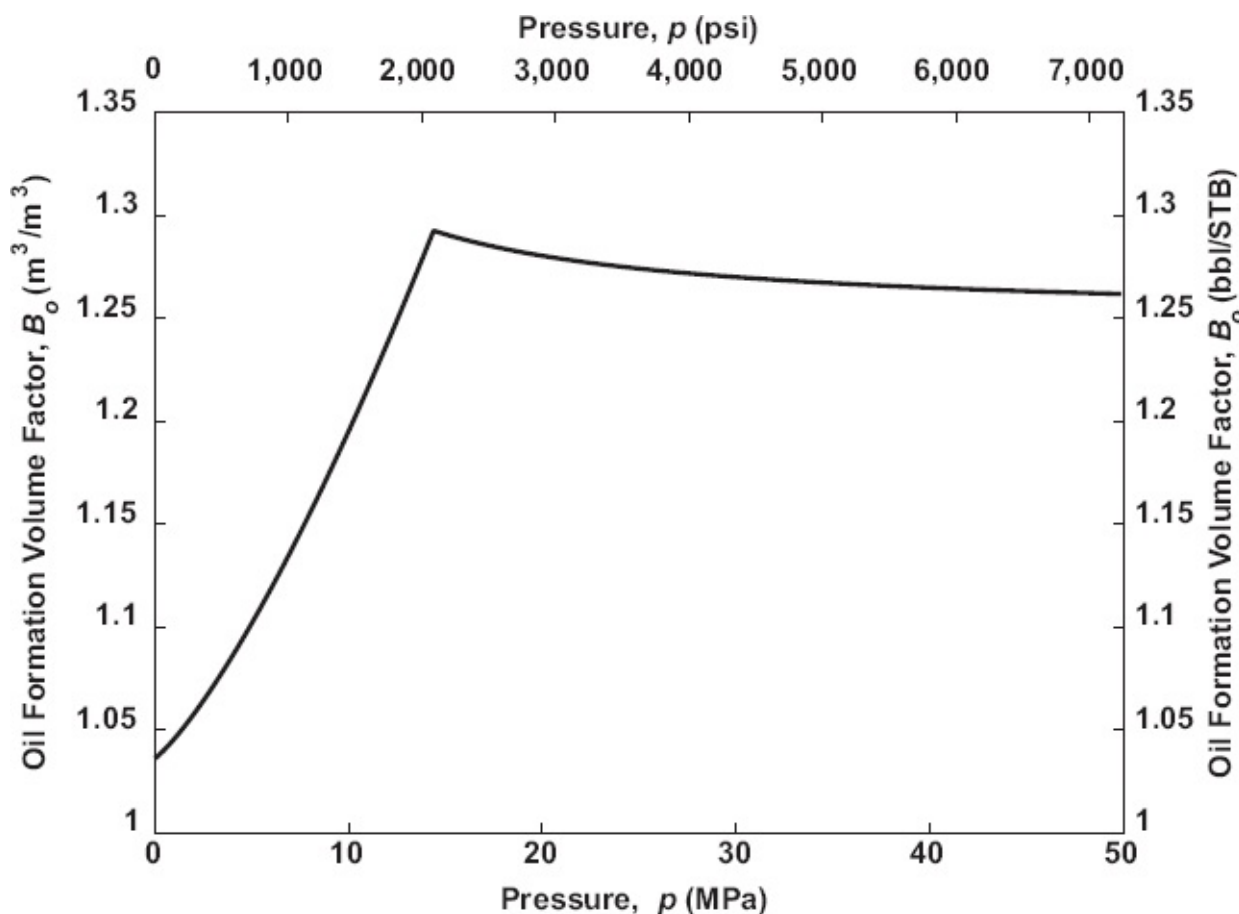


Fig. 2.6—Oil formation volume factor as a function of pressure. The graph is based on the Standing (1947, 1952) correlations applied to a gas/oil mixture with fluid properties: $\rho_{g,sc} = 0.95 \text{ kg/m}^3$ ($y_g = 0.77$), $\rho_{o,sc} = 850 \text{ kg/m}^3$ ($y_{API} = 35^\circ$), and $R_{sb} = 100 \text{ m}^3/\text{m}^3$ (561 scf/STB) at a temperature of 60°C (124°F). The corresponding bubblepoint pressure is 14.4 MPa (2,089 psi).

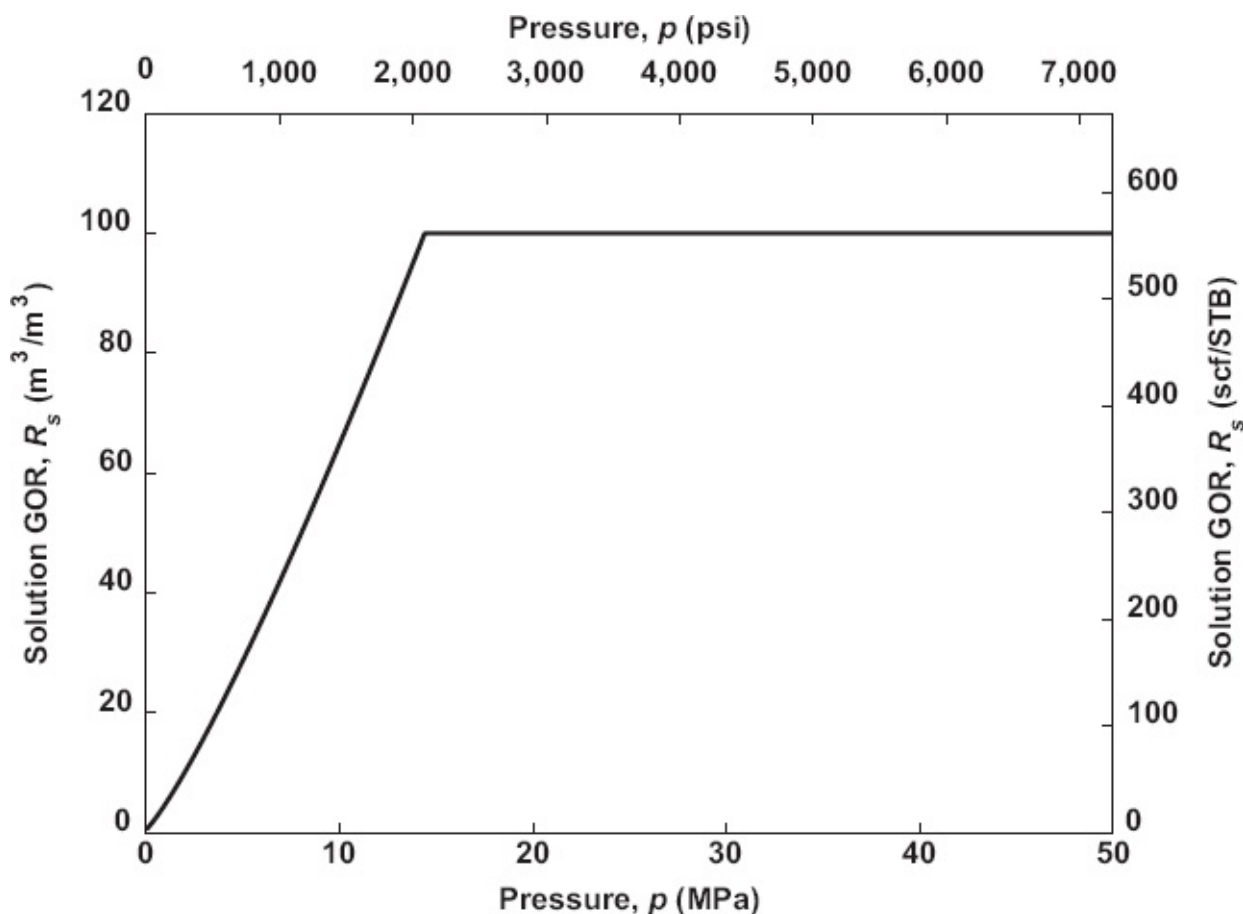


Fig. 2.7—Solution GOR as a function of pressure. The graph is based on the Standing (1947, 1952) correlations applied to a gas/oil mixture with the same fluid properties and at the same temperature as in Fig. 2.6.

- 2.5 Why do we use pseudoreduced pressures and temperatures (and not just reduced values) to compute the Z factor of hydrocarbon mixtures?
- 2.6 Demonstrate that for the volatile oil model we have $\rho_g \cdot q_g + \rho_o \cdot q_o = \rho_{g,sc} \cdot q_{g,sc} + \rho_{o,sc} \cdot q_{o,sc}$. What is the meaning of this equality?
- The PVT data for a volatile oil well producing at 0% water cut and corresponding to a pressure of 50 MPa and a temperature of 50°C are represented as $B_g = 0.0025 \text{ m}^3/\text{m}^3$, $B_o = 1.55 \text{ m}^3/\text{m}^3$, $R_s = 200 \text{ m}^3/\text{m}^3$, and $r_s = 0.0008 \text{ m}^3/\text{m}^3$. What is the local gas/liquid fraction if the well produces 1,000 B/D at a producing GOR of 2000 scf/STB? (Give your answer in SI units).

For questions 2.8 through 2.12, use the oil and gas correlations in Appendix B. The correlations have been programmed in various MATLAB routines (see Appendix H). However, the computations can also be performed by hand calculation.

- 2.7 An oil reservoir has a pressure of $p_R = 17 \text{ MPa}$ at the GOC and a temperature of 76°C. The bubblepoint pressure of the oil is $p_b = 19.5 \text{ MPa}$. The gas and oil densities at standard conditions are $\rho_g = 1.11 \text{ kg/m}^3$ and $\rho_o = 910 \text{ kg/m}^3$. What is the solution GOR of the oil?

- 2.8 Refer to Question 2.8. What is the specific gravity of the gas produced at surface? And what is the density of the gas-cap gas just above the GOC in the reservoir?
- 2.9 Refer to Question 2.8. What are the oil and gas viscosities if the reservoir pressure is 22 MPa and all other parameters remain the same?
- 2.10 Refer to Question 2.8. What is the compressibility coefficient c_o of the oil?
- 2.11 Consider a well that produces dry black oil with a producing GOR of 250 m^3/m^3 . The production history shows no indication of free gas production. The densities of the gas and oil at standard conditions are given by $\rho_{g,sc} = 1.02 \text{ kg/m}^3$ and $\rho_{o,sc} = 805 \text{ kg/m}^3$. What is the oil formation volume factor at the following pressure and temperature combinations: $p = 15 \text{ MPa}$ and $T = 85^\circ\text{C}$, and $p = 30 \text{ MPa}$ and $T = 105^\circ\text{C}$?

2.9 MATLAB Assignment: Hydrocarbon Properties

2.9.1 Objectives

- Perform a simple MATLAB programming exercise and create annotated plots.
- Become familiar with the oil and gas parameters B_g , B_o , r_s , and R_s and their dependency on pressure and temperature.
- Become familiar with the MATLAB function files `black_oil_Stationing.m` and `local_q_and_rho.m` and with the use of tabulated volatile oil parameters.

2.9.2 Assignment

Task 1

- Recreate Figs. 2.6 and 2.7 (i.e., plots of B_o and R_s vs. pressure p) by running script file `example_plot_black_oil_1.m`. Note that in addition to creating plots of B_o and R_s , the file also creates two plots of B_g vs. p , one on a linear scale and one on a semilogarithmic scale.
- Inspect the contents of the script file. It uses a simple *for-loop*, which calls the function file `black_oil_Stationing.m` to obtain the three black oil parameters B_g , B_o , and R_s for increasing values of the pressure p at a fixed temperature T . The values are stored in a matrix named `results` with `n_step` rows and three columns.
- Inspect the contents of `black_oil_Stationing.m` and verify the sequence of computational steps with the aid of the flow chart depicted in Fig. 2.5.

Notes

- All preprogrammed MATLAB function files listed in Appendix H start with a series of comment lines to briefly explain the actions performed in the function and to list the input and output parameters in the *header*, i.e., the first line of the

function. Note that the second line of the function is always a repetition of the header—but with a comment symbol % in front. This is done to echo the header information with the aid of the `help` function. For example, type `help black_oil_Standing` in the MATLAB workspace and watch the result.

- If you are an experienced MATLAB user, you may recognize that the use of a forloop in `plot_black_oil_1.m` could have been avoided by using a technique called *vectorization*. However, in the MATLAB examples used in this book we will not make use of this technique but will instead use classical loops to increase the readability of the code.
- The size of the matrix `results` has been initialized just before the for-loop by defining it as a matrix filled with zeros. This is to avoid the matrix increasing one row in size every time the for-loop is executed, which would slow down the computation.

Question 1

- 1(a) What should be the value of B_o at standard conditions?
- 1(b) Is this in line with the result in your plot. Why not?
- 1(c) Repeat the plot with modified parameter values such that B_o obtains the value corresponding to standard conditions. What did you change?
- 1(d) Why has the B_g curve a (near-)hyperbolic shape? Which equation explains this behavior?

Task 2

- Inspect the function file `local_q_and_rho.m`. The variables `q`, `q_sc`, `rho` and `rho_sc` are column vectors of three elements each. What is their meaning?
- Run script file `example_plot_black_oil_2.m`. It creates plots of local (downhole) oil and gas rates as a function of pressure p and at a fixed temperature T for a given unit surface oil rate and the corresponding surface associated gas rate R_{sb} . The black oil properties are identical to those used in `example_plot_black_oil_1.m`. Inspect the contents of the script file.

Question 2

- 2(a) Why is the local oil rate curve identical to the oil formation volume factor curve plotted under Task 1?
- 2(b) Is the local gas rate curve also identical to the gas formation volume factor curve plotted under Task 1? If not, what explains the difference?

Task 3. Create a MATLAB script file that performs the following steps:

- Load the volatile oil parameter table with the following commands:

```
file name = 'vol oil table 01';
load(file name,'vol oil');
```
- The variable `vol_oil` is a 3D matrix containing values of T , p , B_g , B_o , r_s , and R_s . The first dimension is used to loop over the temperature values; i.e., it just contains integers 1, 2, ..., m , where m is the number of temperature values. The second dimension loops over the pressure values (i.e., integers 1, 2, ...),

n), and the third dimension contains the values of T , p , and the four volatile oil parameters.

- Determine the number of elements in each dimension, as well as the lower and upper bounds of the temperature and pressure ranges, with the following statements:

```
[m, n, k] = size(vol_oil)
T_lo = vol_oil(1,1,1)
p_lo = vol_oil(1,1,2)
T_hi = vol_oil(m,1,1)
p_hi = vol_oil(1,n,2)
```

- Create plots of B_g , B_o , r_s , and R_s , as a function of pressure over the range determined above, for a temperature T of choice (but within the range determined above). For this purpose, save the file `example_plot_black_oil_1.m` under the name `example_plot_volatile_oil_1.m` and, inside this new file, modify the call to function `black_oil_Standing.m` into a call to `volatile_oil.m`. Adjust all comment lines as appropriate.
- Optionally, display two graphs in each plot, one for the lowest and one for the highest value of T as determined above. Hint: Repeat the plot statement and use the command `hold on` between the two plot statements. Add a legend.
- Inspect the contents of `volatile_oil.m` and note how 2D interpolation (i.e., between p values and between T values) is used to obtain the volatile oil parameters.
- Note that when using a volatile oil table, the input parameters $\rho_{g,sc}$, $\rho_{o,sc}$, and R_{sb} should be consistent with those used to generate the tabulated values. In particular, for `vol_oil_table_01` one should use $r_{g,sc} = 0.80 \text{ kg/m}^3$ ($y_g = 0.65$), $\rho_{o,sc} = 800 \text{ kg/m}^3$ ($y_{API} = 45^\circ$), and $R_{sb} = 450 \text{ m}^3/\text{m}^3$ (2,526 scf/STB).

Question 3

- What could be a reason for the minimum in the curves for r_s ?
- What is different in `local_q_and_rho.m` when using a volatile oil table instead of a black oil model?

2.9.3 Deliverables

- MATLAB program listing for Task 3
- Plots
- Answers to the questions

Chapter 3

Single-Phase Flow in Wells and Pipelines

3.1 What Is Covered in This Chapter?

As described in [Chapter 1](#), nodal analysis of a production system is based on a representation of the system in the form of individual elements connected at nodes. In this chapter we will consider elements that describe the flow through circular conduits such as pipelines, flowlines, or wells. We use a 1D description and consider single-phase flow of oil, gas, or water. Multiphase flow will be the topic of the next chapter.

Under the assumption of a known temperature profile along the pipe, we start from differential equations for conservation of mass and momentum and an algebraic EOS in terms of pressures and densities of the fluid. Assuming steady-state conditions, we arrive at a first-order nonlinear ordinary-differential equation for pressure along the pipe, which reveals that there are three contributions to pressure drop: gravity, friction, and acceleration. We discuss how, given a boundary condition, this equation can be integrated numerically with the aid of standard numerical integration routines to produce a *traverse*—i.e., a graph of pressure as a function of distance for a given flow rate. Under simplifying assumptions, the integration can also be performed analytically both for single-phase liquid flow and for single-phase gas flow, although the latter requires some additional tricks to deal with the nonlinear effects of compressibility.

Once we can compute the pressure drop over a pipe for a given flow rate, we can repeat the computation many times for different flow rates, while keeping the pressure at one end of the pipe fixed, to produce a graph of the varying pressure at the other end as a function of rate. This procedure results in (upstream or downstream) *performance curves* that can be used to characterize the flow performance of the pipe element. As discussed in [Chapter 1](#), the use of such performance curves forms a key step in classic nodal analysis.

3.2 Governing Equations

3.2.1 Mass Balance, Momentum Balance, and Equation of State. In this section we will derive the 1D equations for single-phase fluid flow in circular pipes under the assumption that the temperature profile along the pipe is known. For a detailed treatment of the nature of the equations see, e.g., Bird et al. (2002), who also treat the case in which the temperature is not known in advance. Consider a section of an

inclined pipeline with constant cross-sectional area (see [Fig. 3.1](#)). We can write the mass balance per unit time for the section as

$$\underbrace{A\rho v}_{\text{mass rate in}} - \underbrace{A\left(\rho + \frac{\partial \rho}{\partial s}ds\right)\left(v + \frac{\partial v}{\partial s}ds\right)}_{\text{mass rate out}} = \underbrace{A\frac{\partial \rho}{\partial t}ds}_{\text{mass accumulated unit time}}, \quad \dots \dots \dots (3.1)$$

where A is cross-sectional area of the pipe, m^2 ; ρ is fluid density, kg/m^3 ; v is fluid velocity averaged over the cross section, m/s ; s is coordinate along the pipe, m ; and t is time, s . In reality the velocity will change over the cross section of the pipe. It is zero at the wall and reaches its maximum value at the center. However, the use of an averaged velocity is accurate enough for our purpose.

Initially we assume that the fluid velocity is always positive—i.e., that the fluid always flows in the positive coordinate direction. The momentum balance per unit time (Newton's law) can then be written as

$$\begin{aligned} & \underbrace{A\rho v^2}_{\text{momentum rate in}} - \underbrace{A\left(\rho + \frac{\partial \rho}{\partial s}ds\right)\left(v + \frac{\partial v}{\partial s}ds\right)^2}_{\text{momentum rate out}} + \underbrace{Ap - A\left(p + \frac{\partial p}{\partial s}ds\right)}_{\text{pressure forces}} \\ & + \underbrace{F_g(\rho, s)ds}_{\text{gravity force}} + \underbrace{F_f(\mu, \rho, v)ds}_{\text{friction force}} = \underbrace{A\frac{\partial(\rho v)}{\partial t}ds}_{\text{momentum accumulated unit time}}, \end{aligned} \quad (3.2)$$

where p is pressure, Pa ; $F_g(\rho, s)$ is gravity force per unit length, N/m ; $F_f(\rho, \mu, v)$ is friction force per unit length, N/m ; and μ is dynamic viscosity, $\text{Pa}\cdot\text{s}$. The nature of the gravity force $F_g(\rho, s)$ and the friction force $F_f(\mu, \rho, v)$ will be discussed in more detail in Sections 3.22 and 3.23. The viscosity μ is a known function of pressure and temperature, where the temperature is a known function of s . A third equation for the remaining unknown variables ρ , v , and p is given by the equation of state (EOS) for the fluid. For example, if we consider the flow of single-phase gas, we can use [Eq. 2.9](#) derived in [Section 2.5](#); for single-phase oil flow we can use [Eq. 2.17](#). If we expand [Eqs. 3.1](#) and [3.2](#), drop all terms higher than first order in the differential ds , and simplify the results, we can write the three equations as

$$\frac{\partial(\rho v)}{\partial s} = \frac{\partial \rho}{\partial t}, \quad \dots \dots \dots (3.3)$$

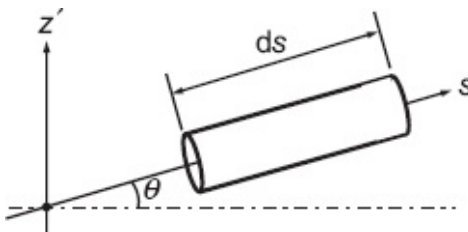


Fig. 3.1—Segment of an inclined pipeline.

$$\frac{\partial(\rho v^2)}{\partial s} = \frac{\partial(\rho v)}{\partial t} - \frac{\partial p}{\partial s} + \frac{F_s}{A} + \frac{F_f}{A}, \dots \quad (3.4)$$

$$\rho = \frac{Mp}{ZRT_{abs}} \text{ for gas, } \dots \quad (3.5)$$

$$\text{or } \rho = \rho_{o,ref} \exp[c_o(p - p_{ref})] \text{ for oil, } \dots \quad (3.6)$$

where the compressibility c_o and the gas deviation factor Z are known functions of p and T ; note that as discussed above, T itself (and therefore also T_{abs}) is a known function of s .

3.2.2 Head Loss. The head loss or gravity loss (i.e., the gravity force per unit length) for a pipe element is defined as

$$F_g(\rho, s) = -\rho g \sin \theta(s) A, \dots \quad (3.7)$$

where g is acceleration of gravity, m/s²; and $\theta(s)$ is pipeline *inclination*, rad. In pipeline engineering, the inclination θ is defined as the angle of the pipeline axis with the respect to the horizontal plane. The term “ $\sin \theta$ ”, which can be positive or negative, is therefore a measure of the change in elevation ζ of the pipeline axis per unit length of measured distance s . The inclination is usually known as a function of s , either theoretically as one of the design parameters of the pipeline or actually from measured data obtained during a pipeline survey. In well engineering it is common practice to define the wellbore geometry with a slightly different set of parameters (see [Fig. 3.2](#)). The inclination α of the well is defined as the angle between the wellbore axis and the vertical direction. The term “ $\cos \alpha$ ” is therefore a measure of the change in *true vertical depth* z , which is measured downward, per unit length of s , which is now known as *along-hole depth* (AHD), or *measured depth*, and naturally is also positive in the downward direction. As a result of the different definition of the inclination and because s is positive going downward, the head loss follows as

$$F_g(\rho, s) = -\rho g \cos \alpha(s) A. \dots \quad (3.8)$$

During the design phase, the *well path*, also known as the *well trajectory*, is specified either in rectangular coordinates or in terms of *survey coordinates*: AHD, inclination, and *azimuth* (i.e., the angle with respect to north). During and after drilling a well, the actual trajectory can be obtained from a *wellbore survey* which can be performed with survey tools run on wireline or with so-called measurement-while-drilling (MWD) tools incorporated in the drillstring. [Appendix C](#) gives an algorithm to convert from survey coordinates to rectangular coordinates, and describes MATLAB functions for survey evaluation and plotting of well trajectories. Note that the choice for a downward positive direction of s also implies that wellbore flow to surface has a negative velocity. We will therefore use the sign convention that flow rates related to

oil, gas, or water production have a negative sign, whereas all flow rates related to injection are positive. We will use this convention for flow in pipelines, flowlines, wellbores, and the near-wellbore region in the reservoir.

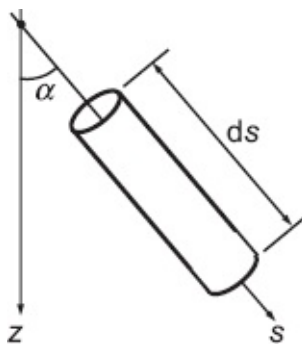


Fig. 3.2—Segment of a deviated well.

3.2.3 Friction Loss. The friction loss for single-phase flow in pipes with a circular cross section can be expressed as

$$\frac{F_f(\mu, \rho, v)}{A} = -\frac{\rho}{2d} f(\mu, \rho, v) \times v|v| = -\frac{8\rho}{\pi^2 d^5} f(\mu, \rho, v) \times q|q|, \dots \quad (3.9)$$

where d is the inside diameter of the pipe, m; f is the Moody *friction factor* (also known as the Darcy-Weisbach friction factor); and $q = v \times A$ is the flow rate, m³/s. Note the use of the absolute sign in the definition of the friction force: The dependency of the friction force on $-v|v|$ (or $-q|q|$) implies that it is always pointing in a direction opposite to the velocity (or the flow rate). For detailed information on the physics underlying the friction loss in pipe flow we refer to Bird et al. (2002) or one of the many other available fluid mechanics textbooks, e.g. White (2016). Here we merely state the key aspects.

The dimensionless friction factor f is a function of μ , ρ , and v (or q) through its dependence on two other dimensionless numbers: the Reynolds number N_{Re} and the scaled pipe roughness ϵ . The Reynolds number is defined as

$$N_{Re} = \frac{\rho d|v|}{\mu} = \frac{4}{\pi} \frac{\rho|q|}{\mu d}, \dots \quad (3.10)$$

where, as discussed before, we assume that μ is a known function of p and $T(s)$. It provides a measure of the relative importance of inertial forces (governed by ρ) and friction forces (governed by μ). The scaled pipe roughness is defined as

$$\epsilon = \frac{e}{d}, \dots \quad (3.11)$$

where e is the pipe roughness expressed in m, which we assume to be constant over the length of the pipe. For Reynolds numbers lower than 2,000 the flow is laminar,

and f is given explicitly by

$$f = \frac{64}{N_{Re}}, \dots \dots \dots \quad (3.12)$$

whereas for Reynolds numbers larger than 3,000 the flow is turbulent and f is given by the Colebrook (1939) equation:

$$\frac{1}{\sqrt{f}} - 1.74 + 2 \log_{10} \left(2\epsilon + \frac{18.7}{N_{Re}\sqrt{f}} \right) = 0. \dots \dots \dots \quad (3.13)$$

Eq. 3.13 is an implicit functional relationship between the three governing dimensionless numbers (f , N_{Re} , and ϵ) and was derived from a large number of experiments by various researchers (see Colebrook 1939, Moody 1944 and references therein). Because of its implicit nature it has to be solved iteratively which is conveniently done numerically, e.g., with Newton-Raphson iteration or the predefined MATLAB function `fzero` (see [Appendix D](#)). Alternatively, one of the several available explicit approximations can be used—e.g., the one of Zigrang and Sylvester (1985), which is defined as

$$f = \left\{ -2 \log_{10} \left[\frac{2\epsilon}{3.7} - \frac{5.02}{N_{Re}} \log_{10} \left(\frac{2\epsilon}{3.7} + \frac{13}{N_{Re}} \right) \right] \right\}^{-2} \dots \dots \dots \quad (3.14)$$

Fig. 3.3, known as the Moody chart, displays the change of friction factor f with increasing Reynolds number N_{Re} for various values of the dimensionless roughness ϵ , as computed with the original implicit [Eq. 3.13](#). For flow in the intermediate regime, characterized by Reynolds numbers between 2,000 and 3,000, one can use a linear interpolation between [Eqs. 3.12](#) and [3.13](#). The figure has been generated with the aid of the MATLAB file `Moody_friction_factor.m` which combines [Eqs. 3.12](#) and [3.13](#) with linear interpolation to cover the entire range of low and high Reynolds numbers. A similar expression that uses the explicit approximation [Eq. 3.14](#) instead of [Eq. 3.13](#), is available as `zig_and_Syl_fric_fact.m`.

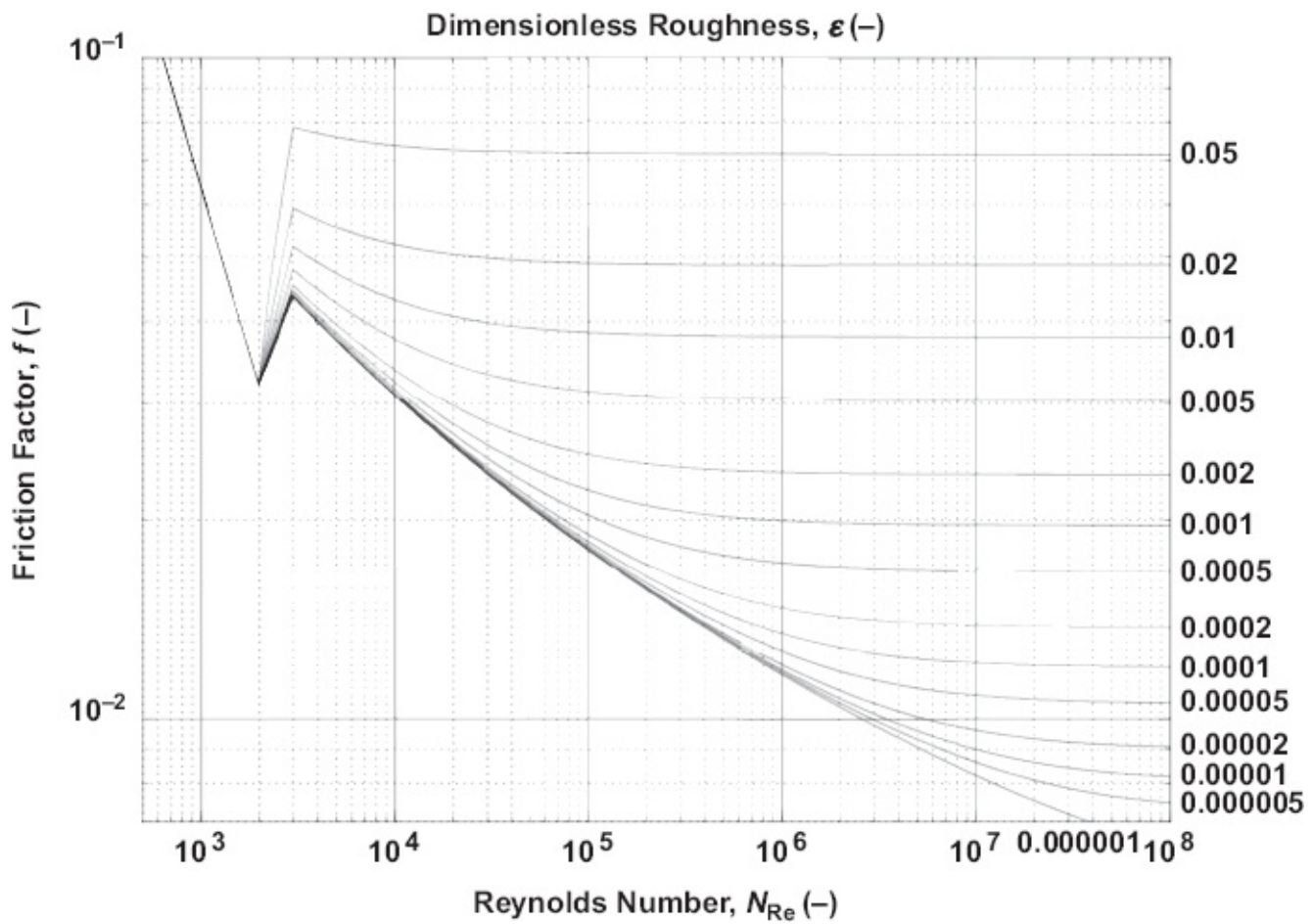


Fig. 3.3—Moody chart: friction factor f as function of Reynolds number N_{Re} for various values of dimensionless roughness ϵ .

3.2.4 Pressure Drop Components. If we restrict the analysis to steady-state flow—i.e., if we assume that ρ , v , and p are functions only of s , not of t —Eqs. 3.3 and 3.4 can be rewritten as

$$\frac{d(\rho v^2)}{ds} = 0, \dots \quad (3.15)$$

$$\frac{d(\rho v^2)}{ds} = -\frac{dp}{ds} + \frac{F_g}{A} + \frac{F_f}{A}. \dots \quad (3.16)$$

Using the equality

$$\frac{d(\rho v^2)}{ds} = \frac{d(\rho v)}{ds} + v + \rho v \frac{dv}{ds}, \dots \quad (3.17)$$

substituting Eqs. 3.7, 3.9, and 3.14, and reorganizing the outcome results in an expression for the pressure drop per unit length dp/ds ,

$$\frac{dp}{ds} = -\rho g \sin \theta - \underbrace{\frac{\rho}{2d} fv|v|}_{\text{friction loss}} - \underbrace{\rho v \frac{dv}{ds}}_{\text{acceleration loss}} \quad \dots \dots \dots \quad (3.18)$$

Here we have taken into account the possibility of negative fluid velocities (which according to our sign convention correspond to production) through the use of the absolute value of the velocity $|v|$. The three terms at the right side of Eq. 3.18 can be interpreted as follows:

- *Head loss or gravity loss* is the static change in pressure caused by the change in the pipe's elevation. In near-horizontal pipelines this component is negligible, but it is usually the most important component in a well. The pressure between surface and well bottom changes greatly, simply because of the weight of the column of fluid in the well, even if it is not flowing.
- *Friction loss* is caused by the dissipation of energy by viscous forces in the fluid. This term depends strongly on the fluid properties, the flow regime (laminar or turbulent), and the fluid velocity. It is usually the most important component in pipelines.
- *Acceleration loss* (sometimes referred to as *kinetic energy loss*) is caused by the change in momentum when the fluid is accelerated in the well because of expansion. Generally this term is less important, but it can become of significance for very high-rate gas wells.

3.3 Single-Phase Oil Flow

Here we focus on single-phase oil flow; we will not treat the case of single-phase water flow separately because it can be directly obtained from the single-phase oil case.

3.3.1 Governing Equations. Maintaining the assumption of steady-state flow, the right side of the mass conservation Eq. 3.3 vanishes, which reduces it to

$$\frac{d(\rho_o v_o)}{ds} = 0. \quad \dots \dots \dots \quad (3.19)$$

This is a first-order ordinary-differential equation, though a trivial one, requiring one boundary condition that can be chosen at an arbitrary reference point $s = s_{\text{ref}}$ as

$$s = s_{\text{ref}} : \rho_o v_o = \frac{\rho_{o,\text{ref}} q_{o,\text{ref}}}{A}. \quad \dots \dots \dots \quad (3.20)$$

Integrating Eq. 3.19 and using the boundary condition in Eq. 3.20, we find that

$$v_o = \frac{\rho_{o,\text{ref}} q_{o,\text{ref}}}{\rho_o A}. \quad \dots \dots \dots \quad (3.21)$$

Next, the acceleration term $\rho v \frac{dv}{ds}$ in Eq. 3.18 can be rewritten as

$$\rho v \frac{dv}{ds} = \rho v \frac{dv}{d\rho} \frac{d\rho}{dp} \frac{dp}{ds} = \rho v \underbrace{\left(-\frac{v}{\rho} \right)}_{\frac{dv}{d\rho}} \underbrace{c\rho}_{\frac{d\rho}{dp}} \frac{dp}{ds} = -c\rho v^2 \frac{dp}{ds}, \quad \dots \dots \dots \quad (3.22)$$

where we dropped the subscripts o to improve the readability of the expression, and where we made use of Eqs. 3.6 and 3.21 to compute dp/dp and $dv/d\rho$. Combining Eqs. 3.6, 3.18, 3.21, and 3.22, we can now write the governing equation for steady-state single-phase oil flow as

$$\frac{dp}{ds} = (1 - c\rho v^2)^{-1} \left(-\rho g \sin \theta - \frac{\rho}{2d} fv|v| \right), \quad \dots \dots \dots \quad (3.23)$$

where v and ρ are given by Eqs. 3.21 and 3.6 respectively (while continuing to drop subscripts). Eqs. 3.6, 3.21, and 3.23 together form a set of three differential-algebraic equations for the three unknowns ρ , v , and p . (Note that in some publications μ is considered a fourth unknown variable, in which case a fourth equation is introduced in the form of the relationship between μ , p , and T , sometimes referred to as a second equation of state.)

Comparison with Eqs. 3.3 through 3.6 shows that the mass balance differential Eq. 3.3 has now been replaced by an algebraic equation (Eq. 3.21) as a result of the restriction to steady state. The set of three equations can be simplified by recognizing that the compressibility of single-phase liquids is often quite small, which implies that the acceleration term (i.e., the first term at the right side of Eq. 3.23) is nearly equal to unity. If we furthermore make use of Eqs. 2.28 and 2.31 (with $R_s = R_{sb}$) and Eq. 2.38, the simplified set of equations for single-phase oil flow becomes

$$\frac{dp}{ds} = -\rho g \sin \theta - \frac{\rho}{2d} fv|v|, \quad \dots \dots \dots \quad (3.24)$$

$$v = \frac{B_o q_{o,sc}}{A}, \quad \dots \dots \dots \quad (3.25)$$

$$\rho = \frac{R_{sb} \rho_{g,sc} + \rho_{o,sc}}{B_o}. \quad \dots \dots \dots \quad (3.26)$$

Alternatively, we can combine Eqs. 3.24 through 3.26 in a single differential equation. Using the fact that for circular conduits it holds that $A = \frac{1}{4}\pi d^2$, this results in

$$\frac{dp}{ds} = -\frac{R_{sb} \rho_{g,sc} + \rho_{o,sc}}{B_o} g \sin \theta - \frac{8B_o (R_{sb} \rho_{g,sc} + \rho_{o,sc})}{\pi^2 d^5} f q_{o,sc} |q_{o,sc}|. \quad \dots \dots \dots \quad (3.27)$$

For dead oil we have $R_{sb} = 0$. If we further assume that the oil is incompressible we also have $B_o = 1$ such that $\rho_o = \rho_{o,sc}$ and $q_o = q_{o,sc}$, and Eq. 3.27 further simplifies to

$$\frac{dp}{ds} = -\rho g \sin \theta - \frac{8\rho}{\pi^2 d^5} f q |q| \dots \dots \dots \quad (3.28)$$

3.3.2 Solutions. Each of the differential equations Eqs. 3.23, 3.24, 3.27, and 3.28 is of first order and therefore requires one boundary condition, specifying the pressure p at a certain value of s :

$$s = \hat{s} : p = \hat{p}, \dots \dots \dots \quad (3.29)$$

where we have used a hat above the variables to indicate that their value is prescribed. The solution to, e.g., Eq. 3.24 can now be expressed as

$$p = \hat{p} \int_{\hat{s}}^s \left(\rho g \sin \theta + \frac{\rho}{2d} f v |v| \right) ds \dots \dots \dots \quad (3.30)$$

In the general case, where θ is a function of s , and f is a function of μ and therefore of $T(s)$, it will usually not be possible to obtain the integral in closed form, in which case it could be obtained numerically. In particular, the MATLAB file `oil_dpds.m` computes the pressure drop for single-phase oil flow. It contains Eqs. 3.24 through 3.26 and can be called on by one of the standard numerical integration routines in MATLAB (see Section D-2 in Appendix D).

Under some simplifying assumptions the integral can be solved analytically. For example, consider the case of a pipeline with constant inclination θ transporting dead oil. If, furthermore, we assume incompressible flow (i.e., a constant ρ) and a constant temperature along the line, the viscosity also remains constant and therefore the friction factor f . Alternatively, we could approximate nonconstant inclinations and friction factors with their average values θ_{av} and f_{av} . The integration then becomes trivial, and the pressure p is a linear function of the measured distance s :

$$p = \hat{p} \left(\rho g \sin \theta_{av} + \frac{\rho f_{av}}{2d} v |v| \right) (s - \hat{s}) = \hat{p} \left(\rho g \sin \theta_{av} + \frac{8\rho f_{av}}{\pi^2 d^5} q |q| \right) (s - \hat{s}). \dots \dots \dots \quad (3.31)$$

3.4 Single-Phase Gas Flow

3.4.1 Governing Equations. In the case of steady-state single-phase gas flow, we can rewrite the acceleration term in Eq. 3.18 as

$$\rho v \frac{dv}{ds} = \rho v \underbrace{\frac{dv}{d\rho} \frac{d\rho}{dp} \frac{dp}{ds}}_{\frac{dv}{dp}} = \rho v \underbrace{\left(-\frac{v}{\rho} \right)}_{\frac{dv}{dp}} \underbrace{\left(\frac{\rho}{p} - \frac{\rho}{Z} \frac{dZ}{dp} \right)}_{\frac{dp}{dp}} \frac{dp}{ds} = -\rho v^2 \left(\frac{1}{p} - \frac{1}{Z} \frac{dZ}{dp} \right) \frac{dp}{ds}, \dots \dots \dots \quad (3.32)$$

where we used Eq. 3.5 to derive the expression for dp/dp . The governing set of equations for steady-state single-phase gas flow through a pipeline now follows by combining Eqs. 3.5, 3.18, 3.21, and 3.32, modifying them where necessary to be

applicable to gas:

$$\frac{dp}{ds} = \left[1 - \rho v^2 \left(\frac{1}{p} - \frac{1}{Z} \frac{dZ}{dp} \right) \right]^{-1} \left(-\rho g \sin \theta - \frac{\rho}{2d} f v |v| \right). \quad (3.33)$$

$$v = B_g \frac{q_{g,sc}}{A} \quad (3.34)$$

$$\rho = \frac{Mp}{ZRT_{abs}} = \frac{\rho_{g,sc}}{B_g}, \quad (3.35)$$

where we also made use of [Eq. 2.28](#) and 2.31 with $q_{o,sc} = 0$. Just as for single-phase liquid flow, [Eq. 3.33](#) requires a single boundary condition. A difference with the single-phase liquid equations ([Eqs. 3.24 through 3.26](#)) is the presence of the acceleration term between square brackets at the right side of [Eq. 3.33](#). The pressure drop dp/ds approaches infinity when this term approaches zero. This happens when the absolute value of the velocity approaches

$$v_s = \sqrt{\left[\rho \left(\frac{1}{p} - \frac{1}{Z} \frac{dZ}{dp} \right) \right]^{-1}} = \sqrt{\frac{dp}{d\rho}}, \quad (3.36)$$

which can be interpreted as the sonic velocity for gas under isothermal conditions. The ratio $|v|/v_s$ is therefore a measure for the importance of acceleration losses. Generally, they can be neglected. Only in extremely high-rate gas wells, or in a situation of uncontrolled gas flow, such as a wellbore blowout, might the gas velocity in a well approach the sonic velocity. However, in that case the flow can no longer be approximated as isothermal; i.e., temperature effects start to become important, and a more elaborate analysis is required, which is beyond the scope of this book. Flow at sonic velocities also plays an important role in the behavior of choke valves, and that aspect is discussed in more detail in [Chapter 5](#).

3.4.2 Solutions. [Eqs. 3.33](#) through [3.35](#), together with a boundary condition, can be solved numerically with the aid of MATLAB (see m-file `gas_dpds.m` and further details in Section D-2 in [Appendix D](#)). An approximate analytical solution can be obtained by assuming that the acceleration losses may be neglected, i.e., that $|v| \ll v_s$ and that f , T_{abs} , θ , and Z may be taken as constant “average” values f_{av} , $T_{av,abs}$, θ_{av} , and Z_{av} over the length of the pipeline. In that case the set of equations reduces to a single differential equation in p :

$$\frac{dp}{ds} = k_1 p + \frac{k_2}{p}, \quad (3.37)$$

where the coefficients k_1 and k_2 are given by

$$k_1 = \frac{Mg \sin \theta_{av}}{Z_{av} RT_{av,abs}}, \dots \dots \dots \quad (3.38)$$

$$k_2 = -\frac{8Z_{av} RT_{av,abs} f_{av} \rho_{g,sc}^2 q_{g,sc} |q_{g,sc}|}{\pi^2 d^5 M}, \dots \dots \dots \quad (3.39)$$

and where we used the relationship $A = \pi d^2/4$. Note that k_1 should be positive for all wells, whereas k_2 should be positive for producers and negative for injectors. (Watch out for the difference between α and θ and the associated signs: $\theta = \alpha - \pi/2$.) Eq. 3.37 can be rewritten as

$$2p \frac{dp}{ds} = 2k_1 p^2 + 2k_2 \dots \dots \dots \quad (3.40)$$

and therefore as

$$\frac{d(p^2)}{ds} = 2k_1 p^2 + 2k_2, \dots \dots \dots \quad (3.41)$$

which has the solution

$$p^2 = C \exp(2k_1 s) - \frac{k_2}{k_1}. \dots \dots \dots \quad (3.42)$$

If we use boundary condition (Eq. 3.29) to solve for the integration constant C , we arrive at

$$p = \sqrt{\left(\hat{p}^2 + \frac{k_2}{k_1}\right) \exp[2k_1(s - \hat{s})] - \frac{k_2}{k_1}}. \dots \dots \dots \quad (3.43)$$

Usually it will be necessary to perform one or more iterations to obtain the average values f_{av} , $T_{av,abs}$, θ_{av} , and Z_{av} because they depend on the unknown pressure $p(s)$. For horizontal flowlines, $\theta_{av} = 0$ and therefore $k_1 = 0$, and thus the solution (Eq. 3.43) breaks down; but starting from Eq. 3.41, it is easily shown that in that case the solution becomes

$$p = \sqrt{\hat{p}^2 + 2k_2(s - \hat{s})}. \dots \dots \dots \quad (3.44)$$

3.5 Tubing Performance and Intake Curves

Referring back to Section 1.5, we can now determine the element equations for single-phase well or pipeline flow that were already specified in concise form in Eq. 1.4 as

$$p_{out} = f(p_{in}, q_{sc}). \dots \dots \dots \quad (3.45)$$

If we choose the boundary condition at one end of the element (i.e., $\hat{p} = p_{in}$), we can compute the pressure p_{out} at the other end through numerical integration of Eqs. 3.24 through 3.26 or Eqs. 3.33 through 3.35, or directly from the analytical expressions Eq. 3.31 or Eq. 3.43, depending on the assumptions and the required accuracy. The velocity v appearing in all these expressions can be related to q_{sc} with the aid of Eq. 3.21 or its equivalent for gas, Eq. 3.34, keeping in mind that negative values of v and q indicate flow in a production situation.

The MATLAB file `pipe.m` provides an element equation according to expression Eq. 3.45, which can be used to compute the pressure drop over an element of a well or a flowline. The file can also be used to compute the pressure drop over an entire well or flowline as long as the geometrical properties of the pipe (diameter, roughness) do not change along its length. This allows, e.g., for the computation of the flowing tubinghead pressure (FTHP) p_{tf} of a single-phase liquid or gas well for a known flowing bottomhole pressure (FBHP) p_{wf} , or, conversely, p_{wf} for a known p_{tf} . Similarly the file can be used for flowlines to compute the manifold pressure for a given flowline pressure and vice versa. Examples of how to use the MATLAB file are provided by the MATLAB script files `example_flowline.m` and `example_well.m`.

With the aid of `pipe.m` it is also possible to create plots of the wellbore pressure p as a function of AHD s. Such plots are often referred to as *traverses*, and an example of how to create them is given in the script file `example_traverse.m`. Another file, `example_traverse_deviated.m`, gives an example of how the traverse of a deviated well can be obtained using a survey file to specify the well trajectory. Moreover, it is possible to repeat the computation of the FTHP, at a fixed FBHP, for a large number of flow rates. This results in a so-called *tubing performance curve*, which depicts the FTHP as a function of flow rate. (Confusingly, the term tubing performance curve is also used for a graph that represents the combined pressure drop over the tubing and the near-well reservoir area.) Alternatively, one can repeat the computation of the FBHP, at a fixed FTHP, for varying flow rates. This results in a so-called *tubing intake pressure curve*, which depicts the FBHP as a function of flow rate (see the script file `example_intake_curve.m`). Shorter names are *tubing intake curve* or *intake pressure curve*.

Figs. 3.4 and 3.5 depict traverses for a dry gas well with parameters given in **Table 3.1**. They were both computed for the same FBHP, but with different flow rates and therefore different FTHPs. Fig. 3.4 corresponds to a relatively low rate, where gravity losses dominate the pressure drop over the well. Fig. 3.5 corresponds to twice the rate, and it can be seen that friction losses play a much larger role. Acceleration losses are of no significance, and only in Fig. 3.5 can they be noticed for very low pressures close to the surface. Going from the bottom of the well to the surface, the gravity losses gradually decrease because the density of the gas decreases, as can clearly be observed in Fig. 3.5. Because the mass flow rate remains the same, the reduction in density with elevation also causes an increase in volume flow rate and therefore in gas velocity. The increased velocity, in turn, results in an increase in friction losses, which is also clearly visible in Fig. 3.5.

An example of a tubing performance curve has been displayed in [Fig. 3.6](#), where the FBHP was kept constant at 29.0 MPa (4,206 psi). The figure illustrates that for decreasing FTHP a point is reached at which the curve becomes vertical (i.e., a point where no further increase in gas flow rate is possible because the gas velocity has reached the sonic velocity). [Fig. 3.7](#) displays the tubing intake curves for fixed FTHPs of 1.5 MPa (218 psi) and 19.2 MPa (2,785 psi).

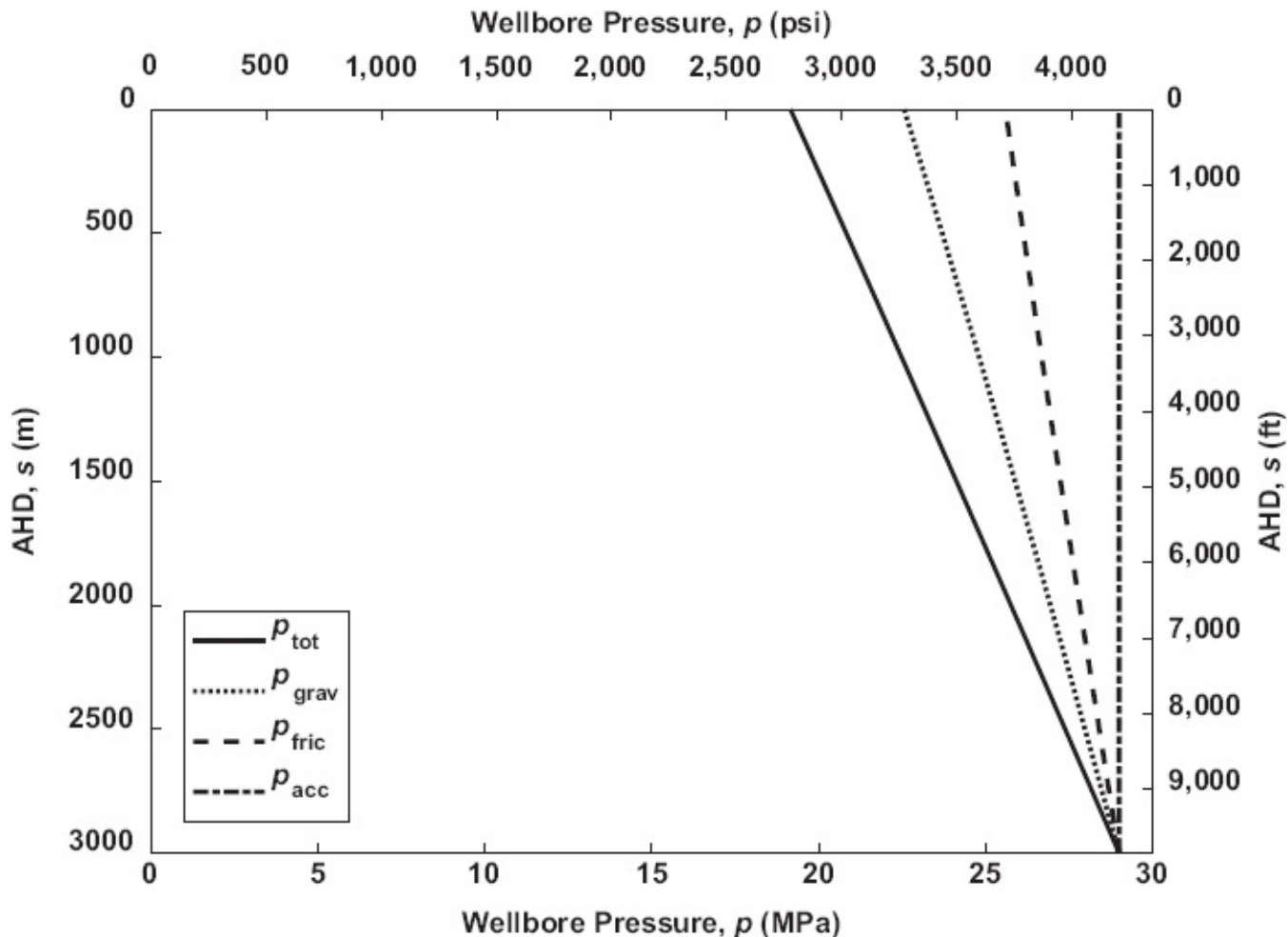


Fig. 3.4—Traverse for a low-rate single-phase gas well with parameters given in [Table 3.1](#).

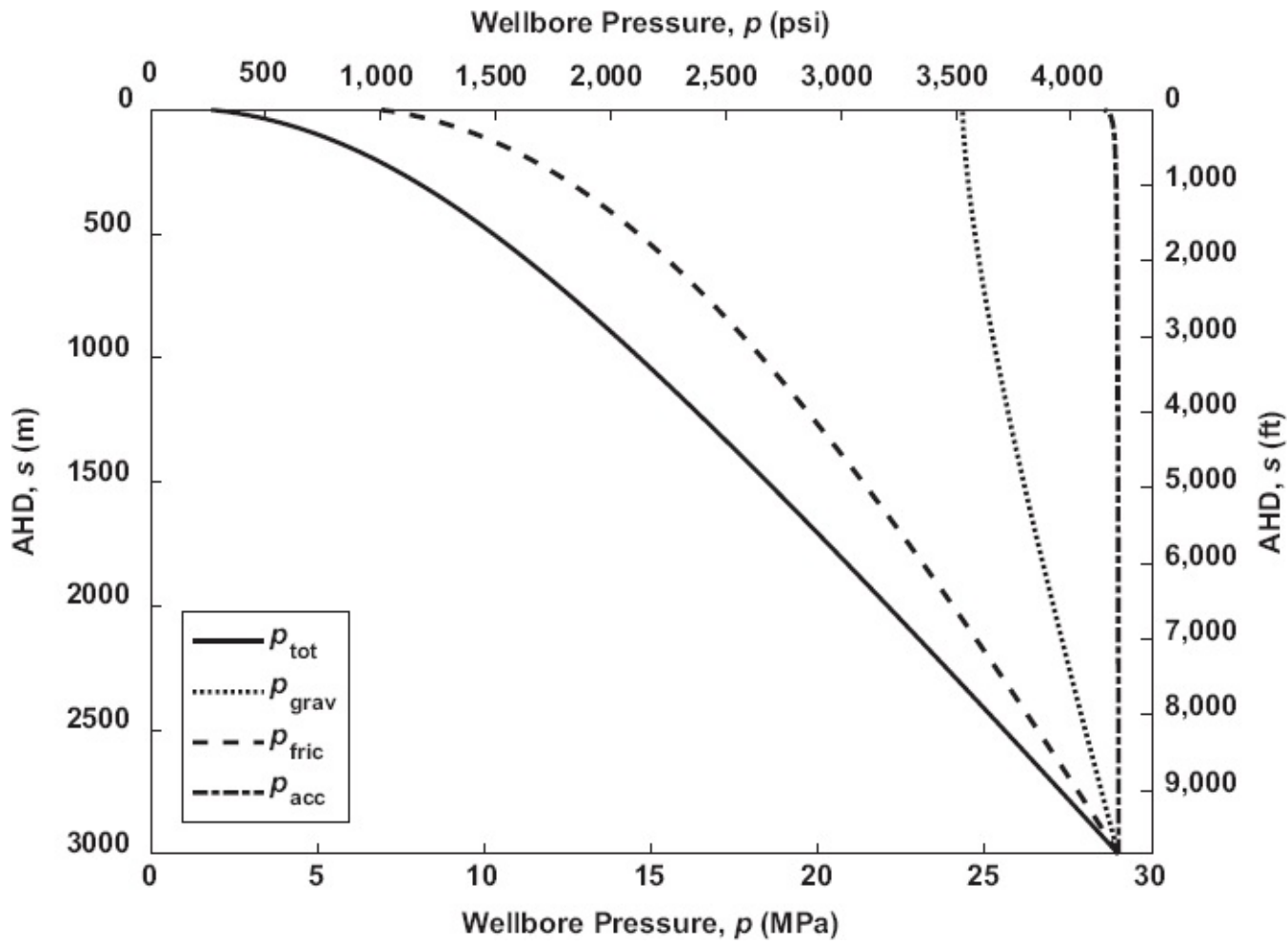


Fig. 3.5—Traverse for the same well as in Fig. 3.4 but at a higher rate.

Parameter	SI Units	Field Units
Tubing diameter, d	62.3×10^{-3} m	2.453 in.
Roughness, e	30×10^{-6} m	0.0012 in.
FBHP, p_{wf}	29.0×10^6 Pa	4,206 psi
FTHP Fig. 3.4, p_{tf}	19.2×10^6 Pa	2,785 psi
FTHP Fig. 3.5, p_{tf}	1.5×10^6 Pa	218 psi
Rate Fig. 3.4, $q_{g,sc}$	$-4.31 \text{ m}^3/\text{s}$	$-13.15 \times 10^6 \text{ scf/D}$
Rate Fig. 3.5, $q_{g,sc}$	$-8.62 \text{ m}^3/\text{s}$	$-26.27 \times 10^6 \text{ scf/D}$
FBHT, T_{wf}	120°C	248°F
FTHT, T_{tf}	30°C	86°F
Well depth, z_{tot}	3,000 m	9,843 ft
Inclination, α	0 rad	0°
Density/gravity, $\rho_{g,sc}/\gamma_g$	0.95 kg/m ³	0.77
Viscosity, μ_g	Carr et al. (1954) correlation	
Equation of state	Standing and Katz (1942) Z factor	

Table 3.1—Parameter values for Figs. 3.4 and 3.5.

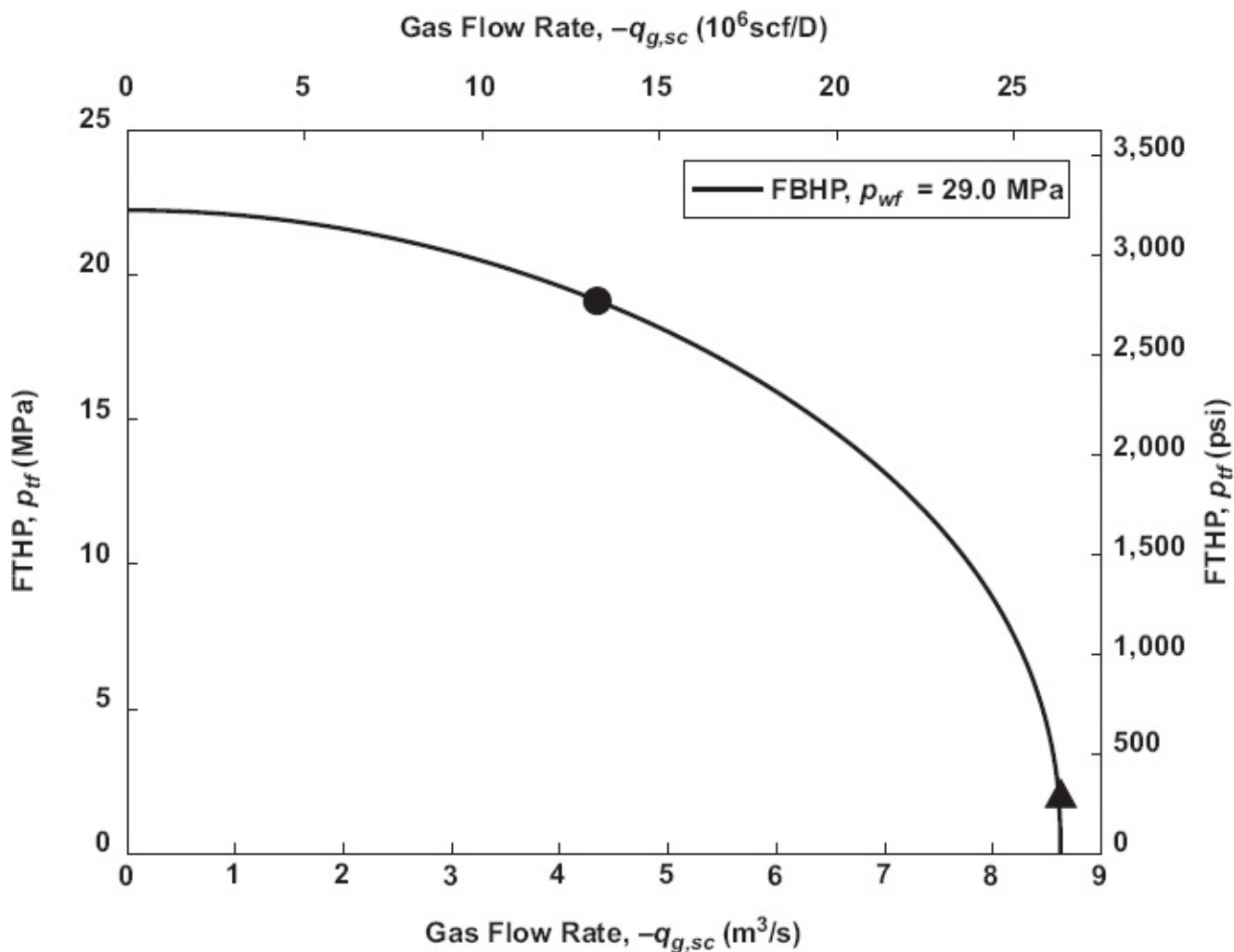


Fig. 3.6—Tubing performance curve for the same well as in Fig. 3.4. The dot and the triangle correspond to the low- and high-flow-rate cases as specified in Table 3.1.

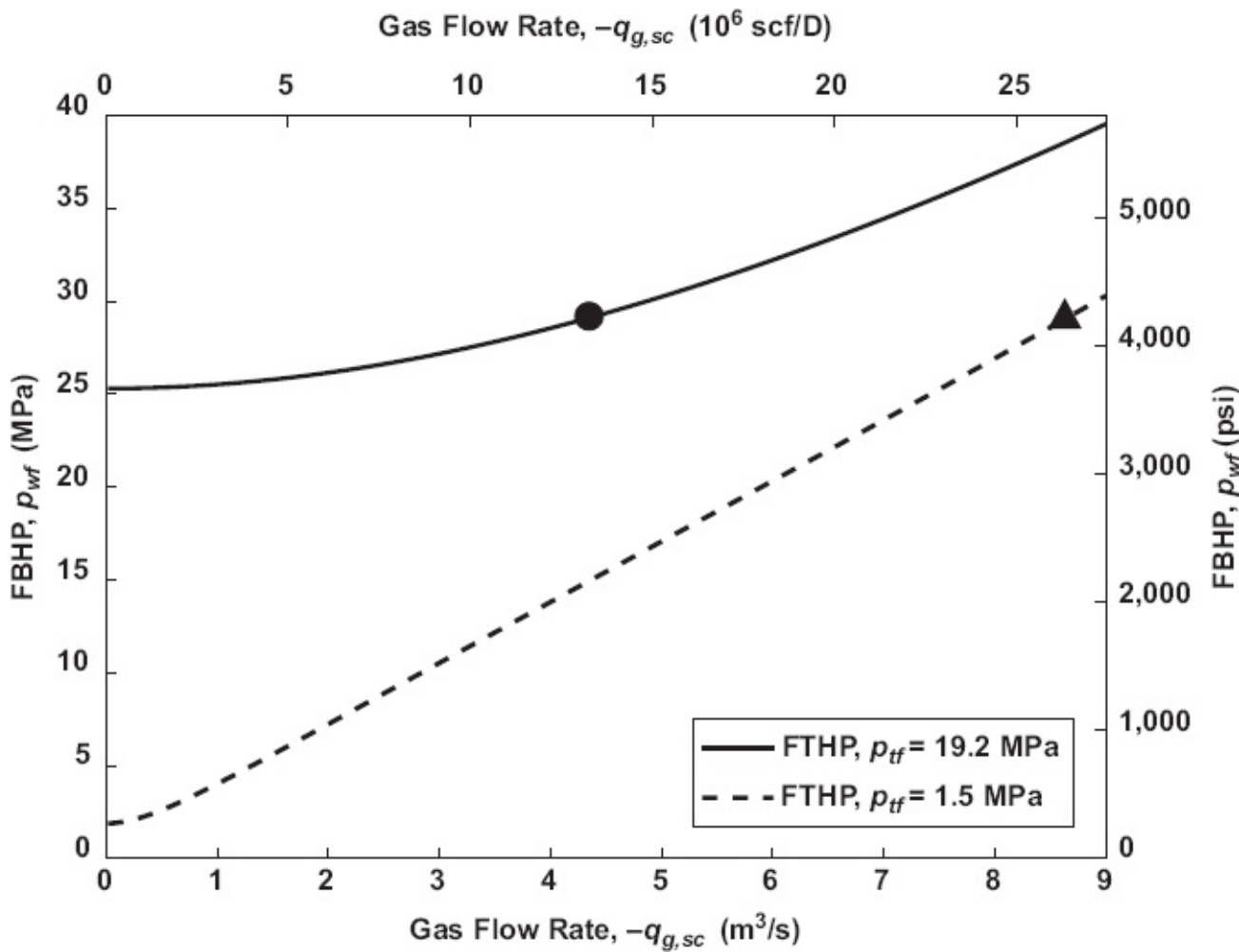


Fig. 3.7—Tubing intake curves for the same well as in Fig. 3.4. The dot and the triangle correspond to the low- and high-flow-rate cases as specified in Table 3.1.

3.6 Flow in an Annular Geometry

An approximate way to compute the pressure drop in an annular geometry (e.g., between casing and tubing) makes use of the hydraulic radius concept. The hydraulic radius r_h is defined as the cross-sectional area A , divided by the wetted perimeter P_w , and it is assumed that conduits with identical hydraulic radii experience identical pressure drops per unit length. For a circular pipe with inner diameter d the wetted perimeter for internal flow is simply the perimeter πd , and the hydraulic radius therefore becomes

$$r_h = \frac{A}{P_w} = \frac{\frac{1}{4}\pi d^2}{\pi d} = \frac{d}{4}. \quad (3.46)$$

For a casing/tubing annulus we find

$$r_{h,ann} = \frac{A_{ann}}{P_{w,ann}} = \frac{\frac{1}{4}\pi(d_c^2 - d_t^2)}{\pi(d_c + d_t)}, \quad (3.47)$$

where d_c is the casing's inner diameter and d_t the tubing's outer diameter. To represent an annular casing/tubing geometry with an equivalent circular pipe, the equivalent pipe diameter d_{eq} therefore follows from setting $r_h = r_{h,ann}$, resulting in

$$d_{eq} = 4r_{h,ann} = \frac{d_c^2 - d_t^2}{d_c + d_t}. \quad \dots \dots \dots \quad (3.48)$$

3.7 Questions

- 3.1 What is the physical meaning of the Reynolds number?
- 3.2 What are the dominant pressure drop mechanisms in (a) a vertical oil well and (b) a horizontal gas pipeline?
- 3.3 Although we consider only steady-state flow (i.e., flow described with variables that do not change over time), why may there still be an effect of acceleration on the pressure drop?
- 3.4 Consider a gas well that produces at such a high rate that the acceleration component cannot be completely neglected. How do the friction, gravity, and acceleration components of the pressure drop in the well change with depth? Sketch a typical profile. Explain the physical mechanisms.
- 3.5 Derive modified mass and momentum balance Eqs. 3.3 and 3.4 such that they are valid for a pipe with a gradually changing cross-sectional area A .
- 3.6 Single-phase oil is pumped uphill through a pipeline under a 1.5° angle over a length of 3 km. The oil has a density of 850 kg/m^3 , the pipeline has an inside diameter of 232 mm and a roughness of 0.003 mm, the ambient temperature is 45°C , and the pipeline pressure at the inlet is 10 bar. What is the outlet pressure for a flow rate $q_o = -5000 \text{ m}^3/\text{d}$? Hint: Use the Beggs and Robinson (1975) dead oil correlation (Eq. B-10) to compute the viscosity and Eq. 3.31 to compute the pressure drop. Choose the origin at the outlet of the pipeline.
- 3.7 The gas well of Fig. 3.5 (with parameter values given in Table 3.1) has friction and Z factors that change only slightly over the height of the well. Their average values are $Z_{av} = 0.96$ and $f_{av} = 0.0166$. Verify the numerical results of Fig. 3.5 with the aid of the approximate analytical solution described in Section 3.4.
- 3.8 Fig. 3.8 schematically depicts a situation in which produced water is reinjected by pumping it down the annulus between two intermediate casing strings into a deep saltwater aquifer. The top of the perforations in the annulus is at a depth of 3230 m. The sizes of the intermediate strings are $9\frac{5}{8}'' - 29.30\#$ [i.e., 9 $\frac{5}{8}$ -in diameter and 29.30 lbm/ft nominal weight (including couplings)] and $13\frac{3}{8}'' - 48\#$. The corresponding relevant outer diameter (OD) and inner diameter (ID) are 0.2445 and 0.2815 m. The water density is 1070 kg/m^3 , the viscosity $0.38 \times 10^3 \text{ Pa} \cdot \text{s}$, the temperature 20°C (neglect heating while flowing down the annulus), and the casing roughness 0.04 mm. If it is required

to maintain an injection rate of $1200 \text{ m}^3/\text{d}$ at an injection pressure of 40 MPa , what is the pressure at the wellhead?

Questions 3.9 to 3.12 require the use of MATLAB. You may first want to complete the MATLAB assignment in [Section 3.8](#) to obtain experience in using the necessary function files. Some guidance on the use of the required numerical integration routines is given in Section D-2 of [Appendix D](#).

- 3.9 Compare the results of Question 3.6 with the results from using the MATLAB m-file `pipe.m`. Type `help pipe` or open the file in the editor to inspect the input requirements. You may also inspect the file `example_flowline.m` to get started.

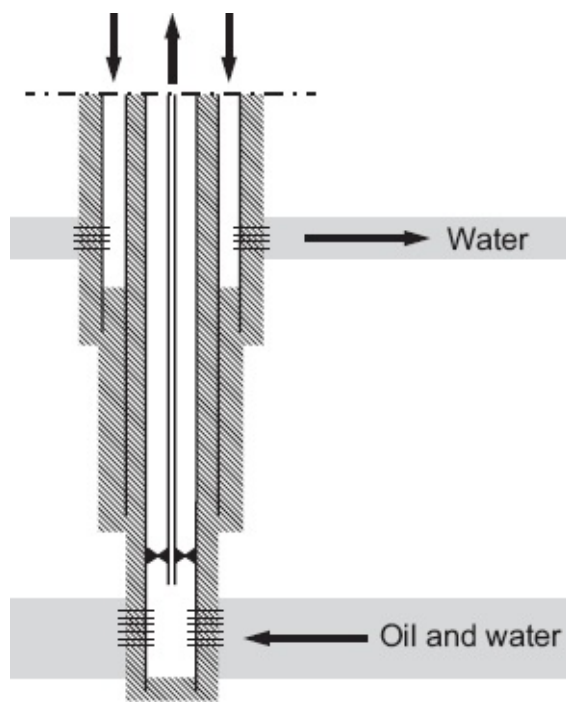


Fig. 3.8—Produced water reinjection through the annulus between two intermediate casing strings. The light gray areas represent layers of highly permeable rock. The shaded areas close to the well represent cement. The thin horizontal lines represent perforations.

- 3.10 Refer to the last paragraph of Section D-2.2 in [Appendix D](#). Use MATLAB file `example_well.m` as a template and write a script file to check the absolute and relative errors in the FBHP for the example of [Fig. 3.5](#). Use the default integration tolerance inside `pipe.m`, i.e., `options = []`. Repeat the exercise using a higher integration tolerance, e.g., `options = odeset('MaxStep', 10, 'RelTol', 1e-3)`. Do not forget to reset the tolerance after completing the exercise to avoid a slow response of `pipe.m` during later use.
- 3.11 Consider a gas pipeline with four different segments as depicted in [Fig. 3.9](#). Use a series of four pipe elements, as shown in [Fig. 3.10](#), to compute the pressure drop over the pipeline for the parameter values given in [Table 3.2](#).

This can be done by repeated calling of `pipe.m` such that the input pressure of an element is equal to the output pressure of the previous element. Choose the coordinate s along the pipeline such that it runs from the gas plant to the platform (Note: This is in line with the assumption that production rates are negative.) Perform the integration backward from $s = l_{\text{tot}}$ to $s = 0$, where l_{tot} is the total pipeline length. Use a linear interpolation for the temperature. Plot the pressure in the pipeline p as a function of distance s from the gas plant.

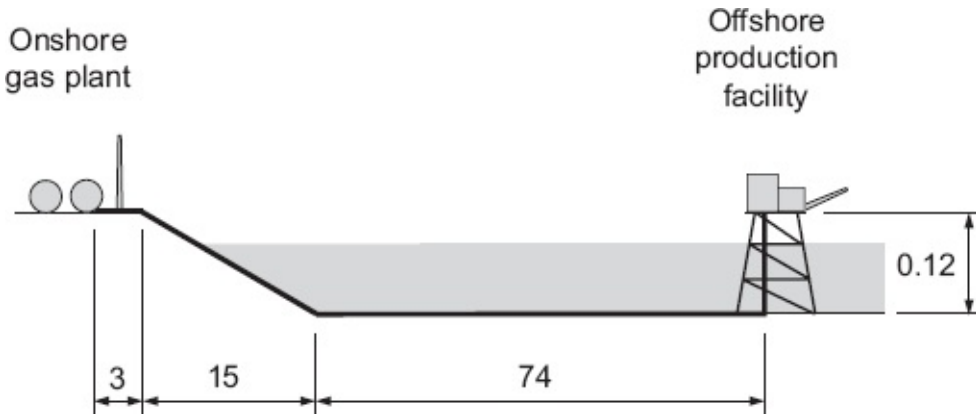


Fig. 3.9—Gas pipeline. All distances in km. Figure not to scale.

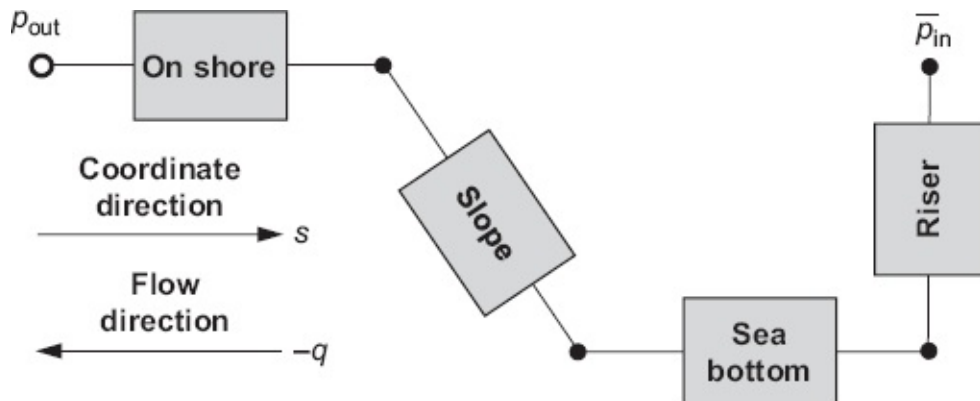


Fig. 3.10—Gas pipeline represented as four elements.

Property	Value
Flow rate (m^3/d)	-1×10^6
Inside diameter (m)	0.30
Roughness (mm)	0.03
Entrance pressure (MPa)	10
Entrance temperature ($^{\circ}\text{C}$)	50
Exit temperature ($^{\circ}\text{C}$)	10
Gas density (kg/m^3)	0.95

Table 3.2—Gas pipeline properties for Question 3.11.

3.12 MATLAB file `pipe.m` computes the pressure drop over a pipe element for a given flow rate. If the pressures at both ends of a pipe are given and the flow rate is the unknown variable, an iterative procedure is required. Use the standard MATLAB routine `fzero` to compute the single-phase gas flow rate through a pipeline for parameters given in [Table 3.3](#). Iterate on $q_{g,sc}$ until $f = \bar{p}_{out} - p_{out} = 0$, where p_{out} is the value as computed with `pipe.m` and \bar{p}_{out} is the value given in [Table 3.3](#). Consult [Appendix D](#) or the online MATLAB help functionality for information on the use of `fzero`. Use low and high flow rates of 20 and 100 m³/s, respectively, to bracket the solution. Alternatively, write your own Newton-Raphson routine to perform the iteration. Use numerical perturbations to compute the derivatives. See [Appendix D](#) for details.

3.8 MATLAB Assignment: Single-Phase Gas Flow

3.8.1 Objectives

- Obtain a feeling for the order of magnitude of single-phase gas flow parameters.
- Become familiar with gas PVT (pressure/volume/temperature) behavior and the associated MATLAB functions.
- Learn to make wellbore pressure drop calculations and create a traverse with MATLAB.
- Learn to use analytical approximations to check numerical results.

Property	Value
d	0.40 m
e	50×10^{-6} m
\bar{p}_n	5×10^6 Pa
\bar{p}_{out}	4×10^6 Pa
S_{in}	0 m
S_{out}	8000 m
T_{in}	25°C
T_{out}	25°C
α	$\pi/2$ rad
$\rho_{g,sc}$	0.95 kg/m ³

Table 3.3—Input data for flow rate calculation for Question 3.12.

3.8.2 Assignment. Consider a gas well with the properties listed in [Table 3.4](#).

Tasks

- Inspect the MATLAB functions `pipe.m` and `gas_dpds.m`.
- Copy the file `example_well.m` and save it under a new name. Use it to compute the FBHP for the parameters given above. Use the MATLAB unit conversion routines to convert the input from field to SI units.
- Keeping the FBHP fixed, compute a new FTHP for a rate that is six times higher than the rate in the example.
- Expand the file to create a pressure traverse for the high flow rate. Refer to script file `example_traverse.m` for guidance.
- Study Section B-3 Gas Correlations, in [Appendix B](#). Inspect the MATLAB functions `pres_pseu_crit_Sutton`, `temp_pseu_crit_Sutton`, `z_factor_DAK.m`, `z_factor_DAK_direct.m`, `gas_viscosity.m`, `Reynolds_number.m` and `Moody_friction_factor.m`.
- Expand your MATLAB routine and compute values for Z -factor, formation volume factor, local density, local flow rate, viscosity, Reynolds number, and friction factor at the top and the bottom of the tubing for the high-flow-rate case.
- Check the FBHP for the high-flow-rate case with the aid of an analytical approximation, starting from the (new) FTHP and using average values f_{av} , $T_{av,abs}$, α_{av} , and Z_{av} and a quadratic pressure relationship (see [Eqs. 3.37](#) through [3.44](#)). Use top and bottom values from your numerical results to compute the averages. The relative error between the analytical and the numerical result should be approximately 5%.
- Now try to do the opposite; i.e., check the FTHP for the high-flow-rate case analytically, starting from the FBHP. Why does this fail? (Or if it does not fail because you made a small error in one of the previous steps, why is there a good chance that it would fail in general?) Hint: Slightly increase (or decrease) the starting value of the FBHP.

Parameter		Field Units	
Inclination	α	30	degrees
Diameter	d	2.453	in.
Roughness	e	0.003	in.
FTHP	p_{tf}	2,900	psi
Rate	$q_{g,sc}$	-3.0×10^6	scf/D
Gas gravity	γ_g	0.85	–
FBHT	T_{wf}	250	°F
FTHT	T_{tf}	115	°F
TVD	S_{tot}	12,124	ft

Table 3.4—Parameter values for MATLAB assignment 3.8.2.

Note that in the analytical approximation, the term “ k_1 ” should be positive for all wells,

whereas " k_2 " should be positive for producers and negative for injectors. Watch out for the difference between α and θ the associated signs ($\theta = \alpha - \pi/2$).

3.8.3 Deliverables

- MATLAB program listing
- Pressure traverse
- Properties at top and bottom
- Analytical approximation of the FBHP for the high-flow-rate case
- Answer to question under last bullet

Chapter 4

Multiphase Flow in Wells and Pipelines

4.1 What Is Covered in This Chapter?

In this chapter we extend the pressure drop analysis of pipes to multiphase flow of gas, oil, and water. A key aspect of such multiphase gas/liquid flow is the occurrence of different flow regimes—i.e., different geometrical configurations of gas and liquid mixtures such as gas bubbles or slugs in liquid, liquid droplets in gas, or segregated liquid and gas layers. Another essential multiphase effect is the occurrence of slip between the liquid and gas phases (i.e., of different liquid and gas velocities where liquid is typically flowing slower than gas). Slip causes the pipe volume to be occupied by a disproportionately large liquid fraction—an effect known as *liquid holdup*—which may result in counterintuitive effects on the pressure drop in multiphase production wells.

Quantitative models for the pressure drop resulting from multiphase flow through pipes have been developed over the past half century in varying levels of detail. They range from simple semiempirical correlations to complex mechanistic models that take into account the details of the interaction between the gas and liquid phases for all possible flow regimes. In [Appendix E](#), we describe a few typical multiphase flow models of medium complexity, which also have been programmed in the accompanying MATLAB code. These enable the creation of traverses and performance curves for use in nodal analysis of multiphase flow through (deviated) wells and pipelines.

4.2 Multiphase Flow Concepts

4.2.1 Flow Regimes. The occurrence of radically different flow regimes (or flow patterns) in multiphase (gas/liquid) flow depends on factors such as the gas/liquid ratio, the gas and liquid velocities, the pipe inclination, and fluid properties. The flow regimes for gas/liquid flow in horizontal pipelines are shown in [Fig. 4.1](#). They are generally known as follows, although some authors use a classification with more categories:

- Single-phase liquid flow
- Bubble flow
- Slug flow
- Stratified flow
- Annular flow

- Mist flow (fully dispersed liquid mist)

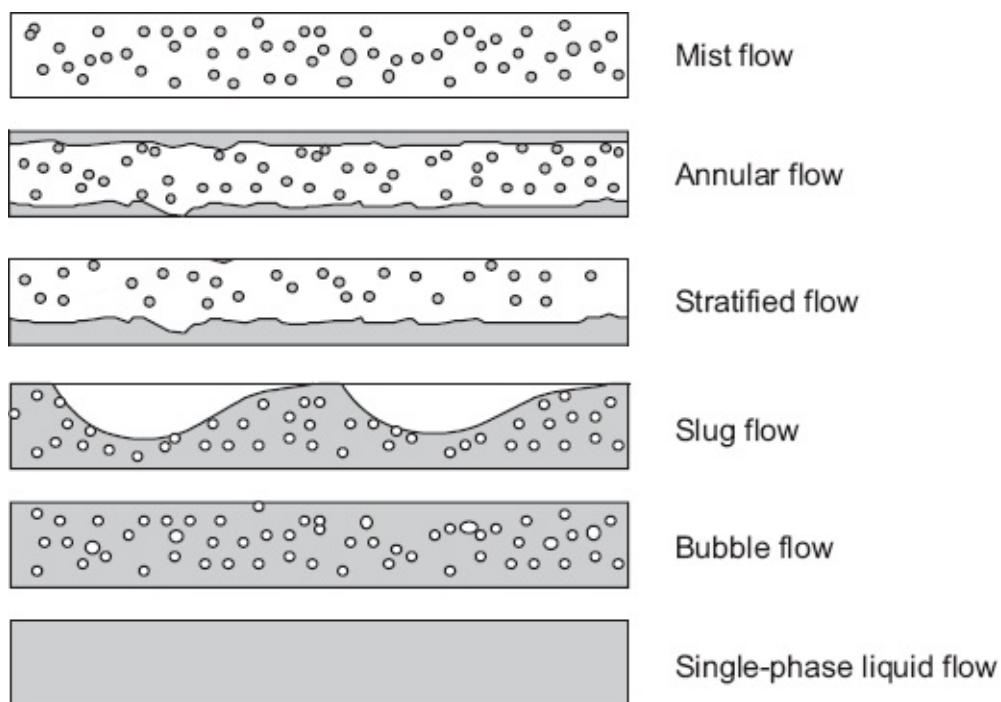


Fig. 4.1—Flow regimes in horizontal flow.

For vertical flow in a well, a similar flow pattern classification can be made. This is shown in [Fig. 4.2](#). The flow regimes are the same as those in horizontal flow except for the absence of stratified flow and the occurrence of churn flow as an intermediate regime between slug and annular flow. Furthermore, the slug flow regime is now somewhat different, displaying bullet-shaped slugs known as *Taylor bubbles*, which remain more or less centered in the wellbore. To describe flow in real pipelines or wells, the inclination of the pipe has to be taken into account to give a full map of multiphase effects. For a treatment of omnidirectional flow maps based on physical principles, see, e.g., Hassan and Kabir (2002) or Shoham (2006). Several simpler, but usually less accurate, approaches based on empirical correlations are discussed, e.g., in Wallis (1969), Brill and Mukherjee (1999), and Govier and Aziz (2008).

In a vertical oil well, the pressure decreases as the oil flows from the bottom to the top of the well. Thus, all the flow patterns shown in [Fig. 4.2](#) may arise. Generally, however, over most of their length most oil wells operate in the bubble flow and slug flow regimes, whereas most gas wells operate in the annular flow regime. It is a formidable task to try to solve the equations based on the laws of physics, which govern these types of flow. There are numerical simulators that attempt this for sensitive industrial processes that need very careful modeling. Within the oil industry, a simpler approach is often adopted. Empirical correlations have been developed based on extensive experiments. Some of these correlations have been published; others remain proprietary to oil companies or service companies. These correlations differ in complexity. Some are proposed as valid for all flow regimes, whereas others have separate correlations for each different regime. Some methods try to include

basic physics, such as modeling the behavior of gas/liquid interfaces, whereas others rely on a purely empirical approach. For an overview we refer again to Brill and Mukherjee (1999) and for more in-depth treatments to Hassan and Kabir (2002), Shoham (2006), and Govier and Aziz (2008). Many of these correlations are usually built into modern well simulators. Care needs to be taken because correlations are often suitable for only certain types of wells. Note that the correlations used for the oil properties will affect the results and may contribute to the inaccuracy.

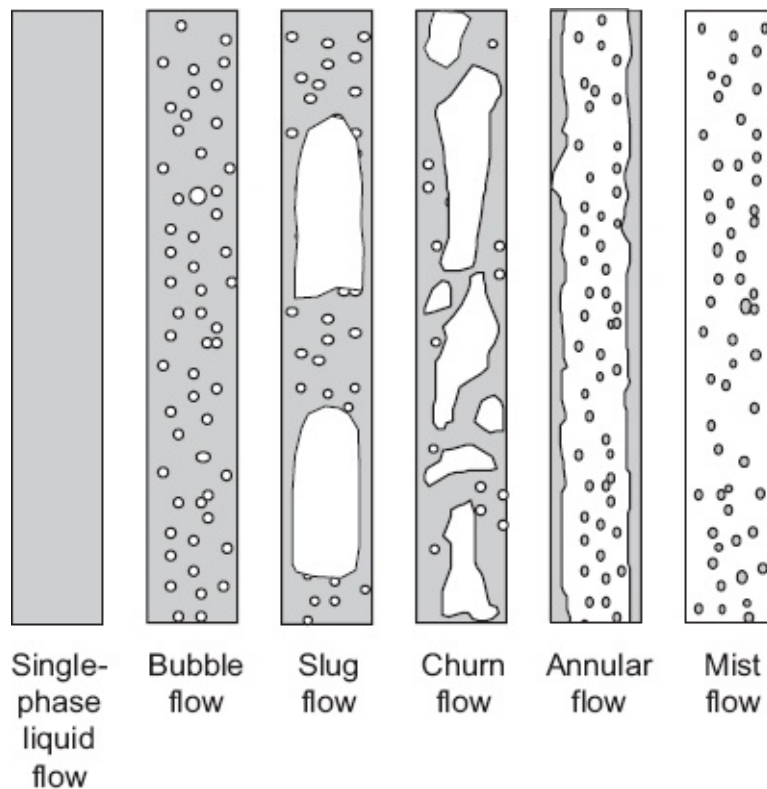


Fig. 4.2—Flow regimes in vertical flow.

4.2.2 Slip and Holdup. One of the complicating factors in the description of multiphase flow is the difference in velocity between the phases. It is generally assumed that water and oil travel at the same speed, known as the *liquid velocity*, although in reality this is not always the case, in particular for stratified flow. However, most computational methods do account for the difference between the liquid velocity and the gas velocity, which is known as *slip* between the two phases. But before considering phase velocities, it is useful to address phase flow rates. In the case of two-phase liquid flow, and assuming that the liquids flow with equal velocities, the local oil and water fractions are defined as

$$f_o = \frac{q_o}{q_l} = \frac{q_o}{q_o + q_w}, \quad \dots \dots \dots \quad (4.1)$$

$$f_w = \frac{q_w}{q_l} = \frac{q_w}{q_o + q_w}. \quad \dots \dots \dots \quad (4.2)$$

Here the word “local” refers to local pressure and temperature conditions (also known as *in-situ conditions*). However, this does *not* imply that “local” refers to a very small length scale—i.e., we are not interested in fluctuations in flow rates or velocities as a result of small-scale flow features such as slugs or bubbles. Instead, all quantities should be interpreted as averaged over a distance much larger than the small-scale features (i.e., on the order of meters). Note that from Eqs. 4.1 and 4.2 it follows that $f_o + f_w = 1$. The gas volume fraction and the liquid volume fraction are defined in the same fashion, although we will indicate them with a λ instead of an f :

$$\lambda_g = \frac{q_g}{q_m} = \frac{q_g}{q_g + q_l}, \quad \dots \dots \dots \quad (4.3)$$

$$\lambda_l = \frac{q_l}{q_m} = \frac{q_l}{q_g + q_l}, \quad \dots \dots \dots \quad (4.4)$$

where the quantity $q_m = q_g + q_l = q_g + q_o + q_w$ is known as the *mixture flow rate* or *total flow rate*. Note that also $\lambda_g + \lambda_l = 1$. Because of slip the fractions of a unit volume of pipe that are occupied by gas and liquid are generally not equal to the gas and liquid fractions as given in Eqs. 4.3 and 4.4. In upward flow, as occurs in a production well or an uphill pipeline, the gas usually travels faster than the liquid, and so liquid *holdup* occurs. In downward flow, as occurs in a downhill pipeline, the liquid may travel faster than the gas, in which case the gas is held up. The expression “holdup” is also often used in the oil industry to indicate the volume fractions occupied by gas and liquid, although in upward flow the gas is not actually held up, but to the contrary is speeded up. The gas and liquid holdups H_g and H_l are defined as

$$H_g = \frac{V_g}{V} = \frac{A_g}{A}, \quad \dots \dots \dots \quad (4.5)$$

$$H_l = \frac{V_l}{V} = \frac{A_l}{A}, \quad \dots \dots \dots \quad (4.6)$$

where V_g and V_l are the fractions of a reference volume of pipe that are being occupied by gas and liquid and $V = V_g + V_l$ is the total reference volume. Similarly, A_g and A_l are the parts of the pipe’s cross-sectional area occupied by the gas and the liquid, respectively, and $A = A_g + A_l$ is the total cross-sectional area. Note that volumes and areas should be interpreted as quantities averaged over a length that is sufficiently large to suppress the effect of small-scale flow features. Just as was the case for the sum of phase volume fractions, the sum of phase holdups is equal to unity. An alternative way to express the equations for phase volume fractions (Eqs. 4.3 and 4.4) and phase holdups (Eqs. 4.5 and 4.6) makes use of variables known as the *local, in-situ, or true phase velocities*

$$v_g = \frac{q_g}{A_g}, \quad \dots \dots \dots \quad (4.7)$$

$$v_l = \frac{q_l}{A_l}, \dots \quad (4.8)$$

the *superficial* phase velocities

$$v_{sg} = \frac{q_g}{A}, \quad \dots \dots \dots \quad (4.9)$$

$$v_{sl} = \frac{q_l}{A}, \dots \quad (4.10)$$

and the mixture velocity

$$v_m = v_{sg} + v_{sl} = \frac{q_g + q_l}{A}. \quad \dots \quad (4.11)$$

Substitution of these expressions in Eqs. 4.3 and 4.4 results in

$$\lambda_g = \frac{v_{sg}}{v_m}, \quad \dots \dots \dots \quad (4.12)$$

and substitution in Eqs. 4.5 and 4.6 gives

$$H_g = \frac{v_{sg}}{v_g}, \dots \quad (4.14)$$

$$H_l = \frac{v_{sl}}{v_l} \quad \dots \dots \dots \quad (4.15)$$

Most computational methods for multiphase flow simulation make use of experimental correlations for the liquid holdup expressed as functions of fluid properties, flow rates, pipe diameter, and well inclination. Eqs. 4.9, 4.10, 4.14, and 4.15 can then be used to compute the gas and liquid velocities for given flow rates according to

$$v_g = \frac{q_g}{H_g A} = \frac{q_g}{(1-H_l)A}, \quad \dots \quad (4.16)$$

$$v_l = \frac{q_l}{H_{t^A}} \dots \quad (4.17)$$

If there is no slip, the local phase velocities v_g and v_l are both identical to the mixture velocity v_m and therefore the holdups as expressed in Eqs. 4.14 and 4.15 become identical to the phase volume fractions as expressed in Eqs. 4.12 and 4.13. Other names for phase volume fraction are therefore *no-slip holdup* or *no-slip volume fraction*. Alternatively, the expressions “phase content” or “input phase fractions” are

used in some publications to identify what we call *phase volume fractions*. Another name for holdup is, somewhat confusingly, *in-situ volume fraction*, and for gas also the term *void fraction* is found. In analogy to porous-media flow the term *saturation* could also be applied. Nonetheless, we will stick to the oil industry convention and speak of gas and liquid holdups. Other multiphase flow concepts used in literature are *slip velocity* defined as

$$v_s = v_g - v_l \quad \dots \dots \dots \quad (4.18)$$

and gas and liquid *mass fractions* x_g and x_l , defined as

$$x_g = \frac{\dot{m}_g}{\dot{m}_g + \dot{m}_l} = \frac{q_g \rho_g}{q_g \rho_g + q_l \rho_l}, \quad \dots \dots \dots \quad (4.19)$$

$$x_l = \frac{\dot{m}_l}{\dot{m}_g + \dot{m}_l} = \frac{q_l \rho_l}{q_g \rho_g + q_l \rho_l} = \frac{q_o \rho_o + q_w \rho_w}{q_g \rho_g + q_o \rho_o + q_w \rho_w}, \quad \dots \dots \dots \quad (4.20)$$

where \dot{m}_g , \dot{m}_o , and \dot{m}_w are the gas, oil, and water mass flow rates and where x_g is also known as the *quality* of the gas/liquid mixture.

To illustrate the effect of slip on the liquid (volume) fraction and the liquid holdup, [Fig. 4.3](#) gives an example of stratified flow where the liquid flow rate equals one-third of the gas flow rate. In case of no slip between the phases, the liquid holdup is equal to the liquid fraction, and 25% of the pipe's cross-sectional area is occupied by liquid. However, if the gas flows twice as fast as the liquid, the liquid fraction remains the same but the liquid holdup increases such that 40% of the area is occupied by liquid.

4.3 Pressure Drop Analysis

4.3.1 Governing Equations. For single-phase flow we derived three governing equations: a mass balance, a momentum balance, and an equation of state (EOS) (see [Eqs. 3.3 through 3.6](#) in [Section 3.1](#)). Therefore, it is to be expected that we can derive six equations for the two-phase flow case: two mass balances, two momentum balances, and two EOSs. Sometimes this approach can indeed be followed, in particular for stratified flow, in which case the interface between gas and liquid is relatively simple and the corresponding interface forces can be modeled in detail. Usually, however, the interaction between gas and liquid is too complex to be taken into account explicitly, and so a different approach is followed. Instead of modeling the dynamics of the two phases individually, mass and momentum balances are derived for the gas/liquid mixture, and two additional closure equations are specified for the relationships between the mixture velocity and the phase velocities, and the mixture density and the phase densities, respectively. The latter two equations are usually empirical or semiempirical. The governing dynamic equations for two-phase flow then become

$$\frac{\partial(\rho_m v_m)}{\partial s} = -\frac{\partial \rho_m}{\partial t}, \dots \quad (4.21)$$

$$\left. \begin{array}{l} \text{No slip: } q_l = \frac{1}{3} q_g \\ v_l = v_g \end{array} \right\} A_l = \frac{q_l}{v_l} = \frac{\frac{1}{3} q_g}{v_g} = \frac{1}{3} A_g$$

$$\lambda_l = \frac{q_l}{q_g + q_l} = \frac{\cancel{\frac{1}{3}}}{1 + \cancel{\frac{1}{3}}} = \frac{1}{4} \quad H_l = \frac{A_l}{A_g + A_l} = \frac{\cancel{\frac{1}{3}}}{1 + \cancel{\frac{1}{3}}} = \frac{1}{4}$$

$$\left. \begin{array}{l} \text{Slip: } q_l = \frac{1}{3} q_g \\ v_l = \frac{1}{2} v_g \end{array} \right\} A_l = \frac{q_l}{v_l} = \frac{\frac{1}{3} q_g}{\frac{1}{2} v_g} = \frac{2}{3} A_g$$

$$\lambda_l = \frac{q_l}{q_g + q_l} = \frac{\cancel{\frac{1}{3}}}{1 + \cancel{\frac{1}{3}}} = \frac{1}{4} \quad H_l = \frac{A_l}{A_g + A_l} = \frac{\cancel{\frac{1}{3}}}{1 + \cancel{\frac{2}{3}}} = \frac{2}{5}$$

Fig. 4.3—Illustration of the effect of slip between the gas and liquid phases on the liquid fraction λ_l (no effect) and the liquid holdup H_l (increases for increasing slip velocity).

$$\frac{\partial(\rho_m v_m^2)}{\partial s} = -\frac{\partial(\rho_m v_m)}{\partial t} - \frac{\partial p}{\partial s} + \frac{F_g}{A} + \frac{F_f}{A}, \dots \quad (4.22)$$

$$\rho_m = \rho_m(\rho_g, \rho_l), \dots \quad (4.23)$$

$$v_m = v_m(v_g, v_l), \dots \quad (4.24)$$

$$\rho_g = \frac{\rho_{g,sc} + r_s \rho_{o,sc}}{B_g}, \dots \quad (4.25)$$

$$\rho_o = \frac{R_s \rho_{g,sc} + \rho_{o,sc}}{B_o}. \dots \quad (4.26)$$

Here the EOS Eqs. 4.25 and 4.26 have been expressed in terms of volatile oil properties with the aid of Eqs. 2.21 through 2.23. Moreover, we use a liquid-mixing rule

$$\rho_l = f_o \rho_o + f_w \rho_w, \dots \quad (4.27)$$

where the weight factors f_o and f_w are the volume fractions defined in Eqs. 4.1 and 4.2. Just as for single-phase flow we can simplify the analysis considerably by considering only steady-state flow, in which case Eqs. 4.21 and 4.22 can be combined to give

$$\frac{dp}{ds} = - \underbrace{\rho_m g \sin \theta}_{\text{head loss}} - \underbrace{\frac{\rho_m}{2d} f v_m |v_m|}_{\text{friction loss}} - \underbrace{\rho_m v_m \frac{dv_m}{ds}}_{\text{acceleration loss}}, \dots \dots \dots \quad (4.28)$$

where we have used the definitions of head and friction losses that were introduced in Sections 3.2.2 and 3.2.3, but are now expressed in terms of mixture velocity v_m and mixture density ρ_m . Several slightly different formulations have been presented by various authors, but they all contain a head loss, friction loss, and acceleration loss component. The equation for the mixture density (Eq. 4.23) can in the simplest case be written as an average of the phase densities weighted by the phase volume fractions:

$$\rho_{mn} = \lambda_g \rho_g + \lambda_l \rho_l, \dots \dots \dots \quad (4.29)$$

where the subscript mn indicates “mixture, no-slip” and reflects that this expression assumes that there is no slip between the phases. The corresponding expression for the mixture velocity (Eq. 4.24) then becomes

$$v_{mn} = \lambda_g v_g + \lambda_l v_l, \dots \dots \dots \quad (4.30)$$

with $v_l = v_o = v_w$; but because of the absence of slip, we also have

$$v_{mn} = v_g = v_l \dots \dots \dots \quad (4.31)$$

Normally, however, we assume that slip occurs, in which case Eq. 4.23 can be written as

$$\rho_{ms} = H_g \rho_g + H_l \rho_l \dots \dots \dots \quad (4.32)$$

where the subscript ms indicates “mixture, slip” and where the gas and liquid holdups are (semi)empirical functions of a large number of parameters such as inclination, pipe diameter, flow rates, densities, viscosities, and surface tensions. The corresponding equation for the mixture velocity is

$$v_{ms} = H_g v_g + H_l v_l, \dots \dots \dots \quad (4.33)$$

as can be verified from Eqs. 4.11, 4.14 and 4.15. In analogy to Eqs. 4.29 and 4.32 we can also define no-slip and slip averaged versions for other fluid properties. For example, for the mixture viscosity we obtain

$$\mu_{mn} = \lambda_g \mu_g + \lambda_l \mu_l, \dots \dots \dots \quad (4.34)$$

$$\mu_{ms} = H_g \mu_g + H_l \mu_l, \dots \dots \dots \quad (4.35)$$

with μ_l expressed in terms of μ_o and μ_w with the no-slip liquid-mixing rule

$$\mu_l = f_o \mu_o + f_w \mu_w \dots \dots \dots \quad (4.36)$$

4.3.2 Holdup and Friction Correlations. Many empirical correlations and semiempirical models have been developed for multiphase flow in pipes. Several of these concern two-phase steam/water flow, especially for the nuclear industry. Others are primarily meant for chemical engineering applications, while also a good number are dedicated to the flow of hydrocarbons in wells and pipelines. We refer to Brill and Mukherjee (1999), Hassan and Kabir (2002), and Shoham (2006) for detailed overviews. In this book we present only three correlations in detail (in Appendix E) as examples of the typical multiphase flow correlations. Brill and Mukherjee (1999) distinguish three types of correlations of increasing complexity, in addition to even more complex *mechanistic models*. The latter involve varying amounts of first-principle physics but are never free from some form of empiricism, which explains why they are also referred to as *semiempirical models*. The simplest group of correlations consists of empirical expressions for the friction factor in terms of no-slip mixture properties. The second category takes slip into account and consists of empirical expressions for holdup and friction, while the third category also considers different flow regimes. The latter two categories typically use a set of dimensionless groups defined in terms of the essential variables to describe the physics of multiphase flow.

In the first systematic dimensional analysis of multiphase flow in oil wells (Ros 1961), 13 variables were identified to describe two-phase flow in near-vertical pipes:

- pipe diameter d [L]
- pipe roughness e [L]
- acceleration of gravity g [L t⁻²]
- pressure p [L⁻¹ m t⁻²]
- gas velocity v_g [L t⁻¹]
- liquid velocity v_l [L t⁻¹]
- well inclination α [-]
- pipe wall–gas wetting angle φ [-]
- gas viscosity μ_g [L⁻¹ m t⁻¹]
- liquid viscosity μ_l [L⁻¹ m t⁻¹]
- gas density ρ_g [L⁻³ m]
- liquid density ρ_l [L⁻³ m]
- liquid/gas interfacial tension σ_{gl} [m t⁻²]

Because these 13 variables are defined in terms of three dimensions (length L , mass M , and time t), it is possible, according to the theory of dimensional analysis, to derive a total of $13 - 3 = 10$ dimensionless groups to completely describe the physics of the problem. Note that the theory of dimensional analysis is described in most textbooks on fluid mechanics—see, e.g. White (2016). For a discussion focused on hydrocarbon pipe flow, see Shoham (2006).

Ros (1961) chose to study the dimensionless pressure gradient $(dp/ds)/(p_l g)$ as a function of nine other dimensionless groups. Further analysis revealed that of those nine, the following four were the most important:

$$\text{Liquid velocity number: } N_v = \left| v_{sg} \right| \sqrt[4]{\frac{\rho_l}{g \sigma_{gl}}}, \quad \dots \dots \dots \quad (4.37)$$

$$\text{Gas velocity number: } N_{gv} = \left| v_{sg} \right| \sqrt[4]{\frac{\rho_l}{g \sigma_{gl}}}, \quad \dots \dots \dots \quad (4.38)$$

$$\text{Pipe diameter number: } N_d = d \sqrt{\frac{g \rho_l}{\sigma_{gl}}}, \quad \dots \dots \dots \quad (4.39)$$

$$\text{Liquid viscosity number: } N_\mu = \mu_l \sqrt[4]{\frac{g}{\rho_l \sigma_{gl}^3}}. \quad \dots \dots \dots \quad (4.40)$$

Among the five groups that were determined to be less important was the wellbore inclination α , because in those days nearly all oil wells were vertical. Clearly, for deviated or horizontal wells the inclination must play an important role. Duns and Ros (1963) used the dimensionless groups (Eqs. 4.37 through 4.40) to design an experimental program that resulted in a set of early popular multiphase flow correlations. Since then, other dimensionless groups have been defined to describe multiphase flow correlations for oil and gas wells, but we will not discuss these and refer instead to the references mentioned above for further information. That also holds for the mechanistic models, which are of a complexity outside the scope of this book.

In Appendix E we discuss three correlations. The first one, from Hagedorn and Brown (1965), is an empirical correlation of the second category; i.e., it gives friction and holdup values. It is valid only for near-vertical wells. The second one is the Mukherjee and Brill (1985b) model. It is a correlation of the third category (i.e., it takes into account flow regimes) and is valid for vertical, deviated, or horizontal wells or pipes. Both these models are defined in terms of the dimensionless groups Eqs. 4.37 through 4.40, as well as, for the Mukherjee and Brill model, the wellbore inclination α . The third model discussed in Appendix E is a so-called *drift flux* model, which uses a particular approach to compute the holdup. The version discussed is a second-category correlation; i.e., it takes into account slip but no distinct flow regimes. It is a popular method for simplified multiphase flow computations inside reservoir simulators because it is fast and results in smooth gradients without the discontinuities that are often present in more complex models and may cause numerical problems. The Hagedorn and Brown, and Mukherjee and Brill correlations have been programmed in the MATLAB function files `Hag_Brown_dpds.m` and `Muk_Brill_dpds.m`. Programming of the drift flux method is left as a MATLAB assignment in Section 4.7. Another popular third-category correlation, by Beggs and Brill (1973), is available in `Beggs_Brill_dpds.m`.

4.3.3 Element Equations. Just as in the single-phase case we can determine element equations for multiphase well or pipeline flow, which can be written concisely in the form of [Eq. 1.4](#) as

$$p_{\text{out}} = f(p_{\text{in}}, q_{g,\text{sc}}, q_{o,\text{sc}}, q_{w,\text{sc}}), \dots \quad (4.41)$$

or alternatively as

$$p_{\text{out}} = f(p_{\text{in}}, q_{o,\text{sc}}, f_w, R_{go}). \dots \quad (4.42)$$

If we choose the boundary condition at one end of the element, (i.e., $\hat{p} = p_{\text{in}}$), we can compute the pressure p_{out} at the other end through numerical integration with the aid of the multiphase functions `Hag_Brown_dpds.m`, `Muk_Brill_dpds.m`, or `Beggs_Brill_dpds.m` in conjunction with a standard MATLAB ordinary-differential equation solver, such as `ode45.m`. This procedure has been implemented in the file `pipe.m`, and examples of how to use these files can be found in `example_flowline.m`, `example_well.m`, and `example_traverse.m`.

[Fig. 4.4](#) displays the traverse of a vertical oil well with properties given in [Table 4.1](#). The figure was created by fixing the flowing tubinghead pressure (FTHP) at 0.5 MPa and integrating from top to bottom, resulting in a flowing bottomhole pressure (FBHP) of 23.9 MPa. Subsequently fixing the FBHP and integrating from bottom to top results in [Fig. 4.5](#). Both figures clearly show that the majority of the pressure drop is caused by head losses, while friction losses play a much smaller role. Acceleration losses can be completely neglected.

[Fig. 4.6](#) displays the results for a deviated well with the same properties given in [Table 4.1](#) except for the FTHP, now taken as 5.4 MPa, and the well depth and the inclination, now determined from survey file `deviated_well_1.txt` which was also used in [Appendix C](#) on wellbore surveying. [Fig. C-4](#), in [Appendix C](#), illustrates that this well has a horizontal section, which explains that in [Fig. 4.6](#) the head losses between measured depths of approximately 2700 and 4600 m are zero.

4.3.4 Gradient Curves. Before modern computers, the practice was to present empirical correlations for wellbore pressure drop in the form of *gradient curves*, which are just traverses for a given set of parameters. An example is given in [Fig. 4.7](#), which was generated with the aid of the Mukherjee and Brill correlation for the parameter values indicated in the chart. Although these curves are hardly used now, they give some insight into the effects of the various parameters. After introduction of the gradient curve concept by Gilbert (1954), large numbers of these curves have been prepared for “typical” well parameters (see, e.g., Beggs 1991). They are valid only for vertical wells. Their vertical axis represents depth measured from surface and the horizontal axis the wellbore pressure computed for the minimum possible (i.e., atmospheric) FTHP. To use the curves for higher FTHPs, the vertical axis can be interpreted as the difference in vertical depth between two points in the wellbore

rather than the absolute depth; and the horizontal axis, the corresponding pressure difference (see Exercise 4.9).

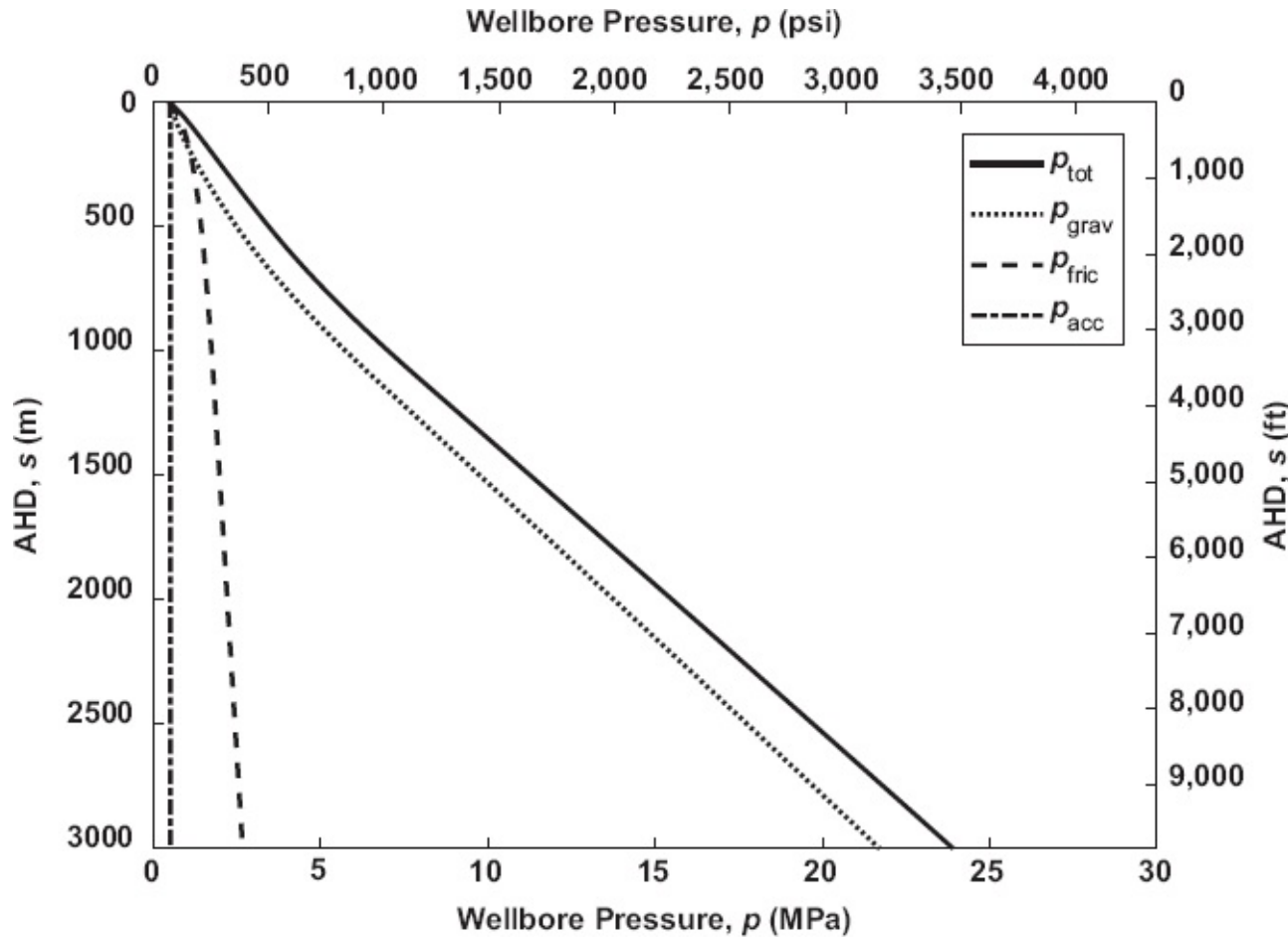


Fig. 4.4—Traverse for a vertical multiphase well with parameters given in Table 4.1. Integration from top to bottom.

4.4 Tubing Intake Curves

As discussed in Section 1.5, the multiphase flow equations for a wellbore element specify a relation between the oil and gas flow rates $q_{o,sc}$ and $q_{g,sc}$ and the wellbore pressure drop $\Delta p = p_{in} - p_{out}$ (see Eq. 1.7). If we know the gas/oil ratio (GOR) R_{go} , we can also determine the flow rates from the pressure drop, although we need to do so in an iterative fashion. However, usually it is one of the pressures that is unknown. If the FBHP p_{wf} is specified, then for a given GOR the FTHP p_{tf} can be computed as a function of $q_{o,sc}$, resulting in a tubing performance curve (see also Section 3.5). Alternatively, p_{tf} may be specified, and p_{wf} computed as a function of $q_{o,sc}$, leading to a tubing intake curve. Fig. 4.8 depicts a typical tubing intake curve for an oil well that has been produced using the data listed in Table 4.1. In comparison to the tubing intake curve for a gas well depicted in Fig. 3.7, there is a marked difference. Whereas the gas curve is monotonously increasing with increasing flow rates, the multiphase curve first decreases before going up. At first sight the gas curve may

seem to be right and the multiphase curve wrong, because increasing the flow rate through a tubing requires an increase in pressure drop (i.e., an increase in FBHP for a given FTHP).

Parameter		SI Units		Field Units	
Tubing diameter	d	62.3×10^{-3}	m	2.453	in.
Roughness	e	30×10^{-6}	m	0.0012	in.
Water cut	f_w	0.2	—	0.2	—
FTHP	p_{tf}	0.5×10^6	Pa	72.5	psi
Gas/oil ratio	R_{go}	50	m^3/m^3	281	scf/STB
FTHT	T_{tf}	30	$^\circ\text{C}$	86	$^\circ\text{F}$
FBHT	T_{wf}	120	$^\circ\text{C}$	248	$^\circ\text{F}$
Well depth	Z_{tot}	3,000	m	9,843	ft
Inclination	α	0	rad	0	degree
Gas viscosity	μ_g	Carr et al. (1954) correlation			
Oil viscosity	μ_o	Beggs and Robinson (1975), Vasquez and Beggs (1980)			
Water viscosity	μ_w	0.35×10^{-3}	$\text{Pa} \cdot \text{s}$	0.35	cp
Gas density/gravity	$\rho_{g,sc}/\gamma_g$	0.95	kg/m^3	0.77	—
Oil density/gravity	$\rho_{o,sc}/\gamma_{API}$	850	kg/m^3	35	$^\circ\text{API}$
Water density	$\rho_{w,sc}$	1,050	kg/m^3	65.5	lbf/ft^3
Gas/oil interf. tension	σ_{go}	0.008	N/m	8	dynes/cm
Gas/w. interf. tension	σ_{gw}	0.04	N/m	40	dynes/cm
Equations of state		Standing (1952), black oil; Standing and Katz (1942), Z factor			
Multiphase flow correlation		Mukherjee and Brill (1985b)			

Table 4.1—Parameter values for Figs. 4.4 to 4.6 and 4.8 to 4.11 (except for deviations as indicated in the figure captions).

To understand what causes the shape of the multiphase curve in Fig. 4.8, consider Fig. 4.9, which is identical to Fig. 4.8 except for a split of the total pressure drop over the tubing into two components: the head loss and the friction loss. It can be seen that the friction loss behaves as expected; i.e., it increases with increasing flow rates. However, the head loss shows a more complex behavior. For increasing flow rates, to the right of the minimum of the curve, the head loss also increases. This is a result of the increased compression of the gas/liquid mixture in the well at higher FBHPs corresponding to higher flow rates. For decreasing flow rates, to the left of the minimum, another effect takes place. The gas increasingly starts slipping through the liquid, resulting in an increasing liquid holdup and therefore an increasing density of the gas/liquid column.

Other types of tubing intake curves are obtained by fixing p_{tf} and $q_{o,sc}$, but varying

one of the process variables, such as the GOR or the tubing size. Some typical examples of tubing intake curves have been displayed in **Figs. 4.10 and 4.11**. Fig. 4.10 shows the tubing intake curve that is generated when the oil production rate $q_{o,sc}$ is held constant while the GOR R_{go} is varied. At zero GOR, the well is producing only liquid. Since the production rate is low, the friction is low, and the intake pressure is close to the hydrostatic pressure of the fluid column. If gas is introduced, the liquid column gets lighter, the hydrostatic pressure decreases, and hence the intake pressure decreases. This effect continues as the GOR increases, but at the same time the friction pressure drop increases because of the increased total mass flow of oil and gas. At a certain point, the friction pressure drop starts to dominate, and then the intake pressure starts to increase again. Apparently, for a well flowing a given volume of liquid, there exists an optimum GOR at which the pressure drop over the tubing is minimal. This effect plays an important role in gas lift optimization. In Fig. 4.11, where the numbers 1 to 5 correspond to tubing sizes given in **Table 4.2**, it can be seen that there exists an optimum tubing size (for a fixed production rate). As expected, to the left of this optimum, the pressure increases as the tubing diameter decreases, given that it is more difficult for fluids to flow through a narrower tube. To the right of the optimum, multiphase effects start to play a role. In a wider tubing it becomes easier for the gas to slip past the liquid and the lifting is less efficient. The downhole pressure required to maintain the flow rate therefore rises.

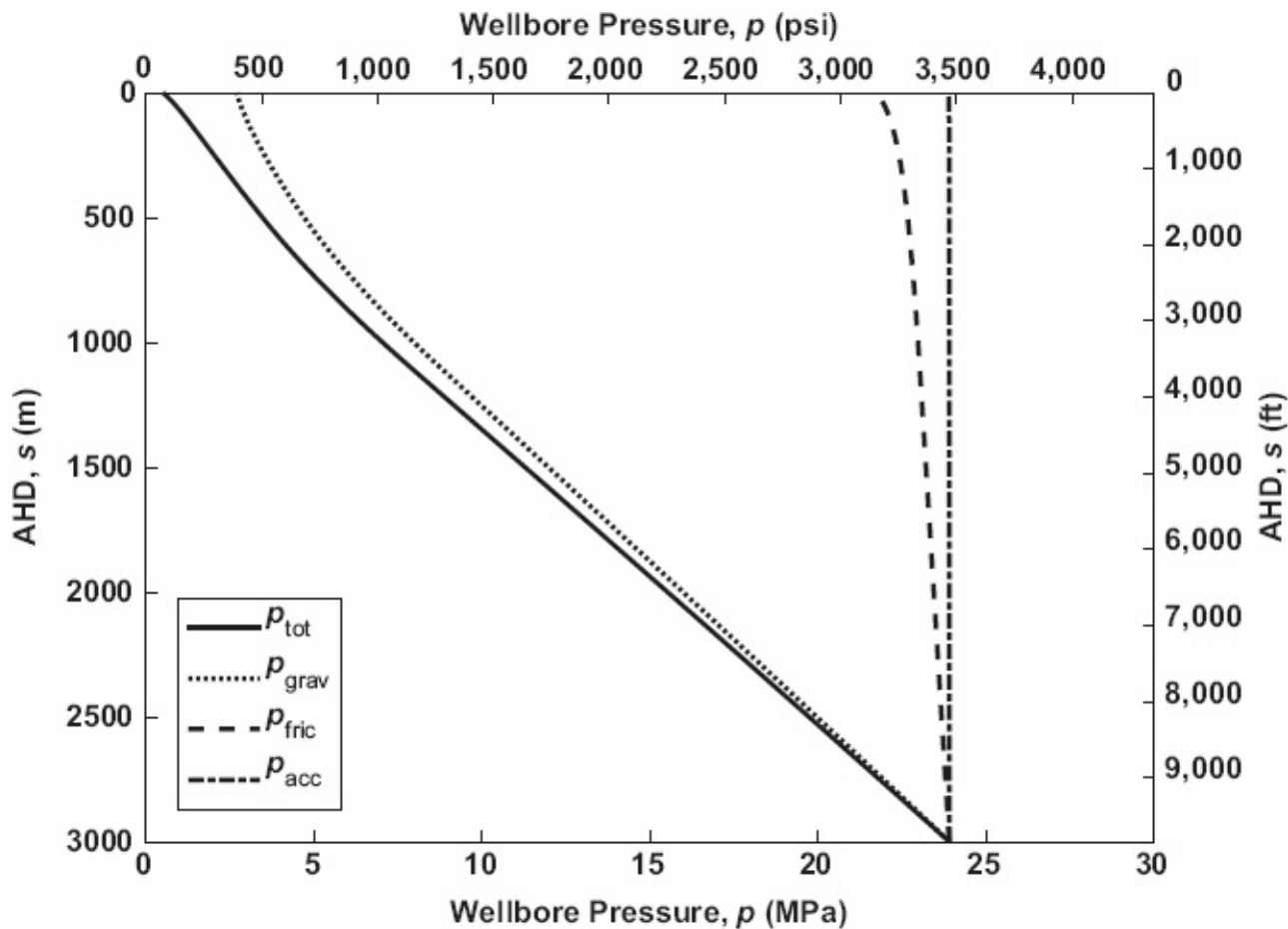


Fig. 4.5—Traverse for a vertical multiphase well with parameters given in **Table 4.1**. Integration from

bottom to top.

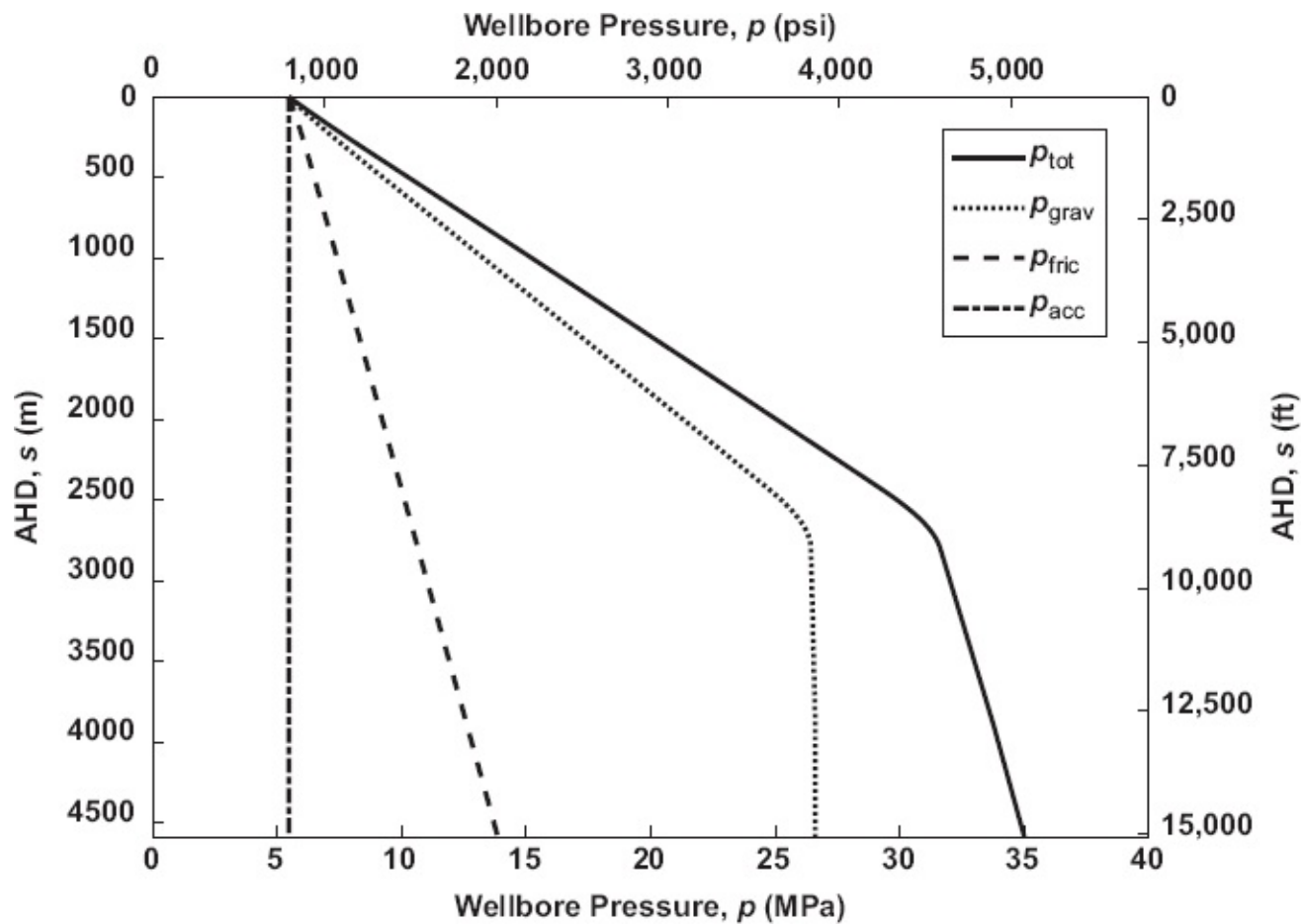


Fig. 4.6—Traverse for a deviated multiphase well with parameters given in Table 4.1, a FTHP of 5.4 MPa, and survey file [deviated_well_1.txt](#). Integration from top to bottom.

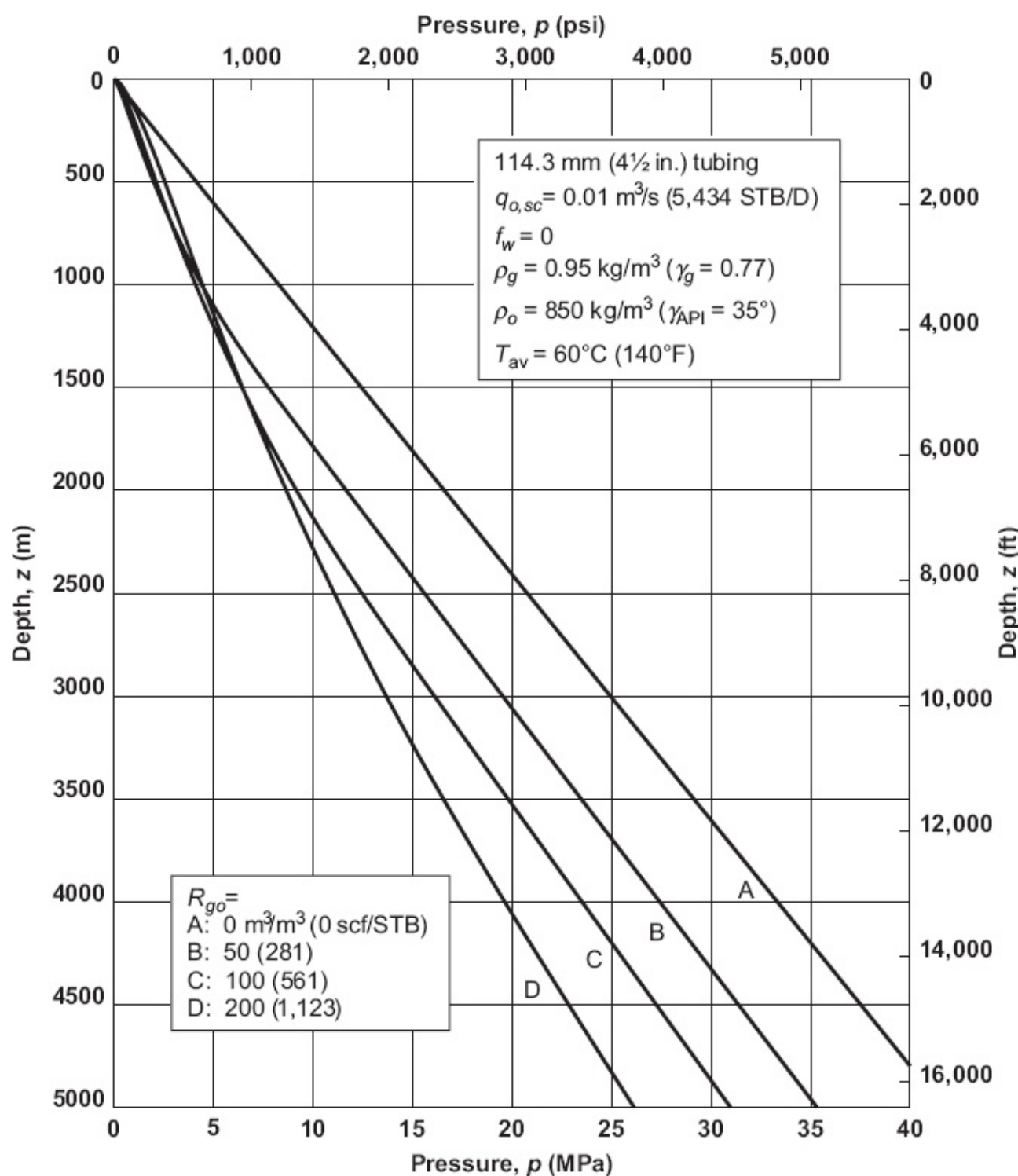


Fig. 4.7—Example of a gradient curve.

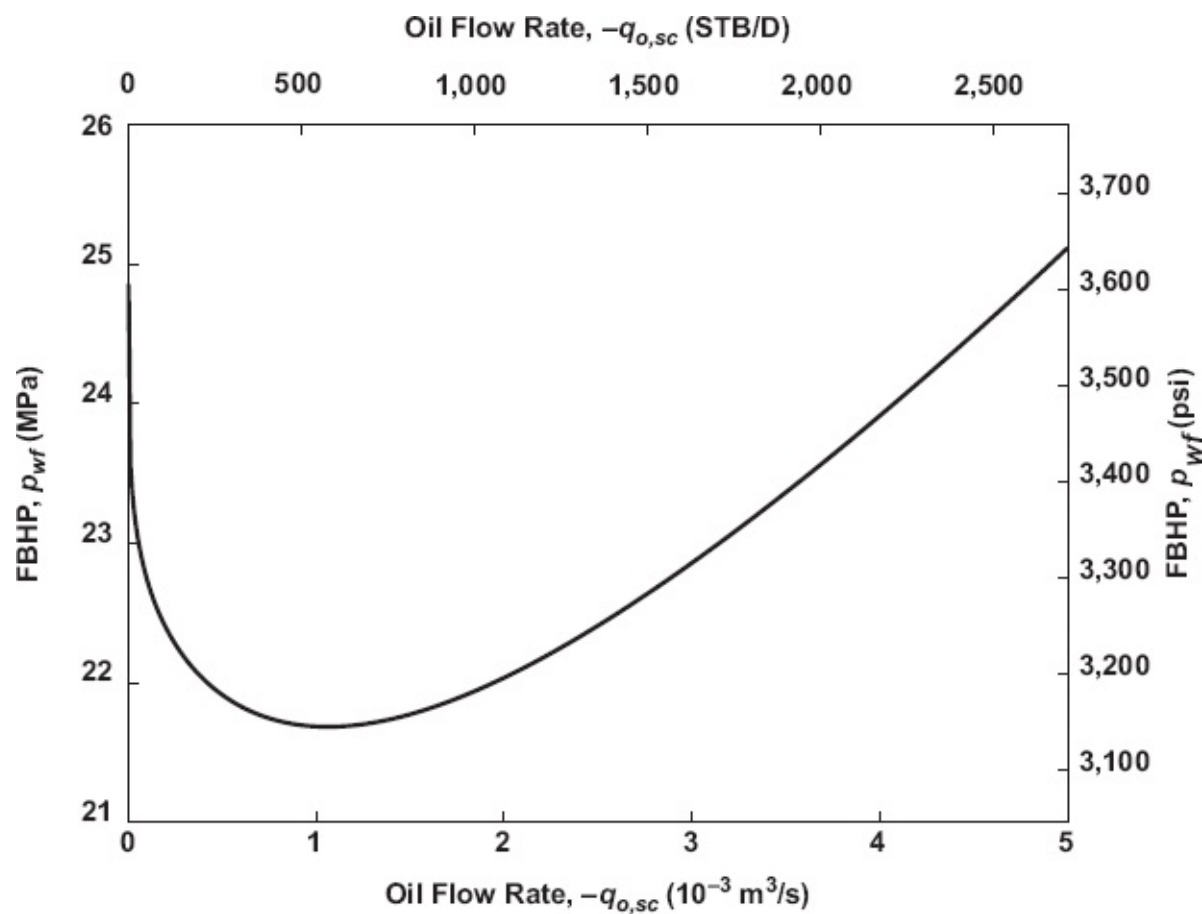


Fig. 4.8—Tubing intake curve for varying production rate.

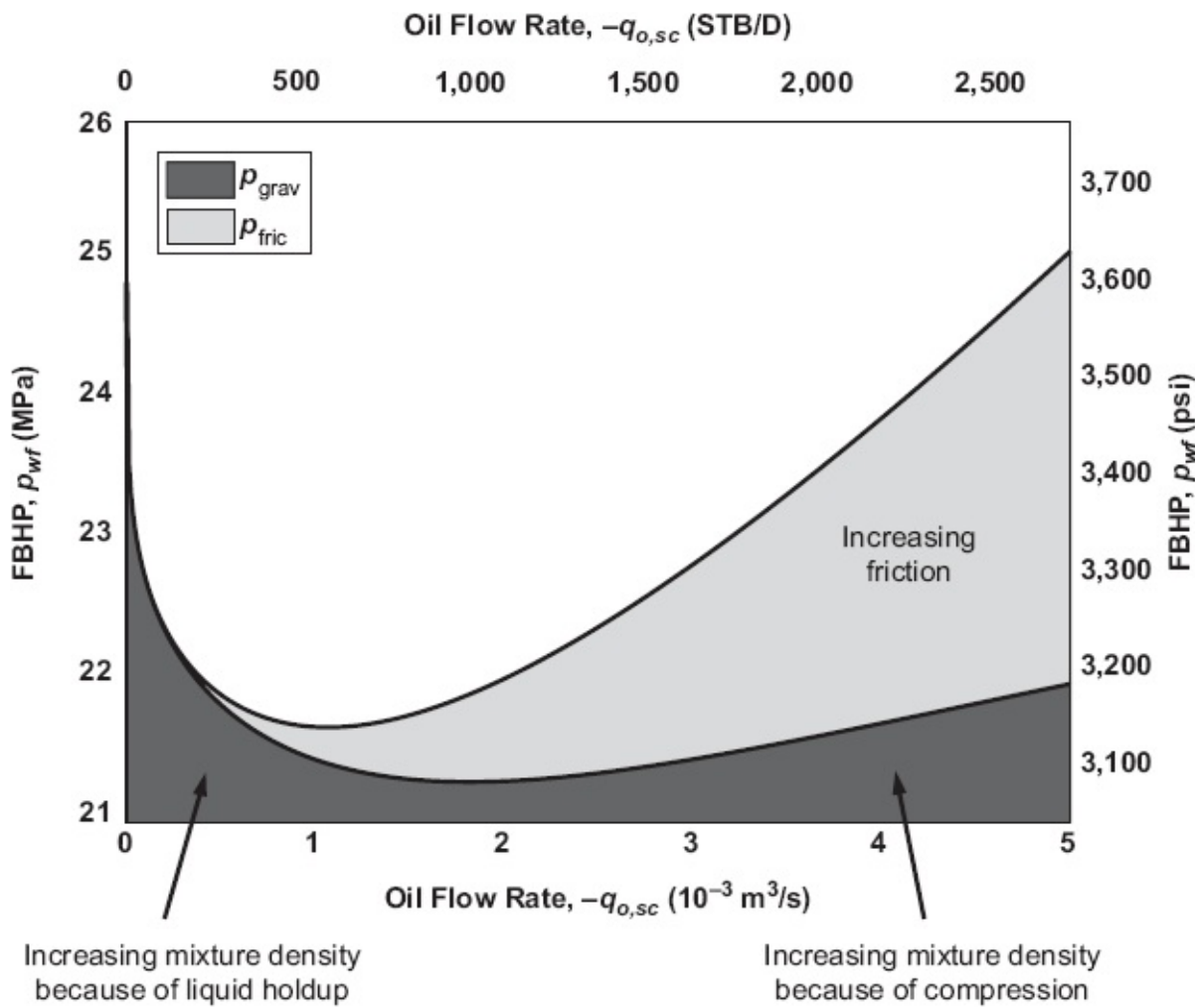


Fig. 4.9—Tubing intake curve for varying production rate with contributions of head loss and friction loss.

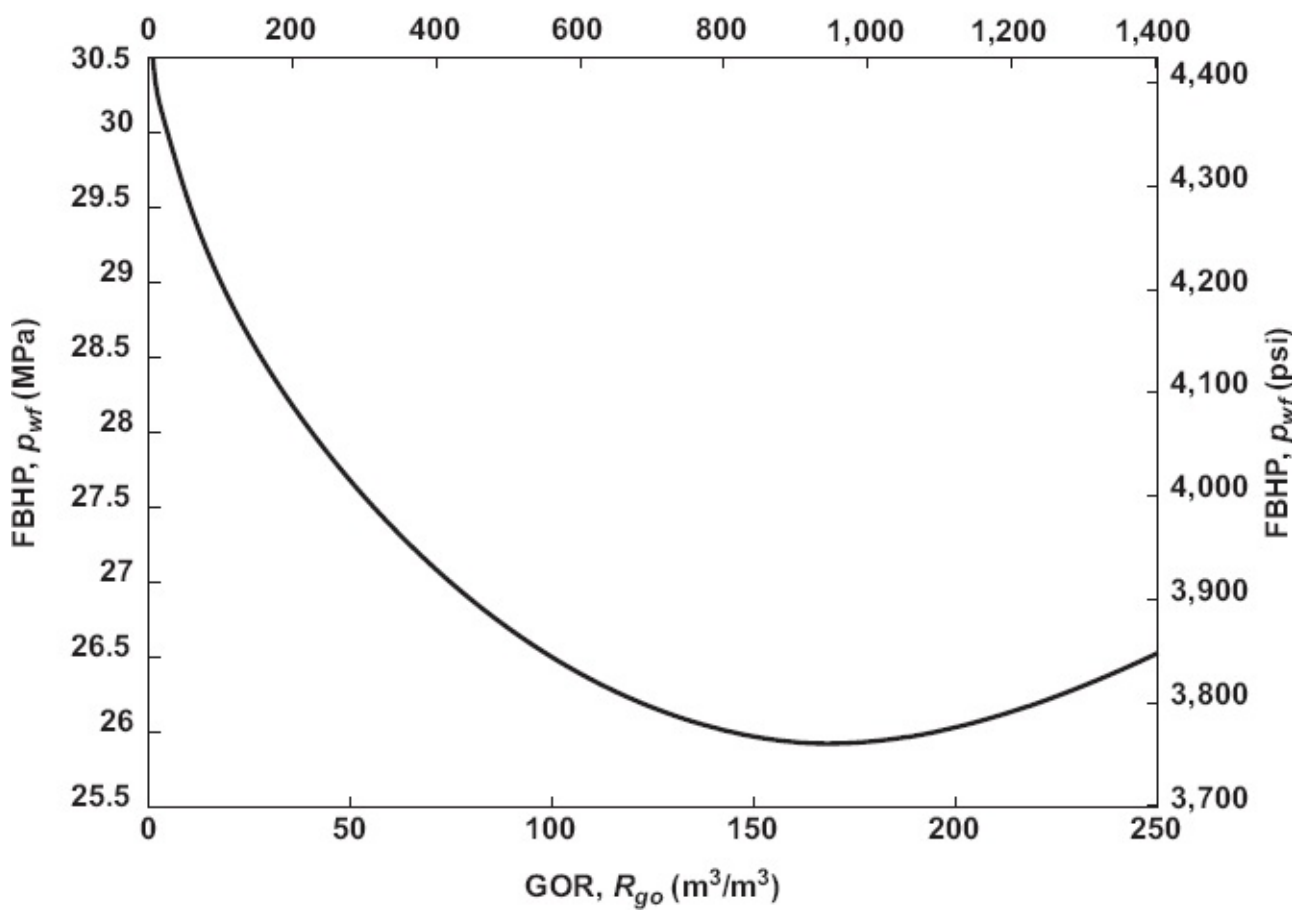
GOR, R_{go} (scf/STB)

Fig. 4.10—Tubing intake curve for varying GORs at a fixed flow rate of $q_{o,sc} = -4 \times 10^{-3} \text{ m}^3/\text{s}$ (2,174 STB/D).

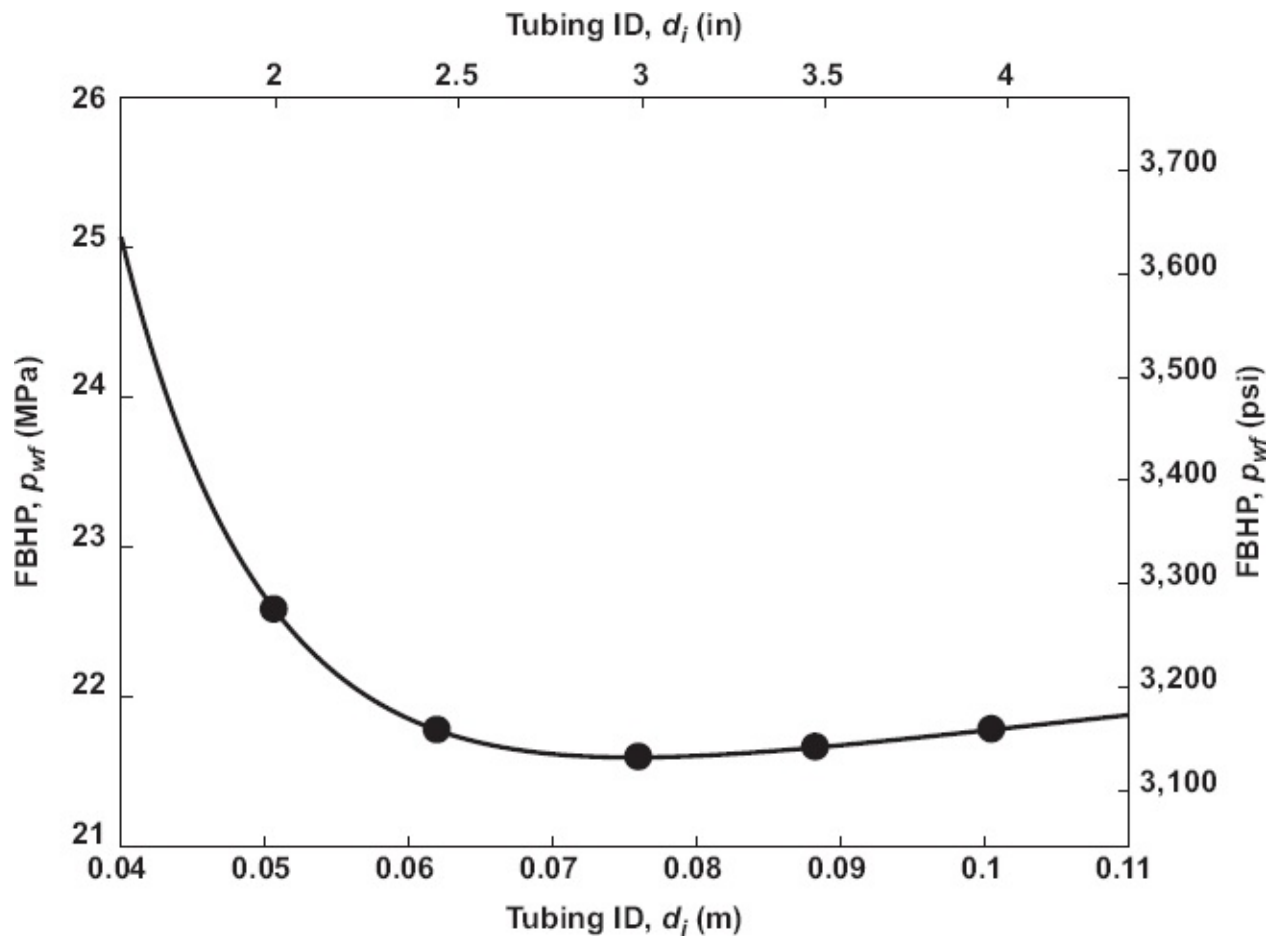


Fig. 4.11—Tubing intake curve for varying tubing inside diameters (ID) at a fixed flow rate of $q_{o,sc} = -1.5 \times 10^{-3} \text{ m}^3/\text{s}$ (815 STB/D) and a fixed GOR of $R_{go} = 50 \text{ m}^3/\text{m}^3$ (281 scf/STB).

4.5 Lift Tables

In numerical reservoir simulation it is necessary to specify the operating conditions of the wells. This can be done in terms of total flow rates q_t or FBHPs p_{wf} . In reality, however, it is usually not the FBHP that is controlled but the FTHP p_{tf} . As discussed above, the FTHP can be computed for given fluid properties, wellbore geometry, phase flow rates; and FBHP. Conversely, the FBHP may be computed for a given FTHP. The computation could be performed with the aid of a wellbore simulator. However, these computations are generally too time consuming to perform every time step of the reservoir simulator. Only for long horizontal wells or for complex well configurations such as multilaterals, the use of a wellbore simulator may be unavoidable, at least for the bottom part of the well. An alternative approach is to perform a large number of wellbore flow simulations upfront to generate a multidimensional table, known as a *lift table* or *flow performance table*, which can be used as a look-up table by the reservoir simulator. Usually the four entries for a lift table are the FTHP and the oil, gas, and water rates, all expressed at standard conditions. (Note that the lift table entries can also be chosen as FTHP, oil rate, gas/oil ratio, and water cut. Whatever the choice of the table entries, it is assumed

that the fluid properties at standard conditions and the wellbore geometry do not change during the reservoir simulation.)

Typically, each of the entries is described with a small number of points, say, 5, in which case the table has $5^4 = 625$ points that correspond to the same number of FBHPs. For intermediate values of the entries a linear or higher-order interpolation is used to compute the corresponding FBHPs, which is much faster than performing a full wellbore flow simulation. Sometimes a higher number of points is needed, at the cost of a longer preprocessing time—e.g., to prevent convergence problems during the numerical solution of the reservoir equations. Lift tables for the commercial reservoir simulators Eclipse and Imex can be generated with MATLAB files `Eclipse_lift_table.m` and `Imex_lift_table.m`. A typical aspect of lift tables is that they are usually “regularized” such that there is no decreasing FBHP for increasing oil flow rates; i.e., the corresponding tubing intake curves have no descending branch. This is done to avoid numerical problems in the reservoir simulator, which usually cannot cope with decreasing wellbore pressure drops for increasing flow rates. The mechanism for regularization is to simply replace the FBHP values in the descending branch of a pressure intake curve (i.e., the values to the left of the minimum) by the minimum value.

Number	OD (in.)	OD (mm)	Nominal Weight (lbm/ft)	ID (mm)
1	2.375	60.3	4.70	50.67
2	2.875	73.0	6.50	62.00
3	3.500	88.9	9.30	76.00
4	4.000	101.6	11.00	88.29
5	4.500	114.3	12.75	100.53

Note: In the oil field literature, tubing dimensions are often referred to as e.g. 2-7/8" 6.5# tubing, meaning tubing with an outside diameter of 2.865 in., and a nominal weight per unit length of 6.5 lbm/ft, where “nominal” means averaged over the length, including the thicker couplings. For a given outside diameter, the inside diameter is therefore a function of the nominal weight.

Table 4.2—Tubing data for Fig. 4.11.

4.6 Questions

- 4.1 Is the liquid holdup in a production well typically larger or smaller than the liquid fraction? Why?
- 4.2 What is the difference between superficial phase velocities and in-situ phase velocities?
- 4.3 One-dimensional single-phase compressible flow with a given temperature distribution can be described with three equations: a mass balance, a momentum balance, and an EOS. Therefore it is to be expected that two-phase flow can be described with six equations: two mass balances, two

momentum balances, and two EOSs. Why is this approach usually not possible? What is the usual alternative approach?

- 4.4 Why have the multiphase flow correlations described in [Appendix E](#) only a limited predictive value for real oil wells?
- 4.5 A tubing intake curve for single-phase flow displays a monotonically increasing relationship between flow rate and FBHP. This is intuitively correct: An increase in flow rate, at a given FTHP, requires an *increase* in FBHP. However, a tubing intake curve for multiphase flow typically displays a minimum. At low flow rates, an increase in rate corresponds to a *decrease* in FBHP. Explain this seemingly counterintuitive behavior.
- 4.6 Consider a gas/liquid mixture with $q_l = 0.3 q_g$ and $v_g = 1.2 v_l$. What are the liquid fraction and the liquid holdup?
- 4.7 A well is completed with a 0.122-m-ID tubing and produces a gas/oil/water mixture with the following properties: $q_{o,sc} = 18.4 \times 10^{-3} \text{ m}^3/\text{s}$, $R_{go} = 238 \text{ m}^3/\text{m}^3$, $f_{w,sc} = 0.23$. You know that you are dealing with a black oil and that at a depth of 400 m the formation volume factors and the solution GOR are given by $B_g = 0.05$, $B_o = 1.15$, $B_w = 1.00$, and $R_s = 10.1$, all expressed in m^3/m^3 . Furthermore, you know that the liquid holdup is 5% higher than the liquid volume fraction. What are the superficial and local gas and liquid velocities?
- 4.8 Consider a deviated oil well with a trajectory as depicted in [Fig. 4.12](#). The well has a constant azimuth; and the “stepout,” displayed on the horizontal axis, is therefore just the horizontal distance from the wellhead s_{hor} . [Fig. 4.13](#) depicts the acceleration, friction, and gravity components of the pressure drop over the well.

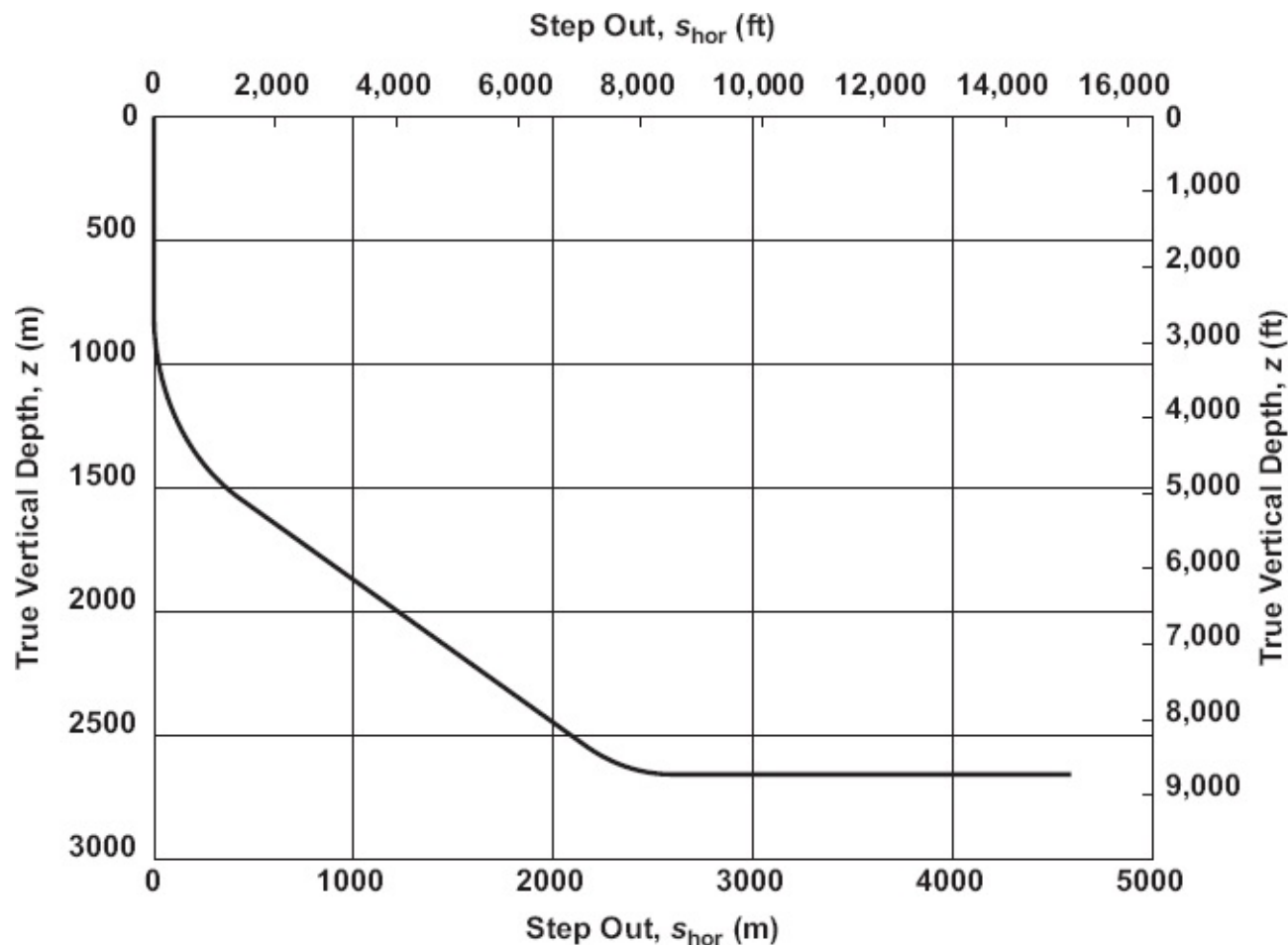


Fig. 4.12—Well trajectory for Question 4.8.

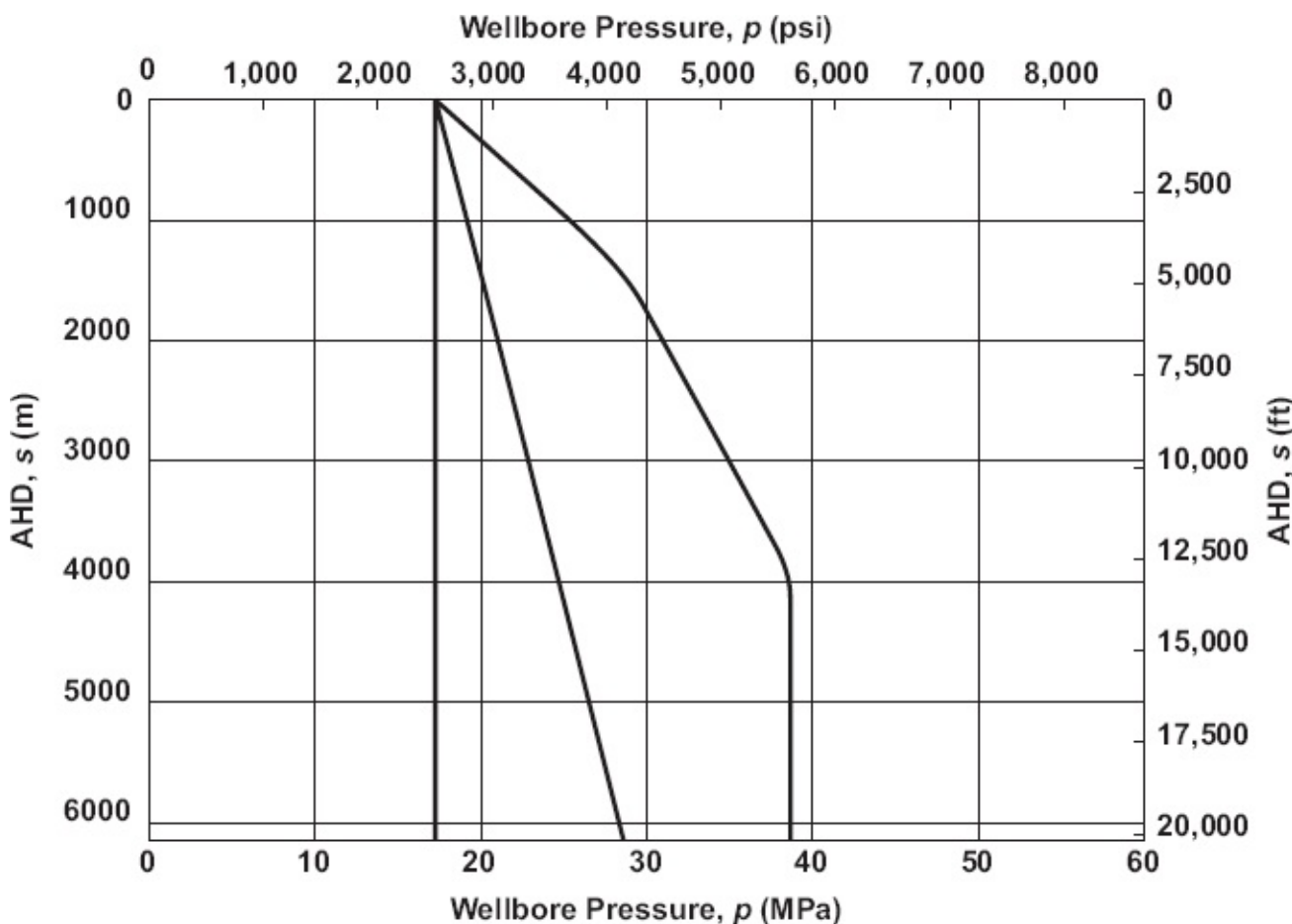


Fig. 4.13—Pressure drop components for Question 4.8.

- (a) Indicate which of the curves correspond to which of the pressure drop components.
- (b) What is the magnitude of the FBHP? Sketch the total pressure drop.
- (c) Consider the same well, producing oil with a much higher solution GOR. Give a qualitative sketch of the corresponding traverses for the pressure drop and its components (i.e., four curves) if the FBHP remains the same. Hint: Pay attention to the shape of the friction and gravity curves close to the surface.
- (d) Which of the following methods could be used to compute the pressure drop over this well: (a) Duns and Ros, (b) Hagedorn and Brown, (c) Brill and Mukherjee, (d) Shi et al. (drift flux)?

4.9 A 3000-m deep vertical oil well is producing at a FTHP of 5 MPa with a GOR of $50 \text{ m}^3/\text{m}^3$. Use the gradient curve in Fig. 4.7 to compute the FBHP.

Questions 4.10 and 4.11 require the use of MATLAB.

4.10 For the same well as in question 4.9 use MATLAB file `pipe.m` to compute the FBHP. Use the operating conditions listed in Fig. 4.7, a tubing ID $d = 0.10053 \text{ m}$, and a pipe roughness $e = 30 \times 10^{-6} \text{ m}$.

4.11 Run MATLAB file `example_intake_curve.m` and verify that the results are identical to those of Fig. 4.8, although in a slightly different layout.

- (a) Rerun the file a few times with an increased FTHP—e.g., choose values of 1, 3, and 5 MPa. (This is simply done by replacing the values for p_{tf} in line 32.) What do you observe? Explain the result. Reset the FTHP to 0.5 MPa.
- (b) Make a copy of the file under a different name. Modify the copied file to produce a tubing performance curve. Leave all well data unchanged. Run the modified file for an FBHP of 26 MPa. Compare the curves to the tubing performance curve for single-phase gas flow in Fig. 3.6. Explain the difference in shape. Repeat the exercise for increasing values of the FBHP—e.g., 28 and 30 MPa. What do you observe? Explain the result.

To answer questions 4.12 through 4.14 you should first study the multiphase flow correlations in Appendix E. The correlations have been programmed in various MATLAB routines (see Appendix H). However, the questions can be answered without performing MATLAB computations.

4.12 For a vertical oil well we have $N_{lv} = 17.6$, $N_{gv} = 237$, $N_d = 45.4$, and $N_\mu = 0.131$. What is the liquid holdup according to the Hagedorn-Brown correlation at the point in the well where the pressure equals 15 MPa? (No need to check if $H_i > \lambda_i$.)

4.13 Fig. 4.14 displays part of the flow chart for the Mukherjee and Brill multiphase flow algorithm (see Appendix E). Enter the following text in the corresponding boxes in the flow chart:

- uphill flow
- horizontal flow
- gas/liquid flow
- liquid-only flow
- injection well
- production well
- interpolate T
- compute v_m

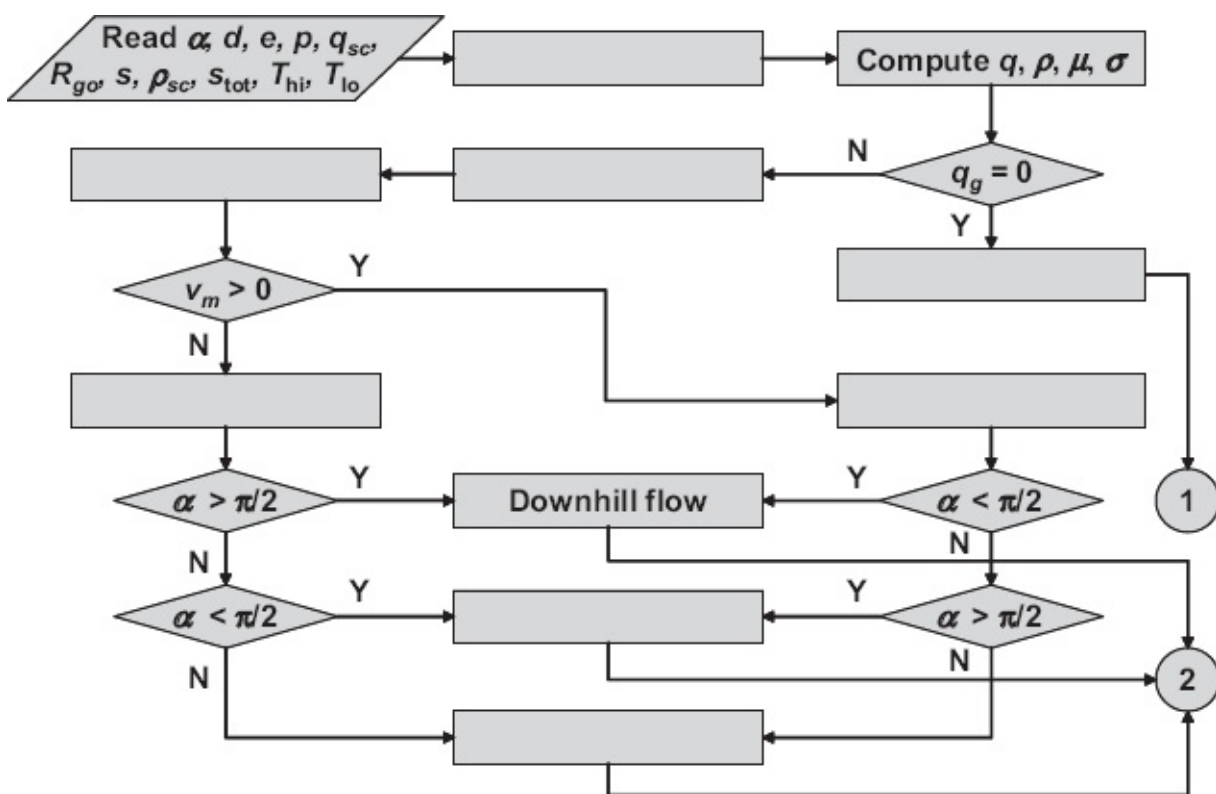


Fig. 4.14—Partial flow chart for Mukherjee and Brill algorithm.

4.14 Consider the following equation:

$$v_d = \frac{m_\alpha (1 - H_g C_0) C_0 K v_c}{H_g C_0 \sqrt{\frac{\rho_g}{\rho_l}} + 1 - H_g C_0}$$

- (a) What does this equation describe? (Hint: Check Appendix E.)
- (b) What can you say about the velocity and concentration profiles if C_0 is equal to unity?
- (c) Why is the ratio $v_{ms}/v_{g,fl}$ typically larger than unity for fully developed annular flow?

4.7 MATLAB Assignment: Drift Flux

4.7.1 Objectives

- Gain insight into the typical contents of a multiphase flow correlation
- Learn to implement such a correlation in MATLAB
- Compare the results to those of another correlation to obtain a feeling for the order of magnitude of the differences

4.7.2 Warning. This MATLAB exercise requires considerably more programming skills than the MATLAB exercises in earlier chapters.

4.7.3 Assignment. The MATLAB function `pipe.m` has the option to call various subfunctions to compute the pressure drop dp/ds over an inclined wellbore or flowline. These include the multiphase flow models `Hag_Brown_dpds.m`, `Muk_Brill_dpds.m`, and `Beggs_Brill_dpds.m`. The user can choose between these submodels by specifying the value of the parameter `fluid` in one of the routines calling `pipe.m` (see, e.g., the calling routine `example_traverse.m`). Program a new correlation `drift_flux_dpds.m` and compare it against an existing routine.

Tasks

- Study the paper by Shi et al. (2005b) and Section E-3 (Drift Flux Models) in [Appendix E](#).
- Inspect the MATLAB functions `pipe.m` and `Muk_Brill_dpds.m`.
- Write a routine `drift_flux_dpds.m` to compute the pressure drop over an inclined well using the Shi et al. drift flux correlation.
- Test the routine by comparing its results against those of `Muk_Brill_dpds.m` when called by `example_intake_curve.m` for a well with a 60° inclination. Do not change the other parameters. Verify the source of the difference in FBHPs by plotting a traverse for the flow rate that corresponds to the largest difference (near $q_{o,sc} = -0.001 \text{ m}^3/\text{s}$). For this purpose modify `example_traverse.m` as appropriate.

4.7.5 Notes

- The gas holdup has to be computed iteratively (see also [Eqs. E-45](#) and [E-46](#) in [Appendix E](#)). Use Picard iteration and terminate it at a preset relative tolerance (e.g., 10^{-3}). Include an exit strategy to terminate the iteration if the computation does not show convergence within a preset number of iterations. You may need a damping factor in the iteration to avoid oscillations (see [Eq. E-46](#)).
- The Shi et al. correlation uses a different definition of the positive flow direction than this book and the existing MATLAB files. Your file should be able to cope with production in an uphill direction. There is no need to consider production in a downhill direction or injection.
- For the pressure drop calculation, copy the code from `Muk_Brill_dpds.m`.

4.7.6 Deliverables

- MATLAB program listing
- A plot with traverses (with detailed contributions from gravity and friction) and a plot with intake curves, each displaying the results for `Muk_Brill_dpds.m` and

Chapter 5

Flow Through Restrictions

5.1 What Is Covered in This Chapter?

In this chapter we discuss the steady-state pressure drop over restrictions to flow, in particular those that are purposely designed to reduce the pressure in a part of the production system. For single-phase liquid flow it is still possible to describe the essential behavior by starting from mass and momentum balance equations and an isothermal equation of state just as in pipe flow. However, unlike in pipe flow, acceleration losses turn out to play a major role in the pressure drop, in particular in the converging part of a restriction.

For single-phase gas flow, the assumption of isothermal flow is no longer valid, and a more elaborate analysis is required to compute the pressure drop. Here we use the classic assumption of isentropic (frictionless-adiabatic) flow to compute the acceleration-dominated flow in the converging part. An essential result is that for an increasing pressure drop the gas velocity may become so high that it reaches the speed of sound in gas, a situation known as *choked flow* or *critical flow*. As a result, the pressure downstream of such a choked restriction is no longer influencing the pressure drop, a decoupling that has important practical implications and also causes theoretical restrictions in nodal analysis.

For multiphase (gas/liquid) flow we develop a description analogous to the one for single-phase gas, using the assumption of polytropic (between isothermal and isentropic) flow. The resulting analytical expression for the pressure drop over a restriction, as well as the expression for the critical pressure drop resulting in choked flow, are now implicit and need to be solved iteratively. This is most easily done numerically. Alternatively, simple semiempirical expressions may be used. Both approaches result in (strongly) approximate results which are, however, good enough for typical nodal analysis calculations for production engineering purposes.

5.2 Restrictions

At several points in the production system the flow may encounter restrictions, such as valves or measurement devices. Usually the pressure drop in these components is not desirable and deteriorates the performance of a production system, in particular when a further reduction of flow area occurs because of deposition of solids such as scale or asphaltenes. Sometimes, however, purposely designed restrictions are used to create a pressure drop or to restrict the flow rate in a controlled fashion. These devices, known as *choke valves*, *chokes*, or *beans*, occur in different forms. Fixed-size chokes require a temporary interruption of the production stream if they need to

be changed out for a choke of a different size. Variable-size chokes can be operated under flowing conditions and may be manually operated or remotely controlled. All chokes work on the same principle of dissipating large amounts of energy over a short distance.

Another reason to restrict the flow on purpose is to measure flow rates: A restriction causes a local reduction in pressure that, for a given geometry of the restriction, is a known function of the flow rate. Measuring the pressure drop, which is relatively simple, can thus be used to indirectly measure the flow rate. [Fig. 5.1](#) displays three schematic restriction geometries. In the bottom geometry the flowlines converge between cross section 1, the entrance, and cross section 3, the throat; thereafter they diverge again until an undisturbed flowline pattern is re-established at cross section 4, the exit. The figure is not to scale, and generally it takes a distance of at least 10 times the diameter reduction ($d_1 - d_2$) before the effects of the restriction on the flowline pattern can no longer be noticed. The top of [Fig. 5.1](#) represents an *orifice plate*, a simple circular plate with a circular hole with diameter d_2 . The maximum flowline contraction in an orifice geometry occurs slightly downstream from the orifice at cross section 3, a point known as the *vena contracta*. The corresponding reduced diameter is d_3 .

The same effect occurs in other restrictions with a sudden change in flow area, such as simple chokes, as shown schematically in the middle of [Fig. 5.1](#). Both the orifice and the choke geometries have a region downstream of the restriction where strongly turbulent flow occurs, which may include large vortices or areas of flow reversal. The turbulent flow results in dissipation of energy and a permanent reduction in pressure between the upstream and the downstream side of the restriction. If such a permanent pressure drop is not desired—e.g., when the restriction is meant only to serve as an indirect flowmeter—a geometry as displayed at the bottom of [Fig. 5.1](#) should be applied. A *venturi*, as this is known, allows for a gradual recovery of the original flowline pattern with a minimum of turbulent dissipation and therefore only a small permanent pressure drop. In contrast, choke valves usually have a geometry that severely disturbs the flow and creates strong turbulence because they are designed to dissipate energy and produce a permanent reduction in pressure.

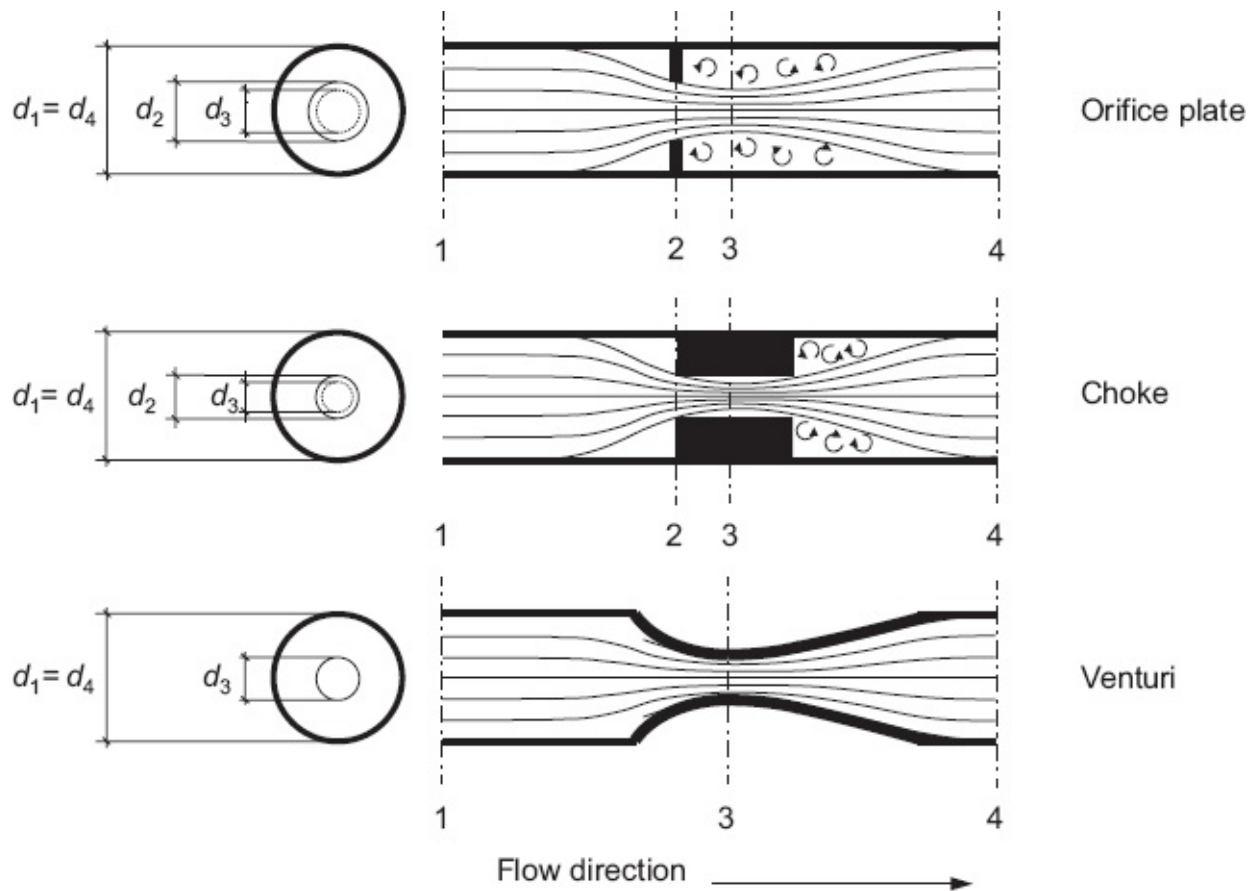


Fig. 5.1—Schematic restriction geometries. The figure is not to scale.

5.3 Single-Phase Oil Flow

5.3.1 Reversible Pressure Drop. A simple semiempirical expression for the pressure drop in incompressible single-phase liquid flow through a sudden restriction is given by

$$p_1 - p_4 = \frac{1}{2} \rho v_2^2 \frac{1}{C_d^2} = \frac{\rho}{2} \frac{q^2}{A_2^2} \frac{1}{C_d^2}, \quad \dots \dots \dots \quad (5.1)$$

where p_1 and p_4 are the pressures at the upstream and the downstream side of the restriction, respectively; $A_2 = \pi (d_2)^2 / 4$ is the throat area; and C_d is an empirical *discharge coefficient*. Eq. 5.1, which has been implemented in MATLAB routine `choke_oil.m`, reflects that the pressure drop over a restriction is proportional to the kinetic energy per unit volume: $E_{\text{kin}}/V = \rho v_2^2/2$, where V is some representative volume for the choke. This is in line with the fact that the flow is highly turbulent, which means that the pressure drop is dominated by inertial forces rather than viscous forces.

A derivation of Eq. 5.1 can be obtained by taking a step back and starting from the pressure drop equation for steady-state pipe flow in a pipe with a diameter that varies along the pipe axis. From experiments it has been determined that the majority of energy dissipation in a restriction occurs in the region of diverging streamlines,

whereas in the converging region the flow experiences only a small friction loss. Therefore we can describe the flow between Points 1 and 3 by disregarding gravity and friction. Following the same approach as in [Section 3.1](#), the steady-state mass and momentum balances can then be written as

$$\underbrace{A\rho v}_{\text{mass rate in}} - \underbrace{\left(A + \frac{\partial A}{\partial s} ds \right) \left(\rho + \frac{\partial \rho}{\partial s} ds \right) \left(v + \frac{\partial v}{\partial s} ds \right)}_{\text{mass rate out}} = 0, \dots \quad (5.2)$$

$$\begin{aligned} & \underbrace{A\rho v^2}_{\text{momentum rate in}} - \underbrace{\left(A + \frac{\partial A}{\partial s} ds \right) \left(\rho + \frac{\partial \rho}{\partial s} ds \right) \left(v + \frac{\partial v}{\partial s} ds \right)^2}_{\text{momentum rate out}} \\ & + \underbrace{Ap}_{\text{left axial force}} + \underbrace{\left(p + \frac{1}{2} \frac{\partial p}{\partial s} ds \right) \left(\frac{\partial A}{\partial s} ds \right)}_{\text{axial force along the pipe}} - \underbrace{\left(A + \frac{\partial A}{\partial s} ds \right) \left(p + \frac{\partial p}{\partial s} ds \right)}_{\text{right axial force}} = 0, \end{aligned} \dots \quad (5.3)$$

where we introduced an extra term to account for the axial component of the force resulting from pressure on the pipe wall. Expanding [Eqs. 5.2](#) and [5.3](#) and dropping all terms higher than first order in the differentials lead to

$$\frac{d(A\rho v)}{ds} = 0, \dots \quad (5.4)$$

$$A\rho v \frac{dv}{ds} + \frac{d(A\rho v)}{ds} v = -A \frac{dp}{ds}, \dots \quad (5.5)$$

from which follows

$$\frac{dp}{ds} = -\rho v \frac{dv}{ds}. \dots \quad (5.6)$$

Note that [Eq. 5.6](#) is no longer dependent on A. Assuming a constant density, the equation can be integrated from s_1 to s_3 according to

$$\int_{p(s_1)}^{p(s_3)} dp = - \int_{v(s_1)}^{v(s_3)} \rho v dv, \dots \quad (5.7)$$

which results in

$$p|_{p_1}^{p_3} = -\frac{1}{2} \rho v^2 \Big|_{v_1}^{v_3}, \dots \quad (5.8)$$

or

$$p_1 + \frac{1}{2} \rho v_1^2 = p_3 + \frac{1}{2} \rho v_3^2. \dots \quad (5.9)$$

[Eq. 5.9](#) is the *Bernoulli equation* for frictionless incompressible flow which can be interpreted as a macroscopic mechanical energy balance (see Bird et al. 2002, §7.4). The frictionless pressure drop over the contracting part of a sudden restriction follows from [Eq. 5.9](#) as

$$p_1 - p_3|_{\text{frictionless}} = \frac{\rho}{2} (v_3^2 - v_1^2) = \frac{\rho}{2} \left(\frac{q^2}{A_3^2} - \frac{q^2}{A_1^2} \right) = \frac{\rho q^2}{2 A_3^2} (1 - \beta_3^2), \quad \dots \quad (5.10)$$

where $A_1 = \pi (d_1)^2 / 4$ is the pipe flow area, $A_3 = \pi (d_3)^2 / 4$ is the area of the vena contracta, and $\beta_3 = A_3 / A_1$. Note that $p_3 < p_1$ (i.e., an increase in velocity corresponds to a decrease in pressure). The true pressure drop in the converging part of a restriction will be somewhat larger than follows from [Eq. 5.10](#) because frictionless flow is an idealization, an effect that can be taken into account by replacing A_3 in [Eq. 5.10](#) by a slightly reduced surface area $\tilde{A}_3 < A_3$. Moreover, Point 3 corresponds to the vena contracta because of the additional streamline contraction downstream of the restriction. To express the pressure drop in terms of the known throat area $A_2 = \pi (d_2)^2 / 4$, one can use a *contraction coefficient*, defined as $\bar{C}_c = A_3/A_2$ for the frictionless case or as $\tilde{C}_c = \tilde{A}_3/A_2 < \bar{C}_c$ for the case with friction. The pressure drop over the converging part of a restriction (i.e., the maximum pressure drop), can now be expressed as

$$p_1 - p_3 = \frac{\rho}{2} \left(\frac{q^2}{\tilde{C}_c^2 A_2^2} - \frac{q^2}{A_1^2} \right) = \frac{\rho q^2}{2 A_2^2} \frac{(1 - \beta_2^2 \tilde{C}_c^2)}{\tilde{C}_c^2}, \quad \dots \quad (5.11)$$

where $\beta_2 = A_2 / A_1$. (Note that some publications define the contraction coefficient as the diameter ratio d_3/d_2 instead of a surface area ratio. Also, β is sometimes defined as a ratio of diameters.) Alternatively, this effect is accounted for with a discharge coefficient \tilde{C}_d in which case [Eq. 5.11](#) becomes

$$p_1 - p_3 = \frac{\rho q^2}{2 A_2^2} \frac{(1 - \beta_2^2)}{\tilde{C}_d^2}. \quad \dots \quad (5.12)$$

Comparison of [Eqs. 5.11](#) and [5.12](#) shows that the contraction and discharge coefficients are related as

$$\tilde{C}_d^2 = \frac{(1 - \beta_2^2) \tilde{C}_c^2}{1 - \beta_2^2 \tilde{C}_c^2} \quad \dots \quad (5.13)$$

For turbulent flow the value of \tilde{C}_c is usually taken as 0.62 for a sharp edged orifice, but it may become even smaller for other types of sudden restrictions. The corresponding value of \tilde{C}_d for an orifice is therefore typically smaller than 0.4. Note that \tilde{C}_d reflects only the losses in the converging part of the restriction, whereas C_d in [Eq. 5.1](#) reflected the losses over the entire restriction.

Because orifices are often used as indirect flowmeters, it is useful to rewrite Eq. 5.12 in terms of the flow rate q as a function of pressure drop, resulting in an expression known as the *orifice equation*:

$$q = -\tilde{C}_d A_2 \sqrt{\frac{2(p_1 - p_3)}{\rho(1 - \beta_2^2)}} = -\tilde{C}_d A_2 \sqrt{\frac{2(p_1 - p_3)}{\rho}}, \dots \quad (5.14)$$

where the approximation is valid for small values of β and where we have used a minus sign under the assumption that the flowmeter is mounted in the production stream. Alternatively, the orifice equation can be expressed in terms of mass flow rate $\dot{m} = \rho q$ as

$$\dot{m} = -\tilde{C}_d A_2 \sqrt{\frac{2\rho(p_1 - p_3)}{(1 - \beta_2^2)}} = -\tilde{C}_d A_2 \sqrt{2\rho(p_1 - p_3)}. \dots \quad (5.15)$$

5.3.2 Permanent Pressure Drop. In theory, a large part of the pressure drop over the converging part of a restriction is reversible because the flow is nearly frictionless. However, in the diverging part there is usually a high amount of energy dissipation, resulting in a limited pressure recovery and, therefore, a considerable permanent pressure drop (see Fig. 5.2). An exception are venturis, which by design have very small permanent losses. In chokes the energy dissipation is usually so high that there is only a very small pressure recovery in the diverging section. For a well-defined and simple geometry, such as an orifice, it is possible to determine the permanent pressure drop theoretically using the Bernoulli equation with an additional loss term (see, e.g., Bird et al. 2002).

For complex geometries, as in chokes, the permanent pressure drop needs to be determined experimentally. The resulting permanent pressure drop $\Delta p_{\text{perm}} = p_1 - p_4$ can then be expressed with the aid of Eq. 5.12 as

$$\Delta p_{\text{perm}} = f_{\text{perm}} \Delta p_{\text{max}} = f_{\text{perm}} (p_1 - p_3) = f_{\text{perm}} \frac{\rho}{2} \frac{q^2}{A_2^2} \frac{(1 - \beta_2^2)}{\tilde{C}_d^2}, \dots \quad (5.16)$$

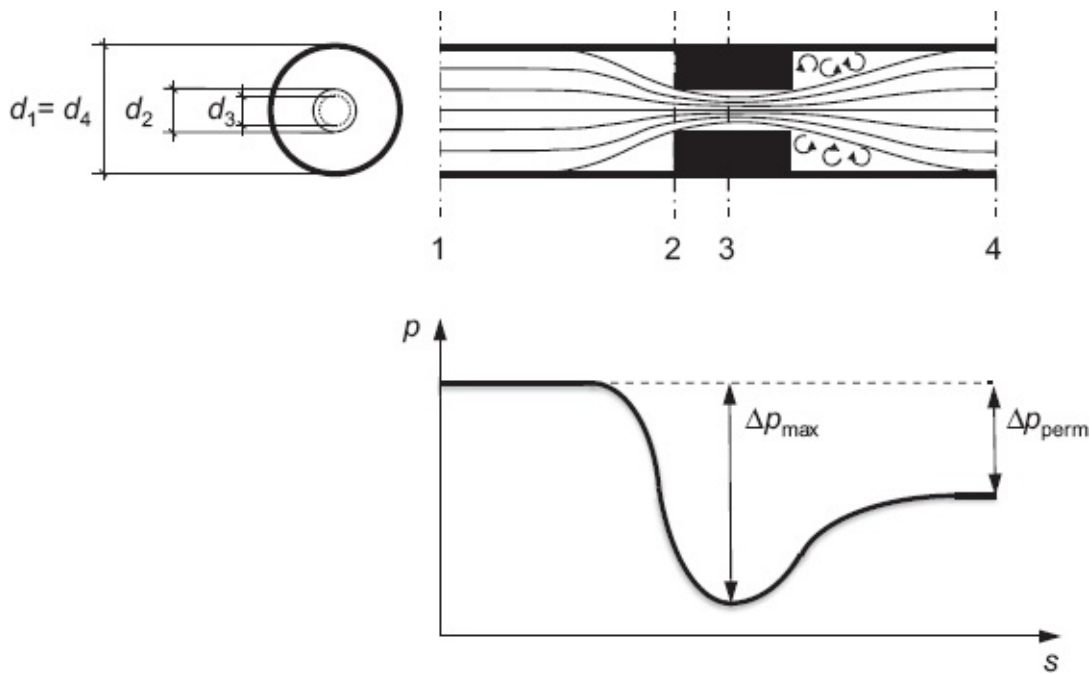


Fig. 5.2—Schematic pressure distribution in a choke. The figure is not to scale.

where f_{perm} is a *permanent pressure drop factor*, which may have values ranging from close to zero, for venturis, to close to unity, for complex-shaped chokes. Note, however, that slightly different definitions may be encountered in the literature. For example, Perry et al. (1997, 8–74) define the *pressure recovery factor* f_{rec} as the square root of the permanent pressure drop factor.

Comparison with Eq. 5.1 shows that the permanent pressure drop can also be expressed with a single discharge coefficient C_d as

$$\Delta p_{\text{perm}} = p_1 - p_4 = \frac{\rho}{2} \frac{q^2}{A_2^2} \frac{1}{C_d^2}, \quad \dots \quad (5.17)$$

such that

$$C_d = \frac{\tilde{C}_d}{\sqrt{f_{\text{perm}}(1-\beta_2^2)}} = \frac{\tilde{C}_c}{\sqrt{f_{\text{perm}}(1-\beta_2^2 \tilde{C}_c^2)}}, \quad \dots \quad (5.18)$$

which accounts for (1) the effects of the term $1-\beta_2^2$; (2) the effect of irreversible losses in the diverging part, as represented by f_{perm} ; and (3) the combined effects of irreversible losses and streamline contraction in the converging part, as represented by either \tilde{C}_d or \tilde{C}_c . Note that because $\Delta p_{\text{perm}} < \Delta p_{\text{max}}$ it is necessary that

$$C_d > \frac{\tilde{C}_d}{\sqrt{1-\beta_2^2}}. \quad \dots \quad (5.19)$$

For most restriction types, the precise values of \tilde{C}_d and f_{perm} are not known.

However, values for C_d have been extensively published in the form of tables and charts for various restriction geometries such as bends or valves. Typical values range from 0.7 to 1.2. Note that in some publications, it is stated that the value of the discharge coefficient can never exceed unity. This is indeed the case for \tilde{C}_d because it reflects only pressure losses not accounted for in the isentropic flow model. However, C_d also reflects pressure recovery and may thus have a value larger than unity. Note also that different definitions of the discharge coefficient and related variables are used throughout the literature.

A related quantity is the *valve coefficient* C_v , also known as the *flow coefficient*, which is sometimes used to quantify the capacity of a valve as determined experimentally by pumping water through it at a known rate and measuring the resulting pressure drop:

$$C_v = \hat{q} \sqrt{\frac{\gamma_w}{\Delta \hat{p}}}, \dots \quad (5.20)$$

where \hat{q} is the flow rate in US gallons per minute, γ_w is the specific gravity of the liquid flowing through the valve, and $\Delta \hat{p}$ is the pressure drop in psi. Note that the dimensions of C_v are gal/min- $\sqrt{\text{psi}}$, whereas C_d is dimensionless. The pressure drop in Pa over a valve with valve coefficient C_v gal/min- $\sqrt{\text{psi}}$ for single-phase flow of a liquid with density ρ (kg/m^3) at a flow rate of q (m^3/s) can therefore be expressed as

$$\underbrace{\frac{\Delta p(\text{Pa})}{6.895 \times 10^3}}_{\text{lbf/in.}^2} = \frac{\left[\frac{q(\text{m}^3/\text{s})}{6.309 \times 10^{-5}} \right]^2 \frac{\rho(\text{kg}/\text{m}^3)}{1000 \text{ kg}/\text{m}^3}}{\underbrace{(gal/min)^2}_{\text{gal}^2 \times \text{in.}^2 / (\text{min}^2 \times \text{lbf})} \underbrace{C_v^2}_{(-)}}, \dots \quad (5.21)$$

from which follows

$$\Delta p = 1.732 \times 10^9 \frac{q^2 \rho}{C_v^2} \text{ Pa}. \dots \quad (5.22)$$

5.3.3 Choke Performance Curves. Fig. 5.3 depicts a *choke performance curve*—i.e., a plot of tubinghead pressure vs. flow rate flow through a wellhead choke—for four different choke sizes as computed with MATLAB file `choke_oil.m`. The corresponding values of d_2/d_1 and β_2 have been displayed in Table 5.1. The discharge coefficient $C_d = 0.7$. In practice, single-phase oil flow through a choke seldom occurs because usually the pressure at the wellhead is below the bubblepoint pressure. However, the figure clearly illustrates the quadratic relationship between pressure drop and flow rate for singlephase liquid flow. Moreover, single-phase liquid flow through a restriction does occur in measurement devices such as orifices or venturis.

5.4 Single-Phase Gas Flow

5.4.1 Isentropic Flow. Unlike what we did for single-phase gas flow through pipes, where we assumed isothermal conditions, we cannot neglect the change in temperature for gas flow through restrictions. A full thermodynamic analysis would require the use of a total energy balance, in addition to the mass balance equation ([Eq. 3.3](#)) and the momentum balance equation ([Eq. 3.4](#)) derived in [Section 3.1](#). We refer to Bird et al. (2002) or a thermodynamics textbook such as Moran and Shapiro (1998) for such a nonisothermal analysis. In the most general case this requires the simultaneous solution of three coupled partial-differential equations together with an algebraic equation of state (EOS) to obtain the unknown values of pressure, density, velocity, and temperature as a function of time and space. Because of the rapid compression and expansion of gas in a restriction, however, there is very little time for energy exchange with the surroundings and the flow can thus be considered *adiabatic*. Furthermore, we may neglect the friction forces when we consider the flow in the converging section of the restriction, just as we did for single-phase oil. This implies that the converging flow may be considered *isentropic*, a thermodynamic condition also indicated as *frictionless-adiabatic* or *reversible-adiabatic*. Under adiabatic conditions, there is no exchange of energy with the surroundings, whereas reversibility implies that there is no change in entropy. A full derivation of the thermodynamic relationship in this section is outside the scope of this text, and we refer to thermodynamics textbooks instead; see, e.g., Moran and Shapiro (1998), [Chapter 6](#), for a detailed description of isentropic processes.

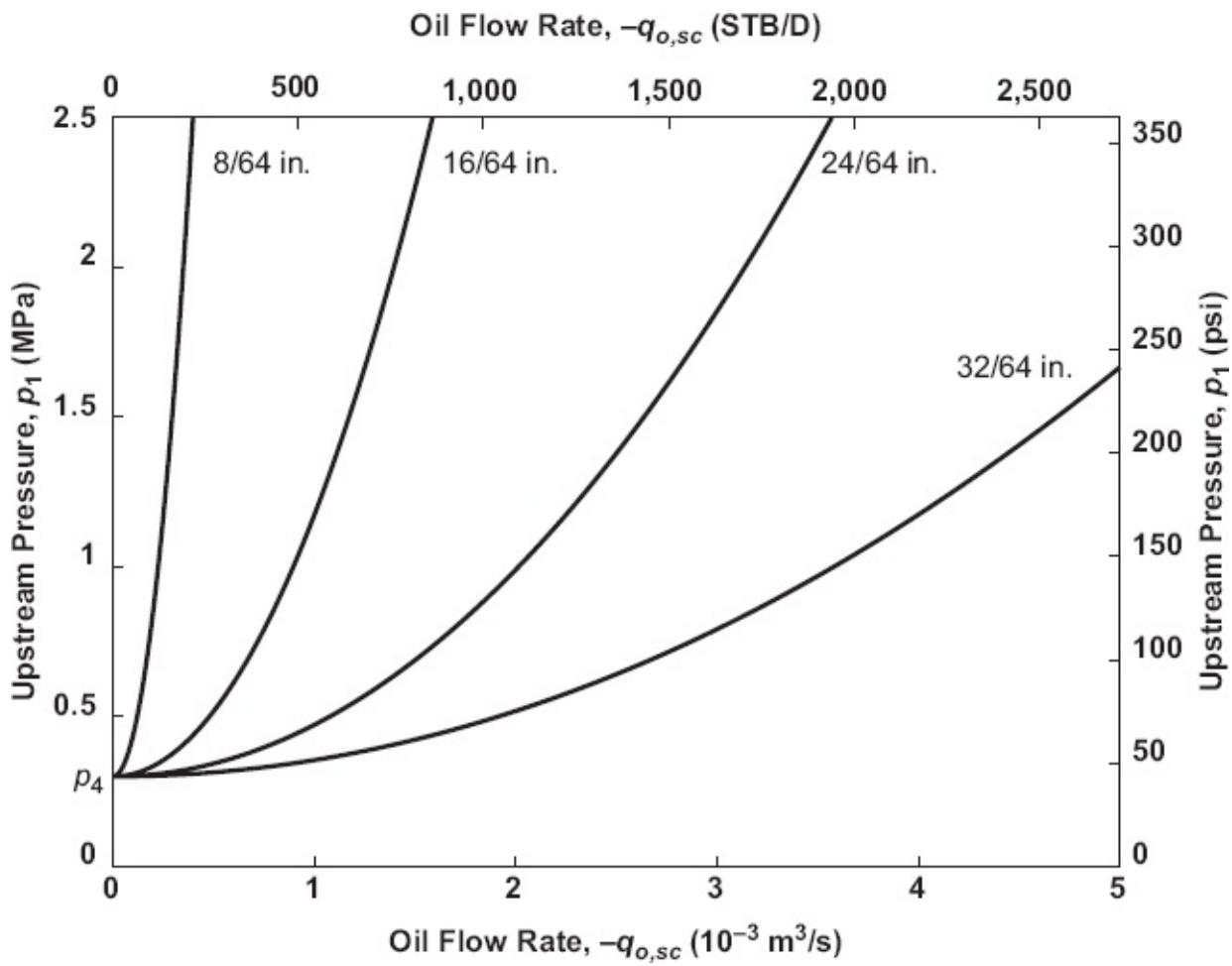


Fig. 5.3—Choke performance curves for single-phase oil flow through four different chokes with $C_d = 0.7$ and sizes 1–4 as specified in Table 5.1. The downstream pressure $p_4 = 0.3 \text{ MPa}$. The other properties have been taken from Table 4.1.

	Size (in.)	Size (mm)	d_2/d_1	β_2
d_1 all chokes	2.453	62.31	—	—
d_2 choke 1	8/64	3.18	0.051	0.002 6
d_2 choke 2	16/64	6.35	0.102	0.010 4
d_2 choke 3	24/64	9.53	0.153	0.023 4
d_2 choke 4	32/64	12.70	0.204	0.041 6
d_2 choke 5	40/64	15.88	0.255	0.064 9
d_2 choke 6	48/64	19.05	0.306	0.093 5

Table 5.1—Choke sizes, corresponding flow diameter ratios d_2/d_1 , and surface area ratios $\beta_2 = (d_2/d_1)^2$ for figs. 5.2, 5.3, and 5.5.

In the case of isentropic flow it is not necessary to solve a differential equation to obtain the change in temperature in the flowing gas. Instead we can use an algebraic relationship between pressure and temperature, which for an ideal gas can be expressed as

$$\frac{p^{\gamma}}{T_{\text{abs}}} = C, \dots \dots \dots \quad (5.23)$$

where C is a constant and where γ is the ratio of specific heat capacities at constant pressure and constant volume:

$$\gamma = \frac{c_p}{c_v} \dots \dots \dots \quad (5.24)$$

The corresponding EOS for an ideal gas under isentropic conditions can be expressed as

$$\frac{p}{\rho^\gamma} = C \dots \dots \dots \quad (5.25)$$

(Note that for isothermal conditions, the EOS for an ideal gas (Eq. 5.25) can simply be expressed as $p/\rho = C$.)

With the aid of Eq. 5.23 we can also write that

$$\frac{T_{1,\text{abs}}}{T_{3,\text{abs}}} = \left(\frac{p_1}{p_3} \right)^{\frac{1}{\gamma}}, \dots \dots \dots \quad (5.26)$$

and then use the definition of the gas formation volume factor (Eq. 2.34) to obtain the relationship

$$\frac{B_1}{B_3} = \left(\frac{p_3}{p_1} \right)^{\frac{1}{\gamma}}, \dots \dots \dots \quad (5.27)$$

where we used $Z_1 = Z_3 = 1$ because we restrict the derivation to ideal gases. (The equivalent expressions for a nonideal gas are more complex and therefore outside the scope of this book.) The value of γ is dependent on the gas composition and pressure. For hydrocarbon gases under moderate pressures γ is usually chosen as a constant with a value somewhere between 1.25 and 1.40.

Just as for single-phase liquid flow, we can now use Eq. 5.6 as a starting point for the derivation of the pressure drop equation. After dividing both sides by ρ we obtain

$$\frac{1}{\rho} \frac{dp}{ds} = -v \frac{dv}{ds}, \dots \dots \dots \quad (5.28)$$

Substitution of Eq. 5.25 in the left side along with integration from s_1 to s_3 results in

$$\int_{s_1}^{s_3} \frac{1}{\rho} \frac{dp}{ds} ds = \int_{s_1}^{s_3} \left(\frac{C}{p} \right)^{\frac{1}{\gamma}} \frac{dp}{ds} ds = C^{\frac{1}{\gamma}} \int_{p_1}^{p_3} p^{-\frac{1}{\gamma}} dp = \frac{C^{\frac{1}{\gamma}} \gamma}{(\gamma-1)} p^{\frac{\gamma-1}{\gamma}} \Big|_{p_1}^{p_3} = \frac{\gamma}{(\gamma-1)} \frac{p}{\rho} \Big|_{p_1}^{p_3}. \dots \dots \dots \quad (5.29)$$

Integration of the right side of Eq. 5.28, and combining the result with Eq. 5.29, gives us the isentropic Bernoulli equation for compressible flow:

$$\frac{\gamma}{\gamma-1} \frac{p_1}{\rho_1} + \frac{1}{2} v_1^2 = \frac{\gamma}{\gamma-1} \frac{p_3}{\rho_3} + \frac{1}{2} v_3^2 \dots \dots \dots \quad (5.30)$$

In analogy to Eq. 5.11 we can now derive an expression for the pressure drop for gas flow through an orifice as

$$\begin{aligned} \frac{p_1}{\rho_1} - \frac{p_3}{\rho_3} &= \frac{1}{2} \frac{\gamma-1}{\gamma} \left(\frac{q_3^2}{\tilde{A}_3^2} - \frac{q_1^2}{A_1^2} \right) \\ &= \frac{1}{2} \frac{\gamma-1}{\gamma} \frac{q_{g,sc}^2}{\tilde{A}_3^2} (B_3^2 - \beta_3^2 B_1^2) \\ &= \frac{1}{2} \frac{\gamma-1}{\gamma} \frac{q_{g,sc}^2}{A_2^2} \left(\frac{B_3^2 - \beta_2^2 B_1^2 \tilde{C}_c^2}{\tilde{C}_c^2} \right), \end{aligned} \quad \dots \dots \dots \quad (5.31)$$

or

$$B_1 p_1 - B_3 p_3 = \frac{\rho_{g,sc}}{2} \frac{\gamma-1}{\gamma} \frac{q_{g,sc}^2}{A_2^2} \left(\frac{B_3^2 - \beta_2^2 B_1^2 \tilde{C}_c^2}{\tilde{C}_c^2} \right), \quad \dots \dots \dots \quad (5.32)$$

where the coefficients β and B indicate surface area ratios and formation volume factors, respectively. In analogy to Eq. 5.12 for single-phase oil flow, we can now also write

$$\begin{aligned} B_1 p_1 - B_3 p_3 &= \frac{\rho_{g,sc}}{2} \frac{\gamma-1}{\gamma} \frac{q_{g,sc}^2}{A_2^2} \left(\frac{B_3^2 - \beta_2^2 B_1^2}{\tilde{C}_d^2} \right) \\ &\approx \frac{\rho_{g,sc}}{2} \frac{\gamma-1}{\gamma} \frac{q_{g,sc}^2 B_3^2}{A_2^2 \tilde{C}_d^2} \end{aligned} \quad \dots \dots \dots \quad (5.33)$$

where the discharge coefficient \tilde{C}_d accounts for the contraction effect and for the irreversible losses in the converging part of the restriction. The approximation $1 - \beta_2^2 B_1^2 / B_3^2 \approx 1$ is justified, given the error already introduced by restricting the analysis to ideal gases.

Although Eq. 5.33 resembles Eq. 5.12, it cannot be solved explicitly for one of the pressures as a function of the other pressure and the flow rate because the formation volume factors are functions of the unknown pressure. Therefore an iterative procedure is needed to compute the maximum pressure drop $\Delta p_{max} = p_1 - p_3$. During the iteration, Eqs. 5.26 and 5.27 should be used to express unknown downstream values T_3 and B_3 in terms of known upstream values T_1 and B_1 , or the other way around. Note that we should still use the formation volume factor with the correct Z value for one of the values B_1 or B_3 because the restriction to ideal gases that applies to Eq. 5.27 is relevant only for the pressure drop over the choke. The iteration

procedure can be implemented in MATLAB with the aid of one of the methods described in [Appendix D](#). For example, if it is required to compute the upstream pressure p_1 for a given downstream pressure p_3 and upstream temperature T_1 , we can combine [Eqs. 5.33](#) and [5.27](#) as

$$f(p_1) = B_1(p_1, T_1) \left[p_1 - \left(\frac{p_3}{p_1} \right)^{\frac{1}{\gamma}} p_3 \right] - \frac{\rho_{g,sc}}{2} \frac{\gamma - 1}{\gamma} \frac{q_{g,sc}^2 \left[\left(\frac{p_3}{p_1} \right)^{\frac{1}{\gamma}} B_1(p_1, T_1) \right]^2}{A_2^2 \tilde{C}_d^2} = 0 \quad (5.34)$$

and solve for the roots of this equation—i.e., the values of p_1 for which $f(p_1)$ becomes equal to zero—with the aid of one of the methods described in [Appendix D](#). Although the pressure drop needs to be computed iteratively, it is still possible to obtain an explicit orifice equation (i.e., an expression for the flow rate $q_{g,sc}$ as a function of the known pressures p_1 and p_3):

$$q_{g,sc} = -\tilde{C}_d A_2 \sqrt{\frac{2p_1}{\rho_{g,sc} B_1} \frac{\gamma}{\gamma - 1} \left[\frac{B_1^2}{B_3^2} - \frac{B_1}{B_3} \left(\frac{p_3}{p_1} \right) \right]}, \dots \quad (5.35)$$

where the minus sign stems from our convention that production flow rates are negative. With the aid of [Eqs. 5.26](#) and [5.27](#), [Eq. 5.35](#) can be rewritten as

$$\begin{aligned} q_{g,sc} &= -\tilde{C}_d A_2 \sqrt{\frac{2p_1}{\rho_{g,sc} B_1} \frac{\gamma}{\gamma - 1} \left[\left(\frac{p_3}{p_1} \right)_{crit}^{\frac{2}{\gamma}} - \left(\frac{p_3}{p_1} \right)_{crit}^{\frac{1+\gamma}{\gamma}} \right]} \\ &= -\tilde{C}_d A_2 \sqrt{\frac{2p_1^2 T_{sc,abs}}{P_{sc} T_{1,abs} Z_1 \rho_{g,sc}} \frac{\gamma}{\gamma - 1} \left[\left(\frac{p_3}{p_1} \right)_{crit}^{\frac{2}{\gamma}} - \left(\frac{p_3}{p_1} \right)_{crit}^{\frac{1+\gamma}{\gamma}} \right]}. \end{aligned} \quad (5.36)$$

or, in terms of the mass flow rate \dot{m}_g , as

$$\dot{m}_g = q_{g,sc} \rho_{g,sc} = -\tilde{C}_d A_2 \sqrt{2p_1 \rho_1 \frac{\gamma}{\gamma - 1} \left[\left(\frac{p_3}{p_1} \right)^{\frac{2}{\gamma}} - \left(\frac{p_3}{p_1} \right)^{\frac{1+\gamma}{\gamma}} \right]}, \dots \quad (5.37)$$

which is the conventional representation in the gas engineering literature.

5.4.2 Critical Flow. [Eq. 5.36](#) is a relation between the flow rate $q_{g,sc}$ and the pressure ratio (p_3/p_1). It can be verified that for a given upstream pressure p_1 , $q_{g,sc}$ has a maximum that occurs when the derivative $d(q_{g,sc})/d(p_3/p_1)$ is equal to zero. To find the corresponding value of the pressure ratio, it is sufficient to take the derivative of the term between square brackets. (This is equivalent to computing the maximum of $q_{g,sc}^2$)

instead of $q_{g,sc}$, which removes the square root from the expression.) Starting from Eq. 5.37 this results in

$$\frac{2}{\gamma} \left(\frac{p_3}{p_1} \right)^{\frac{2-\gamma}{\gamma}} - \frac{1+\gamma}{\gamma} \left(\frac{p_3}{p_1} \right)^{\frac{1}{\gamma}} = 0. \dots \quad (5.38)$$

Eq. 5.38 can be solved for (p_3/p_1) , resulting in

$$\left(\frac{p_3}{p_1} \right)_{\text{crit}} = \left(\frac{2}{1+\gamma} \right)^{\frac{\gamma}{\gamma-1}}. \dots \quad (5.39)$$

For typical values of γ between 1.25 and 1.40, we therefore find

$$0.53 < \left(\frac{p_3}{p_1} \right)_{\text{crit}} < 0.55, \dots \quad (5.40)$$

or

$$1.8 < \left(\frac{p_1}{p_3} \right)_{\text{crit}} < 1.9. \dots \quad (5.41)$$

The velocity corresponding to this *critical pressure ratio* that occurs in the throat of the restriction is equal to the *sonic velocity* (i.e., the speed of sound) under isentropic conditions. The corresponding expression for *critical flow* of an ideal gas can be found by substitution of Eq. 5.39 into Eq. 5.36, which results in

$$\begin{aligned} q_{g,sc} &= -\tilde{C}_d A_2 \sqrt{\frac{2p_1}{\rho_{g,sc} B_1} \frac{\gamma}{\gamma-1} \left[\left(\frac{p_3}{p_1} \right)_{\text{crit}}^{\frac{2}{\gamma}} - \left(\frac{p_3}{p_1} \right)_{\text{crit}}^{\frac{1+\gamma}{\gamma}} \right]} \\ &= -\tilde{C}_d A_2 \sqrt{\frac{2p_1^2 T_{sc,\text{abs}}}{p_{sc} T_{1,\text{abs}} Z_1 \rho_{g,sc}} \frac{\gamma}{\gamma-1} \left[\left(\frac{p_3}{p_1} \right)_{\text{crit}}^{\frac{2}{\gamma}} - \left(\frac{p_3}{p_1} \right)_{\text{crit}}^{\frac{1+\gamma}{\gamma}} \right]}. \end{aligned} \quad (5.42)$$

Rewriting Eq. 5.42 in terms of p_1 results in an expression for the upstream pressure for ideal gas flow through a *critical choke* (i.e., a choke operating under critical conditions):

$$p_1 = -\frac{|q_{g,sc}|}{\tilde{C}_d A_2 \sqrt{\frac{2T_{sc,\text{abs}}}{p_{sc} T_{1,\text{abs}} Z_1 \rho_{g,sc}} \frac{\gamma}{\gamma-1} \left[\left(\frac{p_3}{p_1} \right)_{\text{crit}}^{\frac{2}{\gamma}} - \left(\frac{p_3}{p_1} \right)_{\text{crit}}^{\frac{1+\gamma}{\gamma}} \right]}}, \dots \quad (5.43)$$

which has to be solved iteratively because of the pressure dependence of Z_1 . Note

that the term between square brackets has a fixed value and is not dependent on p_1 . Eq. 5.43 for critical choke flow forms an almost linear relationship between p_1 and $q_{g,sc}$, the small deviation from linearity being caused by the pressure dependence of Z_1 . With the aid of Eqs. 5.26 and 5.39 it follows that the throat temperature T_3 under critical flow conditions becomes

$$T_{3,\text{abs}} = \frac{2}{1+\gamma} T_{1,\text{abs}} \dots \quad (5.44)$$

For typical values of γ between 1.25 and 1.40, this implies a temperature reduction over the converging part of the choke in between $T_{3,\text{abs}} = 0.89 T_{1,\text{abs}}$ and $T_{3,\text{abs}} = 0.83 T_{1,\text{abs}}$. A computation of the critical pressure and temperature ratios for real gases is quite involved and beyond the scope of this book (see, e.g., Cornelius and Srinivas 2004).

The occurrence of critical flow in an orifice used for flow rate measurements is usually avoided to limit the magnitude of the permanent pressure drop. In many other restrictions, however, in particular in choke valves, critical flow frequently occurs. Indeed, the name of such a valve stems from the fact that once the fluid flowing through the valve reaches the critical pressure ratio, the flow is *choked*; i.e., the maximum possible mass flow rate through the choke has been reached (for a given upstream pressure). Another effect of reaching the speed of sound in a choke is that disturbances can no longer travel upstream. The reason for this effect is the finite propagation speed of disturbances. In a 1D conduit filled with a stationary fluid, a small pressure disturbance will result in two waves, both traveling at the speed of sound, away from the point of disturbance and in opposite directions. If the fluid is not stationary but flows through the conduit, the two waves will be influenced such that one will travel faster and the other slower. If the fluid moves so fast that it reaches the sonic velocity, one of the waves will travel at twice the sonic velocity (relative to the conduit) while the other wave will become stationary. As a consequence of this effect any change in back pressure in a gas treatment facility will travel through the flowlines in the direction of the reservoir but will not pass through any choke operating at a critical condition. Although this description is simplistic, it captures the basic idea. For a more detailed thermodynamic analysis of compressible flow in a restriction, see, e.g., Cornelius and Srinivas (2004).

Recall that critical flow was encountered earlier, in [Section 3.4](#), where an isothermal expression for the speed of sound in a gas well was derived. In reality such high flow velocities will not occur in gas wells, except in case of a *blowout* (i.e., an accidental loss of well control). However, in choke valves critical flow occurs frequently.

5.4.3 Pressure Drop in Chokes. *Sub-critical Flow.* The maximum pressure drop $\Delta p_{\max} = p_1 - p_3$ during sub-critical single-phase gas flow in a choke can be computed with the aid of Eq. 5.33, which needs to be solved iteratively because of the pressure

and temperature dependence of B_1 and B_3 . In analogy to Eq. 5.16, the permanent pressure drop during sub-critical flow could, in theory, be approximated with an empirical permanent pressure drop factor f_{perm} according to

$$\Delta p_{\text{perm}} = p_1 - p_4 = f_{\text{perm}} \Delta p_{\text{max}} = f_{\text{perm}} (p_1 - p_3), \dots \quad (5.45)$$

where values of f_{perm} for chokes probably range from 0.5 to 1.0 with most likely values at the high end. However, values for f_{perm} are usually unavailable, and a more pragmatic solution is therefore often introduced through simply replacing the discharge coefficient \tilde{C}_d for the converging part of the choke in Eq. 5.33 by an overall discharge coefficient C_d for the entire choke. Note that because C_d accounts for the partial pressure recovery in the diverging part, it should always hold that $C_d > \tilde{C}_d$. An approximate solution for the pressure drop over the entire choke can therefore be obtained by iteratively solving the equivalent of Eq. 5.33:

$$B_1 p_1 - B_4 p_4 = \frac{\rho_{g,\infty}}{2} \frac{\gamma - 1}{\gamma} \frac{q_{g,\infty}^2 B_4^2}{A_2^2 C_d^2}, \dots \quad (5.46)$$

where the corresponding relationship between B_4 and B_1 follows from Eq. 5.27 as

$$B_4 = \left(\frac{p_4}{p_1} \right)^{\frac{1}{\gamma}} B_1. \dots \quad (5.47)$$

Because of the significant friction losses in the diverging part of the choke, the assumption of isentropic flow is no longer accurate and this relationship is therefore now only a rough estimate. Note that either B_1 or B_4 should be computed in the usual way, using the correct real-gas Z value, whereafter the other value should be approximated with the ideal-gas isentropic relationship shown in Eq. 5.47 (see also the comments after Eq. 5.33).

A more accurate analysis of the pressure recovery in the diverging part of a gas choke would require thermodynamical computations beyond the level of this book. We will also not pursue an analysis of the temperature recovery, but we do know that the downstream temperature T_4 will always be higher than T_3 because of the dissipation of mechanical energy in the form of heat.

Critical Flow. The critical flow boundary in terms of the downstream pressure p_4 can, in theory, be obtained with the aid of Eq. 5.45 as

$$\left(\frac{p_4}{p_1} \right)_{\text{crit}} = 1 - f_{\text{perm}} \left[1 - \left(\frac{p_3}{p_1} \right)_{\text{crit}} \right] \dots \quad (5.48)$$

Although actual values of f_{perm} are usually unknown, Table 5.2 gives an idea of the possible range of critical pressure ratios for f_{perm} values between 0.7 and 1.0 at two different values of γ . Note that if we assume that $f_{\text{perm}} = 1$, Eq. 5.48 reduces to the

equivalent of Eq. 5.39:

$$\left(\frac{p_4}{p_1}\right)_{\text{crit}} = \left(\frac{2}{1+\gamma}\right)^{\frac{\gamma}{\gamma-1}}, \quad \dots \dots \dots \quad (5.49)$$

which seems to be the expression that is most often encountered in the petroleum literature. To compute the upstream pressure in critical choke flow, we can follow the same approach as for sub-critical flow and simply use an overall discharge coefficient C_d . The equivalent of Eq. 5.43 then becomes

	$\gamma \approx 1.25$		$\gamma \approx 1.40$	
f_{perm}	$(p_4/p_1)_{\text{crit}}$	$(p_1/p_4)_{\text{crit}}$	$(p_4/p_1)_{\text{crit}}$	$(p_1/p_4)_{\text{crit}}$
0.7	0.69	1.46	0.67	1.49
0.8	0.64	1.56	0.62	1.61
0.9	0.60	1.68	0.58	1.74
1.0	0.55	1.82	0.53	1.89

Table 5.2—Critical pressure ratios for single-phase gas chokes.

$$p_1 = \frac{|q_{g,sc}|}{C_d A_2 \sqrt{\frac{2T_{sc,\text{abs}}}{p_{sc} T_{1,\text{abs}}} \frac{\gamma}{\gamma-1} \left[\left(\frac{p_4}{p_1}\right)_{\text{crit}}^{\frac{2}{\gamma}} - \left(\frac{p_4}{p_1}\right)_{\text{crit}}^{\frac{1+\gamma}{\gamma}} \right]}}, \quad \dots \dots \dots \quad (5.50)$$

which has to be solved iteratively because of the pressure dependence of Z_1 . A more accurate analysis of the pressure and temperature reversal during critical flow requires thermodynamics theory outside the scope of this book. In simple terms, the gas further accelerates after passing through the throat and reaches a supersonic velocity, which corresponds to a further drop in pressure. The recovery to downstream pressure p_4 then occurs in a thin region where both pressure and temperature increase abruptly in the form of a stationary *shock wave*. It may be assumed that there is no wall friction and no exchange of heat with the surroundings in the diverging part of a choke under critical conditions (i.e., that the flow is *isenthalpic*). However, the change in thermodynamic state is no longer reversible, and inside the shock there is a large conversion of mechanical energy to thermal energy, which is indeed why a choke causes a considerable permanent pressure drop.

Computations. We can use the approximate equations for gas flow through a choke, i.e., those based on an overall discharge coefficient C_d , in the following scenarios:

1. To compute the gas flow rate for a given pressure drop. In this scenario it is

necessary to first compute the effective pressure ratio according to

$$\left(\frac{p_4}{p_1}\right)_{\text{eff}} = \max \left[\left(\frac{p_4}{p_1}\right), \left(\frac{p_4}{p_1}\right)_{\text{crit}} \right], \dots \dots \dots \quad (5.51)$$

where $(p_4/p_1)_{\text{crit}}$ is given by Eq. 5.49, and then use the equivalents of Eqs. 5.36 and 5.42, which, using the effective pressure ratio, can be expressed jointly as

$$\begin{aligned} q_{g,sc} &= -C_d A_2 \sqrt{\frac{2p_1}{\rho_{g,sc} B_1} \frac{\gamma}{\gamma-1} \left[\left(\frac{p_4}{p_1}\right)_{\text{eff}}^{\frac{2}{\gamma}} - \left(\frac{p_4}{p_1}\right)_{\text{eff}}^{\frac{1+\gamma}{\gamma}} \right]} \dots \dots \dots \quad (5.52) \\ &= -C_d A_2 \sqrt{\frac{2p_1^2 T_{sc,abs}}{p_{sc} T_{1,abs} Z_1 \rho_{g,sc}} \frac{\gamma}{\gamma-1} \left[\left(\frac{p_4}{p_1}\right)_{\text{eff}}^{\frac{2}{\gamma}} - \left(\frac{p_4}{p_1}\right)_{\text{eff}}^{\frac{1+\gamma}{\gamma}} \right]}. \end{aligned}$$

2. To compute the pressure drop over a restriction for a given flow rate and a given downstream pressure. In this scenario it is necessary to investigate both critical and sub-critical flow. Assuming sub-critical flow, the upstream pressure can be computed iteratively with the aid of Eq. 5.46. (Refer to the text just after Eq. 5.33 for a discussion on how to perform the iteration in MATLAB.) If the resulting pressure ratio (p_4/p_1) turns out to be smaller than the critical ratio (Eq. 5.48), the flow is critical and the upstream pressure can be computed iteratively with Eq. 5.50.
3. To compute the pressure drop over a restriction for a given flow rate and a given upstream pressure, the same procedure may be followed as under Point 2. In practice, this third scenario is of relevance only for sub-critical flow. For critical flow we will typically find that the computed upstream pressure is different from the given upstream pressure, which implies that the choke model and/or any of the given parameters are inconsistent.

Option 2 has been implemented in the MATLAB routine `choke_gas.m`. Fig. 5.4 depicts the choke performance curves for gas flow through four differently sized chokes, each with a total discharge coefficient $C_d = 0.7$ and specific heat capacity ratio $\gamma = 1.25$. The horizontal dotted line indicates the boundary between sub-critical and critical flow and has been computed with the aid of Eq. 5.49. According to Eq. 5.44, the temperature at the throat of the choke during critical flow in this example drops to $T_3 \approx 0.89 \times (30 + 273.15) - 273.15 = -3.3^\circ\text{C}$ (i.e., to below the freezing point of water). Note that choke temperatures below the freezing point of water may lead to the formation of ice around the outside of the choke, or worse, to the formation of gas hydrates at the inside. This is especially a problem in offshore installations where the gas is already cooled by seawater during its flow through the riser.

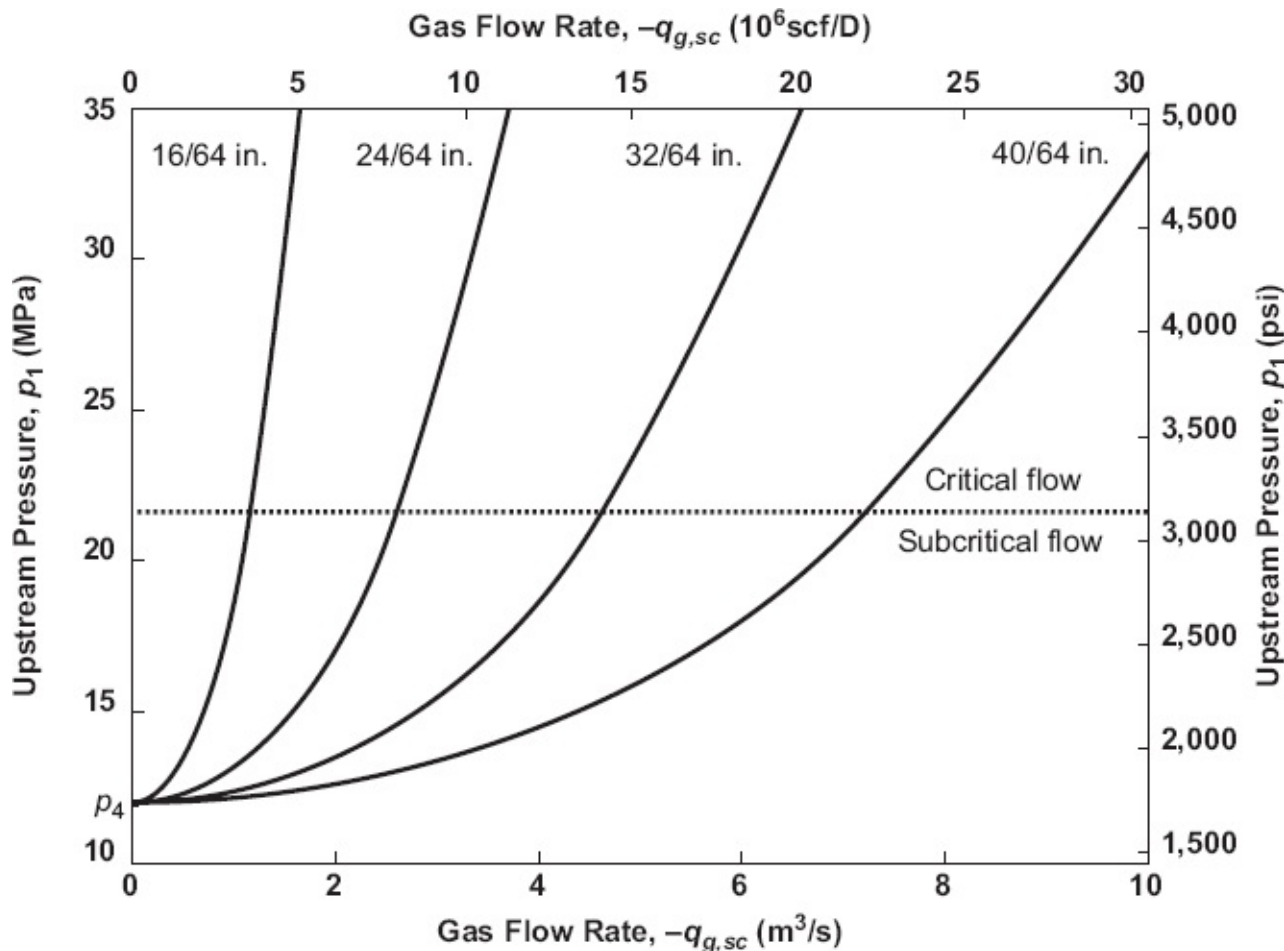


Fig. 5.4—Choke performance curves for the flow of single-phase gas with specific heat capacity ratio $\gamma = 1.25$ through four chokes with discharge coefficient $C_d = 0.7$ and bean sizes 2–5 as specified in Table 5.1. The downstream pressure p_4 and the upstream temperature T_1 are 12 MPa and 30°C respectively. The other properties have been taken from Table 3.1.

5.5 Multiphase Flow: Empirical Models

5.5.1 Multiphase Choke Models. Just as for multiphase flow through pipes, there are many models for multiphase flow through chokes, and they have strongly varying levels of complexity. The simplest models are purely empirical and consist of relationships that have been obtained through curve fitting of experimental data. They are generally applicable to a limited range of choke geometries and fluid properties. At the other end of the scale are detailed models that take into account flashing of components, phase slip, and thermal interactions. These are based on thermodynamics theory that is outside the scope of this book. For a good overview of various choke models and an example of a detailed description see Schüller et al. (2003). Here we will first address some simple empirical models for multiphase choke flow, and thereafter some models at an intermediate level of complexity that have a somewhat more theoretical basis.

5.5.2 Empirical Models for Critical Flow. We define the following variables: $q_{l,sc}$ is

liquid flow rate through the choke, m³/s (STB/D); p_1 is pressure upstream of the choke, Pa (psi); p_3 is pressure at the throat of the choke, Pa (psi); and p_4 is pressure downstream of the choke, Pa (psi).

Just as for single-phase gas flow, for multiphase flow there exists a critical pressure ratio $(p_3/p_1)_{\text{crit}}$. Consider a situation with a constant upstream pressure p_1 and a gradually decreasing downstream pressure p_4 such that the pressure ratio (p_4/p_1) , and therefore also the pressure ratio (p_3/p_1) , gradually decreases. As long as $(p_3/p_1) > (p_3/p_1)_{\text{crit}}$, the flow rate $|q_{l,\text{scl}}|$ increases. This is as expected; the larger the pressure drop, the faster the flow. However, once $p_3/p_1 < (p_3/p_1)_{\text{crit}}$, the flow rate remains constant and a further reduction of p_4 no longer has an effect. Note that it is still possible to increase the flow rate, but only by increasing the upstream pressure p_1 . The importance of critical choke flow for oil well performance is that pressure disturbances downstream can no longer propagate through the choke to the upstream side. Hence the flow behavior becomes independent of the throat pressure p_3 and therefore of the downstream pressure p_4 .

There are advantages in operating the choke at critical conditions. The downstream pressure may vary for many reasons: There may be more wells entering the same manifold, and one of these may be shut in; there may be fluctuations in the processing system; the operating staff may change valve settings in the downstream system; and so on. These effects will not influence the production rate of the well if the choke is operating above critical conditions. Several expressions exist to predict the occurrence of critical multiphase flow through a choke (see, e.g., [Chapter 5](#) of Brill and Mukherjee 1999).

As a rule of thumb, critical flow occurs when the pressure ratio p_4/p_1 is below the critical ratio

$$\left(\frac{p_4}{p_1} \right)_{\text{crit}} \approx 0.6 \approx \frac{1}{1.7}, \dots \quad (5.53)$$

but it should be kept in mind that this is a rather crude approximation of a very complex phenomenon. At sub-critical conditions, the flow rate of a gas/liquid mixture through a choke depends on the specific type of choke, the properties of the multiphase mixture, and so on, and there is no simple pressure drop/flow rate relationship. At critical conditions, there are a number of empirical correlations (see, e.g., Gilbert 1954 or Ros 1960). Other correlations are connected to the names of Baxendell and Achong (see Brill and Mukherjee 1999). Each of these has been determined from a limited set of measurements for specific fluid properties and choke types, and it is therefore not possible to make a general recommendation as to which of them is preferred. The reason to list multiple correlations is, rather, to emphasize the approximate nature of the underlying empirical models and illustrate their range of uncertainty. Moreover, their formulation can serve as a template to develop a new correlation for a specific field situation. All of them have the form

$$p_1 = -A q_{l,sc} \frac{(ER_{gl})^B}{(Fd_{ch})^C} + D, \dots \quad (5.54)$$

where R_{gl} is producing gas/liquid ratio, m^3/m^3 (scf/STB), d_{ch} is choke diameter, m (1/64 in.), and A , B , C , and D are experimentally determined constants given in **Table 5.3**. Here, we have assumed that $q_{l,sc}$ has a negative value in line with our convention that flow rates in production wells are negative. Note that in field units the diameter is specified in 1/64 of an inch. For a given choke size, the choke performance curve is a linear function of the flow rate (see **Fig. 5.5**). (Note that here we plotted just the oil flow rate rather than the liquid flow rate.) For a fixed pressure, the flow rate is approximately equal to the square of the choke diameter (i.e., the cross-sectional area, as might be expected). For upstream pressures below approximately 1.7 times the downstream pressure p_4 , these curves are of course invalid because then the choke operates in the sub-critical regime.

5.5.3 Empirical Models for Sub-critical Flow. An extension of these empirical models to the sub-critical regime can be obtained as follows. From **Eq. 5.54** it follows that the flow rate at the critical pressure ratio is given by

Correlation	SI Units					
	<i>A</i>	<i>B</i>	<i>C</i>	<i>D</i>	<i>E</i>	<i>F</i>
Gilbert	3.75×10^{10}	0.546	1.89	1.01×10^5	5.61	2.52×10^3
Ros	6.52×10^{10}	0.500	2.00	1.01×10^5	5.61	2.52×10^3
Baxendell	3.58×10^{10}	0.546	1.93	1.01×10^5	5.61	2.52×10^3
Achong	1.43×10^{10}	0.650	1.88	1.01×10^5	5.61	2.52×10^3

Correlation	Field Units					
	<i>A</i>	<i>B</i>	<i>C</i>	<i>D</i>	<i>E</i>	<i>F</i>
Gilbert	10.0	0.546	1.89	14.7	1.00	1.00
Ros	17.4	0.500	2.00	14.7	1.00	1.00
Baxendell	9.56	0.546	1.93	14.7	1.00	1.00
Achong	3.82	0.650	1.88	14.7	1.00	1.00

Table 5.3—Coefficients for different choke models.

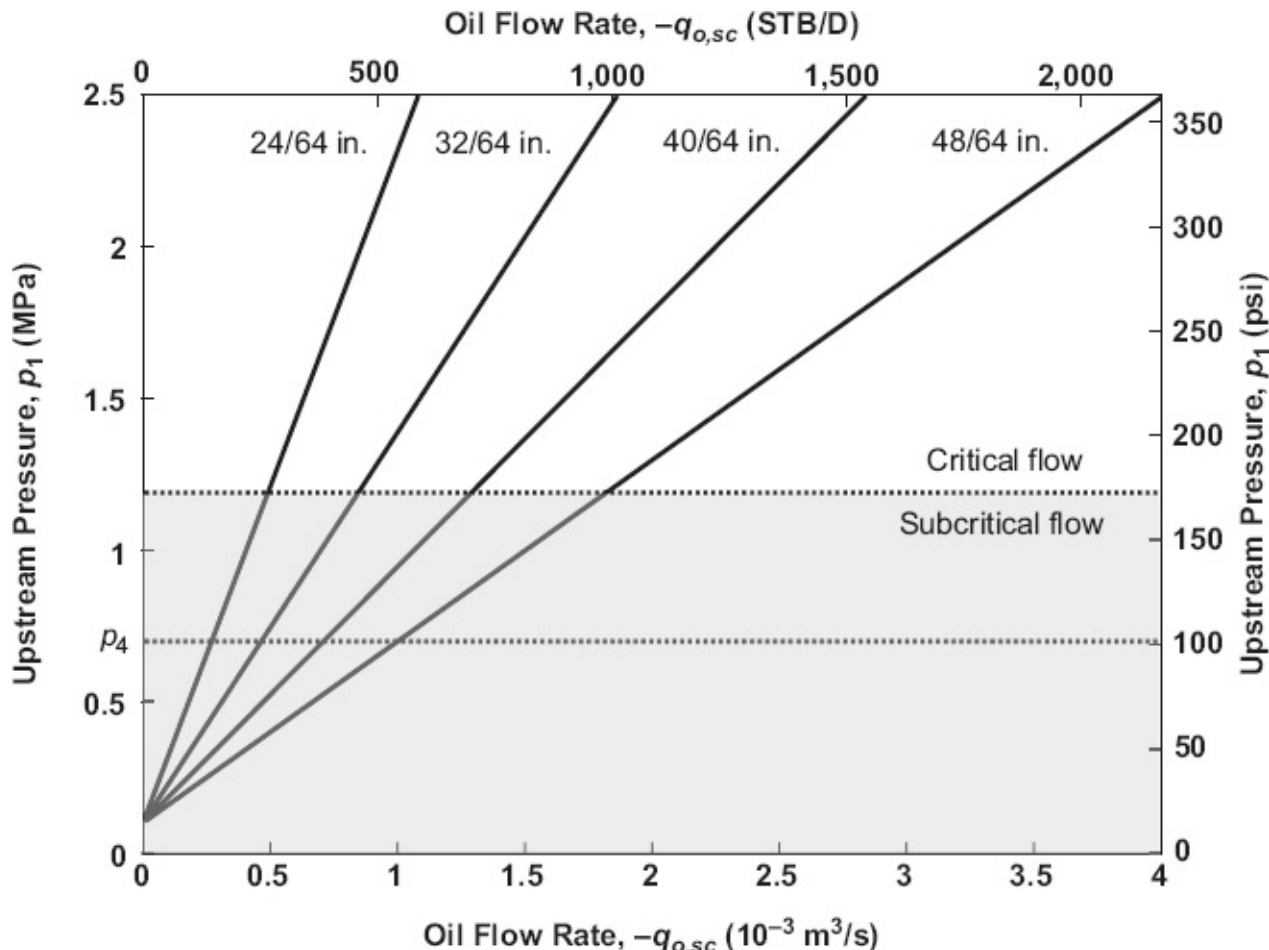


Fig. 5.5—Choke performance curves for multiphase critical flow through four chokes with sizes 3–6 as specified in Table 5.1 and fluid properties according to Table 4.1. The graphs have been obtained with the aid of Eq. 5.54 and the Gilbert correlation. Note that they are valid only in the critical regime, which is outside the gray area.

$$q_{l,sc,crit} = \frac{(D - p_{1,crit})(Fd_{ch})^C}{A(ER_{gl})^B}, \quad (5.55)$$

where, according to Eq. 5.53, $p_{1,crit} \approx 1.7p_4$. We now look for an expression that fulfills the following boundary conditions:

$$q_{l,sc} = 0 \quad : p_1 = p_4, \quad (5.56)$$

$$q_{l,sc} = 0 \quad : \frac{dp_1}{dq_{l,sc}} = 0, \quad (5.57)$$

$$q_{l,sc} = q_{l,sc,crit} : p_1 = p_{1,crit}, \quad (5.58)$$

$$q_{l,sc} = q_{l,sc,crit} : \frac{dp_1}{dq_{l,sc}} = p'_{1,crit}, \quad (5.59)$$

where

$$p'_{1,\text{crit}} = \left. \frac{dp_1}{dq_{l,sc}} \right|_{\text{crit}} = -A \frac{(ER_{gl})^B}{(Fd_{ch})^C}, \quad (5.60)$$

as follows from differentiation of Eq. 5.54. An appropriate expression that can fulfill four boundary conditions is the third-order polynomial

$$p_1 = c_0 + c_1 q_{l,sc} + c_2 q_{l,sc}^2 + c_3 q_{l,sc}^3, \quad (5.61)$$

where the four coefficients can be derived from Eqs. 5.56 through 5.59 as

$$c_0 = p_4, \quad (5.62)$$

$$c_1 = 0, \quad (5.63)$$

$$c_2 = \frac{p'_{1,\text{crit}}}{2q_{l,sc,\text{crit}}} + \frac{3(p_{1,\text{crit}} - \frac{1}{2}p'_{1,\text{crit}}q_{l,sc,\text{crit}} - p_4)}{q_{l,sc,\text{crit}}^2}, \quad (5.64)$$

$$c_3 = -\frac{2(p_{1,\text{crit}} - \frac{1}{2}p'_{1,\text{crit}}q_{l,sc,\text{crit}} - p_4)}{q_{l,sc,\text{crit}}^3}. \quad (5.65)$$

Note that this sub-critical extension of the empirical critical choke model Eq. 5.54 is not based on first-principle physics, but rather a pragmatic correction. Fig. 5.6 depicts the same choke performance curves as in Fig. 5.5, but now with pragmatically corrected sub-critical parts of the curves. The qualitative behavior is the same as for the single-phase gas curves in Fig. 5.4 (by design). The empirical model for sub-critical and critical flow described in this section has been programmed in MATLAB file `choke_multiphase_simp.m`.

5.6 Multiphase Flow: Theoretical Models

5.6.1 Polytropic Flow. Ros (1960), Sachdeva et al. (1986), Perkins (1993), and Al-Safran and Kelkar (2009) presented multiphase choke models of intermediate complexity. The main assumptions in these models are that during passage through the choke

- Flow is 1D
- Acceleration losses form the dominant contribution to pressure drop
- Phase compositions (and therefore R_s) remain constant (a condition known as “frozen” flow)
- The liquid phase density (and therefore B_l) remains constant
- The gas phase expands between isothermally and isentropically
- The gas/liquid mixture expands isentropically
- No slip exists between the gas and liquid phases, except in Al-Safran and

Kelkar (2009), where this assumption is relaxed

In this section we follow a similar approach. Just as in the four papers listed above, the equation of state for the gas is modeled as *polytropic* (i.e., between isothermal and isentropic).

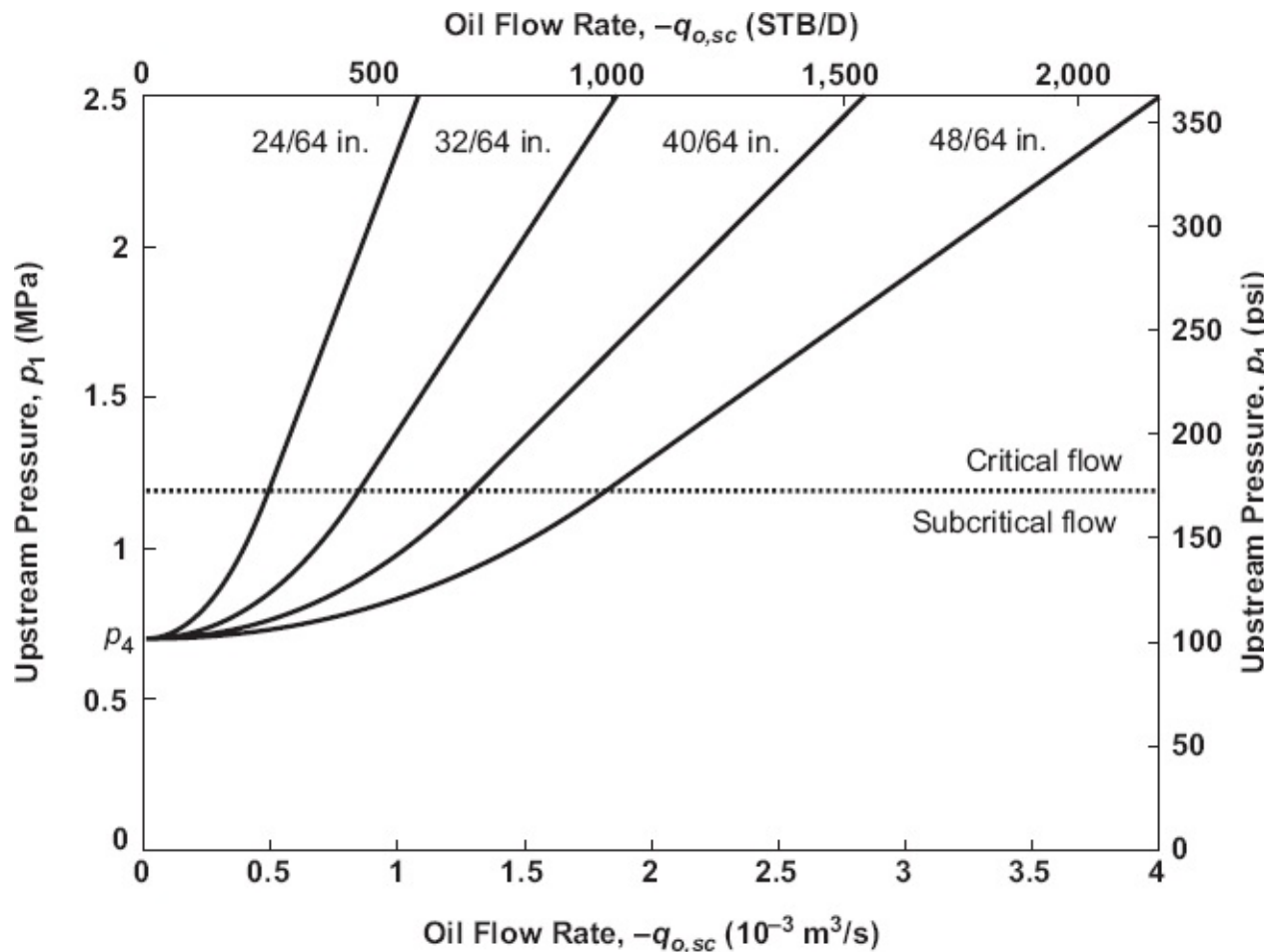


Fig. 5.6—Choke performance curves for multiphase critical flow through four chokes with sizes 3–6 as specified in Table 5.1 and fluid properties according to Table 4.1. The graphs have been obtained with the aid of Eqs. 5.54 and 5.61 and the Gilbert correlation.

This is to account for the fact that the temperature of the expanding gas in multiphase flow drops less than that in single-phase gas flow because it rapidly takes up heat from the surrounding liquid. The relationship between pressure and gas density under polytropic conditions is given by

$$\frac{p}{\rho_g^n} = C, \dots \dots \dots \quad (5.66)$$

where n is the polytropic expansion coefficient. Eq. 5.66 strongly resembles Eq. 5.25 for isentropic expansion, the only difference is that n replaces γ . The polytropic expansion coefficient n is defined as

$$n = 1 + \frac{x_g(c_p - c_v)}{x_g c_v + x_l c_l}, \quad \dots \dots \dots \quad (5.67)$$

where x_g and x_l are the gas and liquid mass fractions defined in Eqs. 4.19 and 4.20; c_p and c_v are, as before, the specific heat capacities for gas at constant pressure and volume, respectively; and c_l is the specific heat capacity for liquid at constant volume. It can be verified that for $\lambda_g = 1$ and $\lambda_l = 0$ (i.e., for single-phase gas flow); n becomes equal to γ , corresponding to isentropic flow; whereas for $\lambda_g = 0$ and $\lambda_l = 1$, n becomes equal to unity, corresponding to isothermal flow. For typical hydrocarbon mixtures the value of n is therefore between 1 and 1.3 depending on the gas/liquid ratio. For a derivation of Eq. 5.67 and a detailed description of the physical mechanisms involved, see Ros (1960).

Just as was the case for isentropic expansion, for polytropic expansion we have an algebraic relationship between pressure and temperature given by

$$\frac{p^{\frac{n-1}{n}}}{T_{\text{abs}}} = C, \quad \dots \dots \dots \quad (5.68)$$

such that we do not have to solve a differential equation to take account of the conservation of total energy over the choke. In analogy to Eqs. 5.26 and 5.27 we can also write

$$\frac{T_{1,\text{abs}}}{T_{3,\text{abs}}} = \left(\frac{p_1}{p_3} \right)^{\frac{n-1}{n}}, \quad \dots \dots \dots \quad (5.69)$$

and

$$\frac{B_1}{B_3} = \left(\frac{p_3}{p_1} \right)^{\frac{1}{n}}, \quad \dots \dots \dots \quad (5.70)$$

where we used $Z_1 = Z_3 = 1$ because we restrict the derivation to ideal gases. To derive the multiphase choke equations, we can now proceed along the same lines as we did for gas flow and start from a momentum balance that considers only acceleration and pressure forces (and no friction or gravity effects):

$$\frac{1}{\rho_{mn}} \frac{dp}{ds} = -v_{mn} \frac{dv_{mn}}{ds}, \quad \dots \dots \dots \quad (5.71)$$

The no-slip mixture velocity v_{mn} and the inverse mixture density $1/\rho_{mn}$ can be written with the aid of Eqs. 4.11, 4.19, 4.20, and 4.29 as

$$v_{mn} = \frac{q_g + q_l}{A} = \frac{q_m}{A} = \frac{B_m q_{m,sc}}{A}, \quad \dots \dots \dots \quad (5.72)$$

$$\frac{1}{\rho_{mn}} = \frac{1}{\lambda_g \rho_g + \lambda_l \rho_l} = \frac{q_g + q_l}{q_g \rho_g + q_l \rho_l} = \frac{x_g}{\rho_g} + \frac{x_l}{\rho_l}. \dots \dots \dots \quad (5.73)$$

(Note that for mixture flow rates, as opposed to mixture velocities, there is no need to make a distinction between slip and no-slip conditions. Therefore we can simply use the subscript m to indicate the mixture flow rate q_m .)

Substitution of Eqs. 5.66 and 5.73 in the left side of Eq. 5.71, along with integration from s_1 to s_3 , results in

$$\begin{aligned} \int_{s_1}^{s_3} \left(\frac{x_g}{\rho_g} + \frac{x_l}{\rho_l} \right) \frac{dp}{ds} ds &= \int_{s_1}^{s_3} \left(\frac{x_g C^{\frac{1}{n}}}{p^{\frac{1}{n}}} + \frac{x_l}{\rho_l} \right) \frac{dp}{ds} ds = x_g C^{\frac{1}{n}} \int_{p_1}^{p_3} p^{-\frac{1}{n}} dp + \int_{p_1}^{p_3} \frac{x_l}{\rho_l} dp \\ &= x_g C^{\frac{1}{n}} \left(\frac{n}{n-1} \right) p^{\frac{n-1}{n}} \Big|_{p_1}^{p_3} + \frac{x_l}{\rho_l} p \Big|_{p_1}^{p_3} = \left(\frac{n}{n-1} \frac{x_g}{\rho_g} + \frac{x_l}{\rho_l} \right) p \Big|_{p_1}^{p_3}. \end{aligned} \dots \dots \dots \quad (5.74)$$

Integrating the right side of Eq. 5.71 and then combining the result with Eq. 5.74 give us the polytropic Bernoulli equation for gas/liquid flow:

$$\left(\frac{n}{n-1} \frac{x_g}{\rho_g} + \frac{x_l}{\rho_l} \right) p_1 + \frac{1}{2} v_{mn,1}^2 = \left(\frac{n}{n-1} \frac{x_g}{\rho_g} + \frac{x_l}{\rho_l} \right) p_3 + \frac{1}{2} v_{mn,3}^2, \dots \dots \dots \quad (5.75)$$

which with the aid of Eqs. 4.19, 4.20, and 5.75 and the equality $q_g \rho_g + q_l \rho_l = q_{m,sc}$ $\rho_{m,sc}$ can be rewritten as

$$\begin{aligned} &\left(\frac{n}{n-1} \frac{B_{g,1} q_{g,sc}}{q_{m,sc} \rho_{m,sc}} + \frac{B_{l,1} q_{l,sc}}{q_{m,sc} \rho_{m,sc}} \right) p_1 - \left(\frac{n}{n-1} \frac{B_{g,3} q_{g,sc}}{q_{m,sc} \rho_{m,sc}} + \frac{B_{l,3} q_{l,sc}}{q_{m,sc} \rho_{m,sc}} \right) p_3 \\ &= \frac{1}{2} \frac{q_{m,sc}^2}{A_2^2} (B_{m,3}^2 - \beta_2^2 B_{m,1}^2). \end{aligned} \dots \dots \dots \quad (5.76)$$

Using the approximation $1 - \beta_2^2 B_1^2 / B_3^2 \approx 1$ and then introducing a discharge coefficient \tilde{C}_d , to account for the contraction effect and for the irreversible losses in the converging part of the restriction, results in

$$\left(\frac{n}{n-1} \frac{B_{g,1} q_{g,sc}}{q_{m,sc} \rho_{m,sc}} + \frac{B_{l,1} q_{l,sc}}{q_{m,sc} \rho_{m,sc}} \right) p_1 - \left(\frac{n}{n-1} \frac{B_{g,3} q_{g,sc}}{q_{m,sc} \rho_{m,sc}} + \frac{B_{l,3} q_{l,sc}}{q_{m,sc} \rho_{m,sc}} \right) p_3 = \frac{1}{2} \frac{q_{m,sc}^2 B_{m,3}^2}{A_2^2 \tilde{C}_d^2}, \quad (5.77)$$

which is analogous to Eq. 5.33 for the pressure drop over a single-phase gas choke as derived in Section 5.4. Continuing the analogy, we can solve Eq. 5.77 for $q_{m,sc}$, resulting in

$$q_{m,sc} = \tilde{C}_d A_2 \sqrt{\frac{2p_1}{\rho_{m,sc} B_{m,3}^2} \left[\left(\frac{n}{n-1} B_{g,1} \lambda_{g,sc} + B_{l,1} \lambda_{l,sc} \right) - \left(\frac{n}{n-1} B_{g,3} \lambda_{g,sc} + B_{l,3} \lambda_{l,sc} \right) \frac{p_3}{p_1} \right]} \\ = \tilde{C}_d A_2 \sqrt{\frac{2p_1}{\rho_{m,sc} B_{m,1} B_{m,3}} \frac{B_{m,1}}{B_{m,3}} \left(\frac{\frac{n}{n-1} B_{g,3} \lambda_{g,sc} + B_{l,3} \lambda_{l,sc}}{B_{m,3}} \right) \left(\frac{\frac{n}{n-1} B_{g,1} \lambda_{g,sc} + B_{l,1} \lambda_{l,sc}}{\frac{n}{n-1} B_{g,3} \lambda_{g,sc} + B_{l,3} \lambda_{l,sc}} - \frac{p_3}{p_1} \right)} \dots \quad (5.78)$$

It can be verified that Eq. 5.78 reduces to its single-phase oil counterpart (Eq. 5.14) for volume fraction values $\lambda_{g,sc} = 0$ and $\lambda_{l,sc} = 1$. Similarly, it reduces to its single-phase gas counterpart (Eq. 5.35) for $\lambda_{g,sc} = 1$ and $\lambda_{l,sc} = 0$.

5.6.2 Critical Flow. To further continue the analogy, we need to define various formation volume factor ratios that are a bit more complicated than for the single-phase gas case. For example, we find that

$$\frac{B_{m,1}}{B_{m,3}} = \frac{B_{m,1} q_{m,sc}}{B_{m,3} q_{m,sc}} = \frac{B_{g,1} q_{g,sc} + B_{l,1} q_{l,sc}}{B_{g,3} q_{g,sc} + B_{l,3} q_{l,sc}} = \frac{\frac{B_{g,1} q_{g,sc}}{B_{g,3} q_{g,sc}} + \frac{B_{l,1} q_{l,sc}}{B_{g,3} q_{g,sc}}}{1 + \frac{B_{l,3} q_{l,sc}}{B_{g,3} q_{g,sc}}} = \frac{(1+\varepsilon) \left(\frac{p_3}{p_1} \right)^{\frac{1}{n}}}{1 + \varepsilon \left(\frac{p_3}{p_1} \right)^{\frac{1}{n}}}, \quad \dots \quad (5.79)$$

and, using similar reasoning, that

$$\frac{\frac{n}{n-1} B_{g,3} \lambda_{g,sc} + B_{l,3} \lambda_{l,sc}}{B_{m,3}} = \frac{\frac{n}{n-1} + \varepsilon \left(\frac{p_3}{p_1} \right)^{\frac{1}{n}}}{1 + \varepsilon \left(\frac{p_3}{p_1} \right)^{\frac{1}{n}}}, \quad \dots \quad (5.80)$$

and that

$$\frac{\frac{n}{n-1} B_{g,1} \lambda_{g,sc} + B_{l,1} \lambda_{l,sc}}{\frac{n}{n-1} B_{g,3} \lambda_{g,sc} + B_{l,3} \lambda_{l,sc}} = \frac{\left(\frac{n}{n-1} + \varepsilon \right) \left(\frac{p_3}{p_1} \right)^{\frac{1}{n}}}{\frac{n}{n-1} + \varepsilon \left(\frac{p_3}{p_1} \right)^{\frac{1}{n}}}. \quad \dots \quad (5.81)$$

The parameter ε can be interpreted as the local liquid/gas ratio:

$$\varepsilon = \frac{q_{l,1}}{q_{g,1}} = \frac{B_{l,1} q_{l,sc}}{B_{g,1} q_{g,sc}} = \frac{B_{l,1}}{B_{g,1}} \frac{1}{R_{gl}}, \quad \dots \quad (5.82)$$

where we used the assumption that B_l remains constant during passage through the choke. With the aid of Eqs. 5.79 through 5.81, Eq. 5.78 can be rewritten as

$$q_{m,sc} = \tilde{C}_d A_2 \sqrt{\frac{2p_1}{\rho_{m,sc} B_{m,1}}} \Theta, \dots \dots \dots \quad (5.83)$$

where

$$\Theta = \frac{(1+\varepsilon) \left(\frac{p_3}{p_1} \right)^{\frac{1}{n}} \times \frac{n}{n-1} + \varepsilon \left(\frac{p_3}{p_1} \right)^{\frac{1}{n}}}{1 + \varepsilon \left(\frac{p_3}{p_1} \right)^{\frac{1}{n}}} \times \left[\frac{\left(\frac{n}{n-1} + \varepsilon \right) \left(\frac{p_3}{p_1} \right)^{\frac{1}{n}}}{\frac{n}{n-1} + \varepsilon \left(\frac{p_3}{p_1} \right)^{\frac{1}{n}}} - \frac{p_3}{p_1} \right] \dots \dots \dots \quad (5.84)$$

For $q_{l,sc} = 0$ (i.e., for $\varepsilon = 0$), this equation reduces to its gas equivalent, Eq. 5.36, whereas for $q_{g,sc} = 0$ (i.e., for $\varepsilon \rightarrow \infty$), it reduces to the single-phase oil expression, Eq. 5.14. Just like the gas flow rate $q_{g,sc}$ in Eq. 5.36, the mixture flow rate $q_{m,sc}$ in Eq. 5.83 obtains a maximum for a critical pressure ratio $(p_3/p_1)_{crit}$. However, unlike for gas flow, it is not possible to obtain a closed-form expression for $(p_3/p_1)_{crit}$, and so we need to search numerically for the maximum of Eq. 5.83 or, equivalently, for the maximum of Θ . In addition, it is necessary to iterate on p_1 because of the pressure dependence of n and of the formation volume factors $B_{g,1}$ and $B_{l,1}$, which appear in the definition of ε . Rewriting Eq. 5.83 in terms of p_1 results in the upstream pressure for multiphase flow through a critical choke:

$$p_1 = \frac{\rho_{m,sc} B_{m,1} q_{m,sc}^2}{2 \tilde{C}_d^2 A_2^2 \Theta_{crit}} = \frac{\rho_{mn,1} q_{m,1}^2}{2 \tilde{C}_d^2 A_2^2 \Theta_{crit}}, \dots \dots \dots \quad (5.85)$$

where Θ_{crit} is the value of Θ corresponding to $(p_3/p_1) = (p_3/p_1)_{crit}$. Eq. 5.85 needs to be solved iteratively because of the pressure dependence of $B_{m,1}$ (or, choosing the last term, the pressure dependence of $\rho_{mn,1}$ and $q_{m,1}$). Although not immediately obvious, it forms a near-linear relationship between the upstream pressure and the flow rate, just as its single-phase gas counterpart, Eq. 5.43.

5.6.3 Pressure Drop in Chokes. Just as for single-phase oil and single-phase gas chokes, the effect of pressure recovery in the diverging part of a multiphase choke can be accounted for pragmatically by replacing the discharge coefficient \tilde{C}_d for the converging part with an overall discharge coefficient $C_d > \tilde{C}_d$. The discussion in Section 5.4.3 for single-phase gas chokes is therefore also valid for multiphase chokes, the only difference being that it is no longer possible to compute the critical pressure ratio in closed form. We will not repeat the discussion except for the most frequently used scenario in which it is required to compute the pressure drop over a choke for a given flow rate and a given downstream pressure. Assuming sub-critical flow, the upstream pressure can then be computed iteratively with the equivalent of Eq. 5.85:

$$p_1 = \frac{\rho_{m,sc} B_{m,1} q_{m,sc}^2}{2C_d^2 A_2^2 \Theta} = \frac{\rho_{m,1} q_{m,1}^2}{2C_d^2 A_2^2 \Theta}, \quad \dots \dots \dots \quad (5.86)$$

where Θ is now defined as

$$\Theta = \frac{(1+\varepsilon) \left(\frac{p_4}{p_1} \right)^{\frac{1}{n}}}{1 + \varepsilon \left(\frac{p_4}{p_1} \right)^{\frac{1}{n}}} \times \frac{\frac{n}{n-1} + \varepsilon \left(\frac{p_4}{p_1} \right)^{\frac{1}{n}}}{1 + \varepsilon \left(\frac{p_4}{p_1} \right)^{\frac{1}{n}}} \times \left[\frac{\left(\frac{n}{n-1} + \varepsilon \right) \left(\frac{p_4}{p_1} \right)^{\frac{1}{n}}}{\frac{n}{n-1} + \varepsilon \left(\frac{p_4}{p_1} \right)^{\frac{1}{n}}} - \left(\frac{p_4}{p_1} \right) \right]. \quad \dots \dots \quad (5.87)$$

(Refer to the text just after Eq. 5.33 for a discussion on how to perform the iteration in MATLAB and how to treat the formation volume factor calculations.) If the resulting pressure ratio (p_4/p_1) turns out to be smaller than $(p_4/p_1)_{crit}$, the flow is critical and the upstream pressure can be computed with the aid of the same Eqs. 5.86 and 5.87 after replacing Θ with Θ_{crit} , and (p_4/p_1) with $(p_4/p_1)_{crit}$, respectively. This scenario has been implemented in the MATLAB routine `choke_multi_phase.m`.

Fig. 5.7 depicts the choke performance curves for multiphase flow through four differently sized chokes. The dashed lines depict the corresponding empirical “Gilbert” lines for critical flow that were shown earlier in Fig. 5.6. In this example, the correspondence between the results of the numerical solution and those of the empirical expression happens to be quite good. However, a much worse correspondence may be encountered for other parameter values. The horizontal dotted line indicates the boundary between sub-critical and critical flow, which, with the aid of the MATLAB file `choke_multi_phase_boundary.m`, has been computed numerically. An example explaining how to plot choke performance curves for either single-phase oil flow, single-phase gas flow, or multiphase flow is given in the MATLAB file `example_choke_performance_curve.m`.

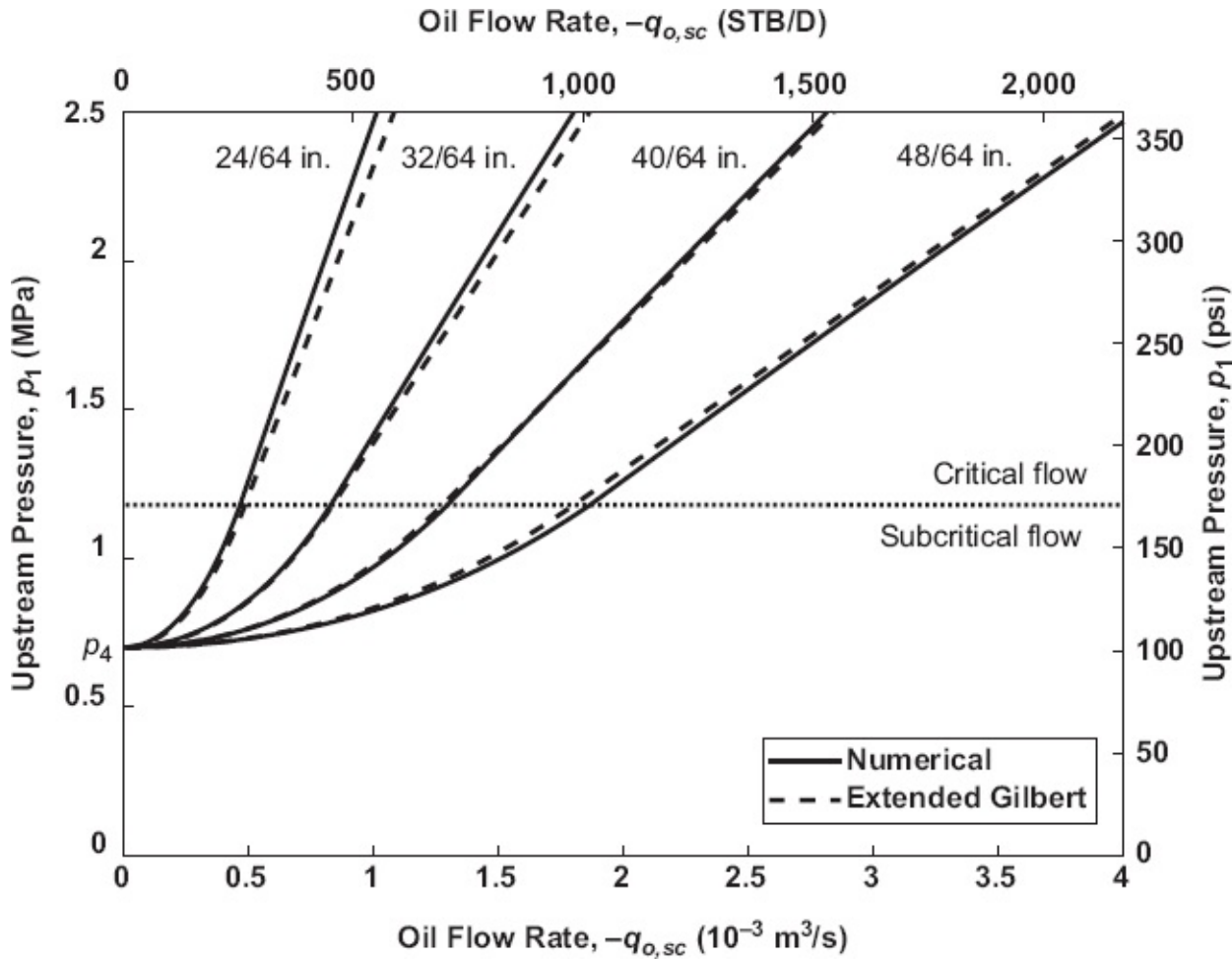


Fig. 5.7—Choke performance curves for multiphase flow with specific heat capacities $c_l = 0.80$, $c_p = 0.25$ and $c_v = 0.20$, through four chokes with discharge coefficient $C_d = 0.7$ and bean sizes 3–6 as specified in Table 5.1. The downstream pressure p_4 and the upstream temperature T_1 are 0.7 MPa and 30°C, respectively (other properties have been taken from Table 4.1, and the dashed lines represent the extended Gilbert curves that were depicted earlier in Fig. 5.6).

5.7 Questions

- 5.1 Why is the Bernoulli equation suitable for modeling the flow in the converging part of a choke, but not in the diverging part?
- 5.2 Which physical mechanisms are causing the maximum and the permanent pressure drop over an orifice plate? What kind of a device would you choose to obtain flow rate measurements with a lower pressure drop than with an orifice plate?
- 5.3 Why is the temperature at the throat of a gas choke lower than at the entrance?
- 5.4 Why is it often desirable to operate a wellhead choke in the critical regime?
- 5.5 Why does critical choke flow not occur for single-phase oil?
- 5.6 Why are the expressions for critical flow over a choke much more approximate than for critical flow over an orifice?

- 5.7 Why do we need the assumption of polytropic conditions instead of isentropic conditions to describe the flow in the converging part of a multiphase choke?
- 5.8 It is sometimes stated that the value of the discharge coefficient C_d of a choke can never exceed unity. Is that correct? Why?
- 5.9 A manufacturer of orifice-type flow measurement devices for single-phase liquid flow provides you with the following specifications: orifice size is 23 mm, to be fitted in a 48-mm pipe (inner diameter); contraction coefficient is 0.62. For a flow rate of $-300 \text{ m}^3/\text{d}$ and oil with a density of 876 kg/m^3 , estimate the maximum pressure drop.
- 5.10 If a restriction has a valve coefficient $C_v = 40 \text{ gal/min}\sqrt{\text{psi}}$, what is the pressure drop over the restriction for flow of single-phase oil with a density of 830 kg/m^3 at a rate of $-0.8 \text{ m}^3/\text{min}$?
- 5.11 Consider flow through an orifice-type dry gas meter. The relevant data are given in **Table 5.4**.
- Is the flow critical or noncritical?
 - What is the flow rate?
- 5.12 Consider multiphase flow through a choke. The relevant data are given in **Table 5.5**.
- What is the upstream pressure, according to the Gilbert correlation?
 - Is the key assumption for validity of the Gilbert correlation satisfied?

Property	Value	Units
A	4.91×10^{-4}	m^2
\tilde{C}_d	0.35	—
c_p	0.26	$\text{J/kg} \cdot \text{K}$
c_v	0.20	$\text{J/kg} \cdot \text{K}$
p_1	4.3	MPa
p_3	3.2	MPa
T_1	65	$^\circ\text{C}$
Z_1	0.94	—
$\rho_{g,sc}$	0.80	kg/m^3

Table 5.4—Input data for dry gas orifice measurement for Question 5.11.

Property	Value	Units
C_d	0.9	—
c_l	0.82	$\text{J/kg} \cdot \text{K}$
c_p	0.26	$\text{J/kg} \cdot \text{K}$

c_v	0.20	J/kg · K
d_{ch}	0.012 7	m
$q_{o,sc}$	-120	m ³ /d
f_w	0.70	—
R_{go}	40	m ³ /m ³
p_4	1.2	MPa
T_1	50	°C
$\rho_{g,sc}$	0.87	kg/m ³
$\rho_{o,sc}$	865	kg/m ³
$\rho_{w,sc}$	1030	kg/m ³

Table 5.5—Input data for multiphase choke flow for Question 5.12.

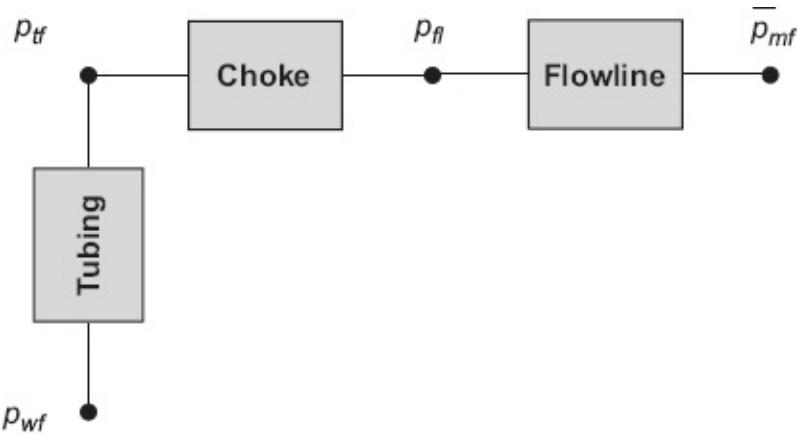
Questions 5.13 and 5.14 require the use of MATLAB.

5.13 Consider the same choke as in Question 5.12.

- (a) Compute the upstream pressure with the aid of MATLAB function `choke_multi_phase.m`. Is the result identical to your answer for Question 5.12?
- (b) Compute the upstream pressure with the aid of MATLAB function `choke_multi_phase.m`. Choose Standing black oil correlations. Is the result identical to your answer for Question 5.12? What is the difference and what are the consequences?

5.14 Consider a flowline/choke/tubing combination as depicted in [Fig. 5.8](#). For the choke and fluid properties, see [Table 5.5](#); for the tubular properties, manifold pressure, and temperatures, see [Table 5.6](#).

- (a) Make copies of `example_choke_performance_curve.m` and `example_intake_curve.m`, and merge and modify the copied files to create a choke performance curve and a tubing intake curve for the flowline/choke/tubing combination. Use flow rates between 0 and -150 m³/d. Explain the difference in shape.
- (b) Expand the file to make a plot of the critical pressure ratio (p_f / p_{tf})_{crit} and the actual pressure ratio (p_f / p_{tf}) as a function of flow rate. For which flow rates is the choke operating in the critical regime? Why is the critical pressure ratio slightly changing with flow rate (unlike in [Fig. 5.7](#), where it is constant)?

**Fig. 5.8—Wellhead choke in between a flowline and a tubing.**

Property	Value	Units
d_t	0.07	m
d_{fl}	0.10	m
$e_t = e_{fl}$	30×10^{-6}	m
L_t	3300	m
L_{fl}	4800	m
P_{mf}	1.2	MPa
T_{mf}	40	°C
T_{wf}	110	°C
α_t	0	degree
α_{fl}	90	degree

Table 5.6—Tubing, flowline, and manifold properties for Question 5.14.

5.8 MATLAB Assignment: Choke Flow

5.8.1 Objectives

- Gain insight into the theory behind the multiphase choke model described in this book and implemented in MATLAB functions `choke_multi_phase.m` and `choke_multi_phase_boundary.m`.
- Gain insight into the effect of slip in multiphase choke flow through modifying the existing MATLAB functions and testing the effect of the modifications.
- Demonstrate the similarities and/or differences between the (modified) multiphase choke model described in this book and other models in the open literature.

5.8.2 Warning. The second optional activity of this MATLAB exercise requires considerably more theoretical analysis than do the MATLAB exercises in the other chapters.

5.8.3 Assignment. The theory behind the multiphase choke model described in Sections 5.6.1 through 5.6.3 and the associated MATLAB functions is related to several choke models presented in the literature. However, one element present in the most recent of these other models is absent: the effect of slip between liquid and gas in the choke throat. You are requested to test the effect of adding slip models and, optionally, to theoretically demonstrate the similarities and/or differences between the modified model and the earlier models.

Tasks

- Read through the papers by Perkins (1993), Sachdeva et al. (1986), Schüller et al. (2003, 2006), and Al-Safran and Kelkar (2009) without studying them in-depth.
- Study Sections 5.6.1 to 5.6.3, dealing with multiphase choke modeling.
- Inspect the MATLAB functions `choke_multi_phase.m` and `choke_multi_phase_boundary.m`. Make a flow chart that illustrates their computational flow.
- Following the approach of Al-Safran and Kelkar (2009), modify the files to implement the Schüller et al. (2006) slip model for critical flow. Study the relevant parts of the papers in depth.
- Test the effect of the addition of slip by running `example_choke_performance_curve.m` for various flow rates, choke diameters, and discharge coefficients. In particular attempt to reproduce the test case used by Al-Safran and Kelkar (2009).
- Optional Activity 1: Also add the “Grolmes and Leung” slip model for sub-critical flow as described in Eq. 6 of Al-Safran and Kelkar (2009), and test the effect.
- Optional Activity 2: Demonstrate theoretically the similarities and/or differences between the multiphase choke model as used in this book (after addition of the slip models) and the models proposed by Perkins (1993), Sachdeva et al. (1986), and Al-Safran and Kelkar (2009).

5.8.4 Deliverables

- Flow chart
- MATLAB program listing
- Plots with choke performance curves illustrating the effect of adding the Schüller et al. (2006) slip model for critical flow
- Optional Activity 1: plots with choke performance curves illustrating the effect of adding the “Grolmes and Leung” slip model for sub-critical flow

- Optional Activity 2: a theoretical analysis demonstrating the similarities and/or differences between the various multiphase choke models

Chapter 6

Inflow Performance: The Basics

6.1 What Is Covered in This Chapter?

Inflow performance is a quantitative measure of the effect of flow resistance in the near-well reservoir and the completion on the production rate of a well. In this chapter we discuss the functional relationship between inflow performance and reservoir properties. Although we restrict the analysis to a simple circular reservoir produced by a vertical well, many of the findings will remain valid for the more-complex well configurations discussed in the next chapter. We start by deriving the governing equations for radial single-phase porous media flow and apply these to describe the inflow performance of single-phase oil and gas wells. In oil wells the relationship between flow rate and *drawdown* (i.e., pressure drop over the near-well reservoir) is linear and can therefore be expressed with a single *productivity index*, while for gas wells it becomes nonlinear. However, in both situations we can usually apply relatively simple analytical expressions to obtain rough estimates of the inflow performance of a well for given reservoir and fluid properties (which typically are known only to a limited extent). More-accurate values of a well's single-phase inflow performance can therefore be obtained only experimentally. To an increased extent, the same holds for multiphase reservoir flow, and so we present some empirical relationships to describe the two-phase (oil/gas) inflow performance of a well producing from an oil reservoir at pressures below the bubblepoint pressure. Finally, we treat the inflow performance of wells producing from multiple reservoirs.

6.2 The Importance of Inflow Performance

This section concerns the relationship between flow rate and pressure in the near-wellbore region. The difference between the reservoir pressure and the flowing bottomhole pressure (FBHP) of a well is the driving force for *inflow* into the wellbore. Resistance to well inflow depends on reservoir rock properties, fluid properties, well trajectory in the reservoir, details of the well completion, and sometimes the late effects of drilling and workover activities. In combination, these factors determine the *inflow performance* or *deliverability* of the well. Because all fluids entering the wellbore have to pass through the narrow area around the wellbore, the highest flow rates in the reservoir occur just there, and any increased resistance to flow has a large effect on the well performance. Because inflow performance plays such an important role, it should be regularly measured through *well testing*—i.e., by connecting the well to a test separator and determining the gas, oil, and water flow rates as functions of different wellbore pressures.

Note that different types of well tests can be distinguished such as *production tests*, which are mainly aimed at measuring the phase rates in a well at a given flowing tubinghead pressure (FTHP), and *pressure transient tests*, primarily aimed at inferring reservoir properties. The latter can be further classified depending on the nature of the well operation: e.g., *pressure buildup tests*, in which a well is closed in and the resulting increase in BHP is measured, or *pressure falloff tests*, in which a closed-in well is suddenly opened and the resulting increase in flow rate and decrease in FBHP is measured. (For further information on well testing see, e.g., Kamal 2009.)

The pressure in the near-wellbore region has to be measured at the bottom of the hole with either a *permanent downhole gauge* (PDG) or a dedicated wireline tool. This regular testing will indicate when a well is producing less than expected because of *impairment* (i.e., blockage of the pores in the near-wellbore region). Remedial measures, such as hydraulic fracturing of the formation through high-pressure pumping of liquids, or stimulation with acids, can then be taken. The results of the well tests can be incorporated in one of the models for inflow performance given below. It is important to realize that these are only models and thus the actual downhole well data must be respected. (For details of inflow performance measurement see, e.g., Golan and Whitson 1991 and Economides et al. 2013.)

As an example of a well's inflow performance, consider a vertical oil well with either an openhole producing zone or a perforated zone. The production performance of this zone is usually described by an *inflow performance relationship* (IPR) between the oil flow rate $q_{o,sc}$ and the BHP p_{wf} . In practice, it is found that the IPR is often a near-linear relationship between $q_{o,sc}$ and p_{wf} , at least when p_{wf} is above the bubblepoint pressure p_b . In that case the IPR can be expressed as a *productivity index* (PI) J defined as the ratio between $-q_{o,sc}$ and the drawdown Δp , which is the difference between the closed-in BHP p_{ws} (also known as the *static* BHP) and the FBHP p_{wf} (also known as the *dynamic* BHP), both measured at the top of the zone or at the top of the perforations (although sometimes the middle of the perforated interval is taken as reference level). If we assume that the static BHP equals the reservoir pressure p_R , we can write

$$J = \frac{-q_{o,sc}}{p_R - p_{wf}}, \quad \dots \dots \dots \quad (6.1)$$

where we adopt the convention that a positive flow rate $q_{o,sc}$ implies injection into the reservoir (with $p_{wf} > p_R$), and a negative flow rate implies production into the well (with $p_{wf} < p_R$). The PI therefore always has a positive value. The units of the PI are $\text{m}^3/\text{s}\cdot\text{Pa}$ ("strict" SI units), $\text{m}^3/\text{d}\cdot\text{kPa}$ ("allowable" SI units), or STB/D-psi (field units). The *reservoir pressure* is the pressure at the boundary of the drainage area of the well. Alternatively, the PI can be defined in terms of the average reservoir pressure $p_{R,av}$ in the drainage area of the well, which results in a somewhat higher value of the PI for the same flow rate. For injection wells it is customary to use the *injectivity*

index (II) as an indication of the injection performance. The definition of the II is completely analogous to that of the PI, with the drawdown now being referred to as the *falloff*. Because both the drawdown/falloff and the flow rate switch signs, the II always has a positive value as well.

Fig. 6.1 depicts the linear IPR for a single-phase oil well. The corresponding reservoir parameters have been given in **Table 6.1**, and their relationship to the IPR is discussed in detail in **Section 6.5**. At a flow rate $q_{o,sc} = 0$ the FBHP p_{wf} equals the static BHP p_R . In the theoretical case of zero pressure at the bottomhole, the flow rate would reach a value known as the *absolute open-flowing potential* (AOFP) of the well. The assumption of a linear PI is justified for single-phase oil or liquid (oil/water) flow and realistic drawdowns. (Note that typical values for drawdown in an oil well are between 0.01 and 5 MPa. At much higher values the pressure dependency of the viscosity will, in theory, cause a nonlinear IPR for single-phase oil. Usually, such higher drawdowns will correspond to a FBHP below the bubblepoint pressure, in which case the IPR becomes nonlinear anyway because of multiphase effects.)

For gas wells, or for oil wells producing from a reservoir below bubblepoint pressure, the IPR is a nonlinear function of the flow rate and can no longer be represented with a straightline PI.

6.3 Well Operation and Reservoir Flow Stages

During the *primary recovery* phase of an oil reservoir—i.e., the period when oil is produced because of reservoir pressure depletion only—wells can be produced at either a constant flow rate and a gradually decreasing FBHP, a constant FBHP and a gradually decreasing rate, or a combination of decreasing rate and FBHP (Walsh and Lake 2003). Constant-rate operation (“plateau production”) is typical for the early life of a well, when surface facility constraints are often limiting the flow rate. Because of reservoir pressure depletion, maintaining the plateau requires a gradual decrease of the FBHP. After reaching the minimum allowable FBHP—i.e., the FBHP required to lift the wellbore contents to surface—a constant-FBHP operation results. During the *secondary recovery* phase, when either water or gas is injected to maintain the reservoir pressure, it is also possible to operate a well at a (near-)constant rate and FBHP.

Inside the reservoir, the following different stages of flow can be distinguished during primary recovery (Walsh and Lake 2003):

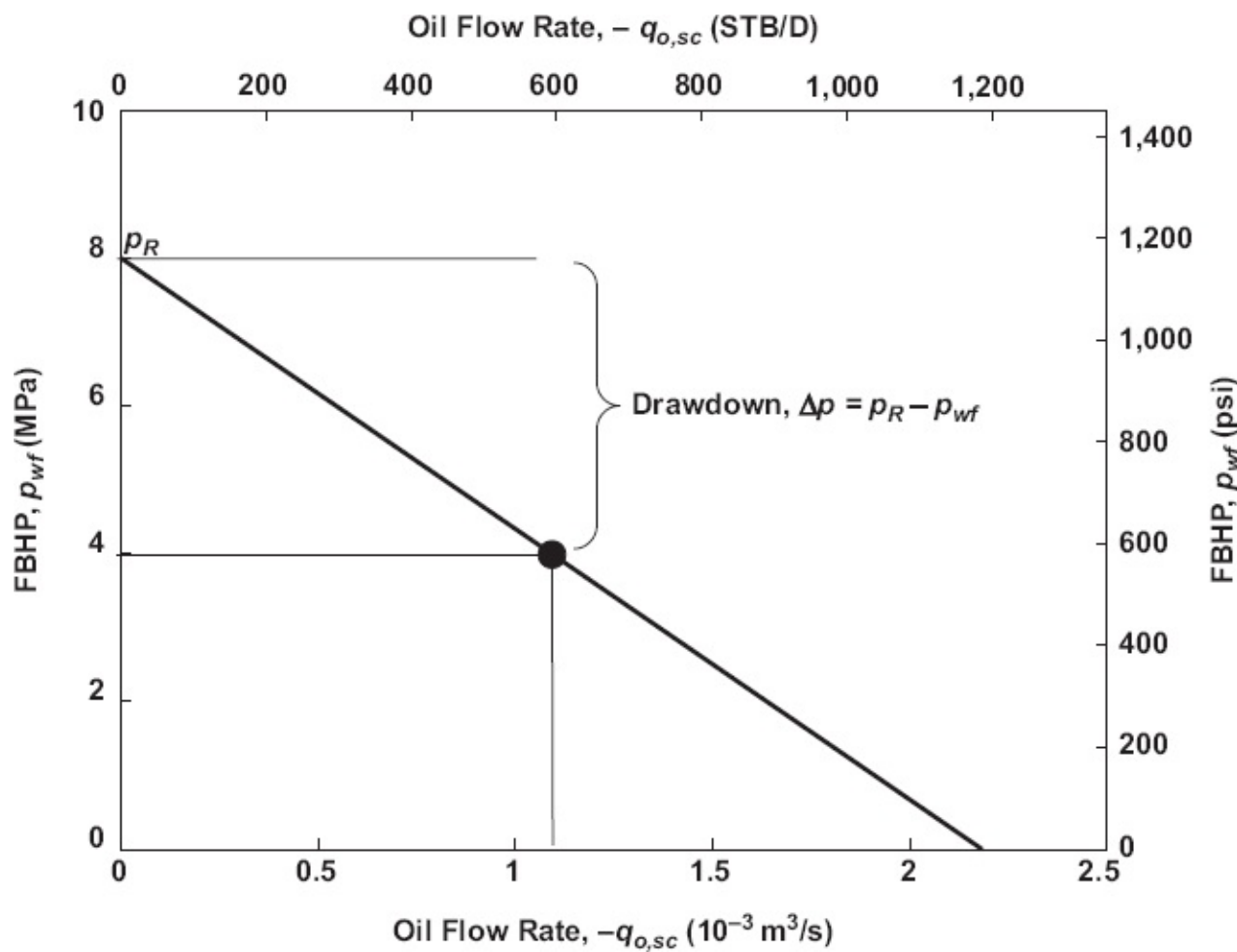


Fig. 6.1—Straightline inflow performance relationship for an oil reservoir with parameters given in Table 6.1. The operating point is indicated with a dot. The corresponding FBHP and flow rate are 4.00×10^6 Pa (580 psi) and 1.09×10^{-3} m³/s (593 STB/D), respectively. The AOFP is 2.18×10^{-3} m³/s (1187 STB/D). The drawdown $\Delta p = 8.00 \times 10^6 - 4.00 \times 10^6 = 4.00 \times 10^6$ Pa (540 psi). The productivity index $J = 2.18 \times 10^{-3}/8.00 \times 10^6 = 2.76 \times 10^{-10}$ m³/s Pa (1.03 STB/D-psi).

Parameter		SI Units		Field Units	
Reservoir height	h	20	m	65.6	ft
Reservoir radius	r_e	500	m	1,640	ft
Well radius	r_w	0.20	m	0.65	ft
Permeability (Fig. 6.1)	k_o	0.35×10^{-13}	m ²	35	mD
(Other figures)		1.00×10^{-13}	m ²	101	mD
Viscosity (Fig. 6.1)	μ_o	1.9×10^{-3}	Pa·s	1.9	cp
(Other figures, analytical)*		5.8×10^{-3}	Pa·s	5.8	cp
(Other figures, numerical)		Beggs and Robinson (1975); Vasquez and Beggs (1980)			
Gas density	$\rho_{g,sc}/\gamma_g$	0.95	kg/m ³	0.77	
Oil density	$\rho_{o,sc}/\gamma_{API}$	850	kg/m ³	35	°API
Sol. gas/oil ratio	R_{sb}	0	m ³ /m ³	0	scf/STB
Oil FVF (Fig. 6.1)	B_o	1	m ³ /m ³	0	bbl/STB

(Other figures, analytical)		1.03	m ³ /m ³	1.03	bbl/STB
Reservoir pressure	p_R	8×10^6	Pa	1,160	psi
Res. temp. (Fig. 6.1)	T_R	120	°C	248	°F
(Other figures)		60	°C	140	°F
Skin	S	0	–	0	–
Flow regime		Steady-state			

* Computed with the aid of the same correlations as used for the numerical solution with $p = p_R$ and $T = T_R$.

Table 6.1—Parameter values for several figures in Chapters 6 and 7.

1. *Transient flow*, also known as *infinite-acting flow*. After opening up a well, a pressure wave will radially travel into the reservoir. Transient flow occurs until the wave approaches either a reservoir boundary or a pressure wave of a neighboring well. This stage typically takes several hours to tens of days for oil reservoirs, and up to several months for gas reservoirs.
2. *Transitional flow*. This occurs once the first boundary effects are felt by the pressure wave, until the effects of all boundaries surrounding the drainage area around a well have exerted their influence on the transient flow. This stage is typically also relatively short (in the order of days) for oil wells and much longer for gas wells.
3. *Semisteady-state flow*. This next stage may last for many years. True semisteady-state flow requires a constant production rate and no inflow through the boundaries of the drainage area. That is, there should be no aquifer influx, and all neighboring wells should be produced at constant rates such that the drainage area of each well remains stationary. In that case, the pressure drops uniformly over the entire reservoir while the flow rates remain constant.
4. *Depletion flow*. This stage starts when the FBHP reaches its minimum allowed pressure and the well starts to be operated at a constant FBHP. As a result both the reservoir pressure, away from the well, and the well flow rates gradually decrease.

During secondary recovery, or in the case of primary recovery in the presence of a very strong aquifer, the reservoir pressure may remain (near-)constant, in which case it is also possible to obtain a fifth stage of flow:

5. *Steady-state flow*. Depending on the properties of the different phases there may occur slow changes over time in the reservoir pressure, the FBHPs, and the flow rates in the wells and the reservoir, corresponding to the movement of the oil/ water and/or oil/gas fronts through the reservoir. In this case we may consider the reservoir to be in near-steady-state condition with slowly varying parameters.

It should be noted that these classifications are highly idealized and in reality a reservoir is nearly always in a continuous pressure transient situation. The closing in and opening up of wells for maintenance, drilling new wells or sidetracks, and the effects of oil/ water or oil/gas fronts that slowly travel through the reservoir, all result in a pressure distribution that continuously changes in space and time. Nevertheless, the analysis of (semi)steady-state flow around a wellbore provides much insight and is often a sufficient approximation to form the basis for useful production engineering models.

6.4 Governing Equations

6.4.1 Mass Balance, Momentum Balance, and Equation of State. In this section we derive the equations for single-phase fluid flow in the near-wellbore region using the same approach used to describe pipe flow in [Chapter 3](#). Consider the classic textbook case of a single vertical well, either openhole or perforated over the entire reservoir height, producing from a circular reservoir (see [Fig. 6.2](#)). (The first book covering this material in depth is the truly classic text by Muskat (1937). It develops analytical solutions for a wide variety of well configurations and, despite its age, anyone interested in analytical expressions to describe inflow performance should consult this book.) It is assumed that the height of a reservoir is small compared to its lateral dimensions such that the flow can be approximated to be 2D. Moreover, the radial symmetry of the configuration allows for the use of polar coordinates. We can then write the mass balance per unit time through a wedge-shaped control volume as (see [Fig. 6.3](#)):

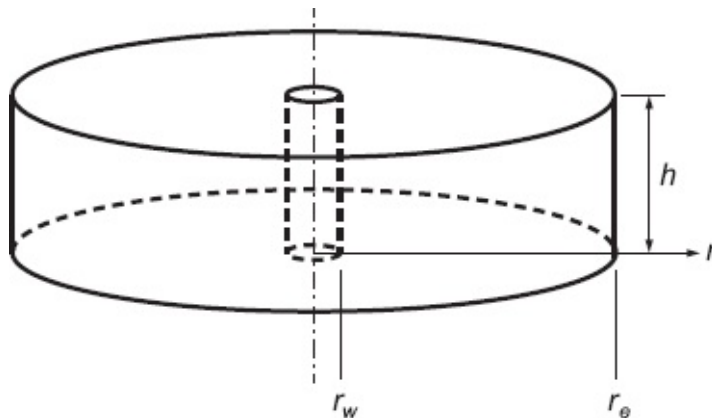


Fig. 6.2—Well in a circular reservoir (with vertical dimension strongly exaggerated).

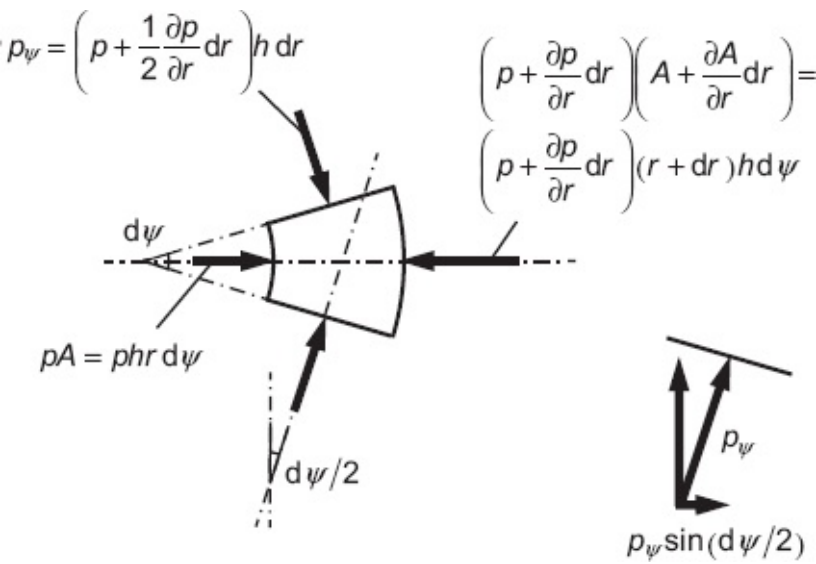


Fig. 6.3—Control volume and pressure forces in polar coordinates.

$$\underbrace{A\rho v}_{\text{mass rate in}} - \underbrace{\left(A + \frac{\partial A}{\partial r} dr \right) \left(\rho + \frac{\partial \rho}{\partial r} dr \right) \left(v + \frac{\partial v}{\partial r} dr \right)}_{\text{mass rate out}} = \underbrace{A\phi \frac{\partial \rho}{\partial t}}_{\text{mass accumulated unit time}}, \dots \quad (6.2)$$

where $A = hrd\psi$ is the cross-sectional area of the control volume in radial direction, m^2 ; h is reservoir height, m ; r is the radial coordinate, m ; ψ is the tangential coordinate, radians; ρ is fluid density, kg/m^3 ; $v = q/A$ is superficial radial fluid velocity, m/s ; q is the radial flow rate, m^3/s ; ϕ is porosity, $-$; and t is time, s . Note that the true fluid velocity v is in general much higher than the superficial velocity because the cross-sectional area A is only partially open to flow, depending on the porosity ϕ . Furthermore, the true fluid velocity field is 3D because the pores form a tortuous 3D network.

A positive velocity implies flow in the positive coordinate direction and therefore corresponds to injection from the well into the reservoir. Maintaining the analogy with pipe flow, the momentum balance can formally be written as

$$\begin{aligned} & \underbrace{A\rho v^2}_{\text{momentum rate in}} - \underbrace{\left(A + \frac{\partial A}{\partial r} dr \right) \left(\rho + \frac{\partial \rho}{\partial r} dr \right) \left(v + \frac{\partial v}{\partial r} dr \right)^2}_{\text{momentum rate out}} \\ & + \underbrace{Ap + 2h \left(p + \frac{\partial p}{\partial r} dr \right) dr \sin \frac{d\psi}{2} - \left(A + \frac{\partial A}{\partial r} dr \right) \left(p + \frac{\partial p}{\partial r} dr \right)}_{\text{pressure forces}} \dots \dots \dots \quad (6.3) \\ & + \underbrace{F_g(\rho, r) dr}_{\text{gravity force}} + \underbrace{F_f(\mu, \rho, v) dr}_{\text{friction force}} = \underbrace{A\phi \frac{\partial(\rho v)}{\partial t} dr}_{\text{momentum accumulated unit time}}, \end{aligned}$$

where the components of the pressure term have been illustrated in Fig. 6.3 and

where p is pressure, Pa; $F_g(\rho, s)$ is gravity force per unit length, N/m; $F_f(\rho, \mu, v)$ is friction force per unit length, N/m; and μ is dynamic viscosity, Pa·s. However, in flow through porous media the velocities v are usually so small that the momentum terms at the left side, which depend on v^2 , play no role. Furthermore, it also can be shown that the momentum term at the right side is negligible and that therefore only the pressure, gravity, and friction terms need to be taken into account (see, e.g., Bear 1972). In our case, we can furthermore disregard gravity because we consider horizontal flow only. The nature of the friction force $F_f(\rho, \mu, v)$ is discussed in more detail in [Section 6.4.2](#).

Just as in the case of pipe flow, we can complete the set of governing equations with the aid of the equation of state (EOS) for the fluid (i.e., [Eq. 2.9](#) for gas or [Eq. 2.18](#) for oil). If we expand [Eqs. 6.2](#) and [6.3](#), substitute $A = hrd\psi$, disregard momentum and gravity, drop all terms higher than first order in the differentials, and simplify the results, we can write the three equations as

$$\frac{\partial(\rho vr)}{\partial r} = -\phi r \frac{\partial \rho}{\partial r}, \dots \quad (6.4)$$

$$\frac{\partial p}{\partial r} = \frac{F_f}{2\pi hr}, \dots \quad (6.5)$$

$$\rho = \frac{Mp}{ZRT_{\text{abs}}} \text{ for gas, or } \dots \quad (6.6)$$

$$\rho = \rho_{o,\text{ref}} \exp[c_o(p - p_{\text{ref}})] \text{ for oil, } \dots \quad (6.7)$$

where the oil compressibility c_o and the gas deviation factor Z are known functions of p and T . (We will not treat the case of single-phase water flow separately because it follows directly from the single-phase oil case by replacing the fluid properties for oil by those for water. Note that unlike in pipe flow, a two-phase liquid mixture—i.e., oil/water—in a porous medium cannot be described with averaged liquid properties; in porous media, the presence of water has a considerable effect on the flow of oil and vice versa.)

The temperature T (and therefore also T_{abs}) can generally be taken as constant because the large heat capacity of the reservoir is usually sufficient to guarantee *isothermal* conditions. Only in high-rate gas wells may some cooling because of expansion of the gas occur in the near-wellbore region, an effect known as the *Joule-Thomson cooling* (see, e.g., Moran and Shapiro 1998).

6.4.2 Friction Force: Darcy's Law. The friction loss for single-phase liquid flow in porous media is described by the experimental relationship known as *Darcy's law*, which can be written in polar coordinates as

$$\frac{\partial p}{\partial r} = -\frac{\mu}{k} v, \dots \quad (6.8)$$

or, with an eye on Eq. 6.5, as

$$\frac{F_f}{2\pi hr} = -\frac{\mu}{k}v, \dots \dots \dots \quad (6.9)$$

where k is rock permeability, expressed in m^2 in SI units or millidarcy (md) in field units. For single-phase liquid flow and a homogeneous reservoir, k is a constant. More generally, the permeability may have different values for flow in different directions (see Section 7.2.5). However, for multiphase mixtures, the permeability for each phase will usually be a nonlinear function of the *phase saturations*, i.e., the proportion of each phase present in the pores). Moreover, the permeabilities may be *path dependent* (i.e., they may depend on the saturation history in the pores. (The nature of this nonlinear behavior is discussed in more detail in Appendix F.) For gas flow, we can use a similar relationship as for liquid flow except for high velocities such as occur in the near-wellbore region of high-rate gas wells. In that case we have to replace Darcy's law with a nonlinear equivalent for which several forms have been proposed (see Bear 1972). A frequently used relationship is given by

$$\frac{F_f}{2\pi hr} = -\frac{\mu}{k}v - \beta\rho|v|v, \dots \dots \dots \quad (6.10)$$

where β is *Forchheimer's coefficient* with dimension L^{-1} (Forchheimer 1901). It represents the inertia effects experienced by gas when it is accelerated and decelerated during its flow through the pore throats. It is also referred to as *inertia coefficient* or *turbulence coefficient*. The latter name is not entirely correct because the inertia effect can be noticed at much lower velocities than the velocity that corresponds to the onset of turbulence in the pores (see, e.g., Bear 1972). The values of k and β should be determined experimentally, either directly through measurements on cores or indirectly from well tests. The relationship between β and k is typically of the form (Dake 1978)

$$\beta = Ak_g^{-B}, \dots \dots \dots \quad (6.11)$$

with k expressed in m^2 and β in $1/\text{m}$ (which implies that the dimensional constant A has units m^{2B-1}).

6.5 Single-Phase Oil Flow

6.5.1 Steady-State Flow. At steady-state conditions the right side of the mass conservation equation (Eq. 6.4) vanishes, which reduces it to

$$\frac{\partial(\rho vr)}{\partial r} = 0. \dots \dots \dots \quad (6.12)$$

This trivial first-order differential equation requires one boundary condition, which can be obtained from the known density and velocity at the wellbore radius:

$$r = r_w : \rho v r = \frac{\rho q r_w}{A_w} = \frac{\rho q r_w}{2\pi r_w h} = \frac{(R_{sb}\rho_{g,sc} + \rho_{o,sc})q_{o,sc}}{2\pi h}, \quad \dots \dots \dots \quad (6.13)$$

where we used Eqs. 2.28 and 2.31 with $R_s = R_{sb}$. Following an approach similar to the one used for single-phase pipe flow in Section 3.3, we can now solve Eq. 6.12 and determine the integration constant with the aid of the boundary condition (Eq. 6.13); combine Eqs. 6.5, 6.7, and 6.9; and use Eqs. 2.28 and 2.31 (with $R_s = R_{sb}$) and Eq. 2.38 to arrive at the following set of equations for single-phase steady-state oil flow in the near-wellbore region:

$$\frac{dp}{dr} = -\frac{\mu}{k} v, \quad \dots \dots \dots \quad (6.14)$$

$$v = \frac{(R_{sb}\rho_{g,sc} + \rho_{o,sc})q_{o,sc}}{2\pi h \rho r} = \frac{B_o q_{o,sc}}{2\pi h r}, \quad \dots \dots \dots \quad (6.15)$$

$$\rho = \frac{R_{sb}\rho_{g,sc} + \rho_{o,sc}}{B_o}, \quad \dots \dots \dots \quad (6.16)$$

where we have dropped some of the subscripts o to improve the readability. This set of differential algebraic equations strongly resembles Eqs. 3.24 through 3.26 as defined in Section 3.3 to describe the steady-state flow of oil in pipes. The equations are nonlinear because ρ and μ are functions of the unknown pressure p . The differential equation (Eq. 6.14) requires one boundary condition, for which we can use

$$r = r_e : p = p_R, \quad \dots \dots \dots \quad (6.17)$$

which represents a constant pressure p_R at the external boundary of the circular drainage area. This situation can, with some imagination, be interpreted as a reservoir with constant pressure support in the form of a strong aquifer.

Just as was done for pipe flow, the equations can be solved with the aid of a standard numerical integration routine in MATLAB, and a numerical implementation can be found in `res.m` and `res_oil_dpdr`. An example of how to use these files to plot pressure vs. radial distance has been programmed in `example_res_pres.m`. A typical result is shown in Fig. 6.4. It displays a steep decrease in pressure close to the wellbore, caused by a radial convergence of the streamlines, which require an increasingly large pressure drop dp/dr to force the oil through an increasingly smaller surface area $2\pi hr$.

6.5.2 Analytical Solution. For oil above the bubblepoint pressure, for realistic drawdowns, it is reasonable to assume that B_o and μ are constants (with a typical

value of B_o slightly below B_{ob} ; see Fig. 2.6). Eqs. 6.14 through 6.16 can then be combined to give the classic linear differential equation for steady-state single-phase radial oil flow near a well (Muskat 1937):

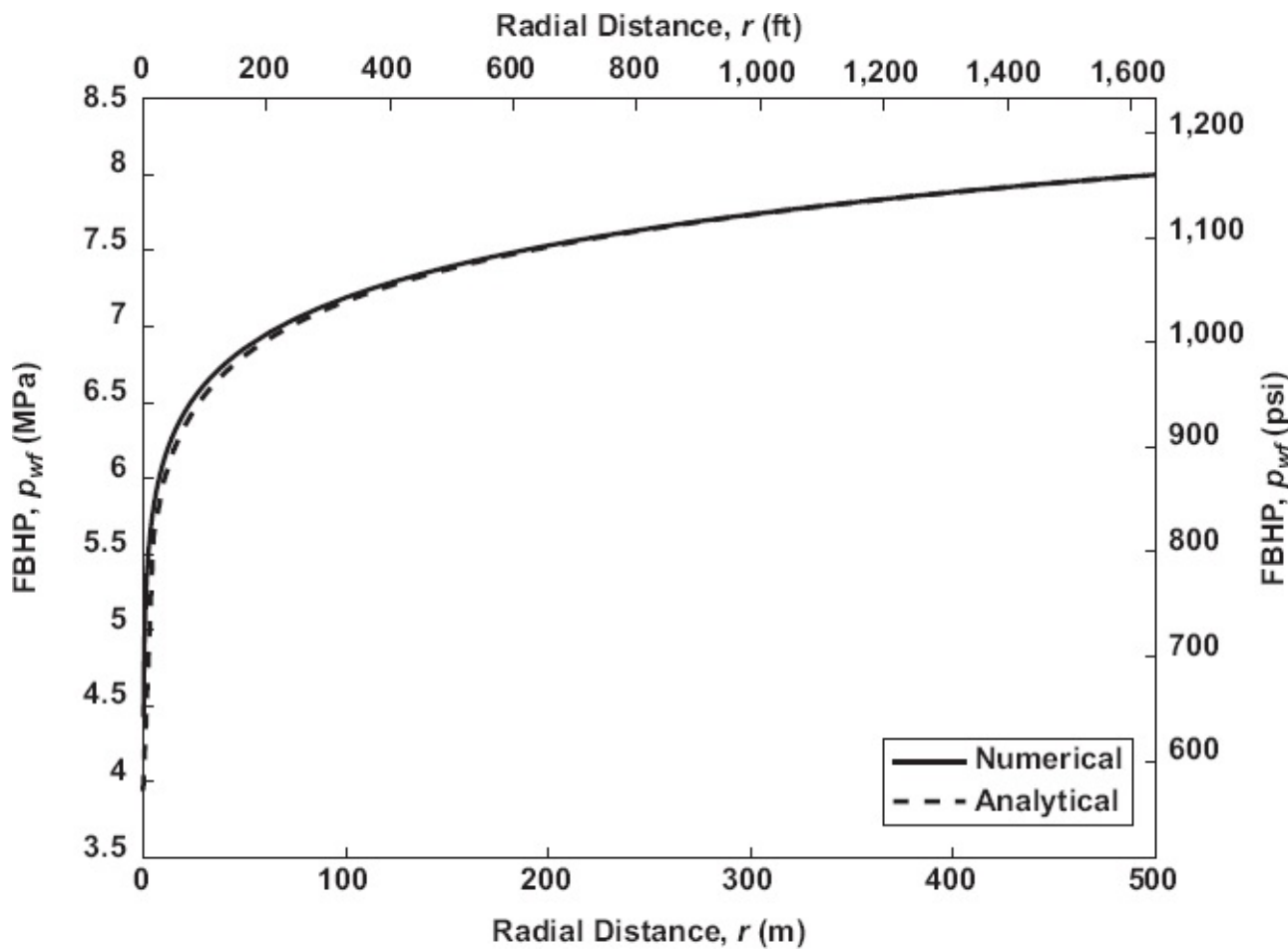


Fig. 6.4—Pressure as function of radial distance from a well in a reservoir with parameters given in Table 6.1 and a flow rate $q_{o,sc} = 1.09 \times 10^{-3} \text{ m}^3/\text{s}$ (593 STB/D). The numerical result for the FBHP is 4.43 MPa (643 psi); the analytical result 3.95 MPa (572 psi).

$$\frac{dp}{dr} = -\frac{\mu B_o q_{o,sc}}{2\pi kh} \frac{1}{r} \quad \dots \quad (6.18)$$

Eq. 6.18 can be integrated analytically to give

$$p = C - \frac{\mu B_o q_{o,sc}}{2\pi kh} \ln r \quad \dots \quad (6.19)$$

The value of the unknown integration constant C can be found with the aid of the boundary condition (Eq. 6.17), and substitution in Eq. 6.19 then gives us the expression for p as a function of r under steady-state flow conditions:

$$p = p_R + \frac{\mu B_o q_{o,sc}}{2\pi kh} \ln \left(\frac{r_e}{r} \right) \quad \dots \quad (6.20)$$

Recall that $q_{o,sc} \leq 0$, such that $p(r) \leq p_R$.

The FBHP for a given flow rate now simply follows by substituting r for r_w and p for p_{wf} . Reorganizing the result such that it becomes an expression for the drawdown as a function of the oil flow rate gives

$$p_R - p_{wf} = -\frac{\mu B_o q_{o,sc}}{2\pi kh} \ln\left(\frac{r_e}{r_w}\right). \quad (6.21)$$

Note that because of our definition of the positive flow direction, a positive drawdown corresponds to a negative flow rate (i.e., to flow toward the well as occurs in a production well). We can now also define the PI, relating the flow rate to the drawdown as

$$J = \frac{-q_{o,sc}}{p_R - p_{wf}} = \frac{2\pi kh}{\mu B_o \ln\left(\frac{r_e}{r_w}\right)}. \quad (6.22)$$

A numerical implementation of Eq. 6.22 can be found in `res_oil_simp.m`. Just like its numerical counterpart, `res.m`, it can be used to create a plot of pressure vs. radial distance from the well (see `example_res_pres.m`). The corresponding result has been plotted as a dashed line in Fig. 6.4.

Although at first sight the analytical and numerical results appear to be very close, there is an increasing discrepancy with increasing proximity to the wellbore, culminating in a difference of approximately 12% in the FBHP. The reason is the pressure dependency of the density and viscosity, which has not been taken into account in the analytical model. However, the drawdown in this example is at the high end of what could be expected in real life. In nearly all circumstances it is fully justified to use the analytical solution to predict a well's inflow performance because uncertainties resulting from reservoir heterogeneity have a much larger influence on the inaccuracy of the prediction than the choice of the solution method.

6.5.3 Average Reservoir Pressure. Alternatively, we may want to express the IPR in terms of the volume-averaged reservoir pressure $p_{R,av}$ defined as

$$p_{R,av} = \frac{\frac{2\pi\phi}{r_w} \int_{r_w}^{r_e} pr dr}{\frac{2\pi\phi}{r_w} \int_{r_w}^{r_e} r dr} = \frac{\frac{2}{r_w} \int_{r_w}^{r_e} pr dr}{\frac{r_e^2 - r_w^2}{r_w}}. \quad (6.23)$$

Substitution of Eq. 6.20 in Eq. 6.23 gives

$$p_{R,av} = \frac{2}{r_e^2 - r_w^2} \int_{r_w}^{r_e} \left[p_R + \frac{\mu B_o q_{o,sc}}{2\pi kh} \ln\left(\frac{r_e}{r}\right) \right] r dr = p_R + \frac{\mu B_o q_{o,sc}}{\pi kh (r_e^2 - r_w^2)} \int_{r_w}^{r_e} r \ln\left(\frac{r_e}{r}\right) dr. \quad (6.24)$$

where the integral can be solved through integration by parts as follows:

$$\int_{r_w}^{r_e} r \ln\left(\frac{r_e}{r}\right) dr = - \int_{r_w}^{r_e} r \ln\left(\frac{r}{r_e}\right) dr = -\frac{1}{2} r^2 \ln\left(\frac{r}{r_e}\right) \Big|_{r_w}^{r_e} + \int_{r_w}^{r_e} \frac{1}{2} r^2 \frac{1}{r} dr = \frac{1}{4} (r_e^2 - r_w^2) - \frac{1}{2} r_w^2 \ln\left(\frac{r_w}{r_e}\right) \quad (6.25)$$

Substitution of this result in Eq. 6.24 gives

$$p_{R,av} = p_R + \frac{\mu B_o q_{o,sc}}{4\pi kh} \left[1 - \frac{2 \frac{r_w^2}{r_e^2} \ln\left(\frac{r_w}{r_e}\right)}{\left(1 - \frac{r_w^2}{r_e^2}\right)} \right] = p_R + \frac{\mu B_o q_{o,sc}}{4\pi kh}, \dots \quad (6.26)$$

where the approximation holds for $r_w \ll r_e$, which is the usual situation. (Recall that $q_{o,sc}$ is negative and therefore $p_{R,av} < p_R$, as expected.) Often the difference between $p_{R,av}$ and p_R is relatively small. Solving for p_R from Eq. 6.26, substituting in Eq. 6.23, and then rearranging the result gives an expression for the drawdown in terms of average pressure:

$$p_{R,av} - p_{wf} = -\frac{\mu B_o q_{o,sc}}{2\pi kh} \left[\frac{1}{1 - r_w^2/r_e^2} \ln\left(\frac{r_e}{r_w}\right) - \frac{1}{2} \right] = -\frac{\mu B_o q_{o,sc}}{2\pi kh} \left[\ln\left(\frac{r_e}{r_w}\right) - \frac{1}{2} \right]. \dots \quad (6.27)$$

6.5.4 Semisteady-State Flow. Most reservoirs are initially produced through pressure depletion (primary recovery). Moreover, even during secondary recovery the injected volumes may not be sufficient to maintain a constant pressure, such that it gradually drops over time. Such a gradual pressure depletion scenario can be schematically represented by a circular reservoir with a boundary condition:

$$r = r_e : \frac{dp}{dr} = 0, \dots \quad (6.28)$$

which implies that there is no pressure gradient and therefore no driving force for flow at the external boundary. This type of no-flow condition typically occurs when a large number of vertical wells producing at constant rates are used to drain a reservoir in a regular pattern. The drainage areas can then be approximated reasonably well by circular cylindrical volumes. A refined approximation can be obtained with the aid of shape factors or equivalent outer radii to account for the fact that the drainage areas are not exactly circular (see Dietz 1965). As a consequence of the absence of flow through the outer boundaries, and of constant oil production rates from the wells, the pressure in the reservoir will steadily decrease, a situation known as *semisteady state* (also known as *pseudosteady state*).

To analyze this situation, we can start from the mass balance (Eq. 6.4), which can be rewritten with the aid of the EOS (Eq. 6.7) as follows:

$$\frac{\partial(\rho vr)}{\partial r} = -\phi r \frac{\partial \rho}{\partial p} \frac{\partial p}{\partial t} = -\phi c_0 \rho r \frac{\partial p}{\partial t}. \dots \dots \dots \quad (6.29)$$

Under semisteady-state conditions the pressure derivative $\partial p / \partial t$ should remain constant—say, equal to an unknown constant C_1 . The mass balance equation therefore reduces to

$$\frac{\partial(\rho vr)}{\partial r} = -C_1 \phi c_0 \rho r. \dots \dots \dots \quad (6.30)$$

If we maintain the assumption that ρ is constant, the first-order differential (Eq. 6.30) can be integrated analytically to give

$$\rho vr = -\frac{1}{2} C_1 \phi c_0 \rho r^2 + C_2. \dots \dots \dots \quad (6.31)$$

We know from the boundary condition (Eq. 6.28) that $v = 0$ at $r = r_e$, which allows us to express C_1 in terms of C_2 . With the aid of the other boundary condition (i.e., Eq. 6.13), which was also used for the steady-state solution, we can now derive

$$v = \frac{(R_{sb}\rho_{g,sc} + \rho_{o,sc})q_{o,sc}}{2\pi h \rho r} \left(1 - \frac{r^2 - r_w^2}{r_e^2 - r_w^2}\right) = \frac{B_o q_{o,sc}}{2\pi h r} \left(1 - \frac{r^2 - r_w^2}{r_e^2 - r_w^2}\right) \approx \frac{B_o q_{o,sc}}{2\pi h r} \left(1 - \frac{r^2}{r_e^2}\right). \dots \dots \dots \quad (6.32)$$

Similarly to what we did in the steady-state situation, we may combine Eqs. 6.5, 6.9, and 6.32 to arrive at the differential equation for semisteady-state radial oil flow:

$$\frac{dp}{dr} = -\frac{\mu B_o q_{o,sc}}{2\pi k h} \left(\frac{1}{r} - \frac{r}{r_e^2}\right). \dots \dots \dots \quad (6.33)$$

Integration of the equation results in

$$p = -\frac{\mu B_o q_{o,sc}}{2\pi k h} \left(\ln r - \frac{1}{2} \frac{r^2}{r_e^2}\right) + C_3. \dots \dots \dots \quad (6.34)$$

We can use the boundary condition (Eq. 6.17) (but now for a slowly decreasing pressure p_R) to solve for the integration constant C_3 , and substitution of the result in Eq. 6.34 gives an expression for p as a function of r under semisteady-state flow conditions:

$$p = p_R + \frac{\mu B_o q_{o,sc}}{2\pi k h} \left[\ln\left(\frac{r_e}{r}\right) - \frac{1}{2} \left(1 - \frac{r^2}{r_e^2}\right)\right]. \dots \dots \dots \quad (6.35)$$

In particular, the drawdown under semisteady-state conditions can now be expressed as

$$p_R - p_{wf} = -\frac{\mu B_o q_{o,\infty}}{2\pi kh} \left[\ln\left(\frac{r_e}{r_w}\right) - \frac{1}{2} \left(1 - \frac{r_w^2}{r_e^2} \right) \right] = -\frac{\mu B_o q_{o,\infty}}{2\pi kh} \left[\ln\left(\frac{r_e}{r_w}\right) - \frac{1}{2} \right]. \dots \dots \dots (6.36)$$

The difficulty with Eqs. 6.35 and 6.36 is that the pressure p_R at the external boundary, which is gradually decreasing, just as the pressure in any point of the reservoir is doing, can usually not be determined. However, the average pressure $p_{R,av}$ can often be determined from the pressure response in a well after shut-in, a well-testing procedure known as *pressure transient analysis* (see, e.g., Dake 1978 or Kamal 2009). To express Eq. 6.36 in terms of the average reservoir pressure, we can use the same approach as in Section 6.5.3, resulting in

$$p_{R,av} - p_{wf} = -\frac{\mu B_o q_{o,\infty}}{2\pi kh} \left[\ln\left(\frac{r_e}{r_w}\right) - \frac{1}{2} \left(1 - \frac{r_w^2}{r_e^2} \right) - \frac{1}{4} \right] = -\frac{\mu B_o q_{o,\infty}}{2\pi kh} \left[\ln\left(\frac{r_e}{r_w}\right) - \frac{3}{4} \right]. \dots \dots \dots (6.37)$$

(For a derivation of this expression, see Question 6.7 in Section 6.11 and its answer in Appendix G.)

6.5.5 Combined Expression. Eqs. 6.21, 6.27, 6.36, and 6.37 can be combined in a single expression:

$$p_{R,ref} - p_{wf} = -\frac{\mu B_o q_{o,\infty}}{2\pi kh} \left[\ln\left(\frac{r_e}{r_w}\right) - f_R \right], \dots \dots \dots (6.38)$$

where f_R and $p_{R,ref}$ are given by

$$f_R = \begin{cases} 0 & \text{for steady-state flow with } p_{R,ref} = p_R, \\ \frac{1}{2} & \text{for steady-state flow with } p_{R,ref} = p_{R,av}, \\ \frac{1}{2} & \text{for semi-steady-state flow with } p_{R,ref} = p_R, \\ \frac{3}{4} & \text{for semi-steady-state flow with } p_{R,ref} = p_{R,av}. \end{cases} \dots \dots \dots (6.39)$$

The corresponding combined expression for the PI becomes

$$J = \frac{-q_{o,\infty}}{p_{R,ref} - p_{wf}} = \frac{2\pi kh}{\mu B_o \left[\ln\left(\frac{r_e}{r_w}\right) - f_R \right]} \dots \dots \dots (6.40)$$

For many practical situations, the value of $\ln(r_e/r_w)$ in Eqs. 6.38 and 6.40 will be between 5 and 10, and the difference between steady state or semisteady state, and between drawdown with respect to reservoir pressure or average reservoir pressure,

becomes unimportant.

Another noteworthy feature of these equations is that the radii r_w and r_e occur within a logarithm. For typical parameter values the sensitivity of J to changes in the radii is therefore relatively small compared to, e.g., changes in k . This is particularly relevant for the sensitivity to uncertainties in the outer radius r_e , because circular reservoirs do not exist and there is usually considerable uncertainty about the shape and “equivalent” radius of the outer boundary. Fortunately, changes in the value of r_e do not strongly influence the results. A downside of this feature is that increasing r_w (i.e., drilling a larger-diameter well) only results in a relatively small increase in production (see also Question 6.6).

6.6 The Skin Factor

6.6.1 Formation Damage. The IPRs derived above assume that the radial permeability is everywhere constant. In practice, this is not the case. In addition to geological heterogeneity, the well may be *impaired*. During the drilling of the well there is penetration of alien fluids into the reservoir rock, which may reduce the permeability of the rock around the well and therefore reduce the rate of oil inflow. This reduction in permeability is called *formation damage* or *impairment*. We currently have a good understanding of the fundamental causes of formation damage, thanks to experimental and theoretical research over the past years. (For an extensive overview, see Civan 2000.) From the moment the drill bit first penetrates the reservoir section until the well is put production, the reservoir rock is exposed to a series of operations that can cause damage:

- *Mechanical interference.* The drilling itself can create mechanical damage, with pore collapse and particle rearrangement.
- *Solids.* Solids come into contact with the rock formation, such as drill cuttings, solid material added to the drilling mud, or metal debris. If small enough, the solids can be swept into the formation and block the pores. If larger, the solid particles cannot enter into the rock pores but are deposited at the borehole wall. Some of these solids will be swept away again when the well is put on production, but not all; **Fig. 6.5** shows a thin layer of residual mud solids on the borehole wall.
- *Fluids.* Fluids used in well construction can also cause formation damage. Such fluids are composed of water, oils, salts, acids, surfactants, and many other chemicals. They may interact with the reservoir rock and fluids, causing detachment of fine particles, flocculation, wettability change, precipitation, emulsion formation, or fluid saturation changes. In particular, the pores may be lined with clay, which may swell disastrously, completely blocking the pores.
- *Phase changes.* Changes in pressure and temperature in the oil and water may result in phase changes, with precipitation of waxes, asphaltenes, or

scale, which are deposited in the pores.

- *Microbial damage.* Last, microbes introduced into the well, or possibly indigenous in the reservoir in a dormant state, may multiply, forming deposits in the pores.

The effect of all these damage mechanisms is to reduce the permeability of the reservoir rock over a relatively small region around the wellbore. This small damaged region is called the *skin* of the well (Van Everdingen 1953). This skin gives rise to an additional pressure drop, as shown in Fig. 6.6, so that the well produces less than expected. The additional pressure drop can be taken into account in the IPR as follows. Eq. 6.38 can now be modified to give

$$p_{R,\text{ref}} - p_{wf} + \Delta p_{\text{skin}} = -\frac{\mu B_o q_{o,\text{sc}}}{2\pi kh} \left[\ln\left(\frac{r_e}{r_w}\right) - f_R \right]. \quad \dots \dots \dots \quad (6.41)$$

6.6.2 Combined Expression. Introducing the dimensionless skin factor S defined through

$$\Delta p_{\text{skin}} = \frac{\mu B_o q_{o,\text{sc}} S}{2\pi kh}, \quad \dots \dots \dots \quad (6.42)$$

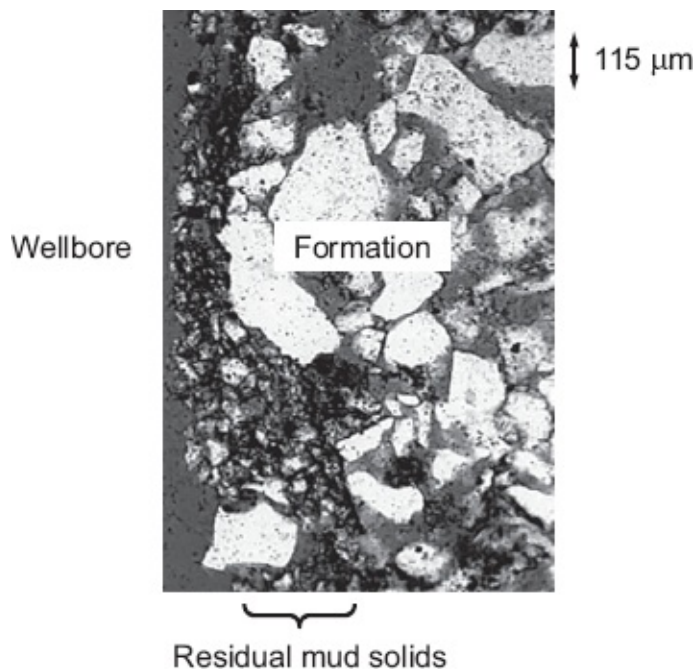


Fig. 6.5—Residual mud solids.

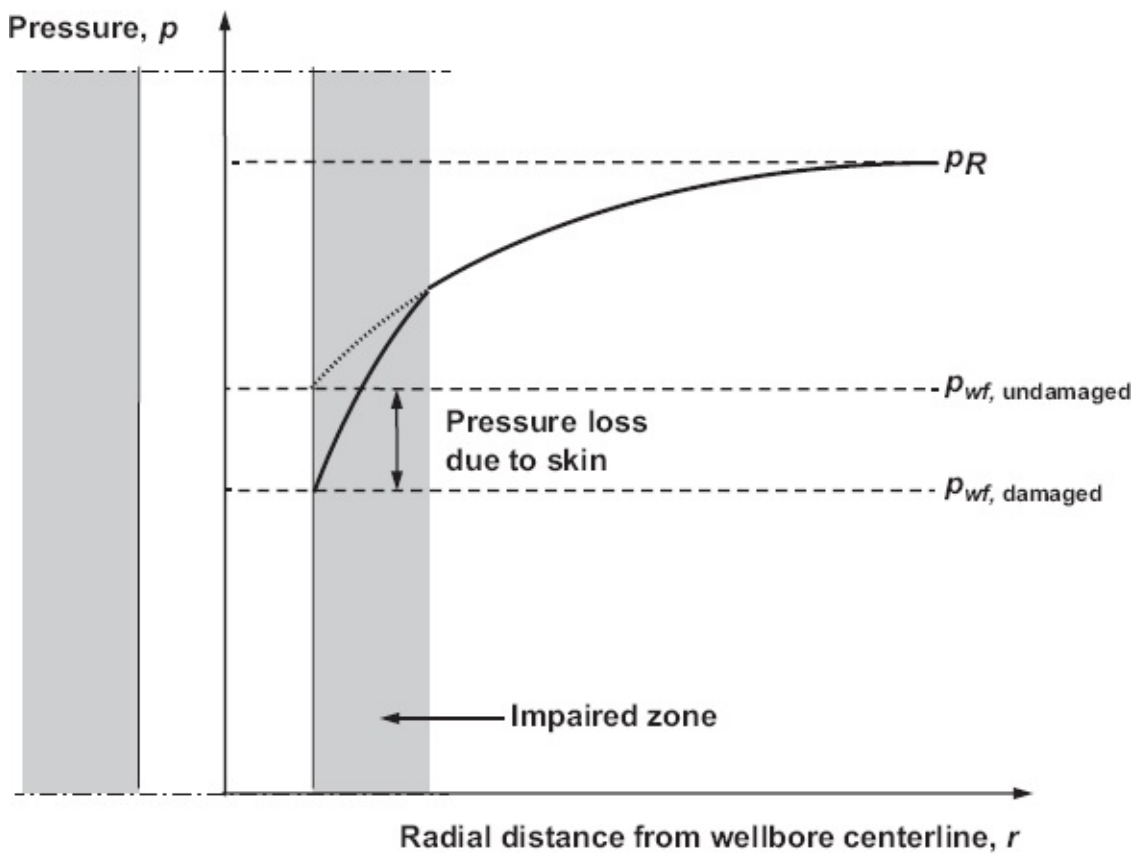


Fig. 6.6—The additional pressure drop caused by skin, at a given flow rate.

we can rewrite the combined expression for the drawdown (Eq. 6.38) as

$$p_{R,\text{ref}} - p_{wf} = -\frac{\mu B_o q_{o,\text{sc}}}{2\pi kh} \left[\ln\left(\frac{r_e}{r_w}\right) - f_R + S \right], \quad (6.43)$$

where

$$f_R = \begin{cases} 0 & \text{for steady-state flow with } p_{R,\text{ref}} = p_R, \\ \frac{1}{2} & \text{for steady-state flow with } p_{R,\text{ref}} = p_{R,\text{av}}, \\ \frac{1}{2} & \text{for semisteady-state flow with } p_{R,\text{ref}} = p_R, \\ \frac{3}{4} & \text{for semisteady-state flow with } p_{R,\text{ref}} = p_{R,\text{av}}. \end{cases} \quad (6.44)$$

The corresponding combined expression for the PI becomes

$$J = \frac{-q_{o,\text{sc}}}{p_{R,\text{ref}} - p_{wf}} = \frac{2\pi kh}{\mu B_o \left[\ln\left(\frac{r_e}{r_w}\right) - f_R + S \right]} \quad (6.45)$$

A numerical implementation of the general single-phase oil pressure drop Eq. 6.43 can be found in `res_oil_simp.m`.

6.6.3 Thick Skin. Alternatively, the skin can be taken into account by simulating the behavior of two or more rings of the near-well reservoir in series, using different permeabilities for the damaged and the undamaged zones (Muskat 1937; Hawkins 1956). **Fig. 6.7** represents an example using two rings. The corresponding pressure drop can be expressed as

$$p_R - p_{wf} = (p_R - p_s) + (p_s - p_w) = -\frac{\mu B_o q_{o,sc}}{2\pi h} \left[\frac{1}{k} \ln\left(\frac{r_e}{r_s}\right) + \frac{1}{k_s} \ln\left(\frac{r_s}{r_w}\right) \right], \dots \quad (6.46)$$

where we used the analytical approximation for steady-state oil flow (Eq. 6.21), where k_s is the reduced permeability, r_s is the external radius of the damaged zone, and p_s is the pressure at r_s . Using the definition for the skin S (Eq. 6.42), we can derive

$$S = \left(\frac{k}{k_s} - 1 \right) \ln\left(\frac{r_s}{r_w}\right), \dots \quad (6.47)$$

which is sometimes referred to as the *finite skin* or *thick skin* approach. The value of the skin S can be determined from transient well tests (see, e.g., Dake 1978, Economides et al. 2013, or more specialized books on well testing such as Kamal 2009). If the value of the skin is high, then remedial measures may be required—e.g., stimulating the well with acid to repair the damage. If a well is tested, it may appear that the skin S is nonzero. However, this may not be a result of formation damage but of the completion. If the well is gravel packed, the permeability of the gravel is likely to be greater than that of the reservoir rock. Thus the gravel pack may give less pressure drop, resulting in negative skin. On the other hand, the gravel pack itself can be heavily impaired during installation or subsequent production, and positive skin could result. Perforations can give rise to negative skin if they provide an effective path for the oil to flow into the well. Often, they contain debris from shooting the perforations and have a zone of crushed rock around them, both effects contributing to positive skin. Fractures, whether natural or produced by hydraulic fracturing, will result in easier inflow and thus negative skin.

6.7 Single-Phase Gas Flow

6.7.1 Numerical Solution. In the case of single-phase gas flow the mass conservation (Eq. 6.4) can be rewritten for steady-state conditions as

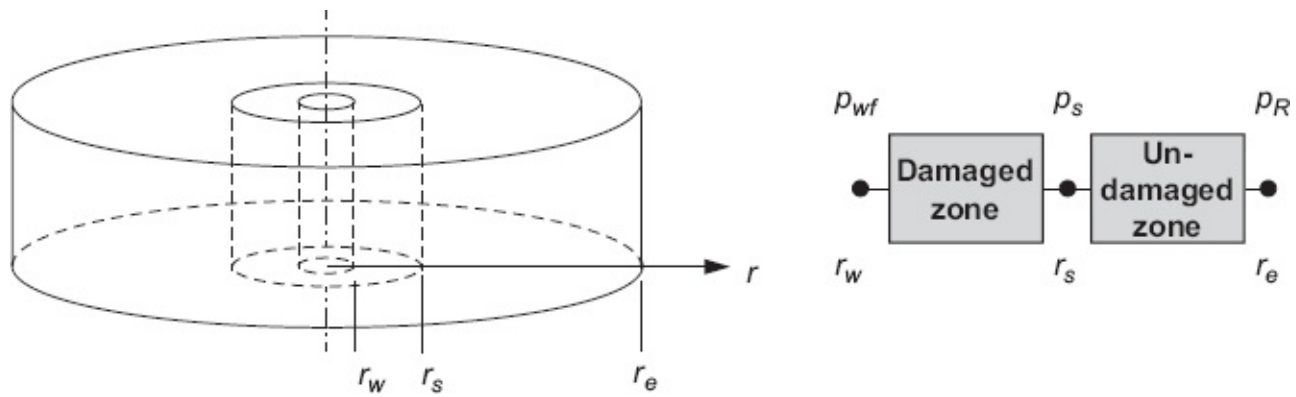


Fig. 6.7—Schematic representation of a damaged near-well reservoir (left) as two pressure drop elements in series (right).

$$\frac{d(v_g \rho_g r)}{dr} = 0. \quad (6.48)$$

The corresponding boundary condition at the wellbore radius becomes

$$r = r_w : \rho_g v_g r = \frac{\rho_g q_g r_w}{A_w} = \frac{\rho_{g,\infty} q_{g,\infty}}{2\pi h}. \quad (6.49)$$

We can now solve Eq. 6.48 and determine the integration constant with the aid of the boundary condition (Eq. 6.49) in the usual fashion. Next we can combine Eqs. 6.5 and 6.10, and together with the EOS for gas (Eq. 6.7), we arrive at the following set of equations to describe single-phase gas flow in the near-wellbore region:

$$\frac{dp}{dr} = -\frac{\mu}{k} v - \beta \rho |v| v, \quad (6.50)$$

$$v = \frac{\rho_{g,\infty} q_{g,\infty}}{2\pi h \rho r} = \frac{B_g q_{g,\infty}}{2\pi h r}, \quad (6.51)$$

$$\rho = \frac{Mp}{ZRT_{abs}} = \frac{\rho_{g,\infty}}{B_g}, \quad (6.52)$$

where we have dropped most of the subscripts g to improve the readability. This set of equations resembles Eqs. 3.33 through 3.35 as defined in Chapter 3 to describe the flow of gas in pipes. The equations are nonlinear because ρ , μ , and Z are functions of the unknown pressure p and because the pressure drop is a quadratic function of the velocity. The differential equation (Eq. 6.50) requires one boundary condition, for which we can use Eq. 6.17. As was the case for single-phase oil flow, the equations can be solved with the aid of a standard numerical integration routine in MATLAB, and a numerical implementation can be found in `res.m` and `res_gas_dpdr.m`. The IPR can then be obtained by plotting p_{wf} as a function of $q_{g,\infty}$ for a given p_R (see `example_res_pres.m`). The solid and dotted lines in Fig. 6.8 depict an example based on the data in Table 6.2 for values of the Forchheimer coefficient $\beta = 0$ and $\beta = 3.5 \times$

10^{10} 1/m, respectively.

6.7.2 Analytical Approximations. Alternatively, the equations can be linearized through the use of a real-gas pseudopressure defined as

$$m(p) = \frac{\mu}{\rho} \left|_{p=p_{ref}} \right. \times \int_{p_{ref}}^p \frac{\rho}{\mu} dp = \frac{\mu Z}{p} \left|_{p=p_{ref}} \right. \times \int_{p_{ref}}^p \frac{p}{\mu Z} dp, \quad \dots \dots \dots \quad (6.53)$$

where p_{ref} is an arbitrary reference pressure. In this formulation the pseudopressure has the dimension of pressure. Often other formulations are used, without the scaling factor $(\mu/\rho)_{p=p_{ref}}$, such that the pseudopressure has a different dimension. (See Al-Hussainy et al. 1966 for the original paper and Hagoort 1988 for practical details.)

The linearization can be obtained as follows. First we combine Eqs. 6.50 through 6.52, while dropping the Forchheimer term, to obtain the pressure drop equation

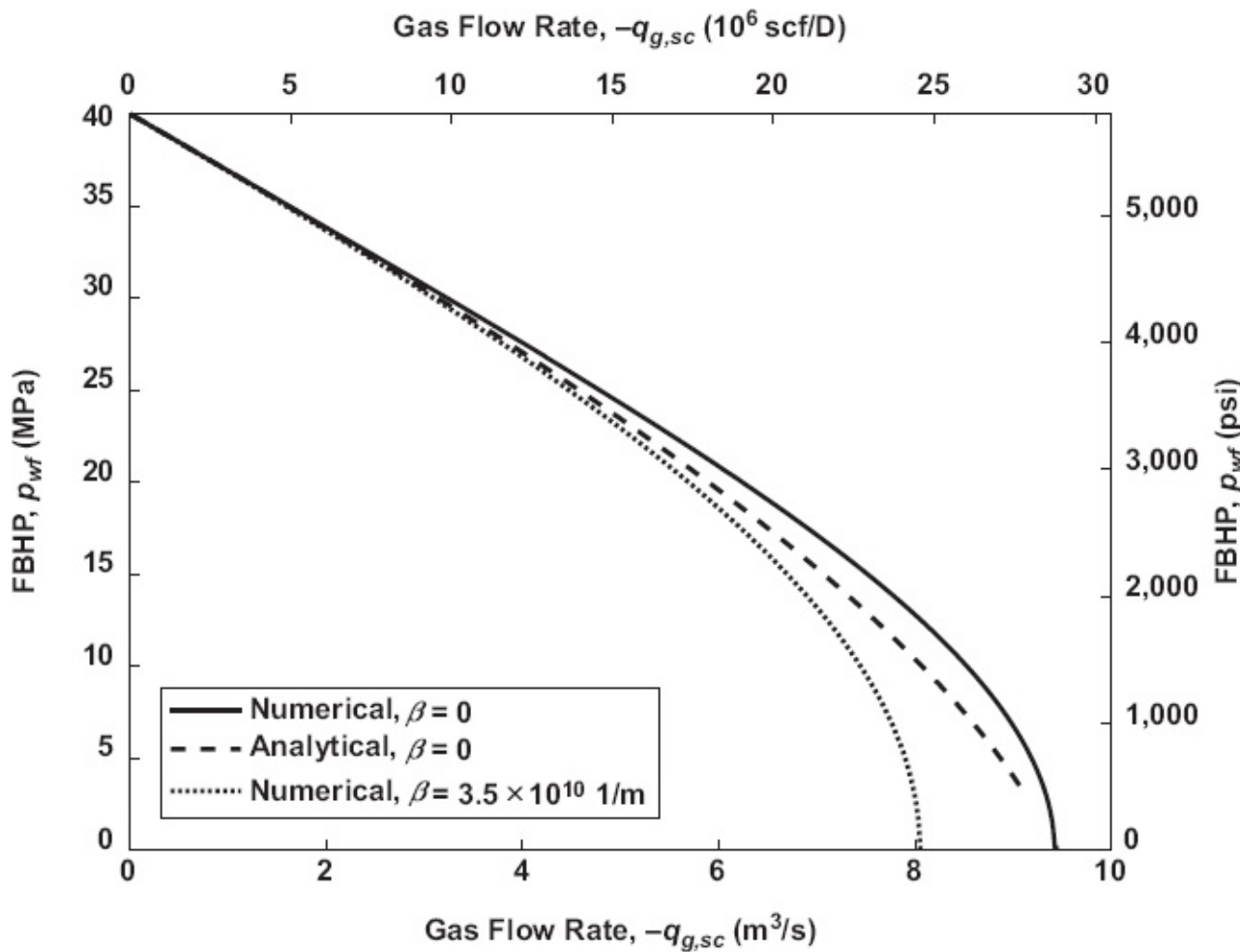


Fig. 6.8—Nonlinear IPR for a gas reservoir with parameters given in Table 6.2.

Parameter		SI Units		Field Units
Reservoir height	h	20	m	65.6 ft
Reservoir radius	r_e	500	m	1,640 ft

Well radius	r_w	0.2	m	0.65	ft
Permeability	k_g	2.0×10^{-15}	m^2	2.0	mD
Forchheimer coeff.	β	3.5×10^{10}	$1/\text{m}$	8.9×10^7	$1/\text{in.}$
Viscosity	μ_g	Carr et al. (1954) correlation			
Density/gravity	$\rho_{g,sc}/\gamma_g$	0.95	kg/m^3	0.77	—
Reservoir pressure	p_R	40×10^6	Pa	5,802	psi
Reservoir temperature	T_R	120	$^\circ\text{C}$	248	$^\circ\text{F}$
Skin	S	0	—	0	—
Flow regime	Steady-state				

Table 6.2—Parameter values for Fig. 6.8.

$$\frac{dp}{dr} = -\frac{\mu Z T_{abs} \rho_{g,sc} q_{g,sc}}{2\pi k h M p} \frac{1}{r} = -\frac{\mu B_g q_{g,sc}}{2\pi k h} \frac{1}{r}, \quad (6.54)$$

which is nonlinear because of the dependence of μ and Z (and therefore of B_g) on p . Next we use the relationship

$$\frac{dm(p)}{dr} = \frac{dm(p)}{dp} \frac{dp}{dr}, \quad (6.55)$$

and Eq. 6.53 to obtain

$$\frac{dm(p)}{dp} = \frac{\mu_{ref} Z_{ref} p}{p_{ref} \mu Z}, \quad (6.56)$$

and therefore

$$\frac{dp}{dr} = \frac{p_{ref} \mu Z}{\mu_{ref} Z_{ref} p} \frac{dm(p)}{dr}. \quad (6.57)$$

Eq. 6.54 can now be rewritten as

$$\frac{dm(p)}{dr} = -\frac{RT_{abs} \mu_{ref} Z_{ref} \rho_{g,sc} q_{g,sc}}{2\pi k h M p_{ref}} \frac{1}{r} = -\frac{\mu_{ref} B_{g,ref} q_{g,sc}}{2\pi k h} \frac{1}{r}, \quad (6.58)$$

which is now a linear equation in terms of the pseudopressure $m(p)$. Here, in line with assumptions made before, we assume that the reservoir temperature T_{abs} remains constant.

For a given gas composition and the corresponding relationships for μ_g and Z as functions of p , we can determine a one-to-one relationship between p and m through numerically integrating Eq. 6.53. We can then simply use all the results that were obtained for single-phase oil flow, replacing p with m and changing the constant oil properties to the corresponding constant gas properties. In other words, the general

single-phase oil equation (Eq. 6.43) can now be used to obtain a corresponding single-phase gas equation:

$$m(p_{R,\text{ref}}) - m(p_{wf}) = -\frac{\mu_{\text{ref}} B_{g,\text{ref}} q_{g,\text{sc}}}{2\pi kh} \left[\ln\left(\frac{r_e}{r_w}\right) - f_R + S \right], \quad (6.59)$$

with f_R and $p_{R,\text{ref}}$ given by Eq. 6.39. The value of the arbitrary reference pressure p_{ref} — not to be confused with $p_{R,\text{ref}}$ — is not relevant to the computation of the pseudopressure because we are interested only in pressure differences, and not in absolute pressures.

Fig. 6.9 depicts an example of the relationship between pressures and pseudopressures. The graph was produced with the aid of MATLAB files `gas_pseu_pres.m` and `gas_dmdp.m`. We refer to Dake (1978) or Hagoort (1988) for further information about the use of pseudopressures for gas engineering calculations. For an extension of the concept of pseudopressures to two-phase (gas/oil) flow, see Walsh and Lake (2003).

If the difference between the reservoir pressure p_R and the FBHP p_{wf} is not too large, we can use constant average values μ_{av} and Z_{av} , evaluated at an average reservoir pressure $p_{R,\text{av}}$, in the definition of the pseudopressure. If we now choose $p_{\text{ref}} = p_{R,\text{av}}$, integration of Eq. 6.53 shows that the pseudopressure reduces to

$$m(p) = \frac{p^2 - p_{R,\text{av}}^2}{2p_{R,\text{av}}}. \quad (6.60)$$

Formally, the average viscosity is generally *not* equal to the viscosity evaluated at the average pressure because $\mu(p)$ is a nonlinear function. However, given the approximate nature of the model, the simplification $\mu_{\text{av}} \approx \mu(p_{\text{av}})$ is justified. The same holds for the average compressibility factor $Z_{\text{av}} \approx Z(p_{\text{av}})$.

Substitution of Eq. 6.60 in the general single-phase gas expression (Eq. 6.59) results in

$$p_{R,\text{ref}}^2 - p_{wf}^2 = -\frac{\mu_{\text{av}} B_{g,\text{av}} q_{g,\text{sc}} P_{R,\text{av}}}{\pi kh} \left[\ln\left(\frac{r_e}{r_w}\right) - f_R + S \right], \quad (6.61)$$

or

$$p_{wf} = \sqrt{p_{R,\text{ref}}^2 + \frac{\mu_{\text{av}} B_{g,\text{av}} q_{g,\text{sc}} P_{R,\text{av}}}{\pi kh} \left[\ln\left(\frac{r_e}{r_w}\right) - f_R + S \right]}. \quad (6.62)$$

Eq. 6.61 can also be obtained without the use of pseudopressures (see, e.g., Russell et al. 1966). Note that we still have the freedom to choose $p_{R,\text{ref}}$ as either p_R or $p_{R,\text{av}}$ with corresponding values of f_R as given in Eq. 6.39. The choice of $p_{R,\text{ref}} = p_{R,\text{av}}$ will be useful if the average reservoir pressure can be obtained from a well test. If we

choose $p_{R,\text{ref}} = p_R$, the average reservoir pressure can be approximated with the aid of Eqs. 6.26 and 6.60 as

$$p_{R,\text{av}} \approx p_R + \frac{\mu_{\text{av}} B_{g,\text{av}} q_{g,\text{sc}}}{4\pi kh}, \dots \quad (6.63)$$

which can then also be used to compute the average values for the gas properties. (The full expression is obtained by solving the quadratic equation in $p_{R,\text{av}}$. The approximation then follows by using a Taylor expansion for the square-root term.) A few iterations may be required to determine the average properties to sufficient accuracy.

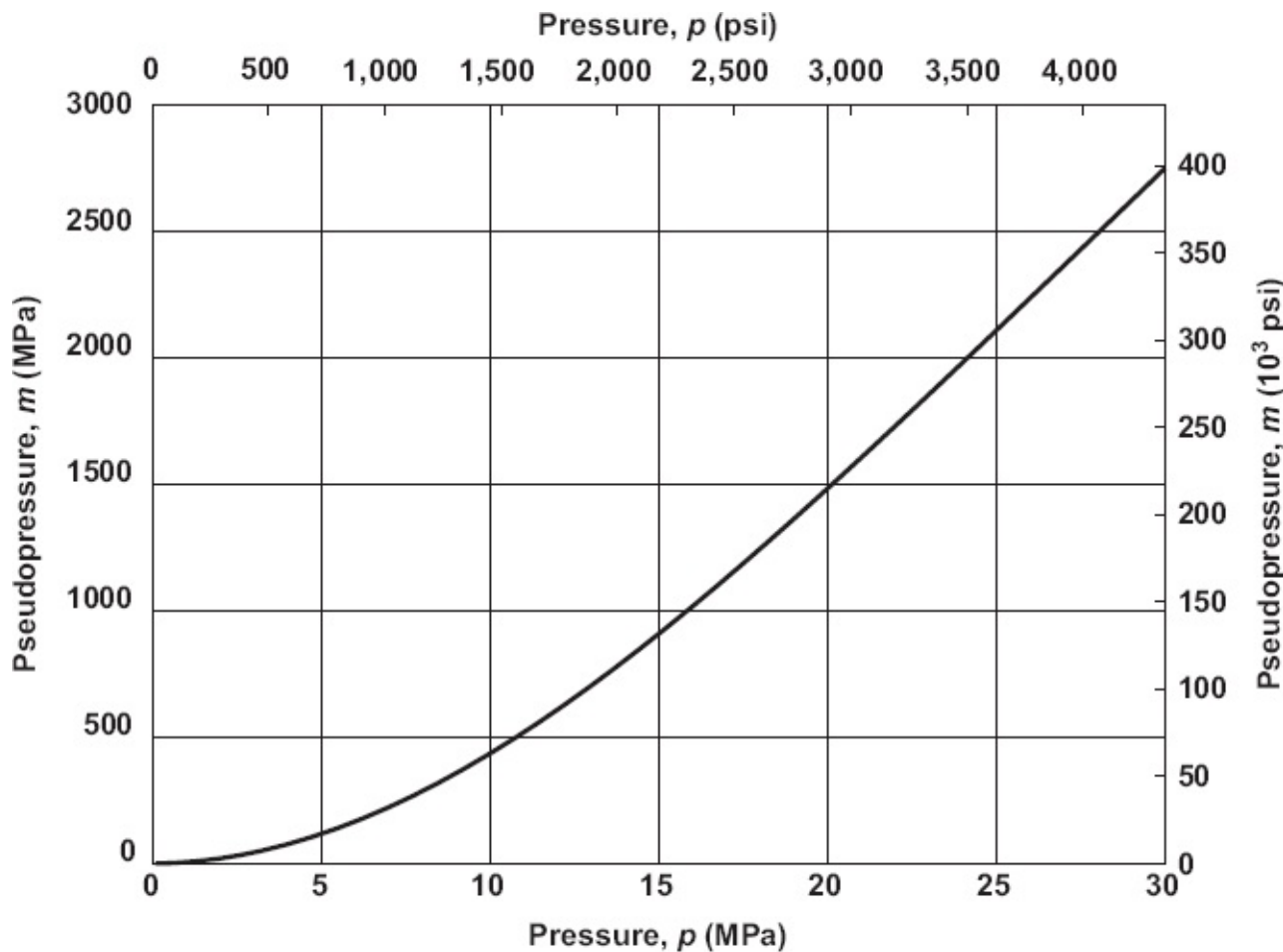


Fig. 6.9—Pseudopressure as a function of pressure for hydrocarbon gas with density $\rho_{g,\text{sc}} = 0.95 \text{ kg/m}^3$ ($y_g = 0.77$), at temperature $T = 75^\circ\text{C}$ (167°F) and pressures $0.1 < p < 30 \text{ MPa}$ ($14.7 < p < 4,351 \text{ psi}$).

Note that this result is valid only for a Forchheimer coefficient β equal to zero, because the nonlinear term $\beta\rho v^2$ was not taken into account in the derivation. For high flow rates (i.e., when β cannot be neglected) we need to add an additional pressure drop term (for details see, e.g., Dake 1978). This approximate inflow relationship (Eq. 6.61) has been implemented in MATLAB file `res_gas_simp.m`, which was used to create the approximate IPR indicated with a dashed line in Fig. 6.8. The difference

with the numerical result, determined with res.m and indicated with a solid line, is not very large even though the drawdown is considerable. However, at higher flow rates (for $|q_{g,sc}| > 9 \text{ m}^3/\text{s}$) the iteration became problematic and no solutions were found. A semi-empirical generalization of Eq. 6.61, known as the *backpressure equation*, can be written as

$$q_{g,sc} = C(p_R^2 - p_{wf}^2)^n, \dots \quad (6.64)$$

where the constants C and n have to be determined from measurements of gas flow rates and bottomhole pressures during a multirate production test. A typical value for n is between 0.5 and 1.

6.8 Multiphase Flow: Empirical Models

Starting from a detailed geological model and measured reservoir and fluid properties, and using numerical reservoir simulation, one could, in theory, obtain a detailed time-varying prediction of the pressure and oil, gas, and water distributions around a well. In practice, predicting the inflow performance of a well under multiphase flow conditions is possible only to a limited extent. However, after a well has been put on stream, we may use data collected during multirate well tests. These can then be used to fit a PI or a nonlinear IPR, which may have some predictive capacity, although extrapolations outside the range of water cuts and gas/oil ratios (GORs) actually observed are still of limited value. Here we first present some examples of such semiempirical IPRs. In Chapter 7, we present a somewhat more physics-based approach to illustrate the effects of the presence of gas in the near-wellbore region around an oil well.

6.8.1 Solution Gas Drive. For primary production of a reservoir below the bubblepoint pressure, several empirical relationships have been established, directly expressed in terms of oil flow rate and FBHP. They are similar to the backpressure equation (Eq. 6.64) for gas wells (which is also sometimes used for oil wells). We mention the ones proposed by Vogel (1968) and Fetkovich (1973), which are valid for gas/oil flow from a reservoir produced by solution gas drive:

$$\text{Vogel: } \frac{q_{o,sc}}{q_{o,sc,\max}} = 1 - \alpha \left(\frac{P_{wf}}{P_{R,\text{ref}}} \right) - (1 - \alpha) \left(\frac{P_{wf}}{P_{R,\text{ref}}} \right)^2, \dots \quad (6.65)$$

$$\text{Fetkovich: } \frac{q_{o,sc}}{q_{o,sc,\max}} = \left[1 - \left(\frac{P_{wf}}{P_{R,\text{ref}}} \right)^2 \right]^n \dots \quad (6.66)$$

Here, $q_{o,sc,\max}$ is the AOFP, i.e., the value of $q_{o,sc}$ when p_{wf} is zero (see Fig. 6.10, left). Note that this zero pressure can normally not be achieved in practice. The reference reservoir pressure $p_{R,\text{ref}}$ may be chosen as either p_R or $p_{R,\text{av}}$. Eqs. 6.65 and 6.66 both

contain two parameters (α in Vogel's, n in Fetkovich's, and $q_{sc,max}$ in both) and therefore need at least two sets of pressure and flow rate measurements from a multirate well test. Based on a large number of numerical simulations, Vogel (1968) recommends choosing $\alpha = 0.2$. In that case at least one single-rate well test is required to estimate $q_{sc,max}$. Fetkovich (1973) reported values of n between 0.57 and 1.00, as observed in a large number of well tests. The shapes of the IPRs corresponding to Eqs. 6.65 and 6.66 are similar to those for gas flow depicted in Fig. 6.8. We refer to Golan and Whitson (1991) and Beggs (1991) for examples of how to determine empirical IPRs from production tests.

6.8.2 Predictive Mode. To use Eqs. 6.65 and 6.66 in a predictive mode, it is necessary to guess the two unknown parameters (i.e., α and $q_{sc,max}$, or n and $q_{sc,max}$). Alternatively, we can use a theoretical estimate of the PI for small flow rates to eliminate one of the two unknowns and use a best guess for the remaining one. For this approach we make use of the observation that for small flow rates the IPR is close to linear such that we can define an approximate initial PI as

$$J^* = \left. \frac{dq_{o,sc}}{dp_{wf}} \right|_{p_{wf} = p_{R,ref}}, \dots \quad (6.67)$$

which for the Vogel relationship (Eq. 6.65) leads to

$$J^* = q_{o,sc,max} \left[-\frac{\alpha}{p_{R,ref}} - \frac{2(1-\alpha)}{p_{R,ref}} \left(\frac{p_{wf}}{p_{R,ref}} \right) \right]_{p_{wf} = p_{R,ref}} = q_{o,sc,max} \left(\frac{\alpha - 2}{p_{R,ref}} \right), \dots \quad (6.68)$$

such that we can express the AOFP as

$$q_{o,sc,max} = J^* \left(\frac{p_{R,ref}}{\alpha - 2} \right). \dots \quad (6.69)$$

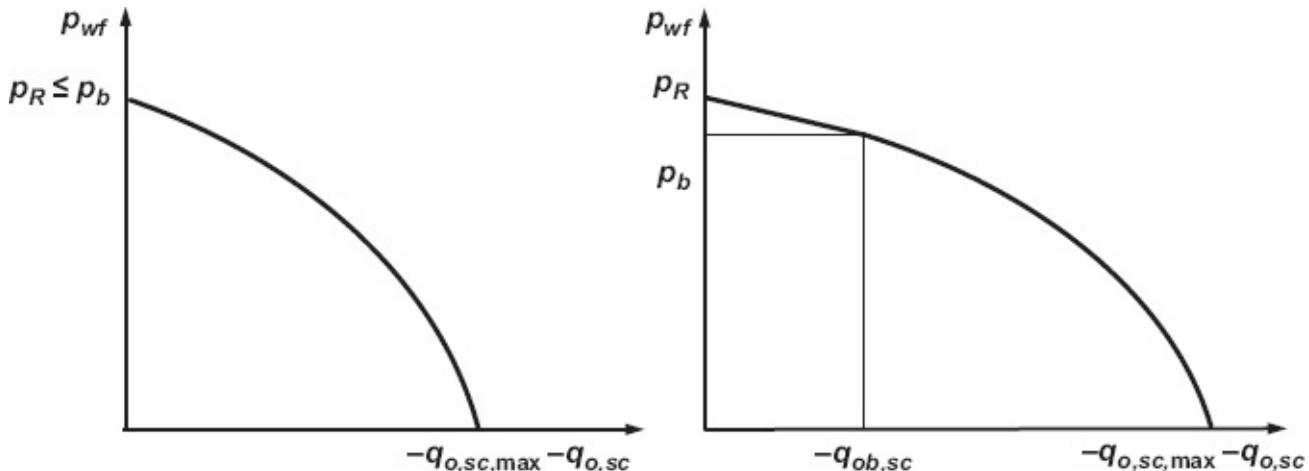


Fig. 6.10—Schematic solution gas drive IPRs for two oils with bubblepoint pressures above the (average) reservoir pressure (left) or below it (right).

(Recall that in our convention $q_{o,sc,max} < 0$.) At the start of production from a solution gas drive reservoir, the value of J^* for pressures at the bubblepoint follows from Eq. 6.45, where the permeability to oil should be taken as $k_o = k \times k_{ro}^0$. After production has resulted in a drop in reservoir pressure and thus an increase in gas saturation and a reduction in oil permeability, the value of J^* may be approximated as

$$J^* = \frac{2\pi k_{o,ref} h}{\mu_{o,ref} B_{o,ref} \ln\left(\frac{r_e}{r_w} - f_R + S\right)}, \quad \dots \quad (6.70)$$

where $k_{o,ref}$ is the (saturation-dependent) permeability to oil, and $\mu_{o,ref}$ and $B_{o,ref}$ are the (pressure-dependent) oil viscosity and the oil formation volume factor, respectively (Standing 1971). The pressure-dependent parameters $\mu_{o,ref}$ and $B_{o,ref}$ can be approximated by using their values evaluated at $p_{R,ref}$. A crude estimate of the saturation-dependent oil permeability $k_{o,ref}$ can be obtained by assuming that the oil saturation decreases linearly with decreasing reservoir pressure such that

$$k_{o,ref}(S_{o,ref}) = k_{o,ref}\left(\frac{p_{R,ref}}{p_b} S_{ob}\right), \quad \dots \quad (6.71)$$

where $S_{ob} = 1 - S_{wi}$ is the oil saturation at (and above) the bubblepoint pressure. An approximate predictive expression for p_{wf} as a function of $q_{o,sc}$ under primary two-phase (gas/oil) production now follows by solving for p_{wf} from Eq. 6.65, which leads to

$$p_{wf} = \frac{p_{R,ref} \left[-\alpha + \sqrt{\alpha^2 - 4(1-\alpha)\left(\frac{q_{o,sc}}{q_{o,sc,max}} - 1\right)} \right]}{2(1-\alpha)}, \quad \dots \quad (6.72)$$

where $q_{o,sc,max}$ should be determined with the aid of Eqs. 6.69 and 6.45 or 6.70, and where, following the original publication of Vogel (1968), the value of α should be taken as 0.2. As before, the reference reservoir pressure $p_{R,ref}$ may be chosen as either p_R or $p_{R,av}$.

6.8.3 Initial Pressure Above Bubblepoint. For a reservoir that has a reservoir pressure above the bubblepoint pressure, but for which the FBHP drops below it, we can derive a modified Vogel expression with the aid of Fig. 6.10 (right) as

$$\frac{q_{o,sc}}{q_{o,sc,max}} = \begin{cases} \frac{J(p_{wf} - p_{R,ref})}{q_{o,sc,max}} & \text{if } p_{wf} > p_b, \\ 1 - \left(1 - \frac{q_{ob,sc}}{q_{o,sc,max}}\right) \left[\alpha \left(\frac{p_{wf}}{p_b}\right) + (1-\alpha) \left(\frac{p_{wf}}{p_b}\right)^2 \right] & \text{if } p_{wf} \leq p_b, \end{cases} \quad \dots \quad (6.73)$$

where $q_{ob,sc} = J (p_b - p_{R,ref})$ is the (negative-valued) flow rate at the bubblepoint pressure, with J given by Eq. 6.45, and where the AOFP should now be determined as

$$q_{o,sc,max} = q_{ob,sc} + J \left(\frac{p_b}{\alpha - 2} \right). \quad \dots \dots \dots \quad (6.74)$$

Eq. 6.73 can be rewritten in a similar form as Eq. 6.72, which leads to

$$p_{wf} = \begin{cases} p_{R,ref} + \frac{q_{o,sc}}{J} & \text{if } |q_{o,sc}| \leq |q_{ob,sc}|, \\ p_b \left[-\alpha + \sqrt{\alpha^2 - 4(1-\alpha) \left(\frac{q_{o,sc} - q_{ob,sc}}{q_{o,sc,max} - q_{ob,sc}} - 1 \right)} \right] & \text{if } |q_{o,sc}| > |q_{ob,sc}|, \end{cases} \quad \dots \dots \quad (6.75)$$

with $q_{o,sc,max}$ given by Eq. 6.74. Eq. 6.75 has been implemented in MATLAB file resVogel.m.

Fig. 6.11 displays two typical Vogel-type IPRs for oils with different solution GORs and reservoir parameters given in **Table 6.3**.

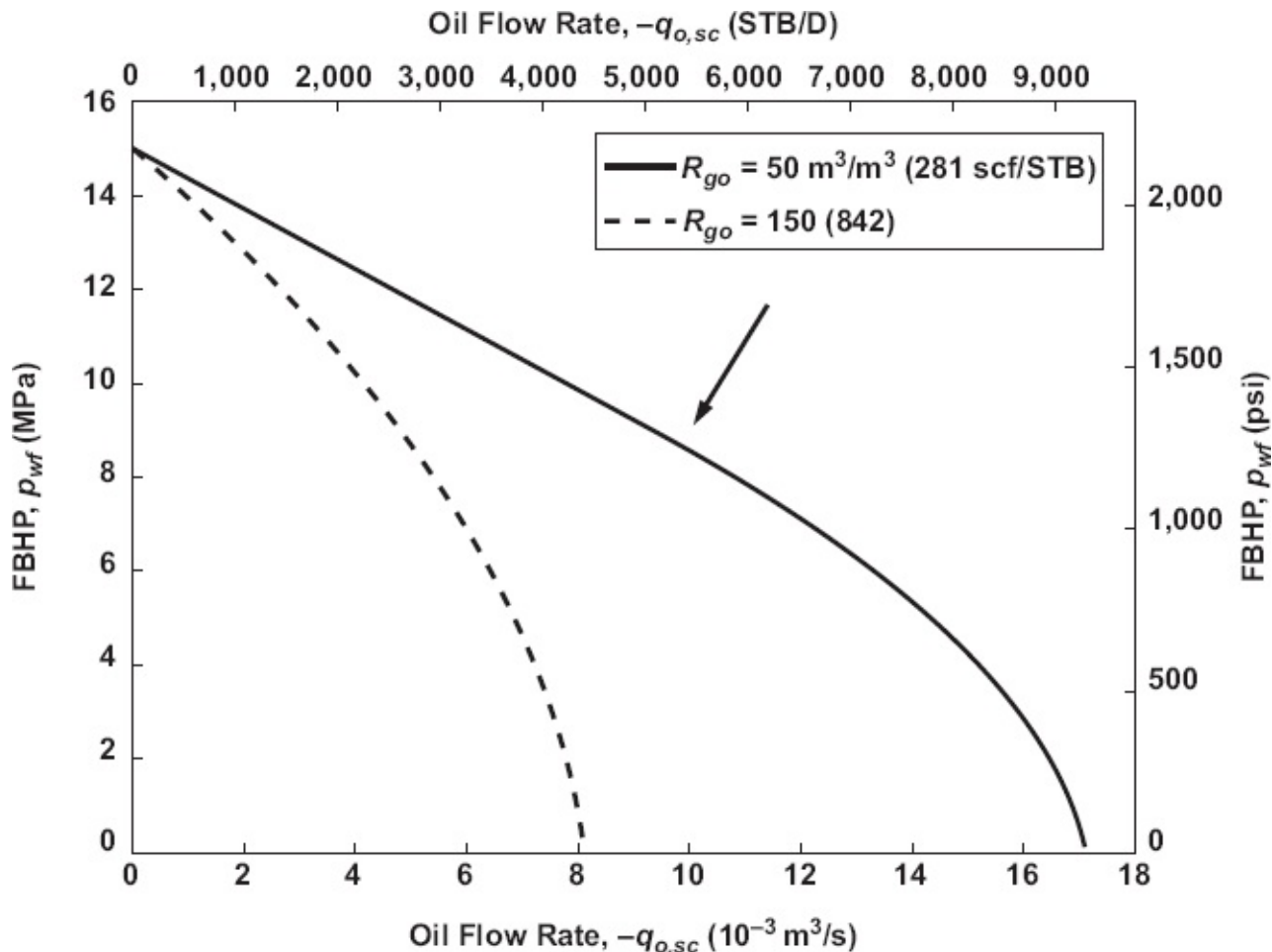


Fig. 6.11—Vogel-type IPRs of an oil well with parameters given in Table 6.3 for two different values of the solution GOR as indicated in the legend. The corresponding bubblepoint pressures are 9.00 MPa (1,306 psi) and 22.7 MPa (3,288 psi) respectively (arrow indicates point at which the low-GOR curve drops below bubblepoint pressure).

Parameter		SI Units		Field Units	
Water cut	f_w	0	—	0	—
Reservoir height	h	20	m	65.6	ft
Reservoir radius	r_e	500	m	1,640	ft
Well radius	r_w	0.2	m	0.65	ft
Permeability	k	1.11×10^{-13}	m^2	101	mD
Forchheimer coeff.	β	3.5×10^{10}	1/m	8.9×10^7	1/in.
Endpoint gas	k_{rg}^0	0.7	—	0.7	—
Endpoint oil	k_{ro}^0	0.9	—	0.9	—
Endpoint water	k_{rw}^0	0.5	—	0.5	—
Corey gas	n_g	3	—	3	—
Corey oil/gas	n_{og}	3	—	3	—
Corey oil/water	n_{ow}	3	—	3	—
Corey water	n_w	3	—	3	—
Critical gas sat.	S_{gc}	0.15	—	0.15	—
Residual oil sat.	S_{or}	0.10	—	0.10	—
Immobile water saturation	S_{wi}	0.15	—	0.15	—
Oil rel. perm.	k_{ro}	Modified Stone II model; Aziz & Settari (1979)			
Gas viscosity	μ_g	Carr et al. (1954) correlation			
Oil viscosity	μ_o	Beggs and Robinson (1975), Vasquez and Beggs (1980)			
Gas density/gravity	$\rho_{g,sc}/\gamma_g$	0.95	kg/m^3	0.77	—
Oil density/gravity	$\rho_{o,sc}/\gamma_{API}$	850	kg/m^3	35	°API
Water density/gravity	$\rho_{w,sc}/\gamma_w$	1050	kg/m^3	1.05	—
Equations of state		Standing (1952), black oil; Standing and Katz (1942) Z factor			
Reservoir pressure	p_R	15.0×10^6	Pa	1,378	psi
Reservoir temp.	T_R	90		194	°F
Skin	S	0	—	0	—
Flow regime		Steady-state			

Table 6.3—Parameter values for Figs. 6.11 and 7.21.

6.9 Multilayer Inflow Performance

If a well is completed in more than one layer, the production from the well is called

commingled. If the layers are separated by impermeable flow barriers, and if they have different permeabilities, *differential depletion* may occur, resulting in gradually increasing differences in the reservoir pressures of the layers. (Here, we disregard the differences in hydrostatic pressure resulting from depth under the assumption that the differences resulting from differential depletion are much larger.) In that case the combined inflow performance can readily be calculated provided that the individual IPRs are both linear.

As shown in [Fig. 6.12](#), for a given value of p_{wf} , the total production rate $q_{o,sc}$ can be determined by calculating the individual contributions $q_{o,sc,1}$ and $q_{o,sc,2}$, and adding them as follows:

$$\begin{aligned} q_{o,sc,1} &= -J_1(p_{R,1} - p_{wf}), \quad q_{o,sc,2} = -J_2(p_{R,2} - p_{wf}), \\ q_{o,sc} &= q_{o,sc,1} + q_{o,sc,2} = -J_1 p_{R,1} - J_2 p_{R,2} + (J_1 + J_2) p_{wf}. \end{aligned} \quad \dots \quad (6.76)$$

Thus the production rate still varies linearly with p_{wf} . Note however that this formula applies only to values of p_{wf} lower than the lowest of the two zone pressures. Above this pressure, part of the production from one zone will be injected into the other zone. This phenomenon, which is often referred to as *crossflow*, is illustrated in [Fig. 6.13](#). If the well is closed in at surface, a steady-state situation will develop in which equal amounts are produced from and injected into the respective reservoir units. Crossflow can seriously impair the reservoir into which the injection takes place. A similar reasoning can be applied in case of nonlinear IPRs (see Question 6.10). For an example of controlled, commingled production from a stacked reservoir, see the MATLAB assignment in [Section 6.12](#).

6.10 Related Topics Not Considered in This Chapter

Many aspects influencing near-wellbore flow have not been considered in this chapter, such as the effect on inflow performance of well deviation, permeability anisotropy, partially penetrating wells, hydraulic fractures, perforation patterns, washed-out well sections, gravel packs, slotted liners, and wire-wrapped screens. We also did not discuss methods used to compute transient reservoir flow, which is important during the early stages of production. Some of these topics will be discussed in [Chapter 7](#), and for some others we refer to the literature. Many publications are available describing pressure drop over specific completion elements such as perforations, slotted liners, or screens. Nearly always the pressure drop over these elements can be considered to be in series with the near-well reservoir pressure drop, such that they may simply be added. For further reading on the topic of inflow performance, see, e.g., the textbooks of Brown (1984), Beggs (1991), Golan and Whitson (1991), and Economides et al. (1998, 2013) as well as the more specialized references mentioned in [Chapter 7](#).

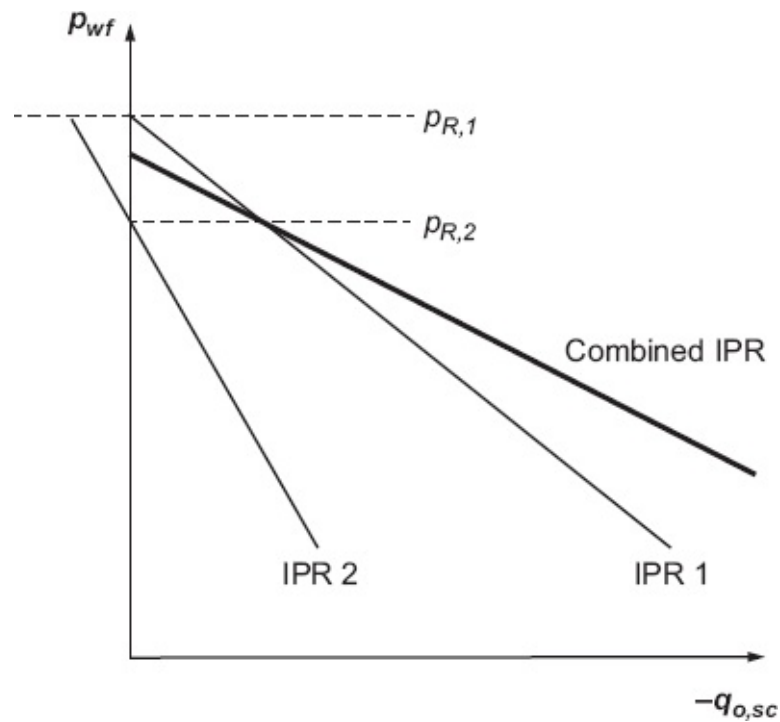


Fig. 6.12—Two-layer inflow performance.

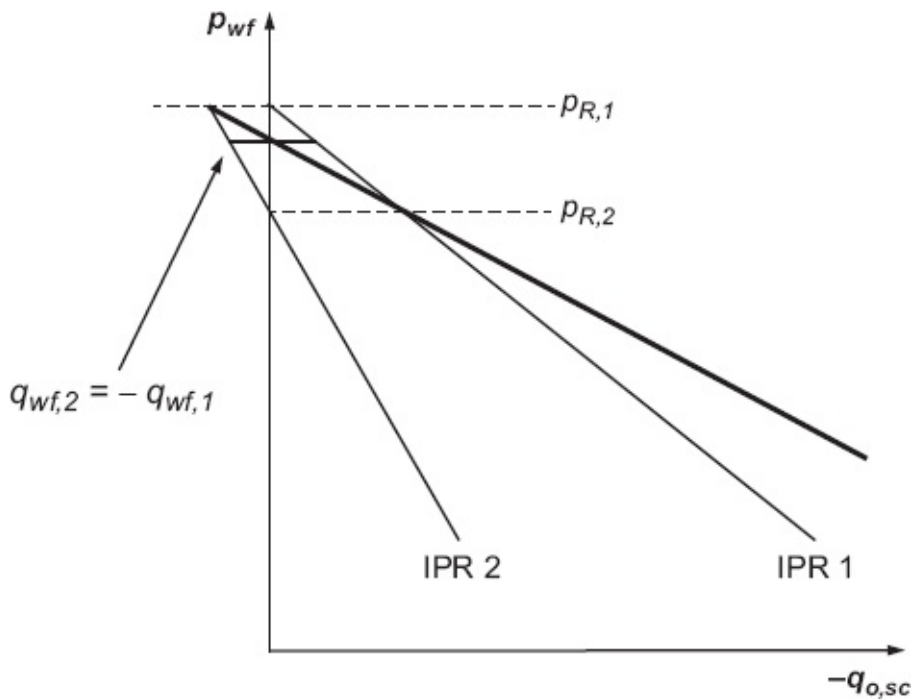


Fig. 6.13—Crossflow between two reservoir units in a closed-in well.

6.11 Questions

- 6.1 Under which conditions does a linear PI provide a good model for well inflow behavior?
- 6.2 What is the difference between steady-state and pseudosteady-state

reservoir flow?

- 6.3 What are the units of the skin factor S in a well inflow equation?
- 6.4 What is the most common reason for crossflow between two zones after closing in a well that has been completed in multiple reservoir zones?
- 6.5 Consider single-phase oil flow under semisteady-state conditions toward a well in the center of a circular reservoir with parameters given in **Table 6.4**. What is the PI expressed in SI units and in field units?
- 6.6 Analyze the sensitivity of the solution to Question 6.5 to changes in k , r_w , and r_e by recomputing the PI for different values of these parameters (e.g., 0.5, 0.75, 1.5, and 2.0 times their original values) and plotting the results in a spider plot—i.e., a plot with the relative change in a parameter value on the horizontal axis and the corresponding relative change in the PI on the vertical axis. What do you conclude?
- 6.7 Starting from the expression for semisteady-state flow toward a vertical well ([Eq. 6.35](#)), derive exact and approximate expressions for the average reservoir pressure and for the corresponding drawdown (i.e., [Eq. 6.37](#)).

Property	Value	Units
B_o	1.12	—
H	35	ft
k_o	84	mD
$p_{R,av}$	5,600	psi
r_e	2,100	ft
r_w	0.33	ft
R_{sb}	145	scf/STB
S	0	—
T_R	230	°F
γ_{API}	29	°API
γ_g	0.78	—
μ_o	2.54	cp

Table 6.4—Input data for well inflow performance for Question 6.5.

- 6.8 A frequently used equation for the inflow performance of a horizontal well was derived by Joshi (1988) and is derived in detail in [Chapter 7](#). He modeled horizontal flow toward a horizontal well of length L oriented along the major axis of an elliptical drainage domain with major axis length a_e and constant height h . He chose the ends of the well to coincide with the foci of the ellipse, and he assumed a vertical constant pressure boundary at the elliptical edge of the domain, as well as two horizontal no-flow boundaries at the top and the bottom with the well midway between. In addition he approximated the flow

resistance in the vertical plane to account for the radial convergence of the flowlines close to the well. The combined effects result in a PI that can, for an oil well, be expressed as

$$J = \frac{-q_{o,sc}}{p_R - p_{wf}} = \frac{2\pi kh}{\mu B_o} \left[\ln \left(\frac{a_e}{L} + \sqrt{\frac{a_e^2}{L^2} - 1} \right) + \frac{h}{L} \ln \left(\frac{h}{2r_w} \right) \right]^{-1} \quad \dots \dots \dots \quad (6.77)$$

Compute the production rate for a horizontal gas well with fluid properties given in [Table 6.2](#), well length $L = 500$ m, reservoir dimensions $h = 20$ m and $a_e = 700$ m, and FBHP $p_{wf} = 20$ MPa. Set the Forchheimer term equal to zero, and use the approximate analytical solution technique with quadratic pressures described in [Section 6.8.2](#). For the average gas properties use $\mu_{g,av} = 23 \times 10^6$ Pa·s and $B_{g,av} = 4.4 \times 10^3$. Compute the average reservoir pressure iteratively with [Eq. 6.63](#); start with a first guess—e.g., $p_{R,av} = (p_{wf} + p_R)/2$ —and perform a single iteration.

- 6.9 A vertical oil well in a reservoir above bubblepoint pressure has a productivity index $J = 4 \times 10^9$ m³/s·Pa (15.0 STB/D-psi). The initial average reservoir pressure is 30 MPa (4351 psi) and the bubblepoint pressure 28 MPa (4,061 psi). Compute the flow rate when the FBHP is lowered to 25 MPa (3,626 psi). Use the Vogel equation with $\alpha = 0.2$.
- 6.10 A vertical gas well's production is commingled from two reservoir layers with different permeabilities. Because of differential depletion, the reservoir pressure in the upper layer has dropped to 9 MPa, whereas the reservoir pressure in the lower layer is still 10 MPa. [Fig. 6.14](#) depicts the IPRs corresponding to the two layers, which are close enough vertically to neglect the effects of gravity. What is the CBHP of the well? Will there be crossflow between the layers? If yes, how much? How much does the well produce at a FBHP of 6 MPa?

Questions 6.11 through 6.14 require the use of MATLAB.

- 6.11 Recompute the answer to Question 6.5 with the aid of MATLAB function `res油simp.m`.
- 6.12 Inspect and run the MATLAB file `example_IPR.m`. Investigate the effect of a skin value $S = 5$. What would be a more effective measure to counteract this amount of wellbore damage for future wells in the same area: (a) performing an acid job to return the skin value to zero again or (b) drilling a well with twice the diameter?
- 6.13 Recompute the answer to Question 6.8 with the aid of pseudopressures. Hint: Inspect MATLAB function `example_gas_pseu_pres.m`. Make a copy and modify it to compute $m(p_R)$, $m(p_{wf})$, $\mu_{g,ref}$, and $B_{g,ref}$ for use in a slightly adapted version of [Eq. 6.77](#). What is causing the small difference with respect to the answer to

Question 6.8? Which of the answers is more accurate?

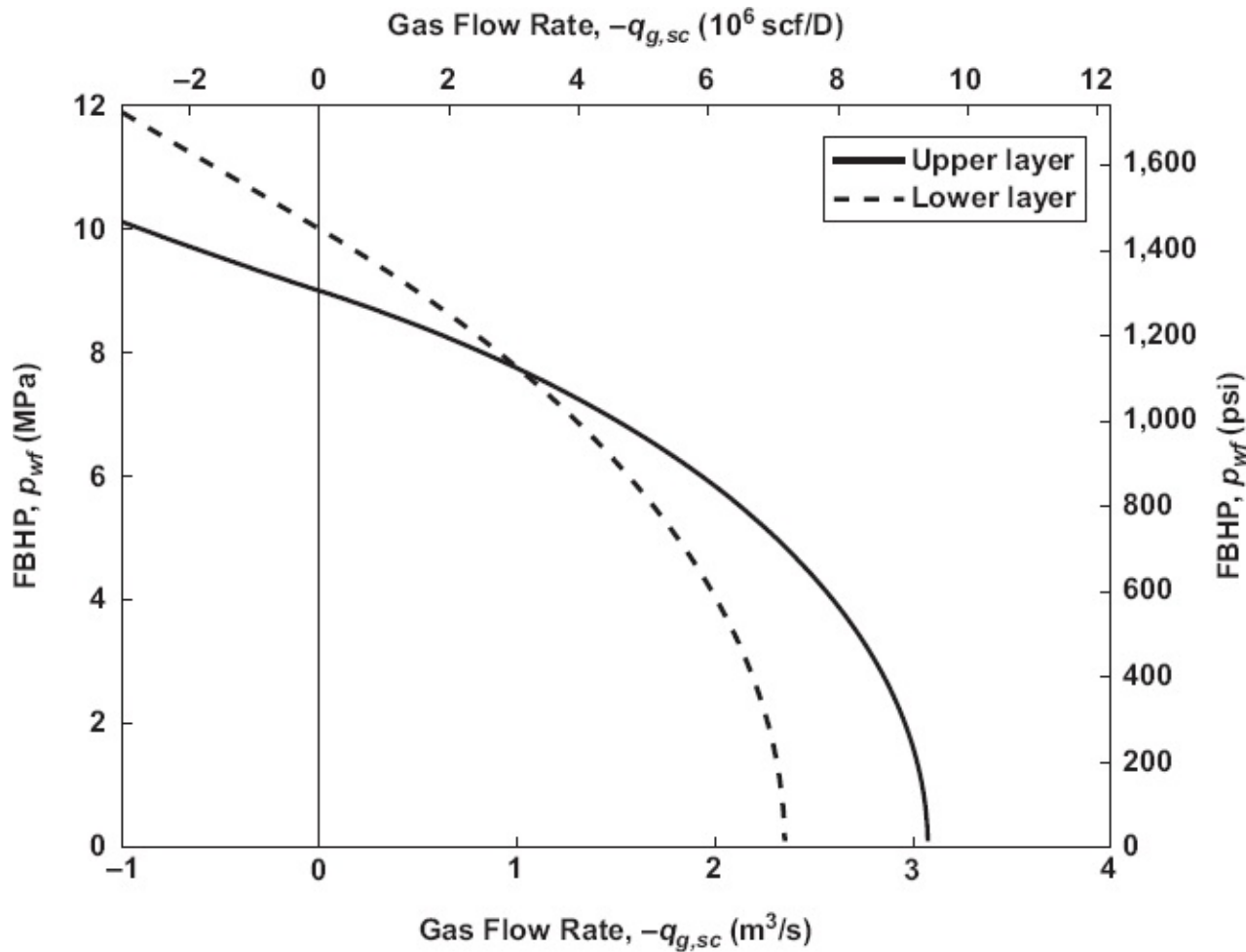


Fig. 6.14—IPRs for a vertical gas well with commingled production.

- 6.14 Have another look at Question 6.10. The corresponding parameters are given in [Table 6.5](#). Use the standard MATLAB routine `fzero` to iteratively compute the closed-in bottomhole pressure (CBHP). Iterate on $q_{g,sc,1}$ ($= -q_{g,sc,2}$) until $p_{wf,1} - p_{wf,2} = 0$ (see [Fig. 6.15](#)). Consult [Appendix D](#) for information on the use of `fzero`. You may also want to review Question 3.12 and its solution as an example of how to implement an iterative procedure.

Property	Value	Units
h	20	m
k_1	1.0×10^{-14}	m^2
k_2	0.5×10^{-14}	m^2
$\bar{p}_{R,1}$	9.0×10^6	Pa
$\bar{p}_{R,2}$	10.0×10^6	Pa
r_e	400	m
r_w	0.20	m

$T_{R,1} = T_{R,2}$	80	°C
β	4.0×10^{10}	1/m
$\rho_{g,sc}$	0.93	kg/m ³

Table 6.5—Input data for CBHP calculation for Question 6.14.

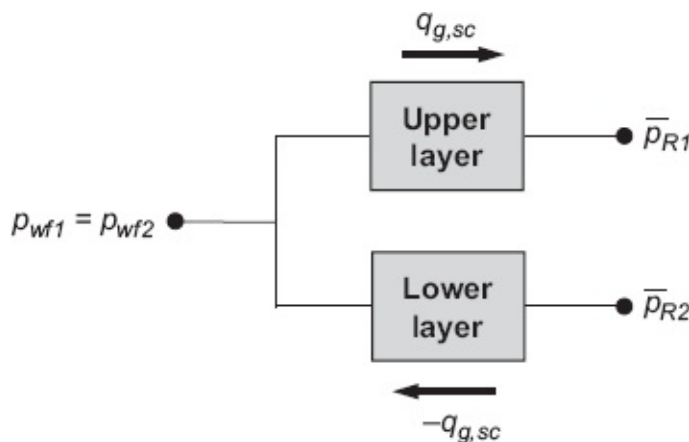


Fig. 6.15—Schematic representation of two crossflowing layers in a closed-in well.

6.12 MATLAB Assignment: Commingled Production With a Smart Well

6.12.1 Objectives

- Become familiar with the concept of smart wells and their use to control commingled production
- Become familiar with the MATLAB function `fsoolve` to perform multivariable root finding (as an extension to single-variable root finding with function `fzero`)

6.12.2 Assignment. *Introduction.* In many oil provinces, hydrocarbons are present in *stacked reservoirs*—i.e., a series of (near-)horizontal permeable layers separated by impermeable boundaries, typically in the form of sand/shale sequences. Most governments have regulations against commingled production from such reservoirs because of the risk of crossflow during well shut-in. Crossflow may cause reservoir impairment and ineffective use of reservoir pressure and therefore a lower ultimate recovery. However, since the beginning of this century the advent of *smart wells* (i.e., wells equipped with sensors and valves to control inflow from each layer) has opened up possibilities for controlled commingled production and even for optimizing the production by balancing the effects of oil, gas, and water production from each layer in a controlled fashion (see, e.g., Naus et al. 2006).

Fig. 6.16 schematically depicts a vertical well producing commingled from three horizontal reservoir layers (also known as *zones*) with the aid of *inflow control valves* (ICVs). ICVs can be operated hydraulically or electrically and can be continuously variable or have a number of discrete settings (valve openings) with the extreme of

being either on or off. Here we consider continuously variable ICVs. Usually smart wells are equipped with pressure sensors inside the tubing and in the annular areas outside each ICV such that it is possible to estimate the (mixture) flow rates from each zone by combining measurements and models for the pressure drop over each of the valves. The combined use of measurements and models of pressure drop to estimate flow rates is known as *soft sensing*. Alternatively, downhole flowmeters are occasionally employed, and it is also possible to estimate zonal inflow through selective production testing of (combinations of) individual zones.

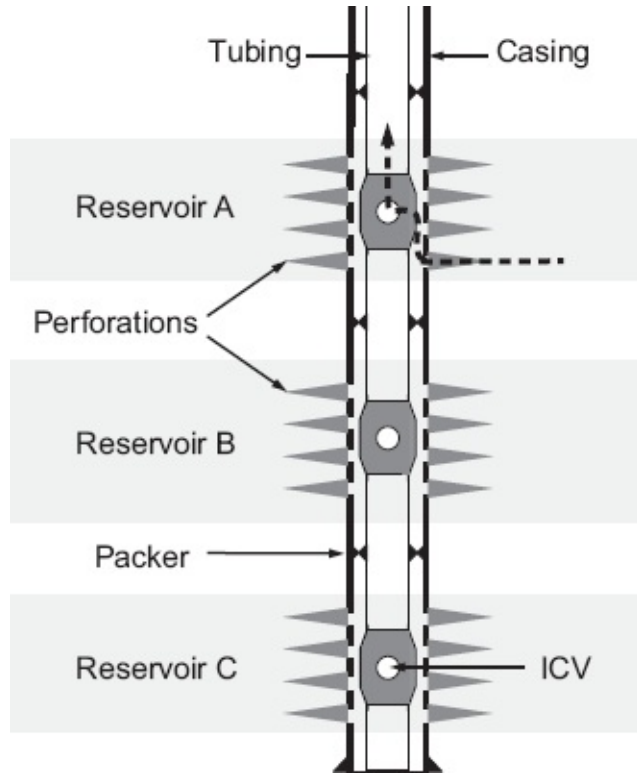
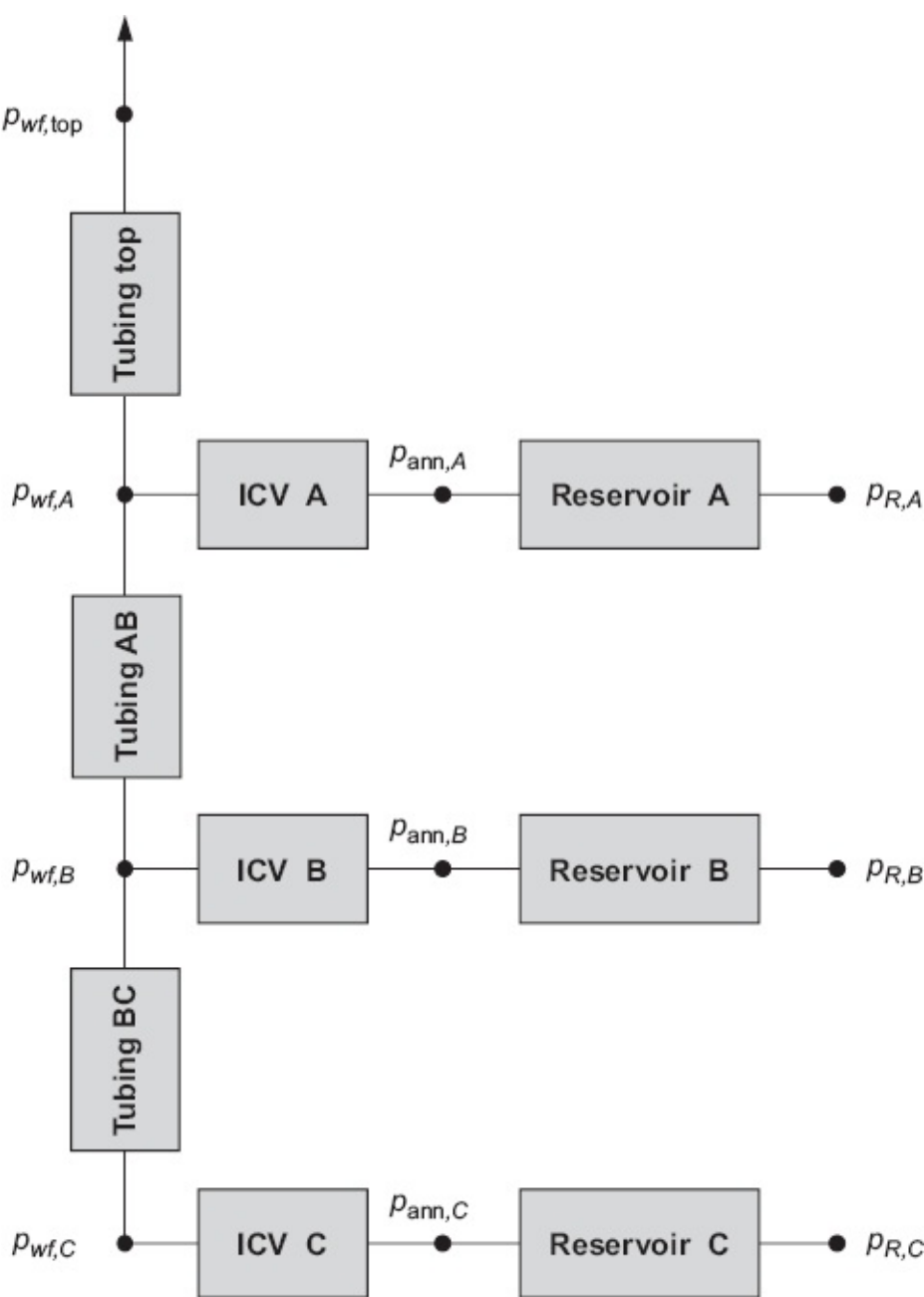


Fig. 6.16—Schematic representation of a smart well producing from three zones (dotted line indicates flow from the near-well reservoir through the perforations and the ICV into the tubing; lateral dimension is exaggerated).

Requirements. This assignment is focused on modeling. Compute the flow rates in the three zones for given ICV settings, reservoir pressures, and the FBHP at the middle of Zone A. The system schematic is given in [Fig. 6.17](#). The largest contributions to the system pressure drop originate from flow through the reservoirs and the ICVs. Pressure drop over the perforations is taken into account with a small positive skin factor. Assume that the zones produce single-phase dry oil from circular drainage areas. All relevant data are given in [Table 6.6](#).

Note. In this assignment you will have to use the black-box MATLAB function `fsoolve`, which forms part of the MATLAB Optimization Toolbox. (For more information, see Section D-1.5 in [Appendix D](#).) This is not necessarily the most efficient way to solve the problem, but more-advanced multivariable optimization approaches and the underlying theory are outside the scope of this book.

**Fig. 6.17—Nodal analysis configuration.**

Variable	Symbol	Unit	Value
Reservoir data			
Height of zone A	h_A	m	13
Height of zone B	h_B	m	15
Height of zone C	h_C	m	7
Permeability of zone A	k_A	m^2	8×10^{-13}
Permeability of zone B	k_B	m^2	4×10^{-13}
Permeability of zone C	k_C	m^2	3×10^{-13}
Drainage radius	r_e	m	300
Skin	S	—	1

Reservoir temperature	T_R	°C	120
Flow regime	Steady-state		
Fluid data			
Solution GOR at bubblepoint	R_{sb}	m^3/m^3	5
Oil viscosity	Beggs and Robinson (1975), Vasquez and Beggs (1980)		
Gas density at standard conditions	$\rho_{g,sc}$	kg/m^3	0.85
Oil density at standard conditions	$\rho_{o,sc}$	kg/m^3	885
Water density at standard conditions	$\rho_{w,sc}$	kg/m^3	1200
Equations of state	Standing (1952), black oil		
Water cut	$f_{w,sc}$	—	0.0
Well data			
Tubing length between compl. top and zone A	L_{top}	m	15
Tubing length between centers zones A and B	L_{AB}	m	16
Tubing length between centers zones B and C	L_{BC}	m	12.5
Wellbore inclination	α	rad	0
Tubing inside diameter	d	m	0.076
Tubing roughness	e	m	30×10^{-6}
Well diameter (for reservoir flow)	r_w	m	0.20
ICV data			
Discharge coefficient	C_d		
Maximum ICV opening	$d_{ICV,max}$	m	0.05
Pressure data			
FBHP at top of completion	$p_{wf,top}$	MPa	28.0
Reservoir pressure at middle of zone A	$p_{R,A}$	MPa	44.0
Reservoir pressure at middle of zone B	$p_{R,B}$	MPa	44.5
Reservoir pressure at middle of zone C	$p_{R,C}$	MPa	39.0

Table 6.6—Data for commingled production with a smart well.**Tasks and Questions**

- Check the data in [Table 6.6](#). What is the thickness of the impermeable layers between the zones?
- Inspect the reservoir pressures. Is the system in hydrostatic equilibrium? If not, in which zones do you expect crossflow to occur when the well is shut in?
- Use MATLAB functions `res_oil_simp.m`, `choke_oil.m`, and `pipe.m` to model the system, and then perform the following steps:
 - Start with a fully open ICV for Zone A and closed ICVs for the other two, and iterate on $q_{o,sc,A}$ until the difference between $p_{wf,top}$ as computed and as specified becomes zero. (Because this is a single-variable root-finding

problem, it may be done with either `fzero` or `fsolve`.) Repeat this step for the other two zones, every time just producing from one zone. The following MATLAB code gives an example of how to compute the flow rates for zone B with `fsolve`:

```
q_o_sc_B = fsolve(@(q_o_sc_B)...
    p_wf_top - cascade_ICV(alpha,av,C_d,d, ...
    d_ICV_B,dir_p,e,fluid,h_B,oil,k_B,p_R_B, ...
    [0,q_o_sc_B,0],r_e,r_w,rho_sc,semi,
    L_top+L_AB,0,S,T_R),q_o_sc_start);
```

Here, the function `cascade_ICV` is defined as an anonymous function with a single argument (in this case `q_o_sc_B`). It generically computes the pressure drop over a cascade of elements (reservoir, ICV, and tubing) for flow from a single zone (in this case zone B). It is specified as

```
function p_out = cascade_ICV(alpha,av,C_d,d, ...
    d_ICV,dir_p,e,fluid,h,oil,k,p_R,q_sc,r_e, ...
    r_w,rho_sc,semi,s_in,s_out,S,T_R)
% Computes the pressure drop over a cascade of
% elements consisting of the reservoir, an ICV
% and a section of tubing.
    p_ann = res_oil_simp(av,h,k,oil,p_R,q_sc,r_e, ...
    r_w,rho_sc,semi,S,T_R); % annulus pr., Pa
    p_wf_int = choke_oil(C_d,d_ICV,dir_p,oil,p_ann, ...
    q_sc,rho_sc,T_R); % intermediate pr., Pa
    p_out = pipe(alpha,d,e,fluid,oil,p_wf_int,q_sc, ...
    rho_sc,s_in,s_out,T_R,T_R); % output pr., Pa
```

2. Next perform multivariable root finding with the aid of `fsolve` and iteratively compute the required flow rates $q_{o,ssc,i}$, $i = A, B, C$ to produce the well for given values of the reservoir pressures $p_{R,i}$ and the FBHP at the top of the completion, $p_{fw,top}$. The corresponding MATLAB code becomes

```
q_o_sc_vect_out = fsolve(@(q_o_sc_vect)...
    system_ICV(alpha,av,C_d,d,d_ICV_A,d_ICV_B, ...
    d_ICV_C,dir_p,e,fluid,h_A,h_B,h_C,L_AB,L_BC, ...
    L_top,oil,k_A,k_B,k_C,p_R_A,p_R_B,p_R_C, ...
    p_wf_top,q_o_sc_vect,r_e,r_w,rho_sc,semi, ...
    S,T_R),q_o_sc_start);
```

Here, the variables `q_o_sc_vect`, `q_o_sc_vect_out`, and `q_o_sc_start` are vectors of three elements (i.e., the three zonal flow rates) each. The anonymous function `system_ICV` is partly specified as follows (code the missing parts indicated with “Etc., etc.” yourself):

```
function p_out = system_ICV(alpha,av,C_d,d,
    d_ICV_A,d_ICV_B,d_ICV_C,dir_p,e,fluid,
    h_A,h_B,h_C,L_AB,L_BC,L_top,oil,k_A,k_B,
    k_C,p_R_A,p_R_B,p_R_C,p_wf_top,
    q_o_sc_vec,r_e,r_w,rho_sc,semi,S,T_R)
% Computes various pressure drops in a system of
% elements consisting of three reservoirs,
% three ICVs, and three sections of tubing.
% Assemble flow rate vectors:
q_sc_A = [0,q_o_sc_vec(1),0];
q_sc_B = [0,q_o_sc_vec(2),0];
```

```

q_sc_C = [0,q_o_sc_vec(3),0];
q_sc_BC = q_sc_B + q_sc_C;
q_sc_ABC = q_sc_A + q_sc_B + q_sc_C;
% Compute horizontal pressure drop over zone C
% to tubing plus vertical pressure drop over
% bottom of completion:
p_ann_C = res_oil_simp(av,h_C,k_C,oil,p_R_C, ...
    q_sc_C,r_e,r_w,rho_sc,semi,S,T_R);
p_wf_C_C = choke_oil(C_d,d_ICV_C,dir_p,oil, ...
    p_ann_C,q_sc_C,rho_sc,T_R);
p_wf_B_C = pipe(alpha,d,e,fluid,oil,p_wf_C_C, ...
    q_sc_C,rho_sc,L_top+L_AB+L_BC,L_top+L_AB, ...
    T_R,T_R);
% Compute horizontal pressure drop over zone B
% to tubing:
p_ann_B = res_oil_simp(av,h_B,k_B,oil,p_R_B, ...
    q_sc_B,r_e,r_w,rho_sc,semi,S,T_R);
p_wf_B_B = choke_oil(C_d,d_ICV_B,dir_p,oil, ...
    p_ann_B,q_sc_B,rho_sc,T_R);
% Compute vertical pressure drop over middle
% of completion:
% Etc., etc.
% Define vector of pressure differences that
% should all be zero:
p_out = [p_wf_top - p_wf_top_ABC;...
    p_wf_A_A - p_wf_A_BC;...
    p_wf_B_B - p_wf_B_C];

```

Use the results obtained under Step 1 as starting values. How large (or small) is the difference with the result obtained under Step 1? What happens if you reduce the tubing size? Explain your answers.

- The sand in the reservoir is loosely consolidated, and therefore the zonal oil production needs to be restricted to avoid sand production. Typical sand production constraints specify either a maximum rate or a maximum drawdown. Constrained optimization is not an option in `fsolve`. Therefore manually iterate on the three valve settings $d_{ICV,i}$ to achieve a maximum production without exceeding a zonal rate of 1,500 STB/D. What are the resulting valve openings?

6.12.3 Deliverables

- MATLAB program listing
- Pressures and flow rates in field units
- Answers to all questions

Chapter 7

Inflow Performance: Further Topics

7.1 What Is Covered in This Chapter?

In this chapter we extend the basic treatment of inflow performance of [Chapter 6](#) to more complex well configurations. Starting with analytical methods to describe single-phase flow toward groups of vertical wells and wells near reservoir boundaries, we progress to discuss various methods to approximate the inflow performance of horizontal wells and multilateral wells. Next we discuss a semianalytical technique to approximate multiphase (gas/oil/water) near-well reservoir flow. Another aspect of complex-well flow is the effect of pressure drop inside the reservoir section of the wellbore, which can become especially significant for high-rate horizontal wells in low-permeability reservoirs. We treat a simplified approach to this coupled reservoir/wellbore-flow problem in the assignment at the end of the chapter. In general, the detailed prediction of multiphase well inflow performance in complex well configurations requires numerical reservoir simulation methods beyond the scope of this book; moreover, we typically need field measurements (production test data) to accurately account for effects that cannot be modeled *a priori* because of lack of information.

7.2 Two-Dimensional Reservoir Flow

7.2.1 The Laplace Equation. Until now we have mainly discussed the inflow performance of vertical wells. One of the underlying assumptions was that the height of a reservoir is usually small compared to its lateral dimensions such that the flow can be approximated to behave two-dimensionally. Moreover, thanks to radial symmetry, the governing differential equations for a single vertical well could be expressed in polar coordinates, resulting in a 1D problem. (Note that only the radial coordinate r plays a role in the differential equations. The angular coordinate ψ is just a constant parameter.) For horizontal wells, we may often maintain the assumption of relatively small reservoir height, but we can no longer make use of the symmetry argument; therefore, we need to express the governing equations in two spatial dimensions. Moreover, in a configuration of multiple vertical wells, the flow field also becomes 2D.

For the control volume depicted in [Fig. 7.1](#) the mass balance equation for single-phase flow can be expressed as

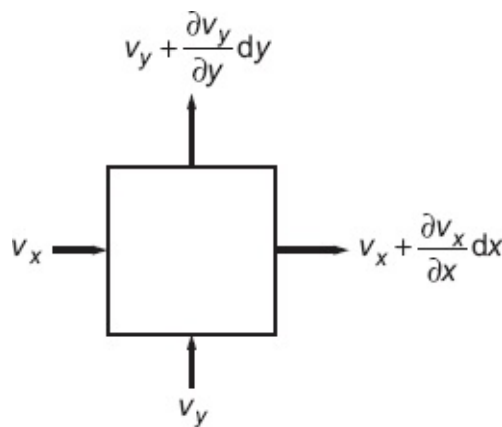


Fig. 7.1—Two-dimensional control volume with dimensions dx and dy in the x and y coordinate directions.

$$\frac{\partial(\rho v_x)}{\partial x} + \frac{\partial(\rho v_y)}{\partial y} = -\phi \frac{\partial \rho}{\partial t} \dots \quad (7.1)$$

(Note the resemblance of Eq. 7.1 to the 1D and radial cases represented in Eqs. 3.3 and 6.4.)

Darcy's law (i.e., the degenerated momentum balance) can be expressed in two dimensions as

$$v_x = -\frac{k}{\mu} \frac{\partial p}{\partial x} \dots \quad (7.2)$$

$$v_y = -\frac{k}{\mu} \frac{\partial p}{\partial y}, \dots \quad (7.3)$$

where we have assumed that the reservoir is homogeneous with scalar permeability k . (See Section 7.2.5 for discussion of a more general expression for nonscalar permeabilities). Substituting Eqs. 7.2 and 7.3 and simplifying the results using the definition of single-phase oil compressibility (Eq. 2.13) lead to

$$\frac{\partial^2 p}{\partial x^2} + \frac{\partial^2 p}{\partial y^2} = \frac{\mu \phi c_o}{k} \frac{\partial p}{\partial t} \dots \quad (7.4)$$

which is known as the *diffusivity equation*. If we restrict the analysis to steady-state flow, the right side of Eq. 7.1 vanishes, resulting in

$$\frac{\partial^2 p}{\partial x^2} + \frac{\partial^2 p}{\partial y^2} = 0, \dots \quad (7.5)$$

known as the *Laplace equation*. (Note that the Laplace equation is often written as $\nabla^2 p = 0$, where ∇ is the gradient operator.) It is a time-independent, linear, homogeneous, second-order, partial-differential equation in two spatial dimensions, and it therefore requires four boundary conditions: two for each coordinate direction. Exactly the same equation describes other physical phenomena such as the steady-

state flow of heat or electric current, in which case p should be replaced by the temperature or the electric potential, respectively. Many single-phase reservoir flow problems can therefore be solved through analogy by using published results from these domains (see, e.g., Morse and Feshbach 1953 or Carslaw and Jaeger 1959).

7.2.2 Polar Coordinates. It is often possible to find a transformation from rectangular coordinates (x, y) to another coordinate system that better suits the geometry of the problem at hand. In [Section 6.4](#) we already used polar coordinates r and ψ , which can be related to rectangular coordinates x and y according to

$$x = r \cos \psi, \dots \quad (7.6)$$

$$y = r \sin \psi, \dots \quad (7.7)$$

where $0 \leq r < \infty$, $0 \leq \psi < 2\pi$. The inverse transformation is given by

$$r = \sqrt{x^2 + y^2}, \dots \quad (7.8)$$

$$\psi = \tan^{-1} \left(\frac{y}{x} \right) \dots \quad (7.9)$$

Lines of constant r form circles, and lines of constant ψ are radial lines (see [Fig. 7.2](#)).

The Laplace equation in polar coordinates can be determined as

$$\frac{\partial^2 p}{\partial r^2} + \frac{1}{r} \frac{\partial p}{\partial r} + \frac{1}{r^2} \frac{\partial^2 p}{\partial \psi^2} = 0. \dots \quad (7.10)$$

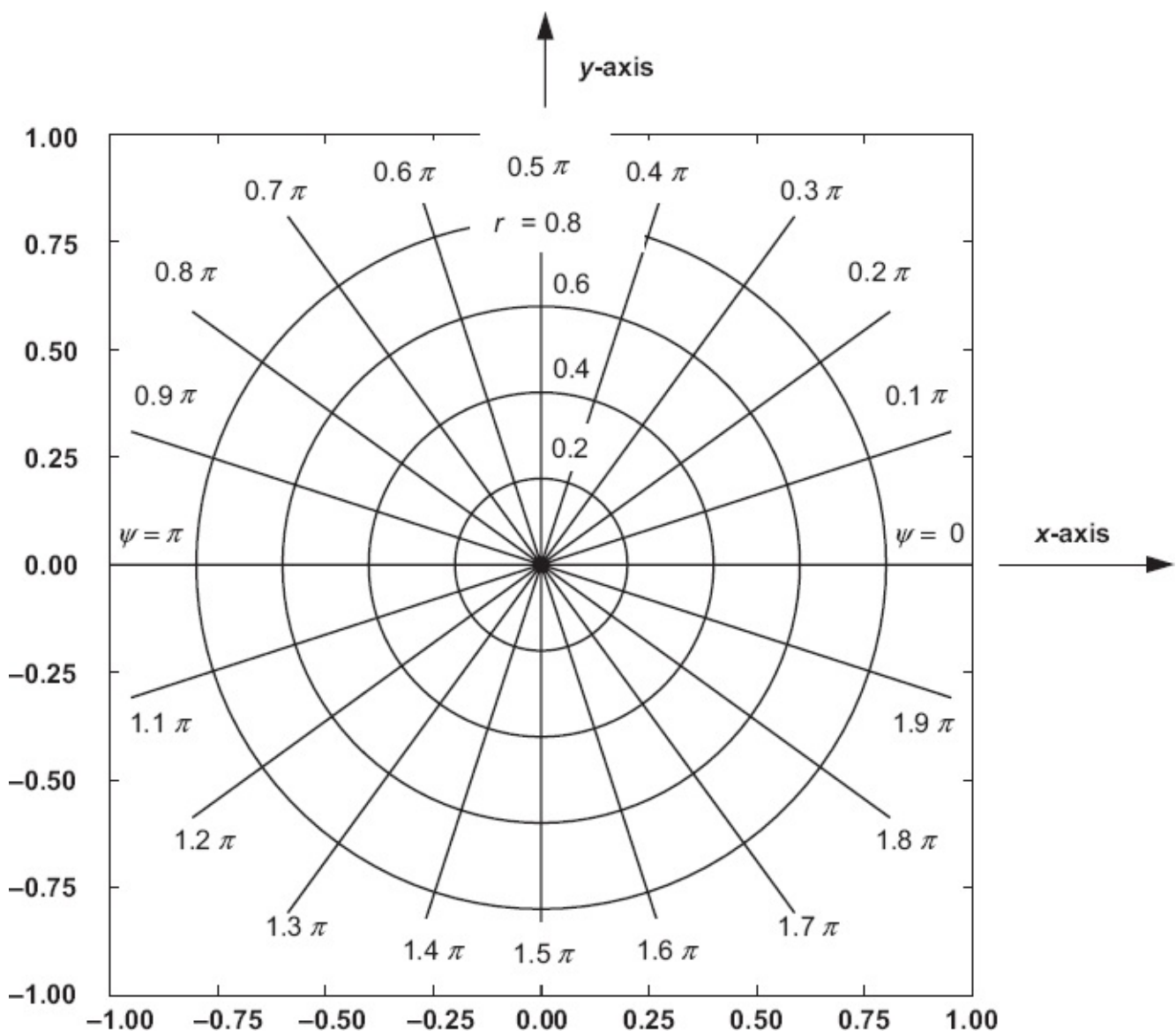


Fig. 7.2—Polar coordinate system with $0 \leq r \leq 0.8$, $0 \leq \psi < 2\pi$.

This is now the equation for single-phase incompressible flow in polar coordinates. [To verify this result, start from $\nabla^2 p = \partial^2 p / \partial x^2 + \partial^2 p / \partial y^2$. Use the chain rule to rewrite the first right-hand-side term as $\partial^2 p / \partial x^2 = \partial / \partial x (\partial p / \partial x) = \partial / \partial x (\partial p / \partial r \partial r / \partial x + \partial p / \partial \psi \partial \psi / \partial x)$. Repeat the chain rule for the second derivative, use the same approach for the term $\partial^2 p / \partial y^2$, compute the derivatives from Eqs. 7.6 and 7.7, and simplify the results.]

In Section 6.5 we expressed the same flow equation as two first-order differential equations and, with the aid of boundary conditions at $r = r_w$ and $r = r_e$, obtained the analytical solution for radial flow given in Eq. 6.20. It can be simply verified by substitution that this expression is also a solution of Eq. 7.10 if we express the boundary conditions as

$$r = r_w : \frac{\partial p}{\partial r} = -\frac{\mu B_o q_{o,sc}}{2\pi k h r_w}, \dots \quad (7.11)$$

$$r = r_e : p = p_R, \dots \quad (7.12)$$

$$\psi = 0 : \frac{\partial p}{\partial \psi} = 0, \quad \dots \dots \dots \quad (7.13)$$

$$\psi = 2\pi : \frac{\partial p}{\partial \psi} = 0. \dots \quad (7.14)$$

Note that in Section 6.5 we never considered the tangential coordinate ψ because we tacitly assumed that radial symmetry implies that $\partial p / \partial \psi = 0$ everywhere. In that case Eq. 7.10 reduces to

$$\frac{\partial^2 p}{\partial r^2} + \frac{1}{r} \frac{\partial p}{\partial r} = 0, \quad \dots \dots \dots \quad (7.15)$$

which can be twice integrated to give the radial pressure distribution

$$p = C_1 + C_2 \ln r, \dots \quad (7.16)$$

where C_1 and C_2 are integration constants that have to be determined from the radial boundary conditions (Eqs. 7.11 and 7.12). Using the first boundary condition leads to

$$p = C_1 + \frac{\mu B_o q_{o,sc}}{2\pi kh} \ln r, \dots \quad (7.17)$$

a result identical to Eq. 6.19, which is sometimes referred to as the *general radial flow solution*. Using the second boundary condition then leads to

$$p = p_R + \frac{\mu B_o q_{o,sc}}{2\pi k h} \ln\left(\frac{r_e}{r}\right), \dots \quad (7.18)$$

which is identical to Eq. 6.20. Alternatively, we may chose the radial boundary conditions as

$$r = r_w : p = p_v \quad \dots \quad (7.19)$$

in which case the solution becomes

$$p = p_R - (p_R - p_{wf}) \frac{\ln r_e - \ln r}{\ln r_e - \ln r_w}. \quad \dots \quad (7.21)$$

The total flow rate from the reservoir into the well can now be computed with the aid of Darcy's law according to

$$q_{o,sc} = -\frac{khr}{\mu B_o} \int_0^{2\pi} \frac{\partial p}{\partial r} d\psi = -\frac{khr}{\mu B_o} \int_0^{2\pi} \frac{p_R - p_{wf}}{(\ln r_e - \ln r_w)r} d\psi = -\frac{2\pi kh}{\mu B_o \ln\left(\frac{r_e}{r_w}\right)} (p_R - p_{wf}), \quad (7.22)$$

which is identical to the result obtained in Eq. 6.21.

The lines of constant r in Fig. 7.2 (i.e., the circles) can be interpreted as contours of constant pressure, called *equipotential lines*, and the lines of constant ψ (i.e., the radii) as *streamlines*. Note that in Fig. 7.2 the coordinates r and ψ have been selected equidistantly but that the corresponding pressure contours will not be equidistant in magnitude because the pressure increases logarithmically with increasing r . In contrast, if we plot pressure contours of equidistant magnitude, the radial coordinates will be logarithmically distributed (see the example in Fig. 7.3).

7.2.3 Linear Superposition. Because the Laplace equation is a linear, homogeneous differential equation, any linear combination of solutions will also be a solution, a property known as the principle of *linear superposition*. Note that this can easily be verified by substitution. For a proof, see any introductory text to differential equations (e.g., Boyce and DiPrima 2012). In general, we can therefore generate new solutions of the form

$$p = c_0 + \sum_{n=1}^N c_n p_n, \quad \dots \quad (7.23)$$

where the coefficients c_0, c_1, \dots, c_N may be chosen such that specific (new) boundary conditions are met. Linear superposition is a valuable property with which to generate solutions for the flow field originating from a number of isolated wells. For example, if we combine two radial solutions, as given in Eq. 6.20, for a *doublet* (i.e., a pair of wells consisting of an injector and a producer) we obtain

$$\begin{aligned} p &= p_R + \frac{\mu B_o q_{o,sc}}{2\pi kh} \left\{ \ln \left[\frac{r_e}{\sqrt{\left(x - \frac{D}{2}\right)^2 + y^2}} \right] - \ln \left[\frac{r_e}{\sqrt{\left(x + \frac{D}{2}\right)^2 + y^2}} \right] \right\} \\ &= p_R + \frac{\mu B_o q_{o,sc}}{4\pi kh} \ln \left[\frac{\left(x + \frac{D}{2}\right)^2 + y^2}{\left(x - \frac{D}{2}\right)^2 + y^2} \right]. \end{aligned} \quad \dots \quad (7.24)$$

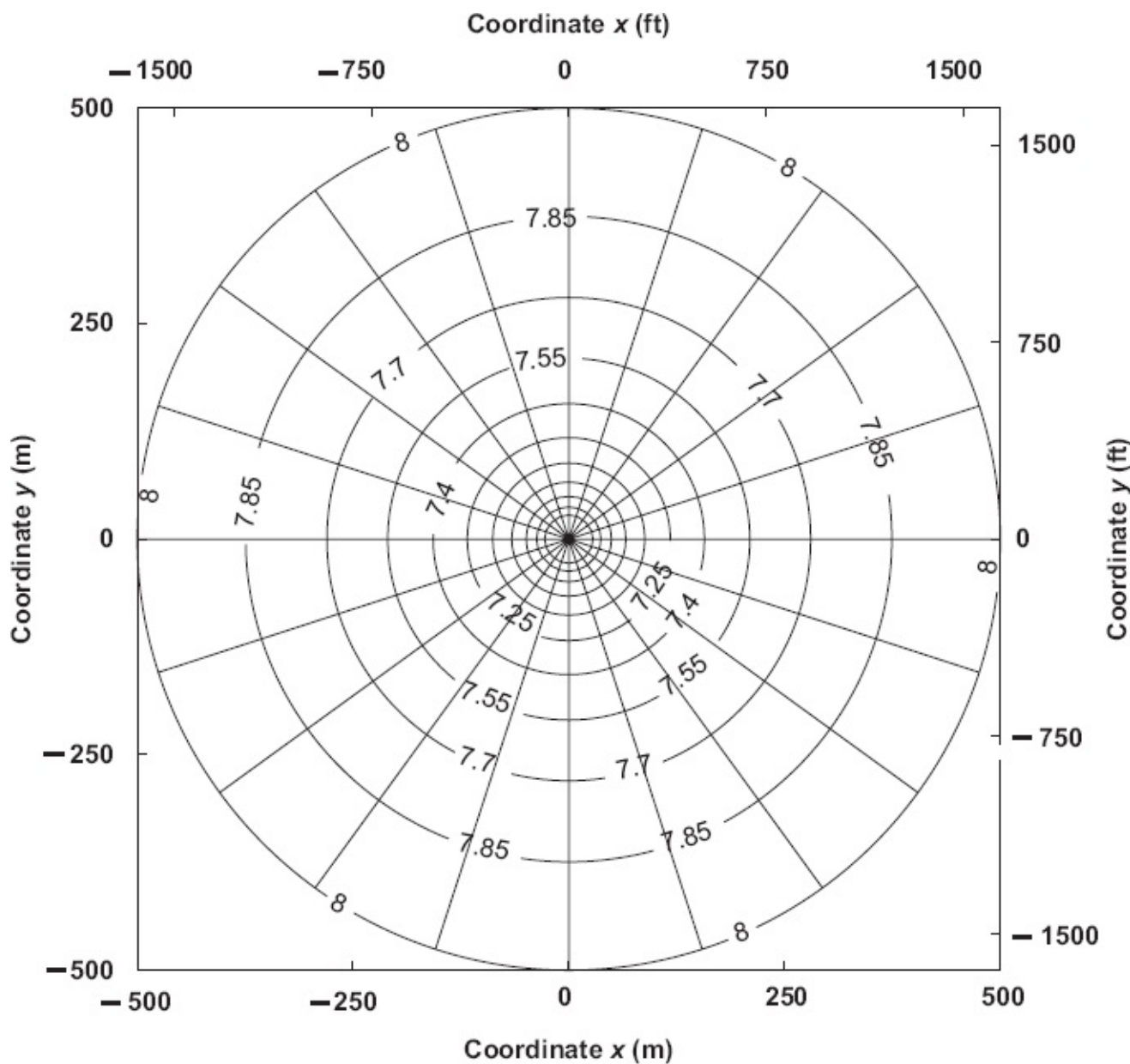


Fig. 7.3—Equipotential lines and streamlines for radial flow with parameters given in [Table 6.1](#) (values for “other figures”) and a flow rate of $-1.09 \times 10^{-3} \text{ m}^3/\text{s}$ (-593 STB/D) (numbers in the plot indicate pressures in MPa).

Here D is the interwell distance which has been chosen along the x -axis. We have used $n = 2$, $c_0 = p_R$, $c_1 = 1$, and $c_2 = -1$; moreover, each of the two solutions was shifted over a distance $\pm D/2$ before addition. [Fig. 7.4](#) displays the corresponding equipotential lines and streamlines for parameters given in [Table 6.1](#), and a value of D equal to 500 m. Note that the outer boundary, r_e , has dropped out of the equation. Thanks to the choice of c_0 , the far-field pressure is equal to p_R . Furthermore, because of symmetry the average reservoir pressure is equal to the far-field reservoir pressure while we have only steady-state flow because the equal injection and production rates result in *voidage replacement* and, thus, a constant reservoir pressure.

For $(x, y) = (-D/2 + r_w, 0)$, Eq. 7.24 gives the pressure in the producer. (Note that the superposition of pressures results in pressure values that are not exactly identical for all points at the wellbore radius. However, this small effect is completely negligible for our purpose.) The steady-state PI for a producer in a doublet therefore becomes

$$J = \frac{-q_{o,sc}}{p_R - p_{wf}} = \frac{2\pi kh}{\mu B_o \ln\left(\frac{r_w}{|r_w - D|}\right)} \approx \frac{2\pi kh}{\mu B_o \ln\left(\frac{r_w}{D}\right)}, \quad \dots \quad (7.25)$$

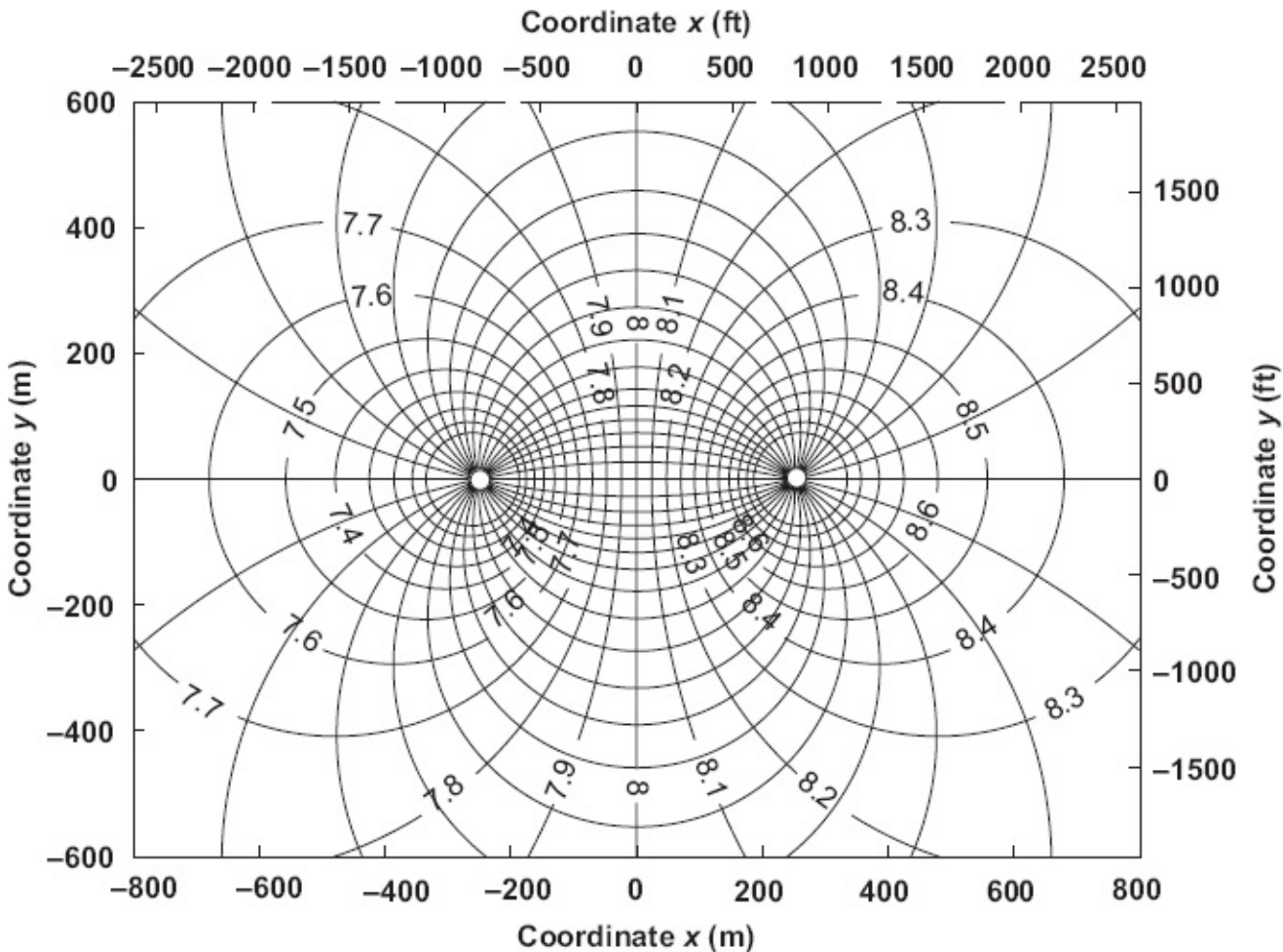


Fig. 7.4—Equipotential lines and streamlines around a doublet with parameters given in Table 6.1 and an inter-well distance $D = 500$ m and flow rates $q_{o,sc} = -1.09 \times 10^{-3}$ m³/s (-593 STB/D) (numbers in the plot indicate pressures in MPa).

where the approximation holds for $r_w \ll D$. As usual, a skin term may be added if required, just as in the standard productivity-index (PI) equation (Eq. 6.45).

7.2.4 Image Wells. Another example of linear superposition of the solution equation (Eq. 6.20) is the case of four producers in a rectangular configuration with interwell distances D_x and D_y along the x - and y -axis, respectively. Together, they result in a pressure distribution:

$$p = p_R + \frac{\mu B_o q_{o,sc}}{4\pi kh} \ln \left(r_e^3 \times \left[\begin{array}{l} \left[\left(x - \frac{D_x}{2} \right)^2 + \left(y + \frac{D_y}{2} \right)^2 \right] \times \left[\left(x + \frac{D_x}{2} \right)^2 + \left(y + \frac{D_y}{2} \right)^2 \right]^{-1} \\ \times \left[\left(x - \frac{D_x}{2} \right)^2 + \left(y - \frac{D_y}{2} \right)^2 \right] \times \left[\left(x + \frac{D_x}{2} \right)^2 + \left(y - \frac{D_y}{2} \right)^2 \right] \end{array} \right] \right), \quad (7.26)$$

where we now used $n = 4$, $c_0 = -3p_R$, and $c_1 = c_2 = c_3 = c_4 = 1$, and where the four solutions were shifted in different combinations in the x - and y -direction over distances $\pm D_x / 2$ and $\pm D_y / 2$ before addition. Note that for this case, with only producers, the external radius r_e still appears in the equation. **Fig. 7.5** displays one quadrant of the resulting double-symmetric configuration of equipotential lines and streamlines. The image can be interpreted as representing flow toward a well near the corner of two no-flow boundaries (along the x - and y -axes) at right angles.

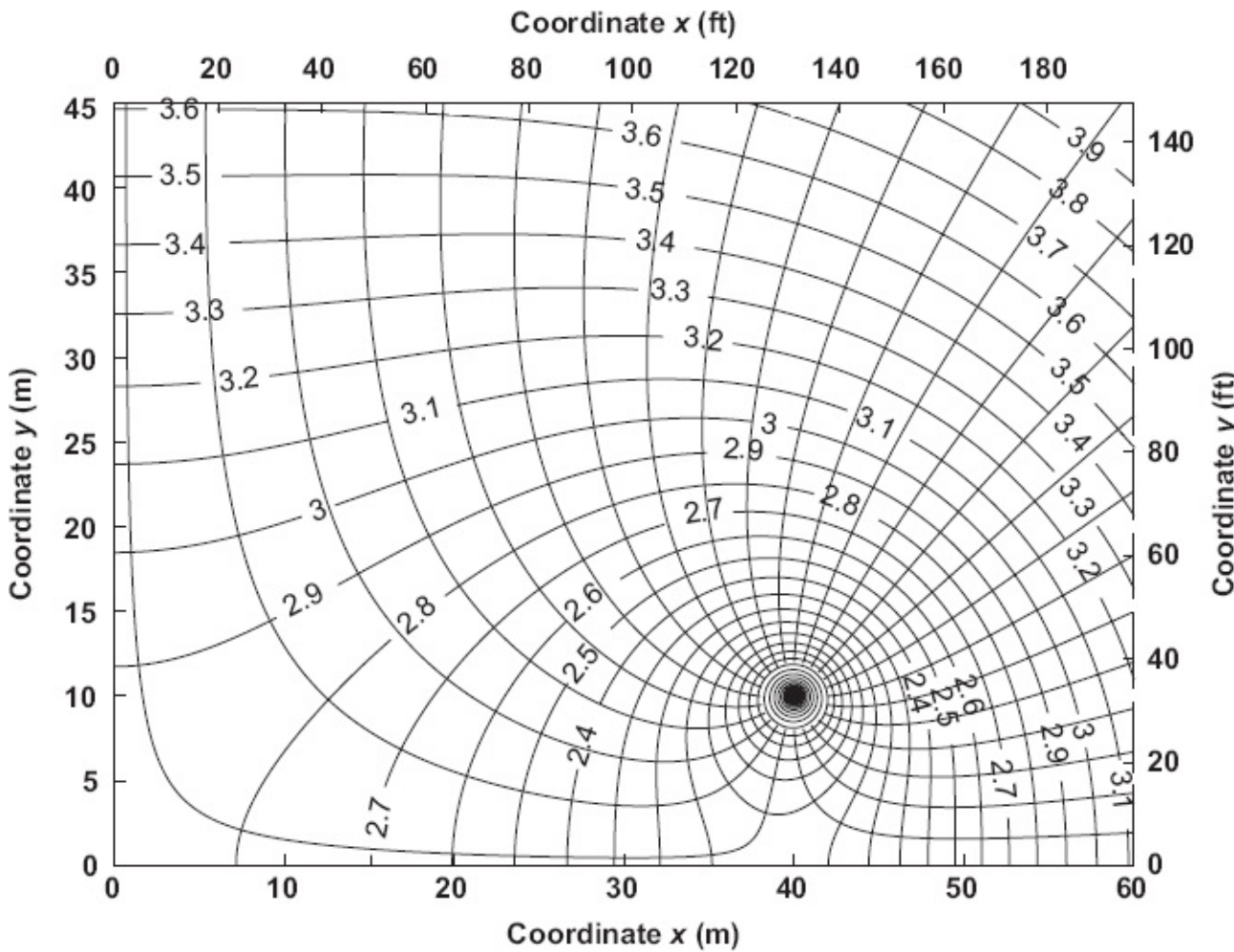


Fig. 7.5—Equipotential and streamlines around a well near a no-flow corner with parameters given in [Table 6.1](#) and a flow rate $q_{o,sc} = -1.09 \times 10^{-3} \text{ m}^3/\text{s}$ (-593 STB/D) (numbers in the plot indicate pressures in MPa).

This example illustrates that we can represent no-flow boundaries with the aid of *image wells*. This property offers many opportunities to create complex flow configurations, especially because we may select any combination of image wells,

even if the pressure field outside the domain of interest becomes physically unrealistic. For several other examples of the use of image wells to model subsurface flow, we refer to Muskat (1937), Verruijt (1970), and Bear (1972). These authors also extensively discuss the use of *conformal mapping*, which is an even more powerful method for obtaining solutions of the Laplace equation in a wide variety of spatial domains. (A conformal map is a transformation that preserves angles. It can be seen in Figs. 7.2 to 7.5 that the angles between the equipotential lines and the streamlines are always 90°, just like those between the x - and y -axis in rectangular coordinates.) The method of conformal mapping makes use of transformations in the complex domain (i.e., using imaginary numbers), which is outside the scope of our book.

Just as in the previous example we can directly compute the PI for this flow field. For $(x, y) = (D_x/2 + r_w/\sqrt{2}, D_y/2 + r_w/\sqrt{2})$, Eq. 7.26 gives the pressure in the producer in the top-right quadrant, and the steady-state PI for a producer near a no-flow corner therefore becomes

$$\begin{aligned} J &= \frac{-q_{o,sc}}{p_R - p_{wf}} \\ &= \frac{4\pi kh}{\mu B_o \ln \left(\frac{r_e^8 \times \left\{ \left(D_x^2 + \sqrt{2}D_x r_w + r_w^2 \right) \times \left(D_y^2 + \sqrt{2}D_y r_w + r_w^2 \right) \right\}^{-1}}{\times \left[D_x^2 + D_y^2 + \sqrt{2}(D_x + D_y)r_w + r_w^2 \right] \times r_w^2} \right)} \quad \dots \dots \dots \quad (7.27) \\ &\approx \frac{4\pi kh}{\mu B_o \ln \left[\frac{r_e^8}{(D_x^2 D_y^4 + D_x^4 D_y^2) r_w^2} \right]}, \end{aligned}$$

where the approximation holds for $r_w \ll D_x \ll r_e$ and $r_w \ll D_y \ll r_e$. It can be verified that the complete expression has the correct limiting behavior: When D_x and D_y approach zero (i.e., when the well approaches the corner), the PI approaches just one-quarter of the single-well PI given in Eq. 6.22. The approximation breaks down for (very) small values of D_x and D_y but gives completely acceptable results for practical purposes, especially in light of the strongly approximate nature of the entire PI concept.

7.2.5 Anisotropic Permeability. Until now we considered *homogeneous* reservoirs (i.e., having properties that do not vary spatially, with an *isotropic* permeability, i.e., a permeability that has equal magnitude for flow in any direction). All realistic reservoirs are *heterogeneous* (i.e., nonhomogeneous). An accurate representation of the governing equations for flow through a heterogeneous reservoir typically requires numerical techniques such as finite volume or finite element methods, which are outside the scope of this book. However, it is often useful to describe reservoirs as homogeneous but *anisotropic*—i.e., with different values of permeability for flow in different directions. In case of 2D flow this requires that we change the definition of

Darcy's law as given in Eqs. 7.2 and 7.3 to

$$v_x = -\frac{k_{xx}}{\mu} \frac{\partial p}{\partial x} - \frac{k_{xy}}{\mu} \frac{\partial p}{\partial y}, \dots \quad (7.28)$$

$$v_y = -\frac{k_{yx}}{\mu} \frac{\partial p}{\partial x} - \frac{k_{yy}}{\mu} \frac{\partial p}{\partial y}, \dots \quad (7.29)$$

where k_{xx} , k_{xy} , k_{yx} , and k_{yy} are the elements of the symmetric 2D permeability tensor,

$$\mathbf{K} = \begin{bmatrix} k_{xx} & k_{xy} \\ k_{yx} & k_{yy} \end{bmatrix}, \dots \quad (7.30)$$

in which $k_{xy} = k_{yx}$. The presence of off-diagonal elements in a permeability tensor implies that a pressure gradient in the x -direction causes flow in the x - and y -direction. It can be shown with physical arguments that a pressure gradient in the y -direction will then also cause flow in the x - and y -directions and that, moreover, the off-diagonal terms k_{xy} and k_{yx} must have the same magnitude. As a result, the permeability tensor is symmetric. Substitution of Eqs. 7.28 and 7.29 in the mass balance (Eq. 7.1) and then simplifying the results using the definition of single-phase oil compressibility (Eq. 2.13) will lead to an anisotropic form of the diffusivity equation (refer to Eq. 7.4):

$$\frac{\partial}{\partial x} \left(k_{xx} \frac{\partial p}{\partial x} + k_{xy} \frac{\partial p}{\partial y} \right) + \frac{\partial}{\partial y} \left(k_{yx} \frac{\partial p}{\partial x} + k_{yy} \frac{\partial p}{\partial y} \right) = \mu \phi c_o \frac{\partial p}{\partial t}, \dots \quad (7.31)$$

which can be more compactly written in vector notation as

$$\begin{bmatrix} \frac{\partial}{\partial x} & \frac{\partial}{\partial y} \end{bmatrix} \cdot \begin{bmatrix} k_{xx} & k_{xy} \\ k_{yx} & k_{yy} \end{bmatrix} \begin{bmatrix} \frac{\partial p}{\partial x} \\ \frac{\partial p}{\partial y} \end{bmatrix} = \mu \phi c_o \frac{\partial p}{\partial t}, \dots \quad (7.32)$$

or

$$\nabla \cdot (\mathbf{K} \nabla p) = \mu \phi c_o \frac{\partial p}{\partial t}, \dots \quad (7.33)$$

where ∇ is the gradient operator. This expression also holds for 3D flow, in which case \mathbf{K} has nine elements (of which, because of symmetry, only six are independent). Often the permeability tensor is diagonal with elements of different magnitude:

$$\mathbf{K} = \begin{bmatrix} k_x & 0 \\ 0 & k_y \end{bmatrix} \dots \dots \dots \quad (7.34)$$

This implies that the flow is aligned with the direction of the pressure gradient, which typically occurs when the coordinate axes are chosen such that they are in alignment with the geological layering of the reservoir.

For the case of a homogeneous anisotropic reservoir it is usually possible to realign the coordinate system through rotation over an angle such that the permeability tensor becomes diagonal. (We will not discuss this any further but for an-in depth description refer to Bear 1972.) Moreover, it is usually possible to obtain an equivalent isotropic system through scaling the coordinate axes (Vreedenburgh 1936; Muskat 1937; Bear 1972). Several choices for scaling are available, and here we choose

$$\hat{x} = \sqrt{\frac{k_y}{k}} x, \dots \dots \dots \quad (7.35)$$

$$\hat{y} = \sqrt{\frac{k_x}{k}} y, \dots \dots \dots \quad (7.36)$$

where

$$\bar{k} = \sqrt{k_x k_y} \dots \dots \dots \quad (7.37)$$

Substitution of Eqs. 7.35 through 7.37 in Eq. 7.31 with $k_{xx} = k_x$, $k_{xy} = k_{yx} = 0$, and $k_{yy} = k_y$ results in

$$\begin{aligned} & \frac{\partial}{\partial x} \left(k_x \frac{\partial p}{\partial x} \right) + \frac{\partial}{\partial y} \left(k_y \frac{\partial p}{\partial y} \right) \\ &= \frac{\partial}{\partial \hat{x}} \frac{\partial \hat{x}}{\partial x} \left(k_x \frac{\partial p}{\partial \hat{x}} \frac{\partial \hat{x}}{\partial x} \right) + \frac{\partial}{\partial \hat{y}} \frac{\partial \hat{y}}{\partial y} \left(k_y \frac{\partial p}{\partial \hat{y}} \frac{\partial \hat{y}}{\partial y} \right) \\ &= \frac{\partial}{\partial \hat{x}} \sqrt{\frac{k_y}{\bar{k}}} \left(k_x \frac{\partial p}{\partial \hat{x}} \sqrt{\frac{k_y}{\bar{k}}} \right) + \frac{\partial}{\partial \hat{y}} \sqrt{\frac{k_x}{\bar{k}}} \left(k_y \frac{\partial p}{\partial \hat{y}} \sqrt{\frac{k_x}{\bar{k}}} \right) \dots \dots \dots \quad (7.38) \\ &= \frac{\partial^2 p}{\partial \hat{x}^2} \bar{k} + \frac{\partial^2 p}{\partial \hat{y}^2} \bar{k} = \mu \phi c_o \frac{\partial p}{\partial t}, \end{aligned}$$

from which follows

$$\frac{\partial^2 p}{\partial \hat{x}^2} + \frac{\partial^2 p}{\partial \hat{y}^2} = \frac{\mu \phi c_o}{\bar{k}} \frac{\partial p}{\partial t}, \dots \dots \dots \quad (7.39)$$

which demonstrates that \bar{k} as defined in Eq. 7.37 is just the equivalent isotropic permeability for the diffusivity equation in scaled coordinates \hat{x} and \hat{y} . By restricting

the analysis to steady-state flow, Eq. 7.39 reduces to the isotropic Laplace equation in scaled coordinates:

$$\frac{\partial^2 p}{\partial \hat{x}^2} + \frac{\partial^2 p}{\partial \hat{y}^2} = 0. \dots \dots \dots \quad (7.40)$$

When applying this scaling method to an inflow equation, it is necessary that all coefficients and boundary conditions that are a function of the reservoir dimensions be scaled accordingly. For circular boundaries, such as a well or the boundary of a circular drainage area, this implies that the circle deforms to an ellipse with (half) axes equal to

$$\hat{r}_x = \sqrt{\frac{k_y}{k}} r, \dots \dots \dots \quad (7.41)$$

$$\hat{r}_y = \sqrt{\frac{k_x}{k}} r, \dots \dots \dots \quad (7.42)$$

and using a simple arithmetic average, we obtain the scaled equivalent radius

$$\hat{r} = \frac{1}{2} \left(\frac{\sqrt{k_x} + \sqrt{k_y}}{\sqrt{k}} \right) r. \dots \dots \dots \quad (7.43)$$

As an example of the use of coordinate scaling to represent reservoir anisotropy, consider Eq. 7.25 for the PI in a doublet with an interwell distance D along the x -axis. If we want to apply this equation to a reservoir with anisotropic permeabilities k_x and k_y we should use

$$J \approx \frac{2\pi \bar{k} h}{\mu B_o \ln\left(\frac{\hat{r}_w}{\hat{D}}\right)} = \frac{2\pi \bar{k} h}{\mu B_o \ln\left[\frac{1}{2} \left(\frac{\sqrt{k_x} + \sqrt{k_y}}{\sqrt{k}} \right) r_w \frac{\sqrt{k}}{\sqrt{k_y} D}\right]} = \frac{2\pi \bar{k} h}{\mu B_o \ln\left[\frac{1}{2} (I_{xy} + 1) \frac{r_w}{D}\right]} , \dots \dots \dots \quad (7.44)$$

where

$$I_{xy} = \sqrt{\frac{k_x}{k_y}} \dots \dots \dots \quad (7.45)$$

is known as the *anisotropy index*.

7.3 Horizontal Wells, Part 1

7.3.1 Box-Shaped Reservoir. Horizontal wells have become ubiquitous since the 1980s, although their first use dates from much longer back (for overviews see, e.g.,

Joshi 1991 and Butler 1994). The first expressions to describe horizontal well inflow considered a box-shaped reservoir geometry as schematically depicted in [Fig. 7.6](#). The reservoir dimensions are specified as length L , height h , and width w . The well is *fully penetrating*— i.e., it runs from the front to the back of the reservoir—and is operated at a constant flow rate $q_{o,sc}$. The x - y planes at $z = \pm h/2$ (i.e., the top and bottom) and the y - z planes at $x = 0$ and $x = L$ (i.e., the front and back) are no-flow boundaries, while the x - z planes at $y = \pm w/2$ (i.e., the sides) are constant pressure boundaries with pressure $p = p_R$. If pressure drop along the wellbore is disregarded, the flow will be perpendicular toward the well; i.e., the flow can be described by considering a slab in the y - z plane with a unit thickness along the x -axis (see [Fig. 7.7](#)). If we consider single-phase incompressible steady-state flow and disregard gravity, it seems reasonable to expect that the flow will be primarily horizontal with some streamline convergence close to the well.

7.3.2 Horizontal Flow. As a precursor to this problem, we first consider a simpler case in which the horizontal well is replaced by a vertical fracture over the entire height and length of the reservoir (see [Figs. 7.8 and 7.9](#)). In this configuration the oil flows purely horizontally from the vertical boundaries to the vertical fracture. For such a linear flow pattern the steady-state mass balance and Darcy's law can be written as

$$\frac{dv}{dy} = 0, \dots \dots \dots \quad (7.46)$$

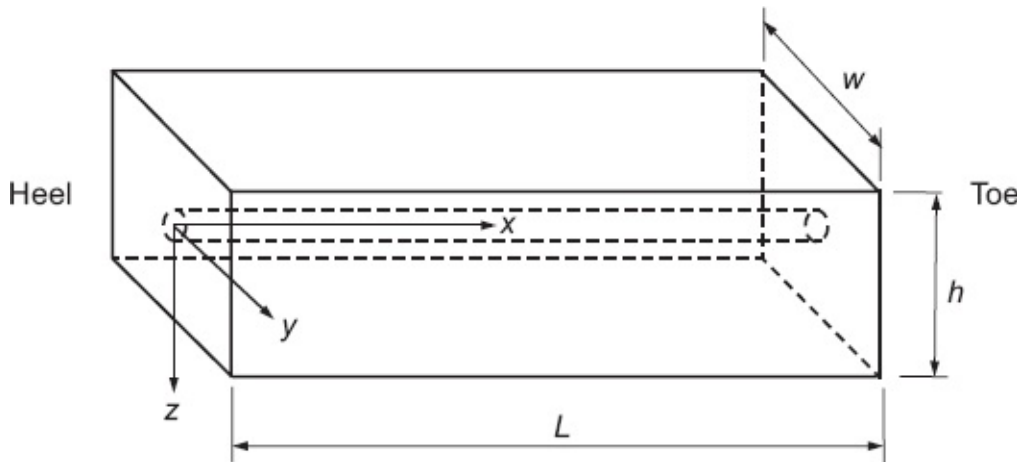


Fig. 7.6—Schematic representation of a box-shaped reservoir with a central horizontal well (with vertical dimension strongly exaggerated).

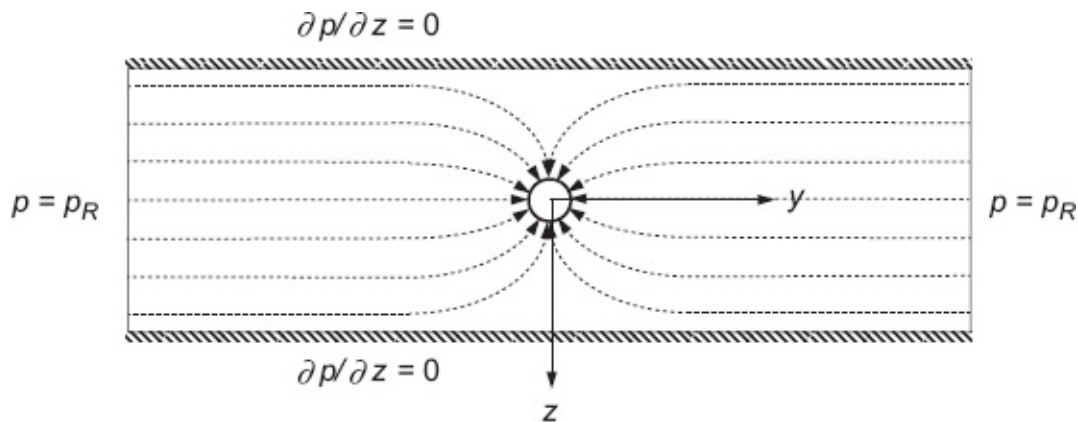


Fig. 7.7—Vertical two-dimensional plane with a central horizontal well, no-flow boundaries at top and bottom, and constant pressure boundaries at the sides (dotted lines represent schematic streamlines).

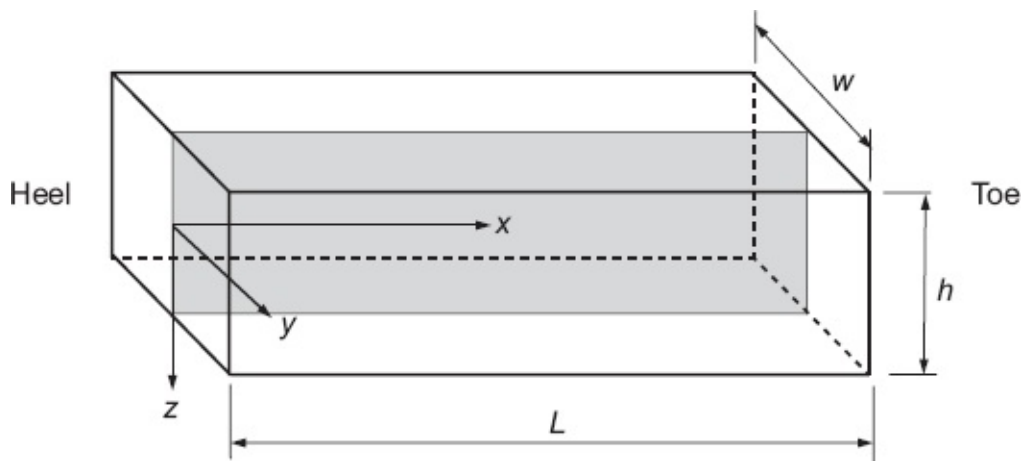


Fig. 7.8—Schematic representation of a box-shaped reservoir with a central vertical fracture.

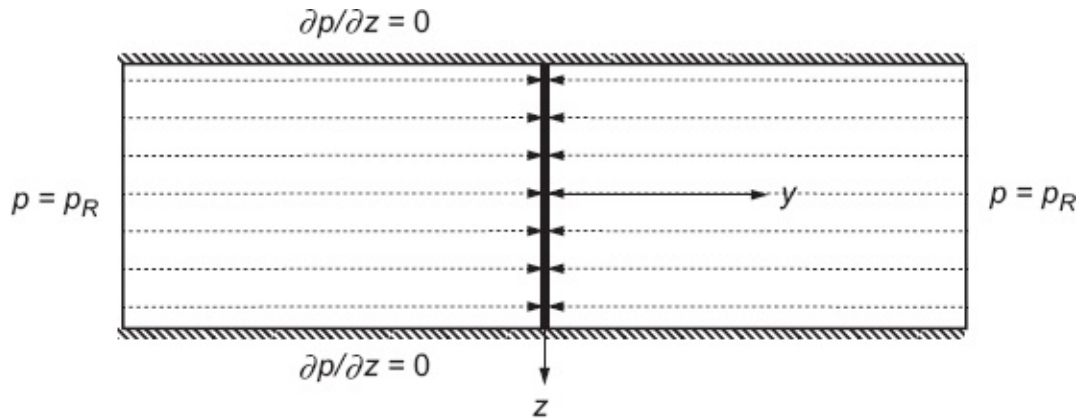


Fig. 7.9—Vertical two-dimensional plane with a central vertical fracture, no-flow boundaries at top and bottom, and constant pressure boundaries at the sides (dotted lines represent streamlines).

$$\frac{dp}{dy} = -\frac{\mu}{k} v, \dots \dots \dots \quad (7.47)$$

and the boundary conditions as

$$y=0: v = \frac{B_o q_{o,sc}}{2Lh} \Rightarrow \frac{dp}{dy} = -\frac{\mu B_o q_{o,sc}}{2kLh}, \dots \dots \dots \quad (7.48)$$

$$y = \frac{\pm w}{2}: p = p_R. \dots \dots \dots \quad (7.49)$$

Note that $q_{o,sc}$ represents the flow rate originating from reservoir inflow from both sides. Differentiation of Eq. 7.47 and substitution of Eq. 7.46 results in the 1D Laplace equation

$$\frac{d^2 p}{dy^2} = 0, \dots \dots \dots \quad (7.50)$$

which can be integrated twice to obtain

$$p = C_1 + C_2 y, \dots \dots \dots \quad (7.51)$$

where the constants C_1 and C_2 can be obtained with the aid of boundary conditions (Eqs. 7.48 and 7.49), resulting in

$$p = p_R + \frac{\mu B_o q_{o,sc}}{2kLh} \left(\frac{w}{2} - y \right) \dots \dots \dots \quad (7.52)$$

The fracture pressure for a given flow rate follows by substituting 0 for y and p_{frac} for p . Reorganizing the results, we obtain the PI for steady-state linear flow toward a vertical fracture:

$$J_{frac} = \frac{-q_{o,sc}}{p_R - p_{frac}} = \frac{4kLh}{\mu B_o w}. \dots \dots \dots \quad (7.53)$$

7.3.3 Near-Well Radial Flow. Returning to the horizontal well problem, we may expect a similar PI but with a slightly lower value because of increased resistance due to radial flow and the associated streamline convergence near the well. The solution for this 2D flow problem in the $y-z$ plane can be obtained using linear superposition with image wells. The effect of top and bottom no-flow boundaries can be represented by image wells, but unfortunately each of these disturbs the pressure field of the other. These disturbances can, in turn, be compensated by new image wells, leading to an infinite array of image wells stretching in the upward and downward direction (see Fig. 7.10).

Because the infinite row of wells stretches beyond the external reservoir boundary r_e , which is present in the conventional radial pressure solution (Eq. 6.20), we start from the general radial flow solution (Eq. 6.19) and will introduce a relevant external reference pressure later. The corresponding expression for the pressure distribution has first been given by Muskat (1937). Using the notation introduced in Eq. 7.23 we can write

$$p = c_0 + \sum_{n=-\infty}^{+\infty} c_n p_n = c_0 - \sum_{n=-\infty}^{+\infty} \frac{\mu B_o q_{o,sc}}{4\pi k L} \ln \left[(z - nh)^2 + y^2 \right], \dots \quad (7.54)$$

where we have left out the constant C under the summation because the constant c_0 , which is as yet undetermined, will be used to fix the pressure. Eq. 7.54 can, after considerable algebraic manipulation, be rewritten as

$$p = c_0 - \frac{\mu B_o q_{o,sc}}{4\pi k L} \ln \left[\cosh \left(2\pi \frac{y}{h} \right) - \cos \left(2\pi \frac{z}{h} \right) \right], \dots \quad (7.55)$$

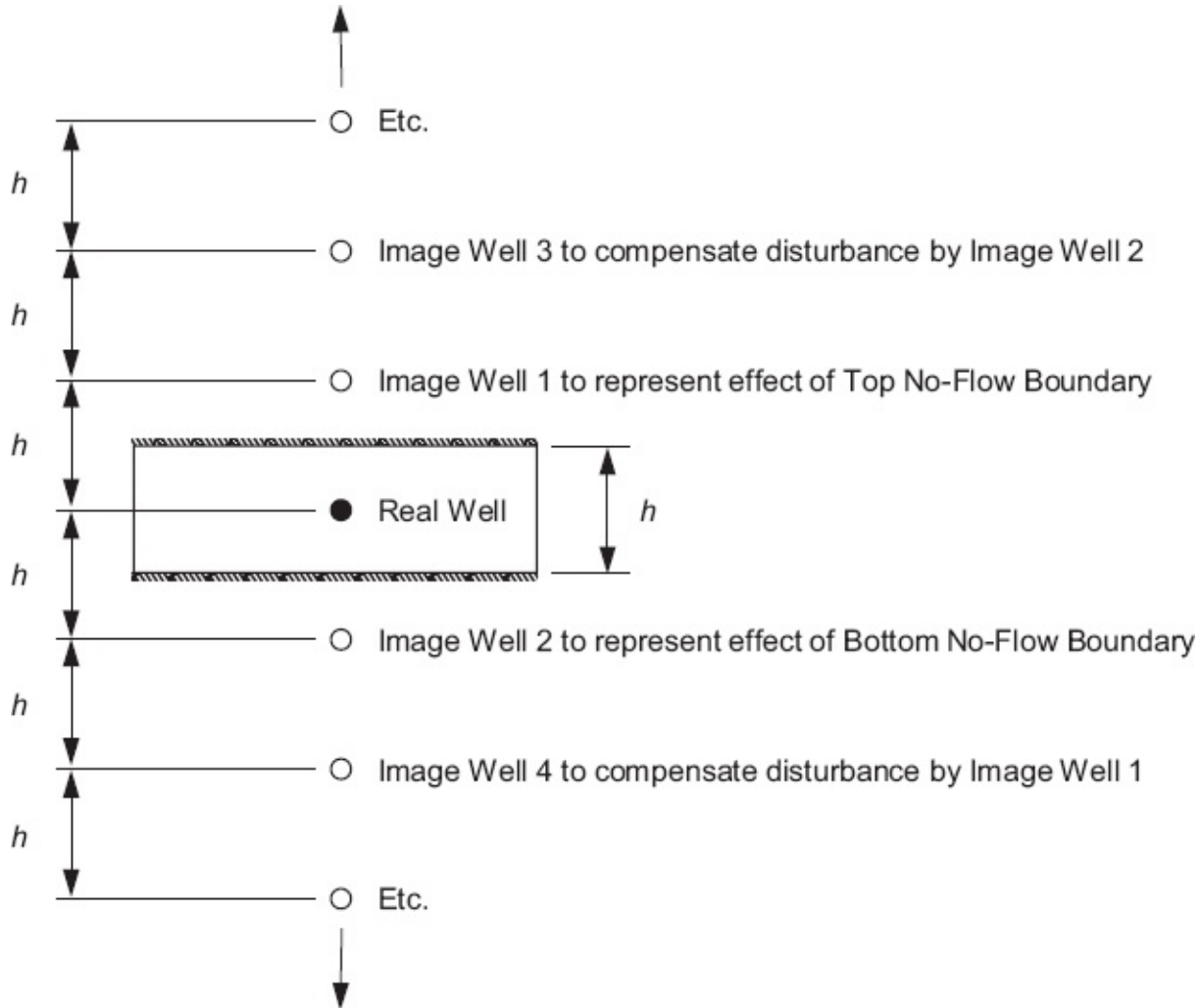


Fig. 7.10—Vertical two-dimensional plane with an infinite array of image wells to represent no-flow boundaries at top and bottom.

where we have neglected several constant terms because their effect will be annihilated once we choose the constant c_0 to fix the reservoir pressure. (The full derivation of Eq. 7.55 is given in question 7.6 in [Section 7.8](#) and its answer in [Appendix G](#)). If we choose to fix the pressure at the external boundaries at the vertical level of the well, we have

$$(y, z) = \left(\pm \frac{w}{2}, 0 \right) : p = p_R, \dots \dots \dots \quad (7.56)$$

which leads to a constant

$$c_0 = p_R + \frac{\mu B_o q_{o,sc}}{4\pi k L} \ln \left[\cosh \left(\pi \frac{w}{h} \right) - 1 \right], \dots \dots \dots \quad (7.57)$$

and therefore to a solution

$$p = p_R + \frac{\mu B_o q_{o,sc}}{4\pi k L} \ln \left[\frac{\cosh \left(\pi \frac{w}{h} \right) - 1}{\cosh \left(2\pi \frac{y}{h} \right) - \cos \left(2\pi \frac{z}{h} \right)} \right] \dots \dots \dots \quad (7.58)$$

As an example, consider a horizontal well in a box-shaped reservoir with parameters given in **Table 7.1**. **Figs. 7.11 and 7.12** depict the equipotential lines and streamlines in the near-well area and in a larger part of the reservoir, respectively. The PI for the well follows by specifying the wellbore pressure as

Property	Symbol	Value	Units
Reservoir height	h	25	m
Reservoir length	L	5000	m
Reservoir width	w	500	m
Permeability	k	2.0×10^{-12}	m^2
Well diameter	d	0.20	m
Oil viscosity	μ	20×10^{-3}	$\text{Pa} \cdot \text{s}$
Oil formation volume factor	B_o	1	—
Reservoir pressure	p_R	33.5	MPa
Oil flow rate	$q_{o,sc}$	-2.28×10^{-4}	m^3/s
Skin	S_v	0	—

Table 7.1—Parameter values for horizontal well in box-shaped reservoir.

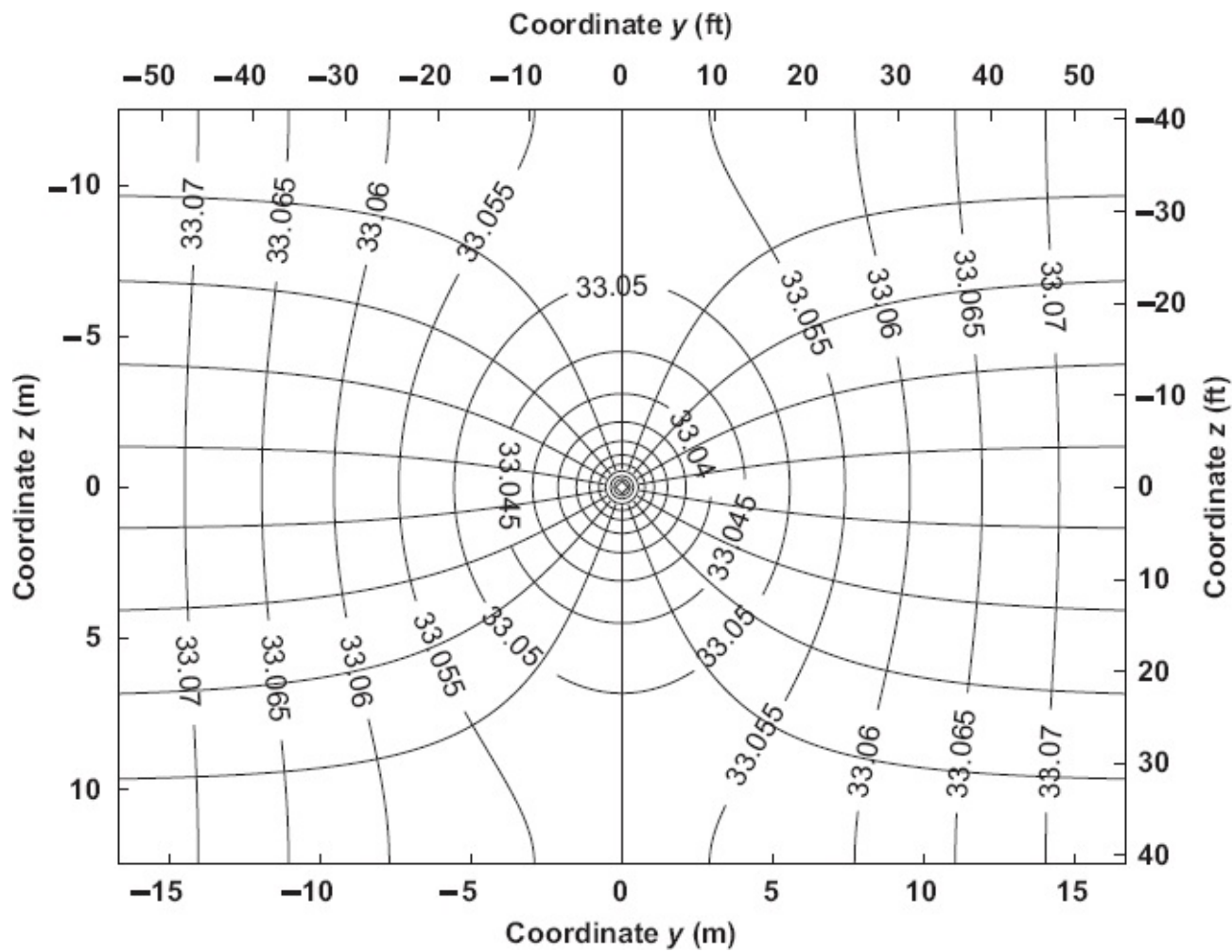


Fig. 7.11—Equipotential and streamlines around a horizontal well with parameters given in Table 7.1. Note that the figure covers the entire reservoir height (25 m) but only a small part (33.3 m) of the reservoir width (500 m) (numbers in the plot indicate pressures in MPa).

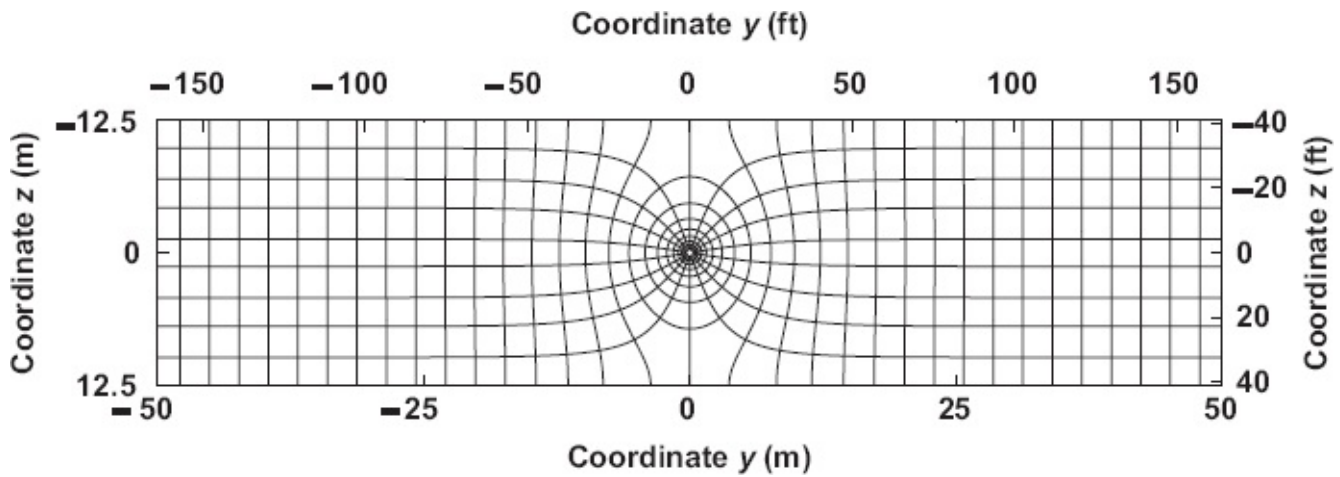


Fig. 7.12—Equipotential and streamlines around a horizontal well with parameters given in Table 7.1. Note that the figure covers the entire reservoir height of 25 m but only 100 m of the 500 m of reservoir width.

$$(y, z) = (\pm r_w, 0) : p = p_{wf}, \dots \quad (7.59)$$

which leads to

$$J = \frac{4\pi kL}{\mu B_o} \left\{ \ln \left[\frac{\cosh\left(\pi \frac{w}{h}\right) - 1}{\cosh\left(2\pi \frac{r_w}{h}\right) - 1} \right] \right\}^{-1} \quad \dots \dots \dots \quad (7.60)$$

For large values of w/h we can write

$$\ln\left(\cosh\pi\frac{w}{h} - 1\right) \approx \pi\frac{w}{h}, \quad \dots \dots \dots \quad (7.61)$$

and for small values of w_R/h_R

$$\cosh\left(2\pi\frac{r_w}{h}\right) \approx 1 + \left(2\pi\frac{r_w}{h}\right)^2, \quad \dots \dots \dots \quad (7.62)$$

and therefore we can derive that

$$J \approx \frac{1}{\frac{\mu B_o w}{4kLh} + \frac{\mu B_o}{2\pi kL} \ln\left(\frac{h}{2\pi r_w}\right)} \quad \dots \dots \dots \quad (7.63)$$

[Eq. 7.63](#) can be interpreted as the harmonic average of two productivity indices:

$$J \approx \frac{1}{\frac{1}{J_{\text{frac}}} + \frac{1}{J_{\text{conv}}}}, \quad \dots \dots \dots \quad (7.64)$$

where J_{frac} is just the PI for linear flow toward a vertical fracture as given in [Eq. 7.53](#), and J_{conv} accounts for the additional pressure drop because of streamline convergence near the well:

$$J_{\text{conv}} = \frac{2\pi kL}{\mu B_o \ln\left(\frac{h}{2\pi r_w}\right)} \quad \dots \dots \dots \quad (7.65)$$

[Eq. 7.65](#) can be interpreted as the PI for radial flow toward a well of length L in a circular reservoir with an equivalent external radius $r_{\text{eq}} = h/(2\pi)$ (refer to [Eq. 6.22](#)). [Fig. 7.12](#) illustrates that the flow in the majority of the reservoir is indeed linear, whereas streamline convergence occurs only close to the well, corresponding to a more radial flow pattern.

These results were published before by Giger (1987) and Butler (1994), who also derived similar expressions for the case of an eccentric horizontal well—i.e., for a situation where the well is positioned above or below the center of the reservoir. Both Giger (1987) and Butler (1994) refer to an earlier Russian publication, notably Borisov

(1964), which has apparently been translated into English but which, unfortunately, could not be located during the preparation of this book. Moreover, according to Butler, the paper by Borisov (1964) refers to other Russian papers, namely, Borisov (1951), Shchurov (1952), and Merkulov (1958), none of which, however, could be found.

7.3.4 Skin and Geometric Skin. Just as in vertical wells, an additional pressure drop may occur because of formation damage. Following the approach of [Section 6.6](#), this effect can be described with a skin factor, and in analogy to [Eq. 6.45](#) we can then rewrite [Eq. 7.63](#) as

$$J = \frac{2\pi kL}{\mu B_o \left[\frac{\pi w}{2h} + \ln\left(\frac{h}{2\pi r_w}\right) + S_h \right]} \quad \dots \quad (7.66)$$

Here, we have added a subscript h to the skin factor S to indicate that it is defined for a horizontal well. Alternatively, we could use the same definition as used for a vertical well (see [Eq. 6.42](#)). This would make sense for a situation in which the skin value is first determined experimentally in a vertical well—e.g., through pressure transient analysis in an exploration or appraisal well—and subsequently used for the design of a horizontal production well. In that case we can rewrite [Eq. 7.63](#) as

$$J = \frac{2\pi kh}{\mu B_o \left[\frac{\pi w}{2L} + \frac{h}{L} \ln\left(\frac{h}{2\pi r_w}\right) + S_v \right]} , \quad \dots \quad (7.67)$$

where

$$S_v = \frac{h}{L} S_h \quad \dots \quad (7.68)$$

The additional pressure drop corresponding to these two definitions follows as

$$\Delta p_{\text{skin}} = \frac{\mu B_o q_{o,\infty} S_h}{2\pi kL} = \frac{\mu B_o q_{o,\infty} S_v}{2\pi kh} \quad \dots \quad (7.69)$$

In addition, the effect of near-well streamline convergence can be interpreted as a *geometric skin factor* defined as

$$S_{\text{conv}} = \ln\left(\frac{h}{2\pi r_w}\right), \quad \dots \quad (7.70)$$

with a corresponding additional pressure drop

$$\Delta p_{\text{conv}} = \frac{\mu B_o q_{o,\infty} S_{\text{conv}}}{2\pi kL}. \quad \dots \quad (7.71)$$

Using this approach, the PI for steady-state flow toward a horizontal well in a homogeneous box-shaped reservoir becomes

$$J = \frac{2\pi kL}{\mu B_o \left[\frac{\pi w}{2h} + S_{\text{conv}} + S_h \right]}, \quad \dots \dots \dots \quad (7.72)$$

or, alternatively,

$$J = \frac{2\pi kh}{\mu B_o \left[\frac{\pi w}{2L} + \frac{h}{L} S_{\text{conv}} + S_v \right]}, \quad \dots \dots \dots \quad (7.73)$$

7.3.5 Average Reservoir Pressure. In Eqs. 7.72 and 7.73 we tacitly used a reference pressure p_{ref} equal to the reservoir pressure p_R . Just as for vertical wells, it may be more convenient to define the PI with respect to a reference pressure equal to the average reservoir pressure $p_{R,\text{av}}$. To do so we can start from Eq. 7.52 for the linear part of the pressure drop:

$$p = p_R + \frac{\mu B_o q_{o,sc}}{2kLh} \left(\frac{w}{2} - y \right). \quad \dots \dots \dots \quad (7.74)$$

An expression for the average reservoir pressure then follows as

$$p_{R,\text{av}} = \frac{\int_0^{w/2} p dy}{\int_0^{w/2} dy} = p_R + \frac{\mu B_o q_{o,sc} w}{8kLh}, \quad \dots \dots \dots \quad (7.75)$$

with which we can derive

$$J = \frac{2\pi kL}{\mu B_o \left(\frac{\pi w}{4h} + S_{\text{conv}} + S_h \right)} \quad \dots \dots \dots \quad (7.76)$$

7.3.6 Semisteady-State Flow. Alternatively, we may consider semisteady-state flow. Starting the derivation again for horizontal flow toward a vertical fracture, the appropriate boundary conditions are now

$$y=0: v = \frac{B_o q_{o,sc}}{2Lh}, \quad \dots \dots \dots \quad (7.77)$$

$$y=\frac{w}{2}: \frac{dp}{dr} = 0. \quad \dots \dots \dots \quad (7.78)$$

Following the same reasoning as in Section 6.5.4, and using boundary conditions

(Eqs. 7.77 and 7.78), we can derive the differential equation for semisteady-state linear flow:

$$\frac{dp}{dy} = -\frac{\mu B_o q_{o,sc}}{2kLh} \left(1 - \frac{2y}{w}\right). \quad (7.79)$$

Integration of the equation results in

$$p = -\frac{\mu B_o q_{o,sc}}{2kLh} \left(y - \frac{y^2}{w}\right) + C. \quad (7.80)$$

Just as in [Section 6.5.4](#), we can use the steady-state boundary condition ([Eq. 7.56](#)) (but now for a slowly decreasing pressure p_R) to solve for the integration constant C , and back substitution of the result in [Eq. 7.80](#) then gives an expression for p as a function of y under semisteady-state flow conditions:

$$p = p_R + \frac{\mu B_o q_{o,sc}}{2kLh} \left(\frac{w}{4} - y + \frac{y^2}{w}\right). \quad (7.81)$$

The PI for semisteady-state linear flow from two sides toward a vertical fracture follows as

$$J_{\text{frac}} = \frac{-q_{o,sc}}{p_R - p_{\text{frac}}} = \frac{8kLh}{\mu B_o w}, \quad (7.82)$$

which is twice as high as the results for steady-state flow (see [Eq. 7.53](#)). The PI for semisteady state flow toward a horizontal well can now be obtained by adding skin factors to represent the effects of near-well streamline convergence and formation damage:

$$J = \frac{2\pi kL}{\mu B_o \left(\frac{\pi w}{4h} + S_{\text{conv}} + S_h\right)}, \quad (7.83)$$

where the reference pressure is the reservoir pressure.

Just as for steady-state flow, we can also express the PI with respect to the average reservoir pressure. (For the derivation, see Question 7.8 in [Section 7.8](#) and its answer in [Appendix G](#).) The corresponding expression for the PI follows as

$$J = \frac{2\pi kL}{\mu B_o \left(\frac{\pi w}{6h} + S_{\text{conv}} + S_h\right)} \quad (7.84)$$

7.3.7 Anisotropic Permeability. As discussed in [Section 7.2.5](#), we can model reservoir anisotropy with the aid of scaled reservoir dimensions. In horizontal wells the difference between horizontal and vertical permeabilities is often significant

because of the nature of geological layering. For example, the presence of horizontal layers with low permeability in an otherwise high-permeability reservoir (as in, e.g., a sand/shale sequence) can result in especially strong anisotropy. If we restrict the analysis to a situation in which the coordinate axes are aligned with the geological layers and consider 2D flow in the vertical y - z plane, we can write

$$\mathbf{K} = \begin{bmatrix} k_y & 0 \\ 0 & k_z \end{bmatrix} = \begin{bmatrix} k_v & 0 \\ 0 & k_h \end{bmatrix}, \dots \quad (7.85)$$

where k_v and k_h are the vertical and horizontal permeabilities. Scaling of the coordinate axes and the relevant parameters and boundary conditions can now be carried out using Eqs. 7.35 through 7.37 and Eqs. 7.43 and 7.45 with an appropriate change in variables. Note that in expressions that combine 1D and 2D flow, only the 2D part requires scaling. As an example, consider the expression for the PI of a horizontal well in an isotropic box-shaped reservoir under steady-state conditions, which contains a linear and a radial flow term in the denominator (Eq. 7.63). The equivalent expression for the anisotropic case becomes

$$J \approx \frac{1}{\underbrace{\frac{\mu B_o w}{4k_h L h} + \frac{\mu B_o}{2\pi \bar{k} L} \ln\left(\frac{\hat{h}}{2\pi \hat{r}_w}\right)}_{\text{1D flow}}} = \frac{1}{\underbrace{\frac{\mu B_o w}{4k_h L h} + \frac{\mu B_o}{2\pi \bar{k} L} \ln\left[\frac{h}{\pi r_w} \left(\frac{1}{I_{vh} + 1}\right)\right]}_{\text{2D flow}}} = \frac{2\pi k_h L}{\mu B_o \left(\frac{\pi w}{2h} + \hat{S}_{\text{conv}}\right)}, \quad (7.86)$$

where the auxiliary variables \hat{r}_w and \hat{h} are given by Eqs. 7.43 and 7.35 (replacing x by h and k_y by k_h), and where the equivalent isotropic permeability \bar{k} , the anisotropy index I_{vh} and the scaled geometric skin \hat{S}_{conv} are now defined as

$$\bar{k} = \sqrt{k_v k_h}, \dots \quad (7.87)$$

$$I_{vh} = \sqrt{\frac{k_v}{k_h}}, \dots \quad (7.88)$$

$$\hat{S}_{\text{conv}} = \frac{1}{I_{vh}} \ln\left[\frac{h}{\pi r_w} \left(\frac{1}{I_{vh} + 1}\right)\right]. \dots \quad (7.89)$$

7.3.8 Combined Expression. Just as we did for vertical wells in Eqs. 6.43 through 6.45, we can combine the various equations for the drawdown of a horizontal well in a box-shaped reservoir into a single expression. Including the effect of k_v/k_h anisotropy, we obtain

$$p_{R,\text{ref}} - p_{wf} = -\frac{\mu B_o q_{o,\text{sc}}}{2\pi k_h L} \left(\frac{\pi w}{c_R h} + \hat{S}_{\text{conv}} + \hat{S}_h \right), \dots \quad (7.90)$$

where \hat{S}_{conv} was already defined in Eq. 7.89, and where

$$\hat{S}_h = \sqrt{I_{vh}} S_h = \frac{L}{h} \sqrt{I_{vh}} S_v, \quad \dots \dots \dots \quad (7.91)$$

with I_{vh} as given in Eq. 7.88, while

$$c_R = \begin{cases} 2 & \text{for steady-state flow with } p_{R,\text{ref}} = p_R, \\ 4 & \text{for steady-state flow with } p_{R,\text{ref}} = p_{R,\text{av}}, \\ 4 & \text{for semisteady-state flow with } p_{R,\text{ref}} = p_R, \\ 6 & \text{for semisteady-state flow with } p_{R,\text{ref}} = p_{R,\text{av}}, \end{cases} \dots \quad (7.92)$$

such that the combined expression for the PI becomes

$$J = \frac{-q_{o,\infty}}{p_{R,\text{ref}} - p_{wf}} = \frac{2\pi k_h L}{\mu B_o \left(\frac{\pi w}{c_R h} + \hat{S}_{\text{conv}} + \hat{S}_h \right)}. \quad (7.93)$$

Eqs. 7.90 through 7.93 have been programmed in MATLAB file `res_oil_box.m`. Examples of how to use this file are given in `example_res_pres_oil_hor.m` and `example_PI_oil_hor.m`.

7.4 Horizontal Wells, Part 2

7.4.1 Partially Penetrating Wells. The horizontal well in a box-shaped reservoir considered in Section 7.3 was assumed to be fully penetrating (i.e., running over the entire length of the reservoir with no-flow boundaries at the heel and the toe). However, in reality horizontal wells are nearly always partially penetrating, resulting in significant additional inflow at the heel and the toe because of the absence of flow barriers.

7.4.2 Elliptic Coordinates. A classic approach to modeling the 2D steady-state pressure distribution around a partially penetrating line source was published by Schlichter (1889, p. 344–347) for groundwater flow and by Muskat (1937) for oil flow. It makes use of the following coordinate transformation:

$$x = \frac{1}{2}L \cosh \xi \cos \eta, \quad \dots \dots \dots \quad (7.94)$$

$$y = \frac{1}{2}L \sinh \xi \sin \eta, \dots \quad (7.95)$$

where $0 \leq \xi < \infty$, $0 \leq \eta < 2\pi$ are known as *elliptic coordinates*. It can be verified by substitution that the inverse transformation is given by

$$\xi = \text{acosh } H_\xi, \quad \dots \quad (7.96)$$

$$\eta = \cos H_\eta, \dots \quad (7.97)$$

where

$$H_{\xi,\eta} = \sqrt{2 \left[\frac{x^2}{L^2} + \frac{y^2}{L^2} + \frac{1}{4} \pm \sqrt{\left(\frac{x^2}{L^2} + \frac{y^2}{L^2} + \frac{1}{4} \right)^2 - \frac{x^2}{L^2}} \right]}, \dots \quad (7.98)$$

with the plus sign referring to H_ξ and the minus sign to H_η . Lines of constant ξ form ellipses, and lines of constant η form hyperbolas (see Fig. 7.13). The parameter L is the distance between the foci of the ellipses. The equation for the line through the foci of the ellipses (the x -axis in Fig. 7.13) is $\xi = 0$ for the part of the line between the foci (the thick black line in Fig. 7.13), and $\eta = 0$ and $\eta = \pi$ for the parts to the right and to the left of the foci respectively. The lengths of the long and short axes of the ellipses are given by

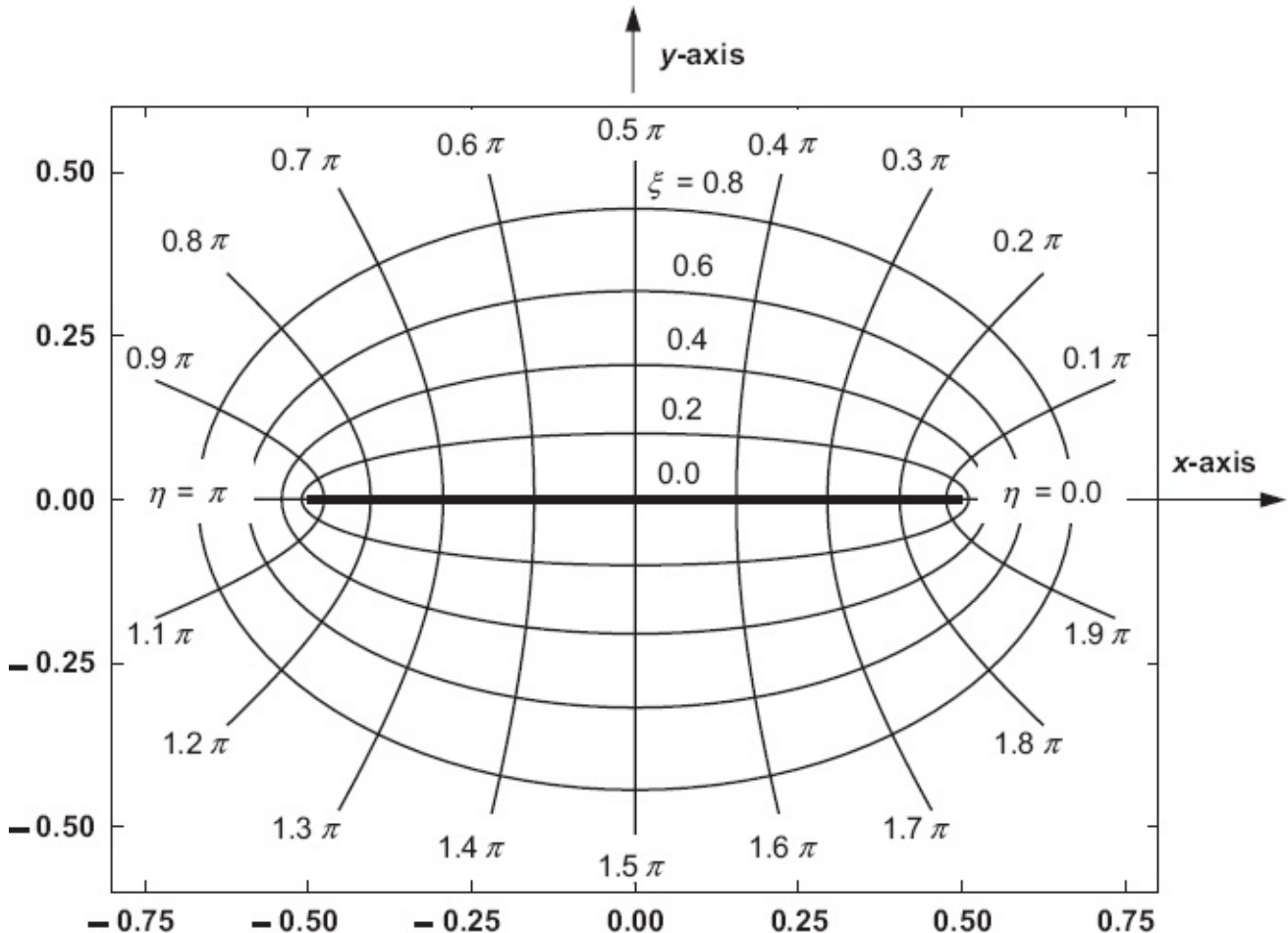


Fig. 7.13— Elliptic coordinate system with $0 \leq \xi \leq 0.8$, $0 \leq \eta \leq 2\pi$ and $L = 1$. The endpoints of the thick horizontal line coincide with the foci of the ellipses.

$$a = L \cosh \xi, \quad (7.99)$$

$$b = L \sinh \xi, \dots \quad (7.100)$$

where a , b , and L are related according to

while the equation for the ellipse in rectangular coordinates is given by

$$\frac{x^2}{a^2} + \frac{y^2}{b^2} = \frac{1}{4} \quad \dots \dots \dots \quad (7.102)$$

With some algebra it can be shown that the expression for $\nabla^2 p$ in elliptic coordinates now becomes

$$\nabla^2 p = \frac{4}{L^2 (\cosh^2 \xi - \cos^2 \eta)} \left(\frac{\partial^2 p}{\partial \xi^2} + \frac{\partial^2 p}{\partial \eta^2} \right). \quad \dots \dots \dots \quad (7.103)$$

[To prove this result, use the chain rule to rewrite the first term between brackets in Eq. 7.103 as $\partial^2 p/\partial\xi^2 = \partial/\partial\xi(\partial p/\partial\xi) = \partial/\partial\xi(\partial p/\partial x \partial x/\partial\xi + \partial p/\partial y \partial y/\partial\xi)$, repeat the chain rule for the second-order derivative, use the same approach for the term $\partial^2 p/\partial\eta^2$, compute the derivatives from Eqs. 7.94 and 7.95, and simplify the results using the equality $\cosh^2(\xi) - \sinh^2(\xi) = 1$.]

From Eq. 7.103, the Laplace equation in elliptic coordinates follows as

$$\frac{\partial^2 p}{\partial \xi^2} + \frac{\partial^2 p}{\partial \eta^2} = 0. \quad \dots \quad (7.104)$$

7.4.3 Horizontal Flow. Just as we did in the case of a boxed-shaped reservoir, we will first consider flow toward a vertical fracture with length L . The corresponding boundary conditions are

$$\xi = 0 : p = p_{wf}, \dots \quad (7.105)$$

$$\xi = \xi_e : p = p_R, \dots \quad (7.106)$$

$$\eta = 0 : \frac{\partial p}{\partial \eta} = 0, \dots \quad (7.107)$$

$$\eta = \pi : \frac{\partial p}{\partial \eta} = 0. \dots \quad (7.108)$$

The first condition prescribes the pressure in the fracture. The second condition prescribes the reservoir pressure at the boundary of an elliptical drainage area with long and short axes a_e and b_e as given in Eqs. 7.99 and 7.100. The last two boundary conditions follow from the argument that the pressure field should be symmetric around the x -axis. (Note that we could just as well have chosen these boundary

conditions at $\eta = \pi/2$ and $\eta = 3\pi/2$ because the pressure field should also be symmetric around the y -axis.)

It can be verified by substitution in Eq. 7.103 that the solution to this problem is simply

$$p(\xi) = p_{wf} + (p_R - p_{wf}) \frac{\xi}{\xi_e} \dots \dots \dots \quad (7.109)$$

The lines of constant ξ (the ellipses) in Fig. 7.14 are equipotential lines, and the lines of constant η (the hyperbolas) are streamlines. Note that for increasing values of ξ the ellipses start increasingly to look like circles; i.e., at a large distance from the well the pressure field becomes nearly identical to the pressure field around a vertical well. The total flow rate from the reservoir into the fracture can be computed with the aid of Darcy's law according to

$$\begin{aligned} q_{o,sc} &= -\frac{2kh}{\mu B_o} \int_0^\pi \frac{\partial p}{\partial \xi} d\eta = -\frac{2kh}{\mu B_o} \int_0^\pi \frac{p_R - p_{wf}}{\xi_e} d\eta = -\frac{2\pi kh}{\mu B_o \xi_e} (p_R - p_{wf}) \\ &= -\frac{2\pi kh (p_R - p_{wf})}{\mu B_o \ln \left(\frac{a_e}{L} + \sqrt{\frac{a_e^2}{L^2} - 1} \right)} = -\frac{2\pi kh (p_R - p_{wf})}{\mu B_o \ln \left(\frac{b_e}{L} + \sqrt{\frac{b_e^2}{L^2} + 1} \right)}, \end{aligned} \quad \dots \dots \dots \quad (7.110)$$

where the latter two equalities have been obtained with the aid of Eqs. 7.99 and 7.100 and the equivalent expressions listed in Table 7.2. The corresponding PI becomes

Function	Equivalent	Derivative	Equivalent
$\sinh x$	$= (e^x - e^{-x})/2$	$\cosh x =$	$(e^x + e^{-x})/2$
$\cosh x$	$= (e^x + e^{-x})/2$	$\sinh x =$	$(e^x - e^{-x})/2$
$\operatorname{asinh} x$	$= \ln(x + \sqrt{x^2 + 1})$	$1/\sqrt{x^2 + 1}$	
$\operatorname{acosh} x$	$= \ln(x + \sqrt{x^2 - 1})$	$1/\sqrt{x^2 - 1}$	

Table 7.2—Derivatives of some hyperbolic and inverse hyperbolic functions and their equivalent expressions.

$$J = \frac{-q_{o,sc}}{p_R - p_{wf}} = \frac{2\pi kh}{\mu B_o \xi_e} = \frac{2\pi kh}{\mu B_o \ln \left(\frac{a_e}{L} + \sqrt{\frac{a_e^2}{L^2} - 1} \right)} = \frac{2\pi kh}{\mu B_o \ln \left(\frac{b_e}{L} + \sqrt{\frac{b_e^2}{L^2} + 1} \right)}. \quad \dots \dots \dots \quad (7.111)$$

7.4.4 Near-Well Radial Flow, Skin, and Anisotropy. To use this result for flow toward a horizontal well, we have to add the additional effect of near-well streamline convergence in the vertical plane. As before, this can be done conveniently with the aid of a geometric skin factor as defined in Eq. 7.70. If we also add the regular skin

factor and account for reservoir anisotropy in the vertical plane with the aid of Eqs. 7.87, 7.88, and 7.90, the result becomes

$$J = \frac{2\pi k_h h}{\mu B_o \left[\ln \left(\frac{a_e}{L} + \sqrt{\frac{a_e^2}{L^2} - 1} \right) + \frac{h}{L} \hat{S}_{\text{conv}} + \hat{S}_v \right]} = \frac{2\pi k_h h}{\mu B_o \left[\ln \left(\frac{b_e}{L} + \sqrt{\frac{b_e^2}{L^2} + 1} \right) + \frac{h}{L} \hat{S}_{\text{conv}} + \hat{S}_v \right]}. \quad (7.112)$$

Note that scaling is required only for the terms related to flow in the vertical plane (because of streamline convergence). The horizontal permeability remains isotropic and is equal to k_h .

An almost identical expression of Eq. 7.112 is often referred to as the Joshi equation. Derived by Joshi (1988) and later slightly modified by Economides et al. (1991), the only difference is the factor $1/\pi$ inside the logarithm of the geometric skin factor (refer to Eq. 7.89):

$$\hat{S}_{\text{conv,Joshi}} = \frac{1}{I_{vh}} \ln \left[\frac{h}{r_w} \left(\frac{1}{I_{vh} + 1} \right) \right] = \hat{S}_{\text{conv}} - \frac{1}{I_{vh}} \ln \left(\frac{1}{\pi} \right) = \hat{S}_{\text{conv}} + \frac{1.14}{I_{vh}}. \quad (7.113)$$

Eq. 7.112 has been programmed in MATLAB file `res_oil_ellipse.m`. Examples of how to use this file are given in `example_res_pres_oil_hor.m` and `example_PI_oil_hor.m`.

7.4.5 Specific PI. Often, the inflow to a horizontal well is expressed in terms of the *specific flow rate* (i.e., the flow rate per unit length):

$$q'_{o,sc} = \frac{q_{o,sc}}{L}. \quad (7.114)$$

For a fully penetrating well in a box-shaped reservoir, and neglecting pressure drop inside the well, the specific flow rate is constant along the well. However, for a well in an elliptical domain the specific flow rate varies as a function of distance along the well. Neglecting the effects of permeability anisotropy and streamline convergence in the vertical plane, we can derive

$$\begin{aligned} q'_{o,sc}(x) &= -\frac{2kh}{\mu B_o} \frac{\partial p(x,y)}{\partial y} \Big|_{y=0} = -\frac{2kh}{\mu B_o} \left(\frac{\partial p}{\partial \xi} \frac{\partial \xi}{\partial y} + \frac{\partial p}{\partial \eta} \frac{\partial \eta}{\partial y} \right)_{y=0} \\ &= \frac{4kh(p_R - p_{wf})}{\mu B_o \xi_e L \sin \eta} = \frac{4kh(p_R - p_{wf})}{\mu B_o \xi_e L \sin \arccos \left(\frac{2x}{L} \right)} = \frac{4kh(p_R - p_{wf})}{\mu B_o \xi_e L \sqrt{1 - \left(\frac{2x}{L} \right)^2}}, \end{aligned} \quad (7.115)$$

where the third equality is obtained with the aid of Eqs. 7.109 and 7.95, and Table 7.2; the fourth one with Eq. 7.94 for $\xi = 0$; and the fifth one with the trigonometric identity $\sin \arccos(x) = \sqrt{1-x^2}$. The inflow is not uniform along the well, with a minimum at $x = 0$. However, the maximum inflow, at $x = 0 \pm 0.5L$, goes to infinity. To overcome this singularity we require the flowing bottomhole pressure (FBHP) to occur at the

wellbore radius—i.e., at $y = r_w$ instead of at $y = 0$. (Here, we tacitly assume that $r_w \ll \xi_e$ such that Eq. 7.109 remains approximately valid.) Eq. 7.115 then has to be replaced by

$$\begin{aligned} q'_{o,sc}(x) &= -\frac{2kh}{\mu B_o} \frac{\partial p(x,y)}{\partial y} \Big|_{y=r_w} = -\frac{2kh}{\mu B_o} \left(\frac{\partial p}{\partial \xi} \frac{\partial \xi}{\partial y} + \frac{\partial p}{\partial \eta} \frac{\partial \eta}{\partial y} \right)_{y=r_w} = -\frac{4kh(p_R - p_{wf})}{\mu B_o \xi_e L \sqrt{\left(\frac{2r_w}{L}\right)^2 + \sin^2 \eta}} \\ &= -\frac{4kh(p_R - p_{wf})}{\mu B_o \xi_e L \sqrt{\left(\frac{2r_w}{L}\right)^2 + \left[\sin \arcsin\left(\frac{2x}{L}\right)\right]^2}} = -\frac{4kh(p_R - p_{wf})}{\mu B_o \xi_e L \sqrt{\left(\frac{2r_w}{L}\right)^2 + 1 - \left(\frac{2x}{L}\right)^2}}. \end{aligned} \quad \dots(7.116)$$

The specific PI (i.e., the PI per unit length) now follows as

$$J'(x) = \frac{-q'_{o,sc}}{(p_R - p_{wf})} = \frac{4kh}{\mu B_o \xi_e L \sqrt{\left(\frac{2r_w}{L}\right)^2 + 1 - \left(\frac{2x}{L}\right)^2}}. \quad \dots(7.117)$$

The total flow rate from the reservoir into the well can, as before, be computed with the aid of Darcy's law according to

$$q_{o,sc} = -\frac{4kh(p_R - p_{wf})}{\mu B_o \xi_e L} \int_{-\frac{L}{2}}^{\frac{L}{2}} \frac{1}{\sqrt{\left(\frac{2r_w}{L}\right)^2 + 1 - \left(\frac{2x}{L}\right)^2}} dx = -\frac{4kh(p_R - p_{wf})}{\mu B_o \xi_e} \arcsin \frac{1}{\sqrt{\left(\frac{2r_w}{L}\right)^2 + 1}}. \quad \dots(7.118)$$

Because $\arcsin(1) = \pi/2$, it follows that Eq. 7.118 reduces to the third equality in Eq. 7.110 when r_w is chosen to be equal to zero. Fig. 7.14 depicts the specific PI as a function of distance along the well for a case where $(2r_w/L) = 0.0001$, which corresponds, e.g., to a well 1800 m (5,906 ft) long with a diameter of 0.18 m (7 in.). It can be seen that a disproportionate amount of the inflow occurs at the ends of the well. In reality the nonlinear effects of friction in the near-wellbore region and the completion will smoothen the inflow profile and the exact values at the ends are therefore not particularly relevant. Moreover, the pressure drop caused by friction inside the horizontal part of the well will result in a higher drawdown at the heel of the well than at the toe, such that the profile becomes asymmetric. Because the pressure drop along the well results in a higher drawdown at the heel than at the toe, water or gas breakthrough is more likely to occur there than at the toe. In long (say, more than 500 m) horizontal wells in highly permeable reservoirs, these effects can be substantial (see Dikken 1990).

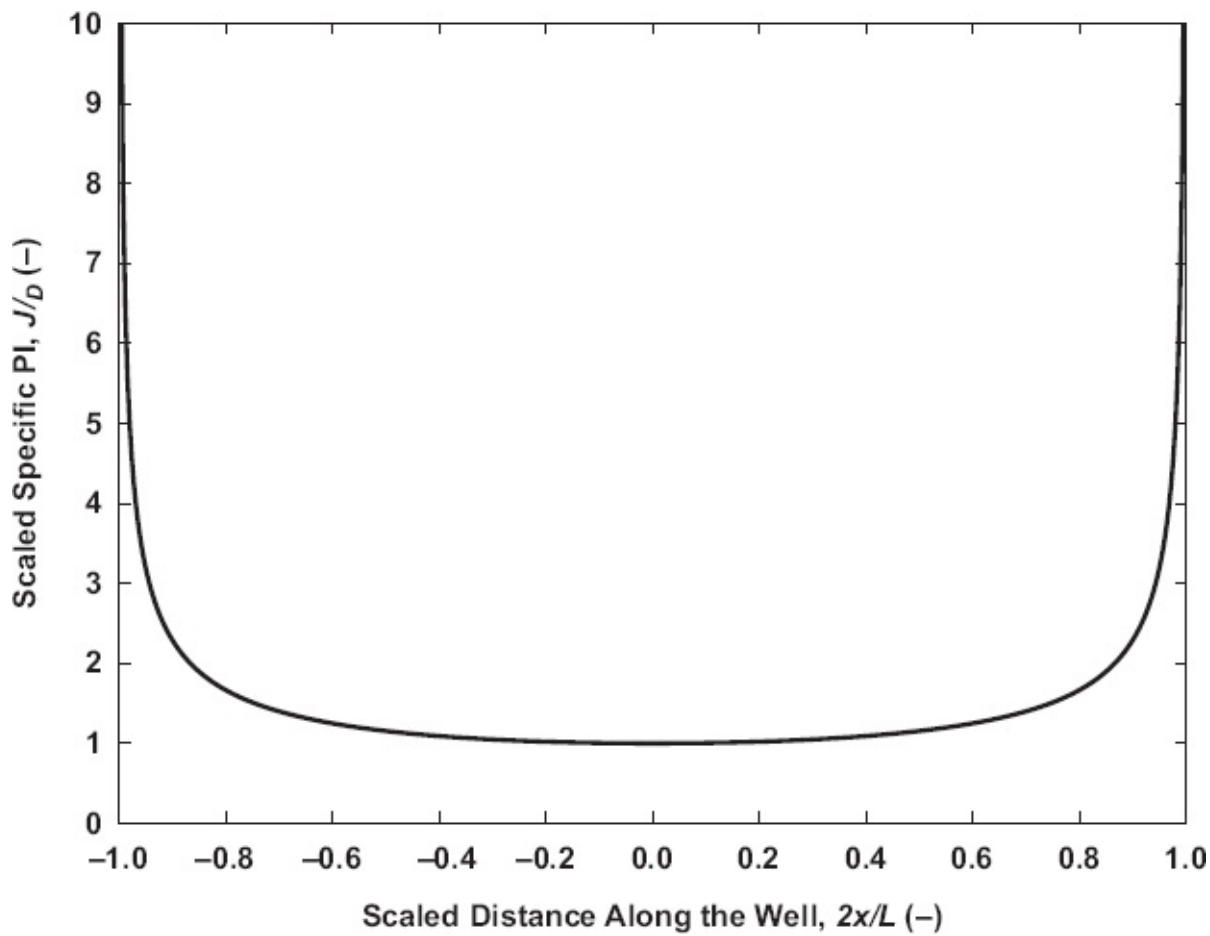


Fig. 7.14—Scaled specific PI $J'_D = J' \mu B_{o,sc} \xi_e L / (4kh)$ as a function of dimensionless distance $x_D = 2x / L$ along the horizontal well for a dimensionless wellbore radius $r_{w,D} = 2r_w / L = 0.0001$. Note: The vertical axis of the figure has been truncated. The largest value of J'_D occurs at $x_D = \pm 1$ and has magnitude $J'_D = 5000$.

7.4.6 Other Horizontal Well Models. Many other horizontal well models have been proposed in the literature. One that is often referred to is by Babu and Odeh (1988), who present an expression for semisteady-state flow toward a partially penetrating well in a box-shaped reservoir. However, as pointed out by Butler (1994), their solution assumes a constant specific inflow that therefore results in a somewhat unrealistically varying wellbore pressure along the well. Another frequently referenced model is the one by Dikken (1990), who included pressure drop inside the wellbore, which may become important for long wells in low-permeability reservoirs where high flow rates result from relatively small drawdowns (i.e., relative to the pressure drop over the well). This Dikken model is the topic of the MATLAB assignment at the end of this chapter. In line with the objectives of our book, we intend not to give a full catalogue of horizontal well models, but to discuss some of the essential modeling aspects as was performed in the previous sections. For extensive discussions and further references on horizontal well inflow performance we refer to Joshi (1991), Butler (1994), and Economides et al. (1998, 2013).

7.5 Semi-Analytical Approach

7.5.1 Complex Well Configurations. After the proliferation of horizontal drilling during the last two decades of the 20th century, the next innovation in drilling technology was the introduction of *multilateral wells* (i.e., of wells with two or more branches). [Fig. 7.15](#) depicts two examples of typical configurations. For a detailed overview of the various types of multilateral wells and completions, see Hill et al. (2008), which also contains a variety of methods to compute inflow performance relationships (IPRs).

7.5.2 Point Sources. Generally, the pressure field around complex well configurations can no longer be described with closed-form analytical solutions as was done for straight vertical and horizontal wells. A detailed description can be obtained with numerical reservoir simulators which, in addition to allowing for a complex well configuration, also allow for incorporating reservoir complexity in the form of layering, fractures, high-permeability streaks, or other geologic heterogeneities. Although such fully numerical reservoir simulation is outside the scope of our book, we next briefly discuss an intermediate, semi-analytical technique that is capable of simulating the pressure around complex wells in homogeneous reservoirs. The basic element of this approach is the use of linear superposition to represent wells in the form of a series of point sources or sinks. (Note that because a sink is just a negative source, from now on we will refer only to sources.)

To illustrate the method, consider again the flow toward a horizontal well, just as in [Subsection 7.3.2](#). The horizontal flow toward the well is, as before, schematized as flow toward a vertical fracture with height h and length L , now oriented along the x -axis between $x = 0$ and $x = L$. Using a similar superposition approach as in [Subsections 7.2.3](#) and [7.2.4](#), we can represent the pressure field around the fracture with the aid of N point sources as follows:

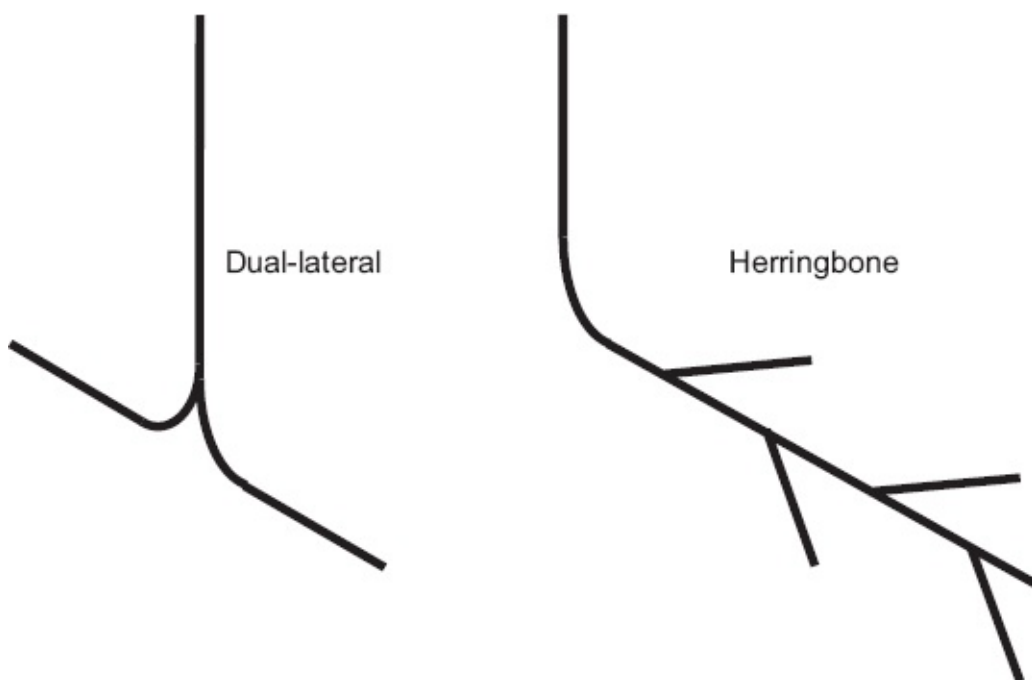


Fig. 7.15—Examples of multilateral well configurations: left, dual-lateral well with opposed branches; right, herringbone well with multiple branches.

$$\begin{aligned} p(x, y) &= p_R + \frac{\mu B_o q_{o,\infty}}{4\pi kh} \sum_{i=1}^N c_i \ln \left[\frac{r_e^2}{(x-x_i)^2 + (y-y_i)^2} \right] \\ &= p_R + \frac{\mu B_o q_{o,\infty}}{4\pi kh} \sum_{i=1}^N c_i \left\{ \ln r_e^2 - \ln \left[(x-x_i)^2 + (y-y_i)^2 \right] \right\}, \end{aligned} \quad (7.119)$$

where x_i and y_i are the positions of the point sources, which in this case are given by

$$x_i = (i-1)\Delta L = (i-1)\frac{L}{N-1}, \quad (7.120)$$

$$y_i = 0. \quad (7.121)$$

According to the notation introduced in [Section 7.2.3](#), we have $n = N$, $c_0 = p_R$, and, as yet, unspecified values of c_i , $i = 1, 2, \dots, N$, while each of the N sources is shifted over a distance ΔL . If we would choose equal weights for the coefficients c_i , the flow rate in each of the point sources would have the same value, but the pressure in each of the sources would be different. For most wells, however, a near-uniform wellbore pressure is the more likely situation. (Note that the pressure drop along a horizontal well may become important at high flow rates. For an analysis of this effect, see the MATLAB assignment at the end of this chapter. Here, we assume that such pressure drop effects are absent.)

If we require the pressure in each of the sources to be identical, this results in unequal flow rates in the sources, in line with the uneven specific inflow distribution along a horizontal well discussed in [Subsection 7.4.5](#). To implement the latter approach, we can use [Eqs. 7.119](#) through [7.121](#) to generate the following set of N equations:

$$\left\{ \begin{array}{lcl} p(x_{p,1}, y_{p,1}) & = & p(0, r_w) = p_R + \frac{\mu B_o q_{o,\infty}}{4\pi kh} \sum_{j=1}^N c_j \left(\ln r_e^2 - \ln \left[-(j-1)\Delta L \right]^2 + r_w^2 \right), \\ p(x_{p,2}, y_{p,2}) & = & p(\Delta L, r_w) = p_R + \frac{\mu B_o q_{o,\infty}}{4\pi kh} \sum_{j=1}^N c_j \left(\ln r_e^2 - \ln \left[[\Delta L - (j-1)\Delta L]^2 + r_w^2 \right] \right), \\ p(x_{p,3}, y_{p,3}) & = & p(2\Delta L, r_w) = p_R + \frac{\mu B_o q_{o,\infty}}{4\pi kh} \sum_{j=1}^N c_j \left(\ln r_e^2 - \ln \left[[2\Delta L - (j-1)\Delta L]^2 + r_w^2 \right] \right), \\ \vdots & = & \vdots = \vdots \\ p(x_{p,N}, y_{p,N}) & = & p(L, r_w) = p_R + \frac{\mu B_o q_{o,\infty}}{4\pi kh} \sum_{j=1}^N c_j \left(\ln r_e^2 - \ln \left[[L - (j-1)\Delta L]^2 + r_w^2 \right] \right), \end{array} \right. \quad (7.122)$$

where $(x_{p,i}, y_{p,i})$, $i = 1, 2, \dots, N$, are the coordinates of the points where we fix the pressures. Note that these fixed-pressure points are almost equal to the source

points but have been shifted slightly to be at the wellbore radius—i.e., at $(x_{p,i}, y_{p,i}) = [(i - 1)\Delta L, r_w]$ —to avoid singularities. (Because we arbitrarily chose the fixed-pressure points to be at the wellbore radius in the positive y -direction, the pressure distribution becomes slightly asymmetric around the x -axis. However, the effect is so small that it may be neglected.)

If we require the pressure in all N sources to be equal to the wellbore pressure p_{wf} , the set of equations (Eq. 7.122) can be rewritten as

$$\underbrace{\begin{bmatrix} A_{11} & A_{12} & A_{13} & \cdots & A_{1N} \\ A_{21} & A_{22} & A_{23} & \cdots & A_{2N} \\ A_{31} & A_{32} & A_{33} & \cdots & A_{3N} \\ \vdots & \vdots & \vdots & \ddots & \vdots \\ A_{N1} & A_{N2} & A_{N3} & \cdots & A_{NN} \end{bmatrix}}_A \underbrace{\begin{bmatrix} c_1 q_{o,sc} \\ c_2 q_{o,sc} \\ c_3 q_{o,sc} \\ \vdots \\ c_N q_{o,sc} \end{bmatrix}}_q = -\frac{4\pi k h}{\mu B_o} (p_R - p_{wf}) \underbrace{\begin{bmatrix} 1 \\ 1 \\ 1 \\ \vdots \\ 1 \end{bmatrix}}_{\Delta p}, \quad \dots \dots \dots \quad (7.123)$$

where we introduced matrix-vector notation with matrix coefficients A_{ij} given by

$$\begin{aligned} A_{ij} &= \ln r_e^2 - \ln \left[(x_{p,i} - x_j)^2 + (y_{p,i} - y_j)^2 \right] \\ &= \ln r_e^2 - \ln \left[[(i-1)\Delta L - (j-1)\Delta L]^2 + r_w^2 \right]. \end{aligned} \quad \dots \dots \dots \quad (7.124)$$

Note that the first line of Eq. 7.124 is valid for any configuration of point sources, whereas the second line is specific for our example of flow toward a well or fracture oriented along the x -axis. Eq. 7.123 constitutes a system of N linear equations for the N unknown vector elements $q_i = c_i q_{o,sc}$, $i = 1, \dots, N$, which can formally be solved as

$$q = A^{-1} \Delta p, \quad \dots \dots \dots \quad (7.125)$$

or, computationally more efficiently, by solving the linear system for q directly. The total flow rate and the PI then follow as

$$q_{o,sc,tot} = \sum_{i=1}^N q_i, \quad \dots \dots \dots \quad (7.126)$$

and

$$J = \frac{-q_{o,sc,tot}}{p_R - p_{wf}}. \quad \dots \dots \dots \quad (7.127)$$

Using MATLAB we can simply use the backslash operator to obtain the result as

```
q = A \ Delta_p;
q_o_sc_tot = sum(q);
J = -q_o_sc_tot / (p_R - p_wf)
```

7.5.3 Near-Well Radial Flow and Skin. To include the effects of skin resulting from near-well streamline convergence and formation damage, we can use Eqs. 7.69 and 7.71 to develop

$$\Delta p_{\text{conv}} + \Delta p_{\text{skin}} = \frac{\mu B_o q_{o,\infty} (S_{\text{conv}} + S_h)}{2\pi k L} = \frac{\mu B_o q_{o,\infty} \left(\frac{h}{L} S_{\text{conv}} + S_v \right)}{2\pi k h}, \quad \dots \dots \dots \quad (7.128)$$

where S_{conv} and S_v are given by Eqs. 7.70 and 7.68, respectively; and then apply this result to modify each of the lines in Eq. 7.122 as

$$p(x_{p,i}, y_{p,i}) = p[(i-1)\Delta L, r_w] = p_R + \frac{\mu B_o q_{o,\infty}}{4\pi k h} \sum_{j=1}^N c_j \left(\ln r_e^2 - \ln \left\{ [(i-1)\Delta L - (j-1)\Delta L]^2 + r_w^2 \right\} \right) \\ + 2 \left(\frac{h}{L} S_{\text{conv}} + S_v \right) \quad \dots \dots \dots \quad (7.129)$$

The matrix coefficients A_{ij} in Eq. 7.123 now become

$$A_{ij} = \ln r_e^2 - \ln \left[(x_{p,i} - x_j)^2 + (y_{p,i} - y_j)^2 \right] + 2 \left(\frac{h}{L} S_{\text{conv}} + S_v \right) \\ = \ln r_e^2 - \ln \left\{ [(i-1)\Delta L - (j-1)\Delta L]^2 + r_w^2 \right\} + 2 \left(\frac{h}{L} S_{\text{conv}} + S_v \right), \quad \dots \dots \dots \quad (7.130)$$

and the resulting equations can be solved as described in the previous section. As an example, Figs. 7.16 and 7.17 depict the pressure field around a horizontal well with length $L = 500$ m, wellbore pressure $p_{wf} = 7$ MPa, external radii $r_e = 1000$ m, and other properties as given in Table 6.1, represented with 5 and 80 point sources, respectively. Fig. 7.18 depicts the error in the PI relative to the analytical solution for an increasing number of point sources. The analytical result obtained is from Eq. 7.112 with $b_e = 2r_e$.

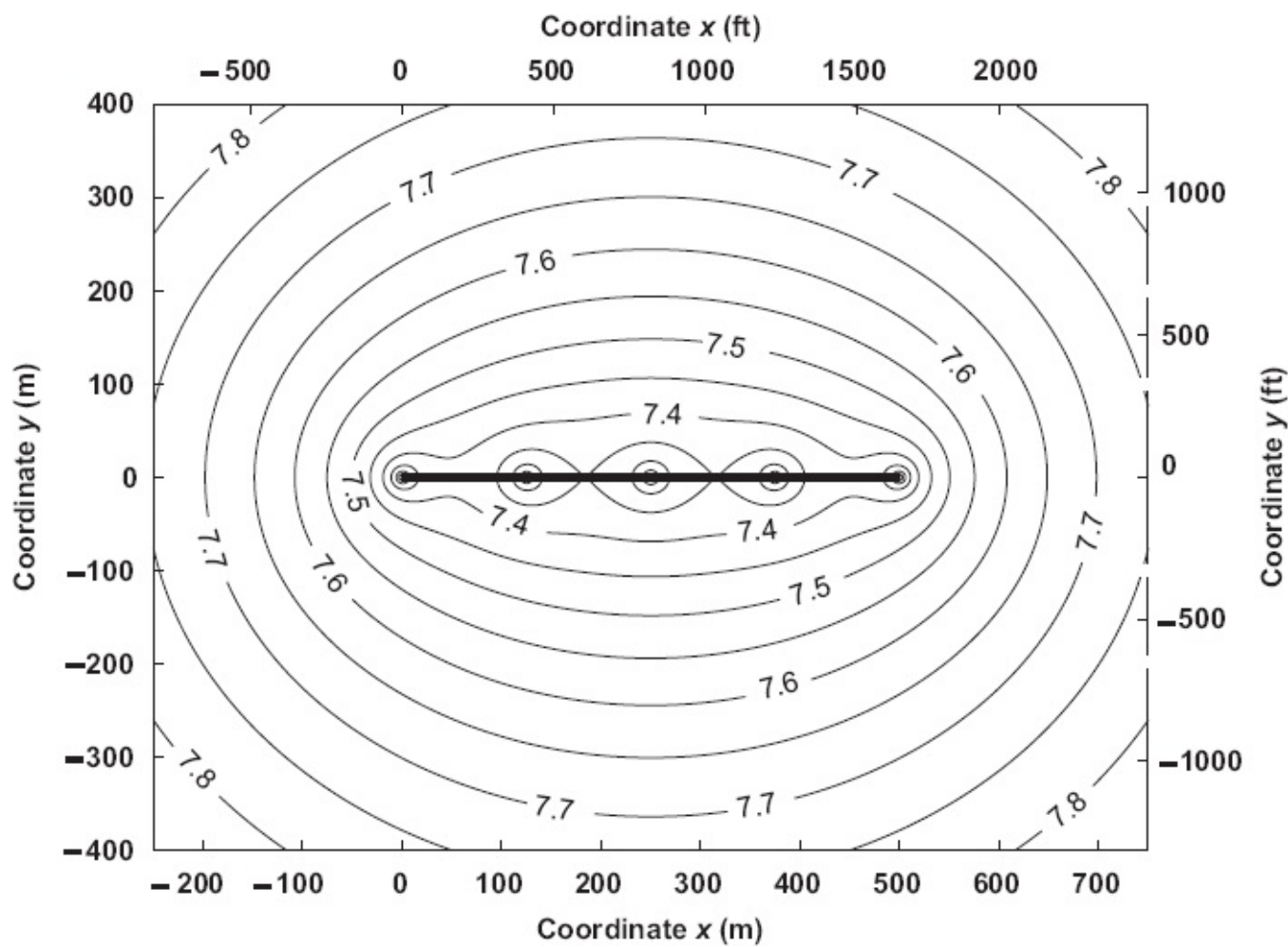


Fig. 7.16—Steady-state pressure field in the horizontal plane (top view) around a horizontal well with length $L = 500$ m (indicated with a fat horizontal line), wellbore pressure $p_{wf} = 7$ MPa, external radii $r_e = 1000$ m, and other properties as given in Table 6.1, represented with five point sources (numbers in the plot indicate pressures in MPa).

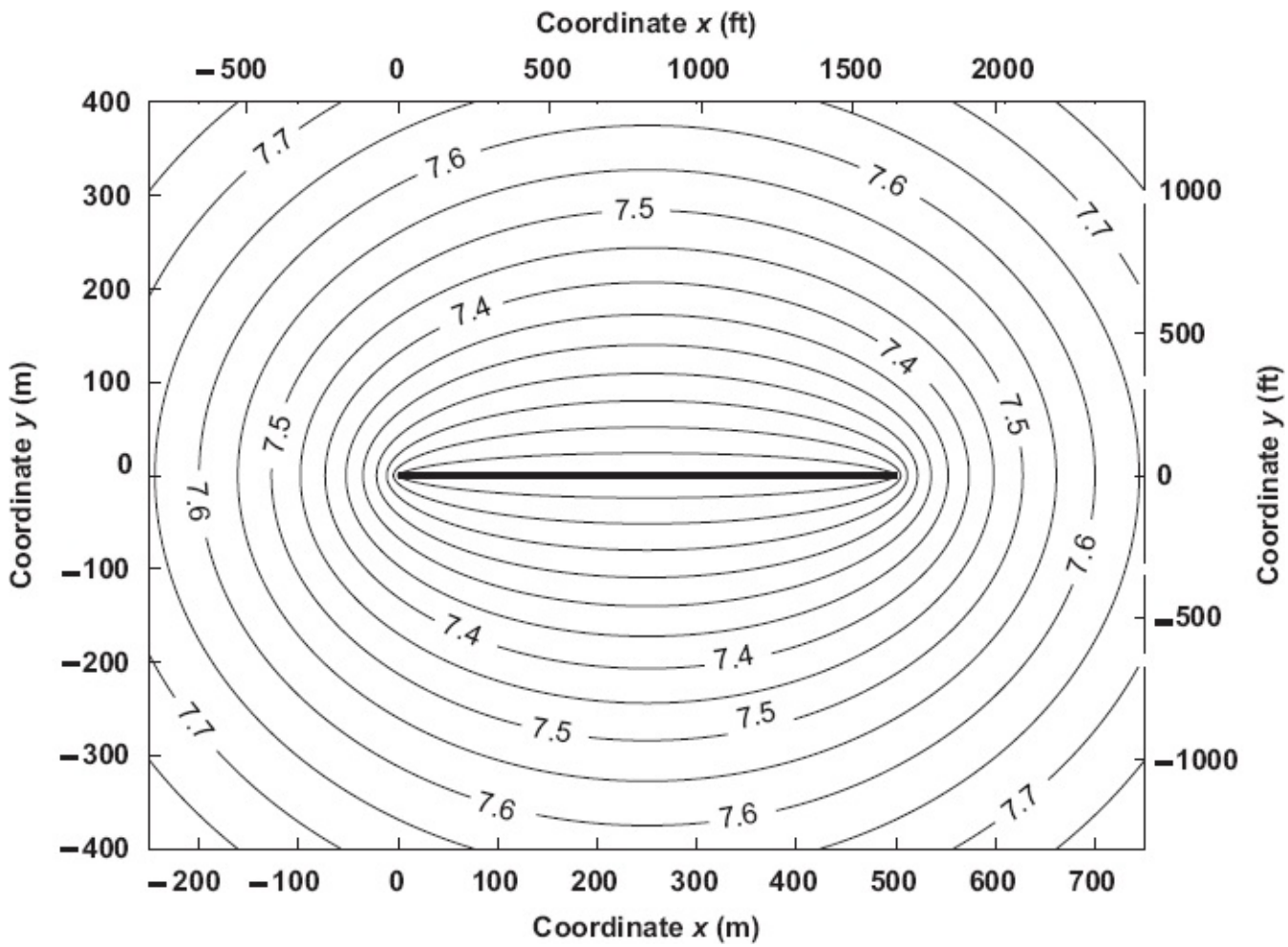


Fig. 7.17—Steady-state pressure field around the same horizontal well as depicted in Fig. 7.16 but now represented with 80 point sources (numbers in the plot indicate pressures in MPa).

7.5.4 Multilateral Wells. As a somewhat more complex example, consider a multilateral well of the herringbone type, like the one depicted in Fig. 7.15. We use the same approach as for the horizontal well in the previous example but with a more elaborate description of the location of the point sources (i.e., of the matrix coefficients A_{ij} in Eq. 7.124). The result is plotted in Fig. 7.19, which represents the same horizontal well as in Figs. 7.16 and 7.17, but now equipped with two 150-m lateral branches. As a result, the PI has increased from 0.95×10^{-9} to 1.02×10^{-9} $\text{m}^3/\text{Pa}\cdot\text{s}$ (3.56 to 3.83 B/D-psi)— i.e., an increase of just 5% even though the total well length has increased 60%. This relatively small increase demonstrates the effect of pressure interference between the branches. (Note that this result relates to steady-state flow. Early during the transient flow period of a multilateral well, a much higher increase of the PI can be observed.) Figs. 7.16, 7.17, and 7.19 can be reproduced with the MATLAB file `example_point_sources.m`, which can also be edited to represent other configurations.

Note that unlike other system element models previously considered, here we compute the flow rate for a given pressure drop (drawdown) rather than the other way around. Of course, it is still possible to create an inflow performance relationship

(i.e., a plot of p_{wf} vs. $q_{o,sc}$) that will be a straight line, just as in Fig. 6.1, because the entire theory of superposition is based on the assumption of linearity of the governing equations. If it is necessary to compute the drawdown as a function of flow rate—e.g., when using a multilateral reservoir model as an element in a cascade of pressure drop elements—it will be required to use an iterative procedure, in which the linear nature of the equations allows for convergence in one iteration.

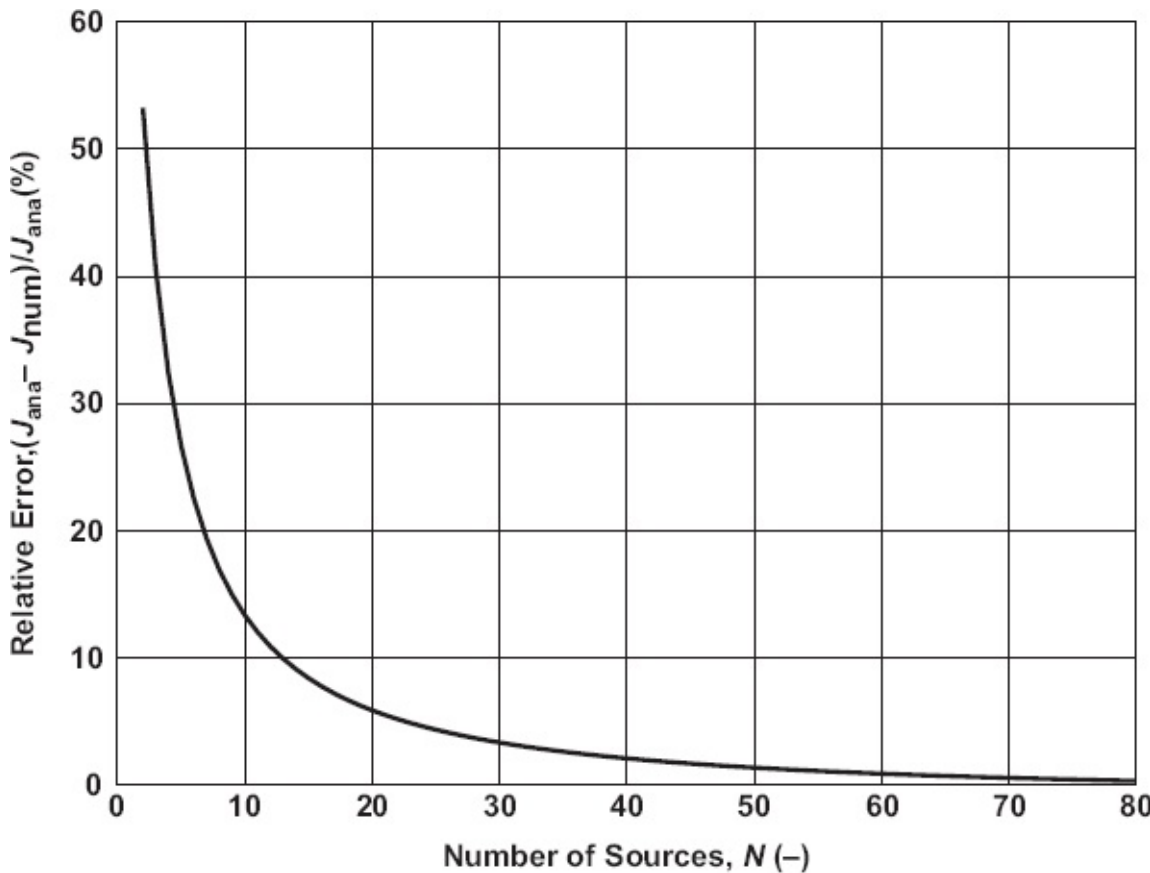


Fig. 7.18—Error in the numerically computed PI, relative to the analytical solution, for a number of point sources increasing from 2 to 80.

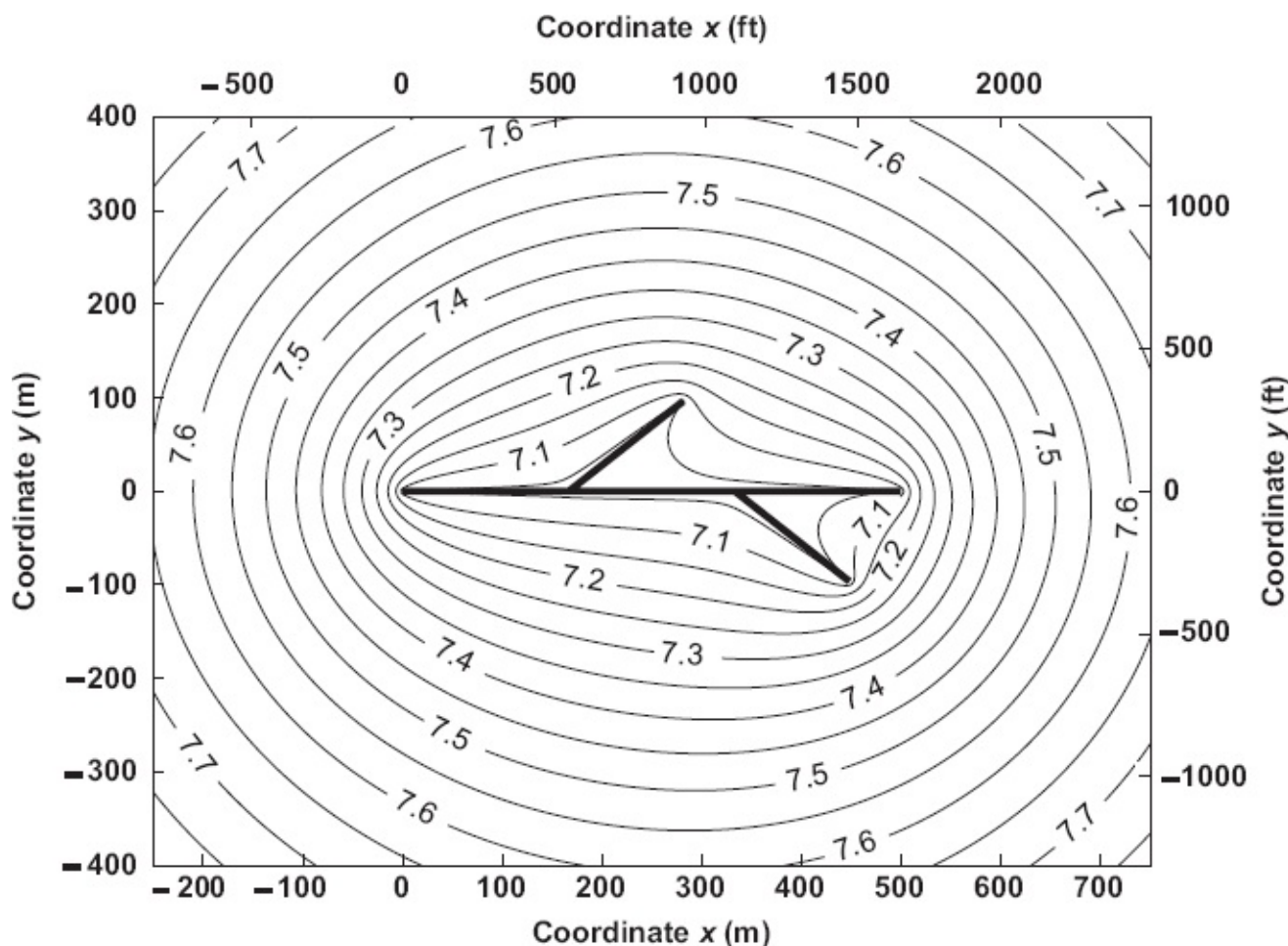


Fig. 7.19—Steady-state pressure field around a multilateral well with a backbone that is identical to the horizontal well depicted in Fig. 7.16 and equipped with two branches. The well is represented with 121 point sources (numbers in the plot indicate pressures in MPa).

7.5.5 Extended Functionality. Linear reservoir behavior is a good approximation for single-phase oil flow. Reservoir anisotropy can be included with some additional programming and using the scaled equations discussed in Sections 7.2.5 and 7.3.7. Moreover, it is relatively straightforward to extend the semianalytical approach with point sources for use in single-phase gas flow with the aid of the pseudopressure formulation that was discussed in Section 6.7.2. The extension to transient or semisteady-state flow is more elaborate, although conceptually the same approach can be used starting from the diffusivity equation rather than the Laplace equation. The next step in complexity is the inclusion of pressure drop in either the branches or the main wellbore. Finally, with some creativity it is possible to approximate two-phase flow under solution gas drive conditions by including Vogel- or Fetkovitch-type relationships as were discussed in Section 6.8.1. However, doing this makes the equations nonlinear and will therefore require an iterative solution strategy—e.g., multivariable Newton-Raphson iteration. We will not discuss these extensions but refer to Ouyang and Aziz (2001) and Hill et al. (2008) for further information.

7.6 Multiphase Flow: Theoretical Models

7.6.1 Relative Permeabilities. As mentioned briefly in [Section 6.4.2](#), in multiphase flow through porous media the permeability for each phase is generally a nonlinear, path-dependent function of the *phase saturations*. The gas, oil, and water saturations, S_g , S_o , and S_w , are defined as the fraction of the pore space occupied by the corresponding phase, such that by definition $S_g + S_o + S_w = 1$. The saturations are equivalent to the holdups or in-situ volume fractions used in multiphase pipe flow. Also, the viscosities of the phases differ, as well as the *mobilities* (i.e., the quotients of permeability and viscosity for each phase). In the case of three-phase gas/oil/water flow we need to replace Darcy's law for single-phase flow, [Eq. 6.9](#), by

$$\frac{F_{fg}}{2\pi hr} = -\frac{\mu_g}{kk_{rg}} v_g, \quad \dots \quad (7.131)$$

$$\frac{F_{fo}}{2\pi hr} = -\frac{\mu_o}{kk_{ro}} v_o, \quad \dots \quad (7.132)$$

$$\frac{F_{fw}}{2\pi hr} = -\frac{\mu_w}{kk_{rw}} v_w, \quad \dots \quad (7.133)$$

where k is the *absolute permeability* (also known as the *homogeneous permeability*) governed by rock properties only, and $0 \leq k_{rg} \leq 1$, $0 \leq k_{ro} \leq 1$, and $0 \leq k_{rw} \leq 1$ are the *relative permeabilities* ("rel perms" for short), which are nonlinear functions of the phase saturations. They represent the reduction of permeability to one phase because of the presence of the other phases. (See [Appendix F](#) for a brief description of the underlying physics and some semiempirical expressions to describe two-phase and three-phase rel perms.) We can now modify the radial wellbore flow treated in the previous sections by introducing relative permeabilities for the phases while maintaining the assumption of steady-state flow. Starting from [Eqs. 6.14](#) to [6.16](#), [Eqs. 6.50](#) to [6.52](#), and their equivalents for water flow, we can write the multiphase Darcy equations as

$$\frac{dp_g}{dr} = -\frac{\mu_g}{kk_{rg}} v_g - \beta \rho_g |v_g| v_g, \quad \dots \quad (7.134)$$

$$\frac{dp_o}{dr} = -\frac{\mu_o}{kk_{ro}} v_o, \quad \dots \quad (7.135)$$

$$\frac{dp_w}{dr} = -\frac{\mu_w}{kk_{rw}} v_w, \quad \dots \quad (7.136)$$

where, for radial flow,

$$v_g = \frac{q_g}{2\pi hr}, \dots \quad (7.137)$$

$$v_o = \frac{q_o}{2\pi hr}, \dots \quad (7.138)$$

$$v_w = \frac{q_w}{2\pi hr}. \dots \quad (7.139)$$

7.6.2 Pressure Gradient. Approximate solutions to Eqs. 7.134 through 7.136 were obtained by Evinger and Muskat (1942) and Wiggins et. al (1992), and the following numerical procedure is inspired by their approach.

Introducing the phase mobilities

$$\lambda_g = \frac{kk_{rg}}{\mu_g}, \dots \quad (7.140)$$

$$\lambda_o = \frac{kk_{ro}}{\mu_o}, \dots \quad (7.141)$$

$$\lambda_w = \frac{kk_{rw}}{\mu_w}, \dots \quad (7.142)$$

Eqs. 7.134 and 7.136 can be simplified to

$$\frac{\lambda_g}{\lambda_o} = R'_{go} + F, \dots \quad (7.143)$$

$$\frac{\lambda_w}{\lambda_o} = R'_{wo}, \dots \quad (7.144)$$

where F is the Forchheimer term

$$F = \beta \rho_g \lambda_g R'_{go} |v_g|, \dots \quad (7.145)$$

and where R'_{go} and R'_{wo} are the in-situ gas/oil and water/oil ratios

$$R'_{go} = \frac{v_g}{v_o} = \frac{q_g}{q_o}, \dots \quad (7.146)$$

$$R'_{wo} = \frac{v_w}{v_o} = \frac{q_w}{q_o}. \dots \quad (7.147)$$

Moreover, introducing the total mobility

$$\lambda_t = \lambda_g + \lambda_o + \lambda_w, \dots \quad (7.148)$$

Eq. 7.135 (i.e., the radial pressure gradient in the oil) can be rewritten as

$$\frac{dp_o}{dr} = -\frac{1}{\lambda_t} \left(\frac{\lambda_g + \lambda_o + \lambda_w}{\lambda_o} \right) v_o, \dots \dots \dots \quad (7.149)$$

and therefore as

$$\frac{dp_o}{dr} = -\frac{1}{\lambda_t(S_g, S_w)} [1 + R'_{go}(p_o) + F(p_o, S_g) + R'_{wo}(p_o)] v_o(p_o), \dots \dots \dots \quad (7.150)$$

where we indicated the dependency of the various terms on $p_o(r)$, $S_g(r)$, and $S_w(r)$. Eq. 7.150 can be integrated numerically, and the pressure-dependent terms F , R'_{go} , R'_{wo} , and v_o can simply be taken into account. However, the coefficients λ_t , and F are also dependent on the phase saturations S_g and S_w , which have yet to be determined.

7.6.3 Phase Saturations. In general, phase saturations in reservoir flow are nonstationary. After all, it is usually the intention to reduce the hydrocarbon saturations in a reservoir to the lowest possible value. In some special cases it is possible to derive relationships between pressure and saturation in a given reservoir geometry and under given production conditions, known as *saturation-pressure paths* (Walsh and Lake 2003). Here we will consider the derivation of a *steady-state path*, which is valid for a circular reservoir with steady-state well production and steady-state boundary inflow of fluids with a constant composition. Such a steady-state relationship between pressure and saturation can be obtained from Eqs. 7.134 through 7.136 by considering that, disregarding capillary pressures, the pressures p_g , p_o , and p_w have to be equal, and therefore also the gradients dp_g/dr , dp_o/dr , and dp_w/dr . We therefore aim to find the saturations S_g and S_w at each point r that result in

$$f_1(S_g, S_w) = \frac{\mu_g}{kk_{rg}(S_g)} v_g + \beta \rho_g |v_g| v_g - \frac{\mu_o}{kk_{ro}(S_g, S_w)} v_o = 0, \dots \dots \dots \quad (7.151)$$

$$f_2(S_g, S_w) = \frac{\mu_o}{kk_{ro}(S_g, S_w)} v_o - \frac{\mu_w}{kk_{rw}(S_w)} v_w = 0. \dots \dots \dots \quad (7.152)$$

The system of nonlinear equations (Eqs. 7.151 and 7.152) cannot be solved explicitly for S_g and S_w because the expressions for the relative permeabilities are too complex. Instead, we can use an iterative method such as the multivariable Newton-Raphson scheme described in Appendix D. Using matrix notation, a single Newton-Raphson step can be expressed as

$$\begin{bmatrix} \frac{\partial f_1}{\partial S_g} & \frac{\partial f_1}{\partial S_w} \\ \frac{\partial f_2}{\partial S_g} & \frac{\partial f_2}{\partial S_w} \end{bmatrix}_k \begin{bmatrix} \Delta S_g \\ \Delta S_w \end{bmatrix}_k = \begin{bmatrix} f_1 \\ f_2 \end{bmatrix}_k, \dots \dots \dots \quad (7.153)$$

$$\begin{bmatrix} S_g \\ S_w \end{bmatrix}_{k+1} = \begin{bmatrix} S_g \\ S_w \end{bmatrix}_k + \begin{bmatrix} \Delta S_g \\ \Delta S_w \end{bmatrix}, \dots \quad (7.154)$$

where k is the iteration counter. Solution of Eq. 7.153 requires solving a linear system of two equations for the two error terms ΔS_g and ΔS_w , after which Eq. 7.154 gives us the new estimates $(S_g)_{k+1}$ and $(S_w)_{k+1}$. Starting values for the gas and oil saturations can be obtained from the closed-form expressions for two-phase flow discussed below. The Newton-Raphson procedure has been implemented in MATLAB file `saturations.m`, which is used by `res_dpdr.m` to numerically integrate Eq. 7.150. Just like the files `res_oil_dpdr.m` and `res_gas_dpdr.m`, the file `res_dpdr.m` can be called by `res.m` to compute the difference between the pressure at the reservoir boundary at $r = r_e$ and the pressure in the wellbore, or to create an IPR (see `example_res_pres.m` and `example_IPR.m`). Note that these files are valid for vertical wells only. However, in theory, similar equations could be implemented for horizontal well flow.

7.6.4 Example Gas/Oil Flow. Fig. 7.20 displays the steady-state IPR for a well with properties given in Table 6.3 for two values of R_{go} , identical to those used in Fig. 6.11. It is assumed that R_{go} is identical to R_{sb} because there is no free gas influx. The water is not mobile and the flow is therefore two-phase. The initial reservoir pressure is above the bubblepoint pressure for the low-GOR case ($R_{go} = 50 \text{ m}^3/\text{m}^3$) and below it for the high-GOR case ($R_{go} = 150 \text{ m}^3/\text{m}^3$). The results in Figure 7.20 have been computed with the aid of `res.m` and `res_dpdr.m`. They correspond reasonably well with the Vogel solutions from Fig. 6.11 (which are here indicated with dotted lines). Note, however, that the steady-state assumption is usually not applicable. Moreover, the approximation of the oil permeability $k_{o,\text{ref}}$ in Eq. 6.71, used to create the low-GOR case in Fig. 6.11, is also debatable, and therefore the discrepancy between the results of empirical and more theoretical models may, in general, be much larger than illustrated in Fig. 7.20.

During the initial stage of a solution gas drive, the gas saturations in the reservoir remain relatively low because only when the saturations in the entire reservoir have reached the critical value S_{gc} does the gas become mobile over larger distances. Moreover, at reservoir pressure gas occupies a relatively small volume, and the much higher mobility of gas than of oil results in a holdup of the flowing oil relative to the flowing gas. This is illustrated in Fig. 7.21, generated for $q_{o,\text{sc}} = -12 \times 10^{-3} \text{ m}^3/\text{s}$, $R_{go} = R_{sb} = 50 \text{ m}^3/\text{m}^3$, and $p_R = 9.5 \text{ MPa}$ (i.e., just above the bubblepoint pressure of 9.0 MPa). A jump in gas saturation occurs at $r = 280 \text{ m}$ (i.e., at the point where the pressure drops below the bubblepoint), and the magnitude of the jump is approximately equal to the critical gas saturation $S_{gc} = 0.15$. In a more realistic, nonsteady-state situation the jump will gradually move outward until it reaches the outer boundary, whereafter the gas becomes mobile throughout the entire reservoir,

resulting in a significant increase in the producing GOR.

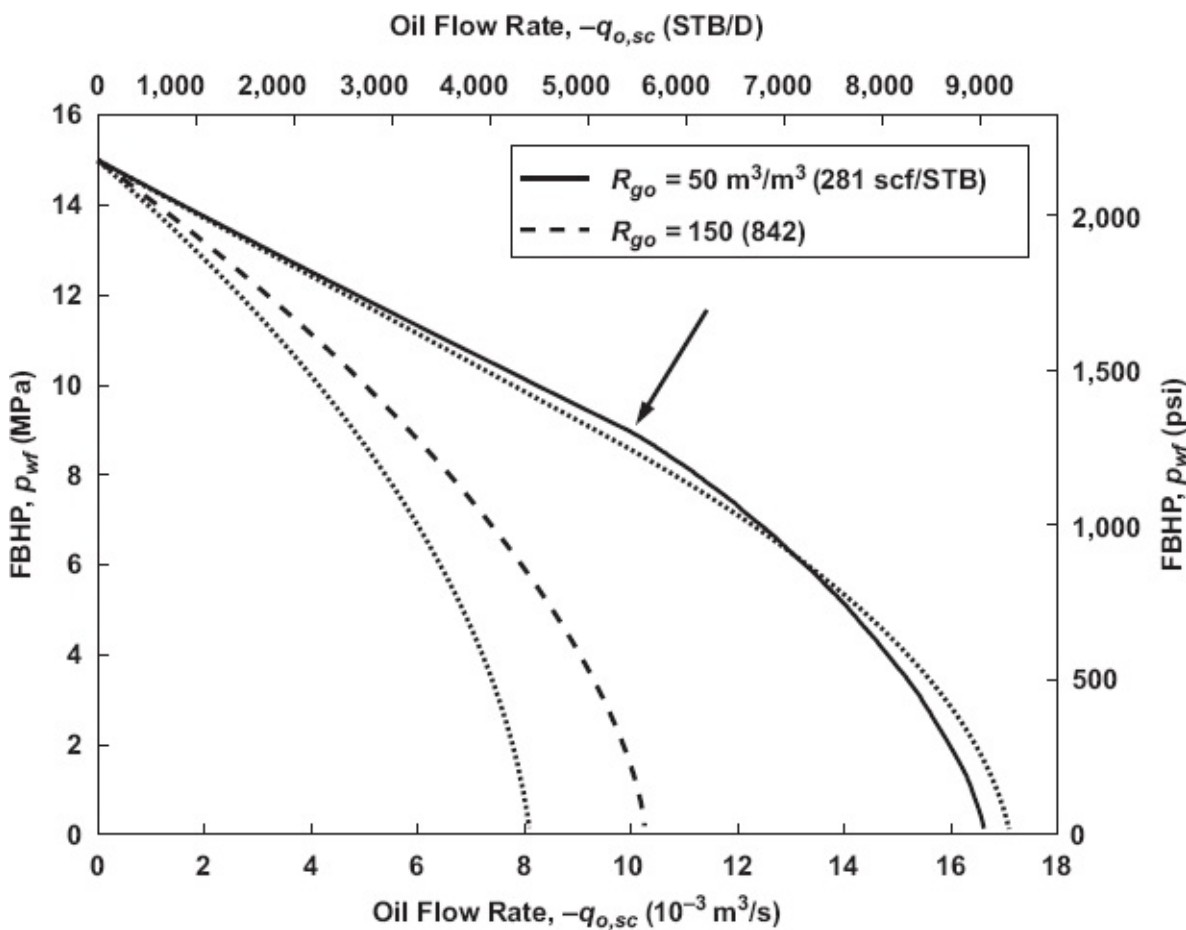


Fig. 7.20—IPR of an oil well with parameters given in Table 6.3 for two different values of the solution GOR as indicated in the legend. The corresponding bubblepoint pressures are 9.00 MPa (1,306 psi) and 22.7 MPa (3,288 psi), respectively (arrow indicates point at which the low-GOR curve drops below bubblepoint pressure, and dotted lines indicate Vogel solutions of Fig. 6.11).

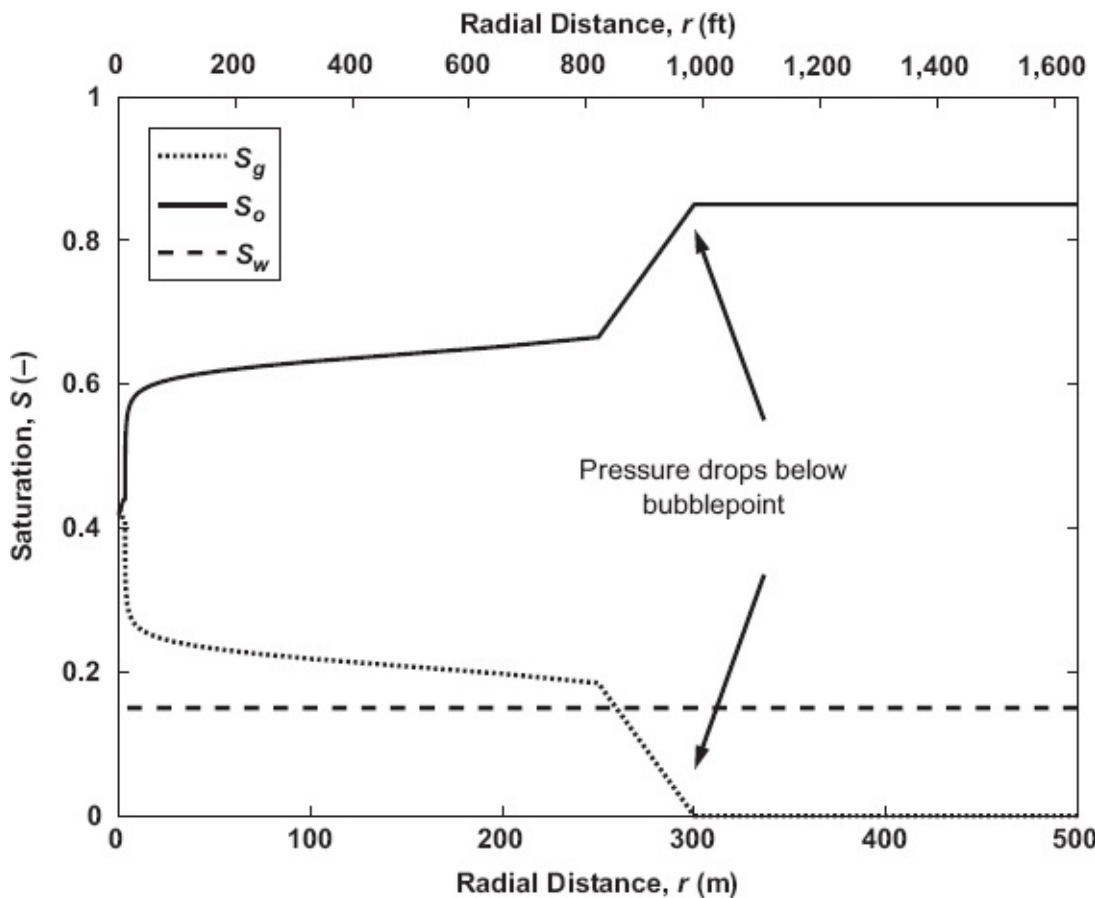


Fig. 7.21—Gas, oil, and water saturations near an oil well with parameters given in Table 6.3. The figure corresponds to a flow rate $q_{o,sc} = -12 \times 10^{-3} \text{ m}^3/\text{s}$ and a GOR of $50 \text{ m}^3/\text{m}^3$. The bubblepoint pressure is 9.0 MPa and the reservoir pressure at the boundary is 9.5 MPa.

7.6.5 Closed-Form Approximations for Primary Recovery. If we consider two-phase (oil/gas) flow and neglect the Forchheimer effect, Eq. 7.151 can be rewritten as

$$\frac{k_{ro}}{k_{rg}} = \frac{\mu_o q_o}{\mu_g q_g}. \quad \dots \quad (7.155)$$

The right side of this expression is a function only of pressure, while the left side is a function only of the oil and gas saturations. With the aid of the Corey expressions for the relative permeabilities, as discussed in Appendix F, this result can also be written as

$$\frac{k_{ro}^0 \times (S_g^*)^{n_g}}{k_{rog}^0 \times (1 - S_g^*)^{n_{og}}} = \frac{\mu_o q_o}{\mu_g q_g}, \quad \dots \quad (7.156)$$

where

$$S_g^* = \frac{S_g - S_{gc}}{1 - S_{gc} - S_{org} - S_{wi}}, \quad 0 \leq S_g^* \leq 1, \quad \dots \quad (7.157)$$

which is the scaled gas saturation. The parameters k_{rg}^0 , k_{rog}^0 , n_g , n_{og} , S_{gc} , S_{org} , and S_{wi} are explained in [Appendix F](#) and are assumed to be known from laboratory experiments. Using the additional assumption that the Corey exponents n_g and n_{og} have an identical magnitude n , [Eq. 7.156](#) can be rewritten as

$$\left(\frac{S_g^*}{1 - S_g^*} \right)^n = \frac{k_{rog}^0 \mu_o q_o}{k_{rg}^0 \mu_g q_g}, \quad \dots \dots \dots \quad (7.158)$$

from which we can solve for S_g as

$$S_g = S_{gc} + (1 - S_{gc} - S_{org} - S_{wi}) \left[1 + \left(\frac{k_{rog}^0 \mu_g q_g}{k_{rg}^0 \mu_o q_o} \right)^{-\frac{1}{n}} \right]^{-1} \quad \dots \dots \dots \quad (7.159)$$

Steady-state gas/oil flow, as described by [Eqs. 7.150](#) and [7.159](#), may occur in a near-well region when the reservoir is initially above bubblepoint pressure but gradually loses pressure, either locally around the well because of drawdown or over the entire reservoir because of depletion.

An expression similar to [Eq. 7.159](#) can be obtained for steady-state oil/water flow:

$$S_w = S_{wi} + (1 - S_{ow} - S_{wi}) \left[1 + \left(\frac{k_{row}^0 \mu_w q_w}{k_{rw}^0 \mu_o q_o} \right)^{-\frac{1}{n}} \right]^{-1} \quad \dots \dots \dots \quad (7.160)$$

It may be of use to describe a gradual increase of water saturation in case of the influx of bottom water or aquifer water into a well. [Eqs. 7.159](#) and [7.160](#) have been implemented in `saturations_gas_oil.m` and `saturations_oil_water.m`.

7.6.6 Water and Gas Fronts in Secondary Recovery. During secondary recovery, water or gas is injected in dedicated injection wells, and the saturation distribution in the reservoir is essentially nonstationary and typically displays abrupt changes. In a single homogeneous layer, such a front may be sharp, and the corresponding water or gas breakthrough in the producers will occur suddenly with corresponding changes in the near-well mobility. If the reservoir is strongly layered or otherwise heterogeneous, the front arrival will be more smeared and the associated mobility change less abrupt.

During secondary recovery, it may still be acceptable to use the (near-)steady-state expression for the radial pressure gradient ([Eq. 7.150](#)), but with slowly time-varying parameters S_g and S_w . Expressions for the saturation change in a circular reservoir during water- or gasflooding can be obtained by starting from conservation equations for the different phases similar to [Eqs. 6.4](#) through [6.7](#) after modifying them to include multiphase flow (i.e., relative permeability) effects. They can be manipulated to produce a differential equation for S_g or S_w as a function of time and

the radial coordinate r , known as the (radial) Buckley-Leverett equation, which allows for an analytical solution. Alternatively, the equations can be solved numerically with the aid of reservoir simulation software, in which case it is also possible to model more realistic heterogeneous, noncircular reservoir geometries. However, both approaches are outside the scope of this book.

7.6.7 Coning and Cusping. A typical multiphase feature of near-wellbore flow is the occurrence of disproportionately high amounts of gas at pressures below the bubblepoint pressure, resulting in producing GORs R_{go} far in excess of the initial GOR of the reservoir fluid R_{sb} . This effect was not captured in the steady-state analysis described above because it was assumed that oil and gas flow as a homogeneous mixture with mass flow rates that remain constant along the radius r . In reality, often a more segregated flow situation occurs in which gas from the gas cap is drawn to the perforations through *coning* or *cusping* (see Fig. 7.22). Because of the extremely high mobility of gas compared to that of oil, even a small contact area between the gas and the wellbore may result in a very large gas influx. A similar effect in the form of water coning may occur for oil/ water flow, especially when the oil viscosity is much higher than the water viscosity. In horizontal wells the cones will be of an elongated shape with a ridge parallel to the well. If pressure drop along a horizontal well plays an important role, coning will first occur at the heel of the well where the drawdown is highest.



Fig. 7.22—Gas coning (left) in a horizontal reservoir, and gas cusping (right) in a dipping reservoir (dashed lines indicate initial GOC).

The combined multiphase flow effects of relative permeabilities (leading to the formation of saturation fronts), gravity (leading to coning), and capillary pressures (leading to more-diffuse saturation distributions) are complex and require advanced numerical simulation of the near-well reservoir flow to be described accurately, which is usually beyond the level of engineering performed in production operations. Moreover, all these effects depend strongly on formation heterogeneities such as

high-permeability lenses, crossbedding, layered stratigraphy, faults, fractures, and cemented regions, the position and size of which are usually poorly known, if known at all. The capacity to theoretically predict the inflow performance of a well under multiphase flow conditions is therefore quite limited.

7.7 Related Topics Not Considered in This Chapter

Chapters 6 and 7 together present an overview of the most important (semi)analytical techniques to compute (semi)steady-state well inflow performance and to generate inflow performance curves for nodal analysis. We did not treat methods for transient reservoir flow, for which we refer to the textbooks mentioned in Section 6.10 and more specialized texts on well testing [e.g., Kamal (2009)]. Transient flow is also important for the development of very-low-permeability reservoirs (e.g. for shale gas production), where it may take a long time before a (semi)steady state is reached. Another aspect of importance for such reservoirs is the use of hydraulic fractures, usually in the form of multiple vertical fractures in horizontal wells, which also require a non-steady-state approach to capture their inflow performance. Moreover, also for (semi) steady-state flow there are analytical approaches available that we did not cover (see, e.g., Chin 2002). Overall, however, the methods discussed in our text should give you sufficient background to read and understand the many conference and journal papers available in this field.

7.8 Questions

- 7.1 In Section 7.2.2 we listed various combinations of radial boundary conditions to solve the Laplace equation in polar coordinates. Would it also be possible to use the following conditions? Explain your answer.

$$r = r_w : \frac{\partial p}{\partial r} = -\frac{\mu B_o q_{o,sc} r_w}{k A_w}, \dots \quad (7.161)$$

$$r = r_e : \frac{\partial p}{\partial r} = -\frac{\mu B_o q_{o,sc} r_e}{k A_e}. \dots \quad (7.162)$$

- 7.2 What is the difference between the skin factors S_h and S_v in Eq. 7.68?
- 7.3 Why is the theoretical prediction of well inflow performance under multiphase conditions possible only to a limited extent?
- 7.4 Derive an expression for the steady-state PI of a vertical well located at a distance $D/2$ from a vertical sealing fault in a circular homogeneous isotropic reservoir with a large drainage radius. How do you interpret your result if D approaches zero?
- 7.5 Starting from the answer to Question 7.4, compute a numerical value for the PI of a well that is located 50 m from the fault. Use the data in Table 6.1 (values for “other figures”) and compare the result to the PI for a well in the

same reservoir without a fault. Does the difference make sense?

- 7.6 Derive Eq. 7.55 starting from Eq. 7.54. (Because this question is somewhat atypical and more a test of algebraic than petroleum engineering skills, you may want to skip it if you are less interested in the former.) Make use of the following identities:

$$\prod_{n=1}^{+\infty} \left(\frac{z}{nh} + 1 \right) \left(\frac{z}{nh} - 1 \right) = \frac{1}{\left(\pi \frac{z}{h} \right)} \sin \left(\pi \frac{z}{h} \right), \quad \dots \dots \dots \quad (7.163)$$

$$\prod_{n=-\infty}^{+\infty} \left[1 + \frac{y^2}{(z-nh)^2} \right] = \frac{\cosh \left(2\pi \frac{y}{h} \right) - \cos \left(2\pi \frac{z}{h} \right)}{1 - \cos \left(2\pi \frac{z}{h} \right)}, \quad \dots \dots \dots \quad (7.164)$$

$$\frac{\sin^2 \left(\pi \frac{z}{h} \right)}{1 - \cos \left(2\pi \frac{z}{h} \right)} = \frac{1}{2}, \quad \dots \dots \dots \quad (7.165)$$

Hint: You may want to first bring the equation in the following intermediate form:

$$2 \ln \prod_{n=1}^{+\infty} (nh)^2 - 2 \ln \left(\frac{\pi}{h} \right) + \ln \left[\left(\frac{\pi z}{h} \right) \prod_{n=1}^{+\infty} \left(\frac{z}{nh} + 1 \right) \left(\frac{z}{nh} - 1 \right) \right]^2 + \ln \prod_{n=-\infty}^{+\infty} \left[1 + \frac{y^2}{(z-nh)^2} \right] \quad \dots \dots \dots \quad (7.166)$$

Note the different summation limits in the infinite products. After using identities (Eqs. 7.163 to 7.165), you will end up with the pressure distributions as a function of coordinates y and z (i.e., Eq. 7.55) and with several additional irrelevant constants. Why are they irrelevant?

Note: for the origin of the expressions in this question, see Eqs. 1.435 and 1.438 in Gradshteyn and Ryzhik (1980). The derivation of the infinite product terms requires analysis beyond the scope of our book (see Section 7.5 of Whittaker and Watson 1915).

- 7.7 Consider a horizontal well in a box-shaped horizontal reservoir like the one depicted in Fig. 7.6.
- (a) If we disregard the effect of streamline convergence and if we choose $P_{\text{ref}} = P_R$, the well has a specific PI of 0.12 B/D-psi-ft. For a reservoir pressure of 5,500 psi, a bottomhole pressure of 5,490 psi, and a well length of 1,500 ft, compute the drawdown and the production rate of the

well.

- (b) The specific PI including the effect of streamline convergence is 0.10 B/D-psi-ft. How large is the pressure drop resulting from streamline convergence?
 - (c) If we take the pressure drop along the well into account and the pressure at the heel of the well (i.e., at $x = 0$) remains the same as before, how does that change the specific inflow along the horizontal well? Give a qualitative answer only, and sketch the inflow profile—i.e., a plot of $q'(x)$ vs. x .
- 7.8 Consider Eq. 7.81 for semisteady-state flow toward a horizontal well. Starting from this equation, derive an expression for the average reservoir pressure and the corresponding PI (i.e., Eq. 7.84).
- 7.9 Repeat Question 7.4 for a situation with anisotropic permeabilities. Express your results in terms of the equivalent isotropic permeability \bar{k} and the anisotropy I_{xy} index as defined in Eqs. 7.37 and 7.45.
- 7.10 (a) Compute the aspect ratio $R_{asp} = a_e / b_e$ and the PI for a partially penetrating horizontal well in an elliptic reservoir with short axis $b_e = 500$ m, $k_h = 5k_v = 2.0 \times 10^{-12}$ m², and all other parameters as given in Table 7.1. Assume steady-state conditions.
- (b) Compute the aspect ratio $R_{asp} = L / w$ and the PI for a fully penetrating horizontal well in a box-shaped reservoir with the same permeabilities as defined under a) and all other parameters as given in Table 7.1. Assume steady-state conditions. Explain the difference with the results obtained under Questions 7.10(a).
- (c) The surface area of an ellipse is defined as

$$A_{ell} = \frac{1}{4}\pi ab. \quad \dots \dots \dots \quad (7.167)$$

Repeat Question 7.10b but choose w such that the horizontal surface area of the box becomes equal to that of the ellipse. What are the corresponding aspect ratio and PI for this new surface area?

- 7.11 Consider a single vertical well draining a near-circular area in an undersaturated reservoir. After opening up the well, the pressure drops below the bubblepoint in the near-wellbore region. Compute the resulting saturations for parameters given in Table 7.3, while neglecting the Forchheimer term.

Question 7.12 requires the use of MATLAB.

- 7.12 Reproduce Fig. 7.17 with the aid of file example_point_sources.m. Increase the formation-damage skin factor to a high value, say 5. Explain the result.

7.9 MATLAB Assignment: Horizontal Well Inflow and Pressure Drop

7.9.1 Objectives

- Become familiar with the Dikken (1990) method to describe combined horizontal well inflow and pressure drop
- Learn to generate an IPR for a long horizontal well
- Learn to solve a two-point boundary value problem in MATLAB with the aid of the shooting method

Property	Value	Units
B_g	0.07	—
B_o	1.20	—
k_{rg}^0	0.70	—
k_{ng}^0	0.95	—
n_g	4	—
n_{og}	4	—
$q_{g,sc}$	3.90	m^3/s
$q_{g,sc}$	65×10^{-3}	m^3/s
r_s	0	m^3/m^3
Rs	55	m^3/m^3
S_{gc}	0.10	—
S_{org}	0.05	—
S_{wi}	0.20	—
μ_g	13.5×10^{-6}	$\text{Pa} \cdot \text{s}$
μ_o	5.8×10^{-3}	$\text{Pa} \cdot \text{s}$
$\rho_{g,sc}$	0.93	kg/m^3
$\rho_{o,sc}$	820	kg/m^3

Table 7.3—Input data for multiphase reservoir flow for Question 7.11.

- Obtain a feeling for the order of magnitude of horizontal well pressure drop as a function of reservoir and fluid parameters

7.9.2 Assignment. For this assignment, consider the same horizontal well configuration used in Question 7.7 and displayed in Fig. 7.6.

Theory. If the pressure drop along the wellbore is taken into account, the wellbore flow and reservoir flow equations need to be considered together. This was first done by Dikken (1990), who observed that the specific reservoir inflow should equal the decrease in wellbore flow rate:

$$\frac{dq(x)}{dx} = -q'(x) = J'(x)[p_R - p(x)], \dots \quad (7.168)$$

where x is the coordinate along the well (with the origin at the heel and positive values in the direction of the toe), q is the wellbore flow rate (expressed at in-situ conditions and taken as positive for flow from the heel to the toe), q' is the specific inflow from the well into the reservoir (expressed at in-situ conditions and taken as positive for injection), J' is the specific PI (which is positive by definition), p is the wellbore pressure, and p_R is the pressure at $0 < x < L$, $y = \pm w/2$, $z = 0$.

A key assumption is that all reservoir flow is perpendicular to the well; i.e., that there is no flow in the reservoir in the along-well direction. If we restrict the analysis to incompressible single-phase oil flow and neglect the effects of acceleration and gravity, the combined equations for wellbore pressure and flow rate are obtained by combining Eqs. 3.28 and 7.168:

$$\frac{dp}{dx} = -\frac{\rho}{2d} f \frac{q|q|}{A^2}, \dots \quad (7.169)$$

$$\frac{dq}{dx} = J'(p_R - p), \dots \quad (7.170)$$

where we refrained from using subscripts o (for oil) to simplify the notation and where all flow rates are expressed at in-situ (local) conditions. Eqs. 7.169 and 7.70 form a system of two coupled first-order differential equations. The boundary conditions can be specified as

$$x = 0 : p = \hat{p}_{wf}, \dots \quad (7.171)$$

$$x = L : q = 0, \dots \quad (7.172)$$

where \hat{p}_{wf} is the prescribed FBHP at the heel of the well and L is the wellbore length. Eq. 7.172 implies that we neglect semiradial inflow at the toe of the well (i.e., that the well is fully penetrating). Unfortunately, the two boundary conditions are specified at different ends of the well, which means that we cannot simply numerically integrate the equations starting from one end of the well to the other. A convenient way to solve such a two-point boundary value problem is to use a *shooting method*, which starts from the known value for $p(0) = \hat{p}_{wf}$ at the heel and a guessed value for $q(0) = \tilde{q}_{tot}$ at that same location. After integration from the heel to the toe, the resulting value of $q(L)$ at the toe is most likely not equal to zero—i.e., not meeting the boundary condition (Eq. 7.172). An iterative procedure can then be applied to change the value of $q(0)$ until the value of $q(L)$ is (almost) zero.

The expression for $J'(x)$ in Eq. 7.170 depends on the reservoir geometry and properties. For this assignment use the (constant) expression for J as given in Eq. 7.60, divided by the well length:

$$J' = \frac{-q'}{p_R - p_{wf}} = \frac{4\pi k}{\mu} \left\{ \ln \left[\frac{\cosh\left(\pi \frac{w}{h}\right) - 1}{\cosh\left(2\pi \frac{r_w}{h}\right) - 1} \right] \right\}^{-1} \quad \dots \dots \dots \quad (7.173)$$

(Note that q' is expressed at in-situ conditions). A first guess \tilde{q}_{tot} of the total well flow rate q_{tot} then follows as

$$\tilde{q}_{tot} = -L J' (p_R - \hat{p}_{wf}), \quad \dots \dots \dots \quad (7.174)$$

which is equal to the result for a horizontal well without pressure drop.

Tasks

- Implement Eqs. 7.169 through 7.172 in a MATLAB file:
 - Create an auxiliary file `hor_dfdx.m` suitable for use with standard MATLAB numerical integration routines, which gives as output $dfdx = [dpdx; dqdx]$ — i.e., the derivatives dp/dx and dq/dx —as function of input values $f = [p, q]$ and other, stationary, parameters:


```
function dfdx = hor_dfdx(~, f, ~, d, e, h, k, mu, p_R, rho, w)
```

 Here the variables p and q should be scalar variables of wellbore pressure and wellbore flow rate at a certain point along the well.
 - Create a second auxiliary file `hor.m` that performs a single integration from $x = 0$ to $x = L$ for given values of $p(0) = \hat{p}_{wf}$ (known) and $q(0) = \tilde{q}_{tot}$ (guessed). If necessary, consult [Appendix D](#) for information on numerical integration in MATLAB, or see `pipe.m` and `oil_dpds.m` for an example. The first output element of `hor.m` should be the flow rate at the toe to enable the direct use of `hor.m` with `fzero`:


```
function [q_toe, p, q, x] = ...
hor(d, e, h, k, L, mu, p_R, p_wf, q_tot, rho, w)
```

 The output variables p , q , and x are now row vectors of wellbore pressure, wellbore flow rate, and coordinates at n points along the well as determined by the numerical integration routine called within `hor.m`. The flow rate at the toe is therefore equal to the last element of q .
 - Call `hor.m` from your main file to iteratively compute the correct value of $q(0)$. Apply the shooting method and use the standard MATLAB routine `fzero` to perform the iteration. If necessary, consult [Appendix D](#) for information on `fzero`, or review Questions 3.12 and 6.14, and their solutions, for examples of its use.


```
q_tot = fzero(@(q_tot) ...
hor(d, e, h, k, L, mu, p_R, p_wf, q_tot, rho, w), q_tot_tilde);
```
- Create plots of the wellbore pressure p , the wellbore flow rate q , and the specific well inflow rate q_s , as a function of distance from the heel x .

- Compute and plot the IPR of the well with parameters given in **Table 7.4**. Here the IPR is a graph of the FBHP at the heel, \hat{P}_{wf} , vs. the total well flow rate q_{tot} . Note that in all previous examples, determining the IPR implied computing the FBHP by varying the well flow rate, whereas here you need to compute the flow rate by varying the FBHP. Choose a pressure range $32.0 \text{ MPa} < \hat{P}_{wf} < 33.5 \text{ MPa}$. Plot your results in both SI and field units.
- Perform a sensitivity study into the effect of the reservoir, fluid, and wellbore parameters on the wellbore pressure drop. Express your results in terms of a dimensionless wellbore pressure drop, defined as the pressure drop between the toe and heel, divided by the drawdown at the heel:

$$\Delta p_D = \frac{p(L) - p(0)}{p_R - p(0)}. \quad (7.175)$$

Property	Symbol	Value	Units
Reservoir height	h	25	m
Reservoir length	L	5000	m
Reservoir width	w	500	m
Well radius	r_w	0.10	m
Well roughness	e	30×10^{-6}	m
FBHP (at the heel)	\hat{P}_{wf}	33.0	MPa
Reservoir pressure	p_R	33.5	MPa
Oil density	ρ	850	kg/m ³
Oil viscosity	μ	20×10^{-3}	Pa · s
Permeability	k	2.0×10^{-12}	m ²
Skin	S_h	0	—

Table 7.4—Parameter values for horizontal well MATLAB assignment.

7.9.3 Deliverables

- MATLAB program listing
- Plots
- Sensitivity study

Chapter 8

Well Performance

8.1 What Is Covered in This Chapter?

In this final chapter we use nodal analysis to describe the combined performance of the various system elements discussed in previous chapters. We address simple production systems in the form of oil and gas wells producing from one or more reservoirs into surface facilities, usually through a choke and flowline. We demonstrate the use of nodal analysis to quantify the effects of changing dimensions or properties of system elements, and to optimize both short- and long-term well performance, including the use of artificial lift methods.

8.2 Analyzing Well Performance

Optimizing a well design or interpreting measurements from a producing well requires tools to analyze the well performance—i.e., its flow behavior under a given set of reservoir and operating conditions. For example, in designing a completion for a new well, we need to assess the effect of the tubing size on well productivity and predict the productivity change as the reservoir pressure declines. Similarly, in a producing well, we need to decide when it makes economic sense to carry out operations to increase the productivity—e.g., whether the skin is significantly affecting production and the well needs stimulating—or when we should change out the tubing. For further reading on well performance in general, we refer to the classic paper of Gilbert (1954) and the textbooks of Nind (1964, 1981), Golan and Whitson (1991), Economides et al. (1998, 2013), and Guo et al. (2007).

8.2.1 Performance of a Well Operating at Given Tubinghead Pressure. Consider a vertical well that is operated at a fixed flowing tubinghead pressure (FTHP) p_{tf} . The flow system between the reservoir and the tubing head can be broken down into

- Inflow into the well
- Flow up the tubing to the tubing head

The total pressure drop between the reservoir and the wellhead is made up of the drawdown associated with the inflow from the reservoir and the vertical flow pressure drop. In oil wells the vertical pressure drop typically makes up 70–90% of the total pressure drop between the reservoir and the wellhead; in a gas well this can be much less because gravity effects are not so important and the pressure drop is dominated by friction. As we have seen in [Chapter 6](#), the inflow into the well is affected by

- Reservoir pressure
- Reservoir geometry
- Reservoir properties
- Skin, including “skin” resulting from the completion
- Properties of the reservoir fluids

As discussed in [Chapter 6](#), for a given reservoir pressure all these effects can be brought into a single relationship between oil flow rate and FBHP, known as the inflow performance relationship (IPR) of the well. Similarly, the flow up the tubing is affected by

- FTHP
- Tubing size and other completion parameters
- Flow regime in which the well operates
- Fluid properties

As discussed in [Chapters 3 and 4](#), for a given FTHP, all these effects can also be brought into a relationship—the tubing intake curve—between oil flow rate and flowing bottomhole pressure (FBHP).

As an example, consider [Fig. 8.1](#), which depicts the IPR of an oil well for fluid properties listed in [Table 4.1](#). The reservoir properties are as shown in [Table 6.3](#), except for the absolute permeability and the reservoir conditions, which have now been chosen as $k = 7.0 \times 10^{-13} \text{ m}^2$ (3,546 mD), $p_R = 25 \text{ MPa}$ (3,626 psi), and $T_R = 120^\circ\text{C}$ (240°F). In this case, because the FBHP remains above the bubblepoint pressure over the entire flow rate range, the IPR is a straight line. [Fig. 8.2](#) depicts the tubing intake curve corresponding to [Table 4.1](#) ([Fig. 4.8](#)). Combining these two curves gives us [Fig. 8.3](#). This is an example of combining the downstream and upstream pressure drop curves (i.e., the tubing intake curve and the IPR) as was discussed in [Section 1.6](#), where we covered nodal analysis. The operating point of the well corresponds to a FBHP of 23.6 MPa (3,423 psi) and an oil flow rate of $-3.7 \times 10^{-3} \text{ m}^3/\text{s}$ ($-2,011 \text{ STB/D}$).

If we lower the FTHP, the FBHP will drop also and the tubing intake curve will shift down. In addition, the curve may somewhat change in shape because the boundaries between the various flow regimes in the tubing may also move. However, the overall effect will be a shift of the operating point to the right, corresponding to an increased flow rate. Conversely, if we increase the FTHP, the production rate will drop; and if we increase it too much, the well will no longer flow at all (see [Fig. 8.4](#)).

A reduction in flow rate also occurs if the FTHP remains constant but the reservoir pressure drops, a situation that frequently happens when an oil field is being depleted. An example is given in [Fig. 8.5](#), where a 10% drop in reservoir pressure results in just a 9% decrease in FBHP but a 54% decrease in oil flow rate. Moreover, the curves now have two intersection points. As will be demonstrated in the next section, one of these points is unstable. The intersection to the right is a stable

operating point and corresponds to the actual FBHP and flow rate, whereas the intersection to the left is an unstable and therefore physically unrealistic operating point. If the reservoir pressure keeps dropping further, a point will be reached at which the well stops flowing. It may sometimes be possible to bring the well back to production by installing a new tubing with a lower pressure drop. It is interesting that this may be either a larger- or smaller-diameter tubing, depending on factors such as the water cut and the gas/oil ratio (GOR). Alternatively, it may be necessary to install a form of artificial lift, such as gas lift, an electrical submersible pump (ESP), or a beam pump.

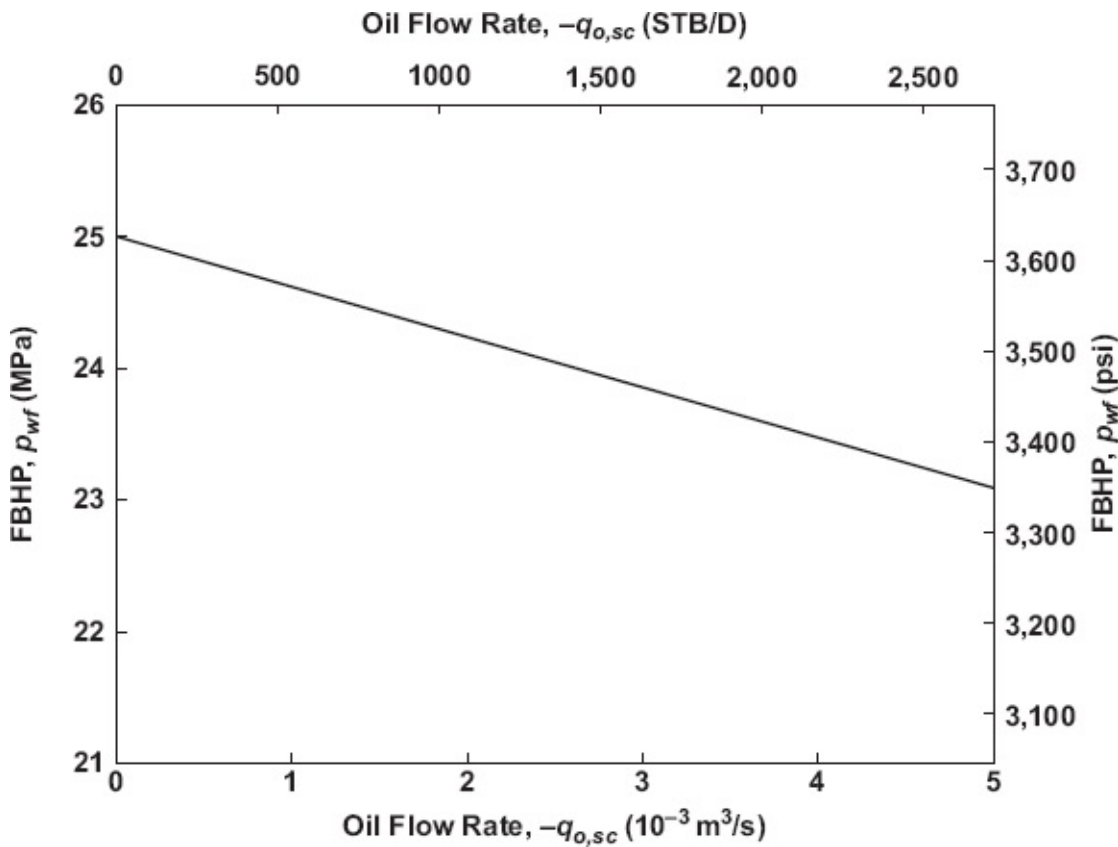


Fig. 8.1—Inflow performance curve of an oil well with reservoir pressure $p_R = 25$ MPa (3,626 psi).

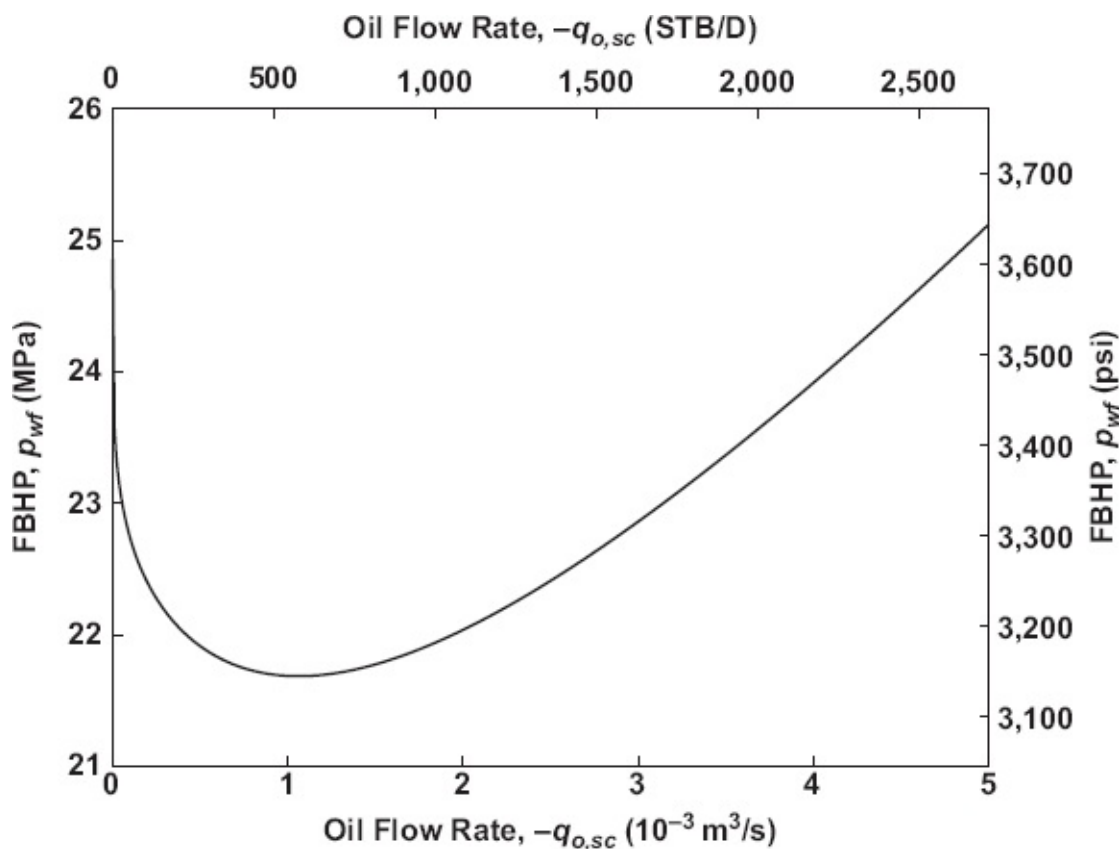


Fig. 8.2—Tubing intake curve of an oil well (identical to Fig. 4.8).

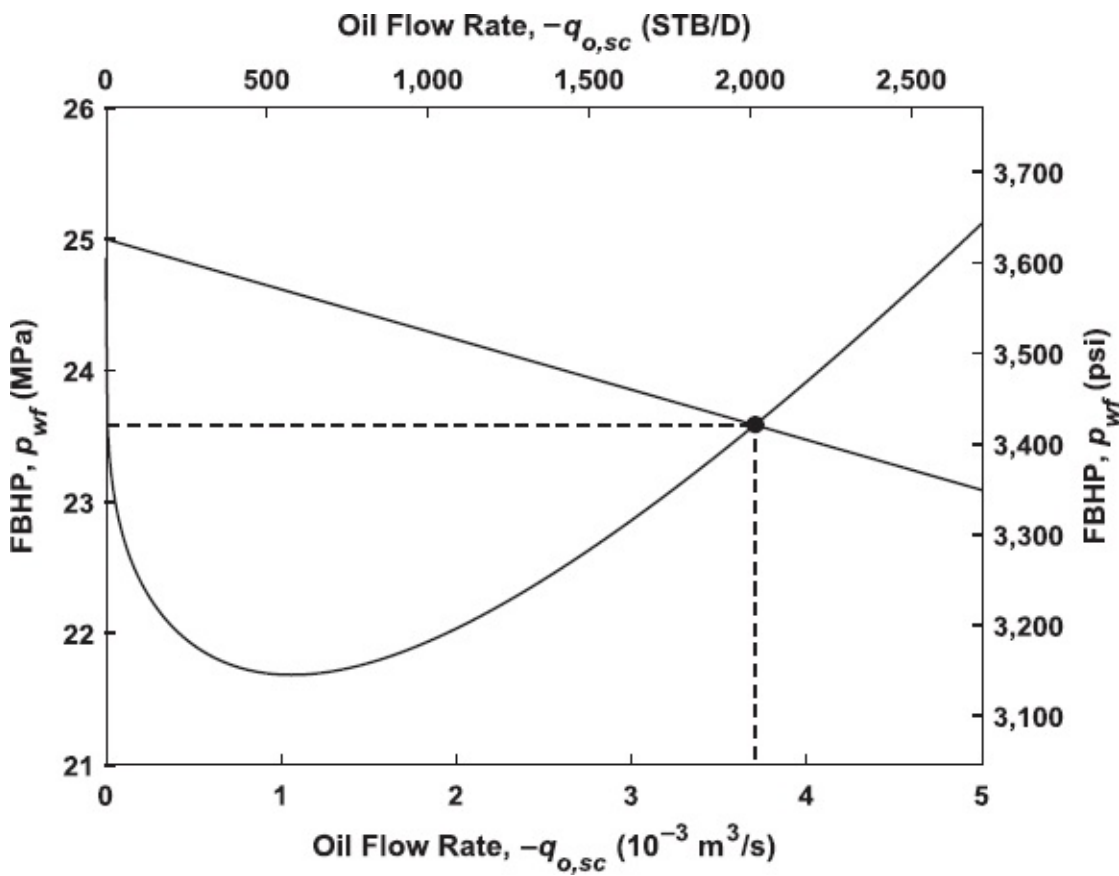


Fig. 8.3—Combined plot of inflow performance and tubing intake curves, determining the FBHP ($p_{wf} = 23.9$

MPa (3,466 psi)) and production rate ($q_{o,sc} = -3.7 \times 10^{-3} \text{ m}^3/\text{s}$ (-2,011 B/D)).

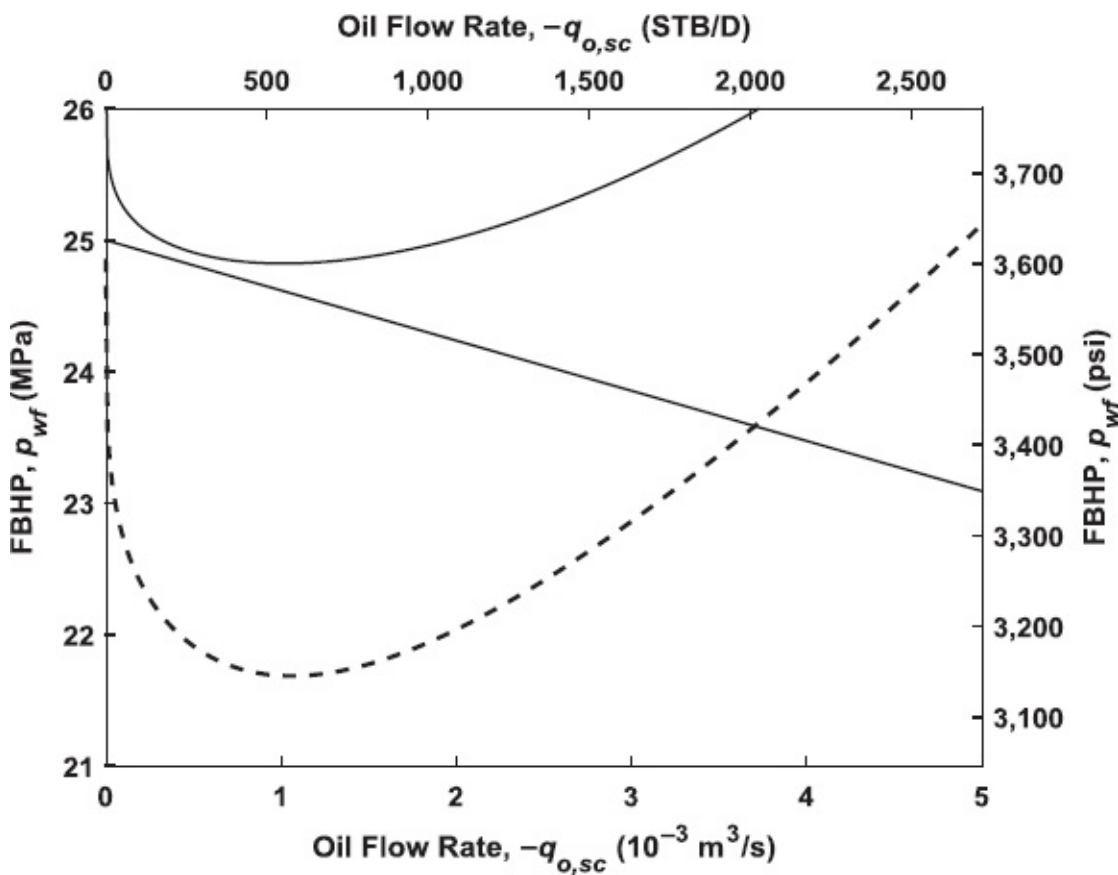


Fig. 8.4—Effect of a too-large increase in FBHP (resulting from a too large increase in FTHP): the tubing intake curve and the IPR no longer intersect. As a result, the well will no longer flow. The minimum rate at which the well can flow is therefore approximately $-0.5 \times 10^{-3} \text{ m}^3/\text{s}$ (-272 B/D).

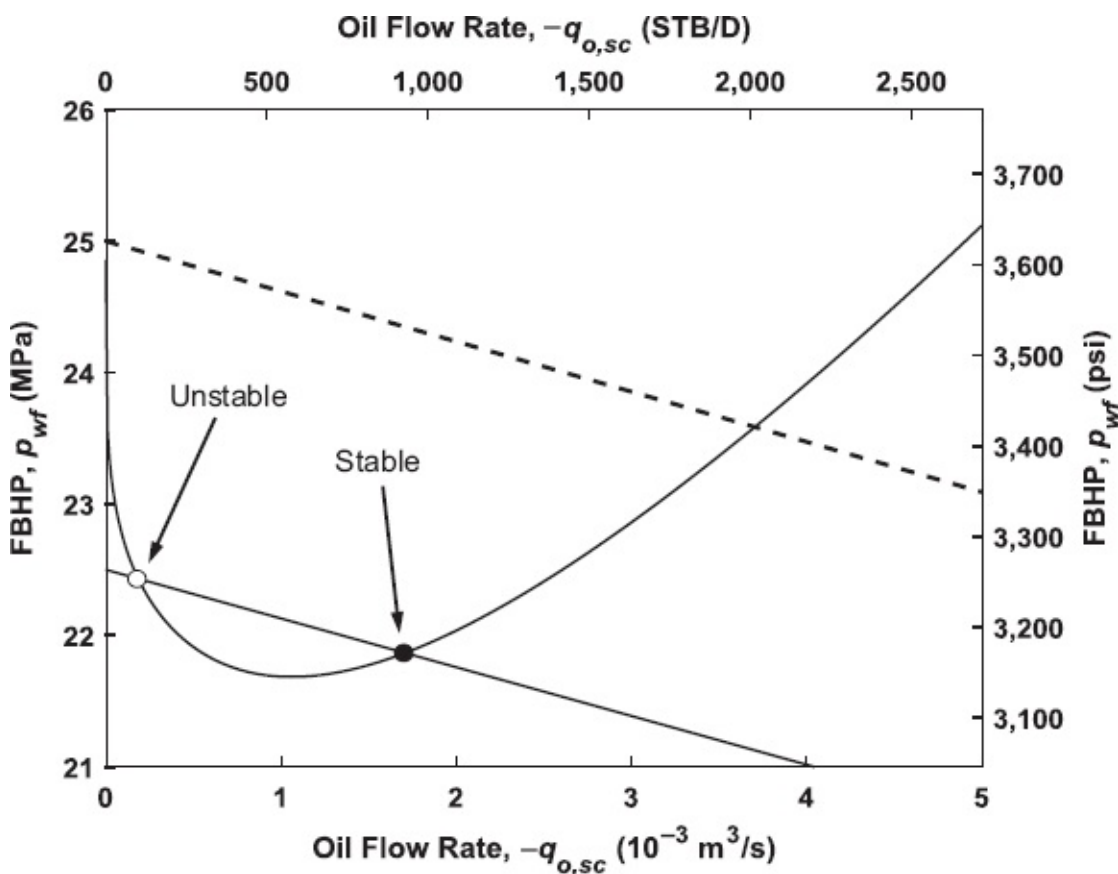


Fig. 8.5—Effect of a drop in reservoir pressure. The reservoir pressure has decreased with 10% from 25 MPa (3,626 psi) to 22.5 MPa (3,263 psi), and as a result the FBHP has decreased with 9% from 23.9 MPa (3,466 psi) to 21.8 MPa (3,162 psi) and the oil production with 54% from $-3.7 \times 10^{-3} \text{ m}^3/\text{s}$ ($-2,011 \text{ B/D}$) to $-1.7 \times 10^{-3} \text{ m}^3/\text{s}$ (-924 B/D). The picture also depicts the presence of two operating points (a stable and an unstable one) for the case of low reservoir pressure.

8.2.2 Intermezzo: Stability of an Operating Point. Because the relationship between pressure drop and flow rate is nonlinear for most elements of the production system, p - q graphs are usually curved. In particular, for wells that produce a mixture of gas and liquids (as do most oil wells), this may lead to a situation in which the graphs intersect at two points (e.g., as depicted in Fig. 8.5). At a first glance we could therefore conclude that such a well could produce at two different flow rates. In reality, however, wells will always produce at only one of these flow rates. The reason is that only one of the operating points is stable, whereas the other one is unstable.

To understand why an operating point can be unstable, we need to consider the dynamics of the system. Nodal analysis, however, usually considers only the steady-state relationship between pressure drop and flow rate. For example, the curves in Fig. 8.5, which were determined from a steady-state analysis, can be represented schematically as

$$p = f_{us}(q), \dots \quad (8.1)$$

$$p = f_{ds}(q), \dots \quad (8.2)$$

where f_{us} and f_{ds} are nonlinear functions representing the upstream and downstream curves (i.e. the IPR and the tubing intake curve), respectively. The flow rate q refers to the oil flow rate at standard conditions $q_{o,sc}$, but in this section we drop the subscript “ o,sc ” to avoid confusion with the subscript “0” (zero) used to indicate an operating point. In an operating point (p_0, q_0) , we find that

$$p_0 = f_{us}(q_0), \dots \quad (8.3)$$

$$p_0 = f_{ds}(q_0). \dots \quad (8.4)$$

We are interested in the effect of small disturbances \tilde{p} on the flow in the neighborhood of an operating point:

$$p_0 + \tilde{p} = f_{us}(q_0 + \tilde{q}), \dots \quad (8.5)$$

$$p_0 + \tilde{p} = f_{ds}(q_0 + \tilde{q}). \dots \quad (8.6)$$

Because we consider only small disturbances, we can linearize f_{us} and f_{ds} . In other words, we can take the Taylor expansions for f_{us} and f_{ds} around q_0 , defined as

$$f_{us} = f_{us}(q_0) + f'_{us}(q_0) \times (q - q_0) + \frac{1}{2} f''_{us}(q_0) \times (q - q_0)^2 + \dots, \dots \quad (8.7)$$

$$f_{ds} = f_{ds}(q_0) + f'_{ds}(q_0) \times (q - q_0) + \frac{1}{2} f''_{ds}(q_0) \times (q - q_0)^2 + \dots, \dots \quad (8.8)$$

where primes indicate differentiation with respect to q . If we substitute the expansions (Eqs. 8.7 and 8.8) into Eqs. 8.3 through 8.6, subtract the results, and maintain only the constant and linear terms, we obtain linear relations for \tilde{p} and \tilde{q} :

$$\tilde{p} = f'_{us} \tilde{q}, \dots \quad (8.9)$$

$$\tilde{p} = f'_{ds} \tilde{q}. \dots \quad (8.10)$$

Small fluctuations in flow rate imply that the flow accelerates and decelerates with small amounts. These accelerations cause pressure fluctuations, which we can incorporate in Eqs. 8.9 and 8.10 by adding inertia terms. As before, we assume that f_{us} and f_{ds} represent the pressure drops over the upstream and downstream parts of our system, respectively. Including inertia, we can write

$$\tilde{p} = f'_{us} \tilde{q} - i_{us} \frac{d\tilde{q}}{dt}, \dots \quad (8.11)$$

$$\tilde{p} = f'_{ds} \tilde{q} + i_{ds} \frac{d\tilde{q}}{dt}, \dots \quad (8.12)$$

where $i_{us} \geq 0$ and $i_{ds} \geq 0$ represent inertia of the fluid upstream and downstream of the

analysis point. The two differential equations (Eqs. 8.11 and 8.12) are dynamic relationships between the pressure and the flow rate in the analysis point as governed by the upstream and the downstream parts of the system. The two acceleration terms have different signs because an increase in pressure in the analysis node causes a deceleration of the flow in the upstream part of the system and an acceleration of the flow in the downstream part. In an operating point the pressures resulting from the upstream and the downstream parts have to be equal, and therefore we can write

$$f'_{us} \tilde{q} - i'_{us} \frac{d\tilde{q}}{dt} = f'_{ds} \tilde{q} + i'_{ds} \frac{d\tilde{q}}{dt}, \dots \quad (8.13)$$

which can be rewritten as

$$(i'_{us} + i'_{ds}) \frac{d\tilde{q}}{dt} - (f'_{us} - f'_{ds}) \tilde{q} = 0. \dots \quad (8.14)$$

Eq. 8.14 is a linear first-order differential equation for \tilde{q} . To obtain a complete solution, we need one initial condition. If we assume that a flow rate disturbance with magnitude \tilde{q}_0 takes place at time $t = 0$, the initial condition becomes

$$t = 0 : \tilde{q} = \tilde{q}_0. \dots \quad (8.15)$$

Solving Eq. 8.14 results in

$$\tilde{q} = C \exp\left(\frac{f'_{us} - f'_{ds}}{i'_{us} + i'_{ds}} t\right), \dots \quad (8.16)$$

where C is an integration constant that can be determined with the aid of the initial condition, expressed in Eq. 8.15. That results in $C = \tilde{q}_0$, and therefore

$$\tilde{q} = \tilde{q}_0 \exp\left(\frac{f'_{us} - f'_{ds}}{i'_{us} + i'_{ds}} t\right). \dots \quad (8.17)$$

Eq. 8.17 represents an exponentially growing or decreasing magnitude of disturbance \tilde{q} with time, depending on the sign of $(f'_{us} - f'_{ds})/(i'_{us} + i'_{ds})$. Because $i'_{us} \geq 0$ and $i'_{ds} \geq 0$, it is the sign of $(f'_{us} - f'_{ds})$ that determines the stability of the flow in an operating point. The terms f'_{us} and f'_{ds} can be interpreted as the slopes of the curves at the operating point. Note that a curve that decreases with increasing q has a negative slope. Referring back to Fig. 8.5, we find that the operating point to the left is unstable, and the one to the right stable. Stable wellbore flow can therefore occur only at the pressure and flow rate corresponding to the operating point to the right. (Note that in a full dynamic analysis, we should also take into account the compressibility of the gas/liquid mixture. In that case we would arrive at a second-order differential equation, which could display oscillatory solutions. However, the

basic results of the stability analysis would not change.)

As discussed below, in practice the criteria for stability of an operating point are chosen slightly differently. However, it is safe to say that in case of two operating points, it will always be the one at the highest flow rate that is stable.

8.2.3 Performance of a Well Operating Through a Surface Choke. In [Section 8.2.1](#), assuming that the FTHP and the reservoir pressure were constant, we calculated the resulting flow rate from the pressure drops over the tubing and the reservoir. Therefore we could analyze the well productivity using nodal analysis with just two elements between three nodes (see [Fig. 8.6, left](#)). However, usually the FTHP itself will also vary with flow rate. To analyze this effect we need also to consider the flow path downstream of the wellhead, up to a point where we can assume that the pressure remains more or less constant. That point will normally be the first separator, which is usually operated with automatic pressure control. The manifold pressure, which is almost the same as the separator pressure, can then be taken as the fixed downstream pressure for a wellbore pressure drop analysis. Recall that we have also assumed constant pressure at the other end of the system, (i.e., in the reservoir), or at least a pressure that varies only very slowly over time. In conclusion, our problem is to determine the flow rate by considering the pressure drop over the following elements:

- Reservoir (including near-wellbore region and completion)
- Tubing up to the tubing head
- Choke
- Flowline

Assume constant pressures in the reservoir and the manifold, and a constant fluid composition [gas/oil ratio (GOR), water cut].

Here we restrict ourselves to the analysis of a three-component system consisting of a choke, a tubing, and the near wellbore. In that case a suitable fixed downstream pressure is the flowline pressure p_f (i.e., the pressure just downstream of the wellhead choke); see [Fig. 8.6, right](#). For this type of analysis it is common practice to choose the analysis node at the top of the tubing and to establish a single performance curve for the choke and a combined performance curve for the tubing and the near wellbore. The latter is obtained by combining the elements for near-wellbore pressure drop and tubing pressure drop in series. For a given reservoir pressure, this gives the tubing performance curve—as you will recall from [Chapter 3](#), this is the relationship between the oil flow rate and the FTHP. The tubing performance curve gives a total picture of the deliverability of the well. Note that the name is slightly misleading because the tubing performance curve is dependent not just on the ability of the tubing to transport the fluids but also on the performance of the near-well reservoir and the completion. As the reservoir pressure declines, the tubing performance curve will change. So a better name would be *well performance*

curve, but this is not normally used. The flow through the choke is governed by a choke performance curve as discussed in [Chapter 5](#). Note that depending on whether the choke flow is critical or not, we do or do not need to specify the downstream pressure (i.e. the flowline pressure).

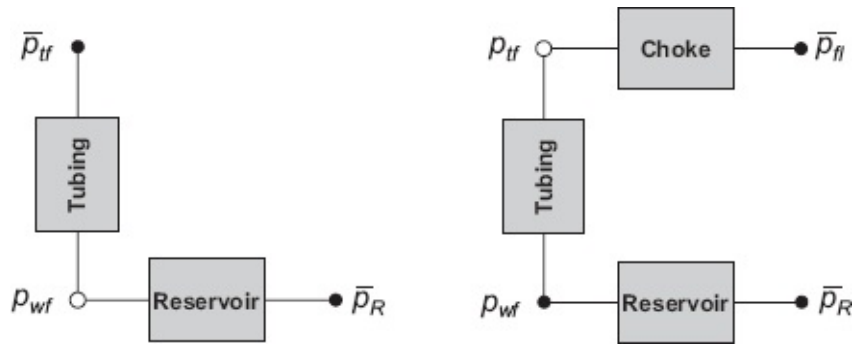


Fig. 8.6—Nodal analysis configurations, with overbars indicating fixed pressures. Left: Fixed FTHP and fixed reservoir pressure; analysis node at the bottom of the well. Right: Fixed flowline pressure and fixed reservoir pressure; analysis node at the top of the well.

We can now plot the choke performance curve and the tubing performance curve together to determine the operating point at the tubing head. As an example consider a gas well with fluid and tubing properties given in [Table 3.1](#) and reservoir properties given in [Table 6.2](#), except for the permeability and the Forchheimer coefficient, which have now been chosen as $k_g = 6.4 \times 10^{-15} \text{ m}^2$ and $\beta = 9.8 \times 10^9 \text{ m}^{-1}$. [Fig. 8.7](#) depicts the IPR and the tubing performance curve in the same graph. Note that the reservoir pressure and the closed-in tubinghead pressure are obtained by reading the graph for zero flow rate. [Fig. 8.8](#) depicts the tubing performance curve of the same well on an expanded scale, and [Fig. 8.9](#) shows the choke performance curves for a number of different choke sizes. The combined performance curves have been plotted in [Fig. 8.10](#), and it can be seen that three of the operating points result in choked flow (i.e., flow in the critical regime where the upstream pressure is independent from the downstream pressure). The other operating point corresponds to sub-critical flow.

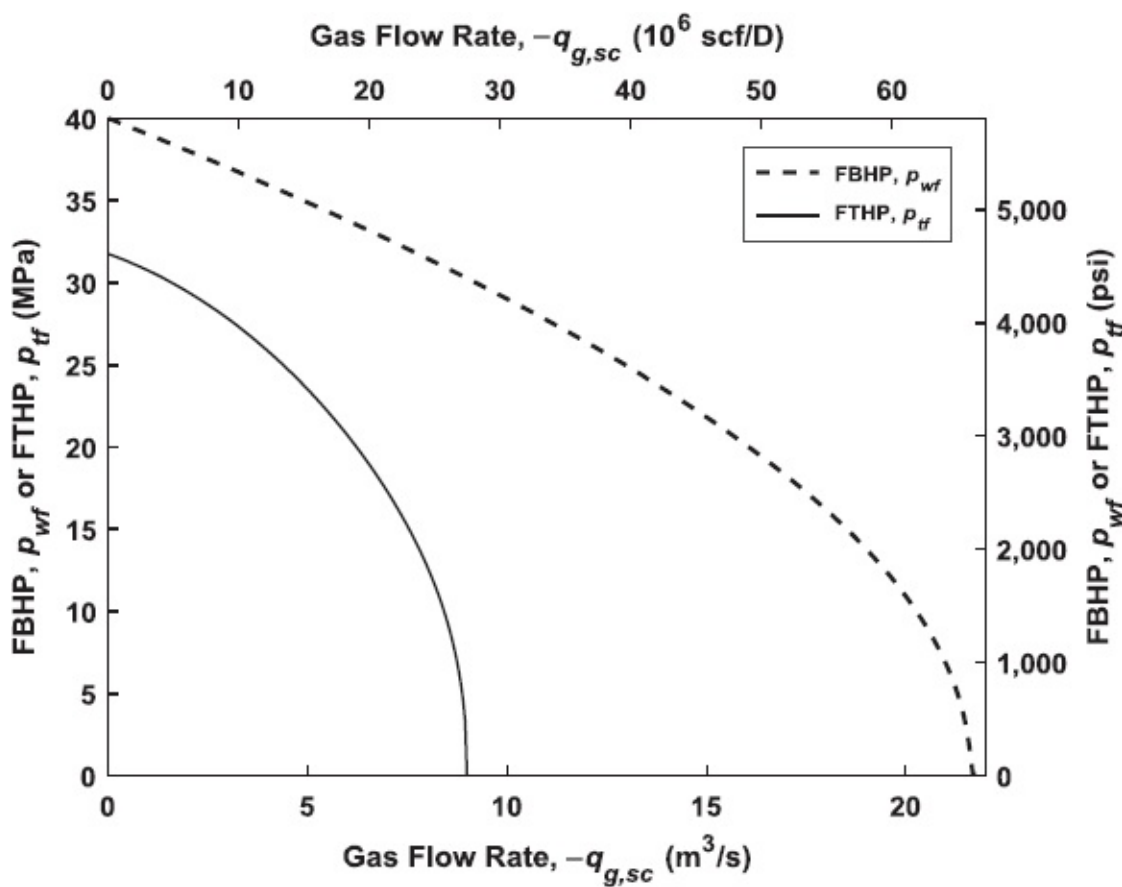


Fig. 8.7—Inflow performance curve and tubing performance curve of a gas well. The reservoir pressure is 40 MPa (5,802 psi), and the closed-in tubinghead pressure is 31.8 MPa (4,612 psi).

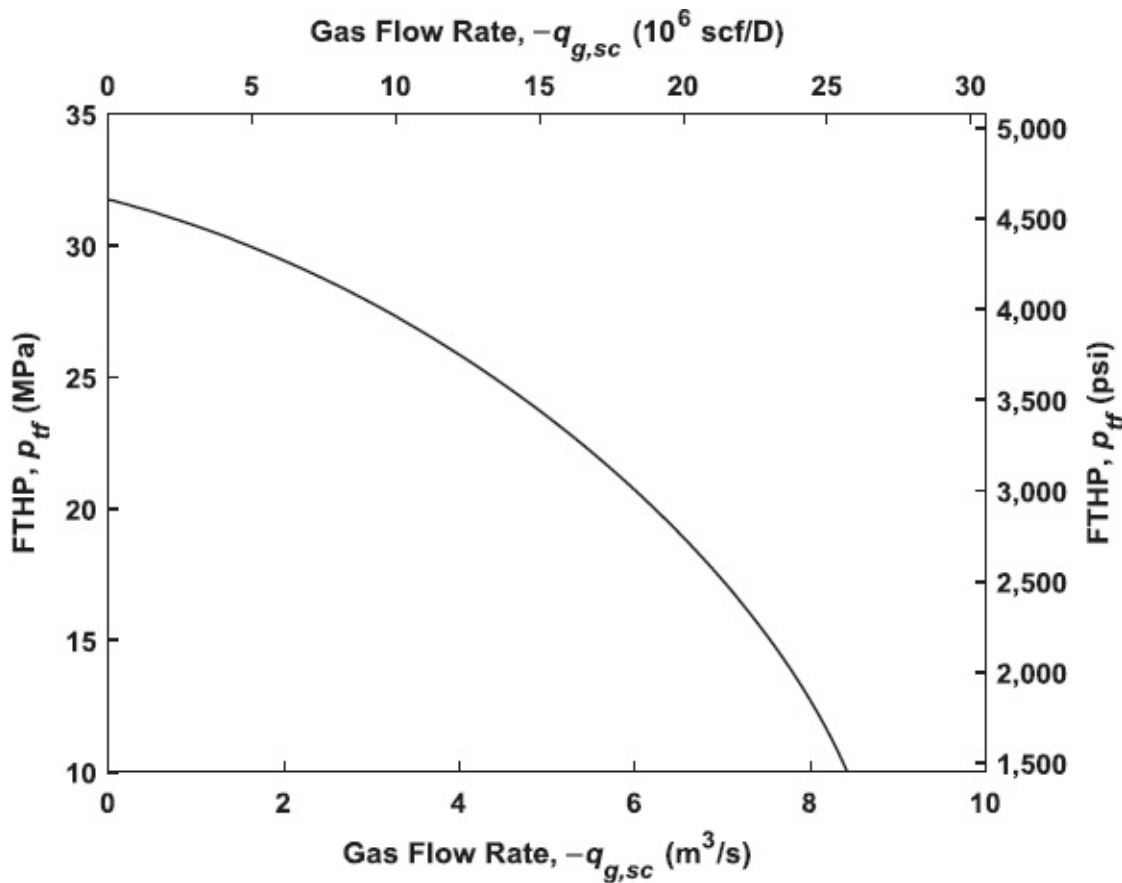
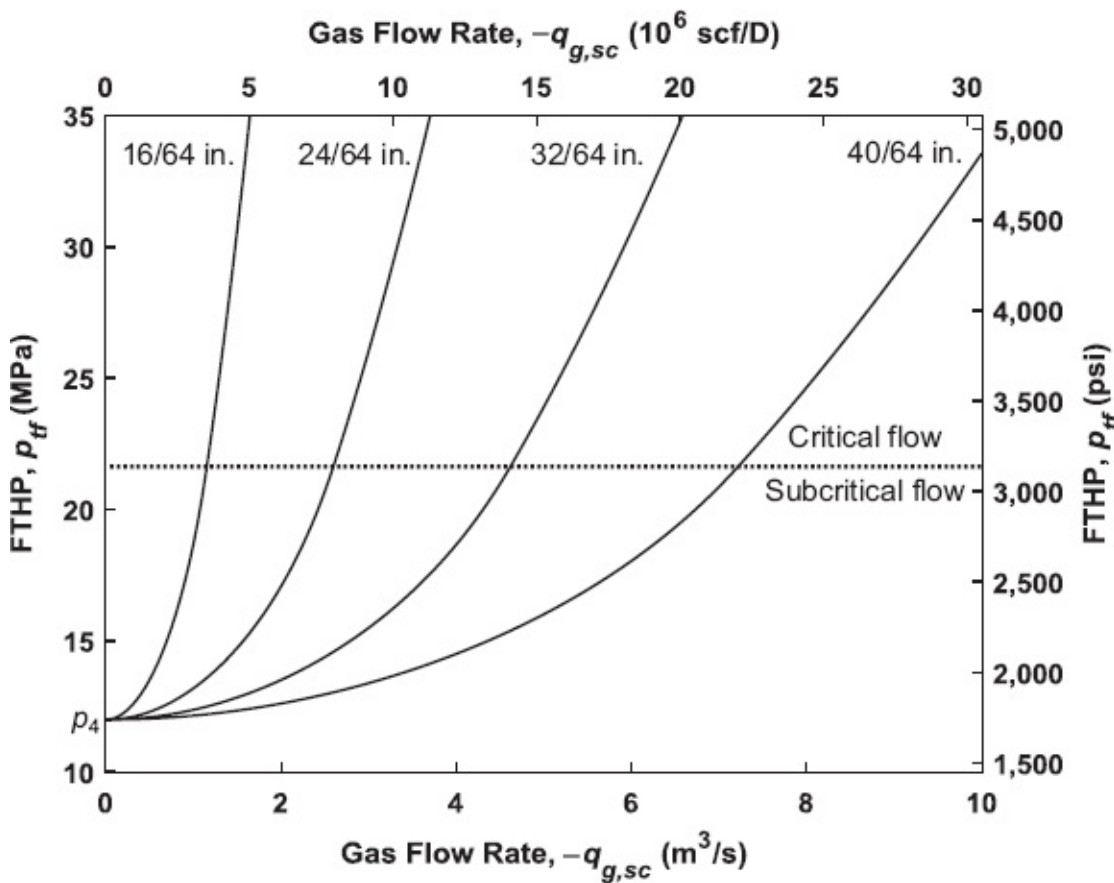


Fig. 8.8—Tubing performance curve of the same gas well on an expanded scale.

Fig. 8.9—Choke performance curves for a gas well (identical to Fig. 5.4 where the upstream pressure p_1 is now the FTHP).

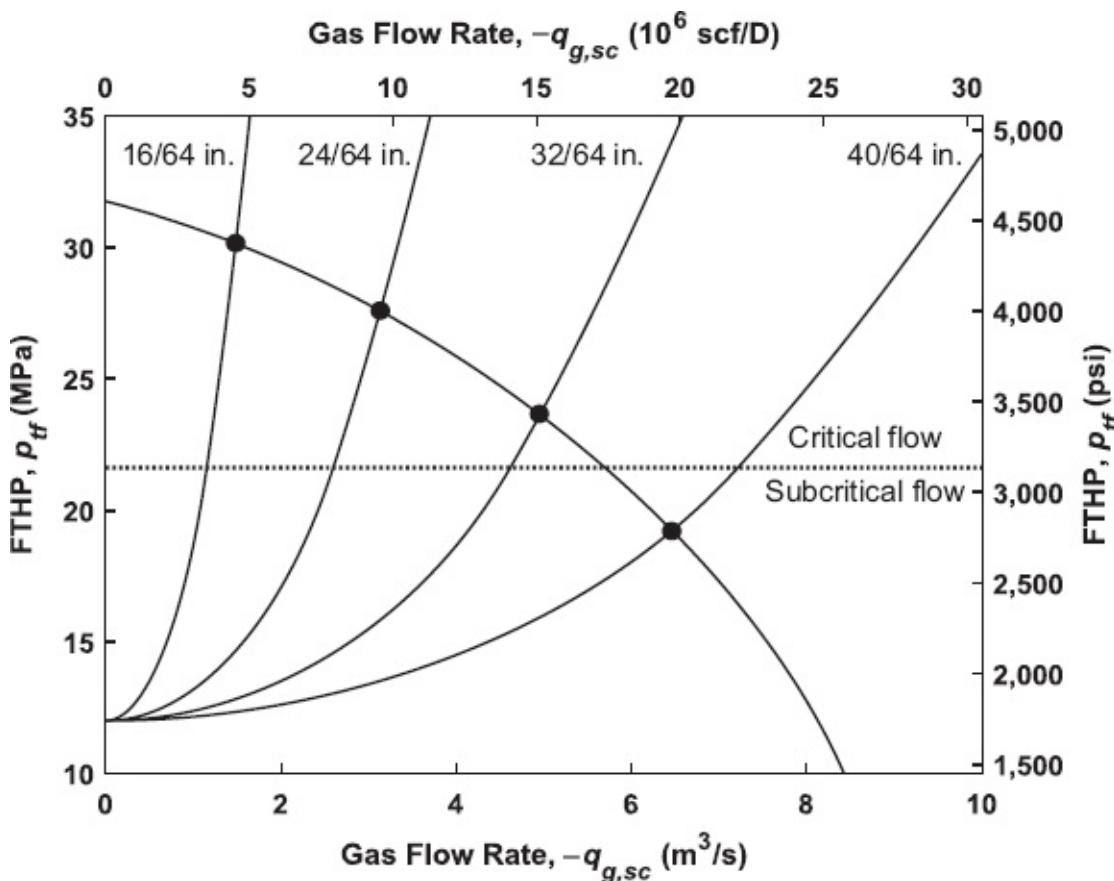


Fig. 8.10—Combined plot of tubing and choke performance curves for a gas well, determining the FTHPs and production rates for different wellhead chokes.

8.2.4 Summary of Analysis Methods. As described, there are two commonly used methods for analyzing the production from oil or gas wells. In each method the behavior of the system is reduced to two relationships between pressure and flow rate. In the first method, the analysis is performed downhole. Using the condition at the tubing head and the pressure drop in the tubing, the tubing intake curve is calculated at the bottom of the well. The intersection of this curve with the IPR determines the production rate. This was illustrated in Fig. 8.3. In the second method, the analysis is performed at the tubing head. Using the inflow performance curve and the pressure drop in the tubing, the tubing performance curve is calculated at the tubing head. The intersection of this curve with the choke performance curve determines the production rate. This was illustrated in Fig. 8.5.

As discussed in Chapter 1, the choice of the analysis nodes at either the top or the bottom of the tubing is rather arbitrary, and before the widespread use of computers, was determined by use of gradient curves for tubing flow. In a cascade system of components the analysis could be performed anywhere at or between the two system boundaries. Indeed, using a computerized analysis method it would be logical to analyze the pressure drop over the entire system with an algorithm marching from one boundary to the other. The program would then need to change the flow rate in an iterative fashion until the pressure drop over the system exactly matches the known difference in pressure between the two boundaries. The advantage of

displaying the traditional combination of two curves is that it provides a quick insight into the flow behavior of two separate system parts in one graph: one downstream and one upstream of the analysis node.

In addition, for chokes operating in the critical regime it is not possible to compute the pressure drop over the choke for a given downstream pressure, and the upstream location (i.e. typically the top of the tubing) is therefore a logical analysis node. Similarly, for semi-empirical IPRs such as the Vogel expression it is not possible to compute the pressure drop over the reservoir for a given upstream pressure, and the downstream location (i.e. typically the bottom of the tubing) is therefore a logical analysis node. For these reasons, most computer programs for nodal analysis still have an option to display the traditional tubing intake and performance curves.

8.3 Field Development Planning and Field Management

Well performance analysis plays a crucial role in field development planning for new fields and the management of producing fields. For a new field, a number of critical questions must be answered:

- What form of completion must be installed in the well, and in particular what size tubing?
- For the chosen tubing size, what is the initial production rate of the well, and how will this vary with time?
- How long will the well be able to produce? When is the optimal time to change the tubing size or switch to artificial lift (pumping or gas lifting)?

For a producing field, the following must be considered:

- Is the well producing as expected?
- Is the well impaired and in need of stimulation to remove the skin?
- Can the well production be improved by changing out the tubing or installing artificial lift? Is the cost justified?
- Can the well performance be improved by increasing the perforated interval?
- Can the well performance be improved by lowering the FTHP or changing out the choke?
- How long will the well produce? Do plans need to be made for artificial lift?

These issues cannot be decided by a production engineer in isolation; it must make economic sense to increase the production of a single well within the total field plan, taking into account the capacity of the surface facilities. However, the production engineer can greatly improve the economic return from a field by continuously monitoring all wells and taking remedial action when production declines.

8.3.1 Improved Inflow Performance. If the well has become impaired, then it can be stimulated (acidized) to improve the inflow performance. Similarly, inflow performance may be improved by additional perforating. To quantify the decreased production from impairment, or the increased production from stimulation, it is useful to analyze what happens downhole. For example, [Fig. 8.11](#) shows the drop in oil production caused by near-well reservoir impairment. In a similar fashion the increase in production can be represented, provided we have good estimates of the original and the impaired permeability.

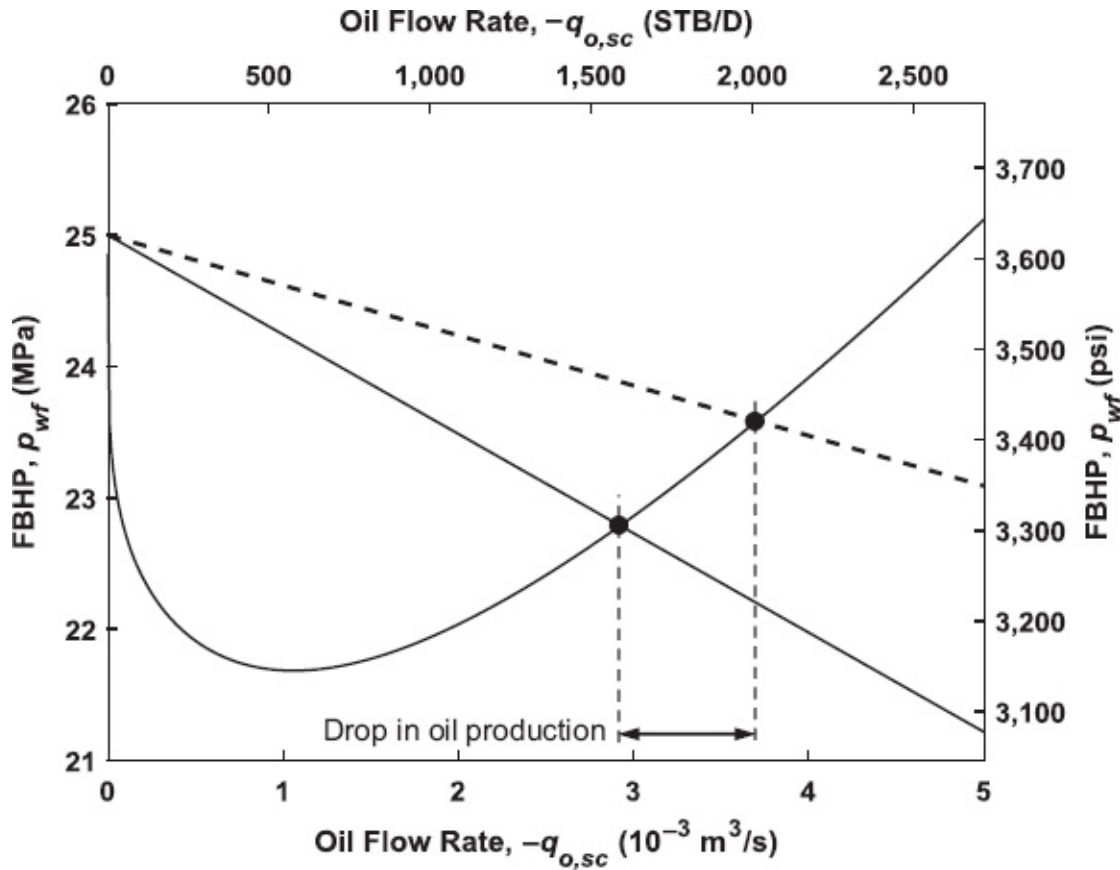


Fig. 8.11—Decreased production due to deteriorated inflow performance resulting from near-well reservoir impairment (“formation damage”).

8.3.2 Changing the Tubing or Choke Size. Increasing or decreasing the tubing diameter can improve production. Changing the choke size can also be of influence. Analysis of choke performance is best done at the tubing head (see, e.g., [Fig. 8.12](#), which depicts a combination of a tubing performance curve and a set of choke performance curves for an oil well). Unlike the tubing performance curve for the gas well depicted in [Fig. 8.8](#), which is monotonically decreasing for an increasing rate, this tubing performance curve has an increasing branch at the left side. The reason is the occurrence of slip in the well at low flow rates, which results in an increased liquid holdup and therefore an increased density of the liquid column. This is exactly the same effect as was observed for multiphase tubing intake curves in [Section 4.4](#).

Changing out a tubing string is expensive and therefore generally needs to be

justified on a long-term basis (see below). Changing out a choke, however, is a low-cost operation. As shown in Fig. 8.13, there is a maximum choke size above which the choke will no longer operate in the critical regime. As explained in Chapter 5, operation in the critical regime is often preferred because it decouples the upstream flow behavior from the downstream behavior and thus shields the well from pressure fluctuations in the production facilities. Associated with the maximum choke size is a maximum flow rate. Sometimes it is required to *bean back* a well (i.e., to reduce the flow rate by installing a smaller choke). A frequently occurring reason for flow reduction is to prevent or delay water or gas coning or to reduce the amount of gas or water produced once the cone has reached the well. As can be seen in Fig. 8.13, there is also a practical minimum choke size and consequently a minimum flow rate, below which the well should not be operated. Reducing the flow rate even further will bring the operating point to the left of the maximum of the tubing performance curve. Although in theory this still results in a stable situation, in practice it is better to avoid operating to the left of the maximum. This is because the very steep drop of the tubing performance curve at low flow rates makes it nearly parallel to the choke performance curves such that small errors in the computation may lead to dramatically different results. The accuracy of pressure predictions using nodal analysis is limited (typically between 5 and 20%), and sensitive results are therefore not very meaningful. For operating points to the right of the maximum the intersection between the curves occurs at a much larger angle, which makes the corresponding flow rate and pressure predictions much more robust.

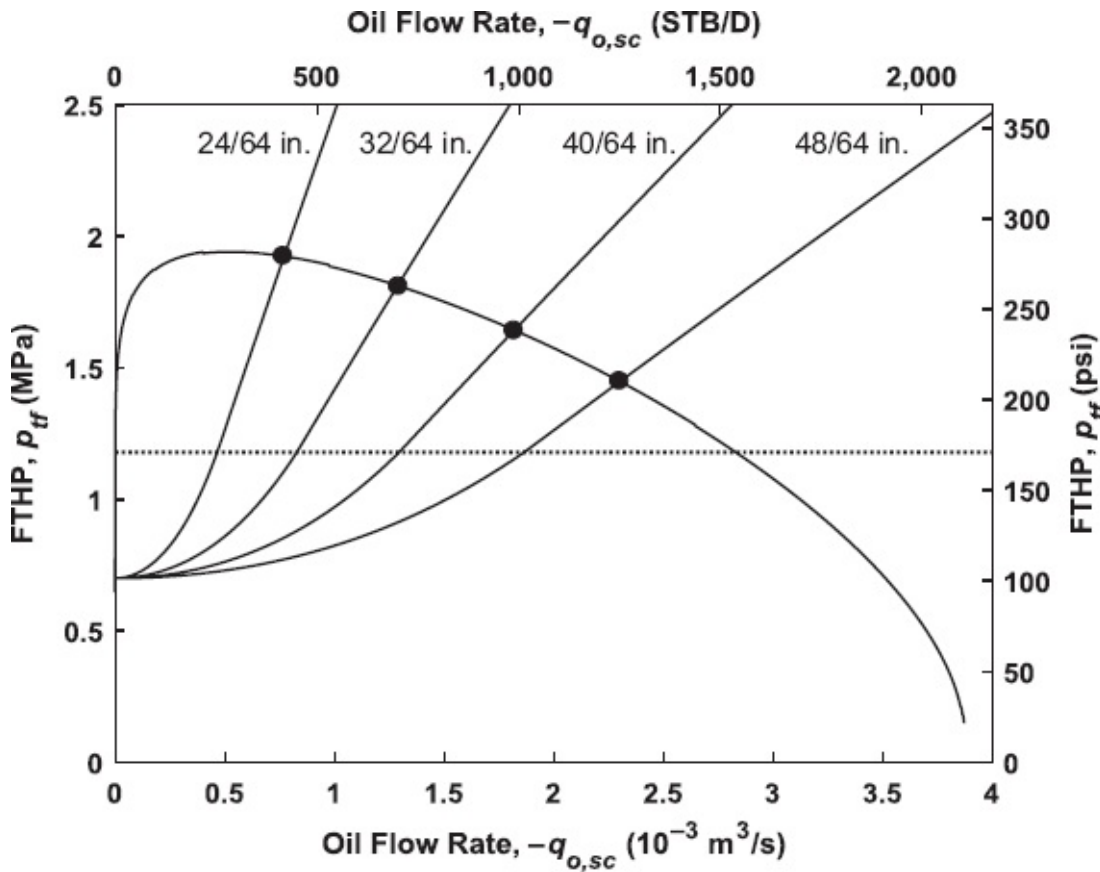


Fig. 8.12—Combined plot of tubing and choke performance curves for an oil well.

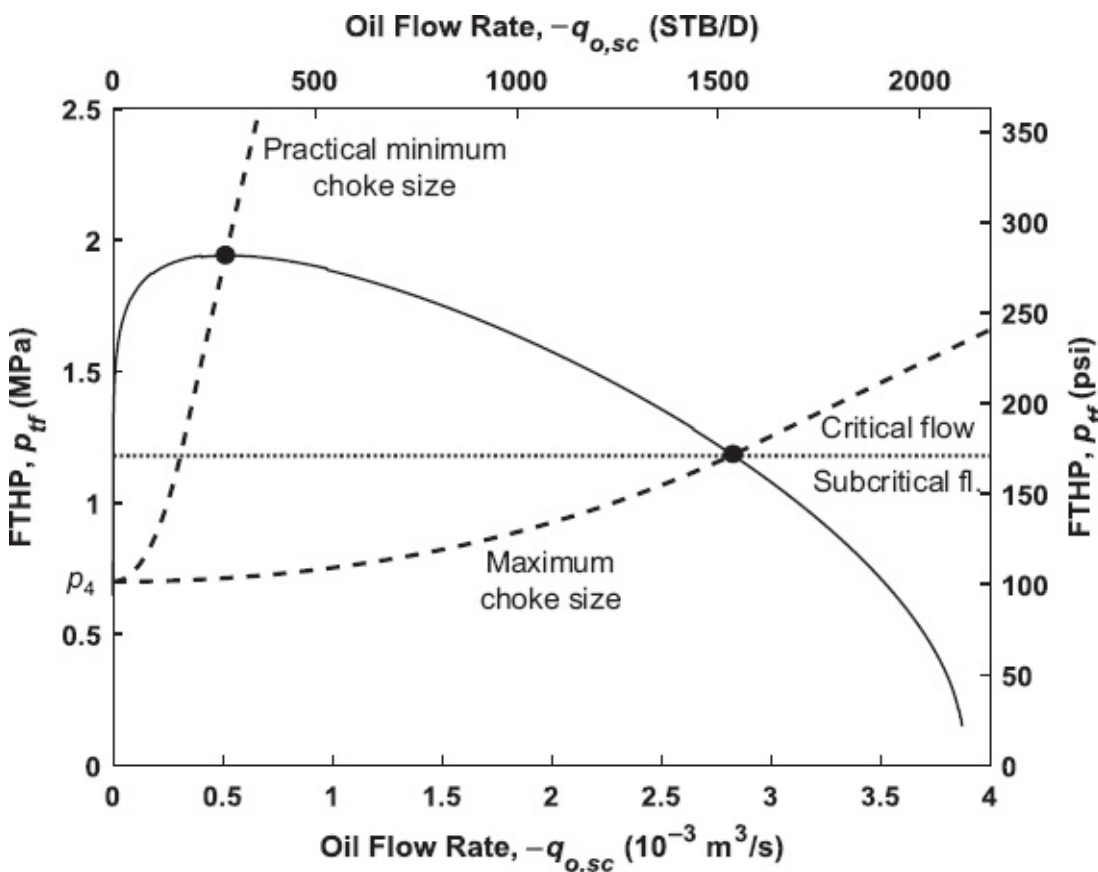


Fig. 8.13—Minimum and maximum choke sizes.

8.3.3 Tubing Change-Out. Analysis of the effect of declining reservoir pressure is best performed downhole using the tubing intake curve. Assuming that the productivity index (PI) remains constant (no impairment) while the reservoir pressure declines, then, as shown in Fig. 8.5, the inflow performance curve will move vertically down the pressure axis with time, keeping the same slope. The corresponding reduction in production can be calculated. If the reservoir pressure drops too far, another and often narrower tubing will need to be installed, as illustrated in Fig. 8.14. By plotting the tubing intake curve for different tubing sizes on the same figure, it will be possible to see how much a tubing change-out will extend the life of the well and to compute whether the cost is justified in terms of the extra oil recovered. Another reason that the 2 $\frac{7}{8}$ -in. tubing in Fig. 8.14 is a better choice than the 4-in. tubing is the position of the operating point with respect to the minimum of the tubing intake curve. Just as for choke performance curves, it is usually advisable to stay to the right of the minimum, a condition that is fulfilled only by the operating point of the 2 $\frac{7}{8}$ -in. tubing. Small errors in either the IPR or the pressure intake curve can have a large effect on the position of the operating point, especially if the two curves are nearly parallel, as is the case to the left of the minimum. To the right of the minimum the curves intersect at a much larger angle, thus reducing the sensitivity to errors in the computation.

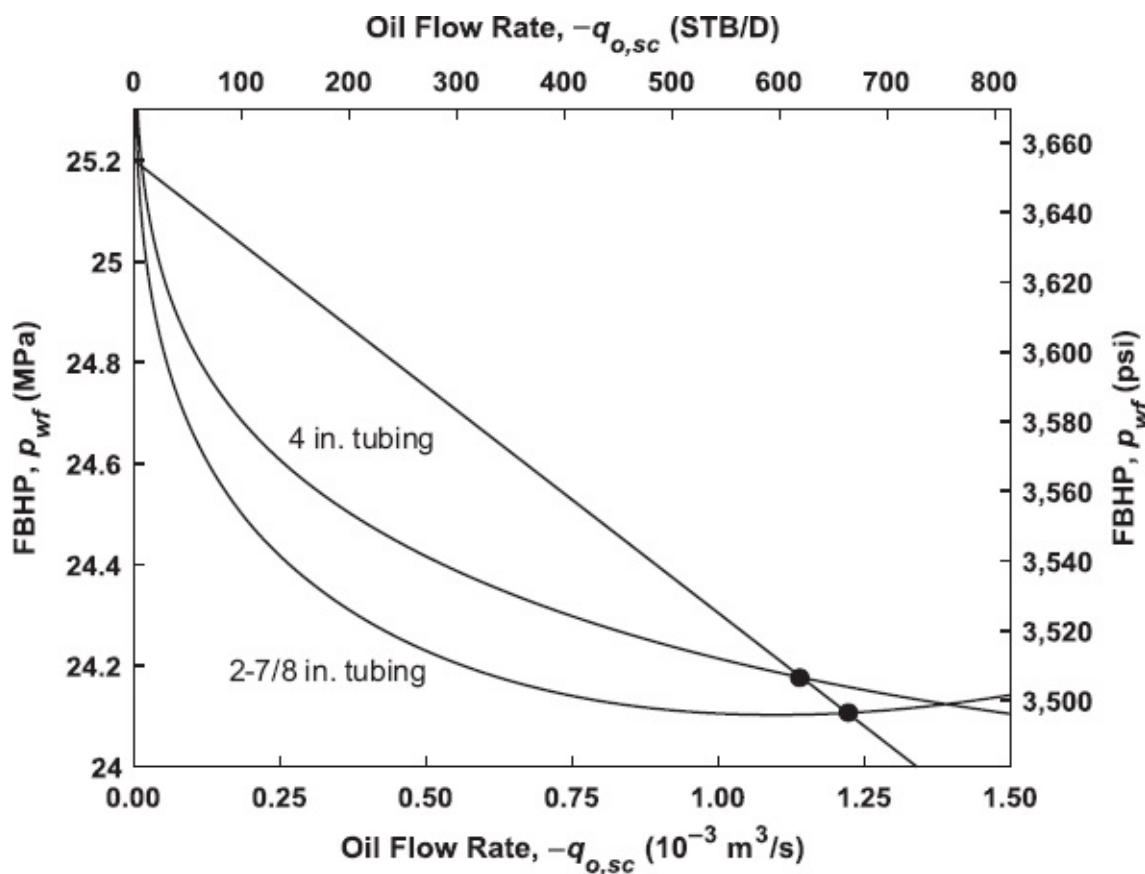


Fig. 8.14—Example depicting a higher flow rate through a smaller tubing.

8.4 Artificial Lift

8.4.1 Gas Lift. Gas lift is one of the most common methods of artificial lift. By injecting extra gas downhole into the tubing, the fluid column becomes lighter and the total production is increased. We have seen in [Chapter 4](#) that there is an optimum GOR that will minimize the pressure drop over the tubing at a given liquid flow rate (see [Fig. 4.10](#)). Too much gas increases the pressure drop because of friction effects. We therefore expect that for a producing well there will be an optimum GOR at which we can inject gas to maximize the oil production rate. This is illustrated in [Fig. 8.15](#), which shows a set of tubing performance curves for varying GORs. The solution GOR of the oil is $30 \text{ m}^3/\text{m}^3$ (168 scf/STB), which implies that higher GOR values result from lift gas injected into the well. If the well should be produced at a minimum FTHP of 2 MPa (290 psi), indicated with the dotted line, the well cannot flow naturally and gas lift will be essential to obtain production. Under these conditions there is indeed an optimum GOR, of approximately $100 \text{ m}^3/\text{m}^3$ (561 scf/STB). See Question 8.12 for an example of the use of nodal analysis of a gas lifted well.

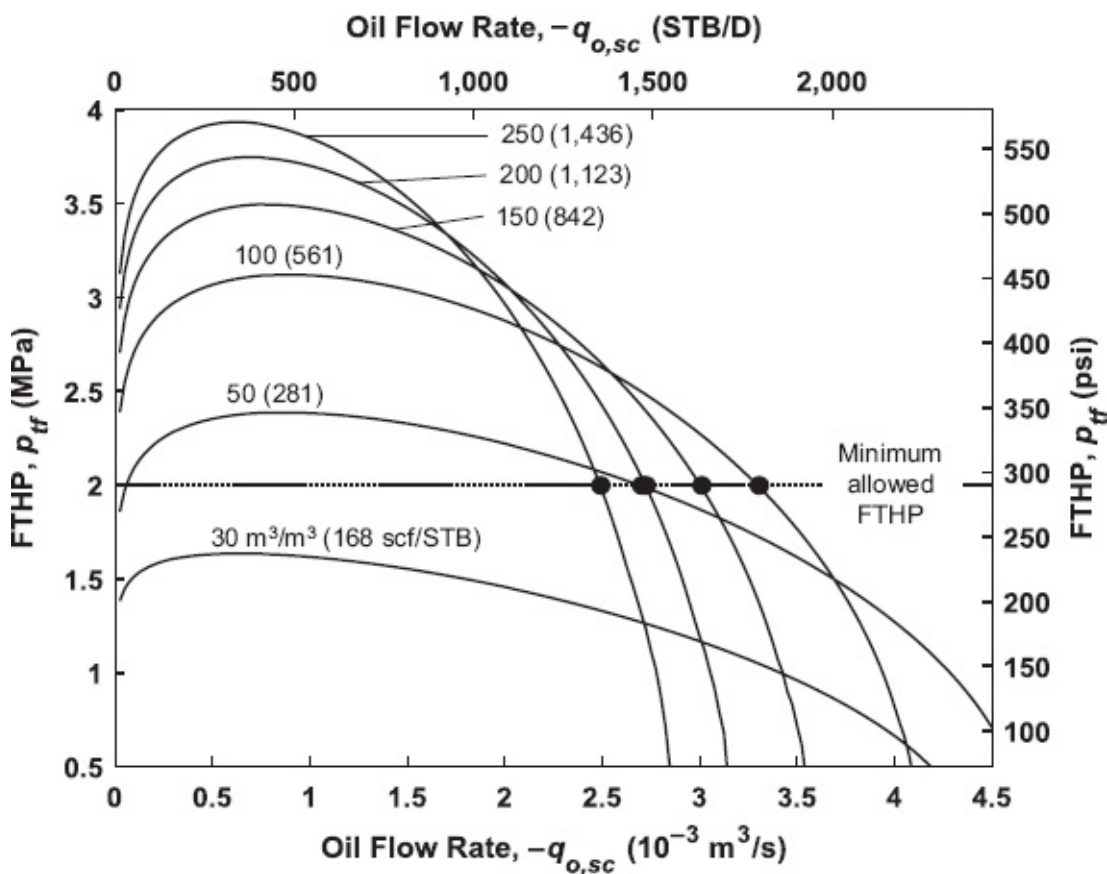


Fig. 8.15—Effect of GOR on the production from a well.

8.4.2 Electric Submersible Pumps. An ESP is a downhole centrifugal pump consisting of a stack (up to several hundreds) of centrifugal impellers (rotors) inside diffusors (stators). The number of stages is directly proportional to the lift capacity of the pump and is therefore a design parameter. The pump is driven by a variable-speed or a fixed-speed electrical motor. Like most pumps, ESPs are most efficient if their throughput is liquid only, although they are capable of handling small amounts of dense gas bubbles. Preferably an ESP should therefore be set deep enough for its suction pressure to be above the bubblepoint pressure. If that is not possible, some form of gas separation can be applied below the pump, whereafter the gas is transported through the annulus, in parallel with the liquid stream through the pump.

The performance of an ESP is characterized by a *pump curve*, which is provided by the manufacturer and typically displays the *head capacity*, or *total (hydraulic) head*, and the efficiency, both as a function of flow rate, for one or more stages (see Fig. 8.16, which gives an example of a pump curve for a fixed-speed ESP with 100 stages). The head capacity, expressed in m (ft), is defined as

$$H = \frac{\Delta p_{\text{lift}}}{g} = \frac{p_{\text{dis}} - p_{\text{suc}}}{\rho_l g} = \frac{p_{\text{dis}} - p_{\text{suc}}}{\left(\frac{\rho_o q_o + \rho_w q_w}{q_o + q_w} \right) g}, \quad \dots \quad (8.18)$$

where Δp_{lift} is the *lift capacity* of the pump, p_{dis} and p_{suc} are the discharge and suction

pressures, g , is the liquid gradient, and g is the acceleration of gravity. (Note that the local oil and water densities ρ_o and ρ_w and flow rates q_o and q_w can be computed with the aid of Eqs. 2.24 and 2.27.) The head capacity in a pump curve is usually specified for water at standard conditions. The corresponding lift capacity in terms of pressure is therefore obtained by multiplying the head by the liquid gradient of the liquid being pumped. For a centrifugal pump, such as an ESP, the head is not influenced by the density of the liquid, although Δp_{lift} and the power consumption do increase with liquid density.

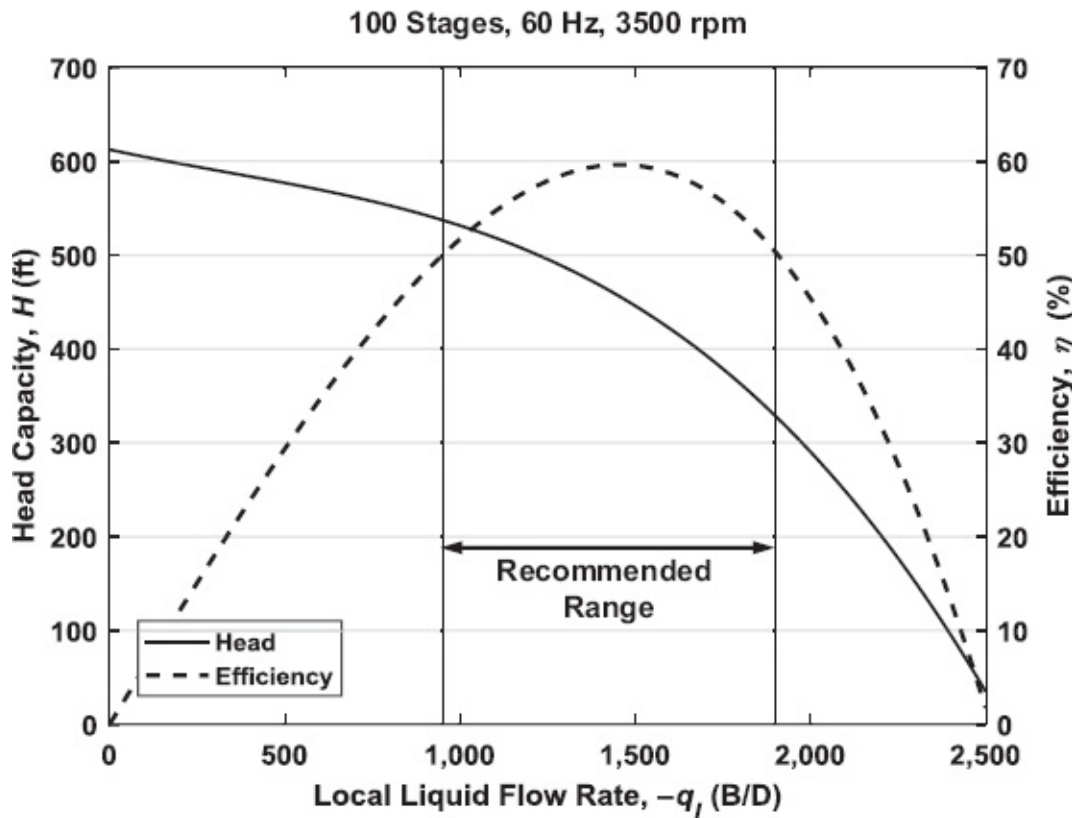


Fig. 8.16—Example of a pump curve for a fixed-speed ESP.

As indicated in the pump curve, an ESP has a limited recommended operating window outside which the efficiency drops considerably. For this particular ESP the optimal flow rate is approximately $-2.8 \times 10^{-3} \text{ m}^3/\text{s}$ ($-1,500 \text{ B/D}$). The required lift capacity as a function of flow rate in a well requiring artificial lift can be displayed in a *lift requirement curve*, which is obtained by taking the difference between the IPR and the tubing intake curve. It should be noted that the pump curve is specified as a function of the local liquid rate, whereas the IPR and intake curve are usually specified as functions of the oil rate under standard conditions. To allow direct comparison with the pump curve, the lift requirement curve should therefore also be plotted as a function of local liquid rate. The vertical axis could display either Δp_{lift} (in units of pressure) or head (in units of length). As an example, consider the lift requirement curve in Fig. 8.17 (dashed line), which was obtained by computing the

difference between the IPR for the low reservoir pressure case ($p_R = 22.5 \text{ MPa}$) and the tubing intake curve in Fig. 8.5, and displaying the result in the form of Δp_{lift} as a function of local liquid rate $-q_l$. (Note that Fig. 8.5 is expressed in oil rates at standard conditions, and Fig. 8.17 in liquid rates at local conditions. It can be seen that a zero lift requirement corresponds to an oil rate $q_{o,sc} = -1.7 \times 10^{-3} \text{ m}^3/\text{s}$ in Fig. 8.5 and to a liquid rate $q_l = -3.7 \times 10^{-3} \text{ m}^3/\text{s}$ in Fig. 8.17.) Fig. 8.17 also displays a second lift requirement curve (solid line), which was computed under the assumption that the reservoir pressure decreased further, to 20 MPa, while at the same time the water cut increased from $f_{w,sc} = 0.2$ to $f_{w,sc} = 0.4$. It can be seen that for the second case, the required Δp_{lift} in Fig. 8.17 at the optimum flow rate for the pump is approximately 3.9 MPa (566 psi). The corresponding liquid gradient can be computed, from additional data not given in this example, as 8396 Pa/m (0.37 psi/ft). The hydraulic head at $2.8 \times 10^{-3} \text{ m}^3/\text{s}$ (1,500 B/D) in Fig. 8.16 is approximately 140 m (460 ft), and because the figure is valid for a pump with 100 stages, the required number of stages can be computed as

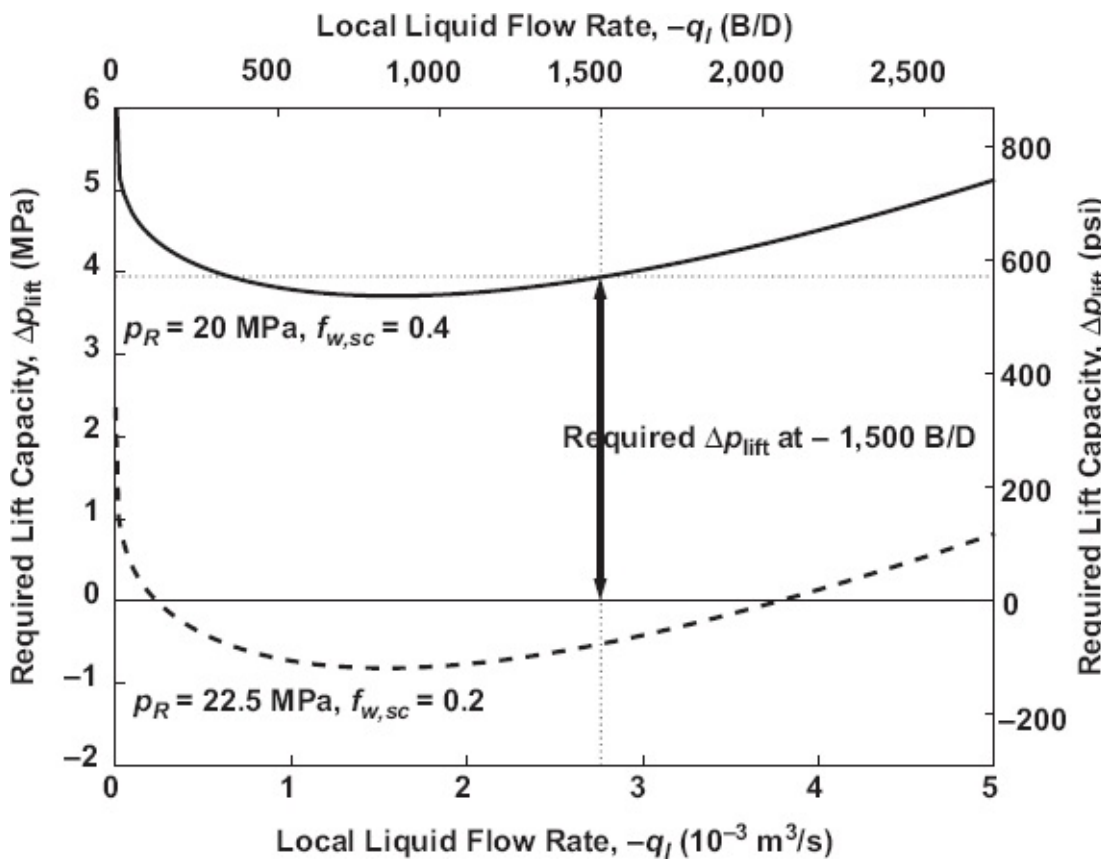


Fig. 8.17—Lift requirement curves for a situation corresponding to Fig. 8.5 (dashed line), and for a further decreased reservoir pressure and increased water cut (solid line).

$$n_{\text{st}} = \frac{\Delta p_{\text{lift}}}{\frac{H}{100} \times g_l} = \frac{3.9 \times 10^6}{\underbrace{\frac{140}{100} \times 8396}_{\text{SI units}}} = \frac{566}{\underbrace{\frac{460}{100} \times 0.37}_{\text{field units}}} = 332. \quad \dots \dots \dots \quad (8.19)$$

The corresponding power requirement of the pump is given by the following equation (see also Eq. 1.1):

$$P = \frac{\Delta p |q|}{\eta} = \frac{3.9 \times 10^6 \times |-2.8 \times 10^{-3}|}{0.60} = 18200 \text{ W}, \dots \quad (8.20)$$

where η is the pump efficiency, which according to Fig. 8.16 is approximately 60% at $-2.8 \times 10^{-3} \text{ m}^3/\text{s}$ ($-1,500 \text{ B/D}$). Note that the electric motor that drives the pump has its own efficiency such that the total electric power required by the ESP is higher than follows from Eq. 8.20.

For use in a computerized nodal analysis procedure, the manufacturer's pump curve from Fig. 8.16 can be converted to a *pump performance curve* either in the form of a look-up table or as a (curve-fitted) equation. This is illustrated in Fig. 8.18, which consists of a combination of the solid lift requirement curve of Fig. 8.17 and the appropriately scaled pump curve of Fig. 8.16.

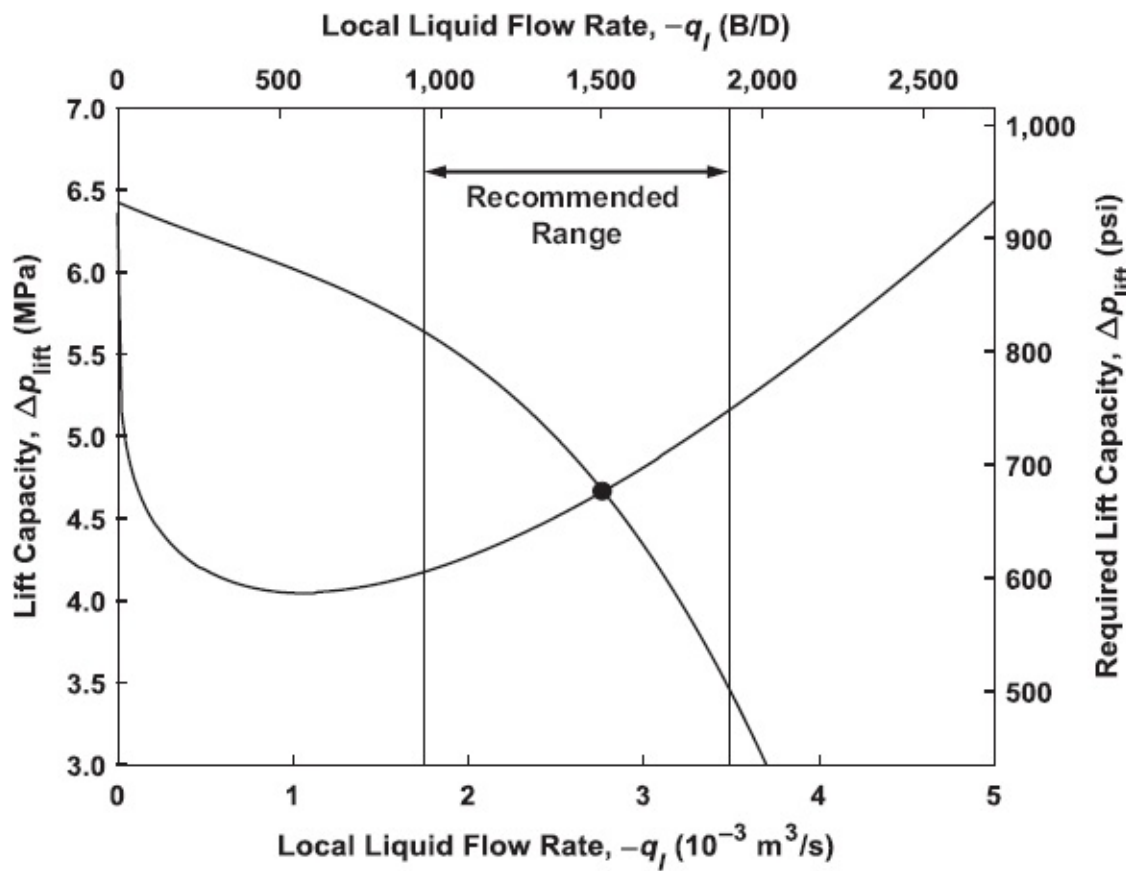


Fig. 8.18—Combined plot of rescaled ESP pump and lift requirement curves.

8.5 Related Topics Not Considered in This Chapter

Not considered in this chapter are several other forms of artificial lift, surface facilities, network topologies with loops, dynamic effects, and temperature effects. Each topic is briefly explained below.

- *Artificial lift.* Apart from gas lift and ESPs, which were briefly mentioned earlier, there are many other artificial lift techniques such as lifting the oil with beam pumps, hydraulic jet pumps, or progressing cavity pumps. The inclusion of a pump in the nodal analysis procedure is straightforward once the relevant pump performance curve is available. Usually such curves are provided by manufacturers in graphical or tabulated form, in which case they need to be converted into computer-legible tables to be used in conjunction with nodal analysis software. Similar relationships are required to model the performance of compressors for gas lift or gas export. For further information, consult Brown (1984).
- *Surface facilities*, such as separators or gas treatment equipment. From a nodal analysis point of view, separators often form a convenient system boundary because they are operated at a constant pressure. The detailed analysis of the flow in separator trains requires the use of compositional analysis of the well stream and flash calculations to optimize the operating pressure such that the yield of liquid hydrocarbons is maximized. Such an analysis is outside the scope of this book.
- *Network topologies with loops.* These topologies occur in pipeline networks or complex production systems with, e.g., parallel flowlines. The analysis of networks requires the derivation of a system of equations in analogy to the analysis of electrical networks with the aid of *Kirchhoff equations*. However, unlike in basic electrical networks, the system elements in the nodal analysis of oil and gas production networks are usually nonlinear. Therefore their solution requires an iterative procedure, typically involving multiple solutions of sets of linearized system equations within a Newton-Raphson procedure. The details of such a general nonlinear network analysis procedure are outside the scope of this book. Note that we did treat the iterative solution of systems with simple branches, in the form of a well producing commingled from two reservoir layers, in Questions 3.12 and 6.14, and from three layers (requiring multivariable root finding) in the MATLAB assignment in [Section 6.12](#).
- *Dynamic effects.* The assumption of steady-state flow which was used in the derivation of the various elements equations is usually justified for production engineering calculation, but not always. For example, during pipeline startup or well testing, *pressure transients* (i.e., the dynamic response to a change in operating conditions), are essential. Also self-excited oscillations, such as low-frequency *slugging* in offshore pipeline riser systems or *heading* (i.e., low-frequency oscillating flow) in low-rate production wells, are dynamic effects that are outside the scope of this book. For an introduction to dynamic well flow modeling, see, e.g., Hassan and Kabir (2002) and Shoham (2006). Moreover, transient reservoir flow (which occurs at much longer time scales than transient pipe flow) is of importance for well testing and for the production of low-permeability reservoirs (see also the discussion in [Section 7.7](#)).
- *Temperature effects.* We did take into account the effect of temperature on

fluid properties, but we did not attempt to compute the temperature distribution in a production system. Instead, we assumed the temperatures to be known. Computing the temperatures would require specification of an energy balance in the formulation of the element equations, in addition to the mass and momentum balances that we used. It would also require specification of the thermodynamic properties of the fluids and heat conduction properties of the various system elements. This would then result in coupled systems of ordinary differential equations for the system elements in terms of both pressure and temperature, which could be solved with a method similar to that we used for pressure only. For a description of such a combined pressure/temperature approach, see, e.g., Brill and Mukherjee (1999), Hassan and Kabir (2002), and Shoham (2006).

8.6 Questions

- 8.1 Nodal analysis concerns the relationship between pressure drop and flow rate in the various elements of a production system. Why, then, are we plotting pressure in a single node vs. flow rate (and not pressure drop over an element vs. flow rate) in a typical nodal analysis plot? What is the underlying assumption to make this work?
- 8.2 Why is the relationship between reservoir pressure decline and production decline usually disproportional? Explain your answer with a picture.
- 8.3 What causes the occasional appearance of two intersections between upstream and downstream performance curves? Which of the corresponding operating points is the physically realistic one? Why is nodal analysis not of any help in indicating which of the points is physically realistic?
- 8.4 Considering the intersection of an IPR and a tubing intake curve, what is the practical rule to avoid unstable flow? Why is this different from the theoretical stability result?
- 8.5 Consider Fig. 8.14. Why is the smaller tubing size the better choice? Give two reasons.
- 8.6 Consider a vertical oil well producing from the oil zone of a reservoir above bubblepoint pressure. The wellhead is close to the separator such that the flowline pressure drop is insignificant. Figs. 8.19 and 8.20 depict two pressure analysis plots for the well.
 - (a) What are the corresponding analysis points?
 - (b) What are the values of reservoir pressure and the separator pressure?
 - (c) Is the choke operating in the critical or the noncritical regime? Why?
 - (d) Why are the flow rates in the operating points in Figs. 8.19 and 8.20 identical?
- 8.7 Consider an oil production system consisting of a slightly inclined (1°) flowline

1500 m in length, a wellhead choke, a 3000-m-deep vertical well, and a near-well reservoir represented as a circular drainage area of 500-m radius (see [Fig. 8.21](#)). The pressure in the production system at a certain flow rate is given in [Fig. 8.22](#).

- What are the magnitudes of the reservoir pressure, the bottomhole pressure, the tubinghead pressure, and the manifold pressure?
- Why is the pressure in the flowline decreasing toward the separator? Why is it decreasing nonlinearly?
- Is the choke operating in the critical regime? (Hint: Use a rule of thumb.) Can you be sure?

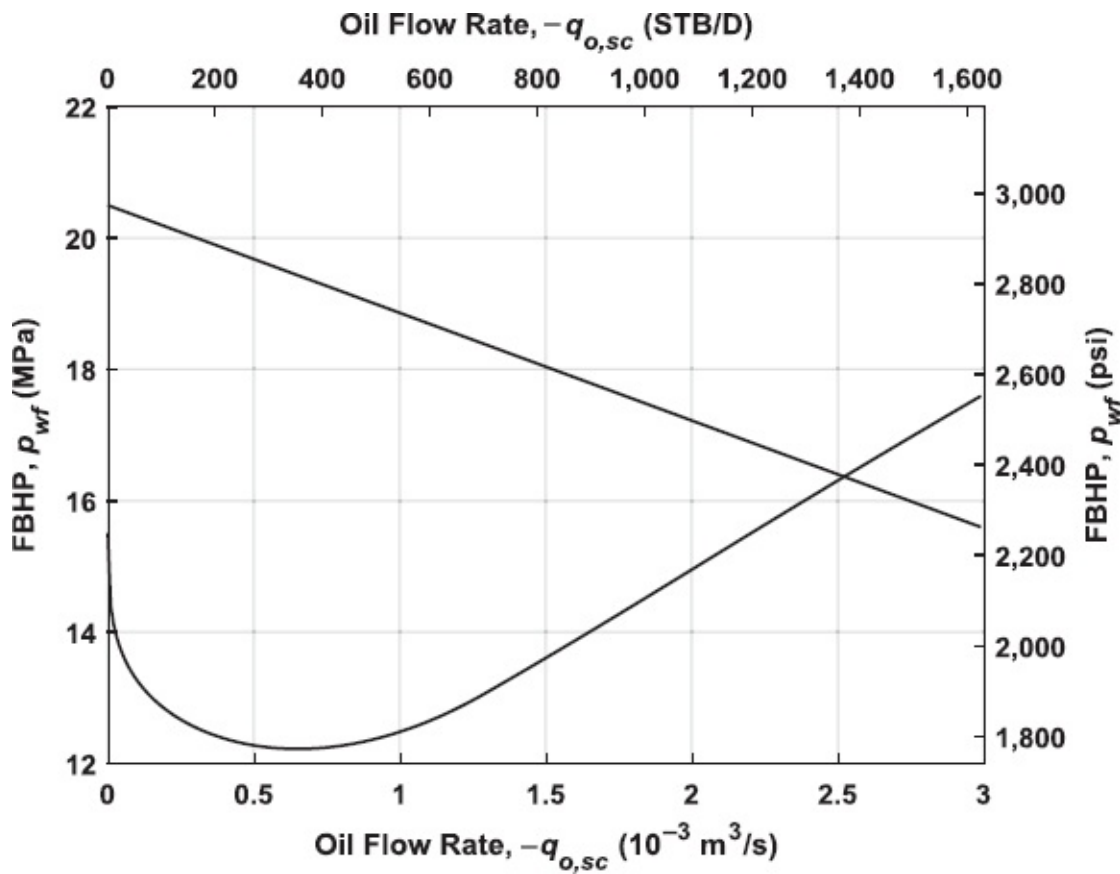


Fig. 8.19—Pressure analysis plot 1 for question 8.6.

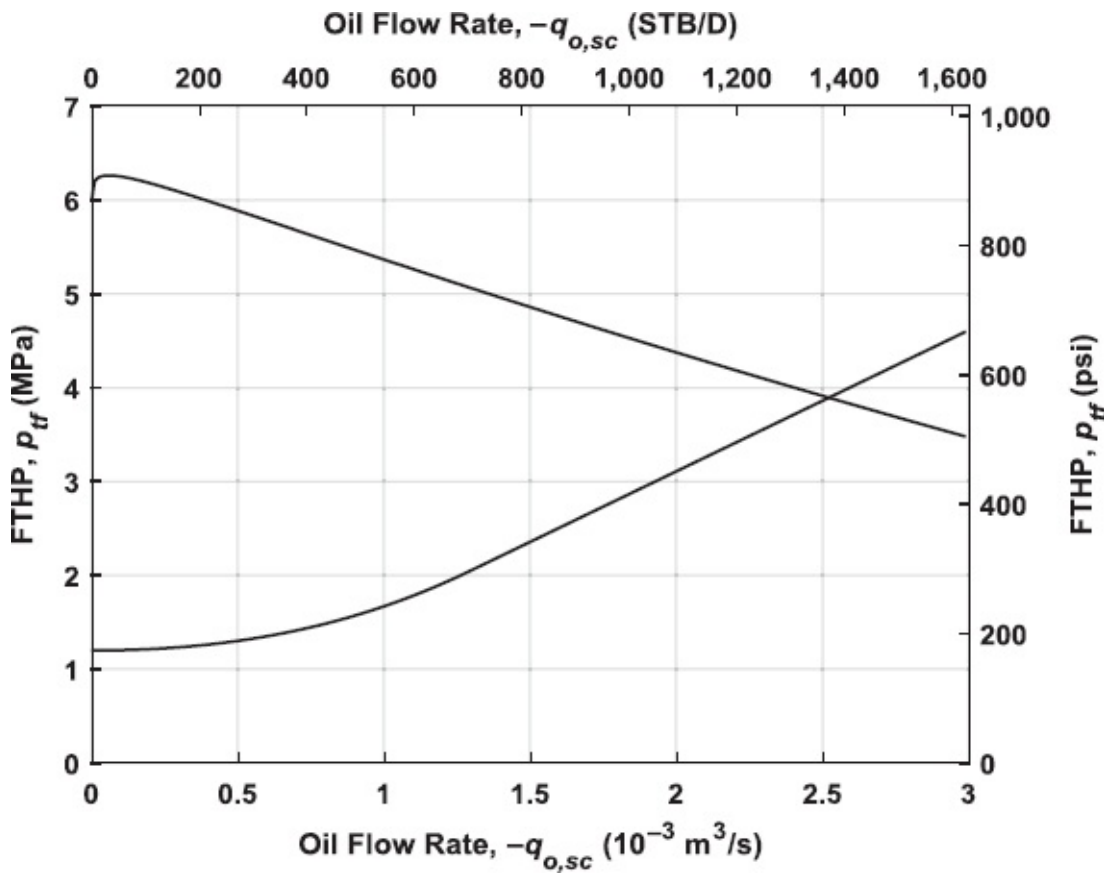


Fig. 8.20—Pressure analysis plot 2 for question 8.6.

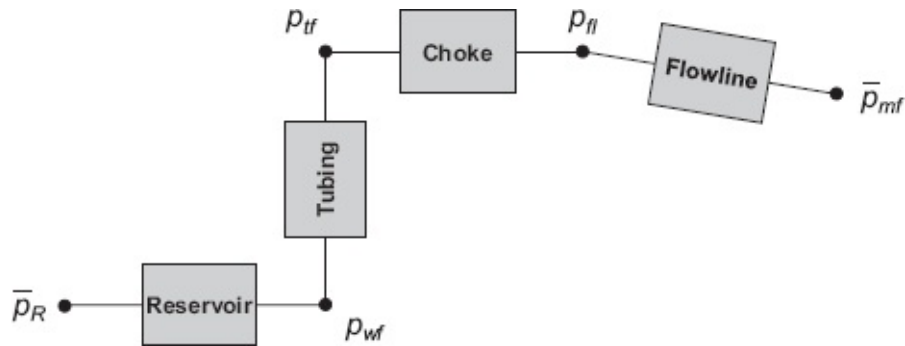


Fig. 8.21—System configuration for question 8.7.

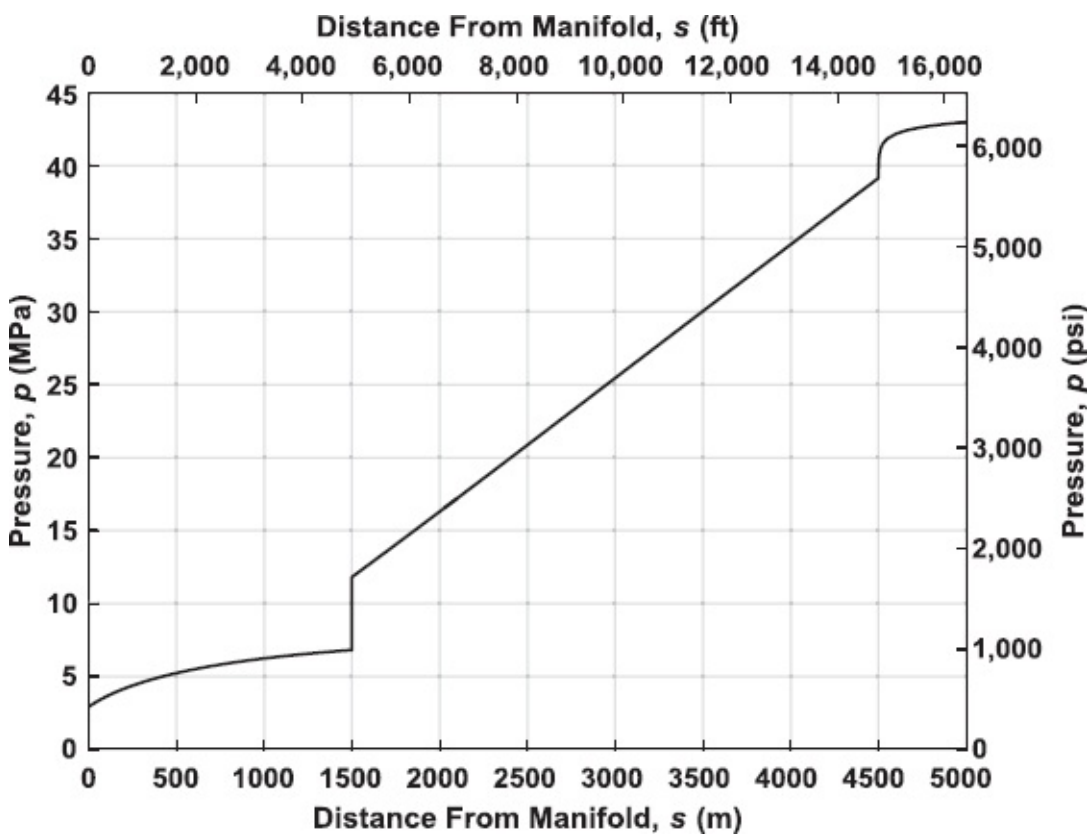


Fig. 8.22—Pressure in the production system at a constant flow rate as a function of distance from the manifold.

8.8 Consider the tubing performance curve in [Fig. 8.23](#).

- (a) Why is the name “tubing performance curve” somewhat misleading?
 - (b) Explain why the left side of the curve is ascending and the right side descending.
 - (c) For a flowline pressure of 1.2 MPa, what are the maximum and the practical minimum flow rates?
 - (d) What is the maximum flow rate if we want to maintain choke flow in the critical regime? (Hint: Use a rule of thumb.)
 - (e) Answer Question 8.8c again for a flowline pressure of 0.8 MPa. Make a sketch of the corresponding choke performance curve.
- 8.9 Consider the nodal analysis plot in [Fig. 8.18](#), which displays an ESP pump performance curve together with the lift requirement curve. The reservoir pressure used to generate the lift requirement curve was 20 MPa. Assuming that the liquid gradient remains unchanged, how much more may the reservoir pressure drop before the ESP runs out of its recommended operating range? Sketch the corresponding nodal analysis plot.

Questions 8.10 through 8.12 require the use of MATLAB. You may want to complete the MATLAB assignment in [Section 8.7](#) first to obtain experience in combining function files for well performance analysis.

- 8.10 **Fig. 8.24** displays the system configuration of a horizontal flowline connected to a deviated well. It is producing from a volatile oil reservoir with a near-circular drainage area. The relevant parameters have been listed in **Table 8.1**. The data have been implemented in MATLAB file `system_02.m`. In that file, the tubing head has been chosen as the analysis node.

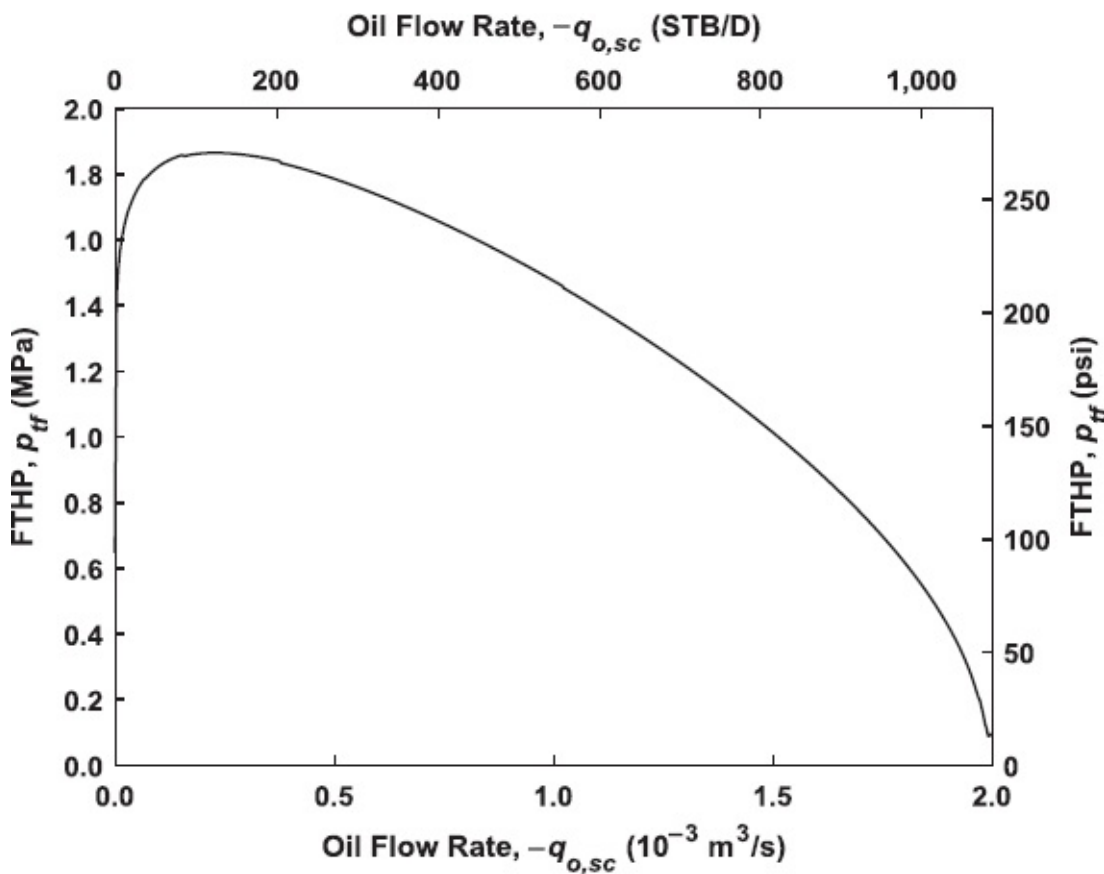


Fig. 8.23—Tubing performance curve for question 8.8.

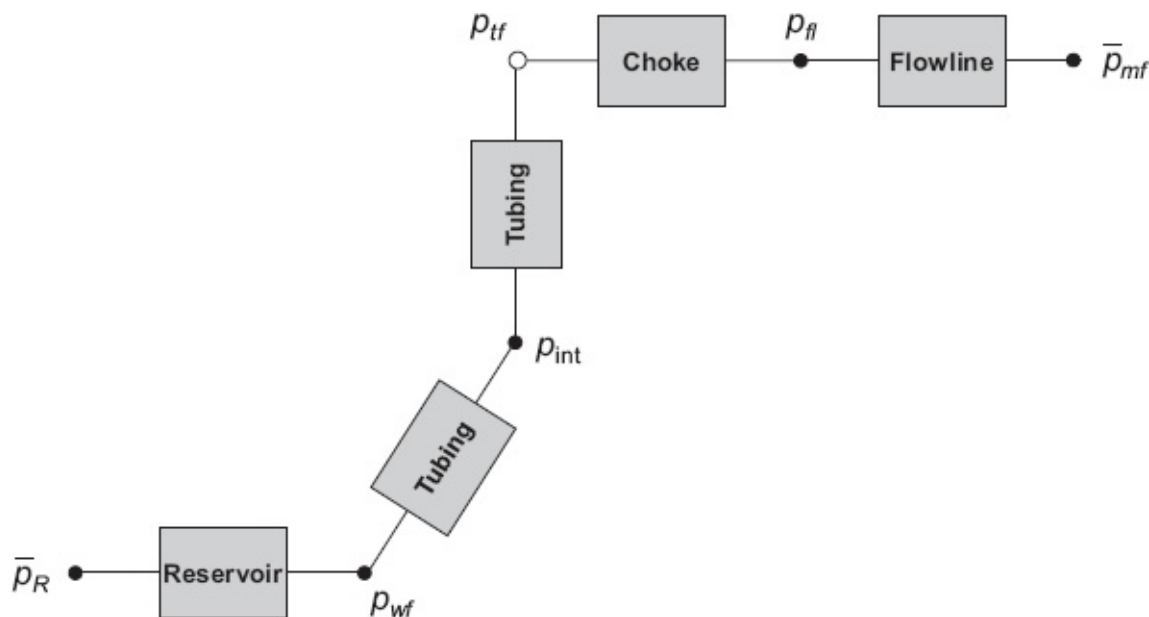


Fig. 8.24—System configuration for question 8.10.

Variable	Symbol	Unit	Value
Production data			
Water cut	$f_{w,sc}$	—	0
Producing GOR	R_{go}	m^3/m^3	450
Manifold pressure	P_{mf}	Pa	3 MPa
Reservoir pressure	P_R	Pa	45 MPa
Fluid data			
Oil model	Volatile oil table 01		
Solution GOR at bubblepoint pressure	R_{sb}	m^3/m^3	450
Gas density at standard conditions	$\rho_{g,sc}$	kg/m^3	0.80
Oil density at standard conditions	$\rho_{o,sc}$	kg/m^3	800
Water density at standard conditions	$\rho_{w,sc}$	kg/m^3	1080
Multiphase flow correlation	Mukherjee and Brill (1985b)		
Reservoir data			
Reservoir height	h_R	m	30
Permeability	k	m^2	1×10^{-14}
Forchheimer coefficient	β	1/m	0
Skin	S	—	0
Reservoir drainage radius	r_e	m	400
Wellbore radius	r_w	m	0.1778
Flow regime	Steady-state		
Relative permeability data			
Endpoint rel. perm. gas	k_{rg}^0	—	0.7
Endpoint rel. perm. oil	k_{ro}^0	—	0.9
Endpoint rel. perm. water	k_{rw}^0	—	0.5
Corey gas	n_g	—	4
Corey oil/gas	n_{og}	—	4
Corey oil/water	n_{ow}	—	4
Corey water	n_w	—	4
Critical gas sat.	S_{gc}	—	0.15
Residual oil sat.	S_{or}	—	0.10
Immobile wat. sat.	S_{wi}	—	0.20
Well data			
AHD until kick-off point	L_{int}	m	3000
Total AHD (from tubing head)	L_{tot}	m	4000
Wellbore inclination, top section	α_{top}	degree	0
Wellbore inclination, bottom section	α_{bot}	degree	50

Tubing inside diameter	d_t	m	0.076 00
Tubing roughness	e_t	m	30×10^{-6}
<u>Choke data</u>			
Choke model	Extended Gilbert (1954)		
Choke size	d_{ch}	1/64 in.	28
<u>Flowline data</u>			
Flowline length	L_{fl}	m	2000
Flowline inclination	α_{fl}	degree	90
Flowline inside diameter	d_t	m	0.100 53
Flowline roughness	e_t	m	30×10^{-6}
<u>Temperature data</u>			
Reservoir temperature	T_R	°C	95
FBHT	T_{wf}	°C	95
Intermediate temperature	T_{int}	°C	90
FTHT	T_{tf}	°C	85
Flowline entry temperature	T_{fl}	°C	80
Manifold temperature	T_{mf}	°C	55

Table 8.1—Data for question 8.10.

- (a) Run the file, inspect the plot, and determine the oil flow rate. Note that depending on your computer system specifications, running the file may take up to a few minutes.
- (b) Modify the file and repeat the analysis for different analysis nodes. Choose the intermediate (kick-off) point, the well bottom, and the reservoir as the analysis nodes. Generate and plot the corresponding performance curves, and verify that they all result in the same oil flow rate.
- (c) Could you also have chosen the flowline entry and the manifold as analysis nodes? Explain your answer. If you are not certain, give it a try.
- (d) For the flow rate determined under 8.10a, do the following:
 - Plot a traverse of the total pressure in the system as a function of distance from the manifold.
 - Plot a traverse of the pressure resulting from gravity.
 - Plot a traverse of the pressure without the gravity contribution—i.e., the pressure resulting from friction and (very little) acceleration.
- (e) Answer the following questions:
 - What are the main causes for the pressure drop over the well?
 - The flowline diameter is larger than the tubing diameter. Nevertheless, the friction loss over the flowline is no smaller than that over the tubing. Why?

- 8.11 (a) Modify MATLAB file `system_02.m` such that the analysis node is at the bottom of the well; i.e., plot the IPR vs. the tubing intake curve. Next, change the production data and fluid properties according to **Table 8.2**, and remove the choke from the system. This should result in the performance plots shown in **Fig. 8.25**. Does the well flow naturally?
- (b) Create a lift requirement curve (at the bottom of the well) in the form of hydraulic head H as a function of local liquid rate q_l .
- (c) Using the ESP pump curve in **Fig. 8.16**, compute the required number of stages.

Variable	Symbol	Unit	Value
<u>New production data</u>			
Water cut	$f_{w,sc}$	—	0.60
Producing GOR	R_{go}	m^3/m^3	20
Manifold pressure	p_{mf}	Pa	0.5×10^6
Reservoir pressure	p_R	Pa	37×10^6
<u>New fluid data</u>			
Oil model	Standing (1952) black oil correlations		
Solution GOR at bubblepoint pressure	R_{sb}	m^3/m^3	20
Gas density at standard conditions	$\rho_{g,sc}$	kg/m^3	0.98
Oil density at standard conditions	$\rho_{o,sc}$	kg/m^3	865
<u>New reservoir data</u>			
Permeability	k	m^2	1.8×10^{-13}

Table 8.2—New data for question 8.11.

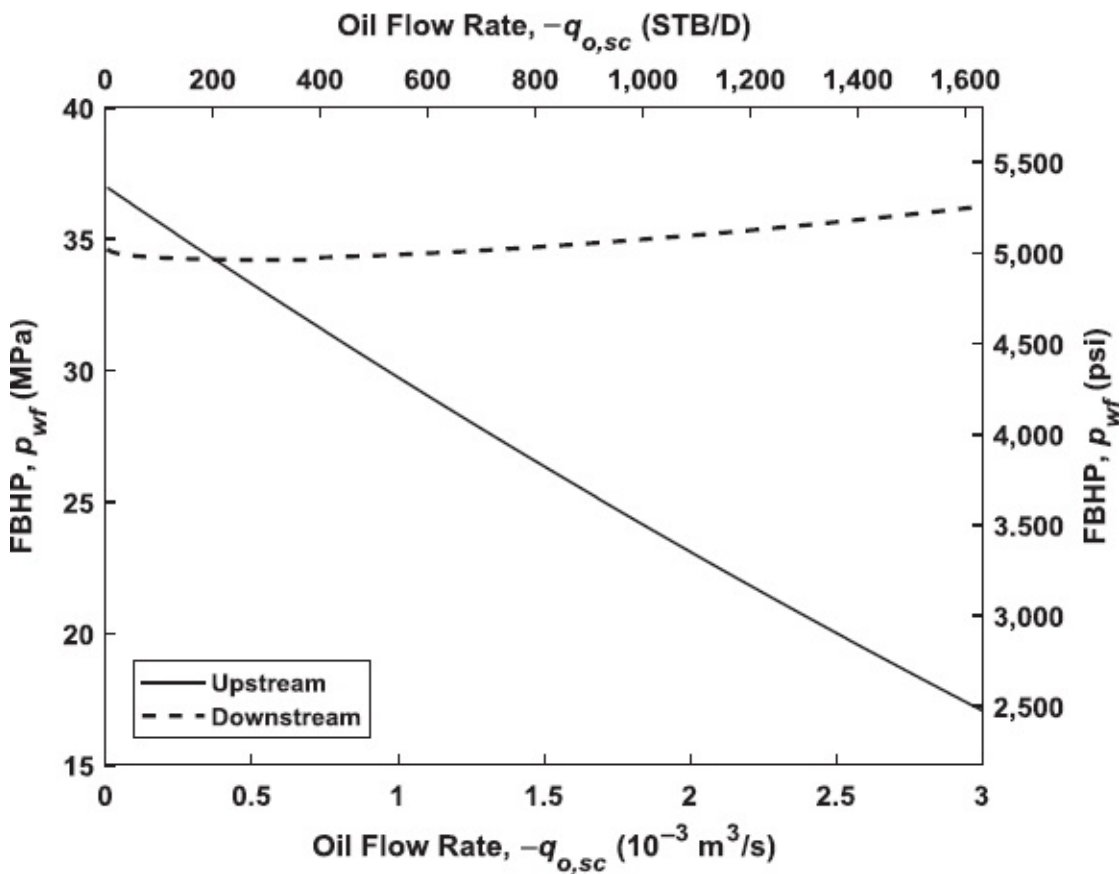


Fig. 8.25—Initial performance plots for question 8.11.

- 8.12 (a) Consider a gas-lifted offshore oil production well with a subsea wellhead connected to a production facility with a flowline, a gas lift line, and risers (see Figs. 8.26 and 8.27). The oil flows to the separator without passing through a choke to minimize the FBHP. The reservoir pressure \bar{p}_6 , the oil manifold pressure \bar{p}_1 , and the gas compressor pressure \bar{p}_7 are fixed, and the lift-gas rate is controlled with a choke at the production platform just downstream of the compressor. A simplified version of this system has been programmed in MATLAB file `system_03_part_1.m`, which models the oil production cascade with lift gas entering directly at the gas lift valve without considering the lift gas cascade. Run the file to produce the upstream and downstream performance curves for an analysis node in the well at the depth of the gas-lift valve. Repeat the analysis for different lift gas rates and determine the optimal rate (i.e., the lift gas rate that maximizes the oil production rate) through trial and error. Plot a set of performance curves in one figure for three lift-gas rates: below, at and above the optimal rate. If the maximum amount of available lift gas is restricted to $q_{g,sc,lift} = 0.10 \text{ m}^3/\text{s}$ ($305 \times 10^3 \text{ scf/D}$), what is the corresponding wellbore pressure at the depth of the gas lift valve?
- (c) Next, inspect and run MATLAB file `system_03_part_2.m`, which models the

flow through the gas lift line. It plots the required compressor discharge pressure as a function of choke diameter for a lift-gas rate $q_{g,sc,lift} = 0.10 \text{ m}^3/\text{s}$ ($305 \times 10^3 \text{ scf/D}$) and the corresponding wellbore pressure at the gas lift valve, p_4 , found under 8.12a. For an available compressor discharge pressure $p_7 = 18 \text{ MPa}$, specify the required choke diameter as a multiple of 1/64 in.

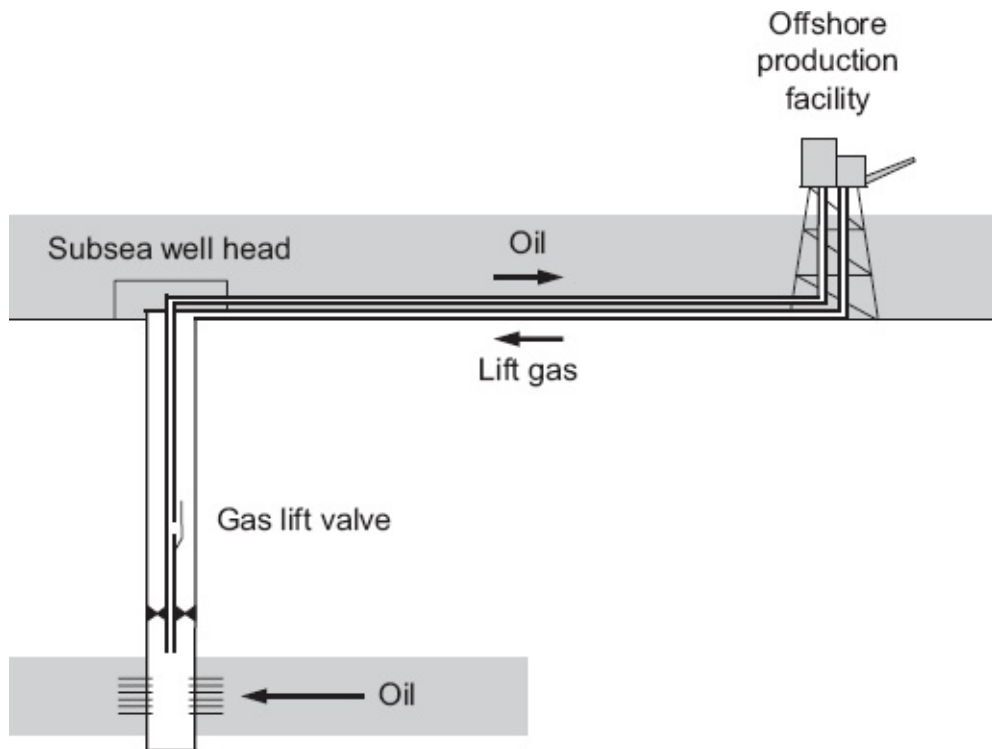


Fig. 8.26—Gas-lifted offshore production well with subsea flowline, gas-lift line, and risers.

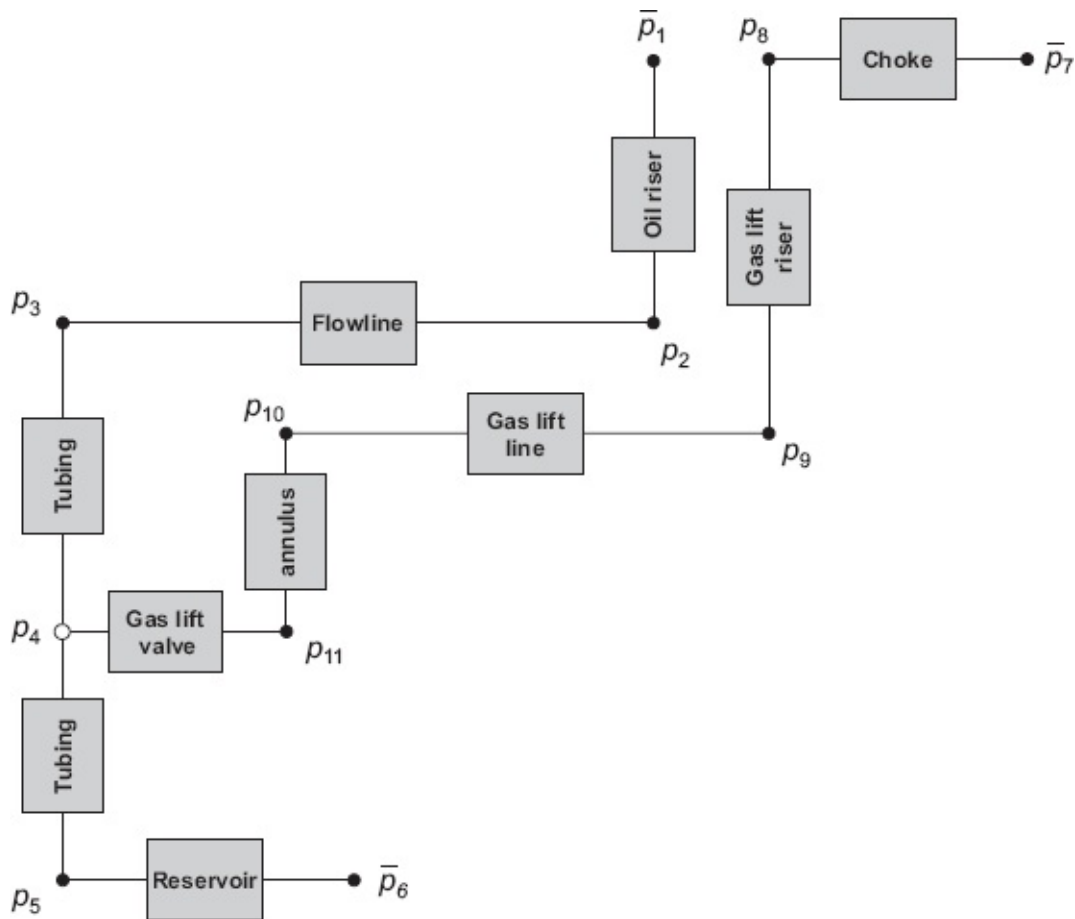


Fig. 8.27—System configuration for question 8.12.

8.7 MATLAB Assignment: Well Performance

8.7.1 Objectives

- Learn to use nodal analysis to determine well performance
- Obtain insight into the effect of tubing size on well performance at different stages of the reservoir life
- Obtain insight into the effect of choke size on well performance

8.7.2 Assignment, Part 1. Consider a multiphase well using the parameters given in **Table 8.3**. Assume that the produced gas is only associated gas.

Task 1

- Inspect the MATLAB files `example_intake_curve.m`, `pipe.m` and `Muk_Brill_dpds.m`.
- Copy `example_intake_curve.m` under a new name and use the new file to create a pressure intake curve for the well from **Table 8.3** for $0 < q_{o,sc} < 3 \times 10^{-3} \text{ m}^3/\text{s}$. Choose parameter `fluid` equal to 4 (Mukherjee and Brill correlation) and `oil` equal to 1 (Standing correlations).

- Expand the script file and create a plot with five intake curves for the tubing diameters given in **Table 8.4**. All other parameters remain the same.
- Compute the bubblepoint pressure at reservoir temperature. Hint: Use `pres_bub_Standin.g.m`.

Variable	Symbol	Unit	Value
Wellbore inclination	α	rad	0
Tubing inside diameter	d	m	0.062
Tubing roughness	e	m	30×10^{-6}
Water cut	$f_{w,sc}$	—	0.0
Flowline pressure	p_{fl}	Pa	0.80×10^6
Flowing tubinghead pressure	p_{tf}	Pa	2.00×10^6
Producing GOR	R_{go}	m^3/m^3	50
Gas density at standard conditions	$\rho_{g,sc}$	kg/m^3	0.95
Oil density at standard conditions	$\rho_{o,sc}$	kg/m^3	850
Water density at standard conditions	$\rho_{w,sc}$	kg/m^3	1050
Bottomhole temperature	T_{wf}	°C	120
Tubinghead temperature	T_{tf}	°C	30
Total true vertical well depth	Z_{tot}	m	3000

Table 8.3—Well data.

OD (in.)	OD (mm)	Nominal Wt (lbm/ft)	ID (mm)
2.375	60.3	4.70	50.67
2.875	73.0	6.50	62.00
3.5	88.9	9.30	76.00
4.0	101.6	11.00	88.29
4.5	114.3	12.75	100.53

Table 8.4—Tubing data for 8.7.2 Assignment, Task 1.

- Inspect the files `example_IPR.m` and `res_oil_simp.m`.
- Further expand the script file and plot the IPR for steady-state flow and the reservoir parameters given in **Table 8.5**. Note: Use the effective permeability for oil.

Question 1

- (a) Is it justified to use the IPR for single-phase oil flow? That is, is it justified to use `res_oil_simp.m`, or should you have used `res.m`?
- (b) What is the PI of the well?
- (c) What is the maximum flow rate of the well at the given FTHP?

- 1(d) What is the corresponding tubing size?
- 1(e) How high can the oil rate become if the FTHP is reduced to 10 bar?
- 1(f) Which factors could determine the lower limit for the FTHP?

8.7.3 Assignment, Part 2. Consider the same multiphase well with the parameters given in [Table 8.3](#)—this time, however, with an increased water cut.

Variable	Symbol	Unit	Value
Forchheimer coefficient	β	1/m	82×10^6
Permeability	k	m ²	4×10^{-14}
Endpoint relative permeability gas	k_{rg}^0	—	0.7
Endpoint relative permeability oil	k_{ro}^0	—	0.9
Endpoint relative permeability water	k_{rw}^0	—	0.5
Corey exponent for gas	n_g	—	3
Corey exponent for oil in gas/oil flow	n_{og}	—	3
Corey exponent for oil in gas/water flow	n_{ow}	—	3
Corey exponent for water	n_w	—	3
Critical gas saturation	S_{gc}	—	0.05
Residual oil saturation	S_{or}	—	0.10
Immobile water saturation	S_{wi}	—	0.15
Average net pay thickness	h	m	20
Radius external drainage boundary	r_e	m	800
Wellbore radius	r_w	m	0.1778
Reservoir pressure	p_r	Pa	26×10^6
Skin	S	—	0

Table 8.5—Reservoir data.

Task 2

- Inspect the files `example_IPR.m`, `res.m` and `res_dpdr.m`.
- Make plots for $f_{w,sc} = 0.1$ and $f_{w,sc} = 0.3$. Use an FTHP of 10 bar and include the intake curves for all five tubing sizes.
- Select a tubing for the case in which $f_{w,sc} = 0.1$ and plot the corresponding traverse.

Question 2

- 2(a) What are the highest possible flow rates and the corresponding tubing sizes for $f_{w,sc} = 0.1$ and $f_{w,sc} = 0.3$?
- 2(b) Why do the curves in the traverse change shape near the surface?

8.7.4 Assignment, Part 3. Consider the same multiphase well with the parameters given in [Table 8.3](#).

Task 3

- Write a MATLAB script file to plot the tubing performance. Make use of the functions `res_oil_simp.m` and `pipe.m` in series. Plot the curve for $f_{wsc} = 0$ and a 2.875-in. tubing. Check if the flow rate at an FTHP of 20 bar corresponds to the flow rate found in Part 1 of the exercise.
- Expand the script file and create a plot with the tubing performance curve and five choke performance curves for choke diameters of 32/64-in., 48/64-in., 64/64-in., 80/64-in., and 96/64-in. Use function `choke_multi_phase_simp.m`, and choose the Gilbert choke model.

Question 3

- 3(a) Which choke diameter results in an FTHP closest to 10 bar?
- 3(b) What is (approximately) the maximum flowline pressure that will still result in critical flow through that choke?

8.7.5 Deliverables (for All Parts)

- MATLAB program listing
- Answers to the questions
- Plots

Appendix A

SI Units and Field Units

A-1 Conversion Factors

To obtain SI units, multiply a quantity given in field units with the conversion factor specified in **Table A-1**.

A-2 SI Prefixes

Table A-2 shows important SI prefixes. Note that out of the seven strict base SI units (m, kg, A, K, mol, and cd), there is one (kg) that has a prefix included in its name. However, the prefixes for mass are based on the gram (g). Therefore, e.g., one-millionth of a kilogram is not a micro kilogram (μkg) but a milligram (mg). This is an unfortunate imperfection in the SI system.

A-3 Standard Conditions

- SI units: 100 kPa and 15°C. Note that sometimes a standard pressure of 101.325 kPa is used (see SPE 1982); the difference is negligible for normal production engineering purposes.
- Field units: 14.7 psia and 60°F.
- Density of air at standard conditions: $\rho_{\text{air,sc}} = 1.23 \text{ kg/m}^3$ ($76.3 \times 10^{-3} \text{ lbm/ft}^3$).
- Density of water at standard conditions: $\rho_{\text{water,sc}} = 999 \text{ kg/m}^3$ (62.4 lbm/ft^3 or 8.34 lbm/gal).

A-4 Pitfalls in Unit Conversions

A-4.1 Force, Mass, and Acceleration of Gravity. The relationship between force and mass is given by Newton's law as "force equals mass times acceleration." This can be expressed in SI units as

$$F = m \frac{d^2x}{dt^2}, \dots \quad (\text{A-1})$$

where F is force, expressed in N; m is mass, expressed in kg; x is distance, expressed in m; and t is time, expressed in seconds. This implies that $\text{N} = \text{kg} \cdot \text{m/s}^2$. As a result, a mass of 1 kg experiences an attractive force because of the Earth's gravitational field, which has a magnitude $g = 9.80665 \text{ m/s}^2$, of

$$F_{\text{grav}} = 1 \text{ kg} \times 9.80665 \text{ m/s}^2 = 9.80665 \text{ kg} \cdot \text{m/s}^2 = 9.80665 \text{ N.} \dots \quad (\text{A-2})$$

Physical Quantity	Dimension	SI Units ¹⁾	Field Units	Conversion Factor From Field Units to SI Units ²⁾
Area	[L ²]	m ²	ft ²	9.290 304 × 10 ⁻² (exact)
		m ²	in. ²	6.451 6 × 10 ⁻⁴ (exact)
		m ²	acre	4.046 856 × 10 ³
Compressibility	[L m ⁻¹ t ²]	1/Pa	1/psi	1.450 377 × 10 ⁻⁴
Density	[L ⁻³ m]	kg/m ³	°API	141.5 × 10 ³ /(131.5 + °API) (exact)
		kg/m ³	lbm/ft ³	1.601 846 × 10 ¹
		kg/m ³	lbm/gal	1.198 264 × 10 ²
Energy	[L m ² t ⁻²]	J	cal	4.184 (exact)
Flow rate	[L ³ t ⁻¹]	m ³ /s	B/D	1.840 131 × 10 ⁻⁶
		m ³ /s	scf/D	3.277 413 × 10 ⁻⁷
		m ³ /s	gal/min	6.309 020 × 10 ⁻⁵
		m ³ /d	B/D	1.589 873 × 10 ⁻¹
Force	[L m t ⁻²]	N	lbf	4.448 222
Gas/oil ratio (GOR)		m ³ /m ³	scf/STB	1.781 076 × 10 ⁻¹
Length	[L]	m	ft	3.048 × 10 ⁻¹ (exact)
	[L]	m	in.	2.54 × 10 ⁻² (exact)
Mass	[m]	kg	lbm	4.535 924 × 10 ⁻¹
Permeability	[L ²]	m ²	mD	9.869 233 × 10 ⁻¹⁶
Power ³⁾	[L m ² t ⁻³]	W	hp	7.456 999 × 10 ²
Pressure ⁴⁾	[L ⁻¹ m t ⁻²]	Pa	psi	6.894 757 × 10 ³
Pressure gradient	[L ⁻² m t ⁻²]	Pa/m	psi/ft	2.262 059 × 10 ⁴
Productivity index (PI)	[L ⁴ m ⁻¹ t]	m ³ /s · Pa	B/D-psi	2.668 884 × 10 ⁻¹⁰
		m ³ /d · Pa	B/D-psi	2.305 916 × 10 ⁻⁵
Specific PI	[L ³ m ⁻¹ t]	m ² /s · Pa	B/D-psi-ft	8.756 182 × 10 ⁻¹⁰
		m ² /d · Pa	B/D-psi-ft	7.565 341 × 10 ⁻⁵
Surface tension	[m t ⁻²]	N/m	Dyne/cm	1 × 10 ⁻³ (exact)
Temperature ⁵⁾	[T]	K	°R	5/9 (exact)
		°C	°F	(°F - 32) / 1.8 (exact)
Velocity	[L t ⁻¹]	m/s	ft/s	3.048 × 10 ⁻¹ (exact)
Viscosity (dynamic)	[L ⁻¹ m t ⁻¹]	Pa · s	cp	1.0 × 10 ⁻³ (exact)
Volume	[L ³]	m ³	ft ³	2.831 685 × 10 ⁻²
		m ³	bbl	1.589 873 × 10 ⁻¹
		m ³	gal	3.785 412 × 10 ⁻³

¹⁾ The expression "SI units" is used loosely to indicate both "strict" SI units and "allowable" units. The strict units can be subdivided in the seven base SI units (m, kg, s, A, K, mol, and cd) and the derived SI such as N, Pa, °C, or J. The allowable SI units are those defined in SPE (1982) and include d (day) and a (year).

²⁾ Conversion factors have been taken from SPE (1982).

³⁾ One hp = 550 ft-lbf/s.

- 4) Pressure in field units can be expressed in psig (gauge pressure) or psia (absolute pressure), where 0 psig = 14.7 psia. Pressure in SI units is often expressed in bars, which is an allowable SI unit, where 1 bar = 10^5 Pa.
- 5) Zero K (Kelvin) is absolute zero in Celsius units. Therefore, the temperature expressed in K equals the temperature expressed in $^{\circ}\text{C}$ + 273.15.
 Zero $^{\circ}\text{R}$ (Rankine) is absolute zero in Fahrenheit units. Therefore, the temperature expressed in $^{\circ}\text{R}$ equals the temperature expressed in $^{\circ}\text{F}$ + 459.67.
-

Table A-1—Conversion factors to convert field units to SI units.

Symbol	Name	Magnitude
n	nano	10^9
μ	micro	10^{-6}
m	mini	10^{-3}
c	centi	10^{-2}
d	deci	10^{-1}
da	deca	10^1
h	hecto	10^2
k	kilo	10^3
M	mega	10^6
G	giga	10^9

Table A-2—SI prefixes.

Field units, however, have been defined purposely such that a mass of 1 lbm experiences an attractive force from the Earth's gravitational field, which has a magnitude $g = 32.174 \text{ ft/s}^2$, of exactly 1 lbf:

$$F_{\text{grav}} = \underbrace{\frac{1}{32.174}}_{g_c} \times 1 \text{ lbm} \times 32.174 \text{ ft/s}^2 = 1 \text{ lbf.} \quad (\text{A-3})$$

This simple result in field units for a mass experiencing the acceleration of gravity leads, however, to a more complicated expression for a mass experiencing an arbitrary acceleration. In that case we should write

$$F = \frac{1}{g_c} m \frac{d^2x}{dt^2}, \quad (\text{A-4})$$

where F is force, lbf; m is mass, lbm; x is distance, ft; t is time, s; and g_c is a dimensionless constant with magnitude 32.174. This implies that $1 \text{ lbf} = 1/g_c \text{ lbm} \cdot \text{ft/s}^2$. Note that the standard acceleration of gravity is specified as 9.80665 m/s^2 (32.174 ft/s^2). In reality, the acceleration of gravity will show slight variations with geographical location and altitude.

A-4.2 Amount of Substance, Molar Mass, and Molecular Weight. In SI units we express the *amount of substance* in mol, defined as “the amount of substance of a system that contains as many elementary entities as there are in 12 g of C₁₂.” The *molar mass*, is specified in kg mol⁻¹. However, for historical reasons one mostly uses the *molecular weight*, which is specified in g mol⁻¹. We will indicate the molar mass with the symbol M and the molecular weight with M_w . An amount of n mol of substance with a molar mass M expressed in kg mol⁻¹ has a mass of $n M$ kg. An amount of n mol of substance with a molecular weight M_w expressed in g mol⁻¹ has a mass of $n M_w$ g.

In field units, the amount of substance is expressed in lbm mol, which is “the amount of substance of a system that contains as many elementary entities as there are in 12 lbm of C₁₂.” The molecular weight is expressed, accordingly, in lbm (lbm mol)⁻¹. It has the same magnitude as when expressed in SI units, and we also indicate it with the symbol M_w . An amount of n lbm mol of substance with a molecular weight M_w expressed in lbm (lbm mol)⁻¹ has a mass of $n M_w$ lbm. For gases, the molar mass M is related to the specific gravity γ_g and the density under standard conditions $\rho_{g,sc}$ according to

$$\text{SI units: } M = \gamma_g M_{\text{air}} = \frac{\rho_{g,sc}}{\rho_{\text{air}}} M_{\text{air}} = \frac{\rho_{g,sc}}{1.23} 28.97 \times 10^{-3} = 23.55 \times 10^{-3} \rho_{g,sc} \text{ kg/mol}, \dots \quad (\text{A-5})$$

$$\text{field units: } M_w = \gamma_g M_{w,\text{air}} = \frac{\rho_{g,sc}}{\rho_{\text{air}}} M_{w,\text{air}} = \frac{\rho_{g,sc}}{76.3 \times 10^{-3}} 28.97 = 379.7 \rho_{g,sc} \text{ lbm/(lbm mol)}. \dots \quad (\text{A-6})$$

A-4.3 Dimensional Constants. The results of experimental data are often presented as correlations with the aid of curve fitting. If the input data and the output data have different physical dimensions, the coefficients of the fitted curve also have physical dimensions. This implies that if you use these expressions in a different unit system, the “constant” coefficients have a different value. To convert such a correlation from field units to SI units, start from the expression in its original form (i.e., as expressed in field units) and

1. Insert the variables in SI units divided by their corresponding field-to-SI conversion factors as given in [Table A-1](#).
2. Solve for the desired left side while combining all numerical factors.

Usually Step 1 is straightforward. Thus, e.g., to convert a pressure variable p expressed in psia to one expressed in Pa, we simply insert

$$\underbrace{\frac{p(\text{Pa})}{6.895 \times 10^3}}_{\text{lbf/in}^2} \dots \dots \dots \quad (\text{A-7})$$

Sometimes Step 1 is slightly more complex. In that case, e.g., to convert a temperature variable T expressed in $^{\circ}\text{F}$ to $^{\circ}\text{C}$, we need to insert

$$\underbrace{1.8T(\text{ }^{\circ}\text{C})+32}_{\text{ }^{\circ}\text{F}} \dots \dots \dots \quad (\text{A-8})$$

As an example of converting a correlation with dimensional constants, consider the Standing correlation for bubblepoint pressure expressed in field units:

$$p_b = 18.2 \left[\left(\frac{R_p}{\gamma_g} \right)^{0.83} \frac{10^{0.00091T}}{10^{0.0125y_{\text{API}}}} - 1.4 \right], \dots \dots \dots \quad (\text{A-9})$$

where p_b is expressed in psi, R_p is expressed in scf/STB, γ_g is dimensionless, T is expressed in $^{\circ}\text{F}$, and y_{API} in $^{\circ}\text{API}$. Following Step 1 as outlined above results in

$$\underbrace{\frac{p_b(\text{Pa})}{6.895 \times 10^3}}_{\text{psi}} = 18.2 \left[\frac{\exp \left\{ 0.00091 \times \underbrace{1.8T(\text{ }^{\circ}\text{C})+32}_{\text{ }^{\circ}\text{F}} \right\}}{\exp \left\{ 0.0125 \times \underbrace{\frac{141.5 \times 10^3}{\rho_o(\text{kg/m}^3)} - 131.5}_{^{\circ}\text{API}} \right\}} - 1.4 \right]. \quad (\text{A-10})$$

Next, solving for p_b and combining all numerical factors leads to

$$p_b = 125 \times 10^3 \left[\left(\frac{716 R_{sb}}{\rho_{g,\infty}} \right)^{0.83} \frac{10^{0.00164T}}{10^{1768/\rho_{o,\infty}}} - 1.4 \right], \dots \dots \dots \quad (\text{A-11})$$

where we used the equality $716^{0.83} = (1.23/1.781076 \times 10^{-1})^{0.83} \exp(0.00091 \times 32 + 0.0125 \times 131.5)$. The result in SI units is identical to [Eq. B-1 in Appendix B](#).

Appendix B

Fluid Properties and Correlations

B-1 Fluid Properties

Properties in **Table B-1** (in SI units) have been computed from the values in **Table B-2** with the aid of the conversion factors presented in **Appendix A**, which were, in turn, taken from SPE (1982). Properties in **Table B-2** (in field units) have been taken from GPSA (1998). Some typical fluid gradients have been listed in **Table B-3**.

Compound	Molar Mass M (10^{-3} kg/mol)	Critical Pres. p_c (10^6 Pa)	Critical Temp. $T_{c,abs}$ (K)	Gas Dens. $\rho_{g,sc}^{1)}$ (kg/m ³)	Liquid Dens. $\rho_{l,sc}^{1)}$ (kg/m ³)
N ₂ (nitrogen)	28.01	3.40	126.2	1.18	809 ²⁾
CO ₂ (carbon dioxide)	44.01	7.37	304.1	1.86	817 ³⁾
H ₂ S (hydrogen sulphide)	34.08	8.96	373.4	1.44	801 ³⁾
H ₂ O (water)	18.02	22.1	647.1	0.77	999
C ₁ H ₄ (methane)	16.04	4.60	190.6	0.68	300 ⁴⁾
C ₂ H ₆ (ethane)	30.07	4.88	305.4	1.27	356 ³⁾
C ₃ H ₈ (propane)	44.10	4.24	369.8	1.86	507 ³⁾
C ₄ H ₁₀ (iso-butane)	58.12	3.64	407.8	2.45	562 ³⁾
C ₄ H ₁₀ (n-butane)	58.12	3.78	425.1	2.45	584 ³⁾
C ₅ H ₁₂ (iso-pentane)	72.15	3.38	460.4	3.05	624
C ₅ H ₁₂ (n-pentane)	72.15	3.37	469.7	3.05	631
C ₆ H ₁₄ (n-hexane)	86.18	3.03	506.4	3.64	663
C ₇ H ₁₆ (n-heptane)	100.20	2.74	539.2	4.23	687
C ₈ H ₁₈ (n-octane)	114.23	2.49	568.4	4.82	706
C ₉ H ₂₀ (n-nonane)	128.26	2.28	594.7	5.42	721
C ₁₀ H ₂₂ (n-decane)	142.29	2.10	617.7	6.00	734

¹⁾ At standard conditions: 100 kPa and 15°C = 288 K.

²⁾ Density at the normal boiling point, i.e., at boiling temperature (78 K) and 100 kPa. The temperature at standard conditions (288 K) is above the critical temperature (126 K).

³⁾ Density at saturation pressure (bubblepoint pressure) and 288 K.

⁴⁾ Estimated value. The temperature at standard conditions (288 K) is above the critical temperature (191 K).

Table B-1—Reservoir fluid properties in SI units.

Compound	Molar Mass M (lbm/lbm · mole)	Critical Pres. p_c (psia)	Critical Temp. T_c (°F)	Gas Specific Gravity ^{1,2)} γ_g (-)	Liquid Specific Gravity ^{1,3)} γ_l (-)
N ₂ (nitrogen)	28.01	492.8	-232.49	0.967 2	0.809 40 ⁴⁾
CO ₂ (carbon dioxide)	44.01	1069.5	87.73	1.519 6	0.818 01 ⁵⁾
H ₂ S (hydrogen sulphide)	34.08	1300.	212.40	1.176 7	0.801 43 ⁵⁾
H ₂ O (water)	18.02	3200.1	705.11	0.622 0	1.000 00
C ₁ H ₄ (methane)	16.04	667.0	-116.66	0.553 9	(0.3) ⁶⁾
C ₂ H ₆ (ethane)	30.07	707.8	90.07	1.038 2	0.356 195)
C ₃ H ₈ (propane)	44.10	615.0	205.92	1.522 6	0.506 985)
C ₄ H ₁₀ (iso-butane)	58.12	527.9	274.41	2.006 8	0.562 86 ⁵⁾
C ₄ H ₁₀ (n-butane)	58.12	548.8	305.51	2.006 8	0.584 02 ⁵⁾
C ₅ H ₁₂ (iso-pentane)	72.15	490.4	368.96	2.491 2	0.624 41
C ₅ H ₁₂ (n-pentane)	72.15	488.1	385.7	2.491 2	0.631 08
C ₆ H ₁₄ (n-hexane)	86.18	439.5	451.8	2.975 5	0.664 04
C ₇ H ₁₆ (n-heptane)	100.20	397.4	510.9	3.459 8	0.688 05
C ₈ H ₁₈ (n-octane)	114.23	361.1	563.5	3.944 1	0.706 78
C ₉ H ₂₀ (n-nonane)	128.26	330.7	610.8	4.428 4	0.721 93
C ₁₀ H ₂₂ (n-decane)	142.29	304.6	652.2	4.912 7	0.734 17

¹⁾ At standard conditions: 14.7 psia and 60°F = 520°F.

²⁾ With respect to air, which has a density at standard conditions of 0.0768 lbm/ft³.

³⁾ With respect to fresh water, which has a density at standard conditions of 62.4 lbm/ft³.

⁴⁾ Density at the normal boiling point, i.e., at boiling temperature (-320°F) and 14.7 psia. The temperature at standard conditions (60°F) is above the critical temperature (-232°F).

⁵⁾ Density at saturation pressure (bubblepoint pressure) and 60°F.

⁶⁾ Estimated value. The temperature at standard conditions (60°F) is above the critical temperature (-117°F).

Table B-2—Reservoir fluid properties in field units.

Fluid	Density (kg/m ³)	Gradient (kPa/m)	Gradient (psi/ft)
Gas	100–300	1.0–2.9	0.04–0.13
Oil	800–900	7.8–8.8	0.35–0.39
Water	1000–1100	9.8–10.8	0.43–0.48

Table B-3—Typical reservoir fluid gradients.

B-2 Oil Correlations

B-2.1 Black Oil Correlations. Black oil correlations are based on laboratory tests, most of which were performed on crudes with a gas/oil ratio (GOR) less than 350 m³/m³ (near 2,000 scf/STB). In practice, black oil correlations are often used above this limit, but with caution. Note that the numerical values in several of these correlations are not dimensionless. The most widely known black oil correlations are the Standing correlations, originally issued in Standing (1947) and Standing (1952). The expressions below have been taken from Appendix II of the 1977 SPE reissue of Standing (1952). They have been derived on the basis of data from 22 Californian crudes under conditions listed in **Table B-4**. (Note that all correlations in this appendix have been implemented in several MATLAB routines, found in [Appendix H](#).)

B-2.2 Bubblepoint Pressure p_b . Standing's correlation to relate the bubblepoint pressure p_b to the bubblepoint gas/oil ratio R_{sb} of a black oil is

$$p_b = 125 \times 10^3 \left[\left(\frac{716 R_{sb}}{\rho_{g,\infty}} \right)^{0.83} \frac{10^{0.00164 T}}{10^{1768/\rho_{o,\infty}}} - 1.4 \right] \dots \quad (\text{B-1})$$

If the producing GOR R_{go} of a well is used to compute p_b with this correlation, the results are valid only if $R_{go} = R_{sb}$ (i.e., if the reservoir pressure is at or above the bubblepoint pressure).

B-2.3 Solution Gas/Oil Ratio R_s . Once we know p_b , and therefore also R_{sb} , we can estimate R_s , the solution gas/oil ratio at a pressure p above or below p_b . If $p > p_b$, the oil is undersaturated, all gas is in solution, and $R_s = R_{sb}$. If $p \leq p_b$, the oil is saturated with gas, there is free gas, and the pressure p must be the bubblepoint pressure of the mixture of oil and still-dissolved gas. Hence R_s is given by the inverse of the above Standing correlation, but with pressure p instead of p_b :

$$p \leq p_b: R_s = \frac{\rho_{g,\infty}}{716} \left[(8 \times 10^{-6} p + 1.4) 10^{1768/\rho_{o,\infty} - 0.00164 T} \right]^{1.2048} \dots \quad (\text{B-2})$$

B-2.4 Oil Formation Volume Factor B_o . As the pressure changes, the volume it

occupies changes as a result of two effects: compressibility effects and, much more importantly, changes in the amount of dissolved gas. If $p \leq p_b$, the oil is saturated and the mixture of oil and still-dissolved gas is at its bubblepoint. We can use Standing's correlation for the oil formation volume factor at the bubblepoint pressure:

Property	SI Units	Field Units
Bubblepoint pressure, p_b	$0.9\text{--}48.3 \times 10^6 \text{ Pa}$	$130\text{--}7,000 \text{ psia}$
Temperature, T	$37\text{--}125^\circ\text{C}$	$100\text{--}258^\circ\text{F}$
Solution GOR, R_s	$3.5\text{--}254 \text{ m}^3/\text{m}^3$	$20\text{--}1,425 \text{ scf/STB}$
Oil density, $\rho_{o,sc}$, and gravity, γ_{API}	$725\text{--}956 \text{ kg/m}^3$	$16.5\text{--}63.8 \text{ }^\circ\text{API}$
Gas density, $\rho_{g,sc}$, and gravity, γ_g	$0.73\text{--}1.17 \text{ kg/m}^3$	$0.59\text{--}0.95 \text{ (air = 1.00)}$

Table B-4—Conditions used to derive Standing correlations.

$$p \leq p_b: B_o = 0.9759 + 12 \times 10^{-5} \left[160 R_s \sqrt{\left(\rho_{g,sc} / \rho_{o,sc} \right)} + 2.25 T + 40 \right]^{1.2} \dots \dots \dots \quad (\text{B-3})$$

If $p > p_b$, the oil is undersaturated and all the gas is dissolved. As pressure changes, all changes result from changes in density of the mixture; no extra gas is dissolved or comes out of solution. Hence

$$p > p_b: B_o = \frac{B_{ob} \rho_{ob}}{\rho_o}, \dots \dots \dots \quad (\text{B-4})$$

where B_{ob} and ρ_{ob} are the oil formation volume factor and the density of the oil at the bubblepoint pressure p_b respectively, and ρ_o is the density at pressure p . As was shown in [Section 2.7.2](#), this can also be written as

$$p > p_b: B_o = B_{ob} \exp[-c_o(p - p_b)], \dots \dots \dots \quad (\text{B-5})$$

where c_o is the isothermal compressibility of the undersaturated oil. A correlation for c_o is given in [Section B-2.6](#).

B-2.5 Densities. Using the principle of conservation of mass, we can derive that

$$p \leq p_b: \rho_o = \frac{\rho_{o,sc} + R_s \rho_{g,sc}}{B_o} \dots \dots \dots \quad (\text{B-6})$$

The oil density at bubblepoint conditions, ρ_{ob} , can be obtained from [Eq. B-6](#) through substitution of $B_o = B_{ob}$. At other pressures, above p_b , the density is given by

$$p > p_b: \rho_o = \rho_{ob} \exp[c_o(p - p_b)], \dots \dots \dots \quad (\text{B-7})$$

(see Eq. 2.18 in Section 2.5.3). Substitution of the Eq. B-7 relationship in Eq. B-4 recovers the Eq. B-5 relationship for B_o quoted above.

B-2.6 Compressibility. Oil compressibility is best measured in the laboratory if accurate values are required for the density or B_o . Correlations do exist for the compressibility. One of these is given by Vazquez and Beggs (1980) and has the form

$$p > p_b: c_o = \frac{-2541 + 27.8R_{sb} + 31.0T - 959\rho_{g,100} + 1784 \times 10^3 / \rho_{o,sc}}{10^5 p}, \dots \quad (B-8)$$

where $\rho_{g,100}$ is the gas density measured at a pressure of 689 kPa (100 psig = 114.7 psia). This pressure was chosen to reflect a typical separator pressure because usually the gas density is determined from a sample taken from a separator (see Vazquez and Beggs 1980). The relationship between $\rho_{g,100}$ and $\rho_{g,sep}$ measured at any other separator pressure p_{sep} and temperature T_{sep} is given by

$$\rho_{g,100} = \rho_{g,sep} \left[1 + 5.912 \times 10^{-5} \left(\frac{141.5 \times 10^3}{\rho_{o,sc}} - 131.5 \right) (1.8T_{sep} + 32) \log \left(\frac{p_{sep}}{790.8 \times 10^3} \right) \right]. \quad (B-9)$$

B-2.7 Viscosity. A commonly used empirical correlation for dead oil is the one from Beggs and Robinson (1975). It can be expressed as

$$\mu_{od} = 10^{-3} (10^a - 1), a = \frac{10^b}{(1.8T + 32)^{1.163}}, b = 5.693 - \frac{2.863 \times 10^3}{\rho_{o,sc}}. \dots \quad (B-10)$$

A correlation for saturated oil viscosity is also given by Beggs and Robinson (1975) as

$$\begin{aligned} \mu_o &= \left[10.72 \times 10^{-3} \times \left(\frac{R_s}{0.178} + 100 \right)^{-0.515} \right] (\mu_{od} \times 10^3)^c, \\ c &= 5.44 \left(\frac{R_s}{0.178} + 150 \right)^{-0.338}. \dots \end{aligned} \quad (B-11)$$

Vazquez and Beggs (1980) determined the following empirical correlation for undersaturated oil:

$$\mu_o = \mu_{ob} \left(\frac{p}{p_b} \right)^d, d = 7.2 \times 10^{-5} p^{1.187} \exp(-11.513 - 1.30 \times 10^{-8} p). \dots \quad (B-12)$$

These expressions illustrate that the oil viscosity increases with increasing oil density and with increasing pressure (for undersaturated oil), and it decreases with increasing temperature and increasing gas saturation (for saturated oil) (see Figs. B-1 and B-2). The physical explanation is, simply said, that the heavier hydrocarbon components

(i.e., the ones with high carbon numbers) consist of long molecules that have a tendency to get entangled. At increasing temperatures these long molecules tend to stretch and untangle, whereas at increasing pressures they are pushed together. Moreover, the addition of short gas molecules results in a molecular mixture of lower viscosity. **Table B-5** gives an overview of the conditions under which these correlations were derived (see Beggs and Robinson 1975 and Brill and Mukherjee 1999).

B-2.8. Example B-1: Oil Formation Volume Factor ($p < p_b$). Consider a well that produces oil and gas at the following rates: $q_{o,sc} = 1000 \text{ m}^3/\text{d}$, and $q_{g,sc} = 200\,000 \text{ m}^3/\text{d}$. The production history shows no indication of gas-cap gas production. The density of the oil and gas at standard conditions are given by $\rho_{o,sc} = 800 \text{ kg/m}^3$ and $\rho_{g,sc} = 0.98 \text{ kg/m}^3$, and the reservoir is at pressure and temperature given by $p_R = 20.00 \text{ MPa}$ and $T_R = 150^\circ\text{C}$.

Question

What is the oil formation volume factor B_o at reservoir pressure and temperature?

Answer

The bubblepoint GOR is given by the producing GOR as

$$R_{sb} = R_{go} = \frac{q_{g,sc}}{q_{o,sc}} = \frac{200000}{1000} = 200 \text{ m}^3/\text{m}^3.$$

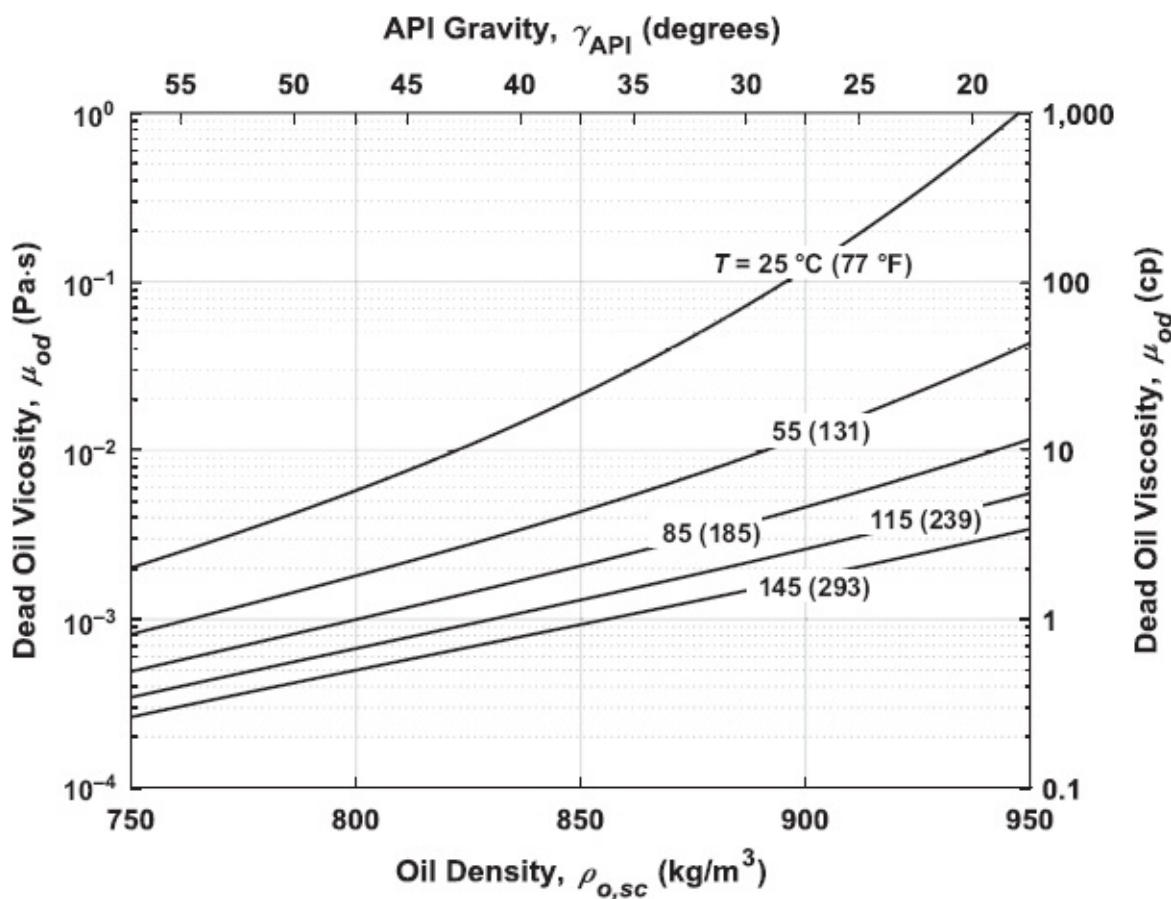


Fig. B-1—Dead oil viscosity as a function of oil density for different temperatures. Graph based on the Beggs and Robinson (1975) correlation.

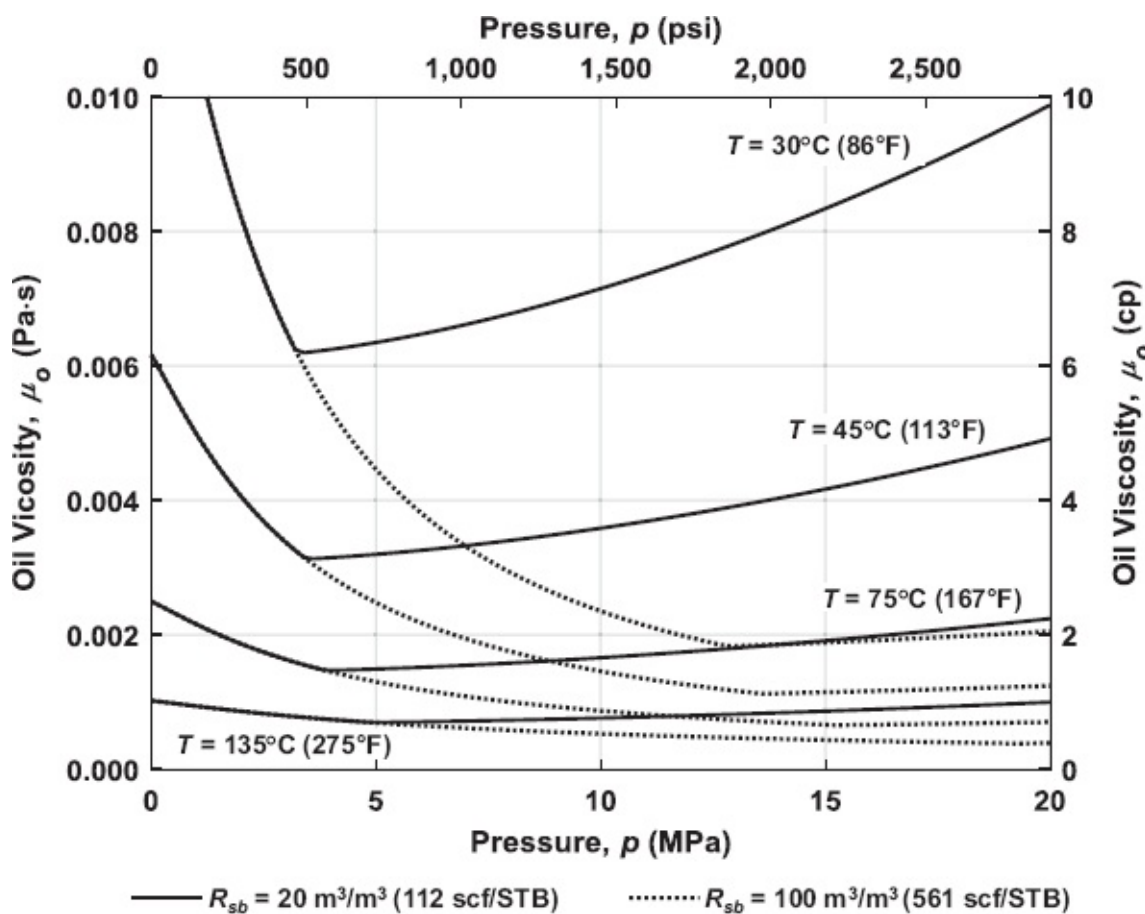


Fig. B-2—Oil viscosity as a function of pressure for two different solution gas/oil ratios and four different temperatures: $\rho_{g,sc} = 0.95 \text{ kg/m}^3$ ($y_g = 0.77$), $\rho_{o,sc} = 850 \text{ kg/m}^3$ ($y_{\text{API}} = 35^\circ$). Graph based on the Beggs and Robinson (1975) and Vazquez and Beggs (1980) correlations.

Property	Eq. B-11	Eq. B-11	Eq. B-12	Eq. B-12
	SI Units	Field Units	SI Units	Field Units
Temperature, T	21–146°C	70–295°F		
Pressure, p_b	0.1–36.3 MPa	15–5,265 psia	1.0–65.6 MPa	141–9,515 psia
Solution GOR, R_s	3.6–369 m^3/m^3	20–2,070 scf/STB	16–392 m^3/m^3	90–2,199 scf/STB
Density, $\rho_{o,sc}$, y_{API}	959–747 kg/m^3	16–58°API	966–739 kg/m^3	15–60°API
Density, $\rho_{g,sc}$, y_g			0.63–1.66 kg/m^3	0.51–1.35
Viscosity, μ_0			0.12–148 $\text{mPa} \cdot \text{s}$	0.12–148 cp

Table B-5—Conditions used to derive viscosity correlations.

With the aid of Eq. B-1 we find that the bubblepoint pressure equals

$$p_b = 125 \times 10^3 \left[\left(\frac{716 \times 200}{0.98} \right)^{0.83} \frac{10^{0.00164 \times 150}}{10^{1768/800}} - 1.4 \right] = 26.1 \text{ MPa},$$

where T has been taken equal to the reservoir temperature. Because the reservoir pressure is below the bubblepoint pressure, we need to compute the solution GOR R_s at reservoir pressure with the aid of Eq. B-2:

$$R_s = \frac{0.98}{716} \left[(8 \times 10^{-6} \times 20.0 \times 10^6 + 1.4) 10^{1768/800 - 0.00164 \times 150} \right]^{1.2048} = 145 \text{ m}^3/\text{m}^3,$$

The oil formation volume factor now follows from Eq. B-3 as

$$B_o = 0.9759 + 12 \times 10^{-5} \left[160 \times 145 \sqrt{(0.98/800)} + 2.25 \times 150 + 40 \right]^{1.2} = 1.57 \text{ m}^3/\text{m}^3.$$

Answer With MATLAB

```
» R_sb = 200000/1000
R_sb = 200
» p_b = pres_bub_Standing(R_sb, 0.98, 800, 150)
p_b = 2.6105e+007
» R_s = gas_oil_rat_Standing(20e6, 0.98, 800, 150)
R_s = 145.4194
» B_o = oil_form_vol_fact_Standing(R_s, 0.98, 800, 150)
B_o = 1.5656
```

Alternatively, the black oil properties can be computed directly as

```
» [B_g, B_o, R_s] = black_oil_Standing
(20e6, 200, 0.98, 800, 150)
B_g = 0.0068
B_o = 1.5656
R_s = 145.4194
```

B-2.9 Example B-2: Oil Formation Volume Factor ($p > p_b$). Consider the same situation as in Example B-1 in Section B-2.8, except for the reservoir pressure, which is now given by $p_R = 40.00 \text{ MPa}$.

Question

What is the oil formation volume factor B_o at this higher reservoir pressure?

Answer

Because the reservoir pressure is now above the bubblepoint pressure, the solution GOR is equal to the bubblepoint GOR:

$$R_s = R_{sb} \cdot 200 = \text{m}^3/\text{m}^3.$$

The corresponding oil formation volume factor B_{ob} is obtained from Eq. B-3 as

$$B_{ob} = 0.9759 + 12 \times 10^{-5} \left[160 \times 200 \sqrt{(0.98/800)} + 2.25 \times 150 + 40 \right]^{1.2} \text{ m}^3/\text{m}^3.$$

We can now compute the oil formation volume factor from Eq. B-5. This requires that we first determine the compressibility c_o from Eq. B-8, which, in turn, requires computation of $\rho_{g,100}$ from $\rho_{g,sep}$ with the aid of Eq. B-9. Because $\rho_{g,sep}$ in our example is equal to $\rho_{g,sc}$, we can enter standard conditions in Eq. B-9. This leads to

$$\rho_{g,100} = 0.98 \left[1 + 5.912 \times 10^{-5} \left(\frac{141.5 \times 10^3}{800} - 131.5 \right) (1.8 \times 15 + 32) \log \left(\frac{100 \times 10^3}{790.8 \times 10^3} \right) \right] = 0.84 \text{ kg/m}^3,$$

$$c_o = \frac{-2541 + 27.8 \times 200 + 31.0 \times 150 - 959 \times 0.84 + 1784 \times 10^3 / 800}{10^5 \times 40 \times 10^6} = 2.27 \times 10^{-9} \text{ 1/Pa},$$

$$B_o = 1.75 \exp \left[-2.27 \times 10^{-9} (40 - 26) \times 10^6 \right] = 1.70 \text{ m}^3/\text{m}^3.$$

Answer With MATLAB. Note that this answer is continued from the previous example.

```

» B_ob = oil_form_vol_fact_Standng(R_sb, 0.98, 800, 150)
B_ob = 1.7515
» rho_g_100 = rho_g_Vazquez_and_Beggs(100e3, 0.98, 800, 15)
rho_g_100 = 0.8407
» c_o = compres_Vazquez_and_Beggs(40e6, R_
sb, rho_g_100, 800, 150)
c_o = 2.2732e-009
» B_o = oil_form_vol_fact_undersat(B_ob, c_o, 40e6, p_b)
B_o = 1.6970

```

Alternatively, the black oil properties can be computed directly as

```

» [B_g, B_o, R_s] = black_oil_Standng
(40e6, 200, 0.98, 800, 150)
B_g = 0
B_o = 1.6970
R_s = 200

```

B-2.10 Example B-3: Oil Viscosity. Consider the same situation as in Example B-2 in Section B-2.9 above.

Question

What is the oil viscosity μ_o at reservoir pressure and temperature?

Answer

With the aid of [Eq. B-10](#) the dead oil viscosity follows as

$$b = 5.693 - \frac{2.863 \times 10^3}{800} = 2.114, a = \frac{10^{2.114}}{(1.8 \times 150 + 32)^{1.163}} = 0.170,$$

$$\mu_{od} = 10^{-3} (10^{0.170} - 1) = 0.48 \times 10^{-3} \text{ Pa} \cdot \text{s}.$$

The oil viscosity at bubblepoint can then be computed with the aid of [Eq. B-11](#) as

$$c = 5.44 \left(\frac{200}{0.178} + 150 \right)^{-0.338} = 0.485,$$

$$\mu_{ob} = \left[10.72 \times 10^{-3} \times \left(\frac{200}{0.178} + 100 \right)^{-0.515} \right] 0.48^{0.485} = 1.93 \times 10^{-4} \text{ Pa} \cdot \text{s},$$

and the viscosity at reservoir pressure with [Eq. B-12](#) as

$$d = 7.2 \times 10^{-5} (40 \times 10^6)^{1.187} \exp(-11.513 - 1.30 \times 10^{-8} \times 40 \times 10^6) = 0.45,$$

$$\mu_o = 1.93 \times 10^{-4} \left(\frac{40 \times 10^6}{26.1 \times 10^6} \right)^{0.45} = 2.34 \times 10^{-4} \text{ Pa} \cdot \text{s}.$$

Answer With MATLAB

```

» mu_od = oil_visc_dead_B_and_R(800,150)
mu_od = 4.7851e-04
» mu_ob = oil_visc_sat_B_and_R(mu_od, 200)
mu_ob = 1.9252e-04
» mu_o = oil_visc_undersat_V_and_B(mu_ob,40e6,26.1e6)
mu_o = 2.3350e-04

```

Alternatively, the oil viscosity can be computed directly as

```

» mu_o = oil_viscosity(40e6,200,0.98,800,150)
mu_o = 2.3348e-04

```

B-3 Gas Correlations

B-3.1 Pseudoproperties. The concepts of critical pressure and temperature are

exactly defined for single components. However, for mixtures the concepts are approximations, as indicated by the use of the terms *pseudocritical* pressure and temperature. We can use the Sutton (1985) correlations to estimate the pseudocritical properties as function of the gas density:

$$p_{pc} = 5218 \times 10^3 - 734 \times 10^3 \rho_{g,sc} - 16.4 \times 10^3 \rho_{g,sc}^2, \quad \dots \quad (\text{B-13})$$

$$T_{pc,abs} = 94.0 + 157.9 \rho_{g,sc} - 27.2 \rho_{g,sc}^2 \quad \dots \quad (\text{B-14})$$

Note that the pseudocritical temperature is expressed in K. If a compositional description of the mixture is available, the pseudocritical properties can be determined more accurately with the aid of *mixing rules*. (For further information, consult the references mentioned in [Section 2.2](#).) The dimensionless *pseudoreduced* pressure p_{pr} and pseudoreduced temperature T_{pr} are defined as

$$p_{pr} = \frac{p}{p_{pc}}, \quad \dots \quad (\text{B-15})$$

$$T_{pr} = \frac{T_{abs}}{T_{pc,abs}}. \quad \dots \quad (\text{B-16})$$

B-3.2 Density. For single-phase gas flow the gas density follows directly from the nonideal gas law as

$$\rho_g = \frac{\rho_{g,sc}}{B_g} = \rho_{g,sc} \frac{p T_{sc,abs} Z_g}{p_{sc} T_{abs} Z} \quad \dots \quad (\text{B-17})$$

In the black oil model, where it is assumed that the gas composition does not change with pressure and temperature, the same expression can be used for the gas density in the two-phase region.

B-3.3 Viscosity. A well-known correlation for gas viscosity was presented in graphical form by Carr et al. (1954). A numerical approximation of this correlation was given by Dempsey (1965) and can be represented in two steps as

$$\mu_g = f(p_{pr}, T_{pr}) \times \mu_{g,p_{sc}}(M, T), \quad \dots \quad (\text{B-18})$$

where

$$f = \frac{1}{T_{pr}} \exp \left[\begin{array}{l} a_0 + a_1 p_{pr} + a_2 p_{pr}^2 + a_3 p_{pr}^3 + T_{pr} (a_4 + a_5 p_{pr} + a_6 p_{pr}^2 + a_7 p_{pr}^3) \\ + T_{pr}^2 (a_8 + a_9 p_{pr} + a_{10} p_{pr}^2 + a_{11} p_{pr}^3) + T_{pr}^3 (a_{12} + a_{13} p_{pr} + a_{14} p_{pr}^2 + a_{15} p_{pr}^3) \end{array} \right], \quad (\text{B-19})$$

with dimensionless coefficients as given in [Table B-6](#). The variable $\mu_{g,p_{sc}}$ is the viscosity at atmospheric pressure for which the correlation can be expressed as

$$\mu_{g,p_x} = b_0 + b_1 T + b_2 T^2 + b_3 M + b_4 TM + b_5 T^2 M + b_6 M^2 + b_7 TM^2 + b_8 T^2 M^2, \quad (\text{B-20})$$

with dimensional coefficients that are also given in [Table B-6](#). The relationships between the molar mass M , the molecular weight M_w , the gas density $\rho_{g,sc}$, and the gas specific gravity y_g are given in [Eqs. A-5](#) and [A-6](#). Correlations B-18 through B-20 are valid for the following ranges of parameter values:

Coefficient	Value	Coefficient	Value
a_0	$-2.462\ 118\ 20 \times 10^{-00}$	a_{13}	$-1.864\ 088\ 48 \times 10^{-01}$
a_1	$2.970\ 547\ 14 \times 10^{-00}$	a_{14}	$2.033\ 678\ 81 \times 10^{-02}$
a_2	$-2.862\ 640\ 54 \times 10^{-01}$	a_{15}	$-6.095\ 792\ 63 \times 10^{-04}$
a_3	$8.054\ 205\ 22 \times 10^{-03}$		
a_4	$2.808\ 609\ 49 \times 10^{-00}$	b_0	$1.112\ 319\ 13 \times 10^{-05}$
a_5	$-3.498\ 033\ 05 \times 10^{-00}$	b_1	$3.019\ 078\ 87 \times 10^{-08}$
a_6	$3.603\ 730\ 20 \times 10^{-01}$	b_2	$6.848\ 080\ 07 \times 10^{-12}$
a_7	$-1.044\ 324\ 13 \times 10^{-02}$	b_3	$-1.094\ 850\ 50 \times 10^{-04}$
a_8	$-7.933\ 856\ 84 \times 10^{-01}$	b_4	$-1.152\ 569\ 51 \times 10^{-07}$
a_9	$1.396\ 433\ 06 \times 10^{-00}$	b_5	$-2.913\ 973\ 49 \times 10^{-10}$
a_{10}	$-1.491\ 449\ 25 \times 10^{-01}$	b_6	$4.577\ 351\ 89 \times 10^{-04}$
a_{11}	$4.410\ 155\ 12 \times 10^{-03}$	b_7	$3.832\ 261\ 02 \times 10^{-07}$
a_{12}	$8.393\ 871\ 78 \times 10^{-02}$	b_8	$1.288\ 652\ 49 \times 10^{-09}$

Table B-6—Coefficients for the Dempsey (1965) approximation of the Carr et al. (1954) gas viscosity correlation.

$$1.0 \leq p_{pr} \leq 20, \quad 1.2 \leq T_{pr} \leq 3.0, \quad 16 \leq M \leq 110, \quad 4^\circ\text{C}(40^\circ\text{F}) \leq T \leq 204^\circ\text{C}(400^\circ\text{F}) \dots \quad (\text{B-21})$$

The Dempsey (1965) approximations have been programmed in MATLAB routines `gas_visc_atm_Dempsey.m` and `gas_visc_ratio_Dempsey.m`, with which [Figs. B-3 and B-4](#) were produced. The graphs are slightly different from the original graphs in Carr et al. (1954), but are accurate enough for most production engineering calculations. In case of the presence of nonhydrocarbon components in the gas, correction factors are needed for the computation of the viscosity at atmospheric pressure (for further information see the original publication of Carr et al. 1954).

[Fig. B-4](#) illustrates that the viscosity of hydrocarbon gases, unlike the viscosity of hydrocarbon liquids, increases with increasing temperature. This is because the increased molecular motion of the small gas molecules at higher temperatures reduces the freedom for molecules to move around. In hydrocarbon liquids this effect is counteracted by the increased freedom of the larger molecules resulting from stretching and disentanglement at higher temperatures.

B-3.4 Z Factor. Standing-Katz Correlation. The widely accepted correlation for the gas compressibility factor (Z factor) for a nonideal gas or gas mixture was presented by Standing and Katz (1942) in graphical form. Various numerical approximations have been developed over time, and an overview is presented in Takacs (1976). Below we reproduce the approximation by Dranchuk and Abu-Kasem (1975), which is given in the form of an implicit function in terms of Z :

$$f(Z) = Z - b_1 Z^{-1} - b_2 Z^{-2} + b_3 Z^{-5} - (b_4 Z^{-2} + b_6 Z^{-4}) \exp(-b_5 Z^{-2}) - 1.0 = 0, \dots \quad (\text{B-22})$$

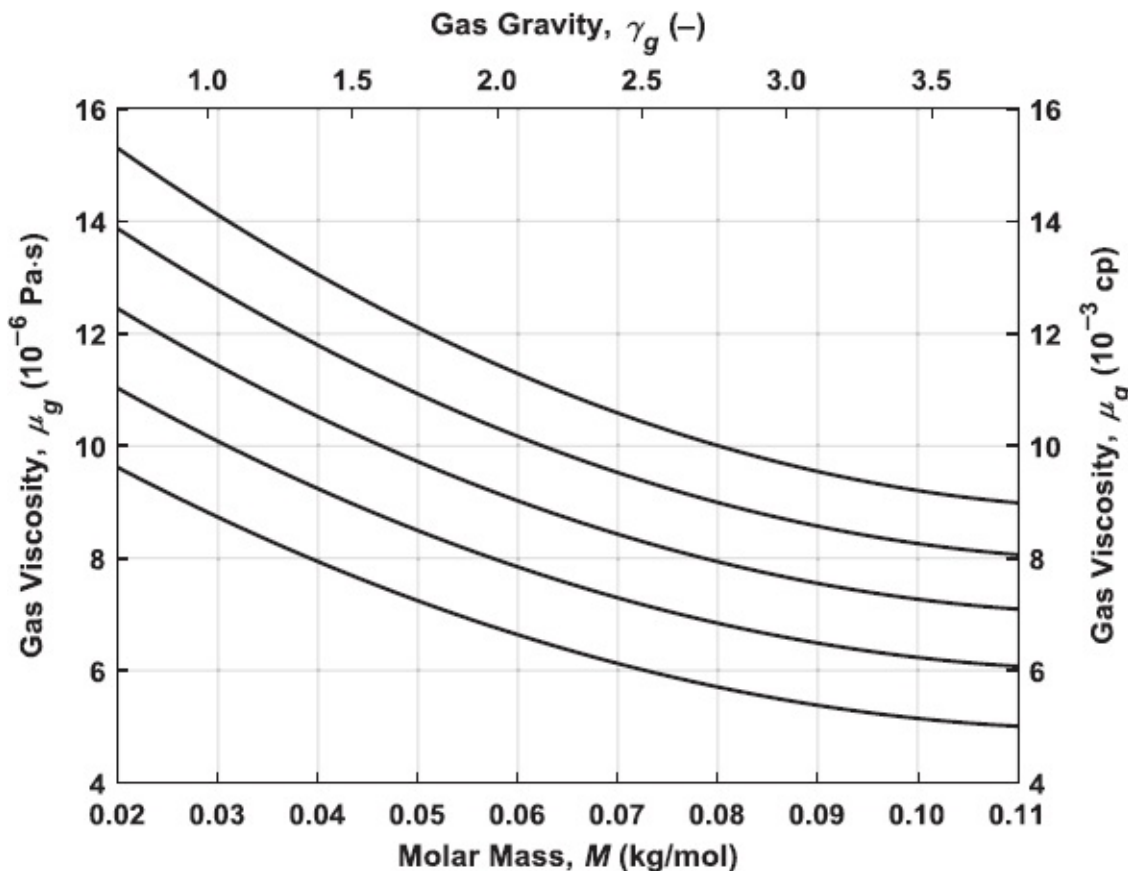


Fig. B-3—Gas viscosity at atmospheric pressure. Graph based on the Dempsey (1965) approximation of the Carr et al. (1954) correlation.

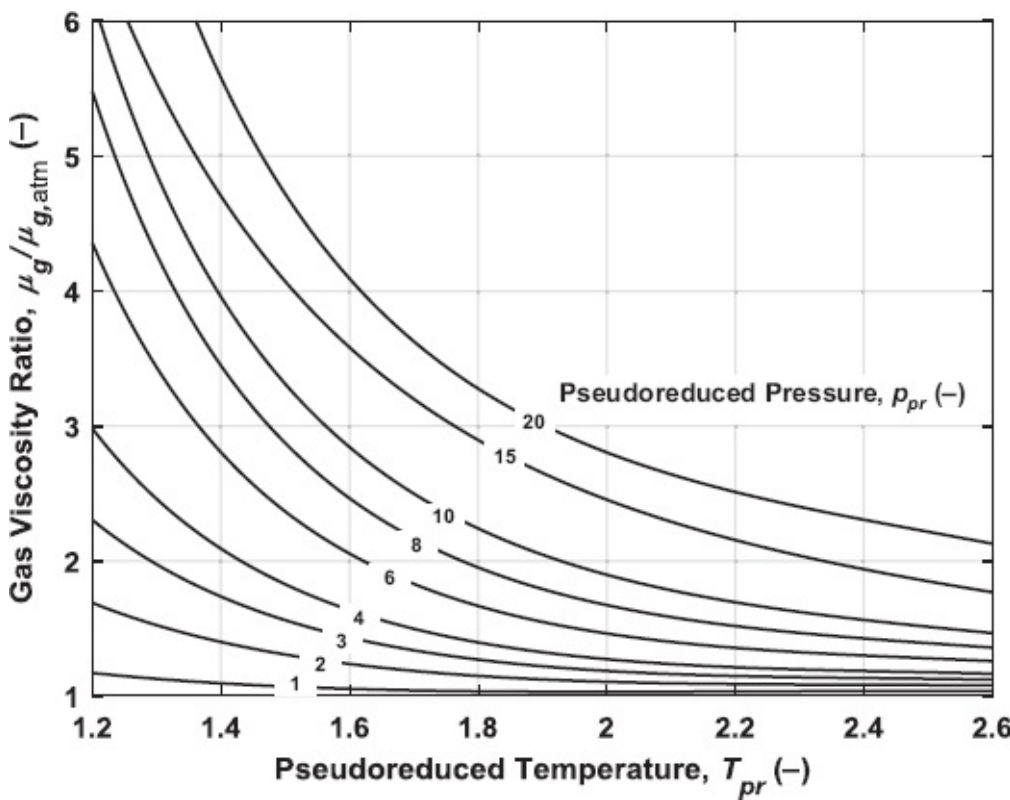


Fig. B-4—Gas viscosity ratio. Graph based on the Dempsey (1965) approximation of the Carr et al. (1954) correlation.

where

$$\begin{aligned} b_1 &= c \left(a_1 + \frac{a_2}{T_{pr}} + \frac{a_3}{T_{pr}^3} + \frac{a_4}{T_{pr}^4} + \frac{a_5}{T_{pr}^5} \right), \quad b_2 = c^2 \left(a_6 + \frac{a_7}{T_{pr}} + \frac{a_8}{T_{pr}^2} \right), \\ b_3 &= c^5 a_9 \left(\frac{a_7}{T_{pr}} + \frac{a_8}{T_{pr}^2} \right), \quad b_4 = c^2 \frac{a_{10}}{T_{pr}^3}, \quad b_5 = c^2 a_{11}, \quad b_6 = b_4 b_5. \end{aligned} \quad (\text{B-23})$$

Here, a_1 through a_{11} are coefficients as specified in [Table B-7](#), and c is a function of the dimensionless pseudoreduced pressure and temperature:

$$c = 0.27 \frac{p_{pr}}{T_{pr}}. \quad (\text{B-24})$$

Numerical Implementation. Because [Eq. B-22](#) is implicit in Z , it needs to be solved iteratively—e.g., with a Newton Raphson algorithm (see [Appendix D](#)), which we can write as

$$(Z)_{k+1} = (Z)_k - \frac{f(Z)_k}{f'(Z)_k}. \quad (\text{B-25})$$

Here k is the iteration counter, and $f'(Z)$ is the derivative of $f(Z)$ with respect to Z given by

$$f'(Z) = 1 + b_1 Z^{-2} + 2b_2 Z^{-3} - 5b_3 Z^{-6} + \\ (2b_4 Z^{-3} - 2b_4 b_5 Z^{-5} + 4b_6 Z^{-5} - 2b_5 b_6 Z^{-7}) \exp(-b_5 Z^{-2}) \dots \dots \dots \quad (\text{B-26})$$

Coefficient	Value
a_1	0.326 5
a_2	-1.070 0
a_3	-0.533 9
a_4	0.015 69
a_5	-0.051 65
a_6	0.547 5
a_7	-0.736 1
a_8	0.184 4
a_9	0.105 6
a_{10}	0.613 4
a_{11}	0.721 0

Table B-7—Coefficients for Dranchuk and Abu-Kasem (1975) approximation.

A convenient starting value for Z is provided by the explicit approximation of Papay quoted in Takacs (1976) as

$$Z = 1 - \frac{3.52 p_{pr}}{10^{0.9813} T_{pr}} + \frac{0.274 p_{pr}^2}{10^{0.8157} T_{pr}} \dots \dots \dots \quad (\text{B-27})$$

Eq. B-25 can then be used to obtain improved approximations to the desired accuracy. Alternatively, we can solve Eq. B-22 with the aid of the standard MATLAB function fzero (see Appendix D). The Dranchuk and Abu-Kasem approximation to the Standing and Katz correlation has been programmed in MATLAB functions `z_factor_DAK.m` and `z_factor_DAK_direct.m`. (Note that these functions take different arguments: `z_factor_DAK.m` requires p_{pr} and T_{pr} as input, whereas `z_factor_DAK_direct.m` requires, p , $\rho_{g,sc}$, and T_{abs} .) The range of validity for the approximation is

$$0.2 \leq p_{pr} \leq 30 \text{ and } 1.05 \leq T_{pr} \leq 3.0, \dots \dots \dots \quad (\text{B-28})$$

which is sufficient for most applications. **Figs. B-5.a and B-5.b** have been generated with the MATLAB routine, and they closely mimic the original graphical Z -factor chart as presented in Standing and Katz (1942).

B-3.5 Example B-4: Gas Properties. Consider the same situation as in Example B-1 in Section B-2.8.

Question

What are the gas formation volume factor B_g and the gas viscosity μ_g at reservoir pressure and temperature?

Answer

With the aid of the Sutton correlations (Eqs. B-13 and B-14) we find the pseudocritical properties of the fluid as

$$p_{pc} = 5218 \times 10^3 - 734 \times 10^3 \times 0.98 - 16.4 \times 10^3 \times 0.98^2 = 4.48 \times 10^6 \text{ Pa},$$

$$T_{pc,abs} = 94.0 + 157.9 \times 0.98 - 27.2 \times 0.98^2 = 223 \text{ K}.$$

The pseudoreduced pressure and temperature at the reservoir follow as

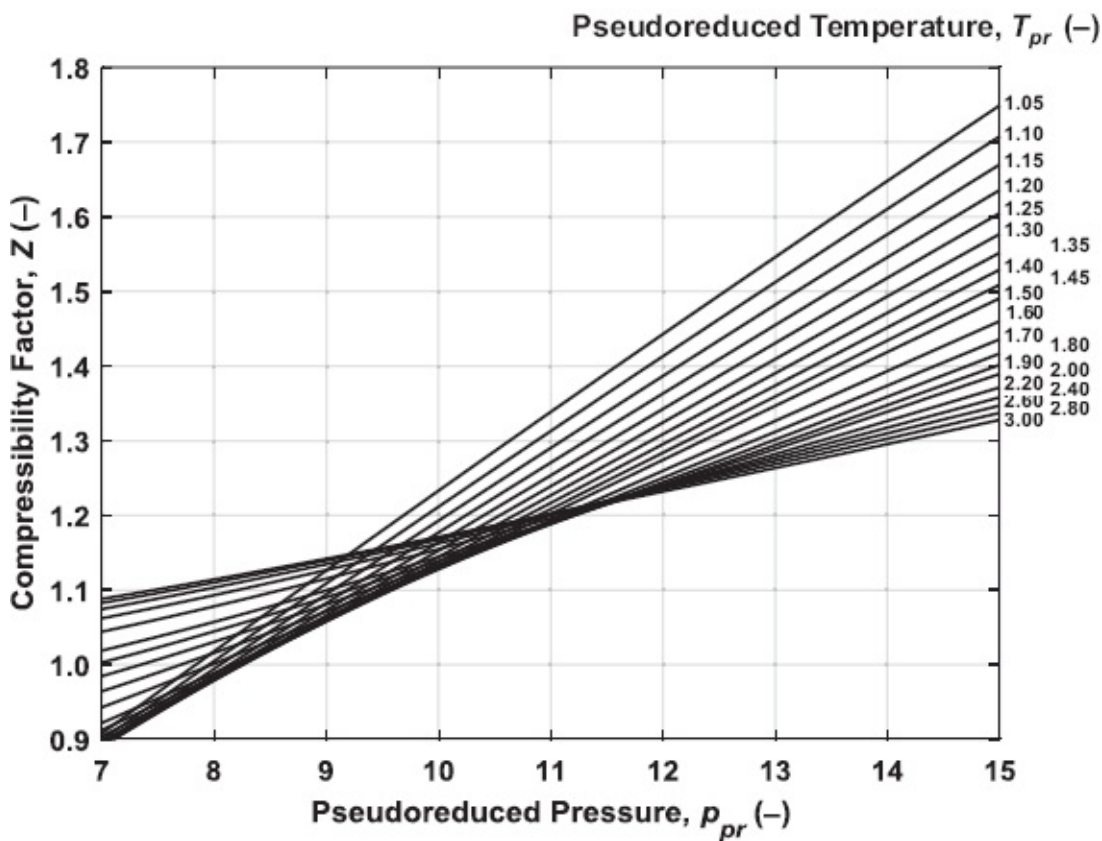
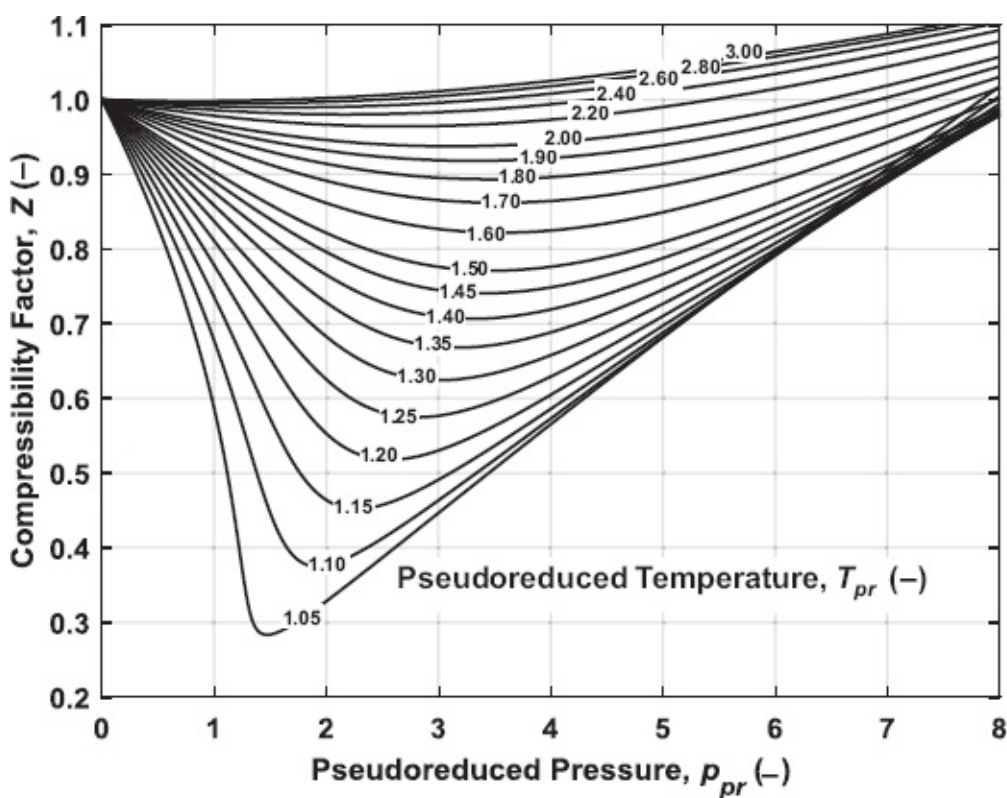
$$p_{R,pr} = \frac{p_R}{p_{pc}} = \frac{20 \times 10^6}{4.48 \times 10^6} = 4.46 \text{ and } T_{R,pr} = \frac{T_R}{T_{pc,abs}} = \frac{150 + 273.15}{223} = 1.90.$$

With the aid of the Standing-Katz chart in Fig. B-5, we find for the compressibility factor, $Z = 0.93$, and with the aid of Eq. 2.34 for the gas formation volume factor,

$$B_g = \frac{100 \times 10^3 \times (150 + 273.15) \times 0.93}{20 \times 10^6 \times (15 + 273.15) \times 1.00} = 6.8 \times 10^{-3} \text{ m}^3/\text{m}^3.$$

The molar mass of the gas follows from Eq. A-5 as

$$M = 23.55 \times 10^{-3} \times 0.98 = 23.08 \times 10^{-3} \text{ kg/mol.}$$



Figs. B-5a and B-5b—Compressibility factor Z as function of pseudoreduced pressure p_{pr} and pseudoreduced temperature T_{pr} . The graph is based on the Dranchuk and Abu Kasem (1975) approximation of the Standing and Katz (1942) correlation.

With the aid of Figs. B-3 and B-4 we now find for the gas viscosity at atmospheric pressure, $\mu_{g,p_c} = 1.3 \times 10^{-5}$ Pa·s, and for the viscosity ratio, $f = 1.4$. The viscosity at reservoir pressure then follows with Eq. B-18 as

$$\mu_g = 1.4 \times 1.3 \times 10^{-5} = 1.8 \times 10^{-5} \text{ Pa}\cdot\text{s}.$$

Answers With MATLAB. The gas formation volume factor is computed by

```
» p_pc = pres_pseu_crit_Sutton(0.98)
p_pc = 4.4829e+006
» T_pc_abs = temp_pseu_crit_Sutton(0.98)
T_pc_abs = 222.6191
» p_R_pr = 20e6 / p_pc
p_R_pr = 4.4614
» T_R_pr = (150 + 273.15) / T_pc_abs
T_R_pr = 1.9008
» Z = Z_factor_DAK(p_R_pr,T_R_pr)
Z = 0.9284
» B_g = gas_form_vol_fact(20e6,150+273.15,Z)
B_g = 0.0068
```

Alternatively, the gas formation volume factor can be computed directly as

```
» B_g = gas_form_vol_fact_direct(20e6,0.98,150+273.15)
B_g = 0.0068
```

Gas viscosity is found by

```
» M = from_kg_per_m3_to_molar_mass(0.98)
M = 0.0231
» mu_g_p_sc = gas_visc_atm_Dempsey(M,150)
mu_g_p_sc = 1.3516e-05
» f = gas_visc_ratio_Dempsey(p_R_pr,T_R_pr)
f = 1.3732
» mu_g = f * mu_g_p_sc
mu_g = 1.8561e-05
```

Gas viscosity can also be computed directly as

```
» mu_g = gas_viscosity(20e6,0.98,150)
mu_g = 1.8561e-05
```

B-4 Water Properties

B-4.1 Water Formation Volume Factor. Fig. B-6 displays the water formation volume factor for a range of pressures and temperatures, based on a correlation by McCain (1990). It is clear that the corresponding volumetric changes in water are much smaller than those in oil (refer to Fig. 2.6). In the examples and questions in this book we therefore simply use a water formation volume factor equal to unity.

B-4.2 Water Density. The water density mainly depends on the amount of dissolved solids it contains. For most formation waters this is primarily NaCl, which may reach such high concentrations that formation water is often referred to as *brine*. Fresh water has a density of 999 kg/m^3 (62.4 lbm/ft^3) at standard conditions, whereas NaCl-saturated brine has a density of 1200 kg/m^3 (75 lbm/ft^3).

B-4.3 Water Viscosity. Water viscosity depends on temperature, salinity, and pressure, but to a much lesser extent than oil viscosity. In the examples and questions in this book we use a constant value corresponding to a temperature of approximately 80°C (176°F): $\mu_w = 0.35 \times 10^{-3} \text{ Pa}\cdot\text{s}$ (0.35 cp).

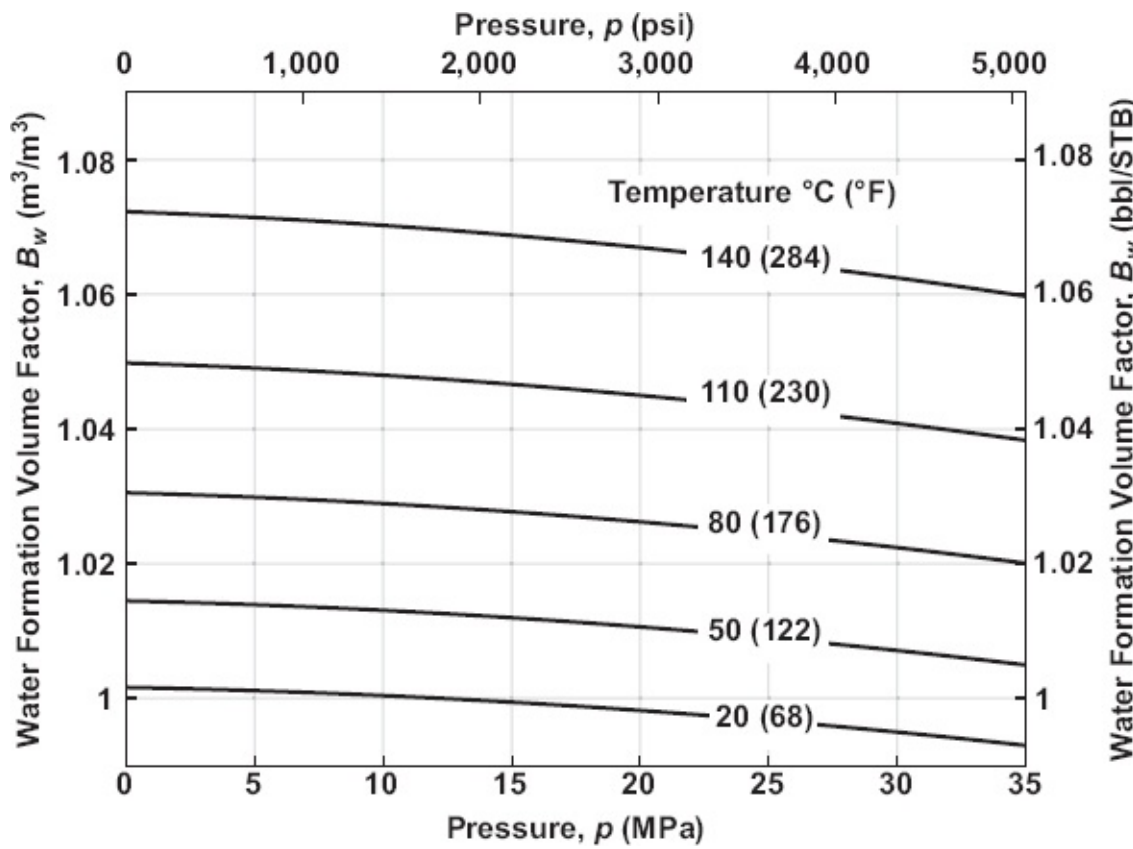


Fig. B-6—Water formation volume factor.

Appendix C

Wellbore Surveying

C-1 Coordinates

The position of a well is usually described in rectangular coordinates, which are referred to as *northing*, *easting*, and *true vertical depth* (TVD) (see [Fig. C-1](#)). These coordinates can be obtained through evaluating a survey file that contains triplets of measured survey data (*survey points*): *along-hole depth* (AHD), *inclination* (the angle with the vertical), and *azimuth* (the angle with north). The AHD is sometimes referred to as *measured depth* (MD). The measurements can be made with a variety of special surveying instruments.

C-2 Survey Evaluation

Consider a set of measured survey data consisting of triplets i of along-hole depth s_i , inclination α_i , and azimuth β_i . Various algorithms exist to reconstruct an estimate of the northing, easting, and TVD corresponding to each triplet. Here, we discuss the most commonly used algorithm known as the *minimum curvature method* or *circular arc method*. The algorithm was first described by Taylor and Mason (1972) and almost at the same time by Zaremba (1973), using goniometric functions. Here, we present an alternative derivation using vector notation.

The survey file evaluation starts at surface and proceeds downward according to a marching algorithm that can be derived as follows. We define orthonormal base vectors $(\mathbf{e}_x, \mathbf{e}_y, \mathbf{e}_z)$ along x , y , and z axes that correspond to north, east, and TVD as depicted in [Fig. C-2](#):

$$\begin{bmatrix} \mathbf{e}_x & \mathbf{e}_y & \mathbf{e}_z \end{bmatrix} = \begin{bmatrix} 1 & 0 & 0 \\ 0 & 1 & 0 \\ 0 & 0 & 1 \end{bmatrix}. \dots \quad (C-1)$$

We define the position of survey points S_i with the aid of position vectors \mathbf{x}_i , and the orientation of the borehole centerline at the survey points with the aid of unit direction vectors \mathbf{e}_i . To simplify the figure, but without loss of generality, we have chosen the position of S_i in [Fig. C-2](#) to be on the z -axis. With the aid of the figure, it can be verified that direction vector \mathbf{e}_i lies in a vertical plane A that is at an angle β_i with respect to the x -axis. We can now write the components of direction vector \mathbf{e}_i as a linear combination of a horizontal direction vector \mathbf{e}_h , which lies in plane A , and the vertical direction vector \mathbf{e}_z :

$$\mathbf{e}_i = \mathbf{e}_h \sin \alpha_i + \mathbf{e}_z \cos \alpha_i \dots \dots \dots \quad (C-2)$$

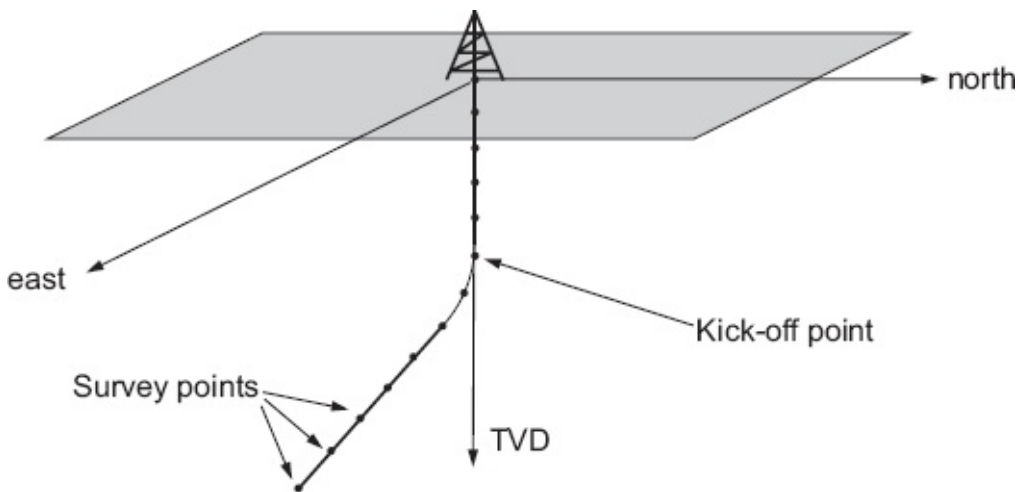


Fig. C-1—Deviated well with survey points and a kick-off point (i.e., where the well trajectory changes from vertical to deviated).

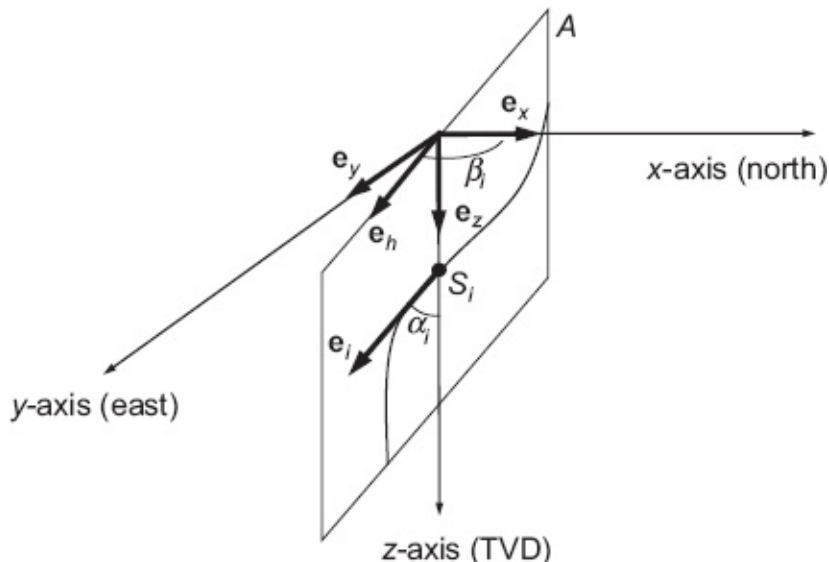


Fig. C-2—Well trajectory in an (x, y, z) coordinate system with unit direction vectors \mathbf{e}_x , \mathbf{e}_y , and \mathbf{e}_z . Direction vector \mathbf{e}_i is tangential to the wellbore axis in survey point S_i , lies in a vertical plane A , and is at an angle α_i (the wellbore inclination) with the vertical. Plane A is at an angle β_i (the wellbore azimuth) with the x -axis.

Direction vector \mathbf{e}_h can be expressed in terms of \mathbf{e}_x and \mathbf{e}_y according to

$$\mathbf{e}_h = \mathbf{e}_x \cos \beta_i + \mathbf{e}_y \sin \beta_i, \dots \dots \dots \quad (C-3)$$

and combination of Eqs. C-1 to C-3 gives us the components of \mathbf{e}_i as

$$\mathbf{e}_i = \begin{bmatrix} \sin \alpha_i \cos \beta_i \\ \sin \alpha_i \sin \beta_i \\ \cos \alpha_i \end{bmatrix}. \dots \dots \dots \quad (C-4)$$

It can be verified that \mathbf{e}_i is a unit vector, given that the squares of its components add up to unity.

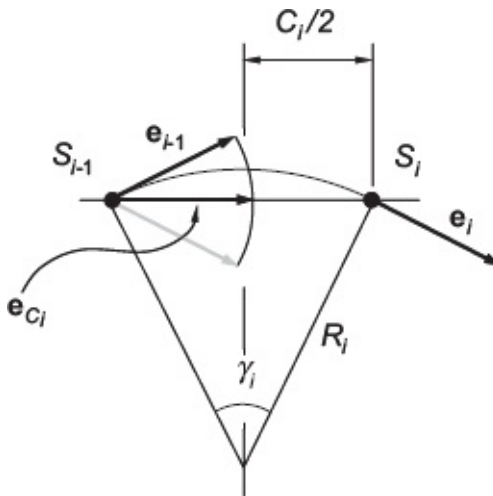


Fig. C-3—Quantities involved in survey evaluation with the minimum curvature method.

Next, we use [Fig. C-3](#) and a well-known property of the inner product of two vectors to derive that $\mathbf{e}_{i-1} \cdot \mathbf{e}_i = \cos y_i$ and therefore that

$$\gamma_i = \cos^{-1}(\mathbf{e}_{i-1} \cdot \mathbf{e}_i) \dots \dots \dots \quad (C-5)$$

The angle y_i is known as the *dogleg* between the two survey points S_{i-1} and S_i . Furthermore, the unit direction vector along the chord C_i from S_{i-1} to S_i can be written as

$$\mathbf{e}_{C_i} = \frac{\mathbf{e}_{i-1} + \mathbf{e}_i}{|\mathbf{e}_{i-1} + \mathbf{e}_i|} \dots \dots \dots \quad (C-6)$$

If we define the increment in AHD as

$$\Delta s_i = s_i - s_{i-1}, \dots \dots \dots \quad (C-7)$$

we can write for the radius of curvature R_i :

$$R_i = \frac{\Delta s_i}{\gamma_i}, \dots \dots \dots \quad (C-8)$$

where γ_i should be expressed in radians. With the aid of [Fig. C-3](#) we can now derive that

$$\sin\left(\frac{\gamma_i}{2}\right) = \frac{C_i}{2R_i}, \dots \dots \dots \quad (C-9)$$

and therefore, using the results of Eqs. C-8 and C-9, we find that

$$C_i = \frac{2\Delta s_i}{\gamma_i} \sin\left(\frac{\gamma_i}{2}\right) \dots \dots \dots \quad (\text{C-10})$$

Initialization:

$$\mathbf{e}_0 = \begin{bmatrix} \sin \alpha_0 & \cos \beta_0 \\ \sin \alpha_0 & \sin \beta_0 \\ \cos \alpha_0 \end{bmatrix}$$

For $i = 1 \dots n$, do:

Step	Equation	Step	Equation
1	$\mathbf{e}_i = \begin{bmatrix} \sin \alpha_i & \cos \beta_i \\ \sin \alpha_i & \sin \beta_i \\ \cos \alpha_i \end{bmatrix}$	4	$\gamma_i = \cos^{-1}(\mathbf{e}_{i-1} \cdot \mathbf{e}_i)$
2	$\mathbf{e}_{c_i} = \frac{\mathbf{e}_{i-1} + \mathbf{e}_i}{\ \mathbf{e}_{i-1} + \mathbf{e}_i\ }$	5	$C_i = \frac{2\Delta s_i}{\gamma_i} \sin\left(\frac{\gamma_i}{2}\right)$
3	$\Delta s_i = s_i - s_{i-1}$	6	$\mathbf{x}_i = \mathbf{x}_{i-1} + C_i \mathbf{e}_{c_i}$

Table C-1 — Minimum curvature algorithm.

The unknown position vector \mathbf{x}_i of survey point S_i can then be obtained explicitly from the known vector \mathbf{x}_{i-1} and the measured survey data as

$$\mathbf{x}_i = \mathbf{x}_{i-1} + C_i \mathbf{e}_{c_i} \dots \dots \dots \quad (\text{C-11})$$

The minimum curvature algorithm as represented by Eqs. C-1 through C-11 is summarized in [Table C-1](#).

The parameter $\gamma_i/\Delta s_i$ is a measure of the local curvature of the borehole and is known as the *dogleg severity* (DLS). Usually the DLS is expressed in degrees/30 m or degrees/100 ft. High dogleg severities are normally not desirable because they give rise to high contact forces between the drillstring and the borehole wall and thereby cause high drillstring drag and torque. Furthermore, high dogleg severities may also cause problems in running the casing in the hole, and in the cased section of the borehole high contact forces may lead to severe casing wear. A typical maximum allowed dogleg severity is on the order of 3°/30 m.

C-3 Numerical Implementation

A MATLAB file, `evaluate_survey.m`, is available to perform a minimum curvature calculation for a given survey file with AHD, inclination, and azimuth values. The survey file should be available in the form of a text file (ASCII file) without comments (see, e.g., the text file `deviated_well_1.txt`). For wellbore flow analysis a survey evaluation is not necessary because it suffices to supply the AHD and inclination

values (see `example_traverse_deviated.m`). However, to interpret the pressure profile along the well, it is usually helpful to visualize the well path. To do so, projections of the well in three planes and a 3D view can be created with the aid of `plot_survey.m`. For an example of how to use this function, see `example_survey.m`. The corresponding plots have been depicted in **Fig. C-4**.

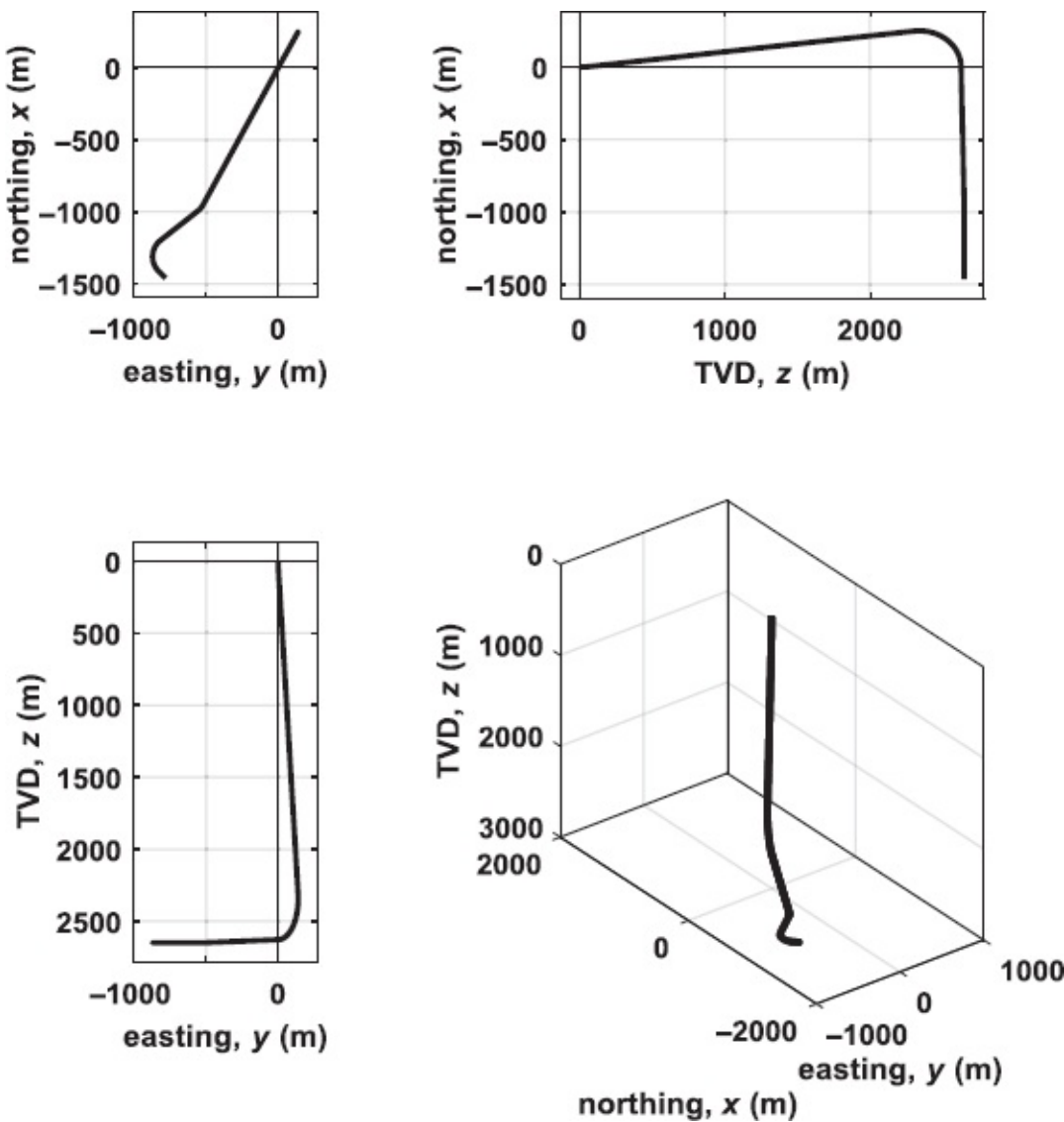


Fig. C-4—Projections and 3D view.

Appendix D

Numerical Methods

D-1 Root Finding

Consider a function $f(x) = 0$ that has at least one root (zero value) in the interval $D = (-\infty, \infty)$, as shown in [Fig. D-1](#). We assume that the function is implicit; i.e., we assume that it is not possible to obtain an explicit expression for the value of x that makes $f(x)$ equal to zero. Therefore we need an iterative procedure to approximate the root, for which various choices are available. Note that root finding is closely related to optimization because finding an optimum of a function (i.e., a minimum or a maximum) corresponds to finding a root of the first derivative of that function. (The requirement that the first derivative of a function is zero in an optimum is a necessary condition. Sufficient conditions also involve higher derivatives.)

D-1.1 Bisection. A very simple approach is the bisection method. It requires two starting values x_0 and x_1 with corresponding function values $f(x_0)$ and $f(x_1)$ of opposite sign, such that the solution is bracketed by the starting values (see [Fig. D-1a](#)). The algorithm proceeds by splitting the interval $I_1 = [x_0, x_1]$ into two equal-length intervals of which the one that brackets the solution is selected as the next interval I_2 . The splitting and selection procedure continues until the difference between the function values is reduced to below a predefined tolerance. The method is guaranteed to converge as long as $f(x)$ is continuous between the starting values. However, this method is slow. The error e_k , which is the maximum possible absolute difference between the true root and the most recent estimate x_k , $k = 2, 3, \dots$, is halved every iteration step, which implies that the method converges linearly.

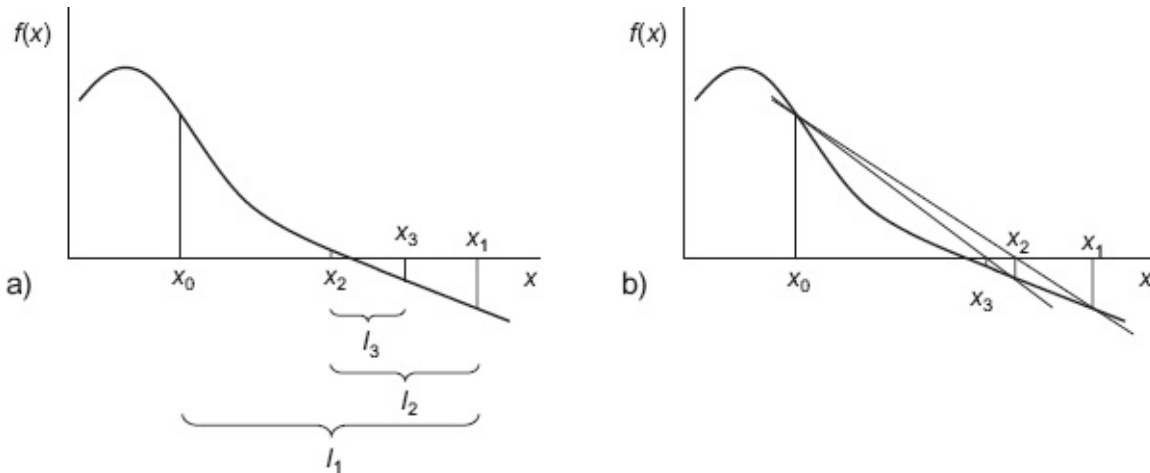


[Fig. D-1a](#)—Two steps of the bisection method; [Fig. D-1b](#)—Two steps of the regula falsi method.

D-1.2 Regula Falsi. The regula falsi method also uses two starting values that bracket the solution. It reduces the size of the bracketing interval I_k every iteration step $k = 2, 3, \dots$ by replacing one of the endpoints of the interval by the point x_i corresponding to the intersection of the x -axis with the line between the points $[x_{k-1}, f(x_{k-1})]$ and $[x_k, f(x_k)]$, as shown in Fig. D-1b. It can be shown that the method converges faster than linearly, but not as fast as the Newton-Raphson method described in the next section.

D-1.3 Newton-Raphson Iteration. The Newton-Raphson method requires that $f(x)$ has a continuous first and second derivative, which implies that the first derivative is smooth and uniquely defined for each value of $x \in D$. Moreover, it is required that the first derivative can actually be computed, either analytically or numerically (i.e., with a finite difference approximation), as opposed to the derivative-free bisection and regula falsi methods. We start the iteration with a first guess x_0 . To improve the estimate, we compute the slope of $f(x)$ —i.e., the derivative $f'(x)$ —in $x = x_0$, which can also be expressed as

$$f'(x_0) = -\tan \alpha = -\frac{f(x_0)}{x_1 - x_0}, \quad \dots \quad (\text{D-1})$$

where α and x_1 have been defined in Fig. D-2a. This expression can be rewritten as

$$x_1 = x_0 - \frac{f(x_0)}{f'(x_0)}, \quad \dots \quad (\text{D-2})$$

which gives us a new estimate x_1 for the root. This procedure, called *Newton-Raphson iteration*, can be generalized by writing

$$x_{k+1} = x_k - \frac{f(x_k)}{f'(x_k)}, \quad \dots \quad (\text{D-3})$$

Eq. D-3 can then be applied until the difference $(x_{k+1} - x_k)$ has been reduced to below a specified value. The derivative $f'(x)$ should preferably be computed analytically, but it may also be obtained with the aid of numerical perturbation:

$$f'(x) = \frac{df}{dx} \approx \frac{\Delta f}{\Delta x} = \frac{f(x + \Delta x) - f(x)}{\Delta x}. \quad \dots \quad (\text{D-4})$$

The choice of the perturbation size Δx is not always trivial. In theory, the smaller the perturbation, the closer the difference $\Delta f/\Delta x$ approaches the differential df/dx , but roundoff errors in a computer implementation may ruin the estimate if the perturbation chosen is too small.

Convergence of the Newton-Raphson process is usually fast and can be shown to be quadratic if the initial estimate is close enough to the root. However, the process

may get in trouble in several situations. It obviously fails for values of $f(x)$ equal to zero (see [Fig. D-2b](#)). A more subtle breakdown occurs when the root is located closely to a change in sign of the first derivative, in which case the process may end up in an endless loop (see [Fig. D-2c](#)). Another type of problem may occur if $f(x)$ has multiple roots in D , in which case the process may show convergence to a root that was not intended to be found. Various controls on the iteration process may be introduced to counteract these problems— e.g., allowing a maximum change in x in each iteration step, or restarting the process with a reduced change in x when the iteration fails to converge in a predefined number of steps. Prior inspection of the nature of the function $f(x)$ before using the Newton-Raphson process may help to reduce the chance of convergence problems.

D-1.4 Multivariable Root Finding. The Newton-Raphson method can easily be extended to multiple variables. Consider a system of n nonlinear algebraic equations in terms of n unknowns:

$$\begin{cases} f_1(x_1, x_2, \dots, x_n) = 0, \\ f_2(x_1, x_2, \dots, x_n) = 0, \\ \vdots \\ f_n(x_1, x_2, \dots, x_n) = 0. \end{cases} \quad \dots \quad (D-5)$$

Using matrix-vector notation, the system can be written in compact form as

$$\mathbf{f}(\mathbf{x}) = \mathbf{0}. \quad \dots \quad (D-6)$$

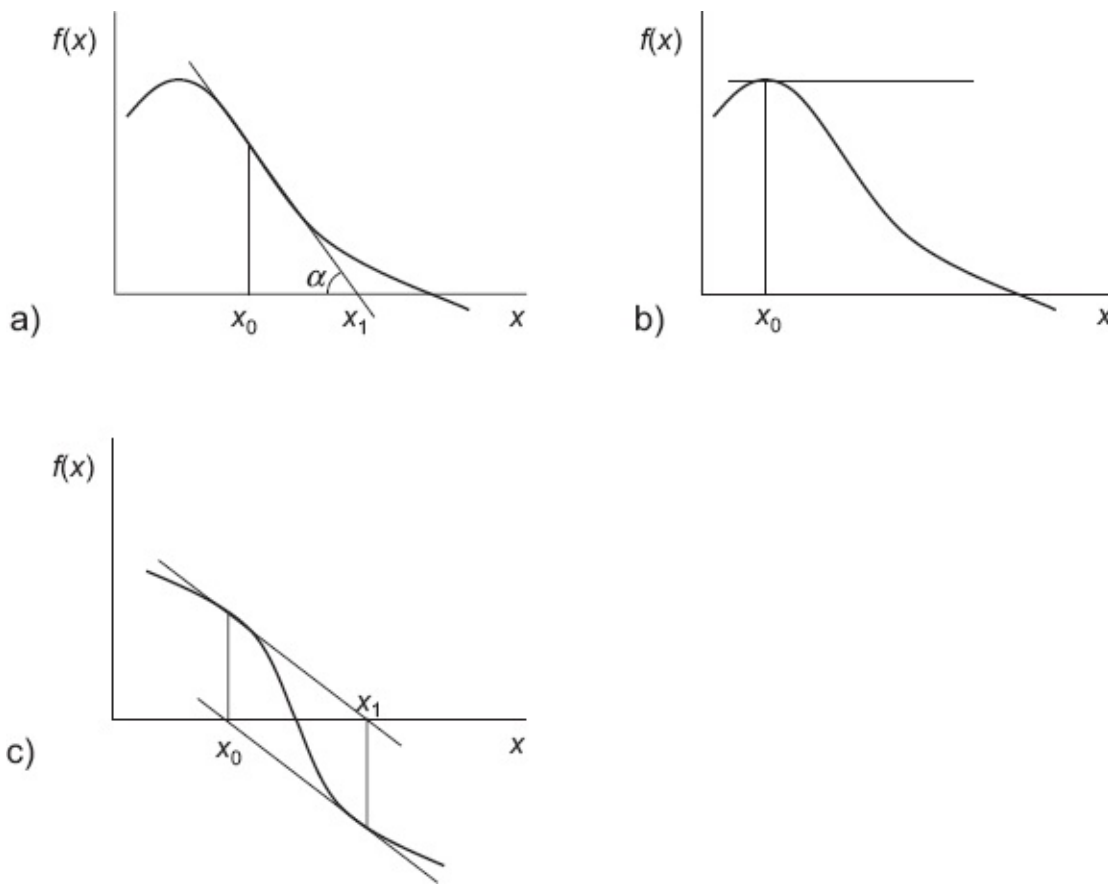


Fig. D-2a—Principle of Newton Raphson iteration; **Fig. D-2b**—Convergence failure caused by a zero value of the derivative in x_0 ; **Fig. D-2c**—Convergence failure caused by an endless loop.

The multivariable equivalent to the single-variable Newton-Raphson update (Eq. D-3) becomes

$$\mathbf{x}_{k+1} = \mathbf{x}_k - \left(\frac{\partial \mathbf{f}(\mathbf{x}_k)}{\partial \mathbf{x}_k} \right)^{-1} \mathbf{f}(\mathbf{x}_k), \dots \quad (\text{D-7})$$

where

$$\frac{\partial \mathbf{f}(\mathbf{x})}{\partial \mathbf{x}} = \begin{bmatrix} \frac{\partial f_1}{\partial x_1} & \frac{\partial f_1}{\partial x_2} & \dots & \frac{\partial f_1}{\partial x_n} \\ \frac{\partial f_2}{\partial x_1} & \frac{\partial f_2}{\partial x_2} & \dots & \frac{\partial f_2}{\partial x_n} \\ \vdots & \vdots & \ddots & \vdots \\ \frac{\partial f_n}{\partial x_1} & \frac{\partial f_n}{\partial x_2} & \dots & \frac{\partial f_n}{\partial x_n} \end{bmatrix}. \dots \quad (\text{D-8})$$

Eq. D-8 is known as the *Jacobian matrix*, or *Jacobian* for short. Just as in the single-variable case, the derivatives should preferably be computed analytically but may also be obtained through numerical perturbation.

In practice, one normally does not actually compute the inverse of the Jacobian but uses the computationally more attractive alternative

$$\frac{\partial \mathbf{f}(\mathbf{x}_k)}{\partial \mathbf{x}_k} (\mathbf{x}_{k+1} - \mathbf{x}_k) = -\mathbf{f}(\mathbf{x}_k), \dots \quad (\text{D-9})$$

which involves solving a system of n linear equations to find the unknown error vector ($\mathbf{x}_{k+1} - \mathbf{x}_k$). In MATLAB we can use the *backslash operator* \ to perform this computation. Using the variable **J** to indicate the Jacobian, we can then write

$$\mathbf{x}(k+1) = \mathbf{x}(k) - \mathbf{J} \backslash \mathbf{f}$$

The iterations are repeated until some convergence criterion is met; this is usually expressed in terms of a norm of the error vector; e.g.,

$$\|\mathbf{x}\| = \sqrt{x_1^2 + x_2^2 + \dots + x_n^2} < \varepsilon \quad (\text{D-10})$$

where ε is small. Alternatively, convergence may be defined in terms of the norm of **f**. Just like in the 1D case, there are various ways in which the iteration procedure may fail. In addition, the Jacobian may be ill-conditioned, and further controls on the iteration process may therefore be required to achieve a robust multivariate Newton Raphson procedure.

D-1.5 Standard MATLAB Functions. Single-Variable Root Finding. Often a good alternative to programming a root-finding algorithm is to simply use a standard MATLAB function. To find the root of a single-variable function, one can use the MATLAB function fzero, which makes use of bisection and other derivative-free optimization methods (see MATLAB 2017). For example, to find the root of $y = \cos(x)$ nearest to an initial guess $x = 1.5$, the syntax is

```
>> fzero(@cos, 1.5)
```

which produces the result

```
ans = 1.5708
```

The symbol @ in front of the function cos serves to specify a *function handle*—i.e., a reference to a function that may be passed as an argument to another function (in this case the function handle @cos is passed to the function fzero). Instead of making an initial guess, it is also possible to specify an interval bracketing the solution. Thus, e.g., to find the root of cos(x) inside the interval [1, 2], we write:

```
>> fzero(@cos, [1 2])
```

```
ans = 1.5708
```

Alternatively one can write

```
>> fzero(@(x) cos(x), [1 2])
```

which produces the same result. In this latter case cos(x) is defined as an

anonymous function with a single argument x as specified by the statement $@(x)$ preceding the function. Anonymous functions can be used to create simple functions in MATLAB without writing an m-file. The general syntax is $\text{fname} = @(arglist) \text{expr}$, where arglist is a comma-separated list of arguments and expr is the function definition. For example, the statement $\text{test} = @(x,y) x^2+y^2$ defines the anonymous function test with arguments x and y , which may be called inside another function. The statement $\text{sqrt}(\text{test}(3,4))$ therefore results in the answer 5. Note that the symbol $@$ now has a different role. In the same way we may call fzero with an ordinary function—i.e., a function defined in an m-file—which may then also contain additional parameters. If, e.g., we want to find the zeros of $y = \cos(x) - a$ for different values of parameter a , we can define y in an m-file as

```
function y = example(x,a)
y = cos(x) - a
```

and then call fzero after first specifying a value for a :

```
>> a = 0.1;
>> fzero(@(x) example(x,a), [1 2])
ans = 1.4706
```

Multivariable Root Finding. To find the roots of a vector-valued multivariable function (i.e., a vector of functions that each depend on multiple variables), one can use the MATLAB function fsolve , which is part of the MATLAB Optimization Toolbox. It performs multivariable optimization (root finding) using a variety of optimization algorithms that are hidden to the user. In this sense it is a multidimensional version of fzero (see MATLAB 2017). The syntax is also partly an extension of the syntax for fzero . For example, to find the root of the vector-valued function $[y_1 \ y_2] = [\cos(x_1) - a \ \sin(x_2) + b]$ for different values of parameters a and b nearest to an initial guess $[x_1 \ x_2] = [1.5 \ 0.5]$, we can define y in an m-file as

```
function y = example(x,a,b)
y(1) = cos(x(1)) - a;
y(2) = sin(x(2)) + b;
```

and then call fsolve after first specifying values for a and b :

```
>> a = 0.1;
>> b = 0.2;
>> x start = [0,0]; % starting values for x(1) and x(2)
>> fsolve(@(x) example(x,a,b), x start)
ans = 1.4706 -0.20136
```

Note that in this simple example each of the function vector elements y_1 and y_2 depends on just one variable—i.e., x_1 and x_2 , respectively. However, it is possible to

specify n function vector elements that can each be a function of up to n variables. Consult the online MATLAB help function for more information on the use of `fsove`.

D-2 Differential Equations

D-2.1 Initial Value Problems. All steady-state pressure drop equations for pipeline or wellbore flow, such as [Eqs. 3.24](#) or [3.33](#), can be expressed as

$$\frac{dp}{ds} = g(s, p), \dots \quad (\text{D-11})$$

where g is a known nonlinear function of s and p . [Eq. D-11](#) is a first-order ordinary differential equation that needs one boundary condition specifying a certain value \hat{p} for the pressure at a certain point \hat{s} along the pipeline or the well:

$$s = \hat{s} : p = \hat{p}. \dots \quad (\text{D-12})$$

To obtain the pressure p at any point along the pipeline, we can integrate [Eq. D-11](#) starting from the boundary condition ([Eq. D-12](#)):

$$p = \hat{p} + \int_{\hat{s}}^s g(s, p) ds. \dots \quad (\text{D-13})$$

This kind of equation is often used to describe problems that depend on time (instead of on distance s , as in our case), in which case the boundary condition is usually specified at the start of the time interval. Therefore the boundary condition is often referred to as an *initial condition*, and the problem as an *initial valueproblem*.

D-2.2 Numerical Integration. Generally, the integral in [Eq. D-13](#) cannot be solved analytically but needs to be evaluated through numerical integration. The simplest approach is to discretize [Eq. D-11](#) by replacing the differential dp/ds by a difference $\Delta p/\Delta s$ and to rewrite the result as

$$\Delta p = g(s, p) \Delta s. \dots \quad (\text{D-14})$$

This gives us an algorithm to compute an approximate new value p_{k+1} at s_{k+1} from a known value p_k at s_k :

$$p_{k+1} = p_k + \Delta p = p_k + g(s_k, p_k) \Delta s, \dots \quad (\text{D-15})$$

where $\Delta s = s_{k+1} - s_k$ and $g(s_k, p_k)$ are a shorthand notation to indicate the evaluation of function $g(s, p)$ at $s = s_k$. More formally, the same result is obtained by using a Taylor expansion for p at s_k ,

$$p_{k+1} = p_k + \left[\frac{dp}{ds} \right]_k \Delta s + \frac{1}{2} \left[\frac{d^2 p}{ds^2} \right]_k (\Delta s)^2 + \dots \dots \dots \quad (D-16)$$

and maintaining only the first-order term. This also illustrates that the truncation error in Eq. D-15, known as an *explicit first-order Euler scheme*, is of the order of $(\Delta s)^2$.

Although conceptually quite simple, the first-order Euler scheme is not very efficient for use in wellbore flow calculations, and so alternative algorithms, with a much smaller error for the same step size, should be applied. A popular class of integration algorithms are the Runge-Kutta routines, which use multiple evaluations of the function $g(s,p)$ on the interval Δs , instead of only a single evaluation at the beginning of the interval as in the first-order Euler scheme. Especially in combination with an automated strategy to adapt the step size in order to achieve a predefined accuracy, they are very powerful. Many other schemes have been developed that may have a superior computational performance or accuracy depending on the nature of the function $g(s,p)$ (see, e.g., Press et al. 2007).

For our purpose the fourth-order Runge-Kutta scheme with variable step size that is readily available in MATLAB provides a fit-for-purpose solution. A simple check on the accuracy of the numerical integration of wellbore or pipeline pressure drop computations can be made by repeating the integration in the opposite direction. For example, after computing the flowing tubinghead pressure (FTHP) through bottom-up integration starting from a known FBHP, the FBHP is recalculated through top-down integration starting from the FTHP. The difference between the two flowing bottom-hole pressure (FBHP) values forms a good indication of the accuracy of the numerical integration. Typically a difference of less than 1% of the total pressure drop would be acceptable, although often a much better performance can be achieved. Note, however, that although a small difference is a necessary condition, it is not a sufficient one.

D-2.3 Numerical Implementation. The fourth-order Runge-Kutta routine with variable step size in MATLAB is named `ode45`. To compute a pressure $p = p_{out}$, at $s = s_{out}$ starting from a known value $p = \hat{p}_{in}$ at $s = \hat{s}_{in}$, the following commands can be used:

```

» interval = [s_in,s_out];
» boundcon = p_in;
» options = [];
» [s,p] = ode45('g_dpds',interval,boundcon,options,p1,p2);
» n = length(p);
» p_out = p(n)

```

The variable `options` is a vector with parameters to control the numerical integration; the default is an empty vector: `options = []`. Useful parameters to control are the maximum step size `MaxStep` and the relative tolerance `RelTol`, which can be set with `options = odeset('MaxStep',value1,'RelTol',value2)`. Default values are `MaxStep`

`= 0.1*interval and RelTol = 1.e-3.` The variable 'g_dpds' (between quotes) that forms the first element of the argument list is the name of the user-defined MATLAB function (m-file) that defines the function $g(s,p)$. It is called many times by `ode45` during the Runge-Kutta integration. The function most likely requires various parameters, which can be passed by means of the argument list after options; here we used parameters `p1` and `p2` as examples. The function would typically look something like this:

```
function dpds = g_dpds(s, p, flag, p1, p2)
%
% User-defined function to compute the derivative dp/ds.
%
% dpds = pressure gradient, Pa/m
% flag = dummy variable, -
% p = pressure, Pa
% p1 = parameter, -
% p2 = parameter, -
% s = along-hole coordinate, m
%
dpds = ...;
```

The three dots on the last line should be replaced by the appropriate function definition in terms of `s`, `p`, `p1`, and `p2`. The first two elements of the argument list in the function header contain the independent and dependent variables `s` and `p`. The dummy variable `flag` is not used but has to be present as the third element of the argument list. Thereafter follow the parameters. Note that the arguments in the calling sequence of `ode45` are not identical to those in the header of `g_dpds`. The output of `ode45` consists of two column vectors with values of the independent and the dependent variables (here `s` and `p`) for regularly spaced values of `s`. The last element of vector `p` is the required output pressure `p_out`.

It is possible to integrate a system of first-order differential equations, rather than a single equation, in the same fashion. This requires only that the dependent variable and the function definition be defined as vectors instead of scalars. We make use of this feature to compute the individual contributions of gravity, friction, and acceleration losses to the total pressure drop in a wellbore. For example, the function `gas_dpds` has the following header:

```
function dpds = gas_dpds(s, p, flag, ...)
```

where the dots indicate parameters. Now, `dpds` is a four-element vector defined as

```
dpds = [dpds_tot; dpds_grav; dpds_fric; dpds_acc]
```

while the variable `p` in the argument list is also a vector, defined as

p = [p_tot;p_grav;p_fric;p_acc]

Appendix E

Multiphase Flow Correlations

E-1 Hagedorn and Brown

E-1.1 Pseudoholdup Correlations. Hagedorn and Brown (1965) developed a set of correlations to compute the pressure drop of gas/liquid flow in vertical wells. They performed a large number of experiments using mixtures of air and water, and air and crude in a test well approximately 450 m (1,500 ft) deep and with tubing sizes up to 38 mm (1.5 in.). They measured pressures at various points along the well but did not measure liquid holdup. Instead, they computed pseudoholdup values by backcalculating the theoretical holdup values that best corresponded with the measured pressures. The pseudoholdup values were presented with the aid of graphical relationships in the form of three charts for various auxiliary parameters defined in terms of the dimensionless groups (Eqs. 4.37 through 4.40). Here we present equations obtained by curve fitting the original charts published by Hagedorn and Brown (1965). The first chart (see Fig. E-1) defines a relationship between the liquid viscosity number,

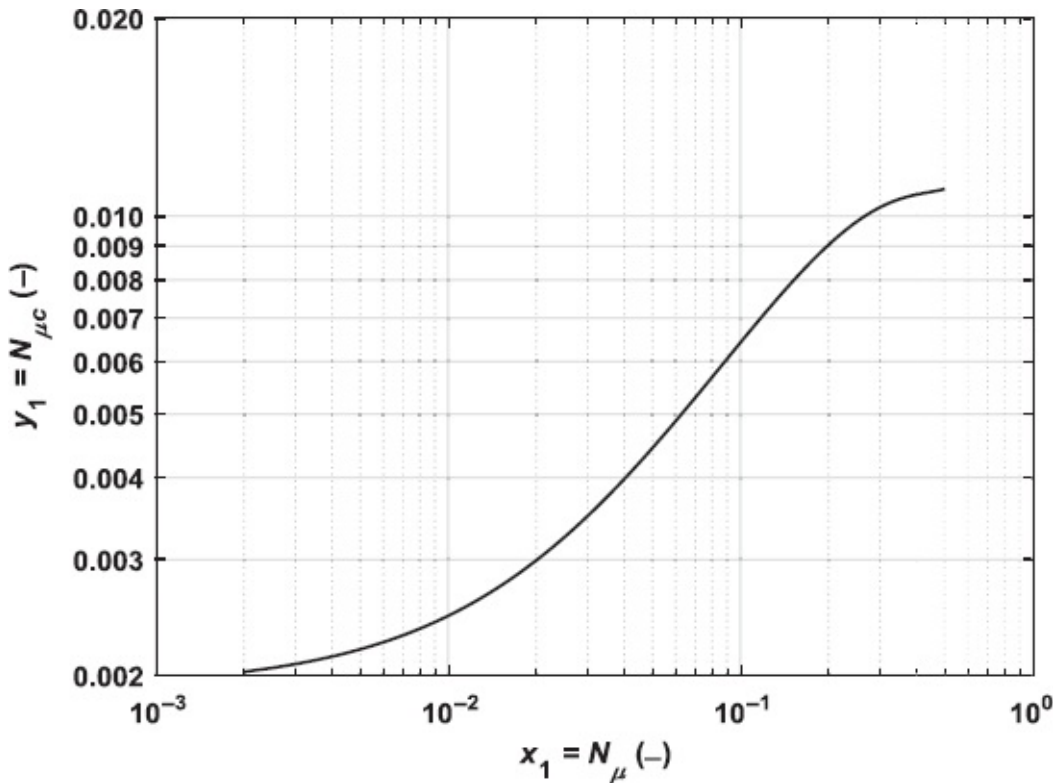


Fig. E-1—Chart 1 for Hagedorn and Brown correlation, corresponding to Eq. E-3.

$$x_1 = N_\mu, \dots \quad (\text{E-1})$$

and a corrected liquid viscosity number,

$$y_1 = N_{\mu c}, \dots \quad (\text{E-2})$$

according to

$$y_1 = a_3 x_1^3 + a_2 x_1^2 + a_1 x_1 + a_0, 0.002 \leq x_1 \leq 0.5, \dots \quad (\text{E-3})$$

where the coefficients a_0 to a_3 have been listed in **Table E-1**. The second chart (**Fig. E-2**) defines a relationship between

$$x_2 = \frac{N_{gv} N_\mu^{0.380}}{N_d^{2.14}} \dots \quad (\text{E-4})$$

and the correction factor

$$y_2 = \psi, \dots \quad (\text{E-5})$$

according to

$$y_2 = \frac{b_3 x_2^3 + b_2 x_2^2 + b_1 x_2 + b_0}{c_4 x_2^4 + c_3 x_2^3 + c_2 x_2^2 + c_1 x_2 + c_0}, 0.01 \leq x_2 \leq 0.088, \dots \quad (\text{E-6})$$

$$y_2 = 1, 0.00 \leq x_2 < 0.01, \dots \quad (\text{E-7})$$

with coefficients listed in **Table E-1**. The third chart (**Fig. E-3**) gives a relationship between

$$x_3 = \frac{N_{lv}}{N_{gv}^{0.575}} \left(\frac{p}{p_{sc}} \right)^{0.10} \frac{N_{\mu c}}{N_d}, \dots \quad (\text{E-8})$$

where p_{sc} is the pressure at standard conditions, and the required liquid holdup (divided by the correction factor ψ)

$$y_3 = \frac{H_l}{\psi}, \dots \quad (\text{E-9})$$

according to

$$y_3 = \frac{d_1 x_3 + d_0}{e_2 x_3^2 + e_1 x_3 + e_0}, 2.1000 \times 10^{-6} \leq x_3 \leq 4.6423 \times 10^{-5}, \dots \quad (\text{E-10})$$

$$y_3 = \frac{f_2 x_3^2 + f_1 x_3 + f_0}{g_1 x_3 + g_0}, 4.6423 \times 10^{-5} < x_3 \leq 5.0000 \times 10^{-3}, \dots \quad (\text{E-11})$$

$$y_3 = 0.98, 5.0000 \times 10^{-3} < x_3, \dots \quad (\text{E-12})$$

with coefficients listed in Table E-1. Note the various lower and upper limits for the x values in these expressions. The correlations (fitted from the charts) should not be used outside their limits because they may display erratic behavior. If it is required to use values outside the limits, the necessary values should be obtained by graphical extrapolation in the charts, and not by numerical extrapolation using the correlations. Occasionally the holdup values H , computed with Eqs. E-10 and E-11 are below the liquid volume fraction λ , which is physically impossible. In that case it is customary to use the volume fraction instead. Eqs. E-1 through E-12 have been programmed in MATLAB file `Hag_Brown_hold_up.m`, which forms a subroutine in `Hag_Brown_dpds.m` but may also be used on a standalone basis to recompute the holdups in a post-processing step—e.g., after computing a traverse with `Hag_Brown_dpds.m`.

Coefficient	Value
a_0	1.9122×10^{-3}
a_1	5.6348×10^{-2}
a_2	-1.2183×10^{-1}
a_3	9.0950×10^{-2}
b_0	1.8089×10^{-5}
b_1	-1.2769×10^{-3}
b_2	1.0029×10^{-2}
b_3	3.6917×10^{-1}
c_0	1.9585×10^{-5}
c_1	-1.2769×10^{-3}
c_2	2.7058×10^{-2}
c_3	-4.8940×10^{-2}
c_4	1.000×10^0
d_0	4.3260×10^{-11}
d_1	-3.7902×10^{-5}
e_0	-3.7520×10^{-10}
e_1	-1.9323×10^{-4}
e_2	1.0000×10^0
f_0	6.4898×10^{-5}
f_1	1.1470×10^0
f_2	$-1.8530 \times 10^{+1}$
g_0	4.5319×10^{-4}
g_1	1.0000×10^{10}

Table E-1—Coefficients for Eqs. E-3, E-6, E-10, and E-11.

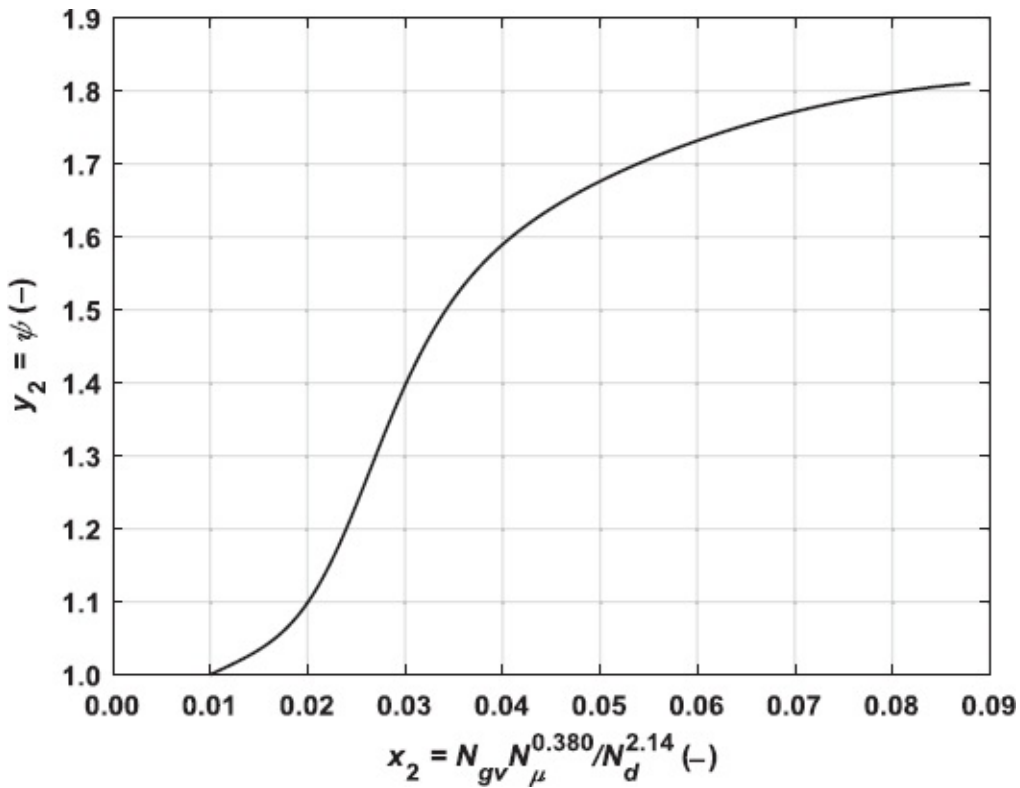


Fig. E-2—Chart 2 for Hagedorn and Brown correlation, corresponding to Eq. E-6.

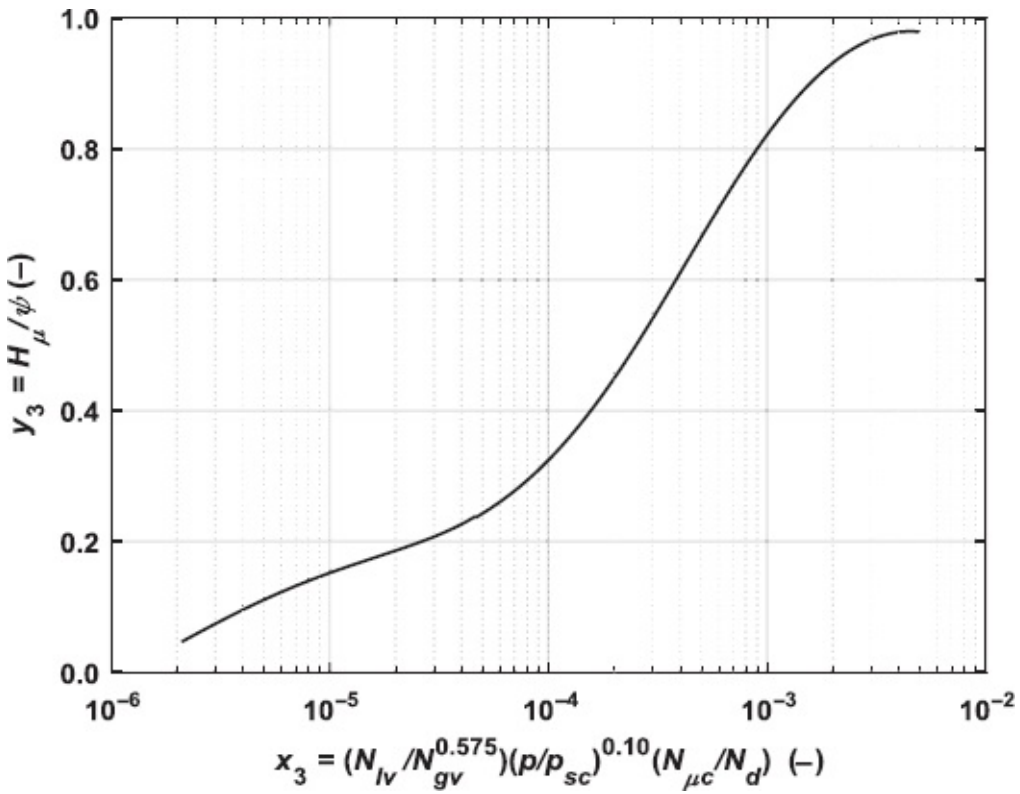


Fig. E-3—Chart 3 for Hagedorn and Brown correlation, corresponding to Eqs. E-10 and E-11.

E-1.2 Pressure Drop Analysis. Once the holdup values have been computed, the mixture velocities can be computed using Eqs. 4.32, 4.33, and 4.35 as presented in the body of the text. The mixture friction factor f_{ms} can then be obtained with the aid of Eqs. 3.12 and 3.13 or the corresponding Moody friction factor chart (Fig. 3.3) by replacing the single-phase properties μ , ρ , and v by the mixture properties μ_{ms} , ρ_{ms} , and v_{ms} . The pressure drop can then be computed with the aid of the expression as proposed in the original publication of Hagedorn and Brown (1965):

$$\frac{dp}{ds} = \underbrace{\rho_{ms}g}_{\text{head loss}} - \underbrace{\frac{\rho_{ms}^2}{2\rho_{ms}d} f_{ms} v_{ms} |v_{ms}|}_{\text{friction loss}} + \underbrace{\rho_{ms} \frac{\Delta v_{ms}^2}{2\Delta s}}_{\text{acceleration loss}}, \quad \dots \quad (\text{E-13})$$

where Δv_m is the velocity increment over a numerical integration interval Δs . The acceleration term in Eq. E-16 is valid only for positive acceleration (i.e. increasing absolute value of the velocity) in a production well. To capture the general case of positive and negative acceleration in injection and production wells, the term should be rewritten as $-\rho_{ms}|\Delta v_{ms}|\Delta v_{ms}/2\Delta s$. (Note, however, that this is of only theoretical interest because acceleration hardly ever plays a significant role except at the top of high-rate gas production wells, where very high velocities may occur.)

For the friction factor, Hagedorn and Brown (1965) suggested using the single-phase Moody diagram with a multiphase Reynolds number defined as

$$N_{Re} = \frac{\rho_{ms} v_{ms} d}{\mu_{ms}}, \quad \dots \quad (\text{E-14})$$

and a mixture viscosity defined as

$$\mu_{ms} = \mu_l^{H_l} \times \mu_g^{H_g}. \quad \dots \quad (\text{E-15})$$

Note that this is an unusual mixture viscosity definition. Most multiphase flow correlations use Eq. 4.35.

Alternatively, the friction loss can be computed according to Eq. 4.28, while the acceleration loss term is often replaced by multiplication of the head and friction terms with an acceleration factor, similar to what was done in the expressions for single-phase oil flow (Eq. 3.23) and single-phase gas flow (Eq. 3.33). For a vertical well—i.e., for $\sin(\theta) = -1$ —the resulting pressure drop expression then becomes

$$\frac{dp}{ds} = \frac{1}{1 - E_{k,D}} \left(\rho_{ms} g - \frac{\rho_{ms}}{2d} f_{ms} v_{ms} |v_{ms}| \right), \quad \dots \quad (\text{E-16})$$

where $E_{k,D}$ is a dimensionless mixture kinetic energy term defined by Beggs and Brill (1973) as

$$E_{k,D} = \frac{\rho_{ms} v_g v_{ms}}{p}. \quad \dots \quad (\text{E-17})$$

Note that the acceleration term in Eq. E-16 is valid only for positive accelerations (see also the comments following Eq. E-13). Eq. E-16, with Reynolds number and viscosity definitions shown by Eqs. E-14 and E-15, has been implemented in MATLAB file Hag Brown dpds.m.

E-1.3 Example E-1: Hagedorn and Brown Correlation. Consider the oil well with the properties given in Table 4.1. The local flow rates and densities just below the tubing head are $q_g = -0.0391 \text{ m}^3/\text{s}$, $q_o = -0.00406 \text{ m}^3/\text{s}$, $q_w = -0.001 \text{ m}^3/\text{s}$, $\rho_g = 4.58 \text{ kg/m}^3$, $\rho_o = 841 \text{ kg/m}^3$, and $\rho_w = 1.05 \times 10^3 \text{ kg/m}^3$. The viscosities at p_{tf} and T_{if} are $\mu_g = 8.69 \times 10^{-6} \text{ Pa}\cdot\text{s}$, $\mu_o = 0.0122 \text{ Pa}\cdot\text{s}$, and $\mu_w = 0.350 \times 10^{-3} \text{ Pa}\cdot\text{s}$.

Question 1 What is the magnitude of the liquid holdup just below the tubing head?

Answer The local oil and water fractions are

$$f_o = \frac{q_o}{q_o + q_w} = \frac{-0.00406}{-0.00406 - 0.00100} = 0.802, \text{ and } f_w = 1 - f_o = 1 - 0.802 = 0.198.$$

The local liquid properties are therefore

$$q_l = q_o + q_w = -0.00406 - 0.00100 = -0.00506 \text{ m}^3/\text{s},$$

$$\mu_l = f_o \mu_o + f_w \mu_w = 0.802 \times 0.0122 + 0.198 \times 0.35 \times 10^{-3} = 0.00985 \text{ Pa}\cdot\text{s},$$

$$\rho_l = f_o \rho_o + f_w \rho_w = 0.802 \times 841 + 0.198 \times 1050 = 882 \text{ kg/m}^3,$$

$$\sigma_{gl} = f_o \sigma_{go} + f_w \sigma_{gw} = 0.802 \times 0.008 + 0.198 \times 0.04 = 0.0143 \text{ N/m}.$$

The surface area of the tubing is

$$A = \frac{\pi d^2}{4} = \frac{\pi (62.3 \times 10^{-3})^2}{4} = 0.00305 \text{ m}^2,$$

such that the superficial and mixture velocities follow as

$$v_{sg} = \frac{q_g}{A} = \frac{-0.0391}{0.00305} = -12.8 \text{ m/s},$$

$$v_{st} = \frac{q_l}{A} = \frac{-0.00506}{0.00305} = -1.66 \text{ m/s},$$

$$v_{ms} = v_{sg} + v_{st} = -12.8 - 1.66 = -14.5 \text{ m/s}.$$

The dimensionless groups then become

$$N_{bv} = v_{sg} \sqrt[4]{\frac{\rho_l}{g\sigma_{gl}}} = -1.66 \times \sqrt[4]{\frac{882}{9.81 \times 0.0143}} = 14.8,$$

$$N_{gv} = v_{sg} \sqrt[4]{\frac{\rho_l}{g\sigma_{gl}}} = -12.8 \times \sqrt[4]{\frac{882}{9.81 \times 0.0143}} = 114,$$

$$N_d = d \sqrt{\frac{g\rho_l}{\sigma_{gl}}} = 62.3 \times 10^{-3} \times \sqrt{\frac{9.81 \times 882}{0.0143}} = 48.5,$$

$$N_\mu = \mu_l \sqrt[4]{\frac{g}{\rho_l \sigma_{gl}^3}} = 0.00985 \times \sqrt[4]{\frac{9.81}{882 \times (0.0143)^3}} = 0.0774.$$

With the aid of Fig. E-1 (or Eqs. E-1 through E-3), we find that

$$x_1 = N_\mu = 0.0774,$$

which corresponds to

$$N_{\mu c} = y_1 = 0.00559.$$

Also, with the aid of Fig. E-2 (or Eqs. E-4 through E-6), we find that

$$x_2 = \frac{N_{gv} N_\mu^{0.380}}{N_d^{2.14}} = \frac{114 \times (0.0774)^{0.380}}{(48.5)^{2.14}} = 0.0106,$$

which corresponds to

$$\psi = y_2 = 1.00.$$

Finally, with the aid of Fig. E-3 (or Eqs. E-8, E-9 and E-11), it follows that

$$x_3 = \frac{N_{bv}}{N_{gv}^{0.575}} \left(\frac{p}{p_{sc}} \right)^{0.10} \frac{N_{\mu c}}{N_d} = \frac{14.8}{(114)^{0.575}} \left(\frac{0.5 \times 10^6}{0.1 \times 10^6} \right)^{0.10} \frac{0.00559}{48.5} = 0.132 \times 10^{-3},$$

which results in a liquid holdup of

$$H_l = y_3 \psi = 0.369.$$

It remains only to be checked that the computed holdup is realistic (i.e., that it is not less than the liquid volume fraction λ_l):

$$\lambda_l = \frac{q_l}{q_g + q_l} = \frac{-0.00506}{-0.0391 - 0.00506} = 0.115 < 0.369, \text{ which is indeed correct.}$$

Question 2 What is the corresponding magnitude of the pressure gradient? Use Eq. E-16 with Reynolds number and viscosity definitions shown by Eqs. E-14 and E-15.

Answer The necessary mixture properties can be computed as

$$H_g = 1 - H_l = 1 - 0.369 = 0.631,$$

$$\mu_{ms} = \mu_g^{H_g} \times \mu_l^{H_l} = (8.69 \times 10^{-6})^{0.631} \times (0.00985)^{0.369} = 1.16 \times 10^{-4} \text{ Pa} \cdot \text{s},$$

$$\rho_{ms} = H_g \rho_g + H_l \rho_l = 0.631 \times 4.58 + 0.369 \times 882 = 328 \text{ kg/m}^3,$$

such that the mixture Reynolds number becomes

$$N_{Re} = \frac{\rho_{ms} v_{ms} d}{\mu_{ms}} = \frac{328 \times (-14.5) \times 62.3 \times 10^{-3}}{1.16 \times 10^{-4}} = 2.55 \times 10^6.$$

With a dimensionless roughness,

$$\epsilon = \frac{e}{d} = \frac{30.0 \times 10^{-6}}{62.3 \times 10^{-3}} = 0.482 \times 10^{-3},$$

and with the aid of the Moody chart (Fig. 3.3), we find a friction factor

$$f_{ms} = 0.0168,$$

such that the friction loss becomes

$$\left. \frac{dp}{ds} \right|_{fric} = -\frac{\rho_{ms}}{2d} f_{ms} v_{ms} |v_{ms}| = -\frac{328}{2 \times 62.3 \times 10^{-3}} \times 0.0168 \times (-14.5) \times 14.5 = 9.30 \times 10^3 \text{ Pa/m}.$$

The head loss follows as

$$\left. \frac{dp}{ds} \right|_{grav} = \rho_{ms} g = 328 \times 9.81 = 3.22 \times 10^3 \text{ Pa/m},$$

and with a dimensionless kinetic energy,

$$E_{k,D} = \frac{\rho_{ms} v_{sg} v_{ms}}{p} = \frac{328 \times (-12.8) \times (-14.5)}{0.5 \times 10^6} = 0.122,$$

we find an acceleration loss

$$\left. \frac{dp}{ds} \right|_{acc} = \frac{E_{k,D}}{1 - E_{k,D}} \left(\left. \frac{dp}{ds} \right|_{grav} + \left. \frac{dp}{ds} \right|_{fric} \right) = \frac{0.122}{1 - 0.122} (3.22 \times 10^3 + 9.30 \times 10^3) = 1.74 \times 10^3.$$

The total pressure gradient is therefore

$$\frac{dp}{ds} = \left. \frac{dp}{ds} \right|_{\text{grav}} + \left. \frac{dp}{ds} \right|_{\text{fric}} + \left. \frac{dp}{ds} \right|_{\text{acc}} = 3.22 \times 10^3 + 9.30 \times 10^3 + 1.74 \times 10^3 = 14.3 \times 10^3 \text{ Pa/m.}$$

E-2 Mukherjee and Brill

E-2.1 Flow Regimes. Mukherjee and Brill (1983; 1985a,b) performed a large number of tests in a 1.5-in.-diameter flow loop with a U-shaped inclined section that could be raised from horizontal to vertical. In this way they studied the behavior of flow in upward and downward directions over all possible inclinations. They used air as the gas phase and kerosene or lube oil as the liquid phase. Both legs of the U contained a 32-ft transparent section to observe flow regimes and a capacitance measurement device to measure holdups. Through curve fitting of a large number of measurements, they developed a set of numerical expressions for the flow pattern boundaries. These are expressed in terms of the dimensionless numbers (Eqs. 4.37 through 4.40) and a pipeline inclination angle θ_{MB} that can be related to our definition for the wellbore inclination α according to

$$\theta_{MB} = d \left| \alpha - \frac{\pi}{2} \right|, \dots \dots \dots \quad (\text{E-18})$$

where d is the flow direction defined as

$$d = \begin{cases} -1 & \text{if } \left(\alpha < \frac{\pi}{2} \wedge v_{ms} > 0 \right) \vee \left(\alpha > \frac{\pi}{2} \wedge v_{ms} < 0 \right) \\ 0 & \text{if } \alpha = \frac{\pi}{2} \\ 1 & \text{if } \left(\alpha > \frac{\pi}{2} \wedge v_{ms} > 0 \right) \vee \left(\alpha < \frac{\pi}{2} \wedge v_{ms} < 0 \right) \end{cases} \dots \dots \dots \quad (\text{E-19})$$

The boundary between annular mist flow and bubble or slug flow is expressed as

$$N_{gv,sm} = 10^{A_1}, \dots \dots \dots \quad (\text{E-20})$$

where

$$A_1 = 1.401 - 2.694N_\mu + 0.521N_\nu^{0.329}. \dots \dots \dots \quad (\text{E-21})$$

The boundary between bubble flow and slug flow depends on the flow direction. The upflow boundary is given by

$$N_{\nu,bs} = 10^{A_2}, \dots \dots \dots \quad (\text{E-22})$$

where

$$A_2 = \log N_{gv} + 0.940 + 0.074 \sin \theta_{MB} - 0.855 \sin^2 \theta_{MB} + 3.695 N_\mu, \dots \dots \dots \quad (\text{E-23})$$

and the downflow and horizontal boundary is given by

$$N_{gv,bs} = 10^{A_3}, \dots \dots \dots \quad (\text{E-24})$$

where

$$A_3 = 0.431 - 3.003 N_\mu - [1.138 \log N_{lv} + 0.429 (\log N_{lv})^2 - 1.132] \sin \theta_{MB}. \dots \dots \quad (\text{E-25})$$

Finally, the transition between slug flow and stratified flow is given by

$$N_{hv,st} = 10^{A_4}, \dots \dots \dots \quad (\text{E-26})$$

where

$$A_4 = 0.321 - 0.017 N_{gv} - 4.267 \sin \theta_{MB} - 2.972 N_\mu - 0.033 (\log N_{gv})^2 - 3.925 \sin^2 \theta_{MB}. \dots \dots \quad (\text{E-27})$$

The flow regime for a given set of parameters can now be determined by following the flow chart in [Fig. E-4](#). The flow chart logic and [Eqs. E-18 through E-27](#) have been programmed in MATLAB file `Muk_Brill_flow_reg.m`, which forms a subroutine in `Muk_Brill_dpds.m` but may also be used on a standalone basis to recompute the flow regimes in a post-processing step.

E-2.2 Holdup Correlation. Once the flow regime has been determined, the liquid holdup can be computed. Mukherjee and Brill (1983) determined a single holdup correlation for all flow regimes given by

$$H_l = \exp \left[\left(C_1 + C_2 \sin \theta_{MB} + C_3 \sin^2 \theta_{MB} + C_4 N_\mu^2 \right) \left(\frac{N_{gv}^{C_5}}{N_{lv}^{C_6}} \right) \right], \dots \dots \dots \quad (\text{E-28})$$

where the coefficients C_1 through C_6 depend on the flow regime and are given in [Table E-2](#). [Eq. E-28](#) has been programmed in MATLAB file `Muk_Brill_hold_up.m`, which forms a subroutine in `Muk_Brill_dpds.m` but may also be used on a standalone basis to recompute the holdups in a post-processing step.

E-2.3 Pressure Drop Analysis. The pressure drop equation used by Mukherjee and Brill is flow regime dependent. For slug and bubble flow it can be written as

$$\frac{dp}{ds} = \frac{1}{1 - E_{k,D}} \left(\rho_{ms} g \cos \alpha - \frac{\rho_{ms}}{2d} f_{ms} v_{ms} |v_{ms}| \right), \dots \dots \dots \quad (\text{E-29})$$

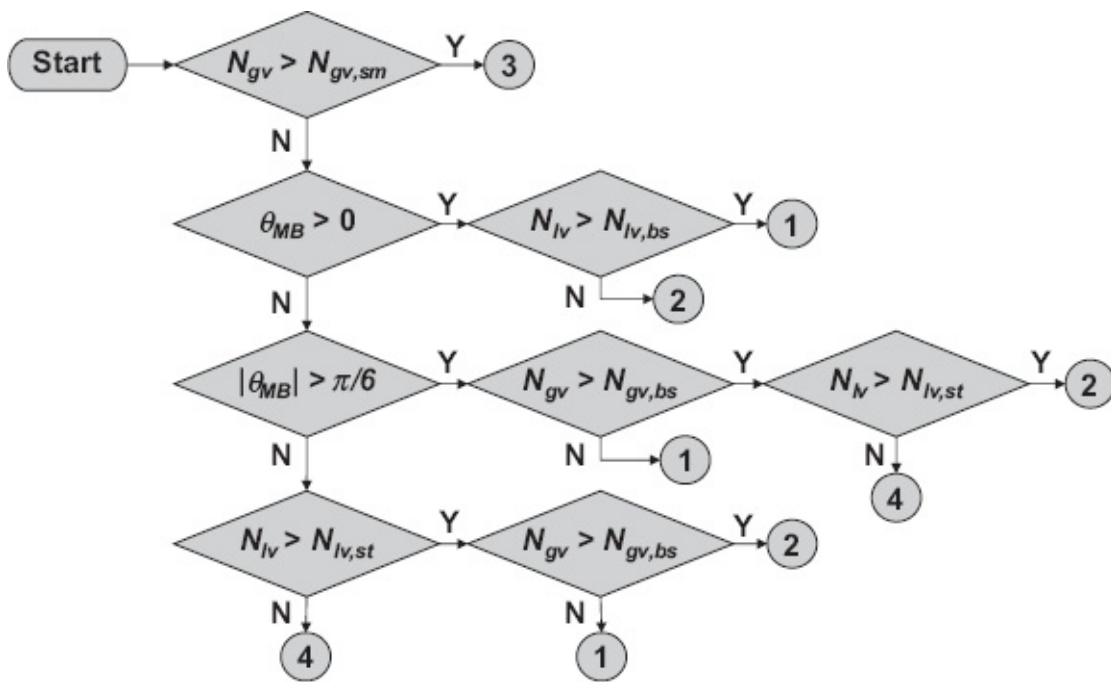


Fig. E-4—Flow chart to determine flow regime: 1, bubble flow; 2, slug flow; 3, annular mist flow; 4, stratified flow. Adapted from Mukherjee and Brill (1985a).

Coefficient	Uphill or Horizontal Flow	Downhill Stratified Flow	Other Downhill Flow
C_1	-0.380 113	-1.330 282	-0.516 644
C_2	0.129 875	4.808 139	0.789 805
C_3	-0.119 788	4.171 584	0.551 627
C_4	2.343 227	56.262 268	15.519 214
C_5	0.475 686	0.079 951	0.371 771
C_6	0.288 657	0.504 887	0.393 952

Table E-2—Coefficients for Eq. E-28, (after Mukherjee and Brill, 1983).

where the dimensionless mixture kinetic energy term $E_{k,D}$ is the one defined in Eq. E-17. The friction coefficient f_{ms} is determined from the Moody diagram (i.e., from Eqs. 3.12 and 3.13) with

$$N_{Re} = \frac{\rho_{mn} v_{ms} d}{\mu_{mn}}. \quad \dots \quad (E-30)$$

For annular flow the same pressure drop Eq. E-29 is used, but with ρ_{ms} in the friction term replaced by ρ_{mn} , and with a friction factor

$$f_{ms} = f_r f_{mn}, \quad \dots \quad (E-31)$$

where f_{mn} is the no-slip Moody friction factor and f_r is a friction factor ratio that depends on the holdup ratio

according to the values in **Table E-3**, which should be linearly interpolated as required.

For stratified flow the friction factor is computed with the aid of a mechanistic model that explicitly accounts for the velocities in the liquid and gas layers, and for the shear forces between the layers and between the fluids and the wall. Here we do not reproduce the corresponding equations, which are quite elaborate, but refer the reader to Mukherjee and Brill (1985b) or Brill and Mukherjee (1999) for further details. Eqs. E-29 through E-32 and the equations for stratified flow have been programmed in MATLAB file `Muk_Brill_dpds.m`.

E-2.4 Example E-2: Mukherjee and Brill Correlation. Consider the same well as in Example E-1.

Question 1 What are the flow regime and the magnitude of the liquid holdup just below the tubing head?

Answer The first steps are identical to those of Example E-1, up to and including the computation of the dimensionless groups N_{lv} , N_{gv} , N_d , and N_μ . Because $v_{ms} < 0$ (upward flow) and $\alpha = 0$ (vertical well), it follows from Eq. E-19 that $d = 1$ and from Eq. E-18 that $\theta_{MB} = \pi/2$. To determine the flow regime, we need to follow the flow chart in Fig. E-4. The first step requires computation of the boundary between annular mist flow and bubble or slug flow according to Eq. E-20:

H_r	f_r
0.01	1.00
0.20	0.98
0.30	1.20
0.40	1.25
0.50	1.30
0.70	1.25
1.00	1.00
10.00	1.00

Table E-3—Coefficients for Eq. E-31.

$$A_1 = 1.401 - 2.694 \times 0.0774 + 0.521 \times (14.8)^{0.329} = 2.46, N_{avsm} = 10^{2.46} = 288.$$

Because $\theta_{MB} > 0$ and $N_{lv} < N_{lv,bs}$ ($114 < 288$) the flow regime is not annular flow, and we proceed to the next step, which requires the boundary between bubble and slug flow for upward flow (see Eq. E-22):

$$A_2 = \log 114 + 0.940 + 0.074 \sin \frac{\pi}{2} - 0.855 \left(\sin \frac{\pi}{2} \right)^2 + 3.695 \times 0.0774 = 2.50, N_{lv,bs} = 10^{2.50} = 316.$$

Because $\theta_{MB} > 0$ and $N_{lv} < N_{lv,bs}$ ($14.8 < 316$), it follows that the flow regime is slug flow. The liquid holdup is given by Eq. E-28 with coefficients from the first column in Table E-2 as

$$H_l = \exp \left\{ \left[-0.380 + 0.130 \times \sin \frac{\pi}{2} - 0.120 \times \left(\sin \frac{\pi}{2} \right)^2 + 2.343 \times (0.0774)^2 \right] \left[\frac{(114)^{0.476}}{(14.8)^{0.289}} \right] \right\} = 0.211.$$

Note the difference between the holdup values computed by the two methods: approximately 0.37 for Hagedorn and Brown (H&B) vs. 0.21 for Mukherjee and Brill (M&B). This gives an indication of the lack of accuracy of these types of empirical correlations. Fig. E-5 illustrates the difference and also displays the liquid volume fractions for both methods (see also Fig. E-4). Note that for depths below about 1150 m, the liquid holdup becomes equal to unity because the pressures become higher than the bubblepoint pressure. The holdup values for both correlations are larger than or equal to the liquid volume fractions—as they should be. Fig. E-5 also depicts the flow regimes for the M&B correlation, and it can be seen that the flow regime changes from single-phase liquid flow (0) for depths below 1150 m to bubble flow (1) between 1150 and 550 m and slug flow (2) above 550 m. An example of how to create a graph of liquid holdup vs. depth is given in MATLAB file `example_hold_up.m`.

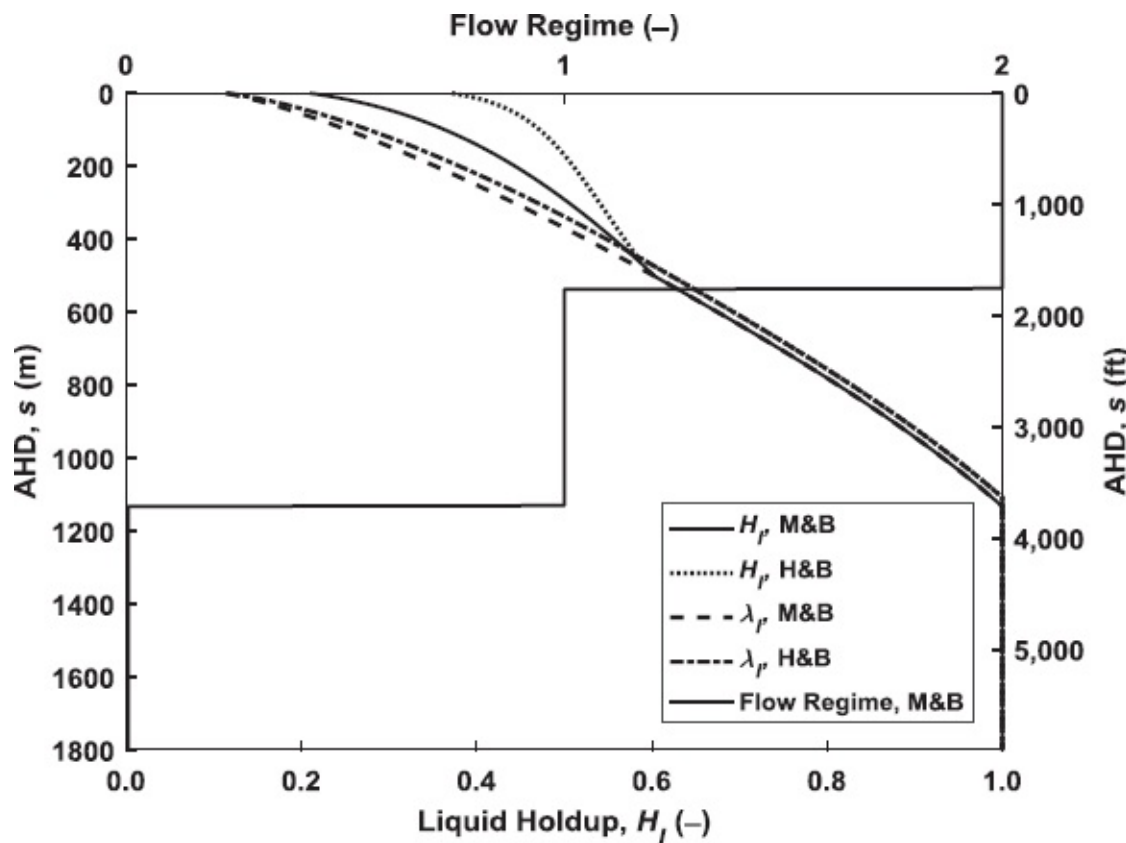


Fig. E-5—Liquid holdups, liquid volume fractions, and flow regimes for a vertical multiphase well with

parameters given in [Table 4.1](#) for comparison between the Mukherjee and Brill (M&B) and the Hagedorn and Brown (H&B) methods. The flow regimes (indicated with a stepped solid line) correspond to the M&B method, with 0 indicating single-phase liquid flow, 1 bubble flow, and 2 slug flow (only the top 1800 m has been displayed).

Question 2 What is the corresponding magnitude of the pressure gradient?

Answer The necessary mixture properties can be computed as

$$\mu_{mn} = \lambda_g \mu_g + \lambda_l \mu_l = 0.885 \times 8.69 \times 10^{-6} + 0.115 \times 0.00985 = 1.14 \times 10^{-3} \text{ Pa} \cdot \text{s},$$

$$\rho_{mn} = \lambda_g \rho_g + \lambda_l \rho_l = 0.885 \times 4.58 + 0.115 \times 882 = 105 \text{ kg/m}^3,$$

$$H_g = 1 - H_l = 1 - 0.211 = 0.789,$$

$$\rho_{ms} = H_g \rho_g + H_l \rho_l = 0.789 \times 4.58 + 0.211 \times 882 = 190 \text{ kg/m}^3.$$

The mixture Reynolds number becomes

$$N_{Re} = \frac{\rho_{mn} |v_{ms}| d}{\mu_{mn}} = \frac{105 \times 14.5 \times 62.3 \times 10^{-3}}{1.14 \times 10^{-3}} = 8.32 \times 10^4.$$

Using a dimensionless roughness,

$$\epsilon = \frac{e}{d} = \frac{30.0 \times 10^{-6}}{62.3 \times 10^{-3}} = 0.482 \times 10^{-3},$$

and with the aid of the Moody chart ([Fig. 3.3](#)), we find a friction factor

$$f_{ms} = 0.0208,$$

such that the friction loss becomes

$$\left. \frac{dp}{ds} \right|_{fric} = -\frac{\rho_{ms}}{2d} f_{ms} v_{ms} |v_{ms}| = -\frac{190}{2 \times 62.3 \times 10^{-3}} \times 0.0208 \times (-14.5) \times 14.5 = 6.67 \times 10^3 \text{ Pa/m}.$$

The head loss follows as

$$\left. \frac{dp}{ds} \right|_{grav} = \rho_{ms} g = 190 \times 9.81 = 1.86 \times 10^3 \text{ Pa/m},$$

and the dimensionless kinetic energy is given by

$$E_{k,D} = \frac{\rho_{ms} v_{sg} v_{ms}}{p} = \frac{190 \times (-12.8) \times (-14.5)}{0.5 \times 10^6} = 0.0705,$$

such that the acceleration loss follows as

$$\left. \frac{dp}{ds} \right|_{acc} = \frac{E_{k,D}}{1 - E_{k,D}} \left(\left. \frac{dp}{ds} \right|_{grav} + \left. \frac{dp}{ds} \right|_{fric} \right) = \frac{0.0705}{1 - 0.0705} (1.86 \times 10^3 + 6.67 \times 10^3) = 0.647 \times 10^3,$$

and the total pressure gradient is given by

$$\frac{dp}{ds} = \left. \frac{dp}{ds} \right|_{grav} + \left. \frac{dp}{ds} \right|_{fric} + \left. \frac{dp}{ds} \right|_{acc} = 1.86 \times 10^3 + 6.67 \times 10^3 + 0.647 \times 10^3 = 9.18 \times 10^3 \text{ Pa/m.}$$

Note that this value is also considerably different from the one previously computed: $14.3 \times 10^3 \text{ Pa/m}$ for H&B vs. $9.18 \times 10^3 \text{ Pa/m}$ for M&B. However, this is a local difference, and at greater depths the discrepancy is much smaller. Overall, the methods produce results that are near-identical (for this example)—i.e., well within the typical accuracy that may be expected for production engineering calculations.

E-3 Drift Flux Models

E-3.1 Profile Parameter. Another class of relatively simple multiphase wellbore flow models is the family of drift flux models, where *drift* refers to the difference between the gas velocity and the mixture velocity (see, e.g., Wallis 1969 and Shi et al. 2005a, b). Shi et al. (2005a, b) performed a series of experiments in a flow loop containing a 0.15-m-diameter transparent pipe section that could be raised from horizontal to vertical. They accurately measured holdups and used their experimental results to tune the free parameters in a drift flux algorithm that is described in broad lines below. Their aim was to develop a fast algorithm for use in a reservoir simulator. Shi et al. (2005b) considered two-phase gas/ liquid and two-phase oil/water flow, and in a follow-up paper they proposed a drift flux formulation for three-phase gas/oil/water flow (Shi et al. 2005a). Here we restrict the analysis to the two-phase gas/liquid situation, in which water and oil flow without slip.

In the drift flux approach, as first proposed by Zuber and Findlay (1965), the difference in phase velocities, and therefore the liquid holdup, is explained as resulting from two physical mechanisms: (1) gas has a tendency to slip through the liquid because of a difference in densities, and (2) gas bubbles have a tendency to concentrate at the center of the wellbore, where the fluid velocities are highest (see **Fig. E-6**). The joint effect of these mechanism can be expressed as

$$v_g = v_d + C_0 v_{ms}, \dots \dots \dots \quad (\text{E-33})$$

where v_g is the gas velocity; v_d is the *drift velocity* or *slip velocity*, defined as the difference between the gas and mixture velocities; C_0 is the *profile* or *distribution parameter*; and v_{ms} is the mixture velocity.

Various studies have reported values for C_0 ; typical values range from 1.0 to 1.5 depending on factors such as the flow regime, pipe diameter, and gas fraction (for a detailed discussion, see Shi et al. 2005b). In general, the profile effect reduces for

increasing gas fractions and increasing mixture velocities. Typical values of C_0 for the bubble flow and annular flow regimes are 1.2 and 1.0, respectively. Shi et al. (2005b) found that for the large pipe diameter used in their experiment the profile effect was also negligible at lower flow rates,—i.e., C_0 should be taken as 1.0—but they suggest that for smaller diameters $C_0 = 1.2$ is a better choice. They proposed the following relationship:

$$C_0 = \frac{C_{0,bub}}{1 + (C_{0,bub} - 1)\gamma^2}, \dots \dots \dots \text{(E-34)}$$

where $C_{0,bub}$ is the value of C_0 in the bubble flow regime and where the parameter γ has a value between zero and unity. The parameter γ should approach its upper limit at high values of H_g or v_{ms} to ensure that C_0 reduces to 1.0. Therefore, the value of γ is obtained from

$$\gamma = \min \left[\max \left(0, \frac{\beta - \bar{\beta}}{1 - \bar{\beta}} \right), 1 \right], \dots \dots \dots \text{(E-35)}$$

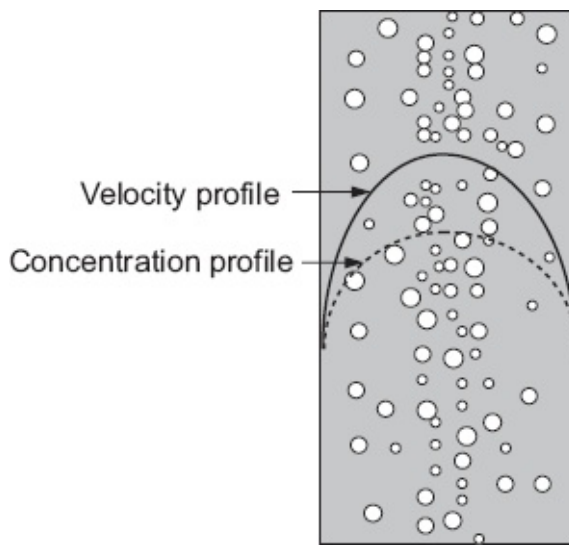


Fig. E-6—Velocity and concentration profiles in upward pipe flow. The gas bubbles tend to be concentrated at the center of the pipe, where the velocity is highest.

where β is also a parameter with a value larger than zero defined as

$$\beta = \max \left(H_g, H_g \frac{v_{ms}}{v_{g,fld}} \right), \dots \dots \dots \text{(E-36)}$$

and $\bar{\beta}$ is the value of β at which C_0 starts to drop below $C_{0,bub}$ (see Fig. E-7).

The variable $v_{g,fld}$ is the *flooding velocity*—i.e., the gas velocity that is just sufficient to support a thin annulus of liquid such that it does not flow back down along the wellbore (Wallis and Makkenchery 1974):

$$v_{g,fl} = \hat{N}_{Ku} \sqrt{\frac{\rho_l}{\rho_g}} v_c, \quad \dots \dots \dots \quad (E-37)$$

where the critical velocity v_c is defined by the following equation (refer to Eq. 4.37; note that in line with the sign convention in our text, we define upward velocities as negative. In the original paper by Shi et al. (2005ab), upward velocities are positive):

$$v_c = -\sqrt[4]{\frac{\sigma_{gl} g (\rho_l - \rho_g)}{\rho_l^2}}, \quad \dots \dots \dots \quad (E-38)$$

and where \hat{N}_{Ku} is the *critical Kutateladze number*, which is a function of a modified pipe diameter number (cf. Eq. 4.39), is

$$\hat{N}_d = d \sqrt{\frac{g (\rho_l - \rho_g)}{\sigma_{gl}}}, \quad \dots \dots \dots \quad (E-39)$$

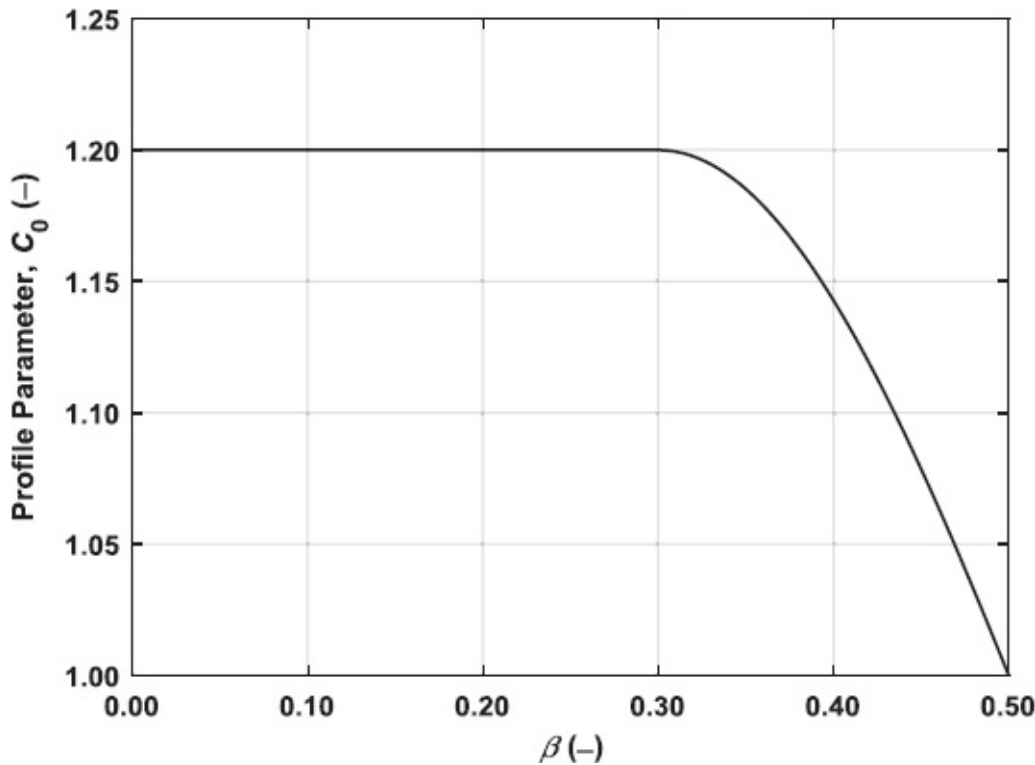


Fig. E-7—Profile parameter as function of β for $C_{0,bub} = 1.2$ and $\bar{\beta} = 0.6$.

according to a graphical correlation displayed in Fig. E-8. Curve fitting of the graph results in

$$\hat{N}_{Ku} = \frac{1.0152 \times 10^{-5} \hat{N}_d^3 - 2.3396 \times 10^{-3} \hat{N}_d^2 + 8.0850 \times 10^{-1} \hat{N}_d - 1.5934}{1.9551 \times 10^{-1} \hat{N}_d + 1.0000}, \quad 2 \leq \hat{N}_d \leq 70. \quad (E-40)$$

The ratio $v_{ms}/v_{g,fl}$ is typically smaller than unity for most flow regimes and may even

be negative in case of countercurrent flow of gas and liquids. It approaches unity at the transition to annular flow, and will exceed unity for fully developed annular flow. Note that in the latter case the value of γ will remain bounded to unity.

E-3.2 Drift Velocity. The drift velocity also depends on the flow regime. Following Shi et al. (2005b), we consider a range of values between two extremes. For bubble flow, corresponding to very low gas fractions, we use an expression for the gas velocity from Harmathy (1960), who determined the rise velocity of small bubbles through a stationary liquid to be

$$v_{g,bub} = 1.53 v_c \quad \dots \dots \dots \quad (\text{E-41})$$

At the other extreme of very high gas holdup values we have to consider annular flow, in which case the gas velocity relative to a stationary liquid becomes equal to the flooding velocity v_{fld} , which was defined in Eq. E-37. Between these two endpoints the values of v_d are given as a function of H_g by a *flooding curve* (see Shi et al. 2005b), defined as

$$v_d = \frac{m_\alpha (1 - H_g C_0) C_0 K v_c}{H_g C_0 \sqrt{\frac{\rho_g}{\rho_l}} + 1 - H_g C_0}, \quad \dots \dots \dots \quad (\text{E-42})$$

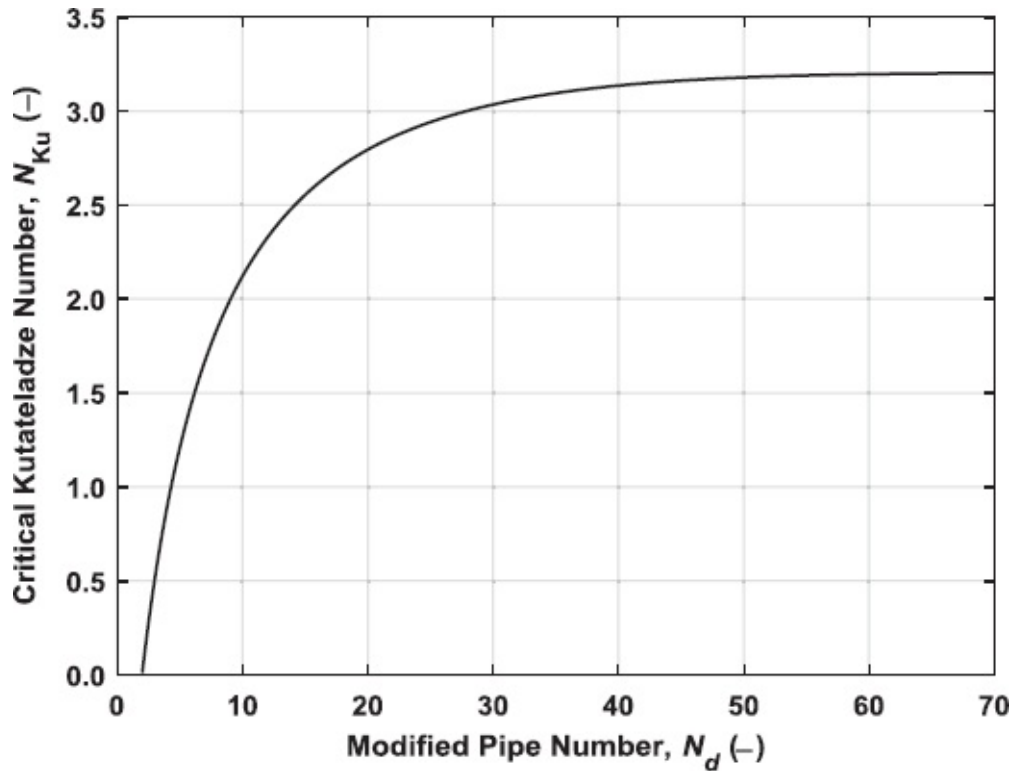


Fig. E-8—Critical Kutateladze number as function of modified pipe number. After Shi et al. (2005b).

where

$$K = \begin{cases} 1.53/C_0 & \text{if } H_g < a_1 \\ \hat{N}_{\text{Ku}} & \text{if } a_2 < H_g \end{cases}, \quad \dots \dots \dots \quad (\text{E-43})$$

with a linear interpolation for values of H_g between the tuning parameters a_1 and a_2 , where $0 < a_1 < a_2 < 1$. The parameter m_α is a multiplier to take account of the effect of the wellbore inclination α , defined as

$$m_\alpha = m_0 (\cos \alpha)^{n_1} (1 + \sin \alpha)^{n_2}, \quad \dots \dots \dots \quad (\text{E-44})$$

where n_1 and n_2 need to be determined experimentally and where m_0 is a nonunit multiplier for vertical flow, which serves as an additional tuning parameter. In the experiments of Shi et al. (2005b) a total of seven parameters for gas/liquid flow were determined by minimizing the root-mean-squared error between a large number of measured and modeled holdup values. The resulting optimal values for large-diameter pipes, as used in their experiments, are displayed in the first row of values in **Table E-4**. The second row of values corresponds to optimal parameters when the values of $C_{0,\text{bub}}$ and $\bar{\beta}$ are fixed at 1.2 and 0.6, respectively, which may provide better results for smaller-diameter pipes (say, below 0.10 m; no specific diameter is mentioned in the original publication).

E-3.3 Holdup. The gas holdup H_g is implicitly related to the profile parameter C_0 and the drift velocity v_d according to

$$H_g = \frac{v_{sg}}{v_g} = \frac{v_{sg}}{v_d(H_g) + C_0(H_g)v_{ms}}, \quad \dots \dots \dots \quad (\text{E-45})$$

and therefore it has to be computed iteratively. A simple numerical implementation is obtained through *Picard iteration* (subsequent substitution) with a damping factor $0 < f < 1$:

$$H_g^{k+1} = (1 - f)H_g^k + f \frac{v_{sg}}{v_d(H_g^k) + C_0(H_g^k)v_{ms}}, \quad \dots \dots \dots \quad (\text{E-46})$$

where k is the iteration counter and where the gas volume fraction forms a convenient starting value: $H_g^0 = \lambda_g$.

E-3.4 Example E-3: Drift Flux Model. Consider the same well as in Example E-1.

Question What are the flow regime and the magnitude of the liquid holdup just below the tubing head?

$C_{0,\text{bub}}$	$\bar{\beta}$	a_1	a_2	m_0	n_1	n_2
1.0	1.0	0.06	0.21	1.85	0.21	0.95

1.2

0.6

0.06

0.12

1.27

0.24

1.08

Table E-4—Parameters for the gas/liquid drift flux model of Shi et al. (2005b).

Answer The drift flux model does not explicitly determine the flow regime. The liquid holdup can be computed iteratively as follows:

- Follow the same steps as in Example E-1, up to and including the computation of

$$v_{sg} = -12.8 \text{ m/s}, v_{sl} = -1.66 \text{ m/s}, v_{ms} = -14.5 \text{ m/s}.$$

- Determine the drift flux parameters. Because the pipe diameter (0.0623 m) is below 0.10 m, we choose the parameters in the second row of Table E-4.
- Choose $\lambda_g = 0.885$ as a first guess H_g^0 for the gas holdup.
- With the aid of Eqs. E-38 and E-39, and either Fig. E-8 or Eq. E-40, determine

$$v_c = -\sqrt[4]{\frac{\sigma_{gl}g(\rho_l - \rho_g)}{\rho_l^2}} = -\sqrt[4]{\frac{0.0143 \times 9.81(882 - 4.58)}{882^2}} = -0.112 \text{ m/s},$$

$$\hat{N}_d = d \sqrt{\frac{g(\rho_l - \rho_g)}{\sigma_{gl}}} = 0.0623 \sqrt{\frac{9.81(882 - 4.58)}{0.0143}} = 48.3,$$

and

$$\hat{N}_{Ku} = 3.17,$$

which, with the aid of Eq. E-37, leads to the flooding velocity

$$v_{g, fld} = \hat{N}_{Ku} \sqrt{\frac{\rho_l}{\rho_g}} v_c = 3.17 \sqrt{\frac{882}{4.58}} 0.112 = -4.93 \text{ m/s}.$$

- Next, use Eqs. E-34 through E-36 to compute a first guess of the profile parameter C_0 as follows:

$$\beta = \max\left(H_g, H_g \frac{v_{ms}}{v_{g, fld}}\right) = \max\left(0.885, 0.885 \frac{-14.5}{-4.93}\right) = 2.60,$$

$$\gamma = \min\left[\max\left(0, \frac{\beta - \bar{\beta}}{1 - \bar{\beta}}\right), 1\right] = \min\left[\max\left(0, \frac{2.60 - 0.6}{1 - 0.6}\right), 1\right] = 1,$$

$$C_0 = \frac{C_{0,bub}}{1 + (C_{0,bub} - 1)\gamma^2} = \frac{1.2}{1 + (1.2 - 1)1^2} = 1.$$

- Compute a first guess of the drift velocity v_d with Eqs. E-42 and E-43 according to

$$v_d = \frac{m_a (1 - H_g C_0) C_0 K v_c}{H_g C_0 \sqrt{\frac{\rho_g}{\rho_l}} + 1 - H_g C_0} = \frac{1.27 (1 - 0.885 \times 1) 1 \times 3.17 \times -0.112}{0.885 \times 1 \sqrt{\frac{4.58}{882}} + 1 - 0.885 \times 1} = -0.289 \text{ m/s},$$

where $m_a = m_0 = 1.27$ because the well is vertical.

7. Compute an improved estimate of the gas holdup with [Eq. E-46](#):

$$\begin{aligned} H_g^1 &= (1 - f) H_g^k + f \frac{v_{sg}}{v_d (H_g^k) + C_0 (H_g^k) v_{ms}} \\ &= (1 - 0.5) 0.885 + 0.5 \frac{-12.8}{-0.289 + 1 \times -14.5} = 0.875, \end{aligned}$$

where we used a damping factor, $f = 0.5$.

8. Repeat Steps 5 through 7, using the damped Picard iteration scheme ([Eq. E-46](#)), until convergence, and compute $H_l = 1 - H_g$.

In this example, one iteration is enough to reduce the absolute error in the gas holdup to below 0.01 and another five to bring it down to below 0.001. The corresponding parameter values are

$$v_{g,fl_d} = -4.93 \text{ m/s}, C_0 = 1, H_g = 0.865, H_l = 0.135.$$

Note that $H_l = 0.130$ is almost identical to $\lambda_l = 0.115$; i.e., there is almost no slip of the gas in this model. This is different from the values for H_l as obtained with both the Hagedorn and Brown and the Mukherjee and Brill methods in Examples E-1 and E-2, which were 0.369 and 0.211, respectively.

Appendix F

Relative Permeabilities

F-1 Physics

The physics of the relative permeability effect is related to the interfacial tension between the phases (which gives rise to capillary pressure), the wettability of the rock, and the geometry of the pore network (see, e.g., Dullien 1979). For the reservoir engineering aspects of relative permeabilities, see, e.g., Muskat (1949), Dake (1978), or Chierici (1994). The products $k_g = k k_{rg}$, $k_o = k k_{ro}$, and $k_w = k k_{rw}$ are known as the *effective permeabilities* to gas, oil, and water, respectively. Here, k is the *absolute permeability* governed by rock properties only, expressed in m^2 (md), and $0 \leq k_{rg} \leq 1$, $0 \leq k_{ro} \leq 1$, and $0 \leq k_{rw} \leq 1$ are dimensionless *relative permeabilities*, which are nonlinear functions of the phase saturations and represent the reduction of permeability to one phase as a result of the presence of the other phases. In most descriptions of two-phase oil/water flow the rock is assumed to be water-wet; i.e., water is the wetting phase and oil the nonwetting phase. Wettability is defined in terms of the *contact angle*, which is the angle between the surfaces of a droplet and a solid in contact, measured at the contact line and through the liquid (see [Fig. F-1](#)).

For water-wet rock, oil production corresponds to *imbibition*, i.e., an increasing wetting-phase saturation. During the migration process of oil from the source rock into the reservoir, the reverse process took place, known as *drainage* (i.e., a decrease of the wetting-phase saturation). In an actual reservoir, the rock may be water-wet, oil-wet, or, as is often the case, mixed-wet—i.e., having a contact angle close to 90° . In case of two-phase gas/water flow, water is always the wetting phase, and gas production therefore also corresponds to imbibition. In case of oil and gas flow, oil is the wetting phase, and we therefore have to consider drainage, at least under a normal production scenario. Under three-phase (gas/oil/water) conditions, the customary approach is to assume that water is the wetting phase, oil the intermediate phase, and gas the nonwetting phase, and that the relative permeabilities are dependent only on the water and gas saturations. Although this very simplistic description is known to be incorrect in most circumstances, it provides a workable description of multiphase permeabilities for numerical reservoir simulation, and various models based on these assumptions have been proposed (see, e.g., Stone 1973, Aziz and Settari 1979, or Chierici 1994).



Fig. F-1—Relation between contact angle and wettability. Left: water droplet on a water-wet surface (contact angle $< 90^\circ$). Right: water droplet on an oil-wet surface (contact angle $> 90^\circ$).

Fig. F-2 depicts a typical set of relative permeability curves for oil and water flow during imbibition in a water-wet rock. The wetting phase (i.e., the water) preferentially occupies the smaller pores. During the water drainage process (i.e., the oil migration process) not all water could be displaced from these small pores, and so at the end of the process some water was left, known as *connate water* or *interstitial* water. The imbibition process (i.e., the oil production process) therefore starts from a situation with an initial water saturation equal to the connate water saturation. Because there is no flow of water until the water saturation exceeds this initial value, it is also referred to as the *immobile* or *critical* water saturation, and we will indicate it with the symbol S_{wi} , where the subscript *i* refers to “immobile.” At the end of the water imbibition process, a certain amount of oil remains trapped in the larger pores from which it cannot be displaced by water. This oil is known as *residual oil*, and the associated saturation S_{orw} as the residual oil saturation after waterflooding. At the beginning and the end of the imbibition process, the presence of connate water and residual oil in the pores results in relative permeabilities below the theoretical maximum of unity. These values, k_{row}^0 and k_{rw}^0 , are known as the *endpoint relative permeabilities* under waterflooding conditions. The more water-wet the rock, the lower the value of k_{rw}^0 .

Fig. F-3 depicts a typical set of relative permeability curves for gas and oil flow during oil drainage. Water is assumed to be present as immobile water, and therefore the relative permeability values should be interpreted as relative to a reduced permeability $k = k_{row}^0$. At increasing gas saturations, the gas does not start flowing until it has reached the critical gas saturation S_{gc} . The critical gas saturation is not very important when oil is forced through the formation but becomes important for solution gas drive (primary recovery), where gas bubbles need to slowly grow into interconnected paths before the oil starts flowing. The endpoint relative permeability k_{rog}^0 is equal to unity; but because we assumed the presence of connate water, the corresponding effective permeability to oil is, in fact, equal to k_{row}^0 . The residual liquid saturation in **Fig. F-3** consists of the sum of the residual oil saturation S_{org} and the immobile water saturation S_{wi} . The value of S_{org} will typically have a finite value in case of primary recovery but may approach zero in case of gasflooding.

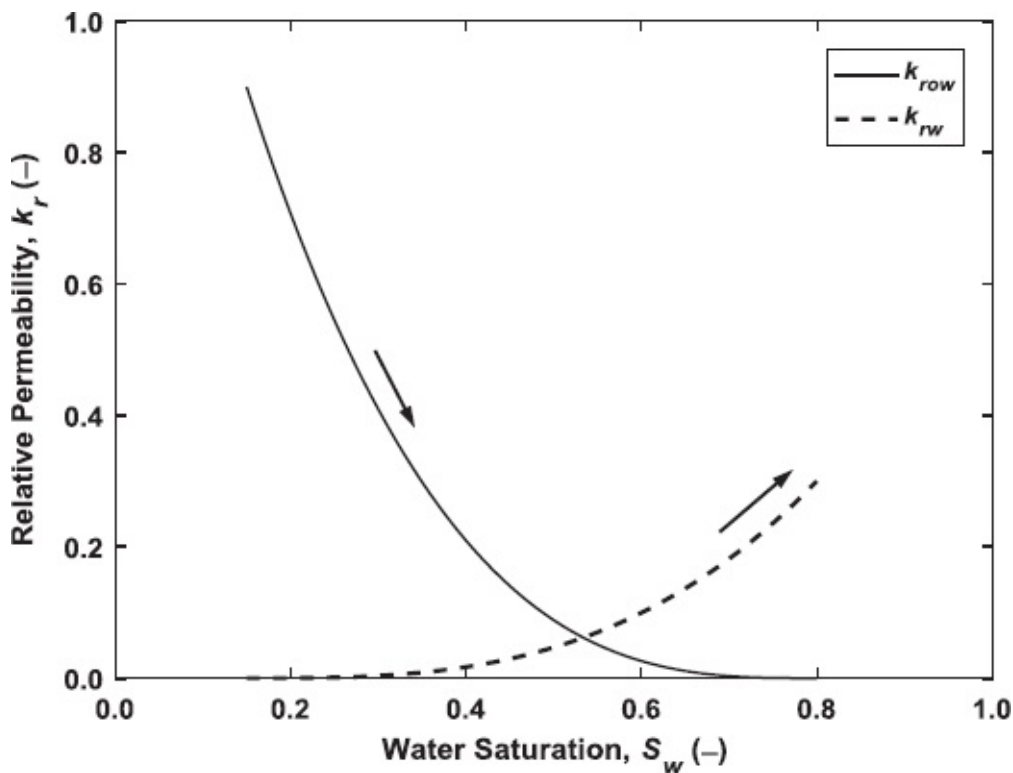


Fig. F-2—Relative permeabilities to oil and water during imbibition (i.e., increasing water saturation). In this example, $k_{roy}^0 = 0.9$, $k_{rw}^0 = 0.3$, $S_{wi} = 0.15$, $S_{orw} = 0.20$, and $n_{ow} = n_w = 3$.

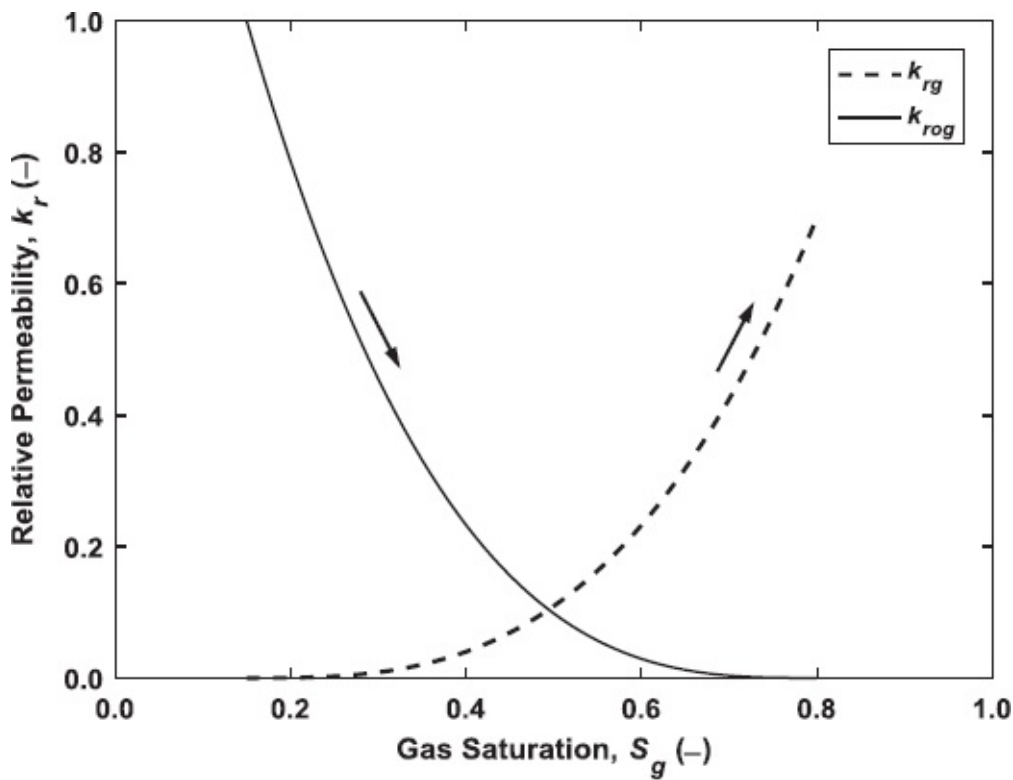


Fig. F-3—Relative permeabilities to gas and oil during drainage (i.e., decreasing oil saturation). In this example, $k_{rog}^0 = 1.0$, $k_{rg}^0 = 0.7$, $S_{gc} = 0.15$, $S_{wi} = 0.15$, $S_{org} = 0.05$, and $n_g = n_{og} = 3$.

F-2 Corey Expressions

Relative permeabilities are strongly dependent on formation and fluid properties and should therefore ideally be determined from laboratory experiments, in particular from coreflooding tests. In the case of heterogeneous reservoir properties, as is nearly always the case, there is a difference between the permeabilities at the core scale and the *upscaled* permeabilities, also known as *pseudopermeabilities*, at the near-well reservoir length scale. In the absence of measured data, it may be necessary to revert to empirical relationships for the relative permeabilities. These relationships are also used to fit measured permeability data and can then be used for upscaling and numerical simulation. For oil/water flow under imbibition conditions (i.e., oil production), we use the relationships

$$k_{row} = k_{row}^0 \left(1 - S_w^*\right)^{n_{ow}}, \quad \dots \dots \dots \quad (\text{F-1})$$

$$k_{rw} = k_{rw}^0 \left(S_w^*\right)^{n_w}, \quad \dots \dots \dots \quad (\text{F-2})$$

where S_w^* is the normalized water saturation defined as

$$S_w^* = \frac{S_w - S_{wi}}{1 - S_{orw} - S_{wi}}, \quad 0 \leq S_w^* \leq 1, \quad \dots \dots \dots \quad (\text{F-3})$$

and where n_{ow} and n_w are known as the *Corey exponents*. They are both larger than 1, with typical values between 2 and 4. For oil/gas flow under drainage conditions (i.e., oil production again), we use

$$k_{rg} = k_{rg}^0 \left(S_g^*\right)^{n_g}, \quad \dots \dots \dots \quad (\text{F-4})$$

$$k_{rog} = k_{rog}^0 \left(1 - S_g^*\right)^{n_{og}}, \quad \dots \dots \dots \quad (\text{F-5})$$

where S_g^* is the normalized gas saturation defined as

$$S_g^* = \frac{S_g - S_{gc}}{1 - S_{gc} - S_{org} - S_{wi}}, \quad 0 \leq S_g^* \leq 1. \quad \dots \dots \dots \quad (\text{F-6})$$

Figs. F-2 and F-3 have been produced with values $n_g = n_{og} = n_{ow} = n_w = 3$. In case of oil/water flow, the total relative permeability to liquid flow is given by $(k_r)_{ow} = k_{row} + k_{rw}$. In case of oil/gas flow, the total relative permeability is given by $(k_r)_{go} = k_{rg} + k_{rog}$; similarly, for three-phase flow, we find that $(k_r)_{gow} = k_{rg} + k_{ro} + k_{rw}$. Many models for gas/oil/water relative permeabilities in three-phase flow have been published, but their details are outside the scope of this book. In these models it is usually assumed that the presence of gas and the presence of water have an influence on the permeability to oil, but that the presence of gas does not influence the permeability to water and vice versa (see, e.g., Stone 1973). The simplest model is then given by

A somewhat more sophisticated example of a three-phase relative permeability model is the so-called modified Stone II equation, which is based on a model of flow in a bundle of parallel tubes (Stone 1973; Aziz and Settari 1979). The relative permeability to oil is then given by

$$k_{ro} = k_{ro}^0 \left[\left(\frac{k_{rog}}{k_{ro}^0} + k_{rg} \right) \left(\frac{k_{row}}{k_{ro}^0} + k_{rw} \right) - (k_{rg} + k_{rw}) \right], \quad \dots \dots \dots \quad (\text{F-8})$$

where k_{rw}^0 is the permeability at residual liquid saturation:

$$k_{\text{ro}}^0 = k_{\text{row}}^0 = k_{\text{rog}}^0 \quad \dots \quad (\text{F-9})$$

Eq. F-8 reduces to the two-phase expressions for the oil/gas and oil/water rel perms in the limits $S_w = S_{wi}$ and $S_g = S_{gc}$, respectively.

Fig. F-4 shows an example, obtained with Eq. F-8, of the relative permeabilities for oil in three-phase flow displayed as a ternary diagram. Note that in a ternary diagram, the horizontal gridlines correspond to the scale at the right (gas saturation in this case), the gridlines running from top-center to bottom-right correspond to the scale at the left axis (water saturation), and those running from bottom-left to top-center to the scale at the bottom axis (oil saturation). It can be seen in **Fig. F-4** that the region of “mobile saturations” is occupying only a part of the total saturation space. The cut-off values are related to the residual or immobile saturations of the phases. The figure also illustrates that in a large region the presence of gas and water strongly reduces the relative permeability to oil and thus the productivity of an oil well producing under three-phase conditions.

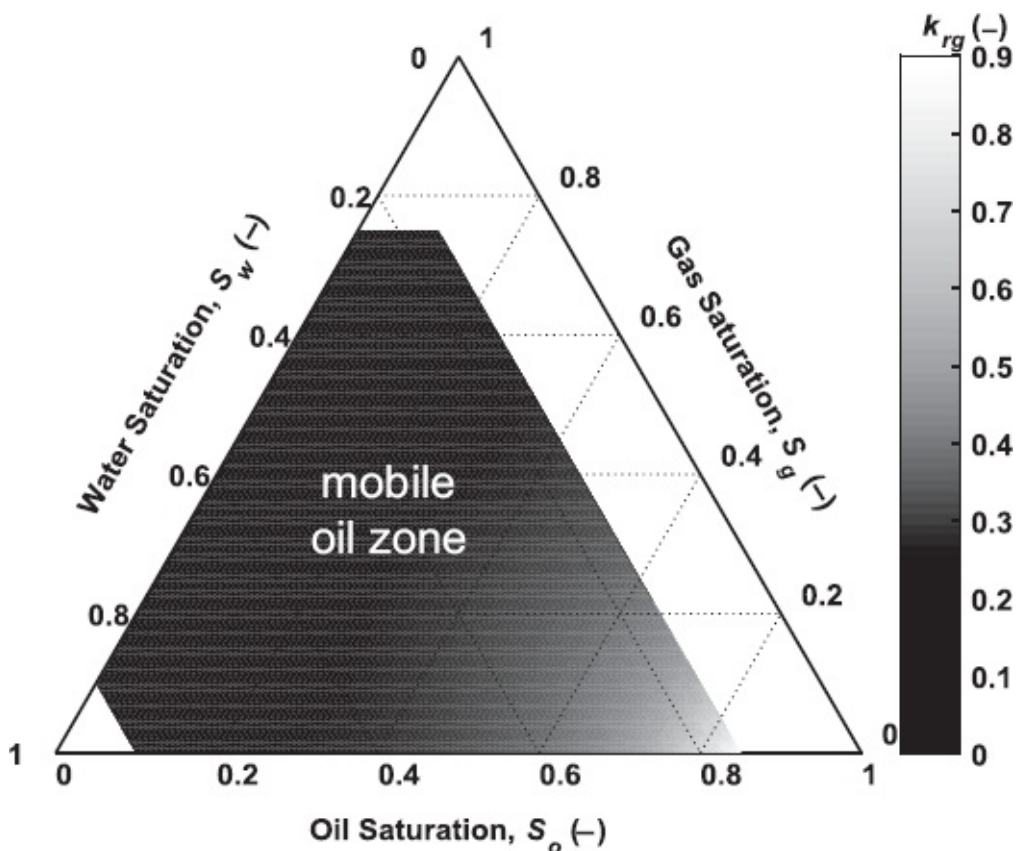


Fig. F-4—Relative permeability to oil under three-phase flow conditions. In this example we have used the following parameter values: $k_{rg}^0 = 0.7$, $k_{ro}^0 = 0.9$, $k_{rw}^0 = 0.5$, $S_{gc} = 0.00$, $S_{org} = S_{orw} = 0.10$, $S_{wi} = 0.15$, and $n_g = n_{og} = n_{ow} = n_w = 3$.

Appendix G

Answers to Questions

G-1 Answers for Chapter 1, Introduction

- 1.1 Performance curves of production system elements display oil or gas flow rate on the horizontal axis vs. pressure at one end of the component on the vertical axis. Because it is tacitly assumed that the pressure at the other end of the component stays fixed, the performance curves therefore also represent pressure drop vs. flow rate.
- 1.2 Because performance curves usually represent nonlinear relationships between flow rate and pressure. As a result, we occasionally encounter two intersections. However, as discussed in detail in [Chapter 8](#), only one of these intersection points represents a physically realistic solution.
- 1.3 Because (a) oil and gas are compressible, and (b) gas may dissolve in oil or oil may vaporize into gas. All these effects result in changes in the oil and gas phase volumes with a change in pressure, whereas the mass rates of the (pseudo)components (both of which are present in both phases in proportions varying with pressure) remain constant. These effects are discussed in detail in [Chapter 2](#).
- 1.4. (a) Yes; one unknown flow rate can, in theory, be determined from a single pressure drop measurement over the tubing.
 (b) Yes; see above.
 (c) Yes; the unknown oil and water flow rates can be determined from a single pressure drop measurement combined with knowledge of the water/oil ratio.
 (d) No; in this case the gas/oil ratio is unknown and therefore the three unknown flow rates cannot be determined individually. Moreover, as discussed in detail in [Chapter 4](#), it is not sufficient just to know the gas/oil ratio because the oil and gas may flow with different velocities.
- 1.5 Refer to [Eq. 1.1](#) and [Table 1.1](#). The power of the motor equals $300 \times 16 = 4800$ W. Because the motor is only 90% effective, the power transmitted through the shaft equals $0.9 \times 4800 = 4320$ W. The shaft of the motor rotates with $240 \text{ rpm} = 240 \times 2\pi / 60 = 25.1 \text{ rad/s}$. The torque is therefore $4320 / 25.1 = 172 \text{ N}\cdot\text{m}$. The reduction gear has an efficiency of 98%, so the remaining power available for the pump is $0.98 \times 4320 = 4234$ W. The pump creates a pressure differential of $160 \times 10^3 \text{ Pa}$ at a flow rate of $22 \times 10^{-3} \text{ m}^3/\text{s}$. The power at the liquid end of the pump is therefore $160 \times 10^3 \times 22 \times 10^{-3} = 3520$ W. The efficiency of the pump now follows as $3520 / 4234 \times 100 \% = 83\%$.

1.6 Oil rate: $12\ 000 \times 1.840 \times 10^{-6} = 0.022 \text{ m}^3/\text{s}$.

Gas rate: $1500 \times 12\ 000 \times 2.831 \times 10^{-2} / (24 \times 3600) = 5.9 \text{ m}^3/\text{s}$.

Oil density: $141.5 \times 10^3 / (131.5 + 38) = 835 \text{ kg/m}^3$.

Gas density: $0.82 \times 1.23 = 1.0 \text{ kg/m}^3$.

» from_bpd_to_m3_per_s(12000) ans = 0.0221

» from_ft3_per_d_to_m3_per_s(1500*12000) ans = 5.8993

» from_deg_API_to_kg_per_m3(38) ans = 834.8083

» from_gas_grav_to_kg_per_m3(0.82) ans = 1.0086

1.7 Molecular weight of $\text{C}_1\text{H}_4 = 16.043$ and of $\text{CO}_2 = 44.010$.

Total mass: $1 \times 16.043 + 0.3 \times 44.010 = 29.25 \text{ lbm}$.

Mass: $4.536 \times 10^{-1} \times 29.25 = 13.27 \text{ kg}$.

Temperature: $83 \times 5/9 = 46.1 \text{ K}$.

Pressure: $(30 + 14.7) \times 6.895 \times 10^3 = 308 \text{ kPa}$.

» from_lbm_to_kg(29.25) ans = 13.2676

» from_deg_R_to_K(83) ans = 46.1111

» from_psi_to_Pa(30 + 14.7) ans = 3.0820e+005

1.8 Pressure = density × gravity × depth + atmospheric pressure = $(1.03 \times 999) \times 9.807 \times 2000 + 0.10 \times 10^6 = 20.28 \times 10^6 \text{ Pa}$. Pressure in psi: $20.18 \times 10^6 / (6.895 \times 10^3) = 2927 \text{ psia}$.

» from_kg_per_m3_to_Pa_per_m(from_liq_grav_to_kg_per_m3(1.03)) * 2000 + 0.1

ans = 2.0181e+007

» from_Pa_to_psi(2.0181e7)

ans = 2.9270e+003

1.9 Step 1: Leave the formula in its original form (i.e., expressed in field units), and insert the variables in SI units divided by their corresponding field-to-SI conversion factors as given in Table A-1.

$$\frac{\Delta p(\text{Pa})}{\text{psi}} = \frac{\rho(\text{kg/m}^3)}{\text{lbf/in}^2} \left[\frac{v(\text{m/s})}{\text{ft/s}^2} \right]^2 \Big/ \underbrace{(288 \times 32.174 \times C^2)}_{\text{dimensionless}}$$

Step 2: Solve for Δp and combine all numerical factors:

$$\Delta p = \frac{\rho v^2}{2C^2}$$

Note that the dimensionless constant C_g has disappeared from the equation.

1.10 $y_{\text{API}} = 30^\circ \Rightarrow \rho_o = 876.16 \text{ kg/m}^3$.

$g_w = 0.45 \text{ psi/ft} \Rightarrow \rho_w = 1037.61 \text{ kg/m}^3$.

$z_{\text{OWC}} = 4250 \text{ ft} = 1295.40 \text{ m}$.

$h_o = 4250 - 4050 = 200 \text{ ft} = 60.96 \text{ m}$.

$p_{\text{OWC}} = z_{\text{OWC}} \times \rho_w \times g + p_{\text{atm}} = 1295.40 \times 1037.61 \times 9.81 + 100\ 000 = 13.29 \times 10^6 \text{ Pa}$.

$p_{\text{GOC}} = p_{\text{OWC}} - h_o \times \rho_o \times g = 13.29 \times 10^6 - 60.96 \times 876.16 \times 9.81 = 12.77 \times 10^6 \text{ Pa}$.

G-2 Answers for Chapter 2, Properties of Reservoir Fluids

- 2.1 The solution GOR, denoted as R_s , is the ratio between the amount of dissolved gas and the amount of oil in which the gas is dissolved (both expressed as volume at standard conditions) at a given pressure and temperature. The producing GOR, denoted as R_{go} , is the ratio between the gas and oil rates (both expressed as volume per unit time at standard conditions) as observed at surface. When producing oil from a reservoir above the bubblepoint pressure, R_{go} will be identical to R_{sb} (i.e., to R_s at bubblepoint pressure and reservoir temperature).
- 2.2 Ordinary condensation occurs when the pressure of a gas/liquid mixture *increases* above the dewpoint line in the phase diagram, at a given temperature (or, more generally, when the pressure/temperature combination passes the dewpoint line from bottom-right to top-left). Retrograde condensation occurs when the pressure *drops* below the dewpoint line (or, more generally, when the pressure/temperature combination passes the dewpoint line from top-right to bottom-left). This somewhat counterintuitive effect is typical for gaseous hydrocarbon mixtures with large amounts of volatile components (wet gas).
- 2.3 The EOS in the black oil model is defined in terms of three parameters: B_g , B_o , and R_s , usually in the form of an empirical correlation. The composition is specified in the form of the solution GOR at bubblepoint, R_{sb} , which gives the ratio between the two pseudocomponents. The oil and gas pseudocomponent properties are often specified with correlations in terms of a single parameter per pseudocomponent, the density: $\rho_{o,sc}$ and $\rho_{g,sc}$ in SI units, or y_o (or y_{API}) and y_g in field units.
- 2.4 The oil phase contains a mixture of oil and gas pseudocomponents with proportions depending on pressure and temperature. The pseudooil component is defined as the oil phase at standard conditions.
- 2.5 Because critical pressures and temperatures (required to compute the reduced values) are defined only for single components. For mixtures, we use approximate pseudocritical pressures and temperatures to compute pseudoreduced values.
- 2.6 With the aid of Eqs. 2.24 and 2.27 it follows that

$$\rho_g q_g + \rho_o q_o$$

$$\begin{aligned}
&= \left(\frac{1}{B_g} \rho_{g,sc} + \frac{r_s}{B_g} \rho_{o,sc} \right) \left(\frac{B_g}{1 - R_s r_s} q_{g,sc} - \frac{B_g R_s}{1 - R_s r_s} q_{o,sc} \right) \\
&\quad + \left(\frac{R_s}{B_o} \rho_{g,sc} + \frac{1}{B_o} \rho_{o,sc} \right) \left(-\frac{B_o r_s}{1 - R_s r_s} q_{g,sc} + \frac{B_o}{1 - R_s r_s} q_{o,sc} \right)
\end{aligned}$$

$$\begin{aligned}
 &= \frac{1}{1-R_s r_s} \rho_{g,sc} q_{g,sc} - \frac{R_s}{1-R_s r_s} \rho_{g,sc} q_{o,sc} + \frac{r_s}{1-R_s r_s} \rho_{o,sc} q_{g,sc} - \frac{r_s R_s}{1-R_s r_s} \rho_{o,sc} q_{o,sc} \\
 &\quad - \frac{R_s r_s}{1-R_s r_s} \rho_{g,sc} q_{g,sc} + \frac{R_s}{1-R_s r_s} \rho_{g,sc} q_{o,sc} - \frac{r_s}{1-R_s r_s} \rho_{o,sc} q_{g,sc} + \frac{1}{1-R_s r_s} \rho_{o,sc} q_{o,sc} \\
 &= \rho_{g,sc} q_{g,sc} + \rho_{o,sc} q_{o,sc}.
 \end{aligned}$$

This equality implies that the mixture mass flow $\rho_m q_m = \rho_g q_g + \rho_o q_o$ expressed at downhole conditions is equal to the mixture mass flow expressed at standard conditions.

- 2.7 In SI: $q_{g,sc} = 0.6555 \text{ m}^3/\text{s}$; $q_{o,sc} = 0.0018 \text{ m}^3/\text{s}$; and $q_{w,sc} = 0.0000 \text{ m}^3/\text{s}$. With the aid of Eq. 2.27, we now find

$$\begin{aligned}
 \begin{bmatrix} q_g \\ q_o \\ q_w \end{bmatrix} &= \begin{bmatrix} \frac{B_g}{1-R_s r_s} & \frac{-B_g R_s}{1-R_s r_s} & 0 \\ \frac{-B_o r_s}{1-R_s r_s} & \frac{B_o}{1-R_s r_s} & 0 \\ 0 & 0 & 1 \end{bmatrix} \begin{bmatrix} q_{g,sc} \\ q_{o,sc} \\ q_{w,sc} \end{bmatrix} \\
 &= \begin{bmatrix} 0.0030 & -0.5952 & 0 \\ -0.0015 & 1.8452 & 0 \\ 0 & 0 & 1 \end{bmatrix} \begin{bmatrix} 0.6555 \\ 0.0018 \\ 0.0000 \end{bmatrix} = \begin{bmatrix} 0.0009 \\ 0.0024 \\ 0.0000 \end{bmatrix},
 \end{aligned}$$

and therefore $R_{gl} = 0.0009/0.0024 \approx 0.4$.

- 2.8 The reservoir is below the bubblepoint pressure, and therefore we can use the Standing correlation shown in Eq. B-2 to calculate the solution GOR:

$$R_s = \frac{1.11}{716} \left[(8 \times 10^{-6} \times 17 \times 10^6 + 1.4) 10^{1768/910 - 0.00164 \times 76} \right]^{1.2048} = 90.5 \text{ m}^3/\text{m}^3.$$

```
» R_s = gas_oil_rat_Standing(17e6, 1.11, 910, 76)
R_s = 90.5408
```

- 2.9 The gas specific gravity at surface (i.e., at standard conditions), is

$$\gamma_g = \frac{\rho_{g,sc}}{\rho_{air}} = \frac{1.11}{1.23} = 0.90 \text{ kg/m}^3.$$

The gas density just above the gas cap (i.e., at reservoir conditions), can be found with the aid of Eq. B-17. For that, we first need to calculate the gas deviation factor Z as follows. With the aid of the Sutton correlations (Eqs. B-13 and B-14), we find the pseudocritical properties of the fluid as

$$\begin{aligned}
 p_{pc} &= 5218 \times 10^3 - 734 \times 10^3 \times 1.11 - 16.4 \times 10^3 \times 1.11^2 = 4.38 \times 10^6 \text{ Pa}, \\
 T_{pc,abs} &= 94.0 + 157.9 \times 1.11 - 27.2 \times 1.11^2 = 236 \text{ K}.
 \end{aligned}$$

The pseudoreduced pressure and temperature at the reservoir follow as

$$P_{R,pr} = \frac{p_R}{p_{pc}} = \frac{17 \times 10^6}{4.38 \times 10^6} = 3.88 \text{ and } T_{R,pr} = \frac{T_R}{T_{pc,abs}} = \frac{76 + 273.15}{236} = 1.48.$$

With the aid of the Standing-Katz chart in Fig. B.5, we find for the compressibility factor, $Z = 0.76$; and then with the aid of Eq. B-17,

$$\rho_{g,R} = 1.11 \times \frac{17 \times 10^6 \times (15 + 273.15) \times 1.00}{100 \times 10^3 \times (76 + 273.15) \times 0.76} = 205 \text{ kg/m}^3.$$

```
» p_pc = pres_pseu_crit_Sutton(1.11)
p_pc = 4.3831e+006
» T_pc_abs = temp_pseu_crit_Sutton(1.11)
T_pc_abs = 235.7559
» p_R_pr = 17e6 / p_pc
p_R_pr = 3.8786
» T_R_pr = (76 + 273.15) / T_pc_abs
T_R_pr = 1.4810
» Z = z_factor_DAK(p_R_pr, T_R_pr)
Z = 0.7637
» B_g = gas_form_vol_fact(17e6, 76+273.15, Z)
B_g = 0.0054
» rho_g_R = 1.11 / B_g
rho_g_R = 203.9255
```

Alternatively, the MATLAB computations can be performed more directly as

```
» B_g = gas_form_vol_fact_
direct(17e6, 1.11, 76+273.15)
B_g = 0.0054
» rho_g_R = 1.11 / B_g
rho_g_R = 203.9255
```

- 2.10 Consult examples B-3 and B-4 in Sections B-2.10 and B-3.5 for the principles of the hand calculation. The reservoir pressure is above the bubblepoint pressure, and therefore the oil is undersaturated. We find for the viscosities $\mu_o = 1.2 \times 10^{-3}$ Pa·s, and $\mu_g = 24 \times 10^{-6}$ Pa·s.

With MATLAB we find for the oil viscosity:

```
» mu_od = oil_visc_dead_B_and_R(910, 76)
mu_od = 0.0070
» R_sb = gas_oil_rat_Standig(19.5e6, 1.11, 910, 76)
R_sb = 106.6472
» mu_ob = oil_visc_sat_B_and_R(mu_od, R_sb)
mu_ob = 0.0011
» mu_o = oil_visc_undersat_V_and_B(mu_ob, 22e6, 19.5e6)
mu_o = 0.0012
```

Alternatively, the oil viscosity can be computed more directly as

```
» mu_o = oil_viscosity(22e6, R_sb, 1.11, 910, 76)
mu_o = 0.0012
```

The MATLAB results for the gas viscosity are

```
» M = from_kg_per_m3_to_molar_mass(1.11)
M = 0.0261
» mu_g_p_sc = gas_visc_atm_Dempsey(M, 76)
```

```

mu_g_p_sc = 1.1148e-05
» p_pc = pres_pseu_crit_Sutton(1.11)
p_pc = 4.3831e+06
» T_pc_abs = temp_pseu_crit_Sutton(1.11)
T_pc_abs = 235.7559
» p_R_pr = 22e6 / p_pc
p_R_pr = 5.0193
» T_R_pr = (76 + 273.15) / T_pc
T_R_pr = 1.4810
» f = gas_visc_ratio_Dempsey(p_R_pr, T_R_pr)
f = 2.1619
» mu_g = f * mu_g_p_sc
mu_g = 2.4101e-05

```

Alternatively, also the gas viscosity can be computed directly as

```

» mu_g = gas_viscosity(22e6, 1.11, 76)
mu_g = 2.4101e-05

```

- 2.11 We can use the Vazquez and Beggs correlation ([Eq. B-8](#)) to calculate c_o . However, we first need [Eq. B-9](#) to convert the gas density $\rho_{g,sc}$ to the density at the reference separator pressure $\rho_{g,100}$, which was used to derive the correlation in [Eq. B-8](#). The values for p_{sep} and T_{sep} are, in our case, simply the standard conditions $p_{sep} = 100$ kPa and $T_{sep} = 15^\circ\text{C}$:

$$\rho_{g,100} = 1.11 \left[1 + 5.912 \times 10^{-5} \left(\frac{141.5 \times 10^3}{910} - 131.5 \right) (1.8 \times 15 + 32) \log \left(\frac{100 \times 10^3}{790.8 \times 10^3} \right) \right] = 1.03,$$

$$c_o = \frac{-2541 + 27.8 \times 90.5 + 31.0 \times 76 - 959 \times 1.03 + 1784 \times 10^3 / 910}{10^5 \times 22 \times 10^6} = 1.71 \times 10^{-9} \text{ 1/Pa.}$$

```

» R_sb = gas_oil_rat_Standing(19.5e6, 1.11, 910, 76)
R_sb = 106.6472
» rho_g_100 = rho_g_Vazquez_and_
Beggs(100e3, 1.11, 910, 15)
rho_g_100 = 1.0266
» c_o = compres_Vazquez_and_Beggs(22e6, R_
sb, rho_g_100, 910, 76)
c_o = 1.7072e-009

```

- 2.12 Consult examples B-1 and B-2 in [Sections B-2.8](#) and [B-2.9](#) for the principles of the hand calculation. For $p = 15$ MPa and $T = 85^\circ\text{C}$, the oil is saturated and we find $B_o = 1.47$. For $p = 30$ MPa and $T = 105^\circ\text{C}$, the oil is undersaturated and we find $B_o = 1.86$.

Using matlab, the results are

```

» p_b = pres_bub_Standing(250, 1.02, 805, 85)
p_b = 2.4529e+007
» R_s = gas_oil_rat_Standing(15e6, 1.02, 805, 85)
R_s = 138.9552
» B_o = oil_form_vol_fact_Standing(R_s, 1.02, 805, 85)
B_o = 1.4666
» p_b = pres_bub_Standing(250, 1.02, 805, 105)
p_b = 2.6467e+007

```

```

» B_ob = oil_form_vol_fact_Standing(250,1.02,805,105)
B_ob = 1.8790
» rho_g_100 = rho_g_Vazquez_and_
Beggs(100e3,1.02,805,15)
rho_g_100 = 0.8785
» c_o = compres_Vazquez_and_Beggs(30e6,250,
rho_g_100,805,105)
c_o = 3.0125e-009
» B_o = oil_form_vol_fact_undersat(B_ob,c_o,30e6,p_b)
B_o = 1.8591

```

Also in this case, the MATLAB computations can performed more directly as

```

» [B_g,B_o,R_s] = black_oil_
Standing(15e6,250,1.02,805,85)
B_g = 0.0067
B_o = 1.4666
R_s = 138.9552
» [B_g,B_o,R_s] = black_oil_
Standing(30e6,250,1.02,805,85)
B_g = 0
B_o = 1.8591
R_s = 250

```

G-3 Answers for Chapter 3, Single-Phase Flow in Wells and Pipelines

- 3.1 The Reynolds number is a dimensionless number that quantifies the relative importance of inertial forces relative to viscous forces in fluid flow. The transition from laminar to turbulent flow is associated with a “critical” value of the Reynolds number with a magnitude that depends on the geometry of the flow conduit. For example, in pipe flow the transition occurs at values of N_{Re} between 2000 and 3000.
- 3.2 (a) Gravity; (b) Friction.
- 3.3 This concerns acceleration in space, not in time. When gas moves up the well, it experiences a reduction in pressure leading to expansion (i.e., a reduction in density). To maintain the same mass flow rate, the velocity has to increase in proportion to the decrease in density. The increase in velocity is by definition the acceleration and, according to Newton’s law, requires a force—and therefore a pressure gradient—in the same direction. This may play a role in gas flow at very high rates. In liquid flow the effect can be completely neglected.
- 3.4 See Fig. 3.5. The gravity component decreases in relative importance closer to the surface because of the decrease in gas density caused by the decrease in pressure. Because the mass flow rate remains constant, a decrease in density implies an increase in velocity. This results in an increase in the relative importance of the friction component (which is strongly velocity dependent). The acceleration component becomes of significance only close to the

surface, where the rapid pressure drop causes a rapid gas expansion and hence a rapid change in velocity (just visible in Fig. 3.5).

3.5 The mass balance (Eq. 3.1) now becomes

$$A\rho v - \left(A + \frac{\partial A}{\partial s} ds \right) \left(\rho + \frac{\partial \rho}{\partial s} ds \right) \left(v + \frac{\partial v}{\partial s} ds \right) = \left(A + \frac{1}{2} \frac{\partial A}{\partial s} ds \right) \frac{\partial \rho}{\partial t} ds,$$

and the momentum balance (Eq. 3.2) becomes

$$\begin{aligned} A\rho v^2 - \left(A + \frac{\partial A}{\partial s} ds \right) \left(\rho + \frac{\partial \rho}{\partial s} ds \right) \left(v + \frac{\partial v}{\partial s} ds \right)^2 \\ + Ap - \left(A + \frac{\partial A}{\partial s} ds \right) \left(p + \frac{\partial p}{\partial s} ds \right) \\ + F_g(\rho, s) ds + F_f(\rho, \mu, v) ds = \left(A + \frac{1}{2} \frac{\partial A}{\partial s} ds \right) \frac{\partial(\rho v)}{\partial t} ds. \end{aligned}$$

Expanding these equations, dropping all terms higher than first order in ds , and simplifying the results gives

$$\frac{\partial(A\rho v)}{\partial s} = -A \frac{\partial \rho}{\partial t},$$

$$\frac{\partial(A\rho v^2)}{\partial s} = -A \frac{\partial(\rho v)}{\partial t} - \frac{\partial(Ap)}{\partial s} + F_g + F_f.$$

3.6 The fluid velocity in the pipeline is given by

$$v = \frac{q}{A} = \frac{q}{\frac{1}{4}\pi d^2} = \frac{-5000/(24 \times 3600)}{\frac{1}{4}\pi 0.232^2} = -1.37 \text{ m/s.}$$

The oil viscosity can be found from the correlation in Eq. B-10 as

$$b = 5.693 - \frac{2.863 \times 10^3}{850} = 2.325, a = \frac{10^{2.325}}{(1.8 \times 45 + 32)^{1.163}} = 0.866,$$

$$\mu = 10^{-3} (10^{0.866} - 1) = 6.3 \times 10^{-3} \text{ Pa} \cdot \text{s.}$$

The Reynolds number and the dimensionless roughness follow from Eqs. 3.10 and 3.11 as

$$N_{Re} = \frac{\rho d |v|}{\mu} = \frac{850 \times 0.232 \times 1.37}{6.3 \times 10^{-3}} = 4.3 \times 10^4 \text{ and } \epsilon = \frac{e}{d} = \frac{3 \times 10^{-6}}{0.232} = 1.3 \times 10^{-5},$$

which allow us to read the friction factor from the Moody diagram in Fig. 3.3 as

$$f(\varepsilon, N_{Re}) = f(1.3 \times 10^{-5}, 4.3 \times 10^{-4})$$

The pipeline inclination, seen from the origin at the manifold, should be negative to correspond to uphill production flow. Expressed in radians, the pipeline inclination therefore becomes

$$\theta = \frac{-1.5 \times \pi}{180} = -0.0262 \text{ rad.}$$

The pressure at the outlet can now be computed with the aid of Eq. 3.31 as

$$\begin{aligned} p_{out} &= \hat{p}_{in} - \left(\rho g \sin \theta + \frac{\rho}{2d} f v |v| \right) (s - \hat{s}) \\ &= 10 \times 10^5 - \left[850 \times 9.81 \times \sin(-0.0262) + \frac{850}{2 \times 0.232} \times 0.021 \times (-1.37) \times 1.37 \right] \\ &\quad \times (0 - 3000) \\ &= 1.29 \times 10^5 \text{ Pa.} \end{aligned}$$

3.7 The average absolute temperature along the well is $T_{av,abs} = 273.15 + (120 + 30)/2 = 348 \text{ K}$. The molar mass follows from Eq. A-5 as

$$M = 23.55 \times 10^{-3} \rho_{g,sc} = 23.55 \times 10^{-3} \times 0.95 = 22.4 \times 10^{-3} \text{ Kg/mol.}$$

The coefficients k_1 and k_2 are given by Eqs. 3.38 and 3.39 as

$$k_1 = -\frac{M g \sin \theta_{av}}{Z_{av} R T_{av,abs}} = -\frac{22.4 \times 10^{-3} \times 9.81 \times \sin(-\pi/2)}{0.96 \times 8.314 \times 348} = 7.91 \times 10^{-5} \text{ 1/m, and}$$

$$\begin{aligned} k_2 &= -\frac{8 Z_{av} R T_{av,abs} f_{av} \rho_{g,sc}^2 q_{g,sc} |q_{g,sc}|}{\pi^2 d^5 M} \\ &= -\frac{8 \times 0.96 \times 8.314 \times 348.15 \times 0.0166 \times 0.95^2 \times (-8.62) \times 8.62}{\pi^2 \times (62.3 \times 10^{-3})^5 \times 22.4 \times 10^{-3}} = 1.19 \times 10^{11} \text{ Pa}^2/\text{m.} \end{aligned}$$

With the aid of Eq. 3.43 we now find that

$$\begin{aligned} p_{wf} &= \sqrt{\left(\hat{p}_{wf}^2 + \frac{k_2}{k_1} \right) \exp \left[2k_1(s - \hat{s}) \right] - \frac{k_2}{k_1}} \\ &= \sqrt{\left(1.5 \times 10^6 \right)^2 + \frac{1.19 \times 10^{11}}{7.90 \times 10^{-5}}} \exp \left[2 \times 7.90 \times 10^{-5} \times (3000 - 0) \right] - \frac{1.19 \times 10^{11}}{7.90 \times 10^{-5}} \\ &= 30.3 \times 10^6 \text{ Pa,} \end{aligned}$$

which is reasonably close to the numerical result of $29.0 \times 10^6 \text{ Pa}$.

3.8 The equivalent diameter is found from Eq. 3.48 as

$$d_{\text{eq}} = \frac{\pi(d_i^2 - d_o^2)}{\pi(d_i + d_o)} = \frac{\pi(0.2815^2 - 0.2445^2)}{\pi(0.2815 + 0.2445)} = 0.037 \text{ m},$$

and the velocity in the annulus as

$$v_{\text{ann}} = \frac{q_{w,\text{sc}}}{0.25\pi(d_i^2 - d_o^2)} = \frac{1200 / (3600 \times 24)}{0.25\pi(0.2815^2 - 0.2445^2)} = 0.908 \text{ m/s}.$$

For the remaining steps, see the answer to Question 3.6. The numerical results are

$$N_{\text{Re}} = \frac{\rho_{w,\text{sc}} d_{\text{eq}} |v_{\text{ann}}|}{\mu_w} = \frac{1070 \times 0.037 \times 0.908}{0.38 \times 10^{-3}} = 1280000,$$

$$\epsilon = \frac{e}{d_{\text{eq}}} = \frac{4 \times 10^{-5}}{0.037} = 0.00108,$$

$$f(\epsilon, N_{\text{Re}}) = f(108 \times 10^{-5}, 128 \times 10^4) = 0.0202,$$

$$\begin{aligned} p_{\text{out}} &= \hat{p}_{\text{in}} - \left(\rho_{w,\text{sc}} g \sin \theta + \frac{\rho_{w,\text{sc}}}{2d_{\text{eq}}} f v_{\text{ann}} |v_{\text{ann}}| \right) (s - \hat{s}) \\ &= 40 \times 10^6 - \left[1020 \times 9.81 \times \sin\left(\frac{-\pi}{2}\right) + \frac{1020}{2 \times 0.037} \times 0.0202 \times 0.908^2 \right] \times (0 - 3230) \\ &= 6.87 \times 10^6 \text{ Pa}. \end{aligned}$$

- 3.9 In line with our sign convention for wellbore flow (positive for injection and negative for production), the MATLAB m-file `pipe.m` has been defined such that the origin of the coordinate along the flowline is at the manifold. Therefore, flow toward the manifold, as occurs in production wells, has a negative sign. Furthermore, a negative value of the flowline inclination indicates a decreasing flowline elevation, seen from the manifold. The m-file can be used for single-phase gas flow, two-phase (oil/water) liquid flow, or multiphase flow, depending on the value of the parameter `fluid`. In the case of single-phase oil flow, the input for gas and water flow rates and densities may be assigned arbitrary values. See script file `answer_question_3_9.m` for the numerical implementation. The output is
`p_mf = 1.2996e+005`

- 3.10 See script file `answer_question_3_10.m` for the numerical implementation. Using a tight tolerance (`options = odeset('MaxStep', 10, 'RelTol', 1e-3)`) in `pipe.m`, the pressure drop over the wellbore is 27.18×10^6 Pa. The error is -27.19 Pa, which gives a relative error with an absolute value of only 1.00×10^{-6} . With the default tolerance, the absolute value of the relative error

increases to 3.72×10^{-6} .

- 3.11 See script file `answer_question_3_11.m` for the numerical implementation. The exit pressure at the gas plant is $p_{out} = 8.97$ MPa. The pressure drop over the line is therefore $\Delta p = p_{in} - p_{out} = 10.00 - 8.97 = 1.03$ MPa. The pressure as a function of distance from the plant is displayed in [Fig. G-1](#).
- 3.12 See script file `answer_question_3_12.m` for numerical implementations using the MATLAB routine `fzero` and using an alternative, user-written Newton-Raphson algorithm. Running the file results in

```
>> answer_question_3_12
q_g_sc = 80.9268
q_g_sc = 80.9268
iter = 7
```

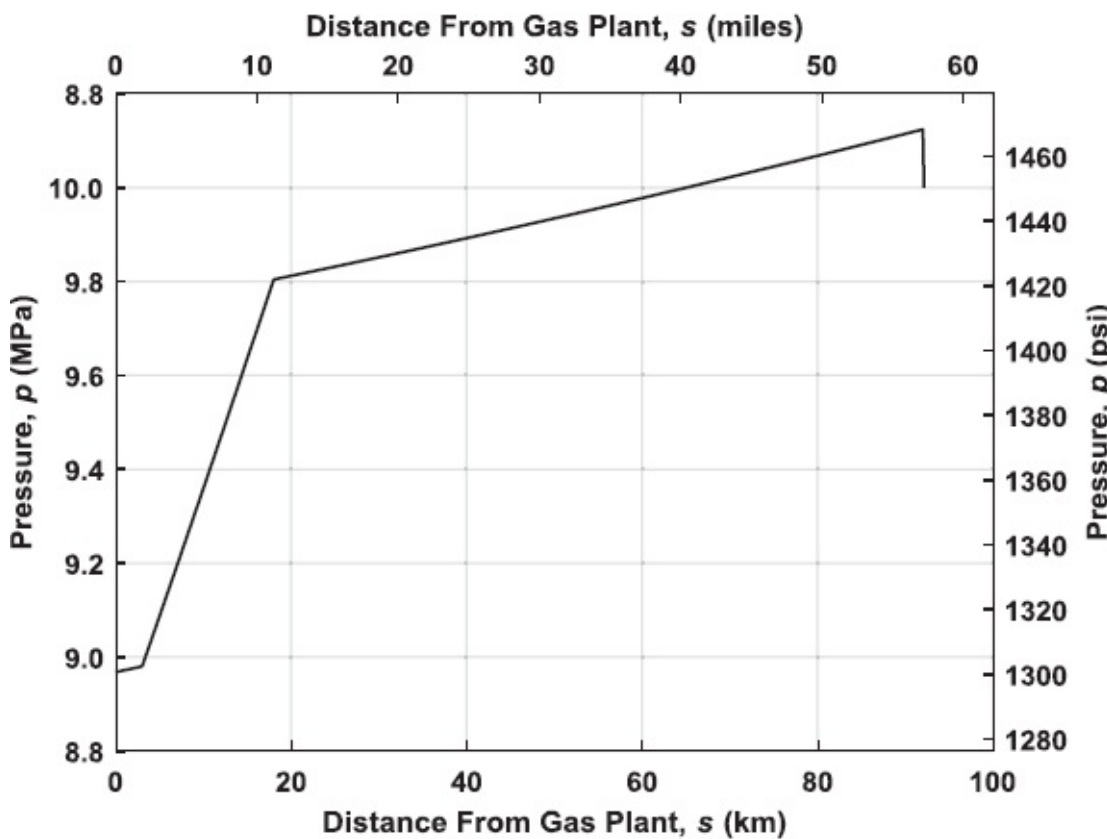


Fig. G-1—Pressure in the gas pipeline.

G-4 Answers for Chapter 4, Multiphase Flow in Wells and Pipelines

- 4.1 In a production well, the liquid holdup is typically larger than the liquid fraction of the fluid flowing through the well because of the slip between the liquid and gas phases.
- 4.2 Superficial phase velocities (i.e., superficial gas or liquid velocities) are equal to the respective phase volume flow rate divided by the *total* pipe cross-sectional area (see [Eqs. 4.9](#) and [4.10](#)). The in-situ phase velocities (i.e., the local or true phase velocities) are equal to the respective phase volume flow

rate divided by the fraction of the pipe's cross-sectional area that is actually occupied by that phase (see Eqs. 4.7 and 4.8). Superficial velocities are therefore always lower than the corresponding in-situ velocities. Superficial velocities are analogous to Darcy velocities in porous media flow. To compute the in-situ velocities from the superficial velocities, it is necessary to first determine the phase holdups—i.e., the relative fractions of the pipe's cross-sectional area that are occupied by the respective phase (see Eqs. 4.14 through 4.17).

- 4.3 Usually the interaction between gas and liquid in two-phase flow is too complex to be described in detail, and the exchange of momentum between the gas and the liquid phase is therefore typically not taken into account explicitly. (Exceptions are stratified or annular flow, which have relatively simple geometries, and sophisticated mechanistic models, which are outside the scope of this book.) The usual solution is to express the mass and momentum balances as mixture equations in terms of a mixture velocity and a mixture density. Two additional closure equations are then specified for the relationships between the mixture velocity and the phase velocities, and the mixture density and the phase densities, respectively. The closure equations are usually empirical or semiempirical.
- 4.4 Because they have been derived from (a) a limited number of experiments on (b) scaled (i.e., not full-size) setups, (c) using a limited range of fluids (sometimes not even hydrocarbons, but, e.g., water and air), (d) at pressures and temperatures that are typically much lower than in real wells.
- 4.5 See Fig. 4.9. The graph has a minimum near $1 \times 10^{-3} \text{ m}^3/\text{s}$. To the right of the minimum, frictional forces dominate, which increase for increasing flow rates, just as in single-phase flow. To the left of the minimum, gravity forces dominate, which increase for decreasing flow rates. This is because at decreasing flow rates the liquid holdup increases as a result of an increasing slip of the gas phase through the liquid phase.
- 4.6 See Fig. 4.3.

$$A_l = \frac{q_l}{v_l} = \frac{0.3 \times q_g}{v_g / 1.2} = 0.36 \times A_g; \lambda_l = \frac{q_l}{q_g + q_l} = \frac{0.3 \times q_g}{(1+0.3)q_g} = 0.23;$$

$$H_l = \frac{A_l}{A_g + A_l} = \frac{0.36 \times A_g}{(1+0.36)A_g} = 0.26.$$

- 4.7 The local phase rates can be obtained from Eq. 2.31 as

$$\begin{bmatrix} q_g \\ q_o \\ q_w \end{bmatrix} = \begin{bmatrix} 0.05 & -0.05 \times 10.1 & 0 \\ 0 & 1.15 & 0 \\ 0 & 0 & 1 \end{bmatrix} \begin{bmatrix} 238 \\ 1 \\ \frac{0.23}{1-0.23} \end{bmatrix} \times 18.4 \times 10^{-3} = \begin{bmatrix} 210 \\ 21.2 \\ 5.5 \end{bmatrix} \times 10^{-3} \text{ m}^3/\text{s}.$$

4.8 The pipe's cross-sectional area is given by $A = \frac{1}{4} \pi d^2 = 0.0117 \text{ m}^2$. Thus we find

$$\lambda_t = \frac{q_t}{q_g + q_t} = \frac{(21.2 + 5.5) \times 10^{-3}}{(210 + 21.2 + 5.5) \times 10^{-3}} = 0.113; H_t = 1.05 \times \lambda_t = 1.05 \times 0.113 = 0.119;$$

$$v_{sg} = \frac{q_g}{A} = \frac{210 \times 10^{-3}}{0.0117} = 17.9 \text{ m/s}; v_{sl} = \frac{q_o + q_w}{A} = \frac{(21.2 + 5.5) \times 10^{-3}}{0.0117} = 2.28 \text{ m/s};$$

$$v_g = \frac{v_{sg}}{(1 - H_t)} = \frac{17.9}{(1 - 0.119)} = 20.3 \text{ m/s}; v_l = \frac{v_{sl}}{H_t} = \frac{2.28}{0.119} = 19.2 \text{ m/s}.$$

4.8 (a) and (b) The FTHP is approximately equal to 17 MPa. At the bottom of the hole, the contribution of acceleration to the pressure drop is zero. The contributions of friction and gravity are approximately $28 - 17 = 11$ MPa and $38 - 17 = 21$ MPa, respectively. The total pressure drop is therefore $11 + 21 = 32$ MPa, and the FBHP follows as $17 + 32 = 49 \approx 50$ MPa, as shown in [Fig. G-2](#).

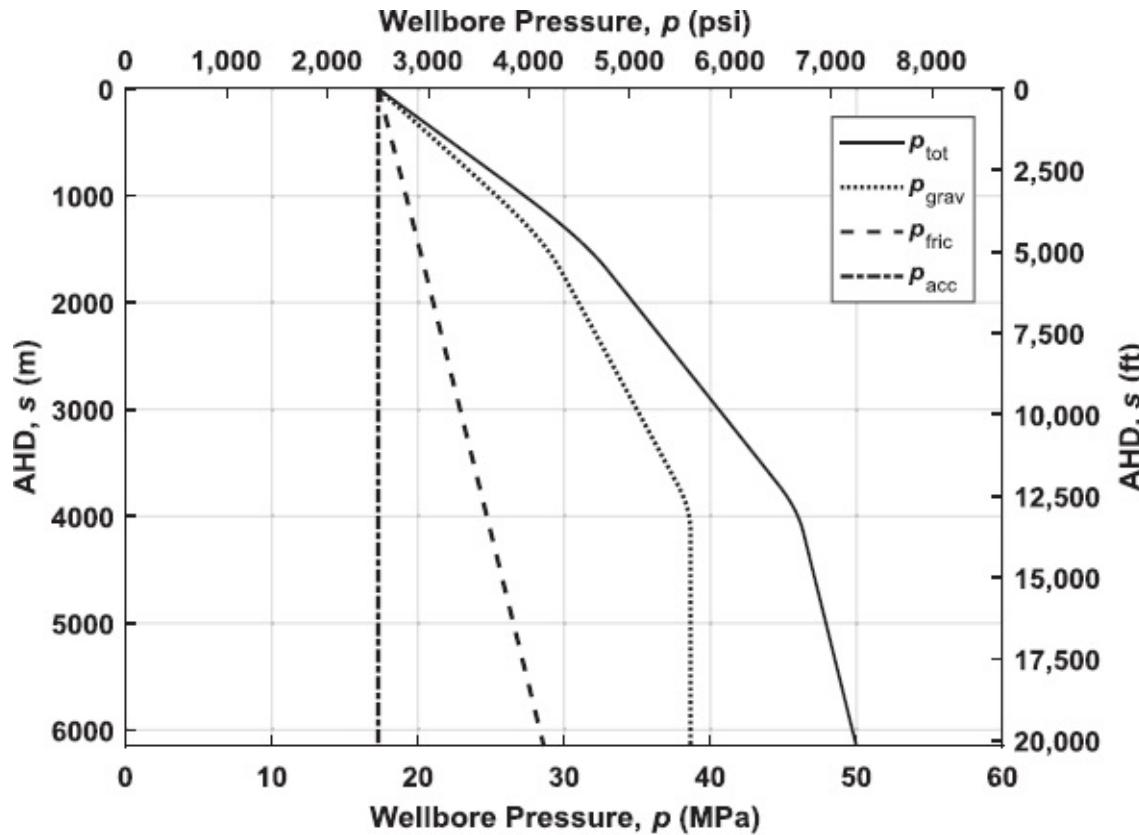


[Fig. G-2](#)—Pressure drop components.

- (c) Note the curvature of the friction curve (slightly concave) and the gravity curve (slightly convex) near the surface, as shown in [Fig. G-3](#).
- (d) Brill and Mukherjee, and Shi et al., because they can cope with deviated

wells.

- 4.9 Read the depth corresponding to a FTHP of 5 MPa from the curve for a GOR of 50 m³/m³. This is approximately 1200 m. Go down 3000 m (the well depth) to 4200 m and read the FBHP. This is approximately 28 MPa.

- 4.10 Type `help_pipe` or open the file in the editor to inspect the input requirements. Use of the Mukherjee and Brill correlation (`fluid = 4`) and the Standing black oil correlations (`oil = 1`) gives

```
>> p_wf = pipe(0,0.1005,30e-6,4,1,5e6, [-50*0.01, - 0.01, 0], [0.95, 850, 1000], 0, 3000, 60, 60)
p_wf = 2.8160e+07
```

- 4.11 (a) In the input data of the example (line 32), replace

`p_tf = 0.5e6; % FTHP, Pa`

by a higher value, e.g.,

`p_tf = 2.0e6; % FTHP, Pa`

At increasing FTHPs the tubing intake curves shift upward because the pressure in the entire well increases. Moreover, the curves become flatter and more and more resemble an intake curve for single-phase flow (see **Fig. G-4**). The reason is that because of the increased pressure, there is less gas coming out of solution and the well starts increasingly to behave as a single-phase well.

- (b) In the input data of the copied file (line 32), replace

`p_tf = 0.5e6; % FTHP, Pa`

by

`p_wf = 26e6; % FBHP, Pa`

In the section for the multiphase case (lines 92 and 93), replace

```
p_wf = pipe (alpha,d,e,fluid,oil,p_tf,q_sc,
rho_sc,0,s_tot,T_tf,T_wf);
results(i,1:2)= [-q_o_sc p_wf];
```

by

```
p_tf = pipe (alpha,d,e,fluid,oil,p_wf,q_sc,
rho_sc,s_tot,0,T_wf,T_tf);
results(i,1:2)= [-q_o_sc p_tf];
```

Note: Here we have highlighted the changes by underlining them, but no underlining is used in the actual MATLAB file.

In the plot commands (line 97) replace

`ylabel('Flowing bottomhole pressure\nit p_{wf},\nrm Pa')`

by

`ylabel('Flowing tubinghead pressure\nit p_{tf},\nrm Pa')`

The tubing performance curve for $p_{wf} = 26$ MPa displays a maximum unlike the single-phase gas curve in **Fig. 3.6**, which decreases monotonically. The explanation is identical to the one for the difference in

tubing intake curves between single-phase and multiphase flow: the effect of gas slipping through the oil at low flow rates causes liquid holdup and therefore increases the head loss. At increasing FBHPs the tubing intake curves shift upward because the pressure in the entire well increases (see [Fig. G-5](#)). Moreover, the curves become flatter and increasingly resemble an intake curve for single-phase flow, just as happened with the tubing intake curves in Part (a) of this question.

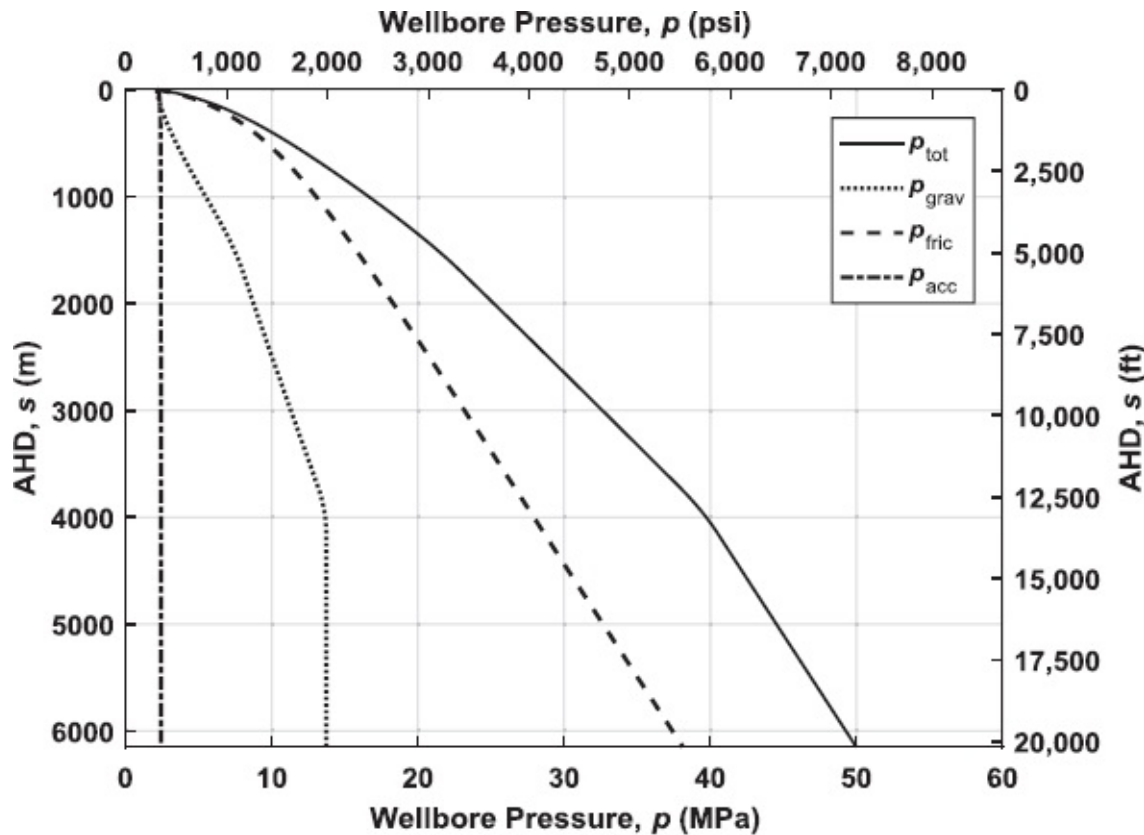


Fig. G-3—Pressure drop components for oil with a much higher solution GOR.

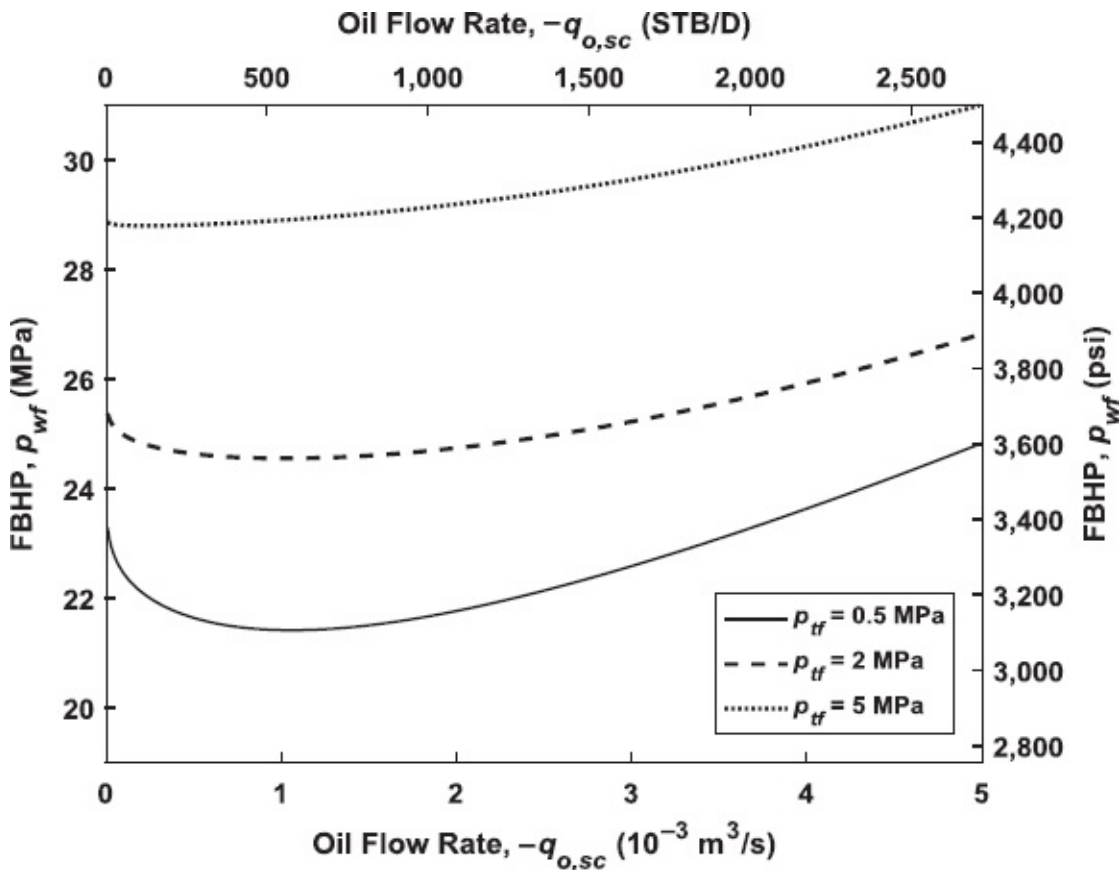


Fig. G-4—Multiphase tubing intake curves for different FTHPs.

4.12 With the aid of Fig. E-1 (or Eqs. E-1 through E-3), we find that

$$x_1 = N_\mu = 0.131,$$

corresponds to

$$N_{\mu c} = y_1 = 0.0074,$$

and with the aid of Fig. E-2 (or Eqs. E-4 through E-6), we find that

$$x_2 = \frac{N_g N_\mu^{0.380}}{N_d^{2.14}} = 0.031,$$

which corresponds to

$$\psi = y_2 = 1.43.$$

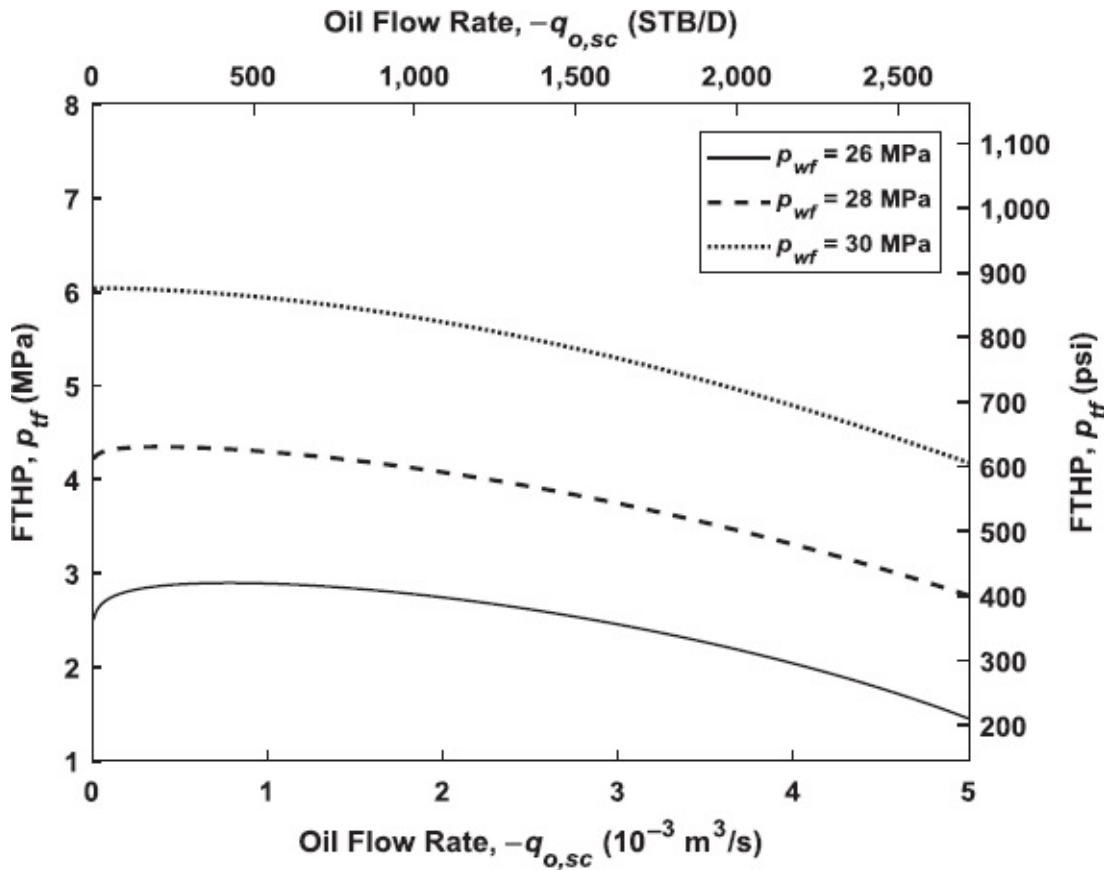


Fig. G-5—Multiphase tubing performance curves for different FBHPs.

Finally, with the aid of Fig. E-3 (or Eqs. E-8, E-9 and E-11), it follows that

$$x_3 = \frac{N_k}{N_{gv}^{0.575}} \left(\frac{p}{p_\infty} \right)^{0.10} \frac{N_{\mu c}}{N_d} = 2.04 \times 10^{-4},$$

which results in a liquid holdup of

$$H_l = y_3 \psi = 0.65.$$

4.13 Fig. G-6 shows a flow chart that has been filled in.

- 4.14 (a) This equation describes a flooding curve, which is the drift velocity v_d as a function of gas holdup H_g in the Shi et al. drift flux model.
- (b) C_0 is the profile parameter, which represents the effect of gas bubbles concentrating at the center of the wellbore, where the fluid velocities are highest. A value of unity implies a flat concentration profile—a situation in which the bubbles are equally distributed over the wellbore area. (Note: This says nothing about the velocity profile.)
- (c) At the transition to annular flow, the ratio $v_g/v_{g,flid} = 1$ and the gas velocity v_g is just sufficient to support a thin annulus of liquid such that it does not flow back down along the wellbore. Although the mixture velocity v_{ms} is

somewhat lower than v_g , because of liquid holdup, the ratio $v_g/v_{g,fl}$ at fully developed annular flow will be much larger than unity, and so also the ratio $v_{ms}/v_{g,fl}$ will exceed unity.

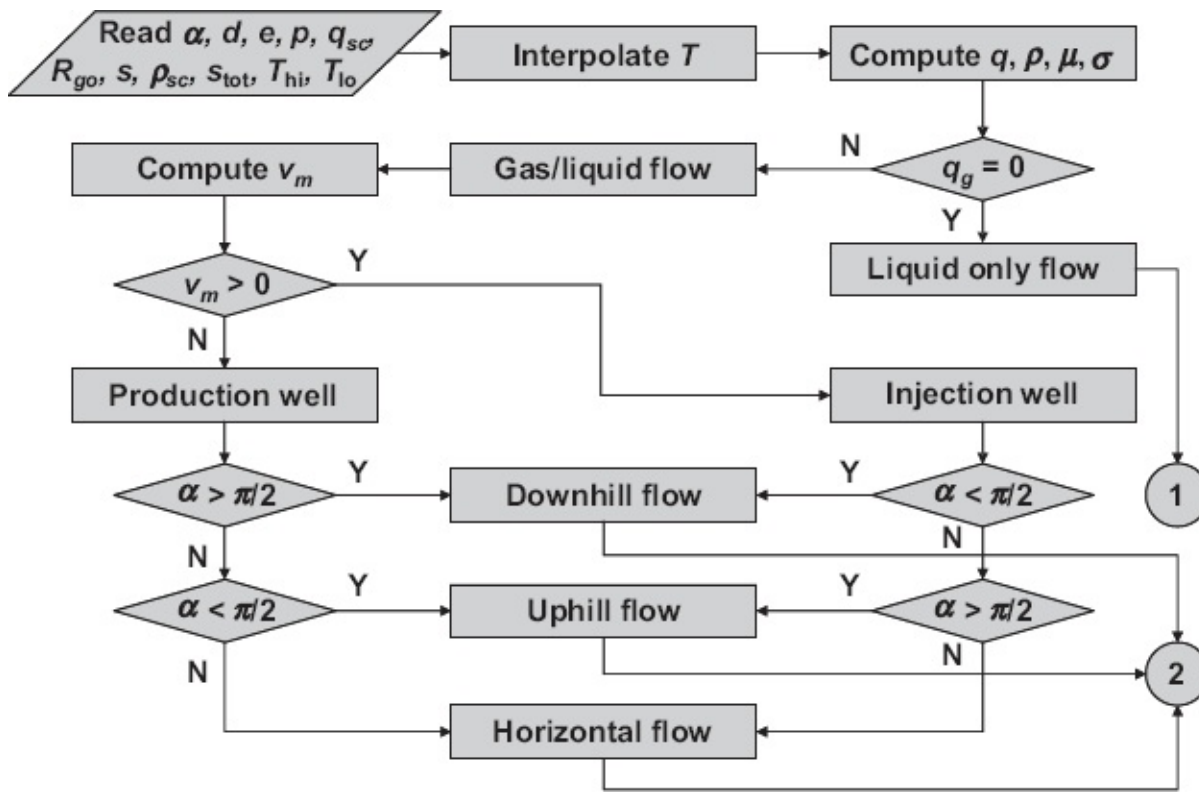


Fig. G-6—Flow chart for Mukherjee and Brill algorithm.

G-5 Answers for Chapter 5, Flow Through Restrictions

- 5.1 Because the main assumption in the derivation of the Bernoulli equation is the occurrence of frictionless flow. This is a reasonable assumption for the converging part of a choke, but not for the diverging part.
- 5.2 The maximum pressure drop is mainly caused by acceleration of the fluid—i.e., by a conversion of potential energy into kinetic energy. A small amount of the maximum pressure drop is caused by dissipation (i.e., by conversion of potential energy into heat). The permanent pressure drop is entirely caused by dissipation. A Venturi flow meter has a lower pressure drop than an orifice meter. Moreover, there are nonintrusive meters that use different physical principles—e.g., acoustic meters, which measure the upstream and downstream sound propagation velocities—and do not cause a pressure drop at all.
- 5.3 For isentropic flow we have

$$\frac{p^{\frac{1}{\gamma}}}{T_{abs}} = C,$$

from which follows that a decrease in pressure leads to a decrease in temperature.

- 5.4 Because then downstream disturbances (in the surface facilities) cannot propagate to the well. Such disturbances may destabilize the wellbore flow or, in the worst case, kill the well.
- 5.5 Because the flow rates remain far below the speed of sound, which is extremely high in nearly incompressible fluids.
- 5.6 Because the expression for critical flow over an orifice can be derived by considering the converging part of the restriction only, for which the theory of isentropic (or polytropic) flow is reasonably accurate (although the restriction to ideal gases already introduces inaccuracies for hydrocarbon flow). However, the expression for critical flow over a choke also involves the partial pressure recovery over the diverging part, which cannot be described accurately without a much more involved thermodynamic analysis. The usual oilfield approach to determine the total pressure drop over the choke with the aid of an overall discharge coefficient C_d is very approximate. Therefore the resulting expression for critical flow is also not too accurate.
- 5.7 An underlying assumption of isentropic flow is that the fluid expansion or compression happens so fast that there is no time for heat exchange with the surroundings (i.e., the flow is adiabatic). This is an accurate assumption for single-phase gas flow. However, in multiphase flow the presence of liquid drops in the gas stream allows for some rapid cooling or heating of the gas (in which case the liquid droplets are considered part of the surroundings of the gas). Because we maintain the assumption of reversibility, the flow will be somewhere between isentropic and isothermal, a condition known as polytropic.
- 5.8 No, this is not correct for C_d . The statement does hold for \tilde{C}_d , which plays a role in quantifying the maximum pressure drop developed over the contracting part of the choke. A value of $\tilde{C}_d = 1$ implies frictionless (i.e., completely reversible) flow, which is theoretically impossible. Any additional loss because of friction results in an increase in the maximum pressure drop, which because \tilde{C}_d appears in the denominator implies a value of \tilde{C}_d below unity. However, C_d , which plays a role in quantifying the permanent pressure drop developed over the total choke, can be larger than unity if the permanent pressure drop is smaller than the frictionless maximum pressure drop.
- 5.9 See [Eq. 5.11](#):

$$q_o = \frac{-300}{3600 \times 24} = -3.47 \times 10^{-3} \text{ m}^3/\text{s},$$

$$A_1 = \frac{\pi d_1^2}{4} = \frac{\pi \times 0.048^2}{4} = 1.81 \times 10^{-3} \text{ m}^2,$$

$$A_2 = \frac{\pi d_2^2}{4} = \frac{\pi \times 0.023^2}{4} = 0.415 \times 10^{-3} \text{ m}^2,$$

$$\beta_2 = \frac{A_2}{A_1} = \frac{0.415}{1.81} = 0.23,$$

$$\begin{aligned}\Delta p_{\max} &= p_1 - p_3 = \frac{\rho}{2} \frac{q^2}{A_2^2} \frac{(1 - \beta_2^2 \tilde{C}_c^2)}{\tilde{C}_c^2} \\ &= \frac{876}{2} \frac{(-3.47 \times 10^{-3})^2}{(0.415 \times 10^{-3})^2} \frac{(1 - 0.23^2 \times 0.62^2)}{0.62^2} = 78.1 \times 10^3 \text{ Pa}.\end{aligned}$$

5.10 See Eq. 5.22:

$$q = \frac{-0.8}{60} = -1.33 \times 10^{-2} \text{ m}^3/\text{s},$$

$$\Delta p = 1.732 \times 10^9 \frac{q^2 \rho}{C_v^2} = 1.732 \times 10^9 \frac{(-1.33 \times 10^{-2})^2 \times 830}{40^2} = 0.16 \times 10^6 \text{ Pa}.$$

5.11 (a) See Eq. 5.39:

$$\gamma = \frac{c_p}{c_v} = \frac{0.26}{0.20} = 1.30,$$

$$\left(\frac{p_3}{p_1}\right)_{\text{crit}} = \left(\frac{2}{1+\gamma}\right)^{\frac{\gamma}{\gamma-1}} = \left(\frac{2}{1+1.3}\right)^{\frac{1.3}{1.3-1}} = 0.55,$$

$$\left(\frac{p_3}{p_1}\right) = \frac{3.2 \times 10^6}{4.3 \times 10^6} = 0.74.$$

Because $(p_3/p_1) > (p_3/p_1)_{\text{crit}}$, the flow is noncritical.

(b) See Eq. 5.36:

$$\begin{aligned}q_{g,\infty} &= -\tilde{C}_d A_2 \sqrt{\frac{2 p_1^2 T_{sc,abs}}{p_{sc} T_{1,abs} Z_1 \rho_{g,\infty}} \frac{\gamma}{\gamma-1} \left[\left(\frac{p_3}{p_1}\right)^{\frac{2}{\gamma}} - \left(\frac{p_3}{p_1}\right)^{\frac{1+\gamma}{\gamma}} \right]} \\ &= -0.35 \times 4.91 \times 10^{-4} \sqrt{\frac{2 \times (4.3 \times 10^6)^2 \times (15 + 273.15)}{0.1 \times 10^6 \times (65 + 273.15) \times 0.94 \times 0.80} \times \frac{1.30}{1.30-1} \left[\left(\frac{3.2 \times 10^6}{4.3 \times 10^6}\right)^{\frac{2}{1.30}} - \left(\frac{3.2 \times 10^6}{4.3 \times 10^6}\right)^{\frac{1+1.30}{1.30}} \right]} = -1.50 \text{ m}^3/\text{s}.\end{aligned}$$

5.12 (a) See Eq. 5.54:

$$q_{o,sc} = \frac{-120}{24 \times 3600} = -1.39 \times 10^{-3} \text{ m}^3/\text{s},$$

$$q_{g,sc} = R_{go} q_{o,sc} = 40 \times -1.39 \times 10^{-3} = -55.6 \times 10^{-3} \text{ m}^3/\text{s},$$

$$q_{w,sc} = \frac{f_w}{1-f_w} q_{o,sc} = \frac{0.70}{1-0.70} \times -1.39 \times 10^{-3} = -3.24 \times 10^{-3} \text{ m}^3/\text{s},$$

$$q_{l,sc} = q_{o,sc} + q_{w,sc} = -1.39 \times 10^{-3} - 3.24 \times 10^{-3} = -4.63 \times 10^{-3} \text{ m}^3/\text{s},$$

$$R_{gl} = \frac{q_{g,sc}}{q_{l,sc}} = \frac{-55.6 \times 10^{-3}}{-4.63 \times 10^{-3}} = 12.0 \text{ m}^3/\text{m}^3,$$

$$\begin{aligned} p_1 &= -A q_{l,sc} \frac{(ER_{gl})^B}{(Fd_{ch})^C} + D \\ &= -3.75 \times 10^{10} \times -4.63 \times 10^{-3} \times \frac{(5.61 \times 12.0)^{0.546}}{(2.52 \times 10^3 \times 0.0127)^{1.89}} + 1.01 \times 10^5 \\ &= 2.57 \times 10^6 \text{ Pa}. \end{aligned}$$

(b) See Eq. 5.53:

$$\left(\frac{p_4}{p_1}\right)_{\text{crit}} \approx 0.6 \approx \frac{1}{1.7},$$

$$\left(\frac{p_4}{p_1}\right) = \frac{1.2 \times 10^6}{2.57 \times 10^6} = 0.47 = \frac{1}{2.1}.$$

Because $(p_4/p_1) < (p_4/p_1)_{\text{crit}}$, the flow is critical.

5.13 (a)/(b) See script file answer_question_5_13.m for the numerical implementation. The result is

```
>> answer_question_5_13
upstream pressure from choke_multi_phase_simp: 2.5722e+06
upstream pressure from choke_multi_phase: 3.00237e+06 critical flow
boundary (p_4/p_1)_crit from choke_multi_phase: 0.544165
p_4/p_1 from choke_multi_phase: 0.399684
critical flow boundary (p_1/p_4)_crit from choke_multi_phase: 1.83768
p_1/p_4 from choke_multi_phase: 2.50198
```

The result from choke_multi_phase_simp.m is identical to the answer to Question 5.12 (which is what you should have found from your hand calculation). The upstream pressure as computed by choke_multi_phase.m is approximately 17% higher. Moreover, the critical flow boundary $(p_4/p_1)_{\text{crit}}$ is 0.54 ($= 1/1.84$) instead of 0.6 ($= 1/1.7$). This illustrates the uncertainty associated with multiphase choke models.

5.14 See script file answer_question_5_14.m for the numerical implementation.

(a) See Figs. G-7 and G-8. The difference in shape between the choke

performance curve and the tubing intake curve is the presence of a minimum in the latter and the absence of such a minimum in the former. The minimum is caused by slip between the gas and liquid phases in the tubing. See also the answer to Question 4.5.

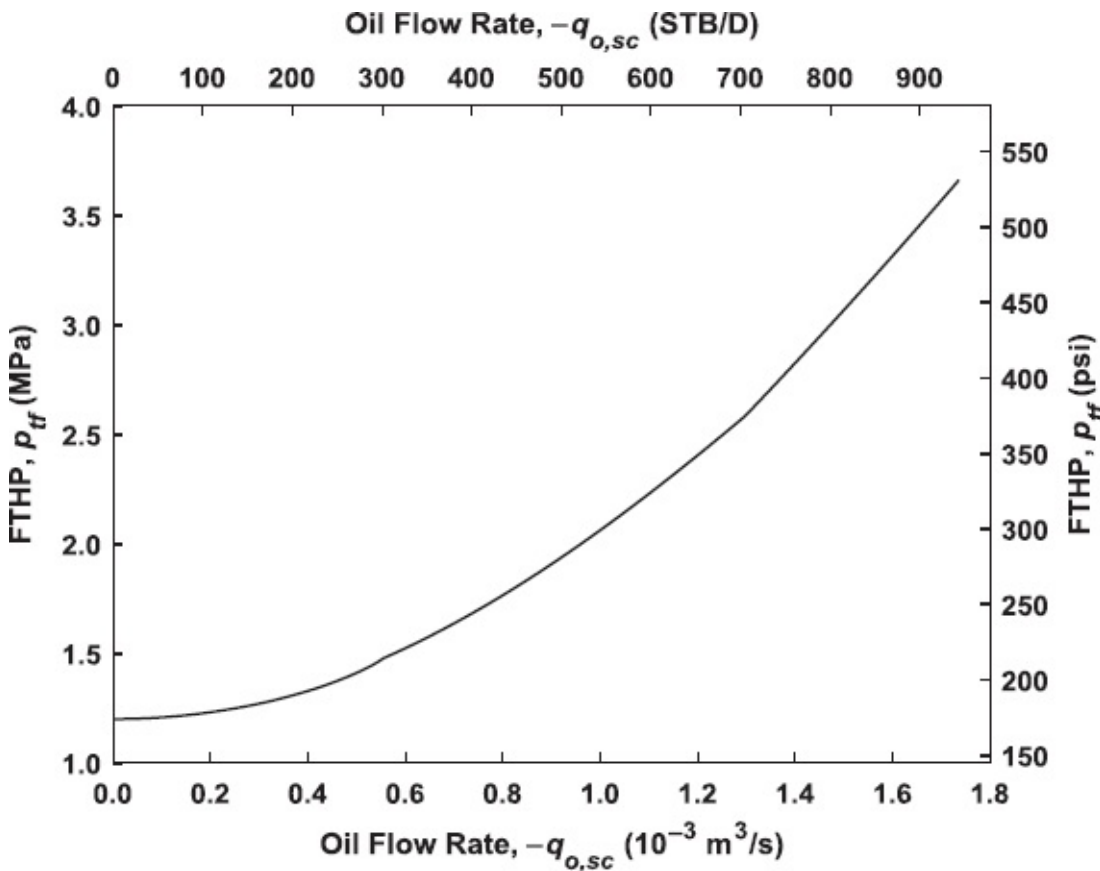


Fig. G-7—Choke performance curve.

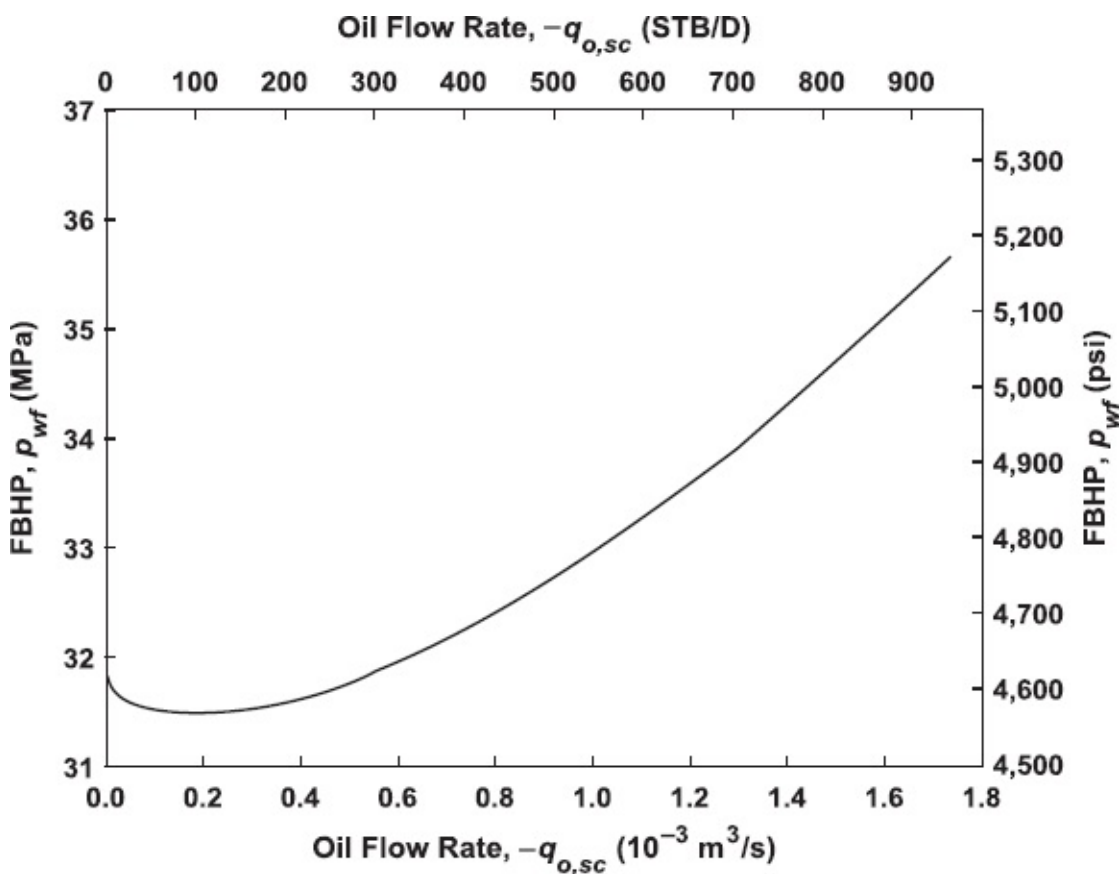


Fig. G-8—Tubing intake curve.

- (b) See Fig. G-9. The choke operates in the critical regime for flow rates above $1.35 \times 10^{-3} \text{ m}^3/\text{s}$. The critical pressure ratio shows a slight drop with increasing flow rates because the downstream pressure is changing with flow rate. This is different from the situation depicted in Fig. 5.7 because in that case the downstream pressure of the choke is kept fixed, whereas here the downstream pressure of the flowline is kept fixed.

G-6 Answers for Chapter 6, Inflow Performance: The Basics

- 6.1 In the case of (nearly) incompressible single-phase liquid (oil or water) flow. In practice the PI is often used when those conditions do not hold, in which case it can be interpreted as a linearized version of the IPR. The range of validity is then limited to operating conditions close to the linearization point (i.e., the point at which the PI has been estimated or computed).
- 6.2 In steady-state reservoir flow, the flow rates and pressures remain constant. In pseudosteady-state reservoir flow, the flow rates stay constant but the pressures decrease linearly with time.
- 6.3 S is dimensionless.
- 6.4 Crossflow occurs when the closed-in pressure of a zone exceeds the closed-in pressure of another zone plus the gravity head between the two zones.

Usually the pressure differences between zones are the result of disproportionate depletion—e.g., because of a large permeability contrast between the two zones.

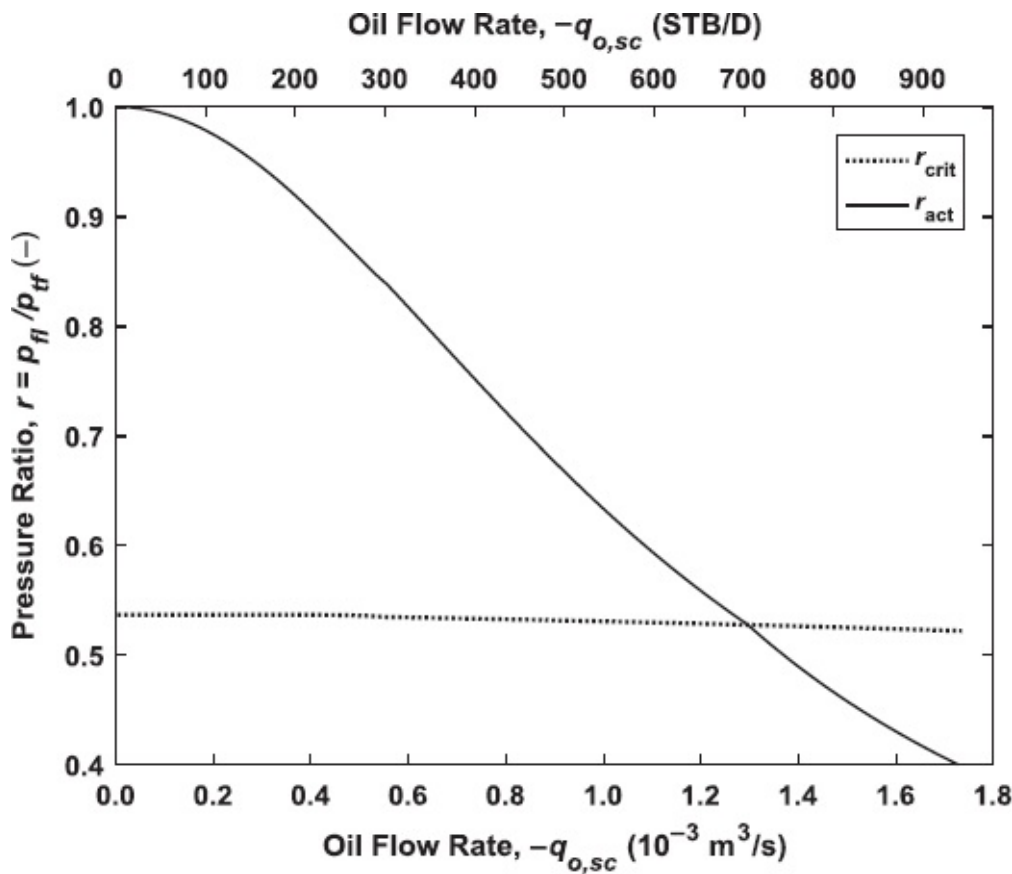


Fig. G-9—Critical and actual pressure ratios.

6.5 See Eq. 6.37:

$$p_{R,av} - p_{wf} = -\frac{\mu_o B_o q_{o,sc}}{2\pi k_o h} \left[\ln\left(\frac{r_e}{r_w}\right) - \frac{3}{4} \right],$$

from which it follows that

$$\begin{aligned} J &= \frac{-q_{o,sc}}{p_{R,av} - p_{wf}} = \frac{2\pi k_o h}{\mu_o B_o} \left[\ln\left(\frac{r_e}{r_w}\right) - \frac{3}{4} \right]^{-1} \\ &= \frac{2\pi \times (84 \times 9.87 \times 10^{-16}) \times (35 \times 0.3048)}{(2.54 \times 10^{-3}) \times 1.12} \left[\ln\left(\frac{2100}{0.33}\right) - \frac{3}{4} \right]^{-1} \\ &= 2.43 \times 10^{-10} \text{ m}^3/\text{Pa} \cdot \text{s}. \end{aligned}$$

In field units this becomes

$$J = \frac{2.43 \times 10^{-10}}{2.669 \times 10^{-10}} = 0.912 \text{ STB/D-psi.}$$

- 6.6 See [Fig G-10](#) for the spider plot. It can be concluded that the sensitivity to changes in the permeability k is much larger than the sensitivity to changes in the radii r_w and r_e . For example, doubling the permeability results in doubling the PI, but doubling the well radius leads only to an increase in the PI with a factor 1.09 and doubling the external radius to a drop in the PI with a factor 0.92. The reason for this difference is the occurrence of the radii inside the logarithm term (see [Eq. 6.37](#)).

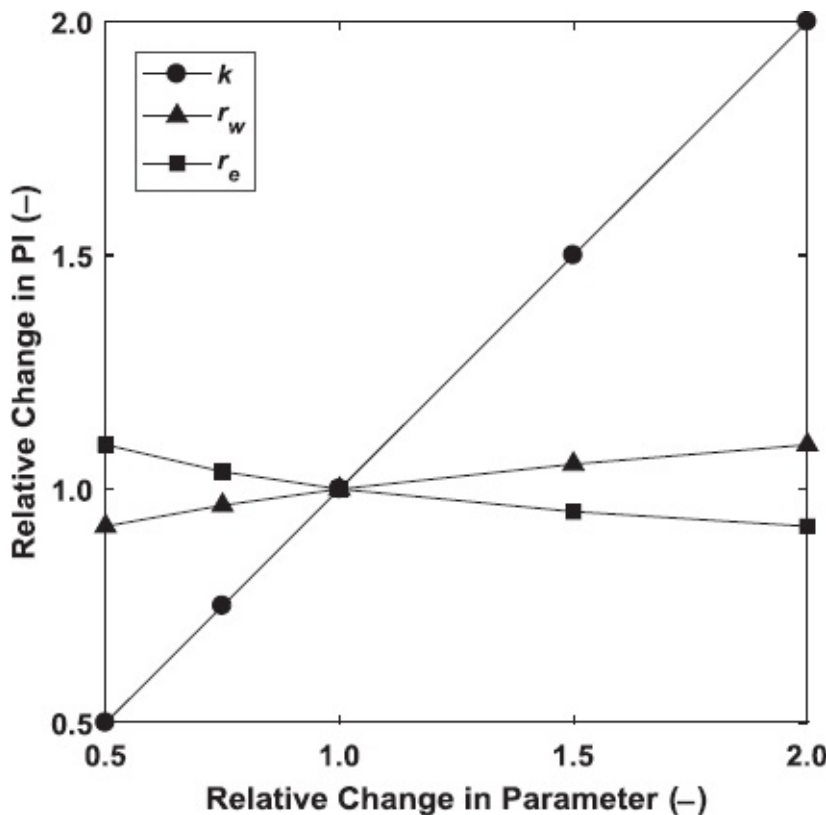


Fig. G-10—Spider plot indicating PI sensitivity to variations in parameter values.

- 6.7 Starting from [Eq. 6.35](#), an expression for the average reservoir pressure can be derived as

$$p_{R,\text{av}} = \frac{\int_{r_w}^{r_e} pr dr}{\int_{r_w}^{r_e} r dr} = p_R + \frac{\mu B_o q_{o,sc}}{\pi kh(r_e^2 - r_w^2)} \int_{r_w}^{r_e} \left[r \ln\left(\frac{r_e}{r}\right) - \frac{1}{2} \left(r - \frac{r^3}{r_e^2} \right) \right] dr,$$

where the first term between square brackets was already given in [Eq. 6.25](#), while the second term follows as

$$\int_w^{r_e} \left[-\frac{1}{2} \left(r - \frac{r^3}{r_e^2} \right) \right] dr = - \left(\frac{1}{4} r^2 - \frac{r^4}{6r_e^2} \right) \Big|_{r_w}^{r_e} = -\frac{1}{4} (r_e^2 - r_w^2) + \frac{(r_e^2 + r_w^2)(r_e^2 - r_w^2)}{8r_e^2}.$$

Substitution of these results gives

$$p_{R,av} = p_R + \frac{\mu B_o q_{o,sc}}{4\pi kh} \left[-\frac{2 \frac{r_w^2}{r_e^2} \ln\left(\frac{r_w}{r_e}\right)}{\left(1 - \frac{r_w^2}{r_e^2}\right)} + \frac{(r_e^2 + r_w^2)}{2r_e^2} \right] \approx p_R + \frac{\mu B_o q_{o,sc}}{8\pi kh}.$$

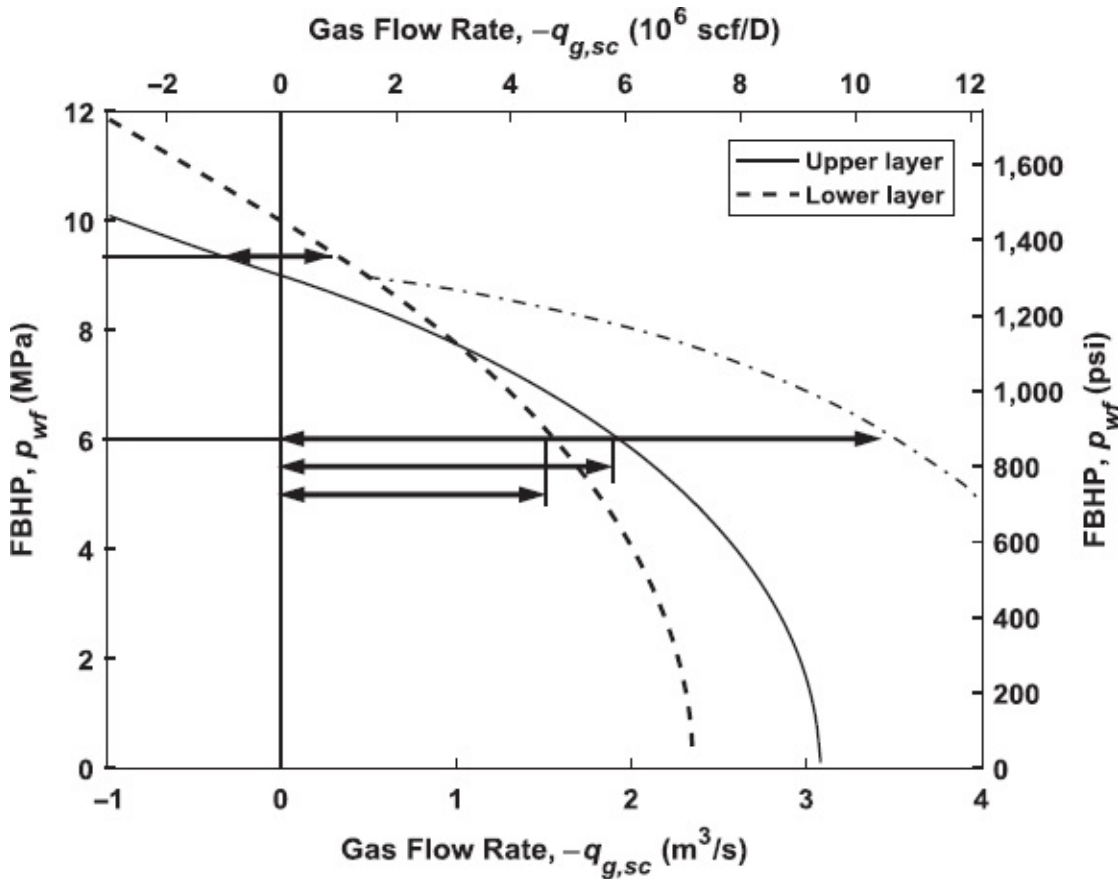


Fig. G-11—Commingled gas production (dash-dotted line represents combined IPR for the well).

Solving for p_R , substituting in Eq. 6.36, and rearranging the result then leads to

$$p_{R,av} - p_{wf} = -\frac{\mu B_o q_{o,sc}}{2\pi kh} \left[\ln\left(\frac{r_e}{r_w}\right) - \frac{1}{2} \left(1 - \frac{r_w^2}{r_e^2} \right) - \frac{1}{4} \right] \approx -\frac{\mu B_o q_{o,sc}}{2\pi kh} \left[\ln\left(\frac{r_e}{r_w}\right) - \frac{3}{4} \right].$$

6.8 First guess for $p_{R,av}$ is

$$p_{R,av} = \frac{(p_{wf} + p_R)}{2} = \frac{(20 \times 10^6 + 40 \times 10^6)}{2} = 30 \times 10^6 \text{ Pa}.$$

Modifying Eq. 6.77 for single-phase gas flow and rewriting the result in terms of flow rate $q_{g,sc}$ as a function of the equivalent drawdown $p_R^2 - p_{wf}^2$ gives

$$q_{g,sc} = \frac{-\pi k_g h (p_R^2 - p_{wf}^2)}{\mu_{g,av} B_{g,av} p_{R,av}} \left[\ln \left(\frac{a_e + \sqrt{a_e^2 - L^2}}{L} \right) + \frac{h}{L} \ln \left(\frac{h}{2r_w} \right) \right]^{-1}$$

$$= \frac{-\pi \times 2.0 \times 10^{-15} \times 20 \times [(40 \times 10^6)^2 - (20 \times 10^6)^2]}{23 \times 10^{-6} \times 4.4 \times 10^{-3} \times 30 \times 10^6}$$

$$\times \left[\ln \left(\frac{700 + \sqrt{700^2 - 500^2}}{500} \right) + \frac{20}{500} \ln \left(\frac{20}{2 \times 0.2} \right) \right]^{-1} = -48.5 \text{ m}^3/\text{s.}$$

With the aid of Eq. (6.63) we find

$$p_{R,av} = p_R + \frac{\mu_{av} B_{g,av} q_{g,sc}}{4\pi kh} = 30 \times 10^6 + \frac{23 \times 10^{-6} \times 4.4 \times 10^{-3} \times -48.5}{4\pi \times 2.0 \times 10^{-15} \times 20} = 30.2 \times 10^6 \text{ Pa.}$$

This is accurate enough, and here is no need to recompute the flow rate.

- 6.9 When the FBHP has dropped to the bubblepoint pressure, the flow rate follows as

$$q_{ob,sc} = J(p_b - p_R) = 4 \times 10^{-9} (28 \times 10^6 - 30 \times 10^6) = -0.008 \text{ m}^3/\text{s.}$$

The AOPF can now be computed with the aid of Eq. 6.74 as

$$q_{o,sc,max} = q_{ob,sc} + J \left(\frac{p_b}{\alpha - 2} \right) = -0.008 + 4 \times 10^{-9} \left(\frac{28 \times 10^6}{0.2 - 2} \right) = -0.0702 \text{ m}^3/\text{s.}$$

When the FBHP drops further to 25 MPa, the flow rate follows with Eq. 6.73 as

$$q_{o,sc} = q_{o,sc,max} \left\{ 1 - \left(1 - \frac{q_{ob,sc}}{q_{o,sc,max}} \right) \left[\alpha \left(\frac{p_{wf}}{p_b} \right) + (1 - \alpha) \left(\frac{p_{wf}}{p_b} \right)^2 \right] \right\}$$

$$= q_{o,sc,max} \left\{ 1 - \left(1 - \frac{-0.008}{-0.0702} \right) \left[0.2 \left(\frac{25 \times 10^6}{28 \times 10^6} \right) + (1 - 0.2) \left(\frac{25 \times 10^6}{28 \times 10^6} \right)^2 \right] \right\}$$

$$= -0.0194 \text{ m}^3/\text{s.}$$

- 6.10 After closing in the well, crossflow will occur (see Fig. G-11). The CBHP is the BHP at which the inflow from the lower layer into the well just balances the outflow from the well into the upper layer. This occurs at a BHP of approximately 9.3 MPa, and the corresponding flow rates are approximately 0.3 m³/s. At an FBHP of 6 MPa the total inflow will be the sum of the inflow from the two layers, which amounts to approximately 3.5 m³/s.

6.11 See script file `answer_question_6_11.m` for the numerical implementation.

Running the file gives

```
>> answer_question_6_11
J = 2.4345e-10
J_fu = 0.9122
```

6.12 See script file `answer_question_6_12.m` for the numerical implementation.

Running the file results in the IPRs depicted in **Fig. G-12**. It is clear that performing an acid treatment is far more effective than drilling a double-diameter well. Moreover, the cost of the acid job will in most circumstances be much lower than the additional drilling costs.

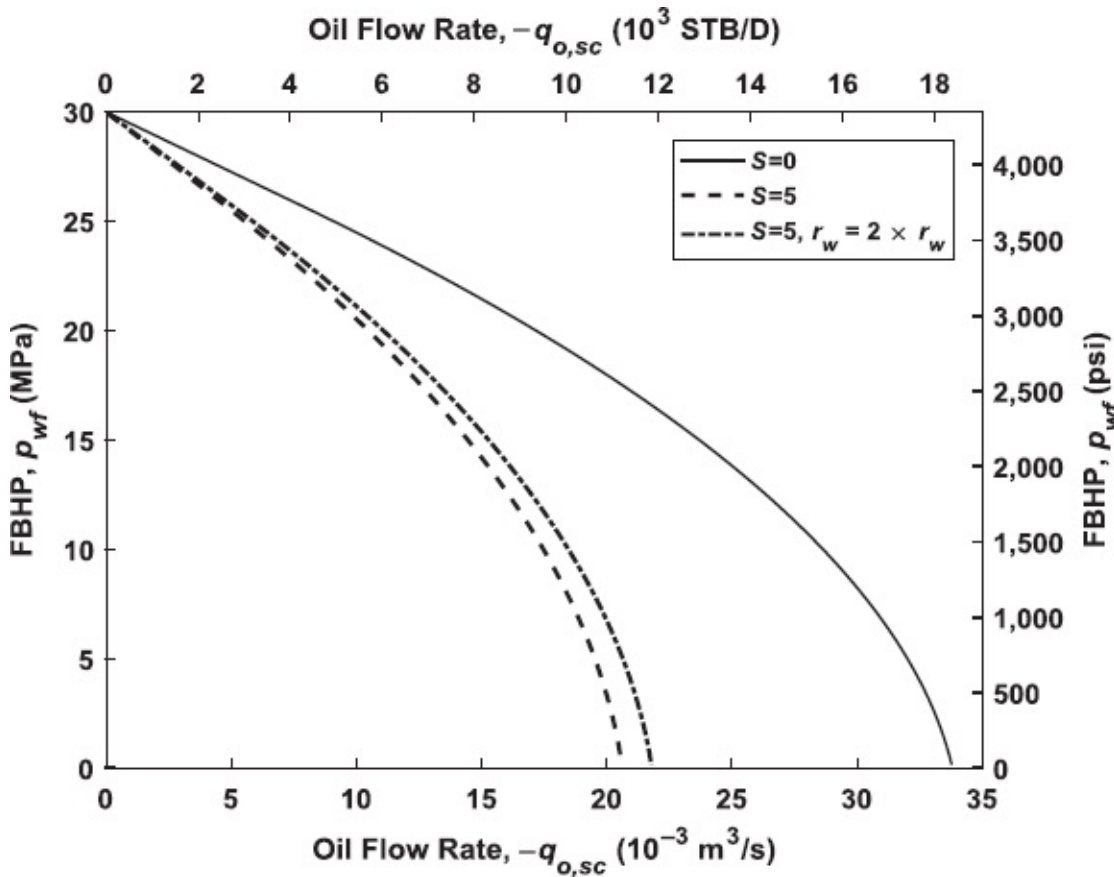


Fig. G-12—IPRs for increased values of skin S and wellbore radius r_w .

6.13 See script file `answer_question_6_13.m` for the numerical implementation.

Running the file results in

```
>> answer_question_6_13
p_wf = 20000000
m_wf = 1.6268e+09
p_R = 40000000
m_R = 4.8051e+09
mu_g_ref = 1.1834e-05
B_g_ref = 1.3627
```

Modifying [Eq. 6.77](#) for single-phase gas flow in terms of pseudopressures and then rewriting the result in terms of flow rate $q_{g,sc}$ as a function of the

drawdown $m_R - m_{wf} = m(p_R) - m(p_{wf})$ give

$$q_{g,sc} = \frac{-2\pi k_g h (m_R - m_{wf})}{\mu_{g,ref} B_{g,ref}} \left[\ln\left(\frac{a_e + \sqrt{a_e^2 - L^2}}{L}\right) + \frac{h}{L} \ln\left(\frac{h}{2r_w}\right) \right]^{-1}$$

$$= \frac{-2\pi \times 2.0 \times 10^{-15} \times 20 \times (4.81 \times 10^9 - 1.63 \times 10^9)}{1.18 \times 10^{-5} \times 1.36}$$

$$\times \left[\ln\left(\frac{700 + \sqrt{700^2 - 500^2}}{500}\right) + \frac{20}{500} \ln\left(\frac{20}{2 \times 0.2}\right) \right]^{-1} = -48 \text{ m}^3/\text{s.}$$

(See Eqs. 6.38 and 6.59 for the similarity to the radial flow case.) The small difference between the answers to Questions 6.6 and 6.13 is caused by the approximation of the average pressure in Question 6.6 and the incomplete iteration. The answer to Question 6.13 is therefore more accurate. However, it should be noted that inflow performance expressions such as Eq. 6.77 are approximate anyway, and the small difference between the answers is therefore probably not relevant for most applications.

6.14 See script file `answer_question_6_14.m` for the numerical implementation.

Running the file results in

```
>> answer_question_6_14
q_g_sc = 0.3279
p_wc = 9.3456e+06
q_g_sc = -3.4960
```

G-7 Answers for Chapter 7, Inflow Performance: Further Topics

7.1 No, that is not possible. To compute a solution to the Laplace equation (i.e., to compute a spatial pressure distribution), it is necessary to specify the pressure in the reservoir at least at one point. Darcy's law only gives us a relationship between flow rate and pressure gradients, and does not allow us to compute absolute pressures without having additional information. As an aside, we note that the boundary conditions (Eqs. 7.161 and 7.162) can be rewritten as

$$r = r_w : \frac{\partial p}{\partial r} = -\frac{\mu B_o q_{o,sc} r_w}{k A_w} = -\frac{\mu B_o q_{o,sc}}{2\pi k h},$$

$$r = r_e : \frac{\partial p}{\partial r} = -\frac{\mu B_o q_{o,sc} r_e}{k A_e} = -\frac{\mu B_o q_{o,sc}}{2\pi k h},$$

which implies that they both prescribe exactly the same flow rate. This is in line with the assumption of steady-state flow such that no storage in the reservoir can take place.

- 7.2 See the explanation in [Section 7.3.4](#). These skin factors both correspond to an additional pressure drop caused by formation damage as defined in [Eq. 7.69](#), but use different geometrical variables depending on their relevance to either horizontal or vertical wells.
- 7.3 See the discussion in [Sections 6.8](#) and [7.6](#). In general, the amounts of oil, gas, and water entering a well vary over time and are strongly influenced by near-well heterogeneities, the size and location of which are poorly known, if they are known at all.
- 7.4 Refer to the image well approach for the four-well configuration in [Section 7.2.4](#). Following a similar approach using just a single image well, the pressure field for the isotropic permeability can be described as

$$p = p_R + \frac{\mu B_o q_{o,\infty}}{4\pi kh} \ln \left(r_e^4 \times \left\{ \left[\left(x - \frac{D_x}{2} \right)^2 + y^2 \right] \times \left[\left(x + \frac{D_x}{2} \right)^2 + y^2 \right] \right\}^{-1} \right),$$

where it has been assumed that the distance D is measured along the x -axis. For $(x, y) = (D_x/2 + r_w, 0)$ [Eq. 7.26](#) gives the pressure in the producer in the top-right quadrant:

$$\begin{aligned} p_{wf} &= p_R + \frac{\mu B_o q_{o,\infty}}{4\pi kh} \ln \left\{ r_e^4 \times \left[\left(\frac{D_x}{2} + r_w - \frac{D_x}{2} \right)^2 \times \left(\frac{D_x}{2} + r_w + \frac{D_x}{2} \right)^2 \right]^{-1} \right\} \\ &= p_R + \frac{\mu B_o q_{o,\infty}}{4\pi kh} \ln \left[\frac{r_e^4}{r_w^2 \times (D_x + r_w)^2} \right] \\ &\approx p_R + \frac{\mu B_o q_{o,\infty}}{4\pi kh} \ln \left(\frac{r_e^4}{D_x^2 r_w^2} \right) = p_R + \frac{\mu B_o q_{o,\infty}}{2\pi kh} \ln \left(\frac{r_e^2}{D_x r_w} \right). \end{aligned}$$

The steady-state PI for a producer near a no-flow boundary therefore becomes

$$J = \frac{-q_{o,\infty}}{p_R - p_{wf}} = \frac{4\pi kh}{\mu B_o \ln \left[\frac{r_e^4}{r_w^2 \times (D_x + r_w)^2} \right]} = \frac{2\pi kh}{\mu B_o \ln \left(\frac{r_e^2}{D_x r_w} \right)}.$$

For D approaching zero, the exact expression reduces to

$$J = \frac{4\pi kh}{\mu B_o \ln \left(\frac{r_e^4}{r_w^4} \right)} = \frac{\pi kh}{\mu B_o \ln \left(\frac{r_e}{r_w} \right)}.$$

This expression represents the PI of a well in a semicircular drainage area. It has half the value of the PI of a well in a circular reservoir as given in [Eq. 6.22](#).

- 7.5 If the well is located 50 m from the fault, we have $D = 100$ m. The PI then

follows as

$$J = \frac{4\pi kh}{\mu B_o \ln \left[\frac{r_e^4}{r_w^2 \times (D_x + r_w)^2} \right]} = \frac{4\pi \times 0.35 \times 10^{-13} \times 20}{5.8 \times 10^{-3} \times 1.03 \times \ln \left[\frac{500^4}{500^2 \times (100 + 0.20)^2} \right]} = 7.80 \times 10^{-11} \text{ m}^3/\text{Pa} \cdot \text{s}$$

The PI of a well in a circular reservoir follows from Eq. 6.22 as

$$J \approx \frac{2\pi kh}{\mu B_o \ln \left(\frac{r_e}{r_w} \right)} = \frac{2\pi \times 0.35 \times 10^{-13} \times 20}{5.8 \times 10^{-3} \times 1.03 \times \ln \left(\frac{500}{0.20} \right)} = 9.41 \times 10^{-1} \text{ m}^3/\text{Pa} \cdot \text{s}$$

The PI for the well near the fault is considerably lower than the PI for the well in the reservoir without a fault, which makes sense. Reducing the value of D to zero leads to a PI with half the value of the PI of the well in the circular reservoir (just as derived in the previous question).

7.6 Starting from Eq. 7.54,

$$p = c_0 + \sum_{n=-\infty}^{+\infty} c_n p_n = c_0 - \sum_{n=-\infty}^{+\infty} \frac{\mu B_o q_{o,sc}}{4\pi k L} \ln \left[(z - nh)^2 + y^2 \right],$$

the infinite sum of logarithmic terms can be rewritten as

$$\begin{aligned} & \sum_{n=-\infty}^{+\infty} \ln \left[(z - nh)^2 + y^2 \right] \\ &= \ln \prod_{n=-\infty}^{+\infty} \left[(z - nh)^2 + y^2 \right] \\ &= \ln \prod_{n=-\infty}^{+\infty} (z - nh)^2 \left[1 + \frac{y^2}{(z - nh)^2} \right] \\ &= \ln \prod_{n=-\infty}^{+\infty} (z - nh)^2 + \ln \prod_{n=-\infty}^{+\infty} \left[1 + \frac{y^2}{(z - nh)^2} \right] \\ &= 2 \ln z + 2 \ln \prod_{n=1}^{+\infty} (z + nh)(z - nh) + \ln \prod_{n=-\infty}^{+\infty} \left[1 + \frac{y^2}{(z - nh)^2} \right] \\ &= 2 \ln z + \ln \prod_{n=-\infty}^{-1} (nh)^2 + \ln \prod_{n=1}^{+\infty} (nh)^2 + 2 \ln \prod_{n=1}^{+\infty} \left(\frac{z}{nh} + 1 \right) \left(\frac{z}{nh} - 1 \right) + \ln \prod_{n=-\infty}^{+\infty} \left[1 + \frac{y^2}{(z - nh)^2} \right] \\ &= 2 \ln \prod_{n=1}^{+\infty} (nh)^2 - 2 \ln \left(\frac{\pi}{h} \right) + \ln \left[\left(\frac{\pi z}{h} \right) \prod_{n=1}^{+\infty} \left(\frac{z}{nh} + 1 \right) \left(\frac{z}{nh} - 1 \right) \right]^2 + \ln \prod_{n=-\infty}^{+\infty} \left[1 + \frac{y^2}{(z - nh)^2} \right]. \end{aligned}$$

With the aid of identities (Eqs. 7.164 through 7.166) it follows that

$$\begin{aligned}
 & 2 \ln \prod_{n=1}^{+\infty} (nh)^2 - 2 \ln \left(\frac{\pi}{h} \right) + \ln \left[\left(\frac{\pi z}{h} \right) \prod_{n=1}^{+\infty} \left(\frac{z}{nh} + 1 \right) \left(\frac{z}{nh} - 1 \right) \right]^2 + \ln \prod_{n=-\infty}^{+\infty} \left[1 + \frac{y^2}{(z-nh)^2} \right] \\
 & = \underbrace{2 \ln \prod_{n=1}^{+\infty} (nh)^2 - 2 \ln \left(\frac{\pi}{h} \right)}_{\text{Irrelevant part}} + \underbrace{\ln \left(\frac{1}{2} \right) + \ln \left[\cosh \left(2\pi \frac{y}{h} \right) - \cos \left(2\pi \frac{z}{h} \right) \right]}_{\text{Relevant part}}.
 \end{aligned}$$

The first three terms are irrelevant for our purpose because they represent a constant pressure. As explained in [Section 7.3.3](#), we still have to define a reference pressure to fix the value of constant c_0 .

- 7.7 (a) The drawdown is, by definition,

$$\Delta p = p_R - p_{wf} = 5500 - 5490 = 10 \text{ psi.}$$

The production rate follows as

$$q = q' L = -J'_{\text{frac}} \Delta p L = -0.12 \times 10 \times 1500 = -1800 \text{ B/D.}$$

- (b) The production rate now reduces to

$$q_{\text{red}} = q'_{\text{red}} L = -J'_{\text{red}} \Delta p L = -0.09 \times 10 \times 1500 = -1350 \text{ B/D.}$$

Furthermore, as evident from [Eq. 7.64](#), we have

$$\frac{1}{J'_{\text{red}}} = \frac{1}{J'_{\text{frac}}} + \frac{1}{J'_{\text{conv}}},$$

and therefore

$$J'_{\text{conv}} = \frac{1}{\frac{1}{J'_{\text{red}}} - \frac{1}{J'_{\text{frac}}}} = \frac{1}{\frac{1}{0.09} - \frac{1}{0.12}} = 0.36.$$

The corresponding pressure drop, caused by streamline convergence, follows as

$$\Delta p_{\text{conv}} = \frac{-q_{\text{red}}}{J'_{\text{conv}} L} = \frac{-1350}{0.36 \times 1500} = 2.5 \text{ psi.}$$

- (c) The effect of pressure drop along the horizontal well would be to reduce the total well flow rate. Going from the toe to the heel of the well, the well-bore pressure would gradually decrease. Therefore also the drawdown and the specific inflow would decrease. This would, schematically, result in the inflow profile shown in [Fig. G-13](#).

- 7.8 Starting from [Eq. 7.81](#), an expression for the average reservoir pressure can be derived as

$$p_{R,av} = \frac{\int_0^{w/2} p dy}{\int_0^{w/2} dy} = p_R + \frac{\mu B_o q_{o,sc}}{2kLh} \frac{\int_0^{w/2} \left(\frac{w}{4} - y + \frac{y^2}{w} \right) dy}{\frac{w}{2}} = p_R + \frac{\mu B_o q_{o,sc} w}{24kLh},$$

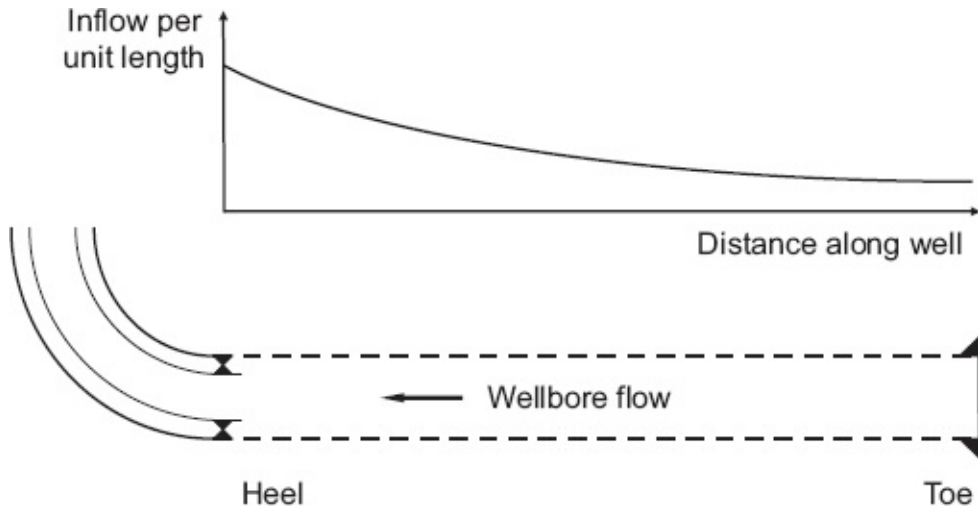


Fig. G-13—Varying specific inflow due to pressure drop in a horizontal well.

with which we find

$$p = p_{R,av} + \frac{\mu B_o q_{o,sc}}{2kLh} \left(\frac{w}{6} - y + \frac{y^2}{w} \right),$$

and

$$J = \frac{-q_{o,sc}}{p_{R,av} - p_{wf}} = \frac{2\pi k L}{\mu B_o \left(\frac{\pi w}{6h} + S_{conv} + S_h \right)}.$$

- 7.9 Refer to the theory in [Section 7.2.5](#). Starting from the approximate result obtained in the answer to Question 7.4, the steady-state PI now becomes

$$\begin{aligned} J &= \frac{2\pi \bar{k} h}{\mu B_o \ln \left(\frac{\hat{r}_e^2}{\hat{D}_x \hat{r}_w} \right)} = \frac{2\pi \bar{k} h}{\mu B_o \ln \left[\frac{\sqrt{\bar{k}}}{\sqrt{k_y} D} \times \frac{1}{2} \frac{(\sqrt{k_x} + \sqrt{k_y})^2}{\bar{k}} r_e^2 \times 2 \left(\frac{\sqrt{\bar{k}}}{\sqrt{k_x} + \sqrt{k_y}} \right) \frac{1}{r_w} \right]} \\ &= \frac{2\pi \bar{k} h}{\mu B_o \ln \left[\frac{(\sqrt{k_x} + \sqrt{k_y}) r_e^2}{\sqrt{k_y} D r_w} \right]} = \frac{2\pi \bar{k} h}{\mu B_o \ln \left[(I_{xy} + 1) \frac{r_e^2}{D r_w} \right]}. \end{aligned}$$

- 7.10 (a) See [Eq. 7.101](#), from which follows

$$a_e = \sqrt{L^2 + b_e^2} = \sqrt{5000^2 + 500^2} = 5025 \text{ m}.$$

$$R_{\text{asp,ell}} = \frac{a_e}{b_e} = 5025 / 500 = 10.05.$$

For the PI, see Eqs. 7.90 and 7.112:

$$\hat{S}_{\text{conv}} = \frac{1}{I_{wh}} \ln \left[\frac{h}{\pi r_w} \left(\frac{1}{I_{wh} + 1} \right) \right] = \frac{1}{\sqrt{1/5}} \ln \left[\frac{25}{\pi \times 0.1} \left(\frac{1}{\sqrt{1/5} + 1} \right) \right] = 8.96 \text{ m.}$$

$$\begin{aligned} J_{\text{ell}} &= \frac{2\pi k_h h}{\mu B_o \left[\ln \left(\frac{b_e}{L} + \sqrt{\frac{b_e^2}{L^2} + 1} \right) + \frac{h}{L} \hat{S}_{\text{conv}} + \hat{S}_v \right]} \\ &= \frac{2\pi \times 2 \times 10^{-12} \times 25}{20 \times 10^{-3} \times 1 \times \left[\ln \left(\frac{500}{5000} + \sqrt{\frac{500^2}{5000^2} + 1} \right) + \frac{25}{5000} \times 8.96 + 0 \right]} \\ &= 1.09 \times 10^{-7} \text{ m}^3/\text{Pa} \cdot \text{s.} \end{aligned}$$

(b) The aspect ratio is given by

$$R_{\text{asp,box}} = \frac{L}{w} = 5000 / 500 = 10.00,$$

which is nearly identical to $R_{\text{asp,ell}}$. For the PI, see Eqs. 7.90 and 7.93:

$$\begin{aligned} J_{\text{box}} &= \frac{2\pi k_h L}{\mu B_o \left(\frac{\pi w}{c_R h} + \hat{S}_{\text{conv}} + \hat{S}_h \right)} \\ &= \frac{2\pi \times 2.0 \times 10^{-12} \times 5000}{20 \times 10^{-3} \times 1 \times \left(\frac{\pi \times 500}{2 \times 25} + 8.96 + 0 \right)} = 7.78 \times 10^{-8} \text{ m}^3/\text{Pa} \cdot \text{s.} \end{aligned}$$

The PI for the elliptical reservoir is approximately 40% higher because the ellipse has inflow from all around, whereas the box-shaped reservoir has no-flow boundaries at the short sides. Moreover, the average distance from the well to the boundaries, in the direction perpendicular to the well, is less in the ellipse than in the box.

(c) The new width becomes

$$A_{\text{box}} = Lw = 5000 \times 500 = 2.50 \times 10^6,$$

$$A_{\text{ell}} = \frac{\pi ab}{4} = \frac{\pi \times 5020 \times 500}{4} = 1.97 \times 10^6,$$

$$w_{\text{new}} = \frac{A_{\text{ell}}}{A_{\text{box}}} w = \frac{1.97 \times 10^6}{250 \times 10^6} \times 500 = 395 \text{ m.}$$

The new aspect ratio and the new PI follow as

$$R_{\text{asp,box,new}} = \frac{L}{W_{\text{new}}} = 5000 / 395 = 12.67,$$

$$\begin{aligned} J_{\text{box,new}} &= \frac{2\pi k_h L}{\mu B_o \left(\frac{\pi w_{\text{new}}}{c_R h} + \hat{S}_{\text{conv}} + \hat{S}_h \right)} \\ &= \frac{2\pi \times 2.0 \times 10^{-12} \times 5000}{20 \times 10^{-3} \times 1 \times \left(\frac{\pi \times 394}{2 \times 25} + 8.96 + 0 \right)} = 9.31 \times 10^{-8} \text{ m}^3/\text{Pa} \cdot \text{s}. \end{aligned}$$

The PI for the elliptical reservoir is now approximately 17% higher.

7.11 See [Eq. 7.159](#). With the aid of [Eq. 2.31](#), it follows that

$$\begin{aligned} S_g &= S_{gc} + (1 - S_{gc} - S_{org} - S_{wi}) \left[1 + \left(\frac{k_{rg}^0 \mu_g q_g}{k_{rg}^0 \mu_o q_o} \right)^{-\frac{1}{n}} \right]^{-1} \\ &= S_{gc} + (1 - S_{gc} - S_{org} - S_{wi}) \left\{ 1 + \left[\frac{k_{rg}^0 \mu_g B_g (q_{g,sc} - R_s q_{o,sc})}{k_{rg}^0 \mu_o B_o q_{o,sc}} \right]^{\frac{1}{n}} \right\}^{-1} \\ &= 0.10 + (1 - 0.10 - 0.05 - 0.20) \\ &\quad \times \left\{ 1 + \left[\frac{0.95 \times 13.5 \times 10^{-6} \times 0.07 \times (3.90 - 55 \times 65 \times 10^{-3})}{0.70 \times 5.8 \times 10^{-3} \times 1.20 \times 65 \times 10^{-3}} \right]^{\frac{1}{4}} \right\}^{-1} \\ &= 0.20. \end{aligned}$$

7.12 Modify `example_point_sources.m` by changing the following lines of code:

```
n_br = 0; % number of branches, -
N_bb = 80; % number of sources to represent back bone between
branches (incl. kick-off pts.), -
S_v = 5; % skin factor (as measured in a vertical well in the same
reservoir), -
```

This will produce the pressure contour plot depicted in [Fig. G-14](#). The skin results in a high pressure drop right at the wellbore. Because the FBHP and the far-field reservoir pressure stay unchanged, the remaining pressure drop in the reservoir is lower than it would be without skin, resulting in a “flat” pressure profile with a large distance between the pressure contours. See script file `answer_question_7_12.m` for the numerical implementation.

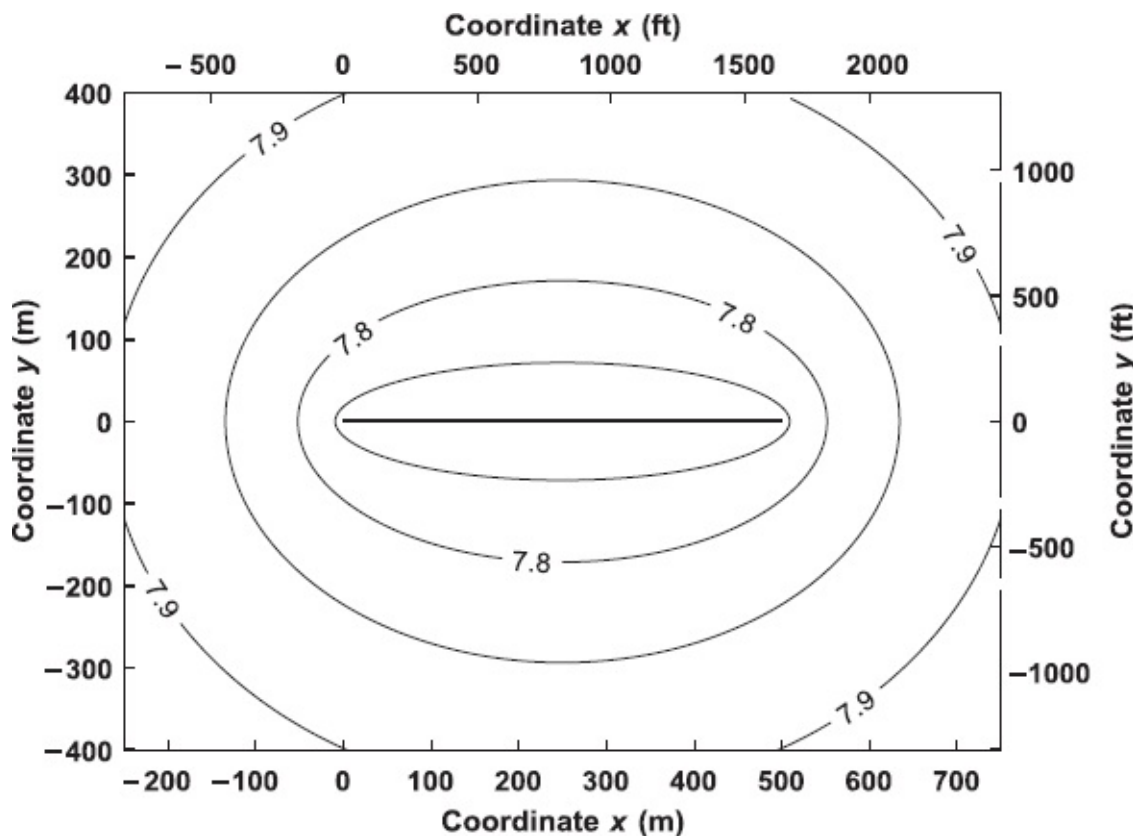


Fig. G-14—Modified version of Fig. 7.17 with increased formation-damage skin factor ($S_V = 5$).

G-8 Answers for Chapter 8, Well Performance

- 8.1 By plotting the pressure in a single (analysis) node vs. flow rate for both the upstream and the downstream part of a system, we can determine the operating point (i.e., the pressure in the analysis node and the flow rate through the entire system). The underlying assumption is that the pressures at the upstream and downstream boundaries of the system remain constant. See also the discussion in Section 1.6.
- 8.2 See Fig. 8.5 and the corresponding text in Section 8.2.1.
- 8.3 The curvature of one or both of the performance curves may lead to two intersections (see Fig. 8.5). The intersection corresponding to the highest flow rate is always the physically realistic (stable) solution. Nodal analysis is based on the assumption of steady-state flow. However, the analysis of the stability of an operating point requires a dynamic (i.e., nonsteady-state) analysis to establish whether small disturbances grow or shrink with time.
- 8.4 The practical rule is to select an operating point to the right of the minimum of the tubing intake curve. Theoretically, an operating point to the left may still be acceptable, but the near-parallel alignment of the curves to the left of the minimum makes the position of the intersection sensitive to small errors. Also, a full dynamic analysis reveals that for points to the left of the minimum, the likelihood of unstable flow is higher than for points farther to the right.

- 8.5 Because it (1) provides a higher flow rate and (2) is less prone to result in unstable flow.
- 8.6 (a) [Fig. 8.19](#): bottom of the tubing; [Fig. 8.20](#): top of the tubing.
- (b) $p_R = 20.5 \text{ MPa}$; $p_s = 1.2 \text{ MPa}$.
- (c) The choke is operating in the critical regime because the FTHP is much higher than 1.7 times the flowline pressure. Also a correct answer: because the operating point is located in the linear part of the choke performance curve.
- (d) Because we consider steady-state flow. In that case the mass flow rate is the same in the entire system, and therefore also the volume flow rate expressed at identical reference conditions (i.e., standard conditions in our case) is the same in the entire system.
- 8.7 (a) Reservoir pressure: 43 MPa
Bottomhole pressure: 39 MPa
Tubinghead pressure: 12 MPa
Manifold pressure: 3 MPa
- (b) The pressure is decreasing, even though the flow toward the manifold is downhill, because the pressure decrease caused by friction exceeds the pressure increase caused by gravity. The effect is nonlinear because the decreasing pressure leads to dissolution of gas, causing an increasing gas flow rate and thus increasing friction. See [Fig. G-15](#), which depicts the detailed contributions of friction, gravity, and (zero) acceleration to the total pressure drop over the flowline.

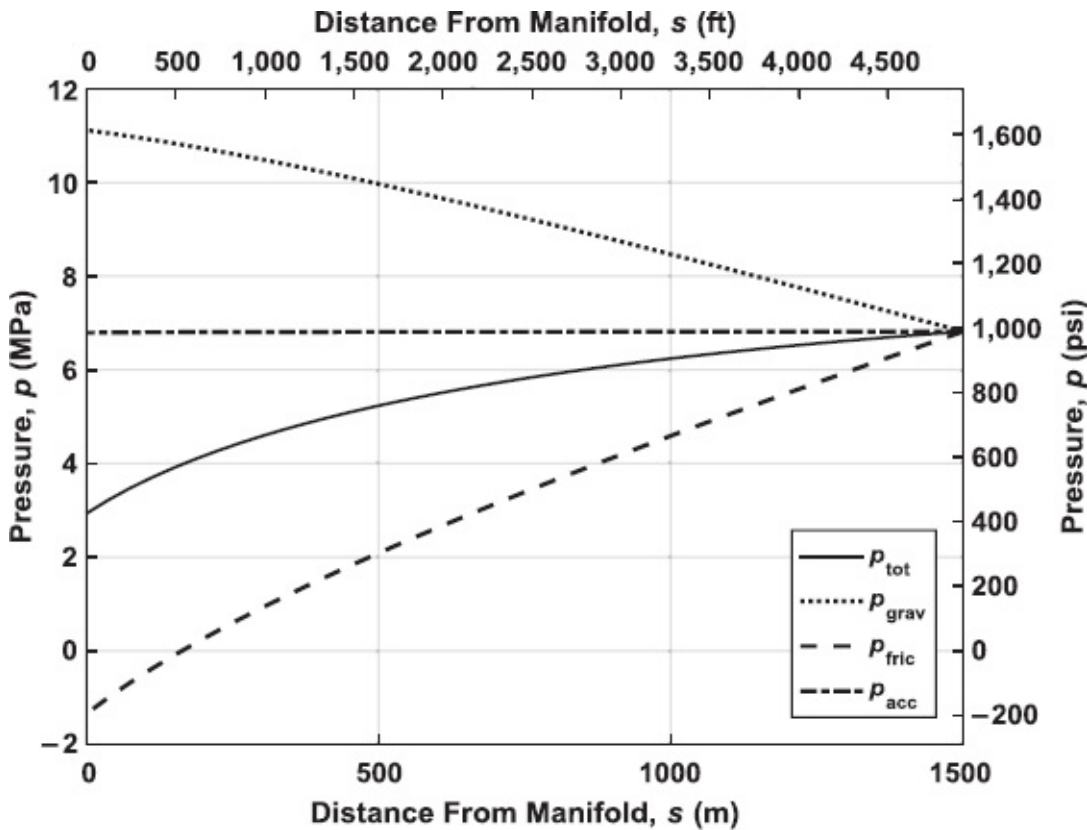


Fig. G-15—Pressure in the flowline with contributions from friction, gravity, and acceleration (relative to the downstream choke pressure).

- (c) The pressure just downstream from the choke is approximately 7 MPa. The ratio between upstream and downstream pressures is therefore approximately $12/7 \approx 1.7$, which is roughly equal to the rule-of-thumb critical boundary, so it is not possible to decide whether the choke operates in the critical regime.
- 8.8 (a) The tubing performance curve represents not only the tubing performance but also the near-wellbore performance. The near-wellbore performance is governed by reservoir and completion properties, not by the tubing properties.
- (b) Left side: Decreasing flow rates result in increasing slip and therefore increasing holdup and increasing head losses. Right side: Increasing flow rates result in increasing friction losses (and also some increased head losses because of an increased density from compression).
- (c) See [Fig. G-16](#). Maximum: approximately $1.32 \times 10^{-3} \text{ m}^3/\text{s}$. Practical minimum: approximately $0.22 \times 10^{-3} \text{ m}^3/\text{s}$.
- (d) Not possible. The critical flow boundary is at a FTHP of approximately 1.7 times the downstream pressure (i.e., at $1.7 \times 1.2 = 2.0 \text{ MPa}$).
- (e) The critical flow boundary is now at approximately $1.7 \times 0.8 = 1.36 \text{ MPa}$. The corresponding flow rate is $1.15 \times 10^{-3} \text{ m}^3/\text{s}$. See [Fig. G-17](#) for the shape of the choke performance curve.

8.9 The reservoir pressure may drop another 1.4 MPa (200 psi), as shown in Fig. G-18.

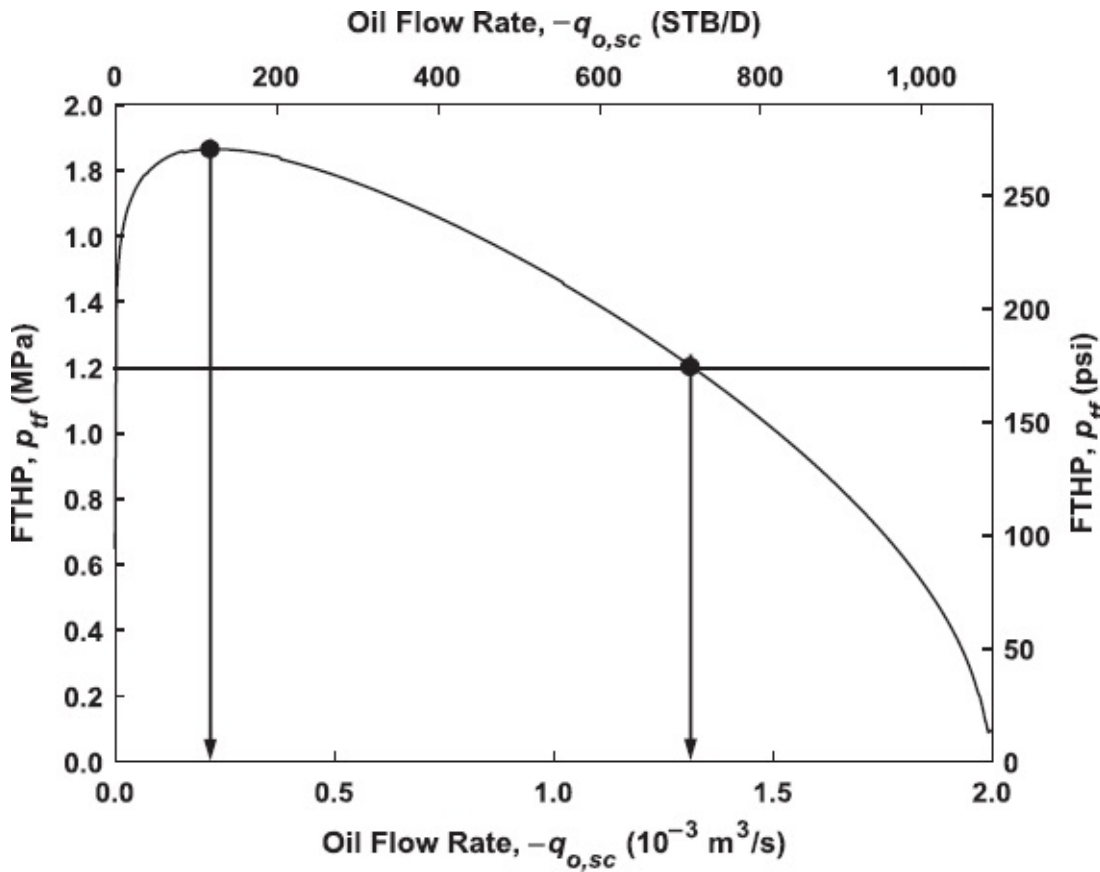


Fig. G-16—Maximum and minimum flow rates.

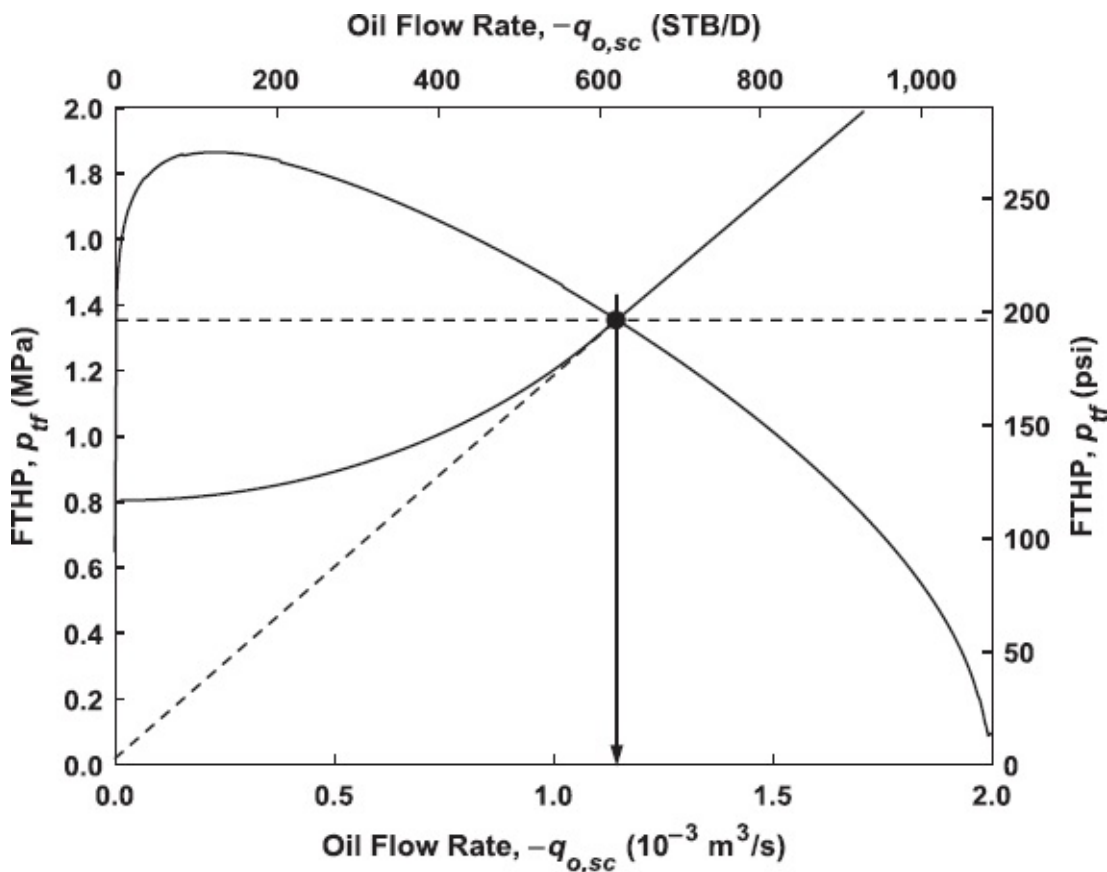


Fig. G-17—Critical flow boundary and corresponding flow rate.

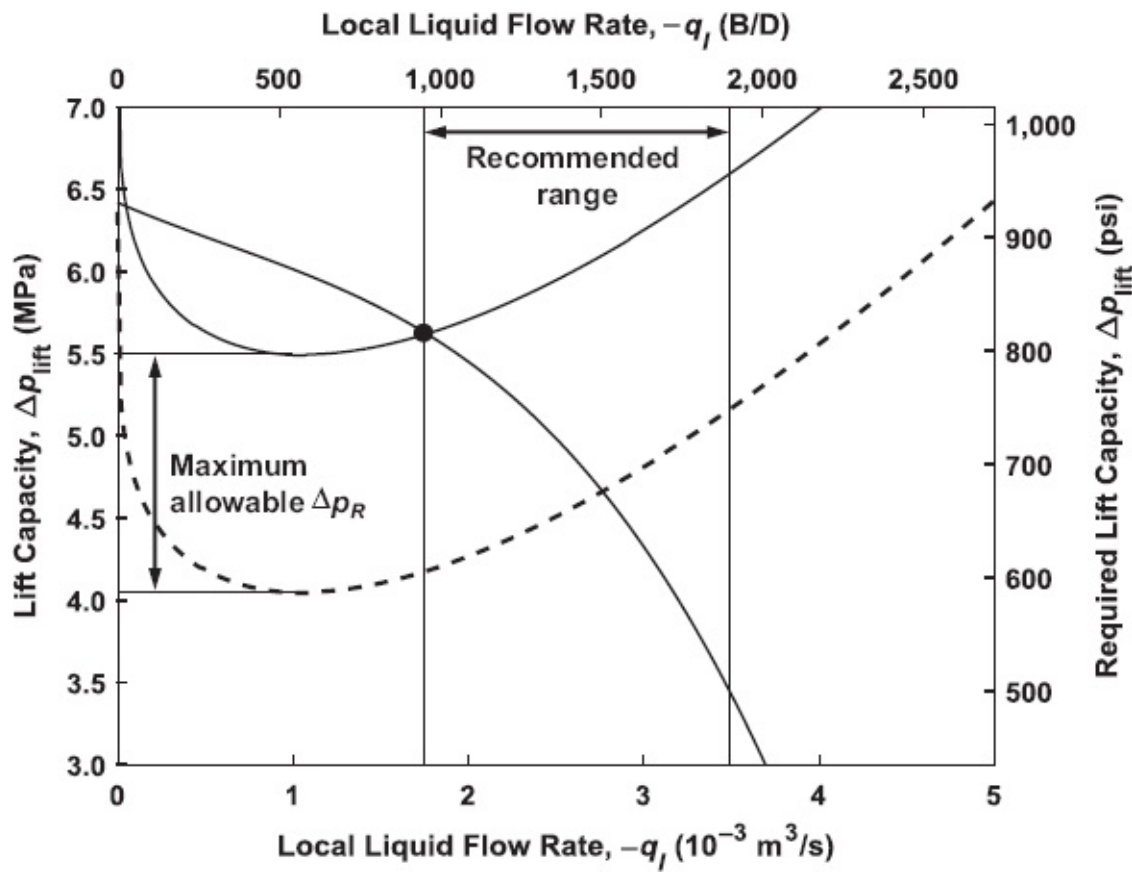


Fig. G-18—Effect of reduced reservoir pressure on lift requirement curve and resulting shift in operating

point to the boundary of the recommended ESP operating range.

- 8.10 (a) (b) See script file `answer_question_8_10_part_1.m` for the numerical implementation and **Fig. G-19** for the results. The oil flow rate through the system is $-2.22 \times 10^{-3} \text{ m}^3/\text{s}$ (i.e., -1206 B/D).
- (c) No. The flow through a choke in the critical regime is completely determined by the upstream pressure, and therefore it is not possible to perform a nodal analysis for the complete range of flow rates starting from the downstream end.
- (d)/(e)/(f) See script file `answer_question_8_10_part_2.m` for the numerical implementation and **Figs. G-20 through G-22** for the results. The main causes for the pressure drop over the well are
- Friction losses over the choke
 - Gravity losses over the wellbore
 - Friction losses in the reservoir

The friction losses over the flowline and the tubing are relatively small. The friction loss over the flowline is no smaller than that over the tubing because the average pressure in the flowline is much lower, causing more gas to come out of solution, which increases the pressure gradient and thus counteracts the effect of a larger-diameter tubing. This type of plot is quite useful for debottlenecking a production system through identifying system elements with undesirably high pressure losses.

- 8.11 (a) See script file `answer_question_8_11.m` for the numerical implementation. The well does flow naturally because the IPR is just crossing the tubing intake curve. However, the uncertainty in production engineering calculations is considerable, so the well may just as well not flow. Anyway, the flow rate is so low that artificial lift is required.

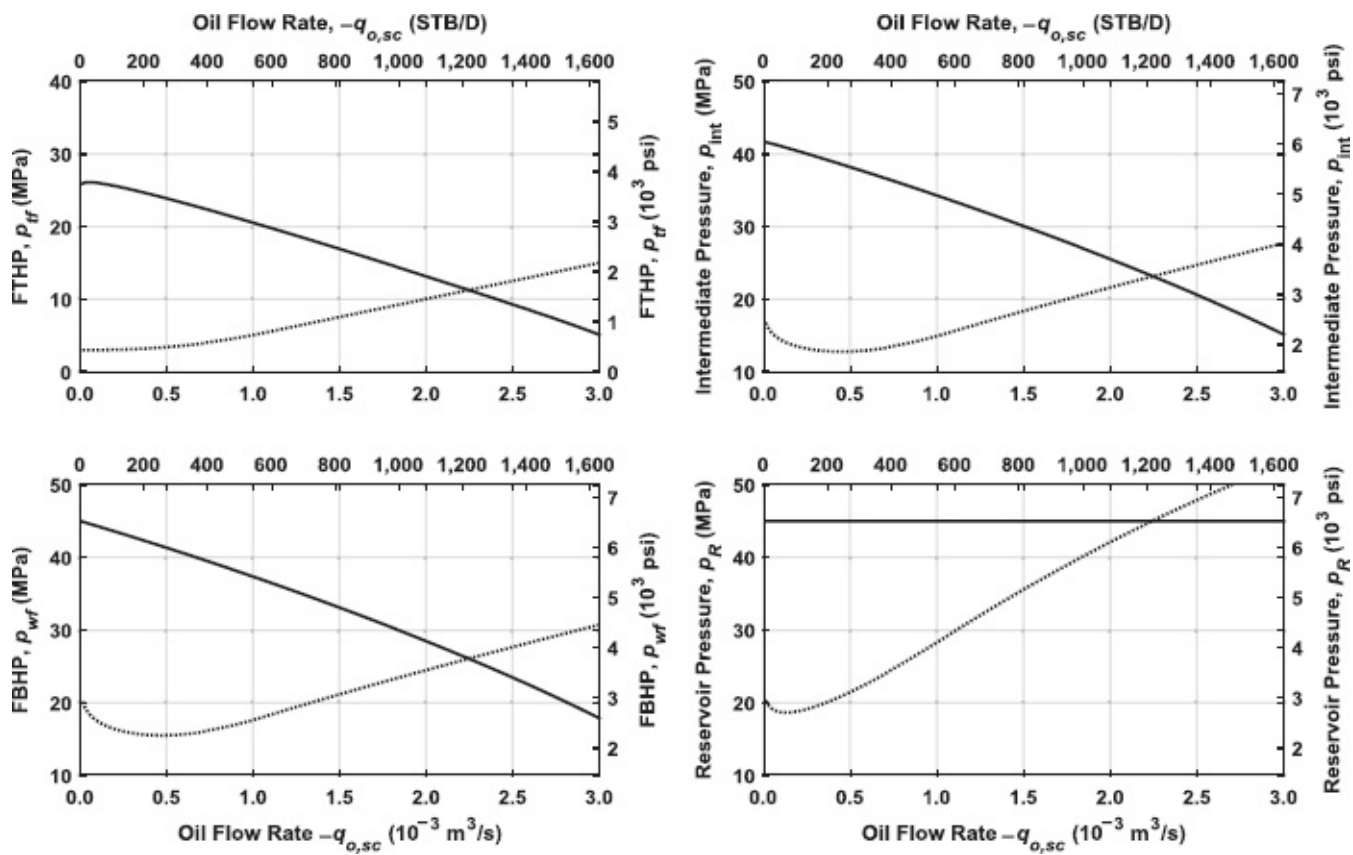


Figure G-19—Nodal analysis of the same system for four different analysis nodes, with all analysis nodes upstream of the choke. Solid lines: upstream performance curves. Dotted lines: downstream performance curves. (Note the shifted vertical scales in the top-left plot.)

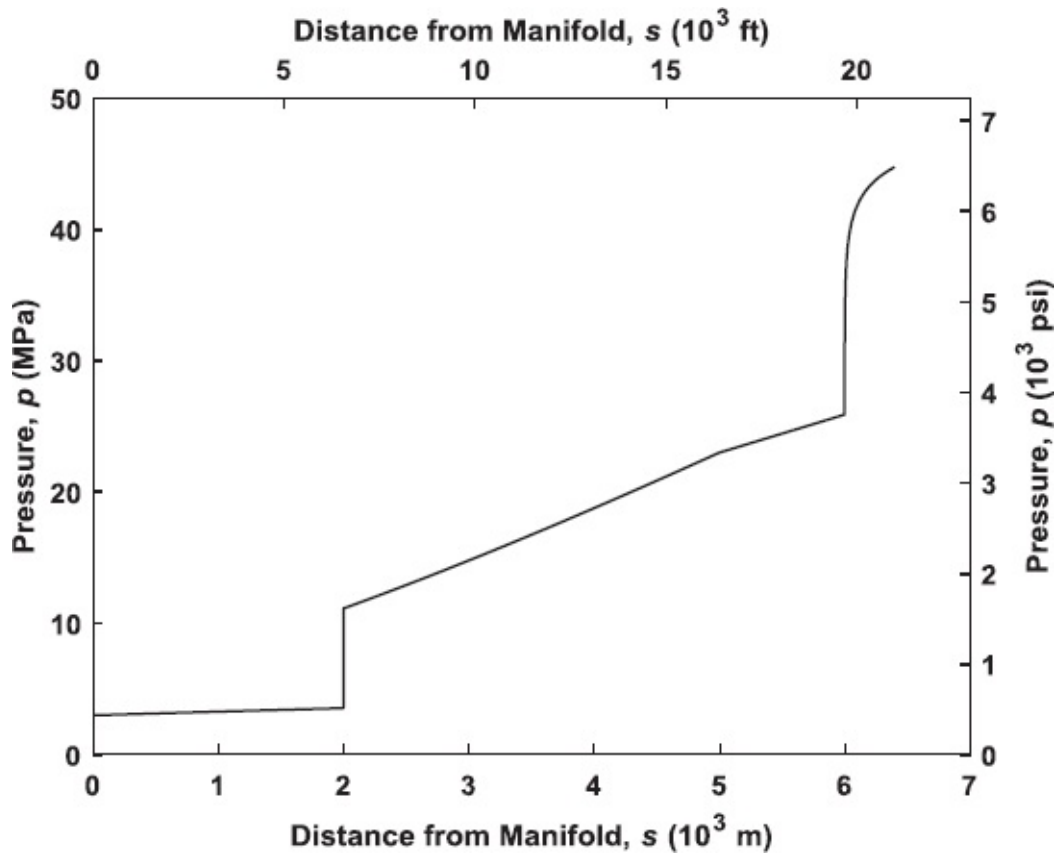


Fig. G-20—Traverse for total pressure.

(b)/(c) See [Fig. G-23](#) for the lift requirement curve. Note that the horizontal axis displays the local liquid rate. The required head at the optimal pump rate of $2.8 \times 10^{-3} \text{ m}^3/\text{s}$ (1500 B/D) is 540 m. According to the pump curve, which is valid for 100 stages, the available head at the optimal pump rate is 140 m (460 ft). The required number of stages is therefore

$$n_{st} = \frac{\frac{540}{140}}{\frac{1}{100}} = 386.$$

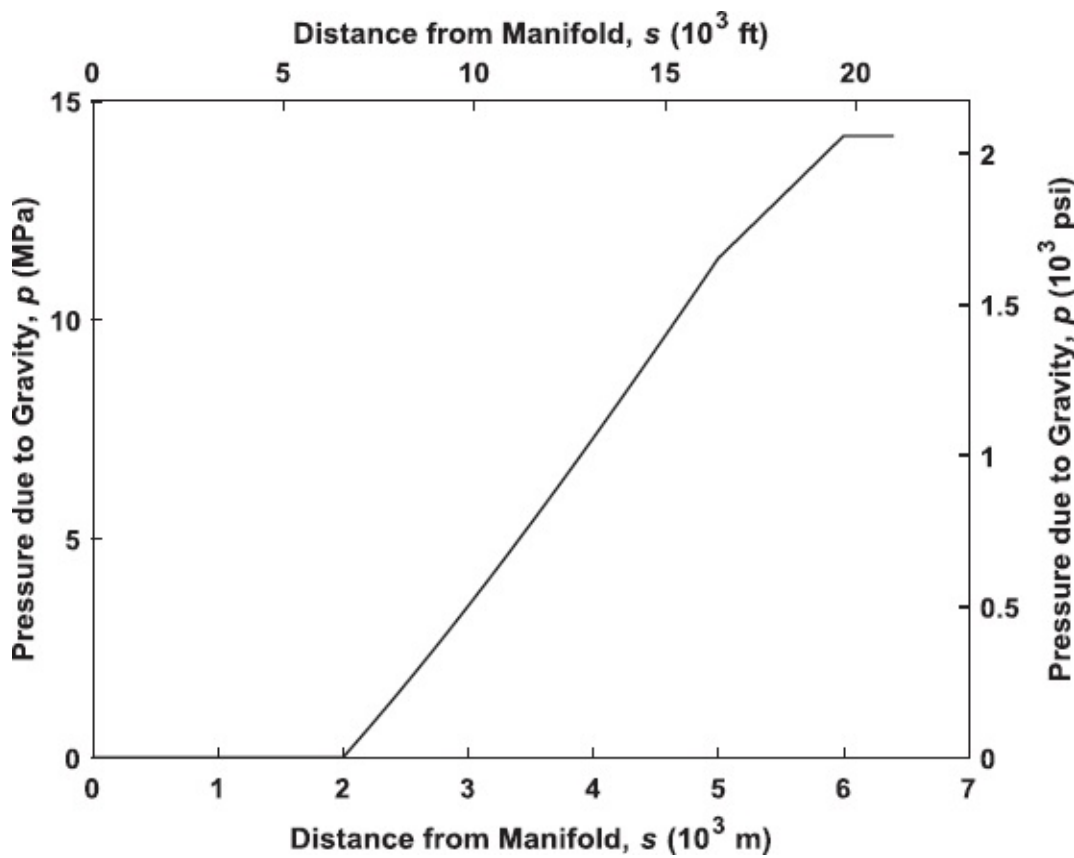


Fig. G-21—Traverse for pressure due to gravity.

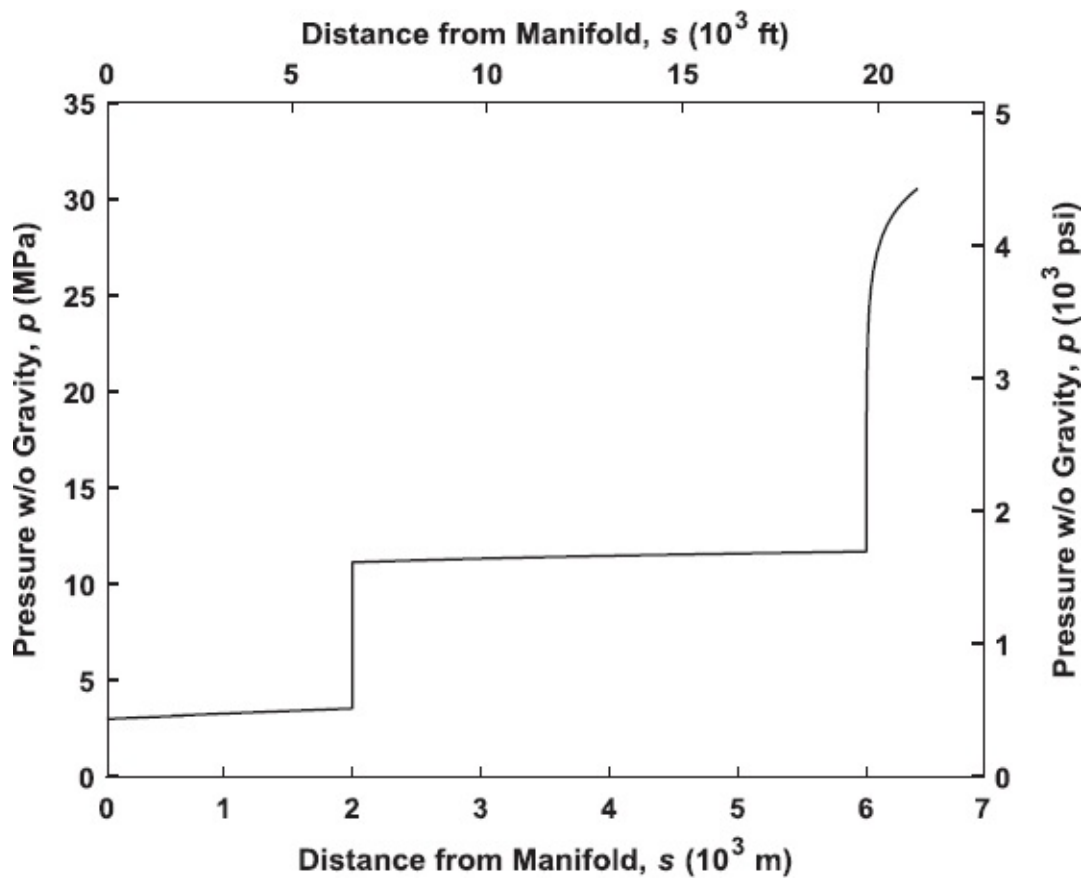


Fig. G-22—Traverse for pressure without gravity effects.

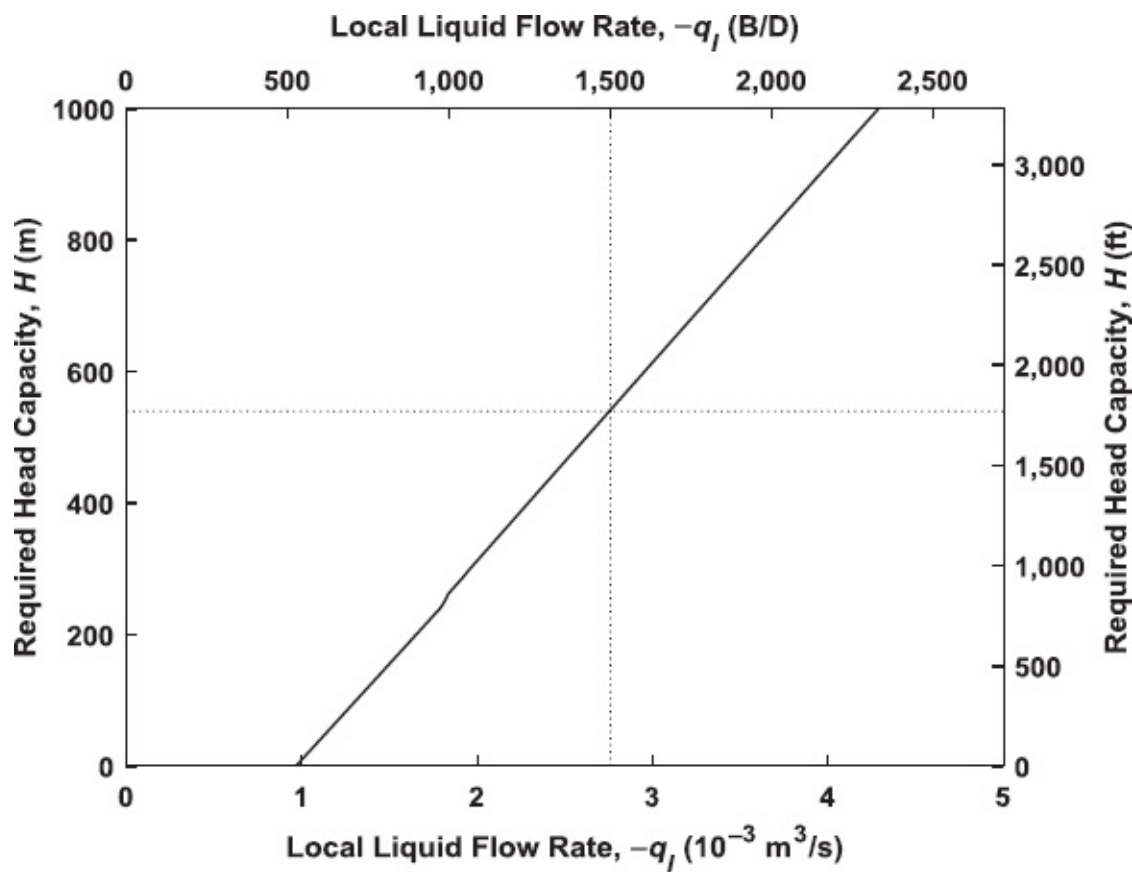


Fig. G-23—Lift requirement curve.

- 8.12 (a) See script file `answer_question_8_12.m` for the numerical implementation. The maximum achievable oil rate of $q_{o,sc} = 4.361 \times 10^{-3} \text{ m}^3/\text{s}$ (2370 B/D) corresponds to an optimal lift gas rate of $q_{g,sc,lift} = 1.00 \text{ m}^3/\text{s}$ ($3051 \times 10^3 \text{ cf/D}$) and a pressure at the gas lift valve of $p_4 = 7.00 \text{ MPa}$ (1,015 psi), as shown in **Figs. G-24 and G-25**. For a restricted maximum lift gas rate of $q_{g,sc,lift} = 0.10 \text{ m}^3/\text{s}$ ($305 \times 10^3 \text{ cf/D}$), the pressure at the gas lift valve is $p_4 = 9.26 \text{ MPa}$ (1343 psi).
- (b) See **Fig. G-26**. The required choke size is $d_{ch} = 5/64 \text{ in.}$

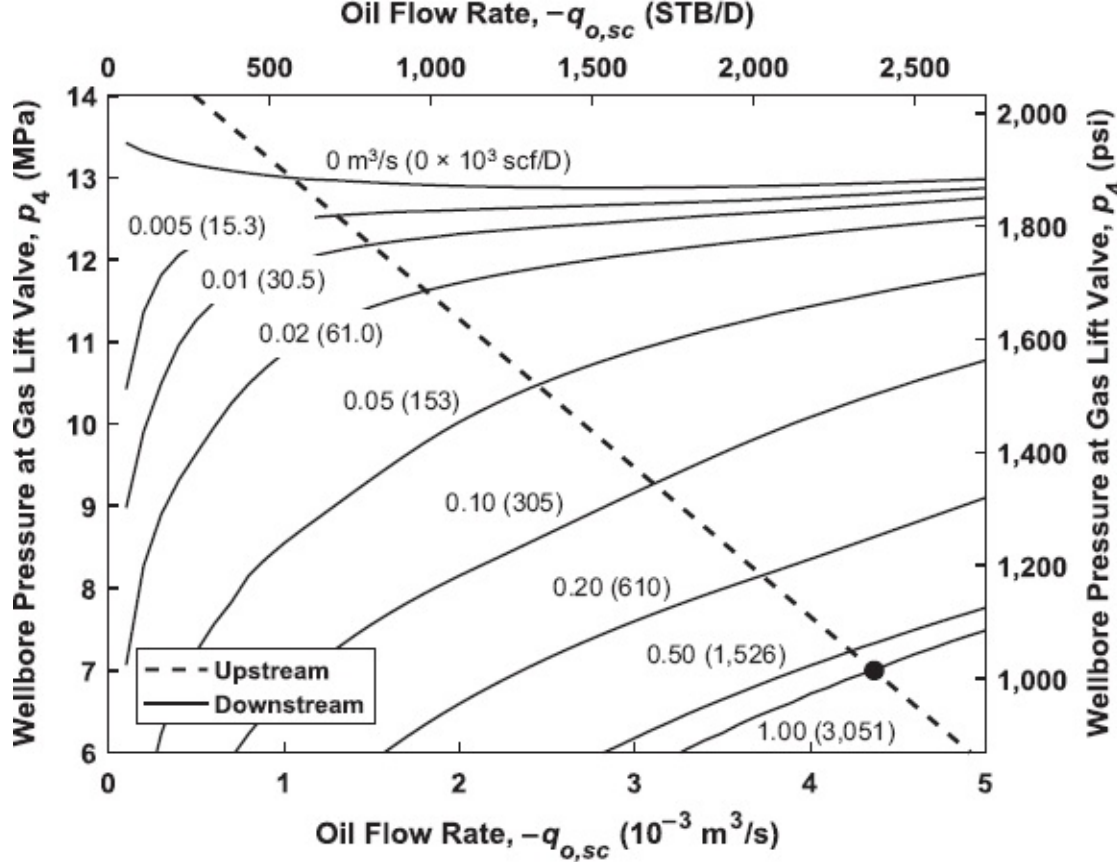


Fig. G-24—Performance curves for different lift-gas rates.

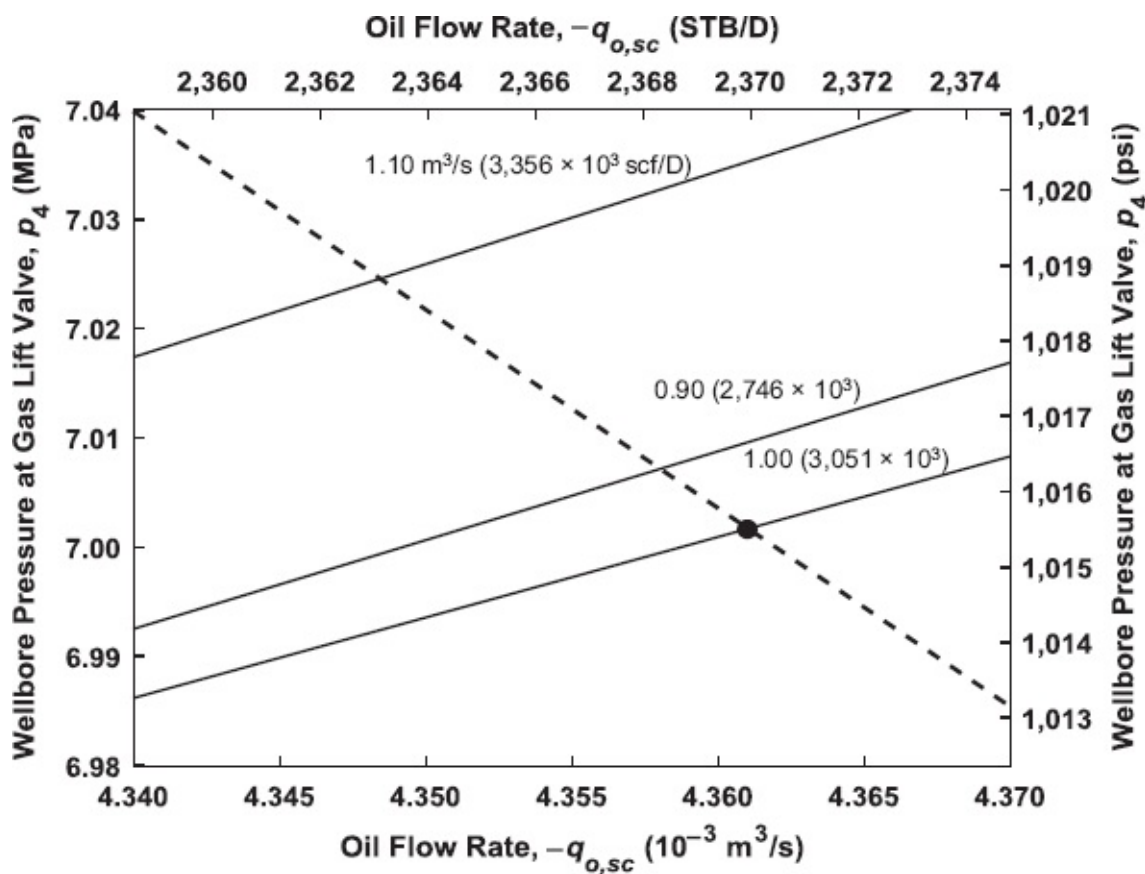


Fig. G-25—Performance curves for different lift-gas rates (detail). The maximum oil flow rate is achieved for an optimal lift-gas rate of $q_{g,sc,lift} = 1.00 \text{ m}^3/\text{s}$ ($3,051 \times 10^3$ scf/D).

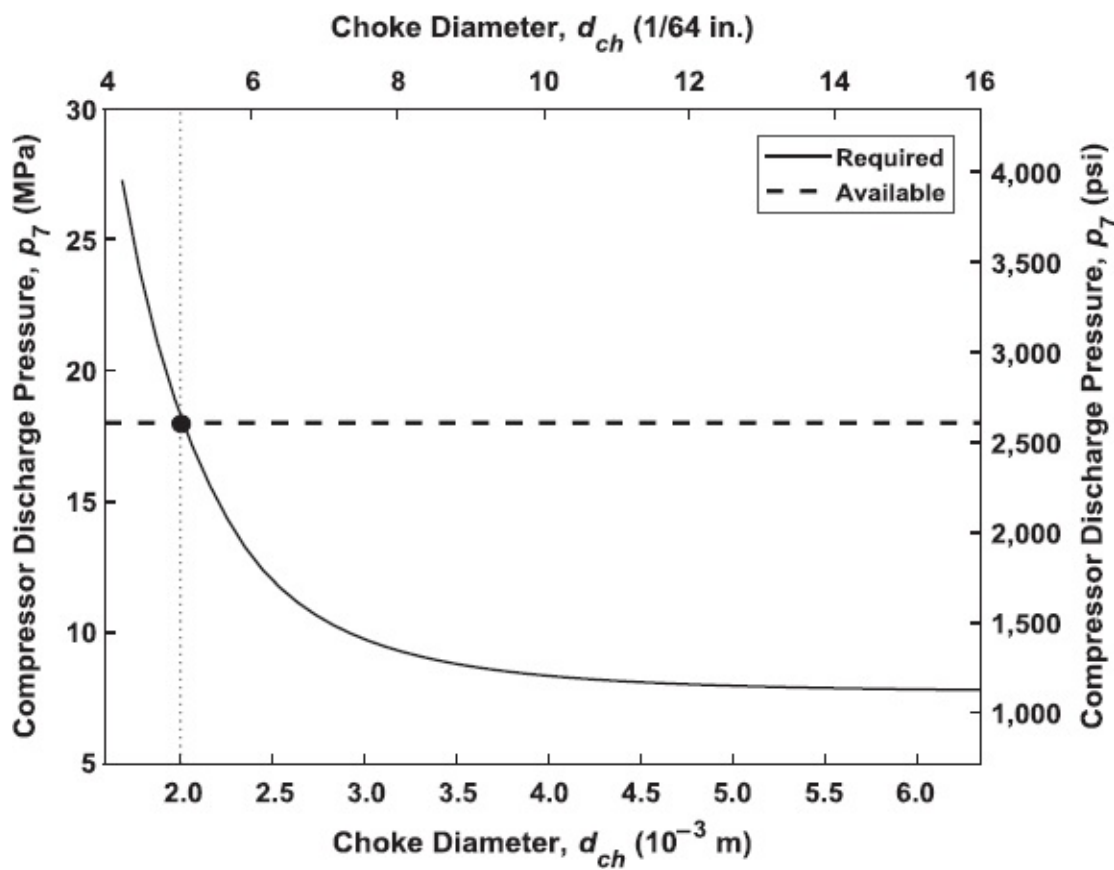


Fig. G-26—Required compressor discharge pressure as a function of choke setting. For an available discharge pressure $p_7 = 18 \text{ MPa}$, the closest choke size expressed in units of 1/64 in. is $d_{\text{ch}} = 5/64 \text{ in.}$

Appendix H

MATLAB Files

H-1 Guidance for Use

The MATLAB files listed here were programmed to illustrate the concepts discussed in the book and to serve as a basis for questions and assignments. They can be downloaded from the web address listed on the title page at time of printing. They must not be used for actual production engineering calculations. For those, refer to professional nodal analysis software packages; among the suppliers of frequently used programs are Pipesim (2017), Prosper (2017), and WellFlo (2017).

The understanding and use of the MATLAB files requires basic programming skills, but no advanced MATLAB knowledge. In particular, the use of compact vector notation as offered by the MATLAB programming language has mostly been avoided, thus somewhat sacrificing computational and notational efficiency for the benefit of readability and educational value.

The files have been tested for all questions and assignments in the book and should therefore run without errors. However, they may crash when used with other parameter settings. In particular, the multiphase routines for choke flow and reservoir flow are not robust for all combinations of parameters. Other reasons for poor performance may be exceedance of the range of validity of the underlying correlations or models, imperfections in the models themselves, or, of course, programming errors. If you spot any bugs, please let us know.

If you run into problems while attempting the questions and assignments, please check the following points, which have proved to be the most frequently occurring source of errors:

- Use strict SI units, either the base unit or the derived units (see [Section 1.2.5](#)). Do not use prefixes—except, of course, in kg, which is a base unit (see also the remark in Section A-2)—or so-called allowable SI units. For example, do not use MPa or m³/d, but use Pa and m/s instead. In the occasional input file that uses field units, the relevant variables have been indicated with an addition _FU.
- Use negative values for production flow rates of oil, gas, and water. Positive values imply injection.
- Specify temperatures in °C, except in some files related to single-phase gas flow that use absolute temperatures, indicated with T_{abs} and expressed in K.

H-2 Conversion Factors

from_bbl_per_ft3_to_m3_per_m3.m
from_bbl_to_m3.m
from_bpd_psi_ft_to_m2_per_d_Pa.m
from_bpd_psi_ft_to_m2_per_s_Pa.m
from_bpd_psi_to_m3_per_d_Pa.m
from_bpd_psi_to_m3_per_s_Pa.m
from_bpd_to_m3_per_d.m
from_bpd_to_m3_per_s.m
from_cal_to_J.m
from_cp_to_Pa_s.m
from_cSt_to_m2_per_s.m
from_deg_API_to_kg_per_m3.m
from_deg_API_to_liq_grav.m
from_deg_C_to_deg_F.m
from_deg_F_to_deg_C.m
from_deg_R_to_K.m
from_deg_to_rad.m
from_dyne_per_cm_to_N_per_m.m
from_ft2_to_m2.m
from_ft3_per_bbl_to_m3_per_m3.m
from_ft3_per_d_to_m3_per_d.m
from_ft3_per_d_to_m3_per_s.m
from_ft3_per_s_to_m3_per_s.m
from_ft3_per_s_to_m3_per_s.m
from_ft3_to_m3.m
from_ft_per_s_to_m_per_s.m
from_ft_to_m.m
from_gal_per_min_to_m3_per_s
from_gas_grav_to_kg_per_m3.m
from_gas_grav_to_mol_weight.m
from_gas_grav_to_molar_mass.m
from_hp_to_W.m
from_in2_to_m2.m
from_in_to_m.m
from_J_to_cal.m
from_K_to_deg_R.m

```
from_kg_per_m3_to_deg_API.m
from_kg_per_m3_to_gas_grav.m
from_kg_per_m3_to_lbm_per_ft3.m
from_kg_per_m3_to_liq_grav.m
from_kg_per_m3_to_mol_weight.m
from_kg_per_m3_to_molar_mass.m
from_kg_per_m3_to_Pa_per_m.m
from_kg_per_m3_to_ppg.m
from_kg_per_m3_to_psi_per_ft.m
from_kg_to_lbm.m
from_lbf_ft_to_N_m.m
from_lbf_to_N.m
from_lbm_per_ft3_to_kg_per_m3.m
from_lbm_per_ft3_to_Pa_per_m.m
from_lbm_per_ft3_to_psi_per_ft.m
from_lbm_to_kg.m
from_liq_grav_to_deg_API.m
from_liq_grav_to_kg_per_m3.m
from_m2_per_d_Pa_to_bpd_psi_ft.m
from_m2_per_s_Pa_to_bpd_psi_ft.m
from_m2_per_s_to_cSt.m
from_m2_to_ft2.m
from_m2_to_in2.m
from_m2_to_mD.m
from_m3_per_d_Pa_to_bpd_psi.m
from_m3_per_d_to_bpd.m
from_m3_per_d_to_ft3_per_d.m
from_m3_per_m3_to_bbl_per_ft3.m
from_m3_per_m3_to_ft3_per_bbl.m
from_m3_per_s_Pa_to_bpd_psi.m
from_m3_per_s_to_bpd.m
from_m3_per_s_to_ft3_per_d.m
from_m3_per_s_to_ft3_per_s.m
from_m3_to_bbl.m
from_m3_to_ft3.m
from_m_per_s_to_ft_per_s.m
```

```
from_m_to_ft.m
from_m_to_in.m
from_mD_to_m2.m
from_mol_weight_to_gas_grav.m
from_molar_mass_to_gas_grav.m
from_mol_weight_to_kg_per_m3.m
from_molar_mass_to_kg_per_m3.m
from_N_m_to_lbf_ft.m
from_N_per_m_to_dyne_per_cm.m
from_N_to_lbf.m
from_Pa_per_m_to_kg_per_m3.m
from_Pa_per_m_to_lbm_per_ft3.m
from_Pa_per_m_to_psi_per_ft.m
from_Pa_s_to_cp.m
from_Pa_to_psi.m
from_per_Pa_to_per_psi.m
from_per_psi_to_per_Pa.m
from_ppg_to_kg_per_m3.m
from_psi_per_ft_to_kg_per_m3.m
from_psi_per_ft_to_lbm_per_ft3.m
from_psi_per_ft_to_Pa_per_m.m
from_psi_to_Pa.m
from_rad_to_deg.m
from_W_to_hp.m
```

H-3 Survey

```
deviated_well_01.txt
deviated_well_02.txt
evaluate_survey.m
example_survey.m
from_alpha_to_theta.m
from_theta_to_alpha.m
plot_survey.m
```

H-4 Fluid Properties

black_oil_Glaso.m
black_oil_Standing.m
compres_Vazquez_and_Beggs.m
example_plot_black_oil_1.m
example_plot_black_oil_2.m
gas_form_vol_fact.m
gas_form_vol_fact_direct.m
gas_oil_rat_Glaso.m
gas_oil_rat_Standing.m
gas_visc_atm_Dempsey.m
gas_visc_ratio_Dempsey.m
gas_viscosity.m
interfacial_tensions.m
local_q_and_rho.m
oil_form_vol_fact_Glaso.m
oil_form_vol_fact_Standing.m
oil_form_vol_fact_undersat.m
oil_visc_dead_B_and_R.m
oil_visc_sat_B_and_R.m
oil_visc_undersat_V_and_B.m
oil_viscosity.m
pres_bub_Glaso.m
pres_bub_Standing.m
pres_bub_volatile_oil.m
pres_pseu_crit_Sutton.m
rho_g_Vazquez_and_Beggs.m
temp_pseu_crit_Sutton.m
volatile_oil.m
vol_oil_table_01 (binary file)
water_viscosity.m
Z_factor_DAK
Z_factor_DAK_direct
Z_factor_Papay

H-5 Pipe Flow

Beggs_Brill_dpds.m
Duns_Ros_dim_less_nrs.m
example_flowline.m
example_hold_up.m
example_intake_curve.m
example_traverse.m
example_traverse_deviated.m
example_well.m
gas_dpds.m
Hag_Brown_hold_up.m
Hag_Brown_dpds.m
local_gas_liq_props.m
Moody_friction_factor.m
Muk_Brill_dpds.m
Muk_Brill_flow_regime.m
Muk_Brill_hold_up.m
oil_dpds.m
pipe.m
Reynolds_number.m
Zig_and_Syl_fric_fact.m

H-6 lift tables

Eclipse_lift_table.m
Imex_lift_table.m

H-7 Choke Flow

choke_gas.m
choke_multi_phase.m
choke_multi_phase_boundary.m
choke_multi_phase_simple.m
choke_oil.m
example_choke_performance_curve.m

H-8 Reservoir Flow

error_drdp.m

example_gas_pseu_pres.m
example_IPR.m
example_PI_oil_hor
example_point_sources.m
example_res_pres.m
example_res_pres_oil_hor
Forchheimer.m
gas_dmdp.m
gas_pseu_pres.m
mobilities.m
rel_perms
res.m
res_dpdr.m
res_gas_dpdr.m
res_gas_simp
res_oil_dpdr.m
res_oil_box.m
res_oil_ellipse.m
res_oil_simp.m
res_Vogel.m.
saturation.m
saturation_gas_oil
saturation_oil_water
Stone_II.m

H-9 Systems

system_01.m
system_02.m
system_03_part_1.m
system_03_part_2.m

H-10 Questions

answer_question_3_9.m
answer_question_3_10.m
answer_question_3_11.m

answer_question_3_12.m
answer_question_5_13.m
answer_question_5_14.m
answer_question_6_10.m
answer_question_6_11.m
answer_question_6_12.m
answer_question_6_13.m
answer_question_7_12.m
answer_question_8_10_part_1.m
answer_question_8_10_part_2.m
answer_question_8_11.m
answer_question_8_12.m

H-11 Graphical User Interface

These files are used by the graphical user interface for the MATLAB exercise in [Chapter 1](#) and should not be edited.

nodal.fig
nodal.m
system_01_downstream_GUI.m
system_01_upstream_GUI.m

H-12 Demo

These executables can be used to run the first MATLAB assignment, Nodal Analysis of a Simple System, in [Chapter 1](#) if you do not have access to MATLAB software. You should first install a run-time compiler by running `MyAppInstaller_web.exe`, which requires Internet access and administrator rights on your computer. Thereafter you can run the file `nodal.exe`.

`MyAppInstaller_web.exe`
`nodal.exe`

Nomenclature

Note: Some symbols occur more than once because they have a different meaning in different parts of the text.

<u>Symbol</u>	<u>Description</u>	<u>Dimension</u>	<u>SI Units</u>
a	long axis of an ellipse	L	m
a	parameter in drift flux model	—	—
A	cross-sectional area	L^2	m^2
A	coefficient	various	various
b	short axis of an ellipse	L	m
B	formation volume factor	—	—
c	coefficient	—	—
c	compressibility	$L m^{-1} t^2$	$1/Pa$
c	specific heat capacity	$L^2 T^{-1} t^{-3}$	$J/(kg \cdot K)$
C	coefficient, constant	various	various
C_0	profile parameter	—	—
d	diameter	L	m
d	direction	—	—
D	distance	L	m
e	pipe roughness	L	m
\mathbf{e}	unit vector	—	—
E	energy	$L^2 m t^{-2}$	$J = N \cdot m$
E	gas expansion factor	—	—
f	fraction	—	—
f	friction factor	—	—
f	function	various	various
\mathbf{f}	vector-valued function	—	—
F	force	$L m t^{-2}$	N
F	force per unit length	$m t^{-2}$	N/m
F	Forchheimer term	—	—
g	function	various	various
g	pressure gradient	$L^{-2} m t^{-2}$	Pa/m
g_c	gravitational constant	—	—
h	height	L	m
H	auxiliary variable (elliptic coordinates)	—	—
H	holdup	—	—

<i>H</i>	hydraulic head	—	m
<i>i</i>	inertia	$L^{-4} m$	kg/m^4
<i>I</i>	electric current	$q \ t^{-1}$	—
<i>I</i>	index	—	—
<i>I</i>	interval	—	—
<i>J</i>	productivity index	$L^5 \ m^{-1} \ t^2$	$m^3/Pa \cdot s$
<i>J*</i>	linearized IPR valid for low flow rates	$L^5 \ m^{-1} \ t^2$	$m^3/Pa \cdot s$
<i>J'</i>	specific productivity index	$L^4 \ m^{-1} \ t^2$	$m^2/Pa \cdot s$
<i>k</i>	coefficient	various	various
<i>k</i>	iteration counter	—	—
<i>k</i>	permeability	L^2	m^2
<i>K</i>	auxiliary variable	—	—
K	permeability tensor	L^2	m^2
<i>L</i>	length	L	m
<i>m</i>	mass	m	kg
<i>m</i>	multiplier	—	—
<i>m</i>	number of components	—	—
<i>m</i>	real-gas pseudopressure	m	Pa
<i>ṁ</i>	mass flow rate	$m \ t^{-1}$	kg/s
<i>M</i>	molar mass	$m \ n^{-1}$	$kg/kmol$
<i>M</i>	torque	$L^2 \ m \ t^{-2}$	N m
<i>n</i>	coefficient	—	—
<i>n</i>	Corey exponent	—	—
<i>N</i>	number	—	—
<i>p</i>	pressure	$L^{-1} \ m \ t^{-2}$	Pa
<i>p̄</i>	derivative of pressure with respect to flow rate	$L^{-4} \ m \ t^{-1}$	$Pa \cdot s/m^3$
<i>P</i>	power	$L^2 \ m \ t^{-3}$	$W = Nm/s$
<i>P</i>	perimeter	L	m
<i>q</i>	flow rate	$L^3 \ t^{-1}$	m^3/s
<i>q̄</i>	specific flow rate	$L^2 \ t^{-1}$	m^2/s
<i>Q</i>	heat flow rate	$L^2 \ m \ t^{-3}$	J/s
<i>r</i>	radial coordinate	L	—
<i>r</i>	(oil/gas) ratio	—	—
<i>R</i>	(gas/oil) ratio	—	—
<i>R</i>	universal gas constant	$L^2 \ m \ n^{-1} \ t^2 \ T^{-1}$	$J/(K \cdot kmol)$
<i>s</i>	distance along well or pipeline	L	m
<i>S</i>	saturation	—	—
<i>S</i>	skin	—	—
<i>t</i>	time	t	s
<i>T</i>	temperature	T	$^{\circ}C$

v	specific volume	$L^3 m^{-1}$	m^3/kg
v	velocity	$L t^{-1}$	m/s
V	electric potential	$L^2 m q^{-1} t^{-2}$	V
V	volume	L^3	m^3
w	width	L	m
x	coordinate	L	m
x	mass fraction	—	—
x	unknown parameter	—	—
\mathbf{x}	vector of unknown parameters	—	—
y	coordinate	L	m
z'	elevation (positive up)	L	m
Z	gas expansion factor	—	—
α	coefficient	—	—
α	inclination	—	radians
β	azimuth	—	radians
β	Forchheimer's coefficient	L^{-1}	$1/m$
β	parameter in drift flux model	—	—
β	ratio of areas	—	—
γ	dogleg (angle)	—	radians
γ	parameter in drift flux model	—	—
γ	ratio of specific heats	—	—
γ	reduction factor	—	—
γ	(specific) gravity	—	—
ε	local liquid/gas ratio	—	—
ε	pipe roughness	—	—
η	efficiency	—	—
η	elliptic coordinate	—	radians
θ	angle with respect to horizontal	—	radians
Θ	auxiliary variable	—	—
λ	fraction	—	—
λ	mobility	$L^3 m^{-1} t$	$m^2/(Pa \cdot s)$
μ	dynamic viscosity	$L^{-1} m t^{-1}$	$Pa \cdot s$
ξ	elliptic coordinate	L	m
P	density	$L^{-3} m$	kg/m^3
σ	interfacial tension	$m t^{-2}$	N/m
ϕ	porosity	—	—
φ	wetting angle	—	—
Φ	factor	$L^6 t^{-2}$	s^2/m^6
ψ	angle, radial coordinate	—	radians
ψ	correction factor	—	—
ω	angular velocity	—	rad/s

Subscripts

0	operating point
abs	absolute
acc	acceleration
act	actual
ana	analytical
ann	annulus
asp	aspect
atm	atmospheric
av	average
B	at bubblepoint
bot	bottom
bub	bubble
c	casing
c	contraction
ch	choke
conv	converging
crit	critical
d	diameter
d	discharge
d	drift
dis	discharge
ds	downstream
D	dimensionless
e	expected
e	external
eff	effective
ell	ellipse
eq	equivalent
f	flow
f	friction
fg	friction, gas
fl	flowline
fld	flooding
fo	friction, oil
frac	fracture
fric	friction
fw	friction, water
g	gas

<i>g</i>	Gravity
<i>gc</i>	gas, critical
<i>gl</i>	gas/liquid
<i>go</i>	gas/oil
<i>gow</i>	gas/oil/water
<i>grav</i>	Gravity
<i>gv</i>	gas velocity
<i>gw</i>	gas/water
<i>h</i>	horizontal
<i>h</i>	hydraulic
<i>hor</i>	horizontal
<i>i</i>	counter
<i>int</i>	intermediate
<i>ip</i>	intake pressure
<i>k</i>	kinetic
<i>kin</i>	kinetic
<i>Ku</i>	kutateladze
<i>l</i>	liquid
<i>lv</i>	liquid velocity
<i>m</i>	mixture
<i>max</i>	maximum
<i>mf</i>	manifold
<i>mn</i>	mixture, no-slip
<i>ms</i>	mixture, slip
<i>MB</i>	Mukherjee and Brill
<i>num</i>	numerical
<i>o</i>	oil
<i>ob</i>	oil at bubblepoint
<i>og</i>	oil/gas
<i>opt</i>	optimal
<i>org</i>	oil, residual, gas
<i>orw</i>	oil, residual, water
<i>ow</i>	oil/water
<i>p</i>	pressure
<i>p</i>	produced
<i>pc</i>	pseudocritical
<i>perm</i>	permanent
<i>pr</i>	seudoreduced
<i>rec</i>	recovery
<i>red</i>	reduced
<i>ref</i>	reference

<i>rg</i>	relative, gas
<i>ro</i>	relative, oil
<i>rog</i>	relative, oil/gas
<i>row</i>	relative, oil/water
<i>rw</i>	relative, water
<i>R</i>	reservoir
<i>Re</i>	Reynolds
<i>sc</i>	at standard conditions
<i>s</i>	in solution (in oil)
<i>s</i>	skin
<i>s</i>	slip
<i>sb</i>	in solution at bubblepoint pressure
<i>sc</i>	standard conditions
<i>sep</i>	separator
<i>sg</i>	superficial, gas
<i>s/l</i>	superficial, liquid
<i>st</i>	stages
<i>suc</i>	suction
<i>sw</i>	in solution in water
<i>t</i>	total
<i>t</i>	tubing
<i>tf</i>	flowing tubinghead
<i>tot</i>	total
<i>us</i>	upstream
<i>v</i>	valve
<i>v</i>	velocity
<i>v</i>	vertical
<i>v</i>	volatilized
<i>v</i>	volume
<i>w</i>	water
<i>w</i>	(molecular) weight
<i>w</i>	well
<i>w</i>	wet
<i>wc</i>	closed-in wellbore
<i>wf</i>	flowing wellbore
<i>wi</i>	water, immobile
<i>wo</i>	water/oil
<i>ws</i>	static wellbore
μ	liquid viscosity
μ_c	corrected liquid viscosity

Superscripts

- 0 endpoint
- g originating from the downhole gas phase
- o originating from the downhole oil phase

Glossary

AHD	along-hole depth
AIChE	American Institute of Chemical Engineers
AIME	American Institute of Mining and Metallurgical Engineers
AOFP	absolute open-flowing potential
API	American Petroleum Institute
ASME	American Society of Mechanical Engineers
bbl	barrel
BHP	bottomhole pressure
BHT	bottomhole temperature
B/D	barrel(s) per day
BSW	base sediment and water
CBHP	closed-in bottomhole pressure
CIM	Canadian Institute of Mining, Metallurgy and Petroleum
CTHP	closed-in tubinghead pressure
CGR	condensate/gas ratio
DLS	dogleg severity
EOS	equation of state
ESP	electrical submersible pump
E&P	exploration and production
FDP	field development plan(ning)
FBHP	flowing bottomhole pressure
FBHT	flowing bottomhole temperature
FTHP	flowing tubinghead pressure
FTHT	flowing tubinghead temperature
FVF	formation volume factor
GLR	gas/liquid ratio
GOC	gas/oil contact
GOR	gas/oil ratio
GUI	graphical user interface
GWC	gas/water contact
H&B	Hagedorn and Brown
ICV	inflow control valve
ID	inside diameter
II	injectivity index
IPR	inflow performance relationship
LC	level control
M&B	Mukherjee and Brill
MD	measured depth
ML	multilateral
MWD	measurement while drilling
OCR	oil/condensate ratio
OD	outside diameter
OGR	oil/gas ratio

OWC	oil/water contact
PC	pressure control
PDG	permanent downhole gauge
PI	productivity index
ppg	lbm per gallon
PVT	pressure/volume/temperature
rpm	revolutions per minute
scf	standard cubic foot
SCSSV	surface-controlled subsurface safety valve
SPE	Society of Petroleum Engineers
STB	stock-tank barrel
STB/D	stock-tank barrels per day
THP	tubinghead pressure
THT	tubinghead temperature
TVD	true vertical depth
VLE	vapor/liquid equilibrium
WOR	water/oil ratio

References

- Al-Hussainy, R., Ramey, H. J., and Crawford, P. B. 1966. The Flow of Real Gases through Porous Media. *Journal of Petroleum Technology* **18** (5): 624–636. <https://doi.org/10.2118/1243-A-PA>.
- Al-Safran, E. M. and Kelkar, M. 2009. Predictions of Two-Phase Critical-Flow Boundary and Mass-Flow Rate Across Chokes. *SPE Production and Operations* **24** (2) 249–256. <https://doi.org/10.2118/109243-PA>.
- Arnold, K. and Stewart, M. 1998. *Surface Production Operations*, second edition, Vols. 1 and 2. Houston, TX: Gulf.
- Aziz, K. and Settari, A. 1979. *Petroleum Reservoir Simulation*. London: Applied Science.
- Babu, D. K. and Odeh, A. S. 1988. Productivity of a Horizontal Well. *SPE Reservoir Engineering* **4** (4): 417–421. <https://doi.org/10.2118/18298-PA>.
- Bear, J. 1972. *Dynamics of Fluids in Porous Media*. Amsterdam: Elsevier. Reprint: New York, NY: Dover, 1988.
- Beggs, H. D. 1991. *Production Optimization Using NODAL Analysis*. Tulsa, OK: Oil and Gas Consultants International Publications.
- Beggs, H. D. and Brill, J. P. 1973. A Study of Two-Phase Flow in Inclined Pipes. *Journal of Petroleum Technology* **25** (5): 607–617. <https://doi.org/10.2118/4007-PA>.
- Beggs, H. D. and Robinson, J. R. 1975. Estimating the Viscosity of Crude Oil Systems. *Journal of Petroleum Technology* **27** (9): 1140–1141. <https://doi.org/10.2118/5434-PA>.
- Bellarby, J. 2009. *Well Completion Design*. Amsterdam: Elsevier.
- Bieker, H. P., Slupphaug, O., and Johansen, T. A. 2007. Real-Time Production Optimization of Oil and Gas Production Systems: A Technology Survey. *SPE Production and Operations* **22** (4): 382–391. <https://doi.org/10.2118/99446-PA>.
- Bird, R. B., Stewart, W. E., and Lightfoot, E. N. 2002. *Transport Phenomena*, second edition. New York, NY: Wiley.
- Boyce, W. E. and DiPrima, R. C. 2012. *Elementary Differential Equations*, tenth edition. New York, NY: Wiley.
- Brill, J. P. and Mukherjee, H. 1999. *Multi-Phase Flow in Wells*. SPE Monograph Series 17. Richardson, TX: SPE.
- Brown, K. E. 1984. *The Technology of Artificial Lift Methods, Volume 4: Production Optimization of Oil and Gas Wells by Nodal Systems Analysis*. Tulsa, OK:

PennWell.

- Brown, K. E. and Lea, J. F. 1985. Nodal Systems Analysis of Oil and Gas Wells. *Journal of Petroleum Technology* **37** (10): 1751–1763. <https://doi.org/10.2118/14714-PA>.
- Butler, R. M. 1994. *Horizontal Wells for the Recovery of Oil, Gas and Bitumen*. Petroleum Society Monograph 2. Calgary, AB, Canada: Petroleum Society of the CIM.
- Carr, N. L., Kobayashi, R., and Burrows, D. B. 1954. Viscosity of Hydrocarbon Gases under Pressure. *Journal of Petroleum Technology* **6** (10): 47–55. <https://doi.org/10.2118/297-G>.
- Carslaw, H. S. and Jaeger, J. C. 1959. *Conduction of Heat in Solids*, second edition. Oxford: Clarendon Press.
- Chierici, G. L. 1994. *Principles of Petroleum Reservoir Engineering*. Berlin: Springer.
- Chilingarian, G. V., Robertson, J. O., and Kumar, S. 1987. *Surface Operations in Petroleum Production*, Vols. 1 and 2. Amsterdam: Elsevier.
- Chin, W. C. 2002. *Quantitative Methods in Reservoir Engineering*. Woburn, TX: Gulf Professional.
- Civan, F. 2000. *Reservoir Formation Damage*. Houston, TX: Gulf.
- Colebrook, C. F. 1939. Turbulent Flow in Pipes with Particular Reference to the Transition Region between the Smooth and Rough Pipe Laws. *Journal of the Institute of Civil Engineers* **11**: 133–156.
- Cornelius, K. C. and Srinivas, K. 2004. Isentropic Compressible Flow for Non-Ideal Gas Models for a Venturi. *Journal of Fluids Engineering* **126** (2): 238–244. <https://doi.org/10.1115/1.1677499>.
- Dake, L. P. 1978. *Fundamentals of Reservoir Engineering*. Amsterdam: Elsevier.
- Danesh, A. 1998. *PVT and Phase Behavior of Petroleum Reservoir Fluids*. Amsterdam: Elsevier.
- Dempsey, J. R. 1965. Computer Routine Treats Gas Viscosity as a Variable. *Oil and Gas Journal*, 16 August, 141–142.
- Dietz, D. N. 1965. Determination of Average Reservoir Pressure from Build-Up Surveys. *Journal of Petroleum Technology* **17** (18): 955–959. <https://doi.org/10.2118/1156-PA>.
- Dikken, B. J. 1990. Pressure Drop in Horizontal Wells and Its Effect on Production Performance. *Journal of Petroleum Technology* **42** (11): 1426–1433. <https://doi.org/10.2118/19824-PA>.
- Dranchuk, P. M. and Abu-Kasem, J. H. 1975. Calculation of Z-Factors for Natural Gasses Using Equations-of-State. *Canadian Journal of Petroleum Technology* **14** (3): 34–36. <https://doi.org/10.2118/75-03-03>.
- Dullien, F. A. L. 1979. *Porous Media—Fluid Transport and Pore Structure*. New York,

- NY: Academic Press.
- Duns, H. and Ros, N. C. J. 1963. Vertical Flow of Gas and Liquid Mixtures in Wells. *Proc., Sixth World Petroleum Congress, Sec. 2*, 451–465, Paper 22-PD6.
- Economides, M. J., Deimbacher, F. X., Brand, C. W. et al. 1991. Comprehensive Simulation of Horizontal-Well Performance. *SPE Formation Evaluation* **6** (4): 418–426. <https://doi.org/10.2118/20717-PA>.
- Economides, M. J., Hill, A. D., Ehlig-Economides, C. et al. 2013. *Petroleum Production Systems*, second edition. Upper Saddle River, NJ: Prentice Hall.
- Economides, M. J., Watters, L. T., and Dunn-Norman, S. 1998. *Petroleum Well Construction*. New York, NY: Wiley.
- Evinger, H. H. and Muskat, M. 1942. Calculation of Productivity Factors for Oil-Gas-Water Systems in the Steady State. *Trans., AIME* **146**: 194–203.
- Fetkovich, M. J. 1973. The Isochronal Testing of Oil Wells. Paper presented at the SPE Fall Meeting, Las Vegas, Nevada, USA, 30 September–3 October. SPE-4529-MS. <https://doi.org/10.2118/4529-MS>.
- Firoozabadi, A. 1999. *Thermodynamics of Hydrocarbon Reservoirs*. New York, NY: McGraw-Hill.
- Forchheimer, P. 1901. Wasserbewegung durch Boden. *Zeitschrift des Vereins deutscher Ingenieure* **45**: 1782–1788.
- Giger, F. M. 1987. Low-Permeability Reservoirs Development Using Horizontal Wells. Paper presented at the Low Permeability Reservoirs Symposium, Denver, Colorado, USA, 18–19 May. SPE-16406-MS. <https://doi.org/10.2118/16406-MS>.
- Gilbert, W. E. 1954. Flowing and Gas-Lift Well Performance. *API Drilling and Production Practice* **143**: 127–157.
- Glasø, O. 1980. Generalized Pressure/Volume/Temperature Correlations. *Journal of Petroleum Technology* **32** (5): 785–795.
- Golan, M. and Whitson, C. H. 1991. *Well Performance*, second edition. Englewood Cliffs, NJ: Prentice Hall.
- Govier, G. W. and Aziz, K. 2008. *The Flow of Complex Mixtures in Pipes*, second edition. Richardson, TX: SPE.
- GPSA. 1998. *Engineering Data Book—FPS*, eleventh edition. Tulsa, OK: Gas Processors Suppliers Association.
- Gradshteyn, I. S. and Ryzhik, I. M. 1980. *Table of Integrals, Series and Products*. London: Academic Press.
- Guo, B., Lyons, W. C., and Ghalambor, A. 2007. *Petroleum Production Engineering: A Computer-Assisted Approach*. Houston, TX: Gulf Professional.
- Hagedorn, A. R. and Brown, K. E. 1965. Experimental Study of Pressure Gradients Occurring During Continuous Two-Phase Flow in Small-Diameter Vertical Conduits. *Journal of Petroleum Technology* **17** (4): 475–484.

<https://doi.org/10.2118/940-PA>.

- Hagoort, J. 1988. *Fundamentals of Gas Reservoir Engineering*. Amsterdam: Elsevier.
- Harmathy, T. Z. 1960. Velocity of Large Drops and Bubbles in Media of Infinite or Restricted Extent. *AIChE Journal* **6** (2): 281–288. <https://doi.org/10.1002/aic.690060222>.
- Hasan, A. R. and Kabir, C. S. 2002. *Fluid Flow and Heat Transfer in Wellbores*. Richardson, TX: SPE.
- Hawkins, M. F. 1956. A Note on the Skin Effect. *Journal of Petroleum Technology* **8** (12): 65–66. <https://doi.org/10.2118/732-G>.
- Hill, A. D., Zhu, D., and Economides, M. J. 2008. *Multilateral Wells*. Richardson, TX: SPE.
- Jansen, J. D., Bosgra, O. H., and van den Hof, P. M. J. 2008. Model-Based Control of Multiphase Flow in Subsurface Oil Reservoirs. *Journal of Process Control* **18** (9): 846–855. <https://doi.org/10.1016/j.jprocont.2008.06.011>.
- Joshi, S. D. 1988. Augmentation of Well Productivity with Slant and Horizontal Wells. *Journal of Petroleum Technology* **40** (6): 729–739. <https://doi.org/10.2118/15375-PA>.
- Joshi, S. D. 1991. *Horizontal Well Technology*. Tulsa, OK: PennWell.
- Kamal, M. M. 2009. *Transient Well Testing*, SPE Monograph Series 23. Richardson, TX: SPE.
- Karnopp, D. C., Margolis, D. L., and Rosenberg, R. C. 2000. *System Dynamics*, third edition. New York, NY: Wiley.
- Lake, L. W., ed. 2007. *Petroleum Engineering Handbook*, Vols. 1–7. Richardson, TX: SPE.
- MATLAB. 2017. <https://mathworks.com/help> (accessed 17 March 2017).
- McCain, W. D. 1990. *The Properties of Petroleum Fluids*, second edition. Tulsa, OK: PennWell.
- Moody, L. F. 1944. Friction Factors for Pipe Flow. *Trans., ASME* **66**: 671–684.
- Moran, M. J. and Shapiro, H. N. 1998. *Fundamentals of Engineering Thermodynamics*, third edition. New York, NY: Wiley.
- Morse, P. M. and Feshbach, H. 1953. *Methods of Theoretical Physics*, Vols. 1 and 2. New York, NY: McGraw Hill.
- Mukherjee, H. and Brill, J. P. 1983. Liquid Holdup Correlations for Inclined Two-Phase Flow. *Journal of Petroleum Technology* **35** (5): 1003–1008. <https://doi.org/10.2118/10923-PA>.
- Mukherjee, H. and Brill, J. P. 1985a. Empirical Equations to Predict Flow Patterns in Two-Phase Inclined Flow. *International Journal of Multi-Phase Flow* **11** (3): 299–315. [https://doi.org/10.1016/0301-9322\(85\)90060-6](https://doi.org/10.1016/0301-9322(85)90060-6).

- Mukherjee, H. and Brill, J. P. 1985b. Pressure Drop Correlations for Inclined Two-Phase Flow. *ASME Journal of Energy Resources Technology* **107** (4): 549–554. <https://doi.org/10.1115/1.3231233>.
- Muskat, M. 1937. *The Flow of Homogeneous Fluids through Porous Media*. New York, NY: McGraw-Hill.
- Muskat, M. 1949. *Physical Principles of Oil Production*. New York, NY: McGraw-Hill.
- Naus, M. M. J. J., Dolle, N., and Jansen, J. D. 2006. Optimization of Commingled Production Using Infinitely Variable Inflow Control Valves. *SPE Production and Operations* **21** (2): 293–301. <https://doi.org/10.2118/90959-PA>.
- Nind, T. E. W. 1964. *Principles of Oil Well Production*. New York, NY: McGraw-Hill.
- Nind, T. E. W. 1981. *Principles of Oil Well Production*, second edition. New York, NY: McGraw-Hill.
- Ouyang, L. B. and Aziz, K. 2001. A General Single-Phase Wellbore/Reservoir Coupling Model for Multilateral Wells. *SPE Reservoir Evaluation and Engineering* **4** (4): 327–335. <https://doi.org/10.2118/72467-PA>.
- Perkins, T. K. 1993. Critical and Sub-Critical Flow of Multi-Phase Mixtures through Chokes. *SPE Drilling and Completion* **8** (4): 271–276. <https://doi.org/10.2118/20633-PA>.
- Perry, R. H., Green, D. W., and Maloney, J. O., eds. 1997. *Perry's Chemical Engineers' Handbook*, seventh edition. New York, NY: McGraw-Hill.
- Pipesim. 2017. <http://www.software.slb.com/products/pipesim#js> (accessed 17 March 2017).
- Press, W. H., Teukolsky, S. A., Vetterling, W. T. et al. 2007. *Numerical Recipes: The Art of Scientific Computing*, third edition. Cambridge: Cambridge University Press.
- Prosper. 2017. <http://www.petex.com/products/?ssi=3> (accessed 17 March 2017).
- Ros, N. C. J. 1960. An Analysis of Critical Simultaneous Gas-Liquid Flow through a Restriction and Its Application to Flow Metering. *Applied Scientific Research* **9** (1): 374–388. <https://doi.org/10.1007/BF00382215>.
- Ros, N. C. J. 1961. Simultaneous Flow of Gas and Liquid as Encountered in Well Tubing. *Journal of Petroleum Technology* **13** (10): 1037–1049. <https://doi.org/10.2118/18-PA>.
- Rossi, D. J., Gurpinar, O., Nelson, R. et al. 2000. Discussion on Integrating Monitoring Data Into the Reservoir Management Process. Paper presented at the SPE European Petroleum Conference, Paris, France, 24–25 October. SPE-65150-MS. <https://doi.org/10.2118/65150-MS>.
- Russell, D. G., Goodrich, J. H., Perry, G. E. et al. 1966. Methods of Predicting Gas Well Performance. *Journal of Petroleum Technology* **18** (1): 99–109. <https://doi.org/10.2118/1242-PA>.
- Sachdeva, R., Schmidt, Z., Brill, J. P. et al. 1986. Two-Phase Flow through Chokes. Paper presented at the SPE Annual Technical Conference and Exhibition, New

Orleans, Louisiana, USA, 5–8 October. SPE-15657-MS.
<https://doi.org/10.2118/15657-MS>.

Schlichter, C. S. 1898. Theoretical Investigation of the Motion of Ground Waters. In *19th Annual Report of the U.S. Geological Survey, 1897–1898, Part 2: Papers Chiefly of a Theoretic Nature*. Washington, DC: USGS.

Schüller, R. B., Munaweera, S., Selmer-Olsen, S. et al. 2006. Critical and Sub-Critical Oil/Gas/Water Mass Flow Rate Experiments and Predictions for Chokes. *SPE Production and Operations* **21** (3): 372–380. <https://doi.org/10.2118/88813-PA>.

Schüller, R. B., Solbakken, T., and Selmer-Olsen, S. 2003. Evaluation of Multi-Phase Flow Rate Models for Chokes under Sub-Critical Oil/Gas/Water Flow Conditions. *SPE Production and Facilities* **18** (3): 170–181. <https://doi.org/10.2118/84961-PA>.

Shi, H., Holmes, J. A., Diaz, L. R. et al. 2005a. Drift-Flux Parameters for Three-Phase Steady-State Flow in Wellbores. *SPE Journal* **10** (2): 130–137. <https://doi.org/10.2118/89836-PA>.

Shi, H., Holmes, J. A., Durlofsky, L. J. et al. 2005b. Drift-Flux Modeling of Two-Phase Flow in Wellbores. *SPE Journal* **10** (1): 24–33. <https://doi.org/10.2118/84228-PA>.

Shoham, O. 2006. *Mechanistic Modeling of Gas-Liquid Two-Phase Flow in Pipes*. Richardson, TX: SPE.

SPE. 1982. *The SI Metric System of Units and SPE Metric Standard*. Richardson, TX: SPE.

SPE. 2015. *SPE Style Guide, 2015-2016 ed*. Richardson, TX: SPE.

Standing, M. B. 1947. A Pressure-Volume-Temperature Correlation for Mixtures of California Oils and Gases. *API Drilling and Production Practice*, 275–287.

Standing, M. B. 1952. *Volumetric and Phase Behavior of Oil Field Hydrocarbon Systems*. New York, NY: Reinhold. Reprint: Dallas, TX: SPE, 1977.

Standing, M. B. 1971. Concerning the Calculation of Inflow Performance of Wells Producing From Solution Gas Drive Reservoirs. *Journal of Petroleum Technology* **23** (9): 1141–1142. <https://doi.org/10.2118/3332-PA>.

Standing, M. B. and Katz, D. L. 1942. Density of Natural Gases. *Trans., AIME* **146**: 140–149.

Stone, H. L. 1973. Estimation of Three-Phase Relative Permeability and Residual Oil Data. *Journal Canadian Petroleum Technology* **12** (4): 53–61. <https://doi.org/10.2118/73-04-06>.

Sutton, R. P. 1985. Compressibility Factors for High-Molecular Weight Reservoir Gases. Paper presented at the SPE Annual Technical Conference and Exhibition, Las Vegas, Nevada, USA, 22–26 September. SPE-14265-MS. <https://doi.org/10.2118/14265-MS>.

Takacs, G. 1976. Comparisons Made for Computer Z-Factor Calculations. *Oil and*

Gas Journal, 20 December, 64–66.

Taylor, H. L. and Mason, C. M. 1972. A Systematic Approach to Well Surveying Calculations. *SPE Journal* **12** (6): 474–488. <https://doi.org/10.2118/3362-PA>.

Van Everdingen, A. F. 1953. The Skin Effect and Its Influence on the Productive Capacity of a Well. *Journal of Petroleum Technology* **5** (6): 171–176. <https://doi.org/10.2118/203-G>.

Vazquez, M. and Beggs, H. D. 1980. Correlations for Fluid Physical Property Prediction. *Journal of Petroleum Technology* **32** (6): 968–970. <https://doi.org/10.2118/6719-PA>.

Verruijt, A. 1970. *Theory of Ground Water Flow*. London: MacMillan.

Vogel, J. V. 1968. Inflow Performance Relationships for Solution-Gas Drive Wells. *Journal of Petroleum Technology* **20** (1): 83–92. <https://doi.org/10.2118/1476-PA>.

Vreedenburgh, C.G.J. 1936. On the Steady Flow of Water Percolating Through Soils With Homogeneous-Anisotropic Permeability. *Proc. First International Conference on Soil Mechanics and Foundation Engineering*, **1** 222-225, Cambridge, Massachusetts, USA, 22-26 June.

Wallis, G. B. 1969. *One-Dimensional Two-Phase Flow*. New York, NY: McGraw-Hill.

Wallis, G. B. and Makkenchery, S. 1974. The Hanging Film Phenomenon in Vertical Annular Two-Phase Flow. *ASME Journal of Fluids Engineering* **96** (3): 297–298. <https://doi.org/10.1115/1.3447155>.

Walsh, M. P. and Lake, L. W. 2003. *A Generalized Approach to Primary Hydrocarbon Recovery*. Amsterdam: Elsevier.

WellFlo. 2017. Weatherford. <http://www.weatherford.com/doc/wft303551> (accessed 17 March 2017).

White, F. M. 2016. *Fluid Mechanics*, 8th ed. McGraw Hill. New York, NY: McGraw-Hill.

Whitson, C. H. and Brûlé, M. R. 2000. *Phase Behavior*. SPE Monograph Series 20. Richardson, TX: SPE.

Whittaker, E. T. and Watson. G. N. 1915. *A Course of Modern Analysis*, second edition. Cambridge: Cambridge University Press.

Wiggins, M. L., Russell, J. E., and Jennings, J. W. 1992. Analytical Inflow Performance Relationships for Three-Phase Flow in Bounded Reservoirs. Paper presented at the SPE Western Regional Meeting, Bakersfield, California, USA, 30 March–1 April. SPE-24055-MS. <https://doi.org/10.2118/24055-MS>.

Zaremba, W. A. 1973. Directional Survey by the Circular Arc Method. *SPE Journal* **13** (1): 5–11. <https://doi.org/10.2118/3664-PA>.

Zigrang, D. J. and Sylvester, N. D. 1985. A Review of Explicit Friction Factor Equations. *ASME Journal of Energy Resources Technology* **107** (2): 280–283. <https://doi.org/10.1115/1.3231190>.

Zuber, N. and Findlay, J. A. 1965. Average Volumetric Concentration in Two-Phase Flow Systems. *ASME Journal of Heat Transfer* **87** (4): 453–468.
<https://doi.org/10.1115/1.3689137>.

INDEX

A

absolute open-flowing potential (AOFP), 117, 137, 138
absolute permeability, 186, 291
acceleration loss, 48
along-hole depth (AHD), 45, 257, 259, 260
analysis node, 14–16, 19, 207, 208, 211, 212
anisotropic permeability
 fully penetrating horizontal wells, 172–173
 two-dimensional reservoir flow, 161–164
annular geometry flow, 56
AOFP. See [absolute open-flowing potential \(AOFP\)](#)
artificial lift, 10
 ESPs, 217–219
 forms, 220
 gas lift, 216
average reservoir pressure, 171

B

barefoot completion, 8
base sediment and water (BSW), 28
base SI units, 3
beam pumps, 10
Bernoulli equation, 88, 89, 94, 107
binary-mixture model, 33
bisection method, 263–264
black oil, 29
 correlations, 38
 model, 35–36
box-shaped reservoir, 164, 165, 168
BSW. See [base sediment and water \(BSW\)](#)
bubblepoint line, 28, 29
bubblepoint pressure, 25
Buckley-Leverett equation, 192

C

choked flow, 85, 209
choke performance curves
 multiphase flow, 102, 103, 105, 109, 110
 single-phase gas flow, 91, 92, 100
 well performance, 209–211, 213–215
condensate/gas ratio (CGR), 25
conformal mapping, 160

coning, 192–193
cricondenbar, 28
cricondentherm, 29
critical flow
 definition, 85
 multiphase flow, 101–102, 107–109
 single-phase gas flow, 95–97
critical point, 28
cuspding, 192–193

D

daily production control, 5
Darcy's law, 122, 157
debottlenecking, 16
depletion flow, 119
derived SI units, 3
dewpoint line, 28
differential equations
 initial value problem, 268
 numerical implementation, 269–270
 numerical integration, 268–269
diffusivity equation, 154
dogleg severity (DLS), 260
drift flux model, 72
dry gas, 29
 reservoirs, 29
dual completion, 8

E

effort variables, 10–12
electric submersible pumps (ESPs), 10, 217–219
element equations
 pressure drop analysis, in multiphase flow, 72
 system models, 11–13
equations of state (EOS)
 single-phase gas, 30–31
 single-phase oil, 31–32
 VLE, 29–30
equipotential lines, 157
ESPs. See [electric submersible pumps \(ESPs\)](#)
exploration and production (E&P), 4, 24, 31
extended black oil model. See [volatile oil model](#)

F

falloff, 116
FBHP. See [flowing bottomhole pressure \(FBHP\)](#)

field development planning
iterative processes, 4
well performance
inflow performance improvement, 212, 213
producing fields, 212
tubing and choke size, 213–215
tubing intake curve, 215–216
field units, 235–236
finite skin approach, 131
flash test, 27
flowing bottomhole pressure (FBHP), 53, 72, 73, 79–80, 202, 204, 205
flowing tubinghead pressure (FTHP), 9, 53, 72, 73, 75, 79, 201–205
flow performance tables. See [lift tables](#)
flow regimes
horizontal flow, 64
vertical flow, 65
flow variables, 10–12
fluid properties, 239–240
Forchheimer's coefficient, 122, 132, 136, 209
formation damage, 128–129
friction loss, 46–48
fully penetrating horizontal wells
anisotropic permeability, 172–173
average reservoir pressure, 171
horizontal flow, 164–166
near-well radial flow, 166–170
semisteady-state flow, 171–172
skin factor, 170–171

G

gas compressibility factor, 31
gas condensate reservoirs, 29
gas correlations, 247–254
gas density at standard conditions, 24
gas deviation factor, 31
gas expansion factor, 27
gas formation volume factor, 25–26, 37
gas lift, 10, 216
gas/liquid ratio (GLR), 27
gas/liquid separator, 9
gas/oil ratio (GOR), 25, 27, 73, 216
general radial flow solution, 156
geometric skin factor, 170–171
Glasø correlations, 38
gradient curves, 72–73
gravity loss, 48

H

Hagedorn and Brown model, 71–72, 271–278

head loss, 45–46, 48

horizontal wells

inflow performance

fully penetrating, 164–174

multilateral wells, 180–186

multiphase flow, 186–193

partially penetrating, 174–180

schematics, 7

hydrocarbon fluids, categories of, 29

I

ICVs. See inflow control valves (ICVs)

ideal-gas law, 30

inclination, 45

inertia coefficient, 122

infinite-acting flow, 118–119

inflow control valves (ICVs), 146, 147

inflow performance

definition, 116

governing equations, 119–122

horizontal wells

fully penetrating, 164–174

multilateral wells, 180–186

multiphase flow, 186–193

partially penetrating, 174–180

importance, 116–117

multilayer performance, 140–141

multiphase flow, 136–140

single-phase gas flow, 131–136

single-phase oil flow, 122–128

skin factor, 128–131

two-dimensional reservoir flow

anisotropic permeability, 161–164

image wells, 159–161

Laplace equation, 153–155

linear superposition, 157–159

polar coordinates, 155–157

well operation and reservoir flow stages, 117–119

inflow performance relationship (IPR), 116, 202, 204, 209, 211, 216, 218

injectivity index (II), 116

interfacial tensions, 26

J

joint node, 14

Joule-Thomson cooling, 122

L

- Laplace equation, 153–155, 160, 166, 176
- lift requirement curve, 218
- lift tables, 79–80
- linear superposition, 157
- liquid holdup, 63, 66

M

- MATLAB assignment
 - choke flow, 113–114
 - Commingled production with a smart well, 145–151
 - drift flux, 83–84
 - horizontal well inflow and pressure drop, 195–199
 - hydrocarbon properties, 40–42
 - multiphase flow, 83–84
 - nodal analysis, 18–21
 - single-phase gas flow, 59–61
 - well performance, 229–232
- MATLAB files
 - black oil correlations, 38
 - choke flow, 87, 91, 95, 100, 109, 345
 - conversion factors, 3, 340–342
 - demo, 346
 - fluid properties, 343–344
 - graphical user interface, 346
 - guidance for use, 339
 - horizontal well inflow performance, 174, 177, 182
 - lift tables, 80, 344
 - Moody friction factor, 48
 - multilateral wells, 184
 - pipe flow, 344
 - reservoir flow, 345
 - routines, 2–3
 - survey, 343
 - systems, 346
 - tubing performance, 53
- measurement-while-drilling (MWD) tools, 46
- mechanical interference, 128
- mechanistic models, 70
- microbial damage, 129
- modified black oil model. See [volatile oil model](#)
- Moody chart, 47
- Moody friction factor, 46
- Mukherjee and Brill correlation, 73, 278–283
- Mukherjee and Brill model, 72
- multilateral wells, 184, 186
- multiphase flow

choke flow

- critical flow empirical models, [101–102](#)
- polytropic flow, [104–107](#)
- pressure drop, [109–110](#)
- sub-critical flow empirical models, [102–104](#)

correlations

- drift flux models, [284–290](#)
- Hagedorn and Brown, [271–278](#)
- Mukherjee and Brill, [278–284](#)

dimensional analysis, [70–71](#)

flow regimes, [63–65](#)

inflow performance, [136–140](#)

- coning, [192–193](#)
- cusping, [192–193](#)
- gas/oil flow, [189–191](#)
- phase saturations, [188–189](#)
- pressure gradient, [187–188](#)
- primary recovery approximations, [191–192](#)
- relative permeabilities, [186–187](#)
- secondary recovery, [192](#)

lift tables, [79–80](#)

MATLAB assignment, [83–84](#)

pressure drop analysis

- element equations, [72](#)
- governing equations, [68–70](#)
- gradient curves, [72–73](#)
- holdup and friction correlations, [70–72](#)

tubing intake curve, [73–79](#)

multivariable root finding, [265–266](#)

N

near-well radial flow

- fully penetrating horizontal wells, [166–170](#)
- multilateral wells, [182–184](#)
- partially penetrating horizontal wells, [177](#)

Newton-Raphson iteration method, [189, 220, 264–265](#)

nodal analysis

- MATLAB assignment, [18–21](#)
- multiphase flow (see [multiphase flow](#))
- performance curves, [16](#)
- principle, [14](#)
- procedure, [15–16](#)
- production optimization, [16–17](#)
- well performance (see [well performance](#))

non-SI units, [3](#)

notation conventions, [3](#)

O

oil and gas production system

 basic elements, 7–9

 feedback control process, 6

 functions, 7

oil correlations, 241–247

oil density at standard conditions, 24

oil formation volume factor, 25, 26, 37

oil/gas ratio (OGR), 25

oil models

 black oil model, 35–36

 compositional model, 32–33

 volatile oil model, 33–35

openhole completion, 8

orifice equation, 89

orifice plate, 86

P

partially penetrating horizontal wells

 elliptic coordinates, 174–176

 horizontal flow, 176–177

 near-well radial flow, 177

 specific PI, 177–179

 well models, 179–180

perforations, 8

permanent downhole gauges (PDGs), 9, 116

petroleum life cycle model, 4–5

phase changes, 129

phase saturations, 186, 188–189

PI. See [productivity index \(PI\)](#)

pipelines, 7

p - q graph, 15–16, 205

pressure buildup tests, 116

pressure drop analysis, in multiphase flow

 element equations, 72

 governing equations, 68–70

 gradient curves, 72–73

 holdup and friction correlations, 70–72

pressure falloff tests, 116

pressure recovery factor, 90

pressure/temperature phase diagram, 28–29

pressure transient analysis, 127

producing gas/oil ratio, 27

producing oil/gas ratio, 27

production engineering, 4–6

production optimization, 5, 16–17

productivity index (PI), 116, 117, 125, 128, 130, 137, 158–161, 168, 172–182, 196, 215

pump curve, 217–219

R

regula falsi method, 264

relative permeabilities

- Corey expressions, 293–295

- multiphase flow, 186–187

- physics, 291–293

reservoir fluids

- equations of state, 29–32

- fluid properties

 - calculations, 37–38

 - standard conditions, 24–26

 - oil models, 32–36

 - pressure/temperature phase diagram, 28–29

 - production variables, 27–28

reservoir management, 5

residual mud solids, 128–129

restrictions, 85–87

retrograde condensation, 29

Reynolds number, 46–47

S

sand control equipment, 8

saturated oil reservoirs, 29

saturation-pressure paths, 188

scaled pipe roughness, 46–47

semiempirical models, 70

semisteady-state flow, 119

separator gas, 24

shrinkage factor, 26

single-phase fluid flow

- equation of state, 44–45

- friction loss, 46–48

- head loss, 45–46

- mass balance, 43–44

- momentum balance, 44

- pressure drop, 48

single-phase gas flow

- governing equations, 51

- inflow performance

 - analytical approximations, 132–136

 - numerical solution, 131–132

- Matlab assignment, 59–61

- restrictions

 - critical flow, 95–97

 - isentropic flow, 91–95

pressure drop, 97–101
solutions, 51–52
single-phase oil flow
governing equations, 49–50
inflow performance
analytical solution, 123–125
average reservoir pressure, 125–126
semisteady-state flow, 126–127
steady-state flow, 122–123
restrictions
choke performance curve, 91, 92
permanent pressure drop, 89–91
reversible pressure drop, 87–89
solutions, 50
SI units, 3
conversion factor, 233–235
dimensional constants, 236–237
force and mass, 233, 235–236
molar mass, 236
prefixes, 233, 235
skin factor, 170–171
slip, 63, 65
solution gas/oil ratio, 25
solution oil/gas ratio, 25
specific heat capacities, 26
SPE Symbols Standard, 3
standard conditions, 12, 13, 19, 23–26, 35
standard MATLAB functions, 266–268
Standing correlations, 38, 237, 241
state variables, 24
steady-state flow, 119
steady-state path, 188
storage tanks, 7
streamlines, 157
strict SI units, 3
surface-controlled subsurface safety valve (SCSSV), 8
surface facilities, 7–9, 212, 220
surveillance, 6
system equations, 13–14
system models
element equations, 11–13
flow and effort variables, 10–12
system equations, 13–14
topology, 10–11

T

Taylor bubbles, 64

test separator, 9
thick skin approach, 131

transient flow, 118–119

transitional flow, 119

tubing, 8

tubing intake curves

- multiphase flow, 73–79

- single-phase fluid flow, 52–56

tubing performance curves

- single-phase fluid flow, 52–55

- well performance, 209, 210

turbulence coefficient, 122

U

undersaturated oil reservoirs, 29

unit systems, 3

V

valve coefficient, 91

vapor/liquid equilibrium (VLE), 29–30

vena contracta, 86

venturi, 87, 89

vertical wells

- gradient curves, 73

- inflow performance, 126, 153

- pseudoholdup correlations, 271

- schematics, 7

- well performance, 201

volatile oil, 29

volatile oil model, 33–35

volatilized oil/gas ratio, 25

volume-averaged reservoir pressure, 125

W

water density at standard conditions, 25, 254

water formation volume factor, 26, 254, 255

water/oil ratio (WOR), 28

water properties, 254–255

wellbore surveying, 46

- evaluation, 257–260

- numerical implementation, 260–261

- rectangular coordinates, 257

wellhead, 8, 91

well performance

- artificial lift

- ESPs, 217–219

forms, 220
gas lift, 216
dynamic effects, 220
field development planning
 inflow performance improvement, 212, 213
 producing fields, 212
 tubing and choke size, 213–215
 tubing intake curve, 215–216
FTHP, 201–205
network topologies with loops, 220
operating point, stability of, 205–208
surface choke, 208–211
surface facilities, 220
temperature effects, 220–221
well trajectory, 45, 53, 81, 258
wet gas, 29, 37
WOR. See [water/oil ratio \(WOR\)](#)

Z

Z factor, 31, 249, 251–252